UNCLASSIFIED

AD NUMBER

AD887071

LIMITATION CHANGES

TO:

Approved for public release; distribution is unlimited.

FROM:

Distribution authorized to U.S. Gov't. agencies only; Test and Evaluation; JUL 1971. Other requests shall be referred to Air Force Weapons Lab., Kirtland AFB, NM 87117.

AUTHORITY

AFWL ltr 29 Apr 1985

THIS PAGE IS UNCLASSIFIED

AD 887071

AUTHORITY: AFWL ltr, 29 Apr 85

AD887071

AFWL-TR-
71-85

THE EFFECTIVE STRESS MECHANICS OF UNDRAINED SHEAR STRENGTH

Douglas H. Merkle
Major USAF
U. S. Air Force Academy

TECHNICAL REPORT NO. AFWL-TR-71-85

July 1971

AIR FORCE WEAPONS LABORATORY
Air Force Systems Command
Kirtland Air Force Base
New Mexico

AD No.
DDC FILE COPY

DDC
RECEIVED
AUG 31 1971
E

Distribution limited to US Government agencies only because of test and evaluation (July 1971). Other requests for this document must be referred to AFWL (DE), Kirtland AFB, NM 87117.

$3.4

UNCLASSIFIED

Security Classification

DOCUMENT CONTROL DATA - R & D

(Security classification of title, body of abstract and indexing annotation must be entered when the overall report is classified)

1. ORIGINATING ACTIVITY (Corporate author) Air Force Weapons Laboratory (DE) Kirtland Air Force Base, New Mexico 87117	2a. REPORT SECURITY CLASSIFICATION Unclassified 2b. GROUP

3. REPORT TITLE

THE EFFECTIVE STRESS MECHANICS OF UNDRAINED SHEAR STRENGTH

4. DESCRIPTIVE NOTES (Type of report and inclusive dates)

5. AUTHOR(S) (First name, middle initial, last name)

Douglas H. Merkle, Major, USAF

6. REPORT DATE July 1971	7a. TOTAL NO. OF PAGES 832	7b. NO. OF REFS
8a. CONTRACT OR GRANT NO. b. PROJECT NO. 683M c. Task 4 d.	9a. ORIGINATOR'S REPORT NUMBER(S) AFWL-TR-71-85 9b. OTHER REPORT NO(S) (Any other numbers that may be assigned this report)	

10. DISTRIBUTION STATEMENT

Distribution limited to US Government agencies only because of Test and Evaluation (July 1971). Other requests for this document must be referred to AFWL (DE), Kirtland AFB, NM 87117.

11. SUPPLEMENTARY NOTES	12. SPONSORING MILITARY ACTIVITY AFWL (DE-I) Kirtland AFB, NM 87117

13. ABSTRACT

(Distribution Limitation Statement B)

On the basis of theory and available experimental data, the influence of stress system (i.e., anisotropy, pore pressure response, rotation of principal planes and the intermediate principal stress) on the undrained shear strength of saturated clay, in terms of effective stress is explained. The developed theory to explain the influence of stress system on the results of model footing test conducted under Project MODIAP at the Massachusetts Institute of Technology is used. The concept of a three-dimensional strength surface is developed to explain the variation of shear strength, in terms of effective stress, in a cross-anisotropic clay. The concept of a three-dimensional pore pressure response surface is developed to explain the variation of pore pressure response in a cross-anisotropic clay. It is then shown that the intersection of these two surfaces defines the variation of undrained shear strength with the orientation of the principal stresses at failure. A numerical example is used to show that the effect of initial consolidation stresses (the q_o effect) cannot be ignored in predicting IN SITU undrained shear strength, when the principal planes rotate during shear. A technique expressing any triaxial stress failure criterion in terms of the octahedral stress invarients is developed and used to analyze strength data from numerous different soils. The Revised Coulomb criterion appears to be the best of the classic failure criteria for soils. However, a large number of soils exhibit a rapid increase in the effective angle of shearing resistance, as the intermediate principal stress begins to exceed the minor

(See next page)

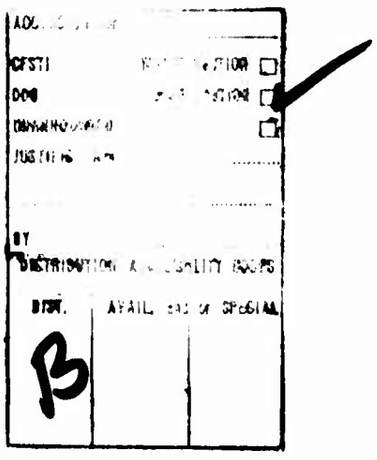

AIR FORCE WEAPONS LABORATORY
Air Force Systems Command
Kirtland Air Force Base
New Mexico 87117

When US Government drawings, specifications, or other data are used for any purpose other than a definitely related Government procurement operation, the Government thereby incurs no responsibility nor any obligation whatsoever, and the fact that the Government may have formulated, furnished, or in any way supplied the said drawings, specifications, or other data, is not to be regarded by implication or otherwise, as in any manner licensing the holder or any other person or corporation, or conveying any rights or permission to manufacture, use, or sell any patented invention that may in any way be related thereto.

This report is made available for study with the understanding that proprietary interests in and relating thereto will not be impaired. In case of apparent conflict or any other questions between the Government's rights and those of others, notify the Judge Advocate, Air Force Systems Command, Andrews Air Force Base, Washington, DC 20331.

DO NOT RETURN THIS COPY. RETAIN OR DESTROY.

14. KEY WORDS	LINK A		LINK B		LINK C	
	ROLE	WT	ROLE	WT	ROLE	WT
Stress mechanics Shear strength Undrained Stress systems Anisotropy Pore pressure response Model footing tests Project MODIAP Civil engineering						

ABSTRACT (cont'd)

principal stress. This same phenomenon is characteristic of a regular packing of equal, rough, rigid spheres, and it is shown that such packings deform in accordance with the normality rule of classical plasticity theory. A simple formula is developed which closely fits the MODIAP bearing capacity test results. The influence of stress system variables is explained in terms of their influence on three parameters defining the formula. Two of these three parameters are predicated independently from the results of conventional triaxial tests. Reliable prediction of the third parameter requires additional computer studies of the type already begun at M.I.T., but when the soil is anisotropic the q_o effect must be taken into account. A generalized stress path method is proposed for formulating deformation-type stress-strain relations when the soil is isotropic.

THE EFFECTIVE STRESS MECHANICS OF UNDRAINED SHEAR STRENGTH

Douglas H. Merkle
Major USAF
U. S. Air Force Academy

TECHNICAL REPORT NO. AFWL-TR-70-185

Distribution limited to US Government agencies only because of test and evaluation (July 1971). Other requests for this document must be referred to AFWL (DE), Kirtland AFB, NM 87117.

ABSTRACT

(Distribution Limitation Statement B)

On the basis of theory and available experimental data, the influence of stress system (i.e., anisotropy, pore pressure response, rotation of principal planes and the intermediate principal stress) on the undrained shear strength of saturated clay, in terms of effective stress is explained. The developed theory to explain the influence of stress system on the results of model footing test conducted under Project MODIAP at the Massachusetts Institute of Technology is used. The concept of a three-dimensional strength surface is developed to explain the variation of shear strength, in terms of effective stress, in a cross-anisotropic clay. The concept of a three-dimensional pore pressure response surface is developed to explain the variation of pore pressure response in a cross-anisotropic clay. It is then shown that the intersection of these two surfaces defines the variation of undrained shear strength with the orientation of the principal stresses at failure. A numerical example is used to show that the effect of initial consolidation stresses (the q_o effect) cannot be ignored in predicting IN SITU undrained shear strength, when the principal planes rotate during shear. A technique for expressing any triaxial stress failure criterion in terms of the octahedral stress invariants is developed and used to analyze strength data from numerous different soils. The Revised Coulomb criterion appears to be the best of the classic failure criteria for soils. However, a large number of soils exhibit a rapid increase in the effective angle of shearing resistance, as the intermediate principal stress begins to exceed the minor principal stress. This same phenomenon is characteristic of a regular packing of equal, rough, rigid spheres, and it is shown that such packings deform in accordance with the normality rule of classical plasticity theory. A simple formula is developed which closely fits the MODIAP bearing capacity test results. The influence of stress system variables is explained in terms of their influence on three parameters defining the formula. Two of these three parameters are predicated independently from the results of conventional triaxial tests. Reliable prediction of the third parameter requires additional computer studies of the type already begun at M.I.T., but when the soil is anisotropic the q_o effect must be taken into account. A generalized stress path method is proposed for formulating deformation-type stress-strain relations when the soil is isotropic.

FOREWORD

This research was peformed under Program Element 63723F, Project 683M, Task 4.

Inclusive dates of research were June 1966 through May 1971. The report was submitted 28 June 1971 by the Air Force Weapons Laboratory Project Officer, Major Paul Y. Thompson (DE-I).

This report is the thesis submitted to the Massachusetts Institute of Technology by Major Douglas H. Merkle in partial fulfillment of the requirements for the degree of Doctor of Philosophy.

This report has been reviewed and is approved.

PAUL Y. THOMPSON
Major, USAF
Assistant Chief, Civil Engineering
Research Division

JEAN M. MARCHAND
Lt Colonel, USAF
Chief, Civil Engineering
Research Division

CONTENTS

Chapter		Page
1	INTRODUCTION	1
	Objective and Scope	1
	Motivation	1
	Technical Considerations	4
2	BASIC SHEAR STRENGTH CONCEPTS	9
	Purpose	9
	Importance of Shear Strength	9
	Consequences of the Nature of Soil	10
	The Revised Coulomb Equation	11
	Experimental Definition of Shear Strength Parameters	14
	Relations Between Principal Effective Stresses at Failure	16
	Thesis Structure	19
3	ANISOTROPY OF SHEAR STRENGTH PARAMETERS	25
	Purpose	25
	Clay Structure	26
	Basic Questions of Anisotropy	26
	Review of Early Work	28
	General Concepts of Anisotropic Shear Strength Analysis	36
	Basic Equations of Anisotropic Shear Strength Analysis	43
	Three-Dimensional Failure Surface	45
	Isotropy as a Limiting Case of Anisotropy	48
	Anisotropic Cohesion Assumed by Jaeger	49
	Anisotropic Angle of Internal Friction	53
	New General Method of Anisotropic Shear Strength Analysis	55
	Experimental Determination of $\bar{c}(\alpha)$ and $\bar{\Phi}(\alpha)$	60
	Discussion of Test Data	62
	Summary	127

CONTENTS (cont'd)

Chapter		Page
4	PORE PRESSURE RESPONSE	287
	Purpose	287
	Historical Development	287
	Pore Pressure Response Prediction	239
	Stress Path Approach	290
	Pore Pressure Response Surface	300
	Influence of the Intermediate Applied Principal Stress Increment	303
	Discussion of Test Data	306
	Summary	309
5	ROTATION OF PRINCIPAL PLANES	319
	Purpose	319
	Variation of Undrained Shear Strength	321
	Numerical Examples	323
	Summary	328
6	INFLUENCE OF THE INTERMEDIATE PRINCIPAL STRESS	335
	Purpose	335
	Interpretation of Test Data	336
	Basic Approaches	341
	The General Approach	341
	The Limited Approach	346
	Discussion of Test Data	354
	An Idealized Strength Model	455
	Summary	456
7	ANALYSIS OF MODIAP FOOTING TEST RESULTS	614
	Purpose	614
	Empirical Settlement Curve	617
	Discussion of Test Data	621
	Predicting the Elastic Subgrade Modulus	625
	Predicting the Bearing Capacity	628
	Predicting the Plastic Settlement Parameter	630

CONTENTS (cont'd)

Chapter		Page
	Useful Range of Elastic Theory in Predicting Initial Settlement	637
	Size Effects	639
	Influence of Stress System	640
	Summary	645
8	GENERAL SUMMARY	685
	BIBLIOGRAPHY	689
	APPENDIXES	
	A EXCESS PORE PRESSURE RESPONSE IN AN ISOTROPIC SOIL	711
	B ANALYSIS OF STRESS IN SOIL	715
	Purpose	715
	Stress Transformation Equations	715
	Principal Stresses	720
	Principal Stress Directions	735
	Cayley-Hamilton Theorem	736
	Simplification of Stress Analysis by Using Principal Stress Axes as Coordinate Axes	739
	Stress Dyadic	740
	Stresses on an Octahedral Plane	741
	Octahedral Plane Stress Plot	743
	Physical Interpretation of the Octahedral Invariants τ_{OCT} and Ψ_2	748
	Mohr's Representation of a Triaxial State of Stress	751
	C STRENGTH OF A FACE-CENTERED CUBIC PACKING OF EQUAL ROUGH RIGID SPHERES	772

LIST OF TABLES

Number	Title	Page
3.1	Anisotropic Strength Data from Unconfined Compression Tests on Vienna and Little Belt Clays	136
3.2(a)	Anisotropic Strength Data from Unconfined Compression and Swedish Cone Tests on Varved Clay from Surte, Sweden	137
(b)	Anisotropic Strength Data from Unconfined Compression and Swedish Cone Tests on Varved Clay from Surte, Sweden	139
3.3	Anisotropic Strength Data from Unconfined Compression on Tests on Homogeneous Post Glacial Clay from Sala, Sweden	140
3.4	Anisotropic Strength Data from Unconfined Compression Tests on Varved Clay from Steep Rock Lake, Ontario	142
3.5(a)	Anisotropic Strength Data from Unconsolidated Undrained Triaxial Tests on Overconsolidated London Clay	143
(b)	Anisotropic Strength Data from Unconsolidated Undrained Triaxial Tests on Overconsolidated London Clay	145
3.6	Anisotropic Strength Data from Unconfined Compression Tests on Slate	146
3.7(a)	Anisotropic Strength Data from Triaxial Compression Tests on Martinsburg Slate	147
(b)	Anisotropic Strength Data from Triaxial Compression Tests on Martinsburg Slate	148
3.8(a)	Stress System Parameters at Failure in $\overline{CIU}$ Hollow Cylinder Tests on Commercial Kaolinite	149
(b)	Anisotropic Strength Data from $\overline{CIU}$ Hollow Cylinder Tests on Commercial Kaolinite	151
(c)	Anisotropic Strength Data from $\overline{CIU}$ Hollow Cylinder Tests on Commercial Kaolinite	152

Number	Title	Page
3.9(a)	Anisotropic Strength Data from Unconfined Compression Tests on Homogeneous Clay from Welland, Ontario	154
(b)	Anisotropic Strength Data from Unconfined Compression Tests on Homogeneous Clay from Welland, Ontario	156
(c)	Anisotropic Strength Data from Unconfined Compression Tests on Homogeneous Clay from Welland, Ontario	157
3.10(a)	Ansiotropic Strength Data from Unconfined Compression Tests on Stratified Clay from Welland, Ontario	159
(b)	Anisotropic Strength Data from Unconfined Compression Tests on Stratified Clay from Welland, Ontario	161
(c)	Anisotropic Strength Data from Unconfined Compression Tests on Stratified Clay from Welland, Ontario	162
3.11	Dimensionless Anisotropic Strength Data from Unconfined Compression Tests on Homogeneous Clay from Welland, Ontario	163
3.12	Anisotropic Strength Data from $\overline{CIU}$ Triaxial Tests on Homogeneous Clay from Welland, Ontario	164
3.13	Anisotropic Strength Data from Unconsolidated Undrained Triaxial Tests on Homogeneous Sarnia Glacial Lake Clay	165
3.14	Anisotropic Strength Data from Triaxial Test on a Varved Glacial Clay	166
3.15	Anisotropic Strength Data from Consolidated Undrained Triaxial Tests on Homogeneous India Black Cotton Clay	167
3.16	Anisotropic Strength Data from Unconsolidated Undrained Triaxial Tests on ASP-900 Kaolinite	168
3.17	Anisotropic Strength Data from Consolidated Undrained Triaxial Tests on ASP-900 Kaolinite	169
3.18	Anisotropic Strength Data from Undrained Plane Strain Tests on San Francisco Bay Mud from Hamilton Air Force Base	170

Number	Title	Page
3.19	Anisotropic Strength Data from Unconsolidated Undrained Triaxial Tests on Undisturbed Samples of San Francisco Bay Mud from Hamilton Air Force Base	171
3.20	Anisotropic Strength Data from Consolidated Undrained Triaxial Tests on Undisturbed Samples of San Francisco Bay Mud from Hamilton Air Force Base	172
3.21	Anisotropic Strength Data from Consolidated Undrained Triaxial Tests on Undisturbed London Clay	173
3.22	Anisotropic Strength Data from Consolidated Drained Triaxial Tests on Undisturbed London Clay	174
3.23	Index Properties of London Clay at the Site of the Ashford Common Shaft	175
3.24	Anisotropic Strength Data from Confined Unconsolidated Undrained Triaxial Tests on Undisturbed London Clay at the Site of the Ashford Common Shaft	176
3.25	Statistical Analysis of Confined Unconsolidated Undrained Triaxial Tests on Vertical Samples of Undisturbed London Clay	177
3.26	Anisotropic Strength Data from Unconsolidated Undrained Triaxial Tests on Resedimented Boston Blue Clay	178
3.27	Anisotropic Strength Ratio from Unconsolidated Undrained Triaxial Tests on Resedimented Boston Blue Clay	181
3.28	Variation of Failure Plane Orientation for UU Triaxial Tests on Resedimented Boston Blue Clay	182
3.29	Effective Stress Strength Data from $\overline{UU}$ Triaxial Tests on Resedimented Boston Blue Clay	184
3.30	Anisotropic Strength Data from Unconsolidated Undrained Triaxial Tests on Undisturbed Boston Blue Clay	185

Number	Title	Page
3.31	Variation of Failure Plane Orientation for UU Triaxial Tests on Undisturbed Boston Blue Clay	186
4.1	Anisotropic Pore Pressure Response Data for Resedimented Boston Blue Clay	310
5.1	Variation of Undrained Shear Strength, Example No. 1	329
5.2(a)	Variation of Undrained Shear Strength, Example No.2 Test Data Reduction	330
(b)	Variation of Undrained Shear Strength, Example No. 2 Pore Pressure Response Surface Contours	331
6.1	Triaxial Strength Data for Carrara Marble	461
6.2	Triaxial Strength Data for Dry German Quartz Sand	462
6.3	Triaxial Compression Data for Vienna Blue Clay	463
6.4	Triaxial Extension Data for Vienna Blue Clay	470
6.5	Triaxial Strength Data for Fontainebleau Sand	473
6.6	Effective Stress Paths Used by Bishop and Eldin (1953) for Triaxial Tests on Brasted Sand	474
6.7(a)	Hollow Cylinder Data for Loch Aline Sand	475
(b)	Triaxial Strength Data for Loch Aline Sand	476
6.8	Triaxial Strength Criteria for Three Sands	478
6.9(a)	Triaxial Strength Data for Remolded Weald Clay	479
(b)	Normalized Triaxial Strength Data for Remolded Weald Clay	485
6.10(a)	Triaxial Strength Data for Remolded London Clay	488
(b)	Normalized Triaxial Strength Data for Remolded London Clay	491
6.11	Triaxial Strength Data for Glen Shira Dam Material	492

Number	Title	Page
6.12	Triaxial Strength Data for a Clayey Silt	493
6.13	Triaxial Strength Data for Brasted Sand	494
6.14(a)	Triaxial Strength Data for Remolded Sault Ste Marie Clay - Batch 1	498
(b)	Triaxial Strength Data for Remolded Sault Ste Marie Clay - Batch 2	500
6.15	Triaxial Strength Data for the 30-50 Fraction of Ottawa Sand	501
6.16	Consolidation Stress Histories for Isotropically Consolidated Triaxial tests on Remolded Weald Clay	503
6.17	Stress Histories for K_o Consolidated Triaxial Tests on Remolded Weald Clay	506
6.18	Strength Data for Isotropically Consolidated Triaxial Tests on Remolded Weald Clay	508
6.19	Strength Data for K_o Consolidated Triaxial Tests on Remolded Weald Clay	512
6.20	Consolidation Stress Histories for Plane Strain Tests on Remolded Weald Clay	514
6.21	Remarks Concerning Plane Strain Tests on Remolded Weald Clay	515
6.22	Strength Data for Plain Strain Tests on Remolded Weald Clay	517
6.23	Average Porosity at Failure for Plane Strain and Triaxial Tests on Belgium Sand	518
6.24	Strength Data from Plane Strain Tests on Belgium Sand	519
6.25	Strength Data from Triaxial Tests on Belgium Sand	520

Number	Title	Page
6.26	Triaxial Strength Data for Commercial Kaolinite	521
6.27	Triaxial Strength Data for Remolded Osaka Alluvial Clay at Maximum Principal Effective Stress Ratio	522
6.28	Triaxial Strength Data for Remolded Osaka Alluvial Clay at Maximum Principal Stress Difference	523
6.29	Triaxial Strength Data for Standard Ottawa Sand	524
6.30	Triaxial Strength Data for a Silty Sand	526
6.31	Triaxial Strength Data for Commercial Kaolinite	527
6.32	Triaxial Strength Data for Standard Ottawa Sand	529
6.33	Average Triaxial Strength Data for Standard Ottawa Sand	531
6.34	Triaxial Strength Data for Resedimented Boston Blue Clay	532
6.35	Influence of the Intermediate Principal Stress on the Strength of Volga Sand	533
7.1	MODIAP Bearing Capacity Test Data	647
7.2	Data for Determining the Elastic Subgrade Modulus, M	652
7.3	Data for Determining the Bearing Capacity, P_{BC}, and the Plastic Settlement Parameter, ρ_{50}	
7.4	Relation Between Load and Settlement Magnification	658
7.5	Comparison of Measured and Calculated Loads	660

Number	Title	Page
7.6(a)	Data for Determining the Initial Tangent Modulus, E_o, for Remolded Boston Blue Clay	663
(b)	Data for Determining the Initial Tangent Modulus, E_o, for Remolded Boston Blue Clay	665
7.7	Predicted Influence of Overconsolidation Ratio on Modulus of Subgrade Reaction	666
7.8	Predicted Influence of Overconsolidation Ratio on Ultimate Bearing Capacity	667
7.9	Predicted Influence of Overconsolidation Ratio on the Plastic Settlement Parameter	668

LIST OF FIGURES

Figure	Title	Page
1.1	Variation of Stress System Orientation at Failure Throughout a Soil Mass	8
2.1	Geometry of the Revised Coulomb Failure Criterion	21
2.2	Revised Coulomb Failure Criterion in $(\bar{p},q)$ Space	22
2.3	Revised Coulomb Failure Criterion in $(\bar{\sigma}_v, \bar{\sigma}_h)$ Space (Rendulic Plot)	23
2.4	Independence of $\bar{\sigma}_2$ in the Revised Coulomb Failure Criterion	24
3.1	Preliminary Geometrical Relationships	187
3.2	Cases Solved Analytically by Casagrande and Carrillo (1944)	188
3.3	Case Solved Analytically by Hand and McCarty (1948)	
(a)	General Problem	189
(b)	Numerical Example	190
3.4	Elliptical Variation Associated with Mohr's Circle	191
3.5	Failure Plane Orientation	192
3.6	Basic Geometric Relations in a Cross Anisotropic Clay at Failure	193
3.7(a)	α Stress Contours for $\beta = 0^o$	194
(b)	α Stress Contours for $\beta = 30^o$	195
(c)	α Stress Contours for $\beta = 60^o$	196
(d)	α Stress Contours for $\beta = 90^o$	197
3.8	α Strength Contours	198

Figure	Title	Page
3.9	State of Stress at Failure in an Anisotropic Clay	199
3.10	Rotation of Principal Planes	200
3.11	Three-Dimensional Surface Defining the Shear Strength of a Cross Anisotropic Clay in Terms of Effective Stress	201
3.12	Variation of $\bar{c}(\alpha)$ Assumed by Jaeger	202
3.13	Football Shaped Constant $\bar{p}_f$ Cross Section of Jaeger's Bi-Conical Failure Surface	203
3.14	Hyperbolic Constant β Cross Section of Jaeger's Bi-Conical Failure Surface	204
3.15	Diagram for Obtaining $q_f(\bar{p}_f, \beta)$ for Jaeger's Bi-Conical Failure Surface	205
3.16(a)	Assumed Anisotropy of the Angle of Internal Friction	206
(b)	Typical Graphical Anisotropic Shear Strength Analysis	207
(c)	Variation of Shear Strength with β for Clay with Anisotropic Angle of Internal Friction	208
(d)	Variation of Failure Plane Orientation with Principal Stress Rotation	209
3.17(a)	Anisotropic Strength Ratio R_u for Vienna Clay IX	210
(b)	Anisotropic Strength Ratio R_u for Little Belt Clay III	211
(c)	Variation of Failure Plane Orientation for Unconfined Compression Tests on Vienna and Little Belt Clays	212
3.18	Anisotropic Strength Ratio R_u for Varved Clay from Surte, Sweden	213
3.19	Anisotropic Strength Ratio R_u for Homogeneous Clay from Sala, Sweden	214

Figure	Title	Page
3.20(a)	Anisotropic Strength Ratio R_u for Varved Clay from Steep Rock Lake, Ontario, Sample 2-62	215
(b)	Anisotropic Strength Ratio R_u for Varved Clay from Steep Rock Lake, Ontario, Sample 2-68	216
3.21	Anisotropic Strength Ratio R_u for London Clay	217
3.22	Unit Vectors Used to Define the Orientation of the Shear Stress Vector Acting on an Arbitrary Plane	218
3.23(a)	Anisotropic Strength Ratio R for Slate	219
(b)	Variation of Failure Plane Orientation for Unconfined Compressive Tests on Slate	220
3.24(a)	Anisotropic Strength Data from Triaxial Compression Tests on Martinsburg Slate	221
(b)	Anisotropic Strength Ratio R_p for Martinsburg Slate	222
(c)	Anisotropic Strength Ratio R_p for Martinsburg Slate	223
(d)	Anisotropic Strength Ratio R_p for Martinsburg Slate	224
3.25	Rotation of Principal Planes in the Hollow Cylinder Test	225
3.26(a)	Anisotropic Strength Data from $\overline{CIU}$ Hollow Cylinder Tests on Commercial Kaolinite	226
(b)	Anisotropic Strength Data from $\overline{CIU}$ Hollow Cylinder Tests on Commercial Kaolinite	227
(c)	Anisotropic Strength Data from $\overline{CIU}$ Hollow Cylinder Tests on Commercial Kaolinite	228
(d)	Anisotropic Strength Data from $\overline{CIU}$ Hollow Cylinder Tests on Commercial Kaolinite	229
(e)	Anisotropic Strength Data from $\overline{CIU}$ Hollow Cylinder Tests on Commercial Kaolinite	230
3.27(a)	Anisotropic Strength Ratio R_p for Commercial Kaolinite	231
(b)	Anisotropic Strength Ratio R_p for Commercial Kaolinite	232
(c)	Anisotropic Strength Ratio R_p for Commercial Kaolinite	233
(d)	Anisotropic Strength Ratio R_p for Commercial Kaolinite	234
(e)	Anisotropic Strength Ratio R_p for Commercial Kaolinite	235

Figure	Title	Page
3.28(a)	Anisotropic Strength Ratio R_u for Homogeneous Welland Clay, Block D	236
(b)	Anisotropic Strength Ratio R_u for Homogeneous Welland Clay, Block H	237
(c)	Variation of Failure Plane Orientation for Unconfined Compression Tests on Homogeneous Welland Clay, Block D	238
3.29(a)	Anisotropic Strength Ratio R_u for Stratified Welland Clay, Block F	239
(b)	Anisotropic Strength Ratio R_u for Stratified Welland Clay, Block K	240
(c)	Variation of Failure Plane Orientation for Unconfined Compression Tests on Stratified Welland Clay, Blocks F and K	241
3.30	Anisotropic Strength Ratio R_u for Homogeneous Welland Clay, Blocks A,B,C,D,E,G,H & I	242
3.31	Mohr Circle Plot of Anisotropic Strength Ratio for Homogeneous Welland Clay, Blocks A,B,C,D,E, G,H & I	243
3.32	Stress Paths for $\overline{CIU}$ Triaxial Tests on Homogeneous Welland Clay, Block I	244
3.33(a)	Anisotropic Strength Ratio R_u for Homogeneous Sarnia Clay, Block 1	245
(b)	Anisotropic Strength Ratio R_u for Homogeneous Sarnia Clay, Block 2	246
3.34	Anisotropic Strength Ratio R_u for a Varved Finnish Glacial Clay	247
3.35	Anisotropic Strength Ratio R_u for Homogeneous India Black Bottom Clay	248
3.36	Anisotropic Strength Ratio R_u for ASP-900 Kaolinite	249
3.37	Anisotropic Strength Data from $\overline{CIU}$ Triaxial Tests on ASP-900 Kaolinite	250

Figure	Title	Page
3.38	Anisotropic Strength Data from Undrained Plane Strain Tests on San Francisco Bay Mud from Hamilton Air Force Base	251
3.39	Anisotropic Strength Ratio R_u for Undisturbed San Francisco Bay Mud	252
3.40	Anisotropic Strength Data from Consolidated Undrained Triaxial Tests on Undisturbed San Francisco Bay Mud from Hamilton Air Force Base	253
3.41(a)	Strength Data from Triaxial Tests on Vertical ($\beta = 0^o$) Specimens of Undisturbed London Clay, Level E	254
(b)	Strength Data from Triaxial Tests on Horizontal ($\beta = 90^o$) Specimens of Undisturbed London Clay, Level E	255
3.42	Strength Data from Triaxial Tests on Vertical and Horizontal Specimens of Undisturbed London Clay, Level E	256
3.43	Depth Variation of Index Properties and Directional Strength of London Clay	257
3.44(a)	Anisotropic Strength Ratio R_u for London Clay from Ashford Common, Level A	258
(b)	Anisotropic Strength Ratio R_u for London Clay from Ashford Common, Level B	259
(c)	Anisotropic Strength Ratio R_u for London Clay from Ashford Common, Level C	260
(d)	Anisotropic Strength Ratio R_u for London Clay from Ashford Common, Level D	261
(e)	Anisotropic Strength Ratio R_u for London Clay from Ashford Common, Level E	262
(f)	Anisotropic Strength Ratio R_u for London Clay from Ashford Common, Level F	263
3.45(a)	Variation of Failure Plane Orientation for Unconsolidated Undrained Triaxial Tests on London Clay from Ashford Common, Level A	264
(b)	Variation of Failure Plane Orientation for Unconsolidated Undrained Triaxial Tests on London Clay from Ashford Common, Level B	265

Figure	Title	Page
3.45(c)	Variation of Failure Plane Orientation for Unconsolidated Undrained Triaxial Test on London Clay from Ashford Common, Level C	266
(d)	Variation of Failure Plane Orientation for Unconsolidated Undrained Triaxial Tests on London Clay from Ashford Common, Level D	267
(e)	Variation of Failure Plane Orientation for Unconsolidated Undrained Triaxial Tests on London Clay from Ashford Common, Level E	268
(f)	Variation of Failure Plane Orientation for Unconsolidated Undrained Triaxial Tests on London Clay from Ashford Common, Level F	269
3.46	Cumulative Distribution Function for 165 Unconsolidated Undrained Triaxial Compression Tests on Vertical Specimens of Undisturbed London Clay from Ashford Common	270
3.47	Stress History for UU Triaxial Test on Resedimented Boston Blue Clay	271
3.48(a)	Anisotropic Strength Data from UU Triaxial Tests on Resedimented Boston Blue Clay, $\beta = 0^{o}$	272
(b)	Anisotropic Strength Data from UU Triaxial Tests on Resedimented Boston Blue Clay, $\beta = 30^{o}$	273
(c)	Anisotropic Strength Data from UU Triaxial Tests on Resedimented Boston Blue Clay, $\beta = 45^{o}$	274
(d)	Anisotropic Strength Data from UU Triaxial Tests on Resedimented Boston Blue Clay, $\beta = 60^{o}$	275
(e)	Anisotropic Strength Data from UU Triaxial Tests on Resedimented Boston Blue Clay, $\beta = 90^{o}$	276
3.49(a)	Anisotropic Strength Ratio R_u for Resedimented Boston Blue Clay, $\bar{\sigma}_s/\bar{\sigma}_{vm} = 0.10$	277
(b)	Anisotropic Strength Ratio R_u for Resedimented Boston Blue Clay, $\bar{\sigma}_s/\bar{\sigma}_{vm} = 0.15$	278
(c)	Anisotropic Strength Ratio R_u for Resedimented Boston Blue Clay, $\bar{\sigma}_s/\bar{\sigma}_{vm} = 0.20$	279
(d)	Anisotropic Strength Ratio R_u for Resedimented Boston Blue Clay, $\bar{\sigma}_s/\bar{\sigma}_{vm} = 0.25$	280

Figure	Title	Page
3.50	Variation of Failure Plane Orientation for UU Triaxial Tests on Resedimented Boston Blue Clay	281
3.51	Effective Strength Data for $\overline{UU}$ Triaxial Tests on Resedimented Boston Blue Clay	282
3.52(a)	Anisotropic Strength Data from UU Triaxial Tests on Undisturbed Boston Blue Clay, $\beta = 0^{o}$	283
(b)	Anisotropic Strength Data from UU Triaxial Tests on Undisturbed Boston Blue Clay, $\beta = 45^{0}$	284
(c)	Anisotropic Strength Data from UU Triaxial Tests on Undisturbed Boston Blue Clay, $\beta = 90^{o}$	285
3.53	Variation of Failure Plane Orientation for UU Triaxial Tests on Undisturbed Boston Blue Clay	286
4.1	Relation Between Effective Stress and Volume Change Characteristics	311
4.2	Total Stress Systems	312
4.3	Intermediate Principal Stress Increment and Intermediate Principal Stress	313
4.4	Mohr Circle Construction for Total Stress	314
4.5	Change in Void Ratio Due to a Change in Hydrostatic Effective Stress	315
4.6	Infinitesimal Changes in Effective Stress	316
4.7	Applied Total Stress Increments	317
4.8	Three-Dimensional Pore Pressure Response Surface for a Cross Anisotropic Clay	318

Figure	Title	Page
5.1	Anisotropic Variation of Undrained Shear Strength, Example No. 1	332
5.2(a)	Anisotropic Variation of Undrained Shear Strength, Example No. 2 - Excluding the q_o Effect	333
(b)	Anisotropic Variation of Undrained Shear Strength, Example No. 2 - Including the q_o Effect	334
6.1	Constant $\bar{\sigma}_2$ Contour of Assumed Failure Surface	534
6.2	Constant μ Contour of Assumed Failure Surface	535
6.3	Physical Significance of Points on a Failure Surface Contour	536
6.4	Relation Between the Parameters $\bar{p}$, q, μ, $\bar{\sigma}_{OCT}$ and τ_{OCT}	537
6.5	Location of a Stress Point in the Octahedral Plane	538
6.6	Octahedral Plane Plot of the Complete Mohr-Coulomb Failure Criterion	539
6.7	Triaxial Strength Data for Carrara Marble	540
6.8	Effect of $\bar{\sigma}_2$ on the Strength of Carrara Marble	541
6.9	Effect of $\bar{\sigma}_2$ on the Strength of Dry German Quartz Sand	542

Figure	Title	Page
6.10(a)	Compression Data for Remolded Vienna Blue Clay, Test No. 8	543
(b)	Compression Data for Remolded Vienna Blue Clay, Test No. 9	544
(c)	Compression Data for Remolded Vienna Blue Clay, Test No. 10	545
(d)	Compression Data for Remolded Vienna Blue Clay, Test No. 11	546
(e)	Compression Data for Remolded Vienna Blue Clay, Test No. 12	547
(f)	Compression Data for Remolded Vienna Blue Clay, Test No. 13	548
(g)	Compression Data for Remolded Vienna Blue Clay, Test No. 14	549
6.11	Stress Paths from Triaxial Compression and Extension Tests on Remolded Vienna Blue Clay	550
6.12	Triaxial Compression and Extension Strength Data for Fontainebleau Sand	551
6.13	Effect of $\bar{\sigma}_2$ on the Strength of Fontainebleau Sand	552
6.14	Effective Stress Paths Used by Bishop and Eldin (1953) for Triaxial Tests on Brasted Sand	553
6.15	Triaxial Strength Data for Loch Aline Sand	554
6.16	Effect of $\bar{\sigma}_2$ on the Strength of Loch Aline Sand	555
6.17	A Generalized Linear Failure Hypothesis for Soil	556
6.18	Effect of $\bar{\sigma}_2$ on the Strength of Three Sands	557

Figure	Title	Page
6.19(a)	Normalized Strength Data from Triaxial Compression Tests on Remolded Weald Clay	558
(b)	Normalized Strength Data from Triaxial Extension Tests on Remolded Weald Clay	559
6.20	Normalized Strength Data from Triaxial Compression Tests on Remolded London Clay	560
6.21	Triaxial Strength Data for Glen Shira Dam Material	561
6.22	Effect of $\bar{\sigma}_2$ on the Strength of Glen Shira Dam Material	562
6.23	Effect of $\bar{\sigma}_2$ on the Strength of a Clayey Silt	563
6.24(a)	Triaxial Strength Data for Brasted Sand	564
(b)	Triaxial Strength Data for Brasted Sand	565
(c)	Triaxial Strength Data for Brasted Sand	566
(d)	Triaxial Strength Data for Brasted Sand	567
6.25(a)	Influence of Density on the Apparent Angle of Internal Friction of Brasted Sand - Plane Strain	568
(b)	Influence of Density on the Apparent Angle of Internal Friction of Brasted Sand - Cylindrical Compression	569
(c)	Influence of Density on the Apparent Angle of Internal Friction of Brasted Sand - Cylindrical Extension	570
6.26	Influence of Density on the Intermediate Principal Stress for Plane Strain Tests on Brasted Sand	571
6.27	Effect of $\bar{\sigma}_2$ on the Strength of Brasted Sand, for Failure Porosities Between 34.0% and 42.0%	572
6.28	Triaxial Compression Strength Data for Remolded Sault Ste. Marie Clay	573

Figure	Title	Page
6.29	Triaxial Extension Strength Data for Remolded Sault Ste. Marie Clay	574
6.30	Effect of $\bar{\sigma}_2$ on the Strength of Remolded Sault Ste. Marie Clay	575
6.31	Triaxial Compression and Extension Strength Data for the 30-50 Fraction of Standard Ottawa Sand	576
6.32	Effect of $\bar{\sigma}_2$ on the Strength of the 30-50 Fraction of Standard Ottawa Sand (e = 0.47 to 0.52)	577
6.33	Effective Stress Paths for Isotropically Consolidated Triaxial Tests Conducted by Sowa (1963)	578
6.34	Effective Stress Paths for K_o Consolidated Triaxial Tests Conducted by Sowa (1963)	579
6.35	Strength Data from Isotropically Consolidated Triaxial Tests on Remolded Weald Clay	580
6.36	Strength Data for K_o Consolidated Triaxial Tests on Remolded Weald Clay	581
6.37	Strength Data for Plane Strain Tests on Remolded Weald Clay	582
6.38	Effect of $\bar{\sigma}_2$ on the Strength of Remolded Weald Clay	583
6.39	Volumetric Strain at Failure in Plane Strain and Triaxial Tests on Belgium Sand	584
6.40 (a)	Influence of Density on the Apparent Angle of Internal Friction of Belgium Sand - Plain Strain	585
(b)	Influence of Density on the Apparent Angle of Internal Friction of Belgium Sand - Cylindrical Compression	586

Figure	Title	Page
6.40(c)	Influence of Density on the Apparent Angle of Internal Friction of Belgium Sand - Cylindrical Extension	587
6.41	Influence of Density on the Intermediate Principal Stress for Plane Strain Tests on Belgium Sand	588
6.42	Effect of $\bar{\sigma}_2$ on the Strength of Belgium Sand, for Failure Porosities Between 37.0% and 44.0%	589
6.43(a)	Effect of $\bar{\sigma}_2$ on the Strength of Remolded Commercial Kaolinite σ_c = 7 PSI	590
(b)	Effect of $\bar{\sigma}_2$ on the Strength of Remolded Commercial Kaolinite $\bar{\sigma}_c$ = 25 PSI	591
(c)	Effect of $\bar{\sigma}_2$ on the Strength of Remolded Commercial Kaolinite $\bar{\sigma}_c$ = 70 PSI	592
6.44	Triaxial Compression and Extension Strenth Data for Remolded Osaka Alluvial Clay at Maximum Principal Effective Stress Ratio	593
6.45	Triaxial Compression and Extension Strength Data for Remolded Osaka Alluvial Clay at Maximum Stress Difference	594
6.46	Effect of $\bar{\sigma}_2$ on the Strength of Remolded Osaka Alluvial Clay at $(\bar{\sigma}_1/\bar{\sigma}_3)_{MAX}$	595
6.47	Effect of $\bar{\sigma}_2$ on the Strength of Remolded Osaka Alluvial Clay at $(\bar{\sigma}_1-\bar{\sigma}_3)_{MAX}$	596
6.48	Relation Between Strain at Maximum Principal Stress Difference and Lode's Parameter for Remolded Osaka Alluvial Clay	597
6.49	Effect of $\bar{\sigma}_2$ on the Strength of Standard Ottawa Sand	598

Figure	Title	Page
6.50	Effect of $\bar{\sigma}_2$ on the Strength of Standard Ottawa Sand - Bell's Failure Criterion	599
6.51	Effect of $\bar{\sigma}_2$ on the Strength of Standard Ottawa Sand - Topping's Failure Criterion	600
6.52	Triaxial Compression Strength Data for a Silty Sand	601
6.53	Effect of $\bar{\sigma}_2$ on the Strength of a Silty Sand	602
6.54	Combined Influence of Anisotropy, the Intermediate Principal Stress and Rate of Applied Stress on the Strength of Commercial Kaolinite	603
6.55	Effect of $\bar{\sigma}_2$ on the Strength of Commercial Kaolinite	604
6.56	Influence of Density on the Apparent Angle of Internal Friction of Standard Ottawa Sand	605
6.57	Effect of $\bar{\sigma}_2$ on the Strength of Standard Ottawa Sand	606
6.58	Triaxial Compression and Extension Strength Data for Resedimented Boston Blue Clay	607
6.59	Influence of Water Content on Lode's Parameter at Failure for Plane Strain Tests on Resedimented Boston Blue Clay	608
6.60	Effect of $\bar{\sigma}_2$ on the Strength of Resedimented Boston Blue Clay	609
6.61	Effect of $\bar{\sigma}_2$ on the Strength of Volga Sand n_i = 39.3%	610

Figure	Title	Page
6.62	Effect of $\bar{\sigma}_2$ on the Strength of Ham River Sand ni = 39.0%	611
6.63	Effect of $\bar{\sigma}_2$ on the Strength of River Welland Sand	612
6.64	Effect of $\bar{\sigma}_2$ on the Strength of Three Different Sands	613
7.1	Idealized Initial Settlement Curve	669
7.2	Settlement Curves for MODIAP Bearing Capacity Tests	670
7.3	Semilogarithmic Plot for Determining the Elastic Subgrade Modulus, M Test No. 105	671
7.4	Modified Southwell Plot for Determing the Bearing Capacity and the Plastic Settlement Parameter Test No. 105	672
7.5	Plastic Settlement Curve for MODIAP Footing Tests	673
7.6	Unified Plastic Settlement Diagram for MODIAP Footing Tests	674
7.7	Comparison of Calculated and Measured Loads for MODIAP Footing Tests	675
7.8(a)	Similogarithmic Plot for Determining the Initial Tangent Modulus, E_o Test $\overline{CIUC}$-1	676
(b)	Semilogarithmic Plot for Determining the Initial Tangent Modulus, E_o Test $\overline{CIUC}$-2	677

Figure	Title	Page
7.8(c)	Semilogarithmic Plot for Determining the Initial Tangent Modulus, E_o Test $\overline{CIUC}$-3	678
(d)	Semilogarithmic Plot for Determining the Initial Tangent Modulus, E_o Remolded Blue Clay	679
7.9	Strain Invariant Contours	680
7.10	Influence of Overconsolidation on the Directional Variation of Undrained Shear Strength	681
7.11	Influence of Inital Stress on the Plastic Settlement Parameter	682
7.12	Predicted Influence of Overconsolidation Ratio on Initial Settlement	683
7.13	Predicted Influence of Overconsolidation Ratio on the Empirical Settlement Parameters	684
B.1	Tetrahedron OABC	761
B.2	Stresses Exerted by Tetrahedron OABC on the Surrounding Material	762
B.3	Infinitesimal Change in a Unit Vector	763
B.4(a)	Representation of the Roots of Equation (B.41) in an Argand Diagram	764
(b)	Relation Between μ and ω	765
B.5	Scaled Octahedral Stress Vector in Principal Stress Space	766
B.6	Geometry of the Octahedral Plane Stress Plot	767
B.7	Equation of a Circle with Center on the X Axis	768
B.8	Mohr Circle Construction for Triaxial Stress	769

Figure	Title	Page
B.9	Graphical Determination of Octahedral Stresses	770
B.10	Mohr Mapping of a Meridian of Longitude on a Unit Sphere	771
C-1	Face-Centered Cubic Array of Equal Spheres	796
C-2	Pyramidal View of the Face-Centered Cubic Array of Equal Spheres	797
C.3	Hexagonal or Tetrahedral View of the Face-Centered Cubic Array of Equal Spheres	798
C.4	Three Views of the Same Dense Packing of Equal Spheres: Face-Centered Cubic, Pyramidal and Tetrahedral	799
C.5	Unit Element Considered in the Strength Analysis of a Face-Centered Cubic (Pyramidal) Packing of Equal Rough Rigid Spheres	800
C.6	Assumed Deformation Pattern	801

CHAPTER 1

INTRODUCTION

Objective and Scope

This thesis deals with the undrained shear strength of saturated clay. The term "undrained" is used to indicate that during the entire shearing process there is no opportunity for pore water flow, and therefore no pore pressure dissipation.

In particular, the objective is to explain, in terms of effective stress, the influence on undrained shear strength of the total stress system. In other words, this thesis explains why the undrained shear strength of a saturated clay may not be a unique value, but may depend on one or more total stress system variables.

The terms "stress system" and "stress tensor" are synonymous. Each is completely and uniquely defined by six independent scalar values. These six values can be either the magnitudes of six stress components, or the

values of the three principal normal stresses, together with three angles which fix the orientations of the principal stress axes, analagous to the Eulerian angles employed in rigid body dynamics; GOLDSTEIN (1950, 107).

Only four stress system variables are considered here: the magnitudes of the three principal stresses, σ_1, σ_2 and σ_3, and the angle β between the major principal stress axis and what will subsequently be defined as the material axis. The principal outcome of the thesis is a rational specification of the variation of undrained shear strength with β, which can be used in the computer solution of problems involving deformation and stability of a saturated clay mass.

Motivation

The motives for this study are two:

1. The desire for a better understanding of factors governing the undrained shear strength of saturated clay, and
2. The pressing need to employ more realistic stress - strain - strength relationships in computer analyses of soil deformation and stability.

The availability of high speed digital computers with large storage capacity has already begun to exert a profound influence on the field of soil mechanics, both in research

and in practice. It has triggered a predictable sequence of events, insofar as the analysis of soil deformation and stability is concerned, as follows:

1. Use available computer programs and classical inelastic stress - strain equations to solve deformation and stability problems, in which the geometery is that of problems encountered in soil mechanics practice.

2. Recognize that the stress - strain equations used so far, and therefore the results obtained from their use, bear at least a debatable relation to the behavior of real soil. At the same time, realize the capacity of the computer to accommodate more complex, but more realistic soil stress - strain equations.

3. Develop more versatile soil testing equipment, capable of yielding data which can serve as the basis for more general soil stress - strain equations, formulated within the framework of Rheology.

4. Use the improved stress - strain equations in computer analyses of soil deformation and stability, and check predicted behavior by field and model tests.

If the above predicted sequence is correct, it promises to give the fields of Soil Behavior and Experimental Soil

Mechanics the biggest incentive they have ever had. This is because it will establish a pressing demand for the results of soil stress - strain tests to be presented in the form of general relationships, instead of essentially raw data. This will, in turn, create a need for more versatile and sophisticated soil testing equipment, improved soil testing techniques, and improved techniques for reducing the degree of disturbance suffered by field samples prior to testing in the laboratory.

In short, the computer has created a demand for many of the products of the soil mechanics industry which, until recently, had essentially no market at all, because they could not be used conveniently in practice. Now, any information which can be accepted by a computer is potentially useful in soil mechanics practice.

Technical Considerations

Shear failure of a soil mass generally occurs by slipping or sliding along characteristic surfaces, called failure surfaces. An example of such a surface is shown in Figure 1.1. The distribution of stress in a soil mass subjected to a local surface load, such as that imposed by a spread footing, is generally such that the orientation of the

stress system at failure will vary from point to point throughout the mass, and the resulting failure surface will be curved. Unless unusual conditions prevail, the undrained shear strength, s_u, defined as

$$s_u = \frac{1}{2} (\sigma_1 - \sigma_3)_f \qquad (1.1)$$

i.e. the radius of the Mohr circle of stress at failure, will vary along the failure surface, depending upon the angle β. The main purpose of this thesis is to explain why s_u varies with β, and to offer means of predicting the variation of s_u with β, for use in computer analyses of deformation and stability.

Briefly, the reasons for variation of s_u with β are:

1. Anisotropy with respect to effective stress shear strength parameters,
2. Anisotropy with respect to pore pressure response, and
3. Anisotropy of the consolidating stress system prior to undrained shear.

In each of the above cases, the term anisotropy means directional dependence. The first two cases refer to directional dependence of soil properties, whereas the

third case refers to directional dependence of normal (and therefore shear) stress in the consolidating stress system prior to undrained shear.

The chapter on anisotropy of effective stress shear strength parameters shows how an assumed directional dependence of cohesion or internal friction can lead to a variation of undrained shear strength with β. It also explains why the actual directional dependencies of cohesion and internal friction are extremely difficult to determine accurately.

As well as discussing the directional dependence of excess pore pressure, the chapter on pore pressure response also attempts to clarify the relationship between excess pore pressure and applied total stress, and to show why the pore pressure response of dilatant soils need not be treated separately, as it has been in the past.

Theory predicts that the undrained shear strength of a saturated, isotropic clay will vary with β when the radius of the initial Mohr stress circle, q_o, is not zero, i.e. when the consolidating stress system is anisotropic. This prediction is a direct consequence of the assumption that excess pore pressure is partly dependent on the radius

of the applied, rather than the resultant total stress circle. This phenomenon will be called the q_o effect, because it is absent when $q_o = 0$.

All three of the above phenomena have to do with the variation of undrained shear strength with β, within the framework of the Revised Coulomb Equation. If that equation were strictly valid, the only possible influence which the intermediate principal stress could have on failure would be through the pore pressure. In fact, this is probably its most important influence. There is, however, considerable evidence to indicate that the Revised Coulomb Equation is not strictly valid, and that the effective stress shear strength parameters are somewhat dependent on the intermediate principal stress. This evidence is examined in the chapter dealing with the influence of the intermediate principal stress on shear strength, using a method for plotting data in the octahedral stress plane devised by the Writer.

Finally, a chapter is devoted to the application of some of the above results to the interpretation of model footing test data obtained by the Writer under Project MODIAP at M.I.T.

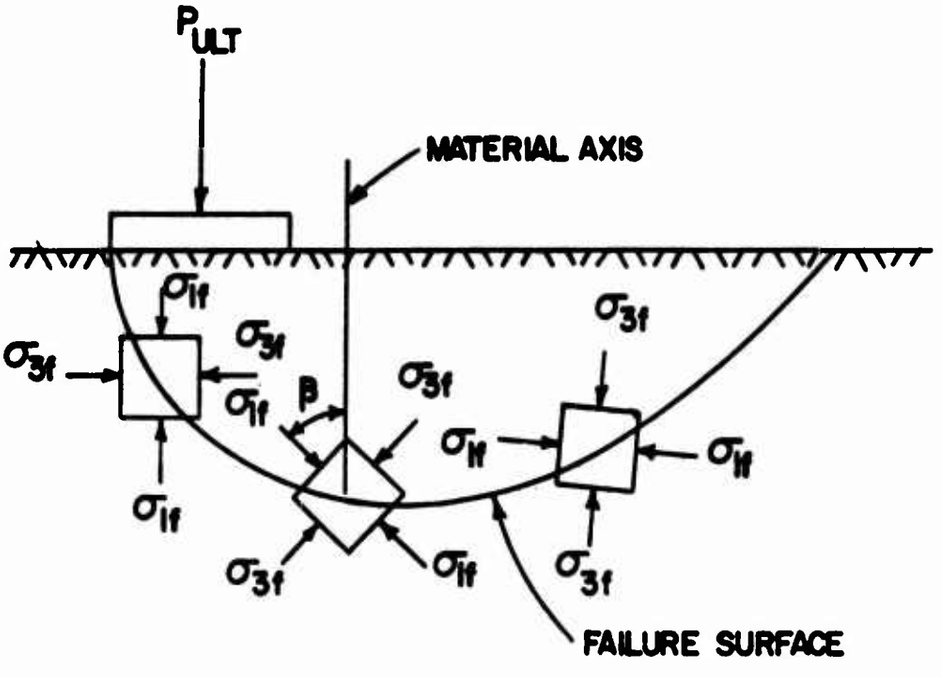

FIGURE 1.1

VARIATION OF STRESS SYSTEM ORIENTATION AT FAILURE THROUGHOUT A SOIL MASS

CHAPTER 2

BASIC SHEAR STRENGTH CONCEPTS

Purpose

The purpose of this chapter is to review basic concepts of soil shear strength, which serve as the framework for the rest of the thesis, and to which frequent reference will be made.

Importance of Shear Strength

The most important structural characteristics of a construction material are its stress - strain relationships. The single most important stress - strain property is strength; WINTER (1961).

Soil is probably the most common construction material with which civil engineers deal. It is difficult to imagine a civil engineering construction project which does not involve soil, and therefore some consideration of soil strength. World economic conditions have reached the point where an increasing number of important foundation engineering problems necessarily involve saturated clays, and

therefore the strength of clays under load has become a subject of considerable practical engineering significance.

Consequences of the Nature of Soil

The feature which most distinguishes soils from other construction materials is their particulate nature; LAMBE AND WHITMAN (1969). The dominant stress - strain and strength characteristics of soils, and of saturated clays in particular, are a direct consequence of their particulate nature:

1. Soils deform mainly by sliding or rolling of individual particles, or groups of particles, with respect to each other.
2. Therefore, when a soil fails under load, the failure is in shear.
3. Shearing stresses tend to produce volumetric, as well as shearing strains in the soil skeleton.
4. Soils are inherently multiphase materials.
5. The phases of a soil interact, both physically and chemically. In particular, the pore water in a saturated, fine-grained soil tends to resist a change in volume of the soil skeleton because of the low compressibility of the water and the

low permeability of the soil skeleton. It is this combination of phase properties which makes the idealization of "undrained" loading of practical value in the analysis of field loading problems involving saturated clay.

The Revised Coulomb Equation

Today the most generally accepted concept of soil shear strength is a combination of Coulomb's failure hypothesis and Terzaghi's principle of effective stress; COULOMB (1773); TERZAGHI (1923). However, in order to be of practical value, the above two concepts must be supplemented by a quantitative relation between applied total stress and pore water pressure; CASAGRANDE (1934), RENDULIC (1936). In fact, the relation between applied total stress and pore water pressure plays a dominant role in the shear strength behavior of cohesive soils, but a clear understanding of this relationship has been difficult to attain.

Coulomb's failure hypothesis can be stated mathematically as follows:

$$\tau_{ff} = c + \sigma_{ff} \tan \Phi \qquad (2.1)$$

where

τ_{ff} = shear stress on the failure plane at failure

σ_{ff} = total normal stress on the failure plane at failure

Φ = material constant, called the angle of internal friction

c = material constant, called cohesion

Failure is assumed to be initiated by sliding along the plane for which Equation (2.1) is first satisfied.

Terzaghi revised Equation (2.1) by proposing that the stress components which control the deformation, and therefore the shear strength behavior of soils are not the total stress components, σ_{ij}, but the effective stress components, $\bar{\sigma}_{ij}$. The effective stress components are related to the total stress components and to the pore water pressure u_w (assuming full saturation, and defining compressive normal stresses to be positive) by the defining equations

$$\bar{\sigma}_{ij} = \sigma_{ij} - u_w \delta_{ij} \qquad (2.2)$$

or, in matrix form

$$\begin{bmatrix} \bar{\sigma}_{11} & \bar{\sigma}_{12} & \bar{\sigma}_{13} \\ \bar{\sigma}_{21} & \bar{\sigma}_{22} & \bar{\sigma}_{23} \\ \bar{\sigma}_{31} & \bar{\sigma}_{32} & \bar{\sigma}_{33} \end{bmatrix} = \begin{bmatrix} \sigma_{11} & \sigma_{12} & \sigma_{13} \\ \sigma_{21} & \sigma_{22} & \sigma_{23} \\ \sigma_{31} & \sigma_{32} & \sigma_{33} \end{bmatrix} - \begin{bmatrix} u_w & 0 & 0 \\ 0 & u_w & 0 \\ 0 & 0 & u_w \end{bmatrix} \qquad (2.3)$$

where

$\bar{\sigma}_{ij}$ = effective stress component

σ_{ij} = total stress component

δ_{ij} = Kronecker delta

u_w = pore water pressure

The pore water pressure is the sum of the static pore water pressure, u_s, and the excess pore water pressure, u.

$$u_w = u_s + u \qquad (2.4)$$

Terzaghi's Revised Coulomb Equation which utilizes the <u>effective stress shear strength parameters</u>, $\bar{c}$ and $\bar{\Phi}$ is therefore

$$\tau_{ff} = \bar{c} + \bar{\sigma}_{ff} \tan \bar{\Phi} \qquad (2.5)$$

Equation (2.5) can also be written as

$$\tau_{ff} = (\bar{\sigma}_{ff} + d) \tan \bar{\Phi} \qquad (2.6)$$

where

$$d = \bar{c} \cot \bar{\Phi} \tag{2.7}$$

The quantity d is called the intrinsic pressure, an example of which is the normal stress caused by the force of attraction between two magnets, which gives rise to frictional resistance without externally applied normal force; TAYLOR (1948, 319).

Experimental Definition of Shear Strength Parameters

The fact that stability and deformation are closely related becomes evident when one addresses the question of what stress values to use in recording the strength of a soil test specimen. When analyzing the results of a conventional undrained triaxial test, it is customary to plot either the normalized principal stress difference, $\frac{\bar{\sigma}_1 - \bar{\sigma}_3}{\bar{\sigma}_{1c}}$, where

$\bar{\sigma}_1$, $\bar{\sigma}_3$ = major and minor principal effective stresses

$\bar{\sigma}_{1c}$ = major principal effective stress at the end of consolidation, prior to undrained shear

or the principal effective stress ratio, $\frac{\bar{\sigma}_1}{\bar{\sigma}_3}$, against the axial strain, ϵ_a, and to define $\bar{\sigma}_{1f}$ and $\bar{\sigma}_{3f}$ as the values of

$\bar{\sigma}_1$ and $\bar{\sigma}_3$ when one of the above stress variables attains its maximum value with respect to ϵ_a; see Figure 2.1. The values of $\bar{c}$ and $\bar{\Phi}$ are then calculated from one of several equations presented in the next section.

Insight into the mobilization of shear strength in an undrained triaxial test, and the relation between the above two stress variables, can be gained by studying a mathematical identity; BJERRUM AND LO (1963).

$$\left(\frac{\bar{\sigma}_1 - \bar{\sigma}_3}{\bar{\sigma}_{1c}}\right) = \left(\frac{\bar{\sigma}_1}{\bar{\sigma}_3} - 1\right)\left(\frac{\bar{\sigma}_3}{\bar{\sigma}_{1c}}\right) = \left(\frac{\bar{\sigma}_1}{\bar{\sigma}_3} - 1\right)\left(\frac{\bar{\sigma}_{3c} + \Delta\sigma_3 - \Delta u}{\bar{\sigma}_{1c}}\right)$$

$$= \left(\frac{\bar{\sigma}_1}{\bar{\sigma}_3} - 1\right)\left(K_o - \frac{\Delta u - \Delta\sigma_3}{\bar{\sigma}_{1c}}\right) \qquad (2.8)$$

Equation (2.8) shows that the normalized principal stress difference can be interpreted as the product of two quantities, the first of which contains $\frac{\bar{\sigma}_1}{\bar{\sigma}_3}$ as the only variable, and the second of which contains as the only variable $\frac{\Delta u - \Delta\sigma_3}{\bar{\sigma}_{1c}}$. Whether the normalized principal stress difference and the principal effective stress ratio attain their respective maximum values at the same or different axial strains depends on the rate of change of the pore pressure function,

$\frac{\Delta u - \Delta\sigma_3}{\bar{\sigma}_{1c}}$, with respect to axial strain. The relationship between this pore pressure function and axial strain in undrained triaxial compression tests has been observed to be relatively independent of both the value of $\bar{\sigma}_{1c}$ and the orientation of the sample axis with respect to the material axis, i.e. the value of the angle β; LAMBE (1963, Fig. 10), LO (1966, Fig. 17). Which of the above stress variables to use in defining $\bar{c}$ and $\bar{\Phi}$, in connection with a particular field problem depends on the expected pore pressure response and the maximum desirable deformation, as well as the strength equation in which the results are to be employed.

Relations Between Principal Effective Stresses at Failure

This section contains several frequently used mathematical relationships. It may be skipped without loss of continuity, and is included only for convenience in reading subsequent portions of the thesis.

It is frequently convenient to express the Revised Coulomb equation in terms of the principal effective stresses at failure. Referring to Figure 2.1, it is easily seen that

$$\tau_{ff} = \left(\frac{\bar{\sigma}_{1f} - \bar{\sigma}_{3f}}{2} \right) \cos \bar{\Phi} = q_f \cos \bar{\Phi} \qquad (2.9)$$

$$\bar{\sigma}_{ff} = \left(\frac{\bar{\sigma}_{1f} + \bar{\sigma}_{3f}}{2} \right) - \left(\frac{\bar{\sigma}_{1f} - \bar{\sigma}_{3f}}{2} \right) \sin \bar{\Phi}$$

$$= \bar{p}_f - q_f \sin \bar{\Phi} \qquad (2.10)$$

and therefore Equation (2.5) can be written in the form

$$q_f \cos \bar{\Phi} = \bar{c} + (\bar{p}_f - q_f \sin \bar{\Phi}) \tan \bar{\Phi}$$

so that, after multiplying both sides by $\cos \bar{\Phi}$, the result is

$$q_f = \bar{c} \cos \bar{\Phi} + \bar{p}_f \sin \bar{\Phi} \qquad (2.11)$$

$$= (\bar{p}_f + d) \sin \bar{\Phi} \qquad (2.12)$$

A plot of Equation (2.11) is shown in Figure 2.2.

If Equation (2.11) is expanded, using the definitions of $\bar{p}_f$ and q_f, the result is

$$\left(\frac{\bar{\sigma}_{1f} - \bar{\sigma}_{3f}}{2} \right) = \left(\frac{\bar{\sigma}_{1f} + \bar{\sigma}_{3f}}{2} \right) \sin \bar{\Phi} + \bar{c} \cos \bar{\Phi} \qquad (2.13)$$

Equation (2.13) leads to the following linear relations between the major and minor principal effective stresses at failure:

$$\bar{\sigma}_{1f} = \left(\frac{1 + \sin\bar{\Phi}}{1 - \sin\bar{\Phi}}\right)\bar{\sigma}_{3f} + \frac{2\bar{c}\cos\bar{\Phi}}{1 - \sin\bar{\Phi}}$$

$$= \left(\frac{1 + \sin\bar{\Phi}}{1 - \sin\bar{\Phi}}\right)\bar{\sigma}_{3f} + \frac{2d\sin\bar{\Phi}}{1 - \sin\bar{\Phi}} \qquad (2.14)$$

$$\bar{\sigma}_{3f} = \left(\frac{1 - \sin\bar{\Phi}}{1 + \sin\bar{\Phi}}\right)\left(\bar{\sigma}_{1f} - \frac{2\bar{c}\cos\bar{\Phi}}{1 - \sin\bar{\Phi}}\right)$$

$$= \left(\frac{1 - \sin\bar{\Phi}}{1 + \sin\bar{\Phi}}\right)\bar{\sigma}_{1f} - \frac{2\bar{c}\cos\bar{\Phi}}{1 + \sin\bar{\Phi}}$$

$$= \left(\frac{1 - \sin\bar{\Phi}}{1 + \sin\bar{\Phi}}\right)\bar{\sigma}_{1f} - \frac{2d\sin\bar{\Phi}}{1 + \sin\bar{\Phi}} \qquad (2.15)$$

Notice that Equation (2.15) can be obtained from Equation (2.14) by interchanging $\bar{\sigma}_{1f}$ and $\bar{\sigma}_{3f}$, and replacing $\bar{\Phi}$ by $-\bar{\Phi}$. A plot of Equations (2.14) and (2.15) is shown in Figure 2.3. The intercepts on the two principal stress axes are necessarily equal, and the slopes are the reciprocal of one another. Equations (2.14) and (2.15) are particularly convenient for treating idealized earth pressure problems.

Thesis Structure

This thesis can be viewed as an examination of each of the terms of the Revised Coulomb Equation, as written in Equation 2.11, when only the direction of the intermediate principal stress axis remains fixed.

Whether or not $\bar{c}$ and $\bar{\Phi}$, the effective stress shear strength parameters, are really constants has been the subject of numerous investigations; HVORSLEV (1960). The possibility of their variation with failure plane orientation is discussed in Chapter 3.

Chapters 4 and 5 are devoted to an investigation of the relation between applied total stresses and the resulting pore water pressure, and to an exploration of the consequences of that relationship for undrained shear strength.

With the aid of Mohr's graphical representation of a state of triaxial stress, it is easily seen that Coulomb's failure hypothesis assumes the intermediate principal stress has no influence on failure; WESTERGAARD (1924). This is shown in Figure 2.4. The possible influence of the intermediate principal stress on $\bar{c}$ and $\bar{\Phi}$, and the limits of applicability of the Revised Coulomb Equation are examined in Chapter 6.

Information on the effective stress mechanics of undrained shear strength of saturated clay, developed in Chapters 2 through 6, is focused on the interpretation of model footing test results in Chapter 7. It was the difficulty of interpreting test results of model footings on clay that originally prompted the Author to undertake this investigation of the effective stress mechanics of undrained shear strength.

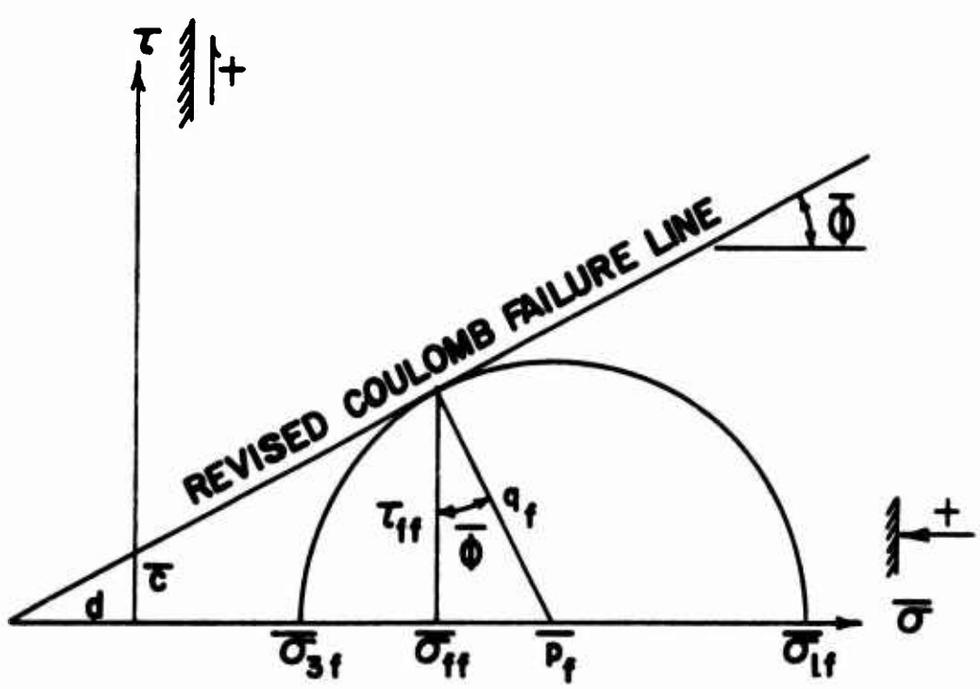

$$\bar{p}_f = \frac{\bar{\sigma}_{1f} + \bar{\sigma}_{3f}}{2}$$

$$q_f = \frac{\bar{\sigma}_{1f} - \bar{\sigma}_{3f}}{2}$$

FIGURE 2.1

GEOMETRY OF THE REVISED COULOMB FAILURE CRITERION

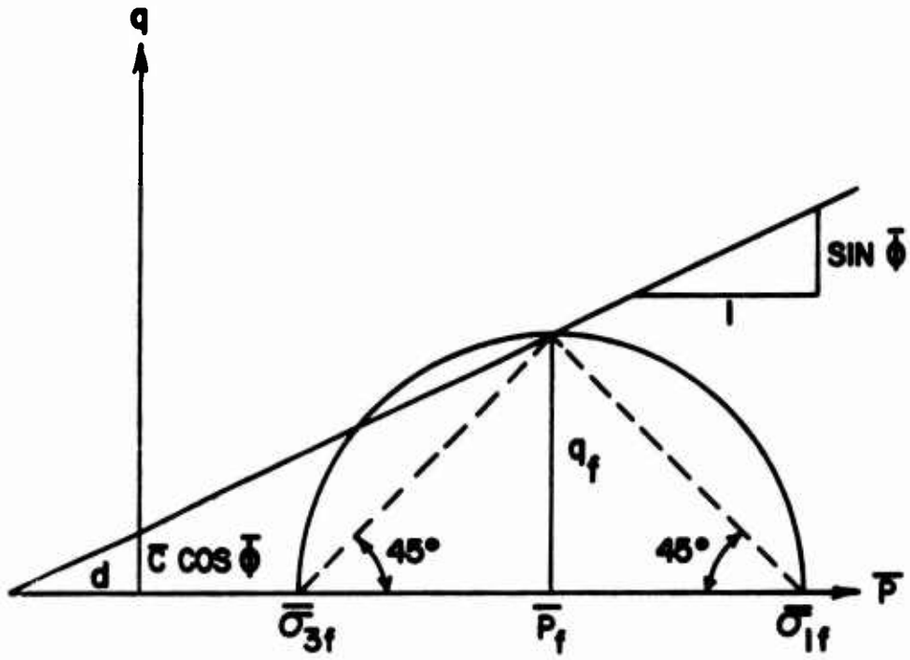

$$\bar{p} = \frac{\bar{\sigma}_1 + \bar{\sigma}_3}{2}$$

$$q = \frac{\bar{\sigma}_1 - \bar{\sigma}_3}{2}$$

FIGURE 2.2
REVISED COULOMB FAILURE
CRITERION IN $(\bar{p},q)$ SPACE

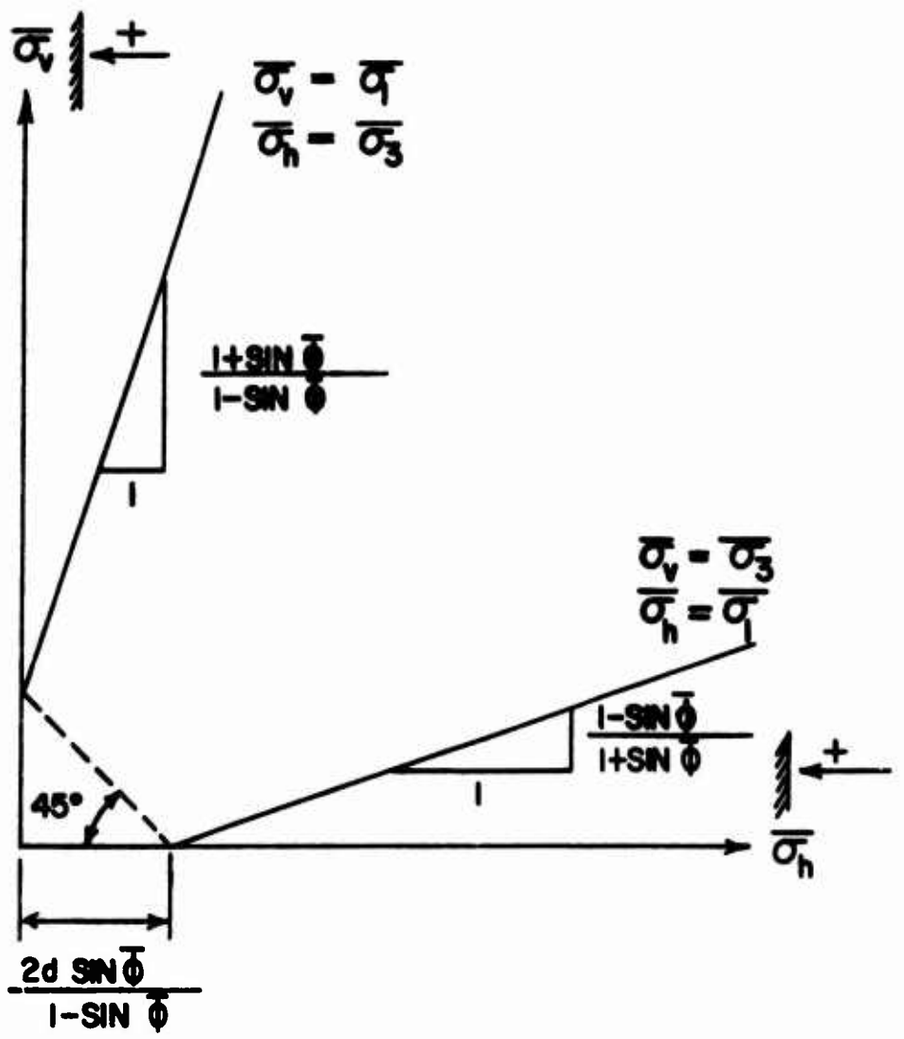

FIGURE 2.3

REVISED COULOMB FAILURE CRITERION IN $(\bar{\sigma}_v, \bar{\sigma}_h)$ SPACE (RENDULIC PLOT)

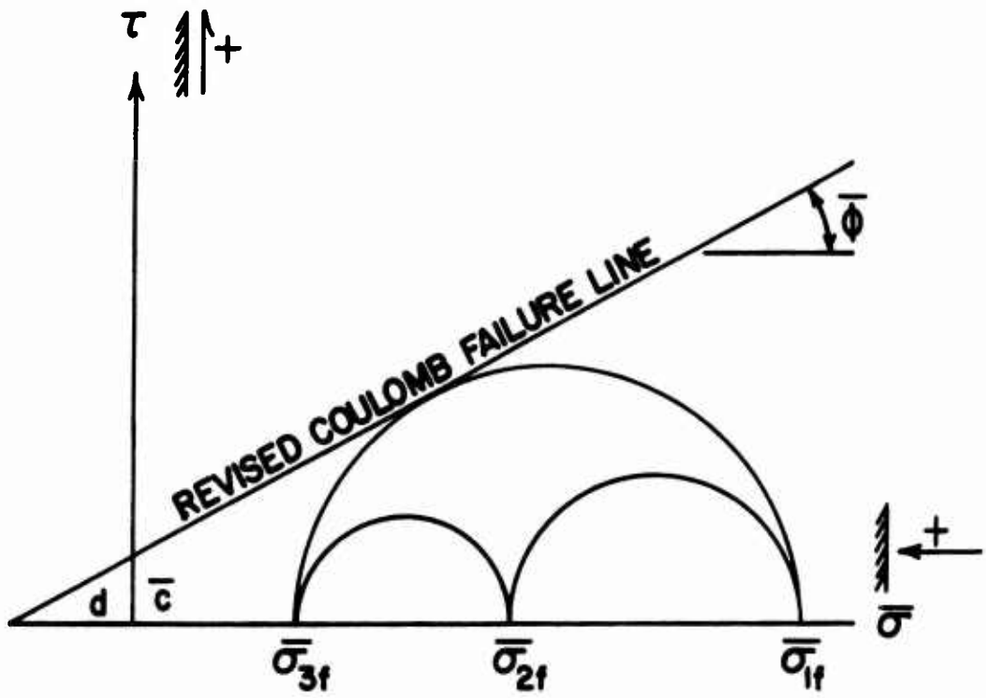

FIGURE 2.4
INDEPENDENCE OF $\bar{\sigma}_2$ IN THE REVISED
COULOMB FAILURE CRITERION

CHAPTER 3

ANISOTROPY OF SHEAR STRENGTH PARAMETERS

Purpose

This chapter examines the influence of anisotropy with respect to the effective stress shear strength parameters, $\bar{c}$ and $\bar{\Phi}$ in the Revised Coulomb Equation, on the directional dependence of shear strength in terms of effective stress. The concept of a three - dimensional failure surface is introduced, which completely describes the shear strength of a soil, within the framework of a Revised Coulomb Equation with anisotropic parameters, provided the direction of the intermediate principal stress axis remains fixed. The influence of pore pressure response on the directional dependence of undrained shear strength is discussed in the following two chapters, but is not explicitly considered in this chapter.

THIS REPORT HAS BEEN DELIMITED
AND CLEARED FOR PUBLIC RELEASE
UNDER DOD DIRECTIVE 5200.20 AND
NO RESTRICTIONS ARE IMPOSED UPON
ITS USE AND DISCLOSURE.

DISTRIBUTION STATEMENT A

APPROVED FOR PUBLIC RELEASE;
DISTRIBUTION UNLIMITED.

Clay Structure

Clays which have been one-dimensionally consolidated from an initial water content at or above the liquid limit are known to possess a structure in which the clay platelets tend to be oriented parallel to the plane of maximum principal stress during consolidation; LAMBE (1953), MARTIN (1962). The stress - strain and shear strength properties of these clays can therefore be suspected of possessing inherent cross anisotropy, characterized by an axis of anisotropic symmetry, called the material axis, parallel to the major principal stress axis during consolidation.* This type of anisotropy results in a variation of effective stress shear strength parameters with the angle between the normal to the failure plane and the axis of anisotropic symmetry.

Basic Questions of Anisotropy

Two main questions arise in dealing with a...otropy of shear strength parameters.

---

*Another material known to possess cross anisotropy is graphite, used in the cores of nuclear reactors; MERKLE, J.G. (1967, 54).

1. Given an assumed variation of effective stress shear strength parameters with failure plane orientation, and the orientation of the principal stresses at failure: on what plane will failure occur, and what will be the corresponding shear strength?
2. What is the actual variation of effective stress shear strength parameters with failure plane orientation?

The above two questions closely parallel the two more general questions which naturally arise in the investigation of the load - deformation response of any material whose stress - strain behavior is not precisely defined, viz.:

A. What are the consequences of an assumed stress - strain realtion?

B. What is the actual stress - strain relation?

The approach guided by Question A can be termed the Axiomatic Approach because it assumes a material characterization, and the consequencies of that assumption are then sought. The approach guided by Question B is the Experimental Approach, because it attempts to measure the actual stress - strain behavior, rather than assume it. Any comprehensive

investigation of load - deformation behavior must employ both the Axiomatic and the Experimental Approaches, with constant feedback between the two. The Axiomatic Approach requires information about the general physical mechanisms which must be reflected in an assumed material characterization, while the Experimental Approach requires a general framework within which to interpret observed behavior. Each approach is therefore dependent on the other for vital information, without which it cannot yield meaningful results.

Review of Early Work

In this section the work of Casagrande and Carrillo, and Hank and McCarty will be reviewed in detail, as a preliminary step toward the treatment of more general problems of shear strength anisotropy. The reason for discussing their work in such detail is that it has frequently been misinterpreted. In particular, Casagrande and Carrillo did not make any assumption concerning the variation of undrained shear strength with orientation of the major principal stress at failure. In fact the bulk of their analysis assumed the principal stress planes to remain fixed, coincident with the planes of maximum and

minimum shear strength. Only a brief qualitiative discussion was devoted to the case in which the principal stress planes do not coincide with the planes of maximum and minimum shear strength. Their analytical results were based, instead, on an assumed variation of shear strength parameters with failure plane orientation.

Referring to Figure 3.1, the following preliminary geometrical relationships can be established:

$$AH = \sqrt{(AF)(AB)} \tag{3.1}$$

$$\frac{KF}{AF} = \frac{HD}{AH} = \frac{GB}{AB} = \tan \Phi \tag{3.2}$$

$$HD = \sqrt{(KF)(GB)} \tag{3.3}$$

$$\frac{KF}{GB} = \frac{AF}{AB} = \tan^2 \left(45 + \frac{\Phi}{2}\right) = \tan^2 \alpha_f \tag{3.4}$$

$$\frac{HC}{HD} = \frac{HD}{ID} = \cos \Phi \tag{3.5}$$

$$HC = \frac{(HD)^2}{ID} = \frac{2(KF)(GB)}{KF + GB} \tag{3.6}$$

$$AE = AD + DE = \left(\frac{AF + AB}{2}\right) + \left(\frac{AF - AB}{2}\right) \cos 2\alpha \qquad (3.7)$$

$$JE = \left(\frac{KF + GB}{2}\right) + \left(\frac{KF - GB}{2}\right) \cos 2\alpha \qquad (3.8)$$

Figure 3.2 shows the cases solved analytically by CASAGRANDE AND CARRILLO (1944), and Figure 3.3(a) shows the case solved analytically by HANK AND McCARTY (1948). While Casagrande and Carrillo posed separate problems for purely cohesive and purely frictional materials, Hank and McCarty treated a material possessing both cohesion and internal friction. Therefore Hank and McCarty's solution can be reduced to either one of those obtained by Casagrande and Carrillo, and so Hank and McCarty's analysis will be discussed here. Emphasis will be placed on the graphical significance of their solution, since it has not been fully appreciated; BARBER (1948).

Hank and McCarty made the assumption that, at failure, the shear strengths in the major and minor principal planes, shown in Figure 3.3(a) are

$$\tau_1 = \bar{c}_1 + \bar{\sigma}_{1f} \tan \bar{\Phi}_1$$
$$\tau_3 = \bar{c}_3 + \bar{\sigma}_{3f} \tan \bar{\Phi}_3 \qquad (3.9)$$

The effective stress shear strength parameters, $\bar{c}_1$, $\bar{c}_3$, $\bar{\Phi}_1$ and $\bar{\Phi}_3$ are assumed known, but $\bar{\sigma}_{1f}$ and $\bar{\sigma}_{3f}$ are not both known. The shear strength in any plane, inclined at an angle α to the material axis, is denoted by $\tau_f(\alpha)$ in Figure 3.3(a), and is assumed to be given by a straight line connecting the points $(\bar{\sigma}_{1f}, \tau_1)$ and $(\bar{\sigma}_{3f}, \tau_3)$. The Mohr circle at failure is then tangent to this line which, according to Equation (3.8) has the equation

$$\tau_f(\alpha) = \left(\frac{\tau_1 + \tau_3}{2}\right) + \left(\frac{\tau_1 - \tau_3}{2}\right) \cos 2\alpha \qquad (3.10)$$

Referring to Figure 3.1, it follows that

$$KF = \tau_1 = \bar{c}_1 + \bar{\sigma}_{1f} \tan \bar{\Phi}_1$$

$$= \bar{c}_1 + (\bar{\sigma}_{3f} + 2q_f) \tan \bar{\Phi}_1$$

$$GB = \tau_3 = \bar{c}_3 + \bar{\sigma}_{3f} \tan \bar{\Phi}_3 \qquad (3.11)$$

Therefore, according to Equation (3.3)

$$q_f = \sqrt{\tau_1 \tau_3} \qquad (3.12)$$

Since τ_1 is a function of q_f, for a given $\bar{\sigma}_{3f}$, according to Equation (3.11), Equation (3.12) yields a quadratic equation for q_f, the solution to which can be expressed in the form

$$\frac{q_f}{\tau_3} = \tan \bar{\Phi}_1 + \sqrt{\tan^2 \bar{\Phi}_1 + \frac{\tau_1'}{\tau_3}} \qquad (3.13)$$

where

$$\tau_1' = \bar{c}_1 + \bar{\sigma}_{3f} \tan \bar{\Phi}_1 \qquad (3.14)$$

Equation (3.13) gives the radius of the Mohr circle at failure when the minor principal effective stress, $\bar{\sigma}_{3f}$, and the strength parameters $\bar{c}_1$, $\bar{c}_3$, $\bar{\Phi}_1$ and $\bar{\Phi}_3$ are known. The quantity τ_1' is the value which τ_1 would assume if

$\bar{\sigma}_{1f}$ were replaced by $\bar{\sigma}_{3f}$. The graphical significance of the quantities τ_3 and τ_1' is easily seen Figure 3.3(a). A numerical example is given below to illustrate the ease of using Equation (3.13).

GIVEN:

$\bar{c}_1 = 100$ psi

$\bar{c}_3 = 250$ psi

$\bar{\Phi}_1 = 25^\circ$

$\bar{\Phi}_3 = 30^\circ$

$\bar{\sigma}_{3f} = 50$ psi

REQUIRED:

$q_f,\ \bar{p}_f,\ \bar{\sigma}_{1f},\ \alpha_f$

SOLUTION:

$$\tau_1' = \bar{c}_1 + \bar{\sigma}_{3f} \tan \bar{\Phi}_1 = 100 + (50)(0.466) = \begin{array}{r} 100.0 \\ \underline{23.3} \\ 123.3 \text{ psi} \end{array}$$

$$\tau_3 = \bar{c}_3 + \bar{\sigma}_{3f} \tan \bar{\Phi}_3 = 250 + (50)(0.578) = \begin{array}{r} 250.0 \\ \underline{28.9} \\ 278.9 \text{ psi} \end{array}$$

$$\frac{q_f}{\tau_3} = \tan \bar{\Phi}_1 + \sqrt{\tan^2 \bar{\Phi}_1 + \frac{\tau_1'}{\tau_3}}$$

$$= 0.466 + \sqrt{0.218 + 0.442} = 1.279$$

$$q_f = 1.279\, \tau_3 = (1.279)(278.9) = \underline{356.1 \text{ psi}}$$

$$\bar{p}_f = \bar{\sigma}_{3f} + q_f \quad \begin{array}{r} 50.0 \\ \underline{356.1} \\ \underline{\underline{406.1 \text{ psi}}} \end{array}$$

$$\bar{\sigma}_{1f} = \bar{\sigma}_{3f} + 2q_f = \begin{array}{r} 50.0 \\ \underline{712.2} \\ \underline{\underline{762.2 \text{ psi}}} \end{array}$$

$$\tau_1 = \bar{c}_1 + \bar{\sigma}_{1f} \tan \bar{\Phi}_1 = 100 + (762.2)(0.466) = \begin{array}{r} 100.0 \\ \underline{355.0} \\ 455.0 \text{ psi} \end{array}$$

From Equation (3.4)

$$\tan^2 \alpha_f = \frac{\tau_1}{\tau_3} = \frac{455.0}{278.9} = 1.631$$

$$\tan \alpha_f = 1.279$$

$$\alpha_f = \underline{\underline{52^\circ}}$$

The above solution is represented graphically in Figure 3.3(b).

The solutions obtained by Casagrande and Carrillo are easily recovered from Equation (3.13). For a purely cohesive material,

$$q_f = \bar{c}_3 \sqrt{\frac{\bar{c}_1}{\bar{c}_3}} = \sqrt{\bar{c}_1 \bar{c}_3}$$

For a cohesionless material,

$$q_f = \bar{\sigma}_{3f} \tan \bar{\Phi}_3 \left[\tan \bar{\Phi}_1 + \sqrt{\tan^2 \bar{\Phi}_1 + \frac{\tan \bar{\Phi}_1}{\tan \bar{\Phi}_3}} \right]$$

$$= \bar{\sigma}_{3f} \tan \bar{\Phi}_1 \tan \bar{\Phi}_3 \left[1 + \sqrt{1 + \cot \bar{\Phi}_1 \cot \bar{\Phi}_3} \right]$$

For an isotropic material,

$$\bar{c}_1 = \bar{c}_3 = \bar{c}$$

$$\bar{\Phi}_1 = \bar{\Phi}_3 = \bar{\Phi}$$

and therefore

$$q_f = (\bar{c} + \bar{\sigma}_{3f} \tan \bar{\Phi}) \left[\tan \bar{\Phi} + \sqrt{\tan^2 \bar{\Phi} + 1} \right]$$

$$= \frac{\bar{c} \cos \bar{\Phi} + \bar{\sigma}_{3f} \sin \bar{\Phi}}{1 - \sin \bar{\Phi}}$$

There seems to be some misunderstanding in the current literature, not only about the ease of obtaining numerical values using the above analytical solution, but also about the physical implications of its formulation. It has been stated that in Hank and McCarty's solution, both $\bar{c}$ and $\bar{\Phi}$ were assumed to vary elliptically between extreme values.

This is not true, as can easily be duduced from Equation (3.10). Rather, the shear strength, $\tau_f(\alpha)$, is the elliptically varying quantity, as shown in Figure 3.4. Even if $\bar{c}$ and tan $\bar{\Phi}$ (not $\bar{\Phi}$) both varied elliptically, $\tau_f(\alpha)$ would still not vary elliptically, because the normal effective stress on a potential failure plane also varies elliptically. The way to obtain an elliptical variation of shear strength is to have $\bar{\Phi}$ remain constant, $\bar{c}$ vary elliptically and the principal planes at failure coincide with the planes of maximum and minimum cohesion.

General Concepts of Anisotropic Shear Strength Analysis

There is no guarantee that the anisotropic shear strength in a clay will vary precisely as prescribed by Equation (3.10) and Figure 3.4. In general, both the cohesion and angle of internal friction may vary with the angle between the normal to a potential failure plane and the material axis. These two axes are shown in Figure 3.5, and it will be assumed that the shear strength in any potential failure plane is given by the equation

$$\tau_f(\alpha) = \bar{c}(\alpha) + \bar{\sigma}_f \tan\left[\bar{\Phi}(\alpha)\right] \qquad (3.15)$$

where

$\tau_f(\alpha)$ = shear strength in a potential failure plane, with normal inclined at an angle α to the material axis.

$\bar{\sigma}_f$ = normal effective stress acting on the potential failure plane

$\bar{c}(\alpha)$ = scalar function of the angle α, called cohesion

$\bar{\Phi}(\alpha)$ = scalar function of the angle α, called angle of internal friction

The key concept of anisotropic shear strength analysis, using Equation (3.15), is the idea of when failure occurs, and on what plane it occurs. Equation (3.15) in effect specifies all limiting combinations of shear and effective normal stress which produce failure, when acting on any plane whose normal is inclined at an angle α to the material axis. Any straight - line plot of $\tau_f(\alpha)$ VERSUS $\bar{\sigma}_f$, found by setting α equal to a constant in Equation (3.15), is called an α strength contour. The complete family of α strength contours for $0^\circ \leq \alpha \leq 90^\circ$, which can be thought of as defining an α strength surface in a three - dimensional space of $(\bar{\sigma}, \tau, \alpha)$, constitutes one of the two basic

elements in the shear strength analysis of a cross anisotropic clay. The other element is the family of α stress contours, any one of which specifies all combinations of shear and effective normal stress which actually act on all planes whose normal is inclined at an angle α to the material axis. The α stress contours can be superimposed upon a three - dimensional Mohr stress circle plot, and can be thought of as defining an α stress surface in the above three - dimensional space. Failure occurs when the α stress surface first contacts the α strength surface, i.e. when an α stress contour first contacts its corresponding α strength contour. The details of this process are discussed below.

All of the analyses to follow are restricted to the case in which the material axis remains in the plane of the major and minor principal stress axes, which includes both axial symmetry and plane strain.

When shear failure occurs in a cross anisotropic clay under the above restriction, three directions are of interest:

1. the direction of the material axis (the axis of strength symmetry),

2. the direction of the major principal stress axis, and

3. the direction of the normal to the failure plane.

The geometric relationships between these directions are shown in Figure 3.6. The X_1, X_2 and X_3 axes are the principal stress axes, and the material axis lies in the first quandrant of the X_1X_3 plane. β is the angle between the material axis and the major principal stress axis, and δ is the angle between the normal to the failure plane and the major principal stress axis. Ψ is the angle between the horizontal projection of the normal to the failure plane and the minor principal stress axis. The angle α between the normal to the failure plane and the material axis can be determined from the condition shown in Figure 3.6,

$$\cos \alpha = \cos \beta \cos \delta + \cos \Psi \sin \beta \sin \delta \qquad (3.16)$$

Using Equation (3.16) one can construct contrours of constant α, for a given value of β, using the curvilinear coordinates δ and Ψ of a three-dimensional Mohr circle mapping. (See Appendix B for a discussion of the three-dimensional Mohr circle.) These contours of constant α are the α stress

contours referred to previously. Each is the Mohr mapping of the intersection of a cone with central angle α with a unit sphere, when the cone apex lies at the sphere center. Hence the $\alpha = 0$ contour is always a single point. Several sets of α stress contours are shown in Figure 3.7, and a hypothetical family of α strength contours is shown in Figure 3.8. As stated previously, failure occurs when the surfaces defined by these two families of contours first come in contact, and the orientation of the failure plane is defined by the coordinates (δ, Ψ) of the contact point, in the Mohr circle mapping.

Inspection of the four sets of α stress contours in Figure 3.7 shows that as the angle β increases from 0° to 90°, the α stress contours progress from circles concentric about the center of the $\sigma_2\sigma_3$ circle to circles concentric about the center of the $\sigma_1\sigma_2$ circle. The points at which these contours intersect the $\sigma_1\sigma_3$ circle remain equally spaced, and rotate counterclockwise by an amount equal to twice the increase in the angle β. The result is that the minimum value of the angle α along any vertical line (i.e. for any given value of normal stress) lies on the upper half of the $\sigma_1\sigma_3$ circle, where the angle Ψ is 0°. The maximum

value of the angle α along a vertical line generally lies somewhere in the interior of the Mohr mapping.

Therefore, provided:

1. the material axis remains in the plane of the major and minor principal stress axes, and
2. both $\bar{c}$ and $\bar{\Phi}$ increase steadily with the angle between the normal to the failure plane and the material axis,

the point of contact between the σ stress and α strength surfaces will always occur on the upper half of the $\sigma_1\sigma_3$ circle, where the angle Ψ is 0^o, and therefore failure will be independent of the intermediate principal stress.

The assumption regarding the variation of $\bar{c}$ and $\bar{\Phi}$ with α is based on the following argument. If clay platelets tend to be oriented parallel to a plane on which the maximum principal stress acts during consolidation, then despite the fact that this is the plane of maximum normal stress during consolidation, it seems reasonable to expect the shear strength parameters $\bar{c}(\alpha)$ and $\tan\left[\bar{\Phi}(\alpha)\right]$ to be minimum for sliding in such a plane. This is because the degree of interlocking mobilized against shearing in this plane would probably be a minimum, as compared to that mobilized against shearing in any other plane. Hence the

second assumption made above. DUNCAN AND SEED (1966a, 45) showed that ψ was equal to 0° for all of 18 $\overline{UU}$ triaxial compression test specimens (16 with $\beta = 90^{\circ}$ and 2 with $\beta = 45^{\circ}$), trimmed from overconsolidated block samples of kaolinite, which had been anisotropically consolidated to $\bar{\sigma}_1 = 9.0$ kg/cm^2 and $\bar{\sigma}_3 = 5.5$ kg/cm^2, then isotropically rebounded to $\bar{\sigma} = 1.0$ kg/cm^2.

An important consequence of the fact that failure will occur on a plane for which $\psi = 0^{\circ}$ is that the angle α will be a minimum, and Equation (3.16) reduces to

$$\cos \alpha = \cos |\delta - \beta| \tag{3.17}$$

In view of the fact that the functions $\bar{c}(\alpha)$ and $\bar{\Phi}(\alpha)$ must be even functions of α, there will be no loss of generality in writing

$$\alpha = \delta - \beta \tag{3.18}$$

in the analyses to follow, and this will be done consistently. The angle α will be considered positive when measured in the opposite direction from β in the X_1X_3 plane, i.e. in the second quadrant.

An equally important consequence of the fact that failure will occur on a plane for which $\psi = 0^{o}$ is that only the two - dimensional Mohr circle determined by the major and minor principal stresses need be considered in a theoretical analysis, since that circle is the $\psi = 0^{o}$ contour.

Basic Equations of Anisotropic Shear Strength Analysis

Consider now the problem of determining the failure plane orientation and the shear strength of a sample when $\bar{c}$ and $\bar{\Phi}$ are known functions of α, for any desired value of $\bar{p}$ and β. Assuming failure will occur on a plane for which $\psi = 0^{o}$, then for any given β, the strength parameters $\bar{c}$ and $\bar{\Phi}$ become functions of δ, according to Equation (3.18). The state of stress at failure in a triaxial sample is shown in Figure 3.9, from which, using the Law of Sines, it can be seen that

$$\frac{q_f}{\bar{c}\cot\bar{\Phi} + \bar{p}_f} = \frac{\sin\bar{\Phi}}{\sin(2\delta - \bar{\Phi})}$$

so that

$$q_f = \frac{\bar{c}\cos\bar{\Phi} + \bar{p}_f \sin\bar{\Phi}}{\sin(2\delta - \bar{\Phi})} \qquad (3.19)$$

where

$$\bar{c} = \bar{c}(\alpha) \tag{3.20}$$

$$\bar{\Phi} = \bar{\Phi}(\alpha) \tag{3.21}$$

Not only must Equation (3.19) be satisfied, but for given values of β and $\bar{p}_f$, failure will occur on the plane corresponding to the value of δ for which Equation (3.19) is first satisfied, as q increases from zero. Mathematically, this requires that the condition

$$\left(\frac{dq_f}{d\delta}\right)_{\beta,\bar{p}_f} = 0 \tag{3.22}$$

be satisfied, in addition to Equation (3.19)

In summary, the governing equations of anisotropic shear strength analysis, subject to the two restrictions explained previously, are the following:

$$\alpha = \delta - \beta \tag{3.18}$$

$$q_f = \frac{\bar{c}\cos\bar{\Phi} + \bar{p}_f \sin\bar{\Phi}}{\sin(2\delta - \bar{\Phi})} \tag{3.19}$$

$$\bar{c} = \bar{c}(\alpha) \tag{3.20}$$

$$\bar{\Phi} = \bar{\Phi}(\alpha) \tag{3.21}$$

$$\left(\frac{dq_f}{d\delta}\right)_{\beta,\bar{p}_f} = 0 \tag{3.22}$$

When Equations (3.18), (3.20) and (3.21) have been introduced into Equation (3.19), Equations (3.19) and (3.22) then constitute a set of two simultaneous equations for the variables q_f and δ.

If the functions $\bar{c}(\alpha)$ and $\bar{\Phi}(\alpha)$ have been obtained experimentally and are not easily expressible in closed form, or if a theoretical analysis becomes excessively tedious, the simultaneous solution of Equations (3.19) and (3.22) can be accomplished graphically or numerically. This will be done for the case of anisotropic friction, as illustrated in Figure 3.16.

Three-Dimensional Failure Surface

The function $q_f(\bar{p}_f, \beta)$ can be interpreted as a surface in a space of three dimensions. However, rather than use the angle β as a rectangular Cartesian coordinate, Figure 3.10 shows that if one uses as rectangular Cartesian coordinates the variables

$$h = \frac{\bar{\sigma}_{zz} - \bar{\sigma}_{rr}}{2} = \frac{\sigma_{zz} - \sigma_{rr}}{2} \tag{3.23}$$

$$\tau = \bar{\sigma}_{rz} = \sigma_{rz} \tag{3.24}$$

$$\bar{p} = \frac{\bar{\sigma}_{zz} + \bar{\sigma}_{rr}}{2} = \frac{\bar{\sigma}_1 + \bar{\sigma}_3}{2} \tag{3.25}$$

which are convenient for computer applications, then the polar coordinates associated with h and τ are q and 2β, because

$$q^2 = h^2 + \tau^2 \tag{3.26}$$

and

$$\tan 2\beta = \frac{\tau}{h} \tag{3.27}$$

Therefore the three-dimensional failure surface which characterizes the shear strength of a cross anisotropic clay, in terms of effective stress, and under the same two previous assumptions (that the material axis remains in the plane of the major and minor principal stress axes and that $\bar{c}$ and $\bar{\Phi}$ increase steadily with increasing inclination of the normal to the failure plane from the material axis), can be expressed by the functional relation

$$F(h, \tau, \bar{p}) = 0 \tag{3.28}$$

The failure surface defined by Equation (3.28) has the general shape of an aircraft fuselage pointed in the $-\bar{p}$ direction, as shown in Figure 3.11. The ribs of the fuselage are closed durves, which define the relation between q_f and β for a particular value of $\bar{p}_f$, by a polar plot which is symmetric about the line $\beta = 0$. The intersection of a radial plane with the failure surface is a curve defining the relation between $\bar{p}_f$ and q_f for a particular value of β.

The above failure surface is one of the two key elements required to define the variation of undrained shear strength with β. The other element is a pore pressure surface, which is discussed in the following two chapters.

The remainder of this chapter is devoted to consideration of the relation between the assumed form of Equations (3.20) and (3.21) and the geometry of the resulting failure surface in Figure 3.11, then to the problem of determining experimentally the actual form of the relations represented by Equations (3.20) and (3.21), and lastly to a discussion of test data.

Isotropy as a Limiting Case of Anisotropy

When $\bar{c}$ and $\bar{\Phi}$ are independent of α, the failure surface in Figure 3.11 becomes a surface of revolution, so that all cross - sections normal to the $\bar{p}$ axis are circles. If, in addition, $\bar{c}$ and $\bar{\Phi}$ are constant, i.e. independent of $\bar{p}$, then the failure surface is a right circular cone. This is because the value of q_f in Equation (3.19) will be a minimum with respect to δ when the denominator reaches its maximum value, since the numerator is assumed constant with respect to δ. This condition will occur when

$$2\,\delta - \bar{\Phi} = \frac{\pi}{2}$$

which leads to the well known results

$$\delta = \frac{\pi}{4} + \frac{\bar{\Phi}}{2}$$

$$q_f = \bar{c} \cos \bar{\Phi} + \bar{p}_f \sin \bar{\Phi}$$

The second expression is the equation of a right circular cone in $(h,\tau,\bar{p})$ space when $\bar{c}$ and $\bar{\Phi}$ are independent of $\bar{p}$.

Anisotropic Cohesion Assumed by Jaeger

A close examination of Figures 3.2 and 3.3 shows that Casagrande and Carrillo, and Hank and McCarty both solved the same problem, but used different expressions for τ_1 and τ_3. The reason the problems they solved were the same is that Equation (3.15) was not used explicitly, but Equation (3.10) was implied in each case. Their problem is a special case of that solved by JEAGER (1960), who did use Equation (3.15), as will be shown by Equation (3.33).

Jaeger assumed that $\bar{\Phi}(\alpha)$ and $\bar{c}(\alpha)$ are given by the equations

$$\bar{\Phi}(\alpha) = \bar{\Phi} = \text{constant} \tag{3.29}$$

$$\bar{c}(\alpha) = \left(\frac{\bar{c}_1 + \bar{c}_3}{2}\right) - \left(\frac{\bar{c}_1 - \bar{c}_3}{2}\right) \cos 2\alpha$$

$$= r - s \cos 2\alpha \tag{3.30}$$

where

$$r = \frac{\bar{c}_1 + \bar{c}_3}{2}$$

$$s = \frac{\bar{c}_1 - \bar{c}_3}{2} \tag{3.31}$$

The assumed variation of $\bar{c}(\alpha)$ with α is shown in Figure 3.12. The minimum value of $\bar{c}(\alpha)$ occurs in the plane normal to the material axis, because of the tendency of the clay platelets to allign themselves parallel to that plane. (Note that Jaeger's original analysis was for rock.)

The shear strength in a plane inclined at an angle δ to the plane of maximum principal stress, when the maximum principal stress axis makes an angle β with the material axis, is

$$\tau_f(\alpha) = \bar{c}(\alpha) + \bar{\sigma}_f \tan \bar{\Phi}$$

$$= r - s \cos(2\delta - 2\beta) + (\bar{p} + q \cos 2\delta) \tan \bar{\Phi} \qquad (3.32)$$

When $\beta = 0^\circ$, δ and α are equal, so that Equation (3.32) reduces to

$$\tau_f(\alpha) = (r + \bar{p} \tan \bar{\Phi}) + (q \tan \bar{\Phi} - s) \cos 2\alpha \qquad (3.33)$$

Equation (3.33) is of the same form as Equation (3.10), hence the previous statement that Jaeger's problem includes that of Casagrande, Carrillo, Hank and McCarty as a special case.

The solution to Jaeger's problem proceeds according to the general method outlined previously. Substitution of Equations (3.29) and (3.30) into Equation (3.19) yields

$$\begin{aligned}&(s \cos \bar{\Phi} \sin 2\beta + q_f \cos \bar{\Phi}) \sin 2\delta \\ &+ (s \cos \bar{\Phi} \cos 2\beta - q_f \sin \bar{\Phi}) \cos 2\delta \\ &= r \cos \bar{\Phi} + \bar{p}_f \sin \bar{\Phi}\end{aligned} \tag{3.34}$$

Differentiating Equation (3.34) with respect to δ and setting $\frac{dq_f}{d\delta}$ equal to zero yields

$$\tan 2\delta = \frac{s \cos \bar{\Phi} \sin 2\beta + q_f \cos \bar{\Phi}}{s \cos \bar{\Phi} \cos 2\beta - q_f \sin \bar{\Phi}} \tag{3.35}$$

The simultaneous solution of Equations (3.34) and (3.35) can be accomplished by obtaining expressions for sin 2δ and cos 2δ from Equation (3.35), then eliminating δ from Equation (3.34) to find q_f. Once q_f is known, δ can then be found from one of the expressions for sin 2δ, cos 2δ or tan 2δ.

Thus,

$$\left.\begin{aligned}\sin 2\delta &= \frac{s \cos \bar{\Phi} \sin 2\beta + q_f \cos \bar{\Phi}}{R} \\ \cos 2\delta &= \frac{s \cos \bar{\Phi} \cos 2\beta - q_f \sin \bar{\Phi}}{R}\end{aligned}\right\} \tag{3.36}$$

where

$$R = \sqrt{q_f^2 + (2s \cos \bar{\Phi} \sin 2\omega) q_f + s^2 \cos^2 \bar{\Phi}} \qquad (3.37)$$

and

$$2\omega = 2\beta - \bar{\Phi} \qquad (3.38)$$

Substitution of Equations (3.36) back into Equation (3.34) and squaring both sides of that result yields

$$R^2 = q_f^2 + (2 s \cos \bar{\Phi} \sin 2\omega) q_f + s^2 \cos^2 \bar{\Phi} \qquad (3.39)$$

$$= (r \cos \bar{\Phi} + \bar{p}_f \sin \bar{\Phi})^2$$

If the following substitution is made in Equation (3.39),

$$\left.\begin{aligned} x &= q_f \cos 2\omega \\ y &= q_f \sin 2\omega \end{aligned}\right\} \qquad (3.40)$$

the result is

$$x^2 + (y + s \cos \bar{\Phi})^2 = (r \cos \bar{\Phi} + \bar{p}_f \sin \bar{\Phi})^2 \qquad (3.41)$$

Equation (3.41) is the equation of a right circular cone, with its axis parallel to the $\bar{p}$ axis along the line $(x = 0, y = -s \cos \bar{\Phi})$. Consequently, sections normal to the $\bar{p}$ axis will be circular, and intersections with planes containing

the $\bar{p}$ axis will be hyperbolic. Since the failure surface must be symmetric with respect to β, Jaeger's failure surface is composed of portions of two right circular cones, with their axes parallel to but displaced symmetrically from the $\bar{p}$ axis. Cross-sections of this surface, for constant $\bar{p}_f$ and for constant β, are shown in Figures 3.13 and 3.14.

For computer applications, it is convenient to solve Equation (3.39) for q_f in terms of β and $\bar{p}_f$. This is done by replotting part of Figure 3.13 in Figure 3.15.

Anisotropic Angle of Internal Friction

When the shear strength of a normally consolidated clay is expressed in terms of effective stress, the contribution of the cohesion term is generally small and often negligible. Therefore the consequences of anisotropic cohesion discussed above, while certainly of academic interest because they are expressable in closed form, may not be as significant in most practical problems as are the consequences of anisotropic friction.

LIVNEH AND SHKLARSKY (1964) discussed the problem of anisotropic friction in general terms, but did not arrive at a complete numerical solution. Also, their choice of orientation of the material axis is open to criticism, and therefore their approach will not be discussed further.

Let it be assumed that Equations (3.20) and (3.21) take the form

$$d = \bar{c} \cot \bar{\Phi} = \text{constant} \tag{3.42}$$

$$\tan \bar{\Phi} = A - B \cos 2\alpha \tag{3.43}$$

Upon expanding Equation (3.19), substituting Equations (3.42) and (3.43) and setting

$$\frac{q_f}{d + \bar{p}_f} = m \tag{3.44}$$

the result is

$$m \left\{ \sin 2\delta - \cos 2\delta \left[A - B \cos(2\delta - 2\beta) \right] \right\}$$

$$= A - B \cos(2\delta - 2\beta) \tag{3.45}$$

However, the transcendental equation for δ obtained by differentiating Equation (3.45) with respect to δ, setting

$$\left(\frac{dm}{d\delta} \right)_{\beta, \bar{p}_f} = 0$$

and then eliminating m between the resulting expression and Equation (3.45) does not appear to be easily solved in closed form. Therefore a new general numerical method, capable of handling any arbitrary variation of $\bar{c}$ and $\bar{\Phi}$

with α will be used. This new method is described in the next section, and an example solution for a particular case of anisotropic friction is then presented.

New General Method for Anisotropic Shear Strength Analysis

In 1935 Casagrande developed a graphical method for anisotropic shear strength analysis, which proceeds as follows:

1. Assume $\bar{\sigma}_{3f}$ to be fixed.
2. Assume a trial value of $\bar{\sigma}_{1f}$, and draw a tentative Mohr stress circle at failure, corresponding to $\bar{\sigma}_{3f}$ and $\bar{\sigma}_{1f}$.
3. Above and below the tentative Mohr stress circle at failure construct a plot of shear strength VERSUS normal stress.
4. Repeat Steps 2 and 3 to find the smallest value of $\bar{\sigma}_1$ for which the Mohr stress circle is tangent to at least one strength curve. When this happens, the orientation of the failure plane is determined by the point of tangency on the Mohr stress circle.

Casagrande's method requires a new set of strength curves for each new trial Mohr stress circle. The new

method, believed to be presented here for the first time, requires only one strength curve, of a slightly different kind from that used by Casagrande.

Referring to Figure 3.9, assume β and $\bar{p}_f$ to be fixed. Then α and δ are uniquely related by the condition

$$\delta = \beta + \alpha \tag{3.46}$$

Call line AC an α strength line and line BC a δ stress ray. Then do the following.

1. Draw α strength lines for several value of α, say $\alpha = 0^o$, 15^o, 20^o, 25^o, 30^o, 35^o, 40^o, 45^o, 50^o, 55^o, 60^o, 65^o, 70^o, 75^o, 90^o.
2. Draw δ stress rays for $\delta = 0^o$ to 90^o at 5^o intervals.
3. Draw a smooth curve through the points of intersection of corresponding strength lines and stress rays, taking account of Equation (3.46). Call this the strength curve. The strength curve is a polar plot of Equation (3.19), with 2δ as the polar angle.
4. Draw the smaller of two circles, with center at B, which are tangent to the strength curve. (The larger circle has no physical significance.)

5. The radius of the above circle is $q_f(\beta,\bar{p}_f)$ and the orientation of the failure plane is determined by the point of tangency on the Mohr stress circle.

In order to construct a plot of q_f VERSUS β for a fixed $\bar{p}_f$, it is suggested that one set of α strength lines be drawn, then a new set of δ stress rays be drawn on tracing paper for each desired value of β.

It is obvious that the above graphical method has a numerical counterpart, suitable for tabular or machine calculation. Details of such a procedure will not be discussed.

Figure 3.16 shows the essential features of a graphical shear strength analysis for a clay possessing anisotropic friction. The assumed frictional variation is

$$\tan \bar{\Phi} = \left(\frac{\tan \bar{\Phi}_{MAX} + \tan \bar{\Phi}_{MIN}}{2}\right) - \left(\frac{\tan \bar{\Phi}_{MAX} - \tan \bar{\Phi}_{MIN}}{2}\right) \cos 2\alpha$$

where

$$\bar{\Phi}_{MIN} = 24.0^{\circ}$$

$$\bar{\Phi}_{MAX} = 36.0^{\circ}$$

The above expression results in the following values of tan $\bar{\Phi}$ and $\bar{\Phi}$:

α DEG.	tan $\bar{\Phi}$	$\bar{\Phi}$ DEG.
0	0.445	24.0
15	0.464	24.9
20	0.478	25.6
25	0.495	26.4
30	0.515	27.3
35	0.537	28.3
40	0.561	29.3
45	0.585	30.4
50	0.609	31.4
55	0.633	32.4
60	0.655	33.2
65	0.675	34.0
70	0.692	34.7
75	0.706	35.2
90	0.725	36.0

Several features of Figures 3.16(c) and 3.16(d) are of interest.

1. m does not appear to be stationary at $\beta = 0^{\circ}$.
2. The variation of m with β is far less than that of tan $\bar{\Phi}$ with α.

3. The reason for Feature 2 is that the material always fails along the plane of least resistance, as shown by Figure 3.16(d). The maximum strength of the material is never utilized, because $|\alpha| < 57^{\circ}$ for all values of β.

4. The least value of m occurs when α is 0°, i.e. when $\beta = 57^{\circ}$.

5. If triaxial tests were conducted on samples of this material with $\beta = 0^{\circ}$, 45° and 90°, and the orientation of the failure plane were ignored, the measured friction angles,

$$\bar{\varphi} = \sin^{-1} m$$

would be as follows:

$$\bar{\varphi}_0 = 33.0^{\circ}$$

$$\bar{\varphi}_{45} = 24.8^{\circ}$$

$$\bar{\varphi}_{90} = 27.2^{\circ}$$

6. The variation of m (or q_f) with β depicted in a plot such as Figure 3.16(c) is not, by itself, a good indication of the IN-SITU variation of q_f with β. This is because the influence of pore pressure response is not reflected.

Experimental Determination of $\bar{c}(\alpha)$ and $\bar{\Phi}(\alpha)$

Figure 3.16(d) shows that it may be impossible to cause failure to occur on a plane for which the angle α exceeds a certain maximum value, in the triaxial test. In order to cause failure to occur on a predetermined plane, some kinematic constraints may have to be introduced, such as exist in the direct shear test. A suggested program for measuring and checking $\bar{c}(\alpha)$ and $\bar{\Phi}(\alpha)$ in the laboratory is as follows.

1. Determine $\bar{c}(\alpha)$ and $\bar{\Phi}(\alpha)$ by means of direct shear tests, assuming the inherent cross anisotropy to be preserved (which may well be an incorrect assumption).
2. Using the variation of $\bar{c}(\alpha)$ and $\bar{\Phi}(\alpha)$ obtained from direct shear tests, predict the variation of q_f with β and $\bar{p}_f$, by means of the general graphical (or numerical) procedure described previously.
3. Check the predicted variation of q_f with β and $\bar{p}_f$ by means of isotropically consolidated triaxial tests, again assuming the inherent cross anisotropy to be preserved.

SOVERI AND HYYPÄ (1967) report having run both test series suggested above on a Finnish varved clay, but do not mention any attempt to correlate the results. It is interesting to note that their data indicate the clay to be anisotropic with respect to cohesion, but isotropic with respect to friction. The values of cohesion reported are shown below.

α DEG	COHESION KG/CM^2
0	0.15
50(?)	0.17
90	0.20

The reported cohesion does increase with the angle α, which is consistent with the previous assumption to that effect, but the friction angle reported is only 6^{o}.

Discussion of Test Data

It has already been stated that there are three possible causes of undrained shear strength anisotropy:

1. anisotropy with respect to the effective stress shear strength parameters in the Revised Coulomb Equation,
2. anisotropy with respect to pore pressure response, and
3. the q_o effect.

The purpose of this section is to present data to substantiate the claim that many clays do exhibit anisotropic undrained shear strength behavior, and to examine in detail what little data exist on shear strength anisotropy in terms of effective stress.

Excluded from this discussion are the vane shear test and the simple shear test. The vane shear test is excluded because:

1. The material axis does not remain in the plane of the maximum and minimum principal stress axes.
2. Failure is forced to occur on a plane on which failure will generally not occur in a triaxial shear test.

3. The state of stress at failure is uncertain.

The simple shear test is excluded because:

1. The state of stress at failure is uncertain.
2. The state of stress in the sample cannot possibly be homogeneous, and therefore progressive failure must play a major role in mobilization of total sample strength. Thus, the soil stress - strain relations are needed to interpret simple shear test strength data, but they are generally unknown. Incremental plastic stress - strain relations presently require knowledge of a yield function, but very little is known about yield functions appropriate for real soils; J.G. MERKLE (1966; 1968a; 1968b); CHRISTIAN (1966).

The fact that clays are composed chiefly of plate-shaped mineral particles has been known for a long time; TERZAGHI (1925; 1960; 47); GRIM (1953, Ch. 2). The hypothesis that the compressibility and elastic rebound of soils are controlled by the percentage of scale - like particles was advanced by TERZAGHI (1927, 42) and thoroughly investigated at M.I.T. by GILBOY (1928).

By the early 1930's foundation engineers had begun to expect that the compressibility of clays might depend on the direction of the applied loading. MARSTON (1932) inquired of Casagrande whether he had found a difference in the compressibility of Laurentian clay when the major principal stress in an oedometer test was applied parallel, rather than normal to the bedding plane. CASAGRANDE (1932) replied that he had attempted to investigate this question, but that samples trimmed with the angle β equal to 90^{o} always broke along planes of stratification and could not be tested. In the same paper Casagrande also discussed the influence of fine layers of cohesionless soil on the compression characteristics of a varved clay. Two years later he presented a more detailed discussion of the lateral restraint provided by thin layers of sand or silt; CASAGRANDE (1934).

The possibility that stratification in clays might lead to anisotropic stress - strain properties was studied experimentally at about the same time by Mason, working under Casagrande at Harvard University and by Hvorslev, working under Terzaghi at the Technical University of Vienna. MASON (1936; 1939; 1940) was concerned primarily with anisotropic deformation characteristics, while

HVORSLEV(1936; 1937; 1938; 1960) was concerned primarily with shear strength. Mason conducted model footing tests and unconfined compression tests, both normal and parallel to the planes of stratification of an undisturbed clay, and found the clay to be stiffer in the horizontal than in the vertical direction. However, he did not publish the numerical results of these tests; see pp. 232-235 of his 1940 paper.

In his 1936 paper, Hvorslev called attention to "the influence of the stratification, arising from a definite orientation of the flaky mineral particles during the re-consolidation process of a remoulded soil". He then explained that, "To investigate a possible variation of the friction and cohesion with respect to the direction of the planes of stratification, simple unconfined compression tests were made on test specimens with various angles between the axis or direction of the compressive force and the planes of stratification. However, on account of undeterminable changes in the capillary pressure during the tests it was not possible to arrive at definite conclusions in regard to the variations of friction and cohesion." In his 1938 paper he stated that in addition to investigating whether the true angle of internal friction, determined from

direct shear tests, is in agreement with the angle of internal friction obtained by means of simple unconfined compression tests and measurements of the angle of inclination of the plane of failure, "...it should be determined if the direction of the principal orientation of the flaky particles in the clay has any influence on the friction and cohesion." To this end Hvorslev reconsolidated large samples of remolded Vienna and Little Belt clays one-dimensionally in a shear box, to a vertical effective stress of 5.0 kg./cm^2. Unconfined compression test specimens with dimensions 2 cm. by 2 cm. by 4 cm. were trimmed from the reconsolidated blocks, with β values of 0^o, 45^o and 90^o. Partial drying during sample preparation raised the equivalent vertical consolidation stress, σ_e, to about 6.0 kg./cm^2. The actual equivalent vertical consolidation stress for each specimen was determined from its measured water content after the unconfined compression test. Results of Hvorslev's tests are tabulated in Table 3.1 and plotted in Figure 3.17.

In order to present test data from the literature in parallel form, the anisotropic strength ratio, R, will be defined as

$$R = \frac{q_f(\beta)}{[q_f(\beta)]_{MAX}} \tag{3.47}$$

The symbols R_u and R_p will be used to denote anisotropic strength ratios for undrained loading and constant $\bar{p}_f$, respectively.

Each figure in Table 3.1 is the average result of the three tests in best agreement out of four. The ratio of horizontal ($\beta = 90^o$) to vertical ($\beta = 0^o$) strengths for the two clays exhibited opposite tendencies. Hvorslev was not able to offer a conclusive explanation for these results, but there is a good possibility that the mechanism primarily responsible was pore pressure response. However, he did clearly recognize the basic causes of undrained shear strength anisotropy. In his 1936 paper, he observed that, "...the compressive strength depends on the value of the coefficient of internal friction, the cohesion, and the capillary pressure. During the test the capillary pressure decreases, but in the case of anisotropic materials this decrease may vary with the angle between the direction of the compressive force and the planes of stratification." Obviously, Hvorslev fully

appreciated the desirability of obtaining pore pressure measurements in tests aimed at studying shear strength anisotropy. Again in 1938 he stated, "The compressive strength q is a function of the friction and cohesion in the plane of failure and of the capillary pressure p_k," and once again in 1960 he stated, "The variations in compressive strength may be caused in part by differences in cohesion and friction parameters and in part by differences in pore-water pressures developed during tests on the three types of specimens." Any of these statements can be viewed as the philosophical foundation of this thesis. In 1960 he also observed, "Difference in friction and cohesion parameters for the test specimens ... cannot be definitely determined by means of the abovementioned theories, since the influence of anisotropy on changes in pore - water pressures is not considered in these theories and was not determined during the tests." He concluded by stating that, "Much more detailed investigations of the influence of orientation of clay particles and of anisotropy in general are needed. Triaxial tests should be performed on specimens with horizontal,

inclined, vertical, and random orientation of the clay particles. The deformation characteristics, inclination of failure planes, pore - water pressures, strength, and the effective cohesion and friction parameters should be determined for each type of orientation of the clay particles."

By 1948, the technique of conducting undrained triaxial compression tests with pore pressure measurements was well known, even if not completely perfected; RENDULIC (1937), TAYLOR (1948), LAMBE (1951, Ch. XIII). However, it was some time before the first triaxial tests with pore pressure measurements were conducted on an anisotropic clay, for the purpose of separating the effects of anisotropic effective stress shear strength parameters and anisotropic pore pressure response. Unconfined compression tests remained popular as a means of demonstrating the existence of anisotropy, but there was little progress made toward investigating its basic causes. Perhaps this was partly because the concept of pore pressure parameters was still new, and not universally accepted, due to their basically empirical nature.

BISHOP (1948) reported results of a series of unconfined compression tests on London Clay, which was to serve

as the foundation for a large earth dam to retain Walton Reservoir No. 1 in the Thames Valley. Preliminary stability analyses disclosed that an important slope failure mode was one in which the failure surface consited largely of a horizontal plane in the overconsolidated London Clay. Consequently the undrained shear strength associated with failure along a horizontal ($\alpha = 0^{o}$) plane was of interest. Since samples near the top of the clay bed exhibited unconfined compressive strengths as low as 10-20 p.s.i., it was proposed to construct the dam slowly, in order to take advantage of the increase in undrained shear strength caused by consolidation under the partial weight of the earth embankment. Both vertical and inclined samples, 4 inches in diameter and 1.25 inches in thickness, were therefore consolidated one-dimensionally in a large oedometer under vertical effective stresses of 1.5 and 3 tons per square foot, and standard 3 inch by 1.5 inch diameter unconfined compression test specimens were then built up of three layers cut from the fully consolidated samples. For the vertical samples, the average value of δ was 56^{o}. The inclined samples were taken (presumably with $\beta \approx 60^{o}$, but this is not stated)

in an effort to cause failure along a horizontal plane in the unconfined compression test. No average value of δ was given for the inclined samples, but the ratio of inclined strength to vertical strength was reported as

$$\frac{\text{inclined strength}(\beta \approx 60^{\circ})}{\text{vertical strength}(\beta = 0^{\circ})} = 0.72$$

Varved clays have provided an incentive for several investigations of shear strength anisotropy. Doubts as to whether unconfined compression tests are suitable for determining the shear strength of varved clays were raised by TSCHEBOTARIOFF (1943), and in reply by TERZAGHI (1943). In order to investigate the matter further TSCHEBOTARIOFF AND BAYLISS (1948) performed unconfined compression tests on tube samples of a plastic glacial varved clay, some of which were obtained and trimmed with a value of β as high as 35° (see their Figure 5, p. 205). However, the authors apparently took no special notice of the value of β, or of any relationship between unconfined compressive strength and β. They were primarily concerned with the influence of the type of sampler on the degree of disturbance, as reflected by the entire stress - strain curve, and with

whether the failure plane intersected rather than followed the planes of stratification. The first failure mode was generally observed.

On September 29, 1950 a huge landslide occurred in varved clay at Surte, Sweden, about 15 kilometers north of Gothenburg on the Gota River. The results of an extensive post-slide geological and soils investigation, performed by the Swedish Geotechnical Institute, are contained in a report by JAKOBSON (1952). In most landslides the slip surface is difficult to locate, being covered by earth masses. However, in this particular instance the slip surface was laid bare in the upper part of the slide area; see Figures 9 and 49 of JAKOBSON (1952), and also Figure 11 of JAKOBSON (1955). A similar situation resulted from the First Avenue Slide in Anchorage, Alaska which occurred during the 1964 Good Friday Earthquake; FISHER AND MERKLE (1965, Figs. 114 to 117). In the case of the Surte landslide a number of superficial samples were taken from the exposed convex slip surface in the upper part of the slide area, simply by driving open brass tubes (such as those used as liners in the piston sampler employed at other locations) into the ground at right angles to the

slip surface. When stored in the air and allowed to dry, the samples clearly showed that the planes of stratification had been parallel to the slip surface; see Figure 40 of JAKOBSON (1952). In an attempt to explain why this was so, three additional series of superficial samples were taken: one series with the angle β equal to 0°, the second with the angle β equal to 45°, and the third with the angle β equal to 90°. The undrained shear strength of the samples was determined by both the unconfined compression test and the cone test; BJERRUM AND FLODIN (1960, 7). The test results are tabulated in Table 3.2 and plotted in Figure 3.18. Although the shear strengths for β equal to 0° and 90° showed opposite trends in the two tests, the differences were slight and of the same general magnitude as the standard deviation. The shear strength for β equal to 45° was, however, consistently the lowest of the three values.

An attempt was made to determine the Hvorslev shear strength parameters for each of the three values of β, by means of drained direct shear tests. However, variations in void ratio within individual samples made the determinations impossible. Jakobson's proposed method of calculating

the Hvorslev parameters is also open to question, since it employed an assumed linear relation between true cohesion and void ratio. In effect Jakobson was attempting to solve for four independent variables, using only three equations.

Following his investigation of the Surte landslide, Jakobson became interested in whether homogeneous sedimentary clays are anisotropic because of the tendency of the clay platelets to achieve parallel orientation; JAKOBSON (1955). He therefore performed three series of unconfined compression tests on a homogeneous post glacial clay obtained from a slope at the Sala brickyard, about 75 miles northwest of Stockholm. The same three values of the angle β were used for the three test series as had been used for the Surte varved clay, viz. 0°, 45° and 90°. The samples were taken at a depth of 3 meters below ground surface, in a line and about 0.4 meters apart, with every third sample having the same value of β. Results of the unconfined compression tests are tabulated in Table 3.3 and plotted in Figure 3.19. Because each of the above means lies within one standard deviation of each of the other two, Jakobson did not feel the data conclusively showed

the Sala clay to be anisotropic, hence the title of the paper, "Isotropy of Clays." The scatter, he felt, was due to inhomogeneity. This paper also contains measurements of permeability and one-dimensional compressibility, in both the vertical and horizontal directions, for a clay from Enkoping, and of permeability in both directions for a clay from Vasby. The Enkoping clay was also investigated extensively by Jakobson in the course of a study of sampling effects, in which the q_o effect was discussed.

Shortly after Jakobson's 1955 paper appeared, W.J. Eden published a study of the engineering properties of a varved glacial lake clay from Steep Rock, Ontario; EDEN (1955). See also MILLIGAN, SODERMAN AND RUTKA (1962) and LAMBE AND WHITMAN (1969, Table 7.5, p.79) for discussion of and additional references to publications on Canadian varved clays. Steep Rock Lake is located in Ontario, Canada, about 130 miles north of Duluth, Minnesota. The lake was drained in 1943-44 by means of a large pumping operation, in order to permit iron ore to be removed by open pit methods by Steep Rock Iron Mines Limited. As the dewatering progressed, serious movements of the exposed soil occurred, which led to detailed geological and soils investigations, some of which are discussed by Eden.

The thickest deposits encountered in the vicinity of Steep Rock Lake are the well laminated varved silts and clays of glacio-lacustrine origin, characterized by their regular bedding. They vary in thickness from a few feet to at least 200 feet. This is the material discussed by Eden, as well as in a previous paper by LEGGET AND BARTLEY (1953), and in a subsequent paper by LEGGET (1958). One of the many interesting features of the Steep Rock varved clay is that the material does not exhibit "light and dark" bands until dried. This same feature is also characteristic of varved clay in Hartford, Connecticut; LANE (1963, 148). However, the most unusual and troublesome feature of the Steep Rock clay is its sensitivity; LEGGET AND BARTLEY (1953, 526), TERZAGHI (1944). The clay was difficult to excavate with a drag line bucket, difficult to shake out of the bucket, but once dropped (and thereby thoroughly remolded) it flowed easily. The same transformation occurred throughout large masses of the clay above points of initially small slides, thus triggering widespread "mud runs." It was the mud runs that led to the detailed soils investigations described in the above

references. Samples were obtained and laboratory tests begun at both the Mine and the University of Toronto. At first the significance of the varves was not apparent and all the early tests were therefore conducted on composite samples, cut indiscriminately through several varves. It was the results of these early tests which revealed the great extent of the varves, and which led to a more sophisticated test program. As the soil investigation progressed, the method of obtaining soil samples also progressed, from the use of a split tube sampler at the bottom of a cased hole sunk by wash boring, to the careful extraction of block samples. Block samples were shipped to laboratories in the United States and Great Britain as well as in Canada.

Early index tests on composite samples revealed that the liquidity index varied randomly with depth about an average value of 150%, which would account for the material's sensitivity. Engineers at the Mine quickly learned that it was desirable to minimize the disturbance suffered by the clay in its natural state. This basic principle had been stated previously by CASAGRANDE (1932).

Early soil tests were aimed at obtaining satisfactory answers to immediately pressing practical engineering problems, such as the design of stable slopes and berms which would permit the open pit mining operation to proceed safely. As these practical problems were solved, attention turned to some of the more fundamental properties of the varved material, such as the difference in particle gradation and Atterberg limits between light and dark layers, then to variations of soil properties within individual layers and finally to shear strength anisotropy of composite specimens. The results of unconfined compression tests on specimens trimmed at various values of the angle β from two block samples are tabulated in Table 3.4 and plotted in Figure 3.20. The difference in the two variations may, as suggested by Eden, be attributable to the relative thicknesses of dark and light varves. The dark layers were about twice as thick as the light layers in Sample 2-62 (Figure 3.20a), whereas the reverse was true for Sample 2-68 (Figure 3.20b) Eden ran direct shear tests on separate samples of dark and light material, but did not report values of effective stress shear strength parameters for either. However, if the Steep Rock clay is similar to the

varved clay at Huntsville, Ontario, it possesses little or no cohesion in either layer, with a considerably higher angle of internal friction in the light layer; MILLIGAN, SODERMAN AND RUTKA (1962, 40).

About this time tunnel construction for subway and water supply purposes was going on in the heavily over-consolidated and highly laminated London clay. The British Building Research Station and Imperial College of the University of London took the opportunity to perform extensive and intensive studies of the engineering properties of London clay. WARD (1957) reported a series of unconsolidated undrained triaxial tests on specimens trimmed from block samples, with values of the angle β equal to 0^{o} and 90^{o}. The stress-strain curves for specimens from Site L, using a confining pressure of 50 p.s.i., showed the following results:

β	Average Unconfined Compression Strength	R_u	Average Strain at Failure
DEG	PSI		%
0	160	0.76	3.50
90	210	1.00	2.75

Some of the tests were not quite carried to failure, because the principal interest was in the soil-structure interaction problem at low strains. Ward's data showed that the strain corresponding to any given stress can be 100% greater for a specimen trimmed from a tube sample than for one trimmed from a block sample with the same value of β. This influence of sample disturbance on strains measured in a laboratory triaxial test is one of at least two reasons why the stress path method is so difficult to apply reliably in engineering practice. The other reason is the difficulty in determining what stresses should be applied to the sample to simulate IN-SITU conditions; MERKLE (1969),LAMBE (1969). See also CASBARIAN (1964, 41).

The effect of sample disturbance on strains measured in unconsolidated undrained triaxial tests on London clay is even more apparent in data published in a subsequent paper by WARD, SAMUELS AND BUTLER (1959). The authors identified three principal structural features of London clay:

1. laminations,
2. fissures, and
3. "backs", which are surfaces of bedding discontinuity, presumably caused by tectonic movement, rather than by the same tensile stresses which cause fissures.

The London clay is described as possessing "orthotropy with one axis of symmetry", which is synonymous with the terms "transverse isotropy" and "cross - anisotropy" used throughout this thesis. Shear strength data for all tests in which the angle β was recorded or can be inferred are tabulated in Table 3.5, and average values are plotted in Figure 3.21. Because of interest in the structure - medium interaction problem at low strains, all specimens were subjected to cyclic loading prior to failure, using a maximum stress value of about 40% of the unconfined compression strength.* There appears to be no systematic variation of the shear strength ratio, R_u, with depth below ground level, natural water content or any of the Atterberg limits. However, extensive fissuring appears to

---

*Specimens for sites A and H were not subjected to cyclic loading, but neither were the values of β recorded.

significantly lower the ratio, e.g. at site G. On the basis of the data shown in Table 3.5b, Ward et.al. concluded that, except for site G, $\frac{q_f(90)}{q_f(0)} \approx 1.3 \pm 0.1$. The total number of tests in which the angle β was measured was 150. Four of these tests were run with the angle β equal to 60^o, and produced failure surfaces approximately parallel to the planes of lamination. No tests were reported in which the angle β was 45^o. DUNCAN AND SEED (1966a, 53) have suggested that the difference between the value of the ratio $\frac{q_f(60)}{q_f(0)}$ reported by Ward, et. al. from that reported by SKEMPTON (1948) may be due to variation in the ratio of horizontal effective to vertical effective stress with depth, as discussed by SKEMPTON (1961). This may well be true, but the occurrence of numerous fissures and "backs" also suggests that some horizontal strain has occurred in the London clay as a result of tectonic movement, so that the ratio of horizontal effective to vertical effective stress IN-SITU has not been determined under K_o conditions at all locations.

Ward et.al. conclude that opening of laminations caused by disturbance during sampling is unlikely to have much effect on shear strength unless the angle α is small,

in which case the shear strength could be appreciably reduced. However, the decrease in shear strength due to overall sample disturbance is unmistakable. In effect, Ward et.al. have shown that the structure of the soil prior to shear does influence undrained shear strength, i.e. the influence of pre-shear structure is not entirely obliterated by the time failure occurs. The question is, how does the pre-shear structure make its influence felt? Available evidence, although sparce, suggests that the principal influence of pre-shear structure is through pore pressure response, rather than through the effective stress shear strength parameters. At any rate, the concept of inherent anisotropy does have a logical basis.

At about the same time, papers on shear strength anisotropy in rocks began to appear in the literature of geology and rock mechanics. WILLIAMS (1958) discussed two possible causes of oblique slip faulting, in which the direction of relative movement does not coincide with either the dip or strike directions of the fault plane. Such faults are common in the southwestern part of the Midland Valley of Scotland. The two explanations for

oblique slip faulting which he advanced were shear strength anisotropy, i.e. preferred planes of failure created by previous faulting, and rotation of principal stessses.

BOTT (1959) reviewed the two mechanisms of oblique slip faulting proposed by Williams, and then investigated theoretically the influence of preferred planes of fracture of arbitrary orientation. He obtained an expression for the first direction of slip within the failure plane, under the influence of an arbitrary stress system. Although this paper contains no test data, the results are of fundamental importance for a clear understanding of both shear strength and the general nature of stress.

Bott reasoned that if slip occured in a preferred plane of fracture, the direction of initial movement would be that of the shear stress vector acting on the failure plane. He therefore set out to calculate the direction of the shear stress vector acting on a plane having an arbitrary orientation with respect to the principal stress axes. Using the notation of Figure 3.22, Bott's results can be summarized as follows.

If

$\sigma_1, \sigma_2, \sigma_3$ = principal stresses

$\alpha_{n1}, \alpha_{n2}, \alpha_{n3}$ = direction cosines of the unit normal to plane ABC, with respect to the principal stress axes

$T_s = \bar{\sigma} \cdot \bar{s}$ = strike component of the shear stress vector acting on plane ABC

$T_d = \bar{\sigma} \cdot \bar{d}$ = dip component of the shear stress vector acting on plane ABC

then

$$T_s = \frac{\alpha_{n1}\,\alpha_{n3}}{\sqrt{1 - \alpha_{n2}^2}} \quad (\sigma_1 - \sigma_3) \tag{3.48}$$

$$T_d = \frac{\alpha_{n2}}{\sqrt{1 - \alpha_{n2}^2}} \quad \left[\alpha_{n2}^2(\sigma_2 - \sigma_3) - \alpha_{n1}^2(\sigma_1 - \sigma_2)\right] \tag{3.49}$$

$$\frac{T_d}{T_s} = \tan \psi$$

$$= \frac{\alpha_{n2}}{2\alpha_{n1}\,\alpha_{n3}} \left[(\alpha_{n3}^2 - \alpha_{n1}^2) + (\alpha_{n3}^2 + \alpha_{n1}^2) \left(\frac{2\sigma_2 - \sigma_1 - \sigma_3}{\sigma_1 - \sigma_3} \right) \right]$$

(3.50)

Notice from Equation (3.48) that the angle ψ will lie in quadrants 1 or 4 provided $\sigma_1 \geq \sigma_3$. The direction of the unit vector $\bar{s}$ in Figure 3.22 has been taken opposite to that assumed by Bott, in order to be consistent with other results derived in Appendix B for the octahedral plane. The expression for the orientation of the octahedral shear stress vector derived in Appendix B can be obtained from the above equations by setting

$$\alpha_{n1} = \alpha_{n2} = \alpha_{n3} = \frac{1}{\sqrt{3}}$$

Bott thus showed that by unrestricted variation of the relative values of the three principal stresses, assuming that the directions of the principal stress axes remain fixed, the direction of maximum shearing stress within a

preferred plane of fracture can be made to lie in any direction, provided the plane is not normal to a principal stress axis. He then related an angle θ, which is equal to $\pi - \psi$, to the tectonic stress regimes defined by HARLAND AND BAYLY (1958).

JAEGER (1959) conducted triaxial tests on rock cylinders with artificial joints, to measure the coefficient of friction for sliding along a preferred plane of fracture as a function of the angle δ. The value of the angle β for his specimens was probably 0° but was not reported. Model joints were cut with a diamond saw, with values of the angle δ at 5° intervals between 25° and 65°. Three joint types were tested:

1. a layer of patching plaster about 1 millimeter thick,
2. bare sawed surfaces, lightly ground and flat to better than 0.05 millimeter, and
3. previous, reasonably flat natural shear surfaces.

Variation of the angles of internal friction for all joint types and all values of the angle δ was between about 22° and 41°, but no clear trend was evident. Because of

scatter of the test results and curvature of the shear strength lines, Jaeger could not determine cohesion values. As a matter of interest, Jaeger made extensive use of the maximum shear stress loci in this paper, and developed an expression for the shear strength in a single plane of weakness similar to Equation (3.19). The maximum shear stress loci had previously been used in the treatment of shear strength of geologic materials by ANDERSON (1951).

A year later JAEGER (1960) published results concerning anisotropic cohesion, the theoretical aspects of which have already been examined earlier in this Chapter. In this paper Jaeger also presented results of unconfined compression tests on slate cylinders, cut with values of the angle β between 0° and 60°. The test results are tabulated in Table 3.6 and plotted in Figure 3.23. The most distinctive feature of this data is the strong anisotropy, reflected by an 90% decrease in unconfined compressive strength as the angle β increases from 0° to 90°. This is much stronger anisotropy than reported for any of 14 anisotropic rocks, including Pennsylvania slate, by OBERT AND DUVALL (1967, Table 15.7.1).

In the same year DONATH AND COHEN (1960) presented preliminary results for triaxial compression tests on several rocks, including the Longwood shale from Highland Mills, New York, which indicated that anisotropy had no appreciable effect on shear fracture for values of the angle β less than 60°. For values of the angle β less than 60° the angle δ was very nearly constant and equal to 60°, increasing to about 70° as the angle β varied between 60° and 90°.

The following year, however, DONATH (1961) presented triaxial compression data for the foliated Martinsburg slate from Bangor, Pennsylvania, which showed a marked variation in compressive strength with the angle β, in addition to a general increase in compressive strength with confining pressure. The slope, μ^*, and intercept, τ_o^*, of the Mohr envelope, for values of the angle β at 15° degree intervals, and confining pressures between 35 and 350 bars, are tabulated in Table 3.7(a). However, despite the fact that Donath referred to μ^* and τ_o^* as the "coefficient of internal friction" and "cohesive resistance," they are not the Mohr-Coulomb shear strength parameters. In addition, the data for values of the angle β greater than 60° must be considered suspect, due to the probability

of end restraint. End restraint must be suspected whenever tan δ approaches or exceeds the specimen height to diameter ratio, which in this case was 2.5 inches/1.0 inch. Had Donath's data allowed him to construct curves of α VERSUS β for each of the confining pressures employed, it would have been possible for him to calculate the Mohr - Coulomb shear strength parameters as functions of failure plane orientation. Apparently scatter prevented such an approach. The values of δ_{AVG} and α_{AVG} in Table 3.7 have been scaled from a curve drawn by eye through Donath's plotted data points, and are not intended as a statement that the relation between the angles α and β is independent of confining pressure.

DONATH (1964) reviewed his data for Martinsburg slate, and supplemented it with the results of additional traixial tests on 0.5 inch diameter by 1.0 inch length specimens at confining pressures of 500, 1000 and 2000 bars. Specimen size did not appear to influence test results. However, at confining pressures of 1000 and 2000 bars, failure tended to be by plastic flow in a restricted zone (ductile faulting), rather than by brittle fracture, and the Mohr envelopes exhibited substantial curvature. These two phenomena,

i.e. plastic flow and nonlinearity of the Mohr envelope could well be related. The data are tabulated in Table 3.7(b) and plotted in Figure 3.24. Figure 3.24 completely defines the three-dimensional failure surface shown in Figure 3.11.

CASBARIAN (1964, 3) intended to study the effect of rotation of the principal stress axes and variation of the intermediate principal stress on the shear strength of a remolded kaolinite, and to exclude the effects of anisotropy. In fact, however, because his hollow cylinder test specimens were isotropically consolidated, he actually excluded the q_o effect. Furthermore, he could not exclude the effects of anisotropy. At present there is also some concern about the degree of homogeneity of stresses in hollow cylindrical soil test specimens, and so the following data must be viewed with caution.

The soil used in Casbarian's investigation was a commercial kaolinite clay, mined in Bath, South Carolina, and having the following index properties:

Liquid Limit	57%
Plastic Limit	32%
Plasticity Index	25%
Clay Fraction (<0.002mm)	41%

Activity	0.61
Specific Gravity of Solids	2.69

This clay has essentially the same activity as Weald clay; LAMBE AND WHITMAN (1969, 34). The clay powder was mixed with tap water by a mechanical mixer to a water content of 48-49%, then stored in a steel container and covered by a plastic sheet, with water poured on top to prevent evaporation. The hollow cylindrical test specimens were formed in a humid room by hand tamping the clay into a mold, using a 0.75 inch diameter rod. The test specimens were 10 inches high, with an outside diameter of 5 inches and a wall thickness of 1 inch. Thus the tamper was 3/4 the thickness of the cylinder wall being molded. The resulting particle structure was probably dispersed (i.e. particles oriented parallel to one another), but whether the orientation was predominatly vertical or horizontal is not clear.

All samples were initially isotropically and normally consolidated. Test letter designations indicated the consolidation pressure, as shown below

TEST LETTER DESIGNATION	CONSOLIDATION PRESSURE
	PSI
A	7.0
B	25.0
C	70.0

Three series of tests were run, reflecting the influence of two variables on shear strength:

β, the angle between the major principal stress axis at failure and the vertical (designated α by Casbarian*)

N, the intermediate principal stress ratio, equal to $\frac{\sigma_2 - \sigma_3}{\sigma_1 - \sigma_3}$

*It is not clear what Casbarian meant by the term rotation of principal stress axes. Although he intended to exclude consideration of inherent anisotropy, he may have intended to study developed anisotropy. The ambiguity arises because when the angle β exceeded 45°, Casbarian reported it as $\beta - 90^{\circ}$ in one place and β in another, using the same symbol, α, for both values.

The intermediate principal stress ratio, N, which BISHOP (1966) denoted by the symbol b, and HABIB (1953) denoted by the symbol λ, is related to Lode's parameter μ, which is used throughout this thesis, by the relation

$$N = b = \lambda = \frac{\mu + 1}{2}$$

The radial stress σ_{rr} was always equal to the intermediate principal stress. As shown in Figure 3.25, when the vertical normal stress σ_{zz} exceeded the tangential normal stress $\sigma_{\theta\theta}$ the test was called a compression test. When $\sigma_{\theta\theta}$ exceeded σ_{zz} the test was called an extension test. Rotation of the major and minor principal stress axes in the tangential plane was induced by applying a torque to the sample. Table 3.8(a) shows the values of β and N corresponding to each test.

In Series I the value of N was held constant, equal to 0.5 ($\sigma_2 = \frac{\sigma_1 + \sigma_3}{2}$), while the angle β was varied between 0^o and 90^o. In Series II N was supposed to be the only variable, but Table 3.8(a) shows that the angle β varied also. In Series III both the angle β and the parameter N were varied intentionally. Only the results of Series I are of interest here, because variation in undrained shear

strength with the angle β could only have resulted from anisotropy. The Series I data are tabulated in Tables 3.8(b) and (c), and plotted in Figures 3.26 and 3.27. The symmetry of the relationship between q_f and the angle β at constant $\bar{p}_f$ is remarkable, almost to the point of being incredulous. However, if the test procedure was as Casbarian described it, then there is little doubt that those values of the angle β which he reported as being greater than 45° were not actually equal to the complement of the reported values. In place of the smooth curves in Figures 3.26(a) through (e) Casbarian drew straight lines, the slopes of which he interpreted as sin $\bar{\Phi}$. Thus he constructed a symmetrical relation

$$\bar{\Phi} = \bar{\Phi}(\beta) = \Phi(90^\circ - \beta)$$

Such a relation is not in agreement with any theoretical treatment of inherent shear strength anisotropy of which the Author is aware, and is certainly not in agreement with the concept of inherent anisotropy upon which this thesis is based. Moreover, since Casbarian was apparently unable to measure the orientation of a distinct failure surface,

it is not possible to use his data to construct the actual relationship between the effective stress shear strength parameters and failure plane orientation.

An alternative interpretation of Casbarian's data is that his samples were inherently isotropic prior to shear, and the variation of undrained shear strength with the angle of rotation of the major principal stress axis during shear was due entirely to developed anisotropy, i.e. to particle reorientation during shear. If this were true, then his compression and extension tests were in fact duplicates of one another, and the fact that they yielded essentially identical results should be extremely gratifying. One would then plot shear strength against the change in the angle β during shear (i.e. $|\beta_f - \beta_o|$), rather than against the angle β itself, and the previous suspicious symmetry would vanish, since one half of each curve in Figure 3.27 would be superimposed on the other. In addition, N would then have been the only variable in Series II. However, this interpretation leads to an inconsistency. The value of $|\beta_f - \beta_o|$ for tests to which Casbarian assigned a value of 45^o to β is actually zero, because no rotation of the principal stress axes took place during these tests.

Therefore, according to the above argument, the results of these tests should have coincided with those for simple compression and simple extension (without any applied torque), when in fact Figure 3.27 shows they were at opposite extremes. It seems probable, therefore, that although Casbarian's material may have developed some additional anisotropy as a result of shearing strain and rotation of principal stress axes, it also possessed considerable inherent anisotropy prior to shear, as a result of the compaction procedure used to form the test specimens. See also LADD AND VARALLYAY (1965, 56).

GIBSON AND MORGENSTERN (1962) calculated the factor of safety of slopes in which the undrained shear strength of the soil is independent of the orientation of the failure plane at any depth, is zero at the top of the slope, and varies linearly with depth beneath the top of the slope.

Their investigation was extended by KENNEY (1963), in a discussion of which SCHMERTMANN (1964) suggested that slope stability calculations be further refined by considering the variation of undrained shear strength at a

point with failure plane orientation. Schmertmann suggested a type of undrained shear strength anisotropy in which undrained shear strength is proportional to the effective normal stress acting on the failure plane prior to shear, and plotted values of an anisotropic slope stability correction factor based on this assumption. When the coefficient of earth pressure at rest equals unity, Schmertmann's correction factor reduces to unity, thus verifying the fact that Schmertmann's hypothetical undrained shear strength variation is related to the q_o effect, and is not the result of true anisotropy with respect to either the effective stress shear strength parameters or pore pressure response. In his closure, Kenney made several remarks concerning undrained shear strength anisotropy:

1. Anisotropic behavior of soil is seldom considered in undrained stability analyses, because estimating average undrained shear strength by means of simple tests (unconfined compression, cone, vane) and using this strength in a static stability analysis appears to yield results which check well with field experience.

2. Undrained shear strength is a behavior, not a property, which can be influenced by stress environment and testing method.

3. Soils exhibit not only anisotropic strength characteristics, but also anisotropic general stress - strain behavior.

4. It would be unwise to begin making corrections to measured shear strengths to account for anisotropy, if the only basis for such corrections were theoretical. An integrated program of theoretical and experimental studies is required to assess the importance of anisotropy in soil mechanics practice.

LO (1965a) extended the above slope stability calculations by considering variation of undrained shear strength with the angle β (which he denoted by the symbol i). Although his approach was general enough to accommodate any arbitrary variation of shear strength with the angle β, he concentrated on variations in which the largest and smallest strengths result when the angle β is either 0° or 90°. The assumption that the undrained shear strength attains its limiting values when the angle β is 0° and 90° was based on the results of

more than 500 unconfined compression tests on 2 inch Shelby tube samples, 3 inch piston samples, and 1½ inch diameter by 3 inch length specimens trimmed from block samples, of lightly overconsolidated (O.C.R. ≈ 2.0) glacio-lacustrine clays from the Welland Canal Tunnel site at Welland Ontario; LO (1965a) LO AND MILLIGAN (1967). To obtain the block samples a 5 foot diameter shaft was sunk to a depth of 77 feet, and 1 foot cube block samples were extracted at every 4 foot interval of depth. Some of the samples were homogeneous and some stratified, as shown in the tabulation below.

BLOCK	DESCRIPTION		DEPTH
	HOMOGENEOUS	STRATIFIED	FT.
A	X		30
B	X		34
C	X		38
D	X		42
E	X		46
F		X	51
G	X		55
H	X		60
I	X		65
K		X	74

Variation of undrained shear strength with the angle β for blocks D, H, F and K is tabulated in Tables 3.9 and 3.10 and plotted in Figures 3.28 and 3.29. For all block samples tested, the value of $R_u(90)$ ranged between 0.64 and 0.80, i.e.

$$0.64 \leq \quad R_u(90) = \frac{q_f(90)}{q_f(0)} \quad \leq 0.80$$

Variation of the angle α with the angle β is also tabulated in Tables 3.9 and 3.10 and plotted in Figures 3.28 and 3.29. From this data, Lo concluded that the angle δ is approximately constant and equal to 56°. This fact indicates that the clay may be isotropic with respect to the effective stress shear strength parameters, so that the anisotropy of undrained shear strength is due entirely to anisotropic pore pressure response.

Lo proposed a variation of undrained shear strength with the angle β which can be written in the form

$$R_u(\beta) = \frac{1 + R_u(90)}{2} + \frac{1 - R_u(90)}{2} \cos 2\beta$$

To test the validity of the above proposal he constructed a polar plot of R_u VERSUS β for blocks A, B, C, D, E, G, H, and I, i.e. for all the homogeneous block samples. His data are tabulated in Table 3.11 and plotted in Figure 3.30. Differences between values for blocks D and H in Tables 3.9(b) and 3.11 could be explained if it were known that values in Table 3.11 were read off smooth curves, rather than being averages of raw data, as are the values in Tables 3.9 and 3.10. An important feature of Lo's proposed Mohr-circle type strength variation is that it predicts R_u to be stationary when the angle β is 0° and 90°, whereas most published data do not exhibit this feature. In fact, Lo's own data do not exhibit this feature either, as shown in Figure 3.30 and also in Figure 3.31, where an attempt has been made to construct a Mohr circle using the data from Table 3.11. Although departure of the measured curve from a circle is everywhere less than 10 percent, the shape of the measured curve does not suggest that a circle is necessarily the best form of approximation to test data.

In a discussion of the results of Lo's stability calculations MEYERHOF (1965) pointed out that Lo's results can be approximated by using the average of $q_f(0)$ and $q_f(90)$ in previously developed solutions for isotropic soils. He also pointed out that the orientation of the true failure surface in anisotropic material tends toward the direction of minimum strength, a factor which becomes increasingly important as the slope angle decreases.

In his discussion, SCHMERTMANN (1966) repeated Hvorslev's earlier request for investigations of shear strength anisotropy to be reported in terms of effective stresses, which means obtaining pore pressure measurements. He also noted that the material axis does not remain in the plane of the major and minor principal stress axes for the cylindrical portion of a vane failure surface, and reasoned that the influence of shear stress direction was probably reflected mainly in pore pressure response.

In his closure, LO (1966) supplied anisotropic shear strength data for block I in terms of effective stress. His stress - strain data are tabulated in Table 3.12 and plotted in Figure 3.32 in the form of effective stress

paths. Lo also gave data at failure, but they were not entirely consistent with his stress - strain data and therefore have been omitted. In three out of four cases, the stated strain at failure did not correspond to either maximum deviator stress or maximum obliquity. No criterion for failure was given. Lo found the excess pore pressure to be an unique function of the axial strain, for all values of the angle β. Figure 3.32 therefore has the property that strain contours are lines of constant $\bar{\sigma}_3$. Anisotropy of both stress - strain behavior and pore pressure response (in terms of applied total stress) is apparent. Why the excess pore pressure should be determined solely by the axial strain is a question which requires more study. See also LO (1965b).

HANNA(1967), in his discussion of LO AND MILLIGAN (1967), presented data from unconsolidated undrained triaxial tests on a homogeneous glacial lake clay near Sarnia, Ontario. The test specimens were trimmed from two 1 foot cube block samples, cut from the side of a deep excavation at a depth of about 40 feet. Values of the angle β were 0°, 45° and 90°. See also HANNA (1966). His data are tabulated in Table 3.13 and plotted in Figure 3.33. In

his discussion, Hanna observed that the influence of the q_o effect is not reflected by an isotropically consolidated laboratory shear test.

In their discussion of LO AND MILLIGAN (1967), SOVERI AND HYYPPA presented results of both direct shear tests and triaxial tests (presumably undrained) on a Finnish varved clay of Pleistocene (glacial) origin. Few details of the tests were given, and it appears that the results of the direct shear tests were reported in terms of total, rather than effective stress, because of the low reported friction angle.

α	c	Φ_T
DEG	KG/CM^2	DEG
0	0.15	6
45	0.17	6
90	0.20	6

Data from the triaxial tests are tabulated in Table 3.14 and plotted in Figure 3.34. This work was apparently accomplished in 1959; SOVERI AND HYYPPA (1959). The authors concluded that the problem of shear strength anisotropy "is more geological and mineralogical than mechanical or

mathematical and it must and can be solved in each country only by close collaboration between geologists and engineers."

Consolidated undrained triaxial tests with pore pressure measurements were conducted on homogeneous Black Cotton clay from India, and the results were described briefly by MATTHAI (1967) in his discussion of LO AND MILLIGAN (1967). The soil was reconsolidated from a slurry in the laboratory (presumably one-dimensionally), and triaxial samples were obtained by a sampling operation, using brass tubes 1 1/2 inches in diameter by 3 inches high, at values of the angle β of 0°, 45° and 90°. Data for samples normally consolidated (presumably isotropically) to 22.5 PSI are tabulated in Table 3.15 and plotted in Figure 3.35.

Following Hvorslev's advice, DUNCAN AND SEED (1965), under the sponsorship of the U.S. Army Engineer Waterways Experiment Station, set out to separate the contributions to undrained shear strength anisotropy, of anisotropy with respect to the effective stress shear strength parameters, anisotropy with respect to pore pressure response and the q_o effect.

To determine the cause of undrained shear strength anisotropy, they conducted both isotropically consolidated and unconsolidated triaxial tests on kaolinite samples which had previously been consolidated one-dimensionally from a slurry. Index properties of the commercial kaolinite, known as ASP-900, were

Liquid Limit	45.0%
Plastic Limit	34.8%
Plasticity Index	10.2%
Percent by Weight of Particles Smaller than 2 Microns	48.0%
Activity	0.212
Consolidation Coefficient	0.01 CM^2/SEC
Compression Index	0.33
Swelling Index	0.06

For a thorough discussion of the index properties of this material, see SEED, WOODWARD AND LUNDGREN (1964). The triaxial samples were prepared by first mixing dry kaolinite powder with deaired tap water, to form a slurry with a water content of 66.2 percent (liquidity index = 3.08). Three

batches of the slurry were then each consolidated one-dimensionally in a 6 inch diameter mold, under a maximum vertical effective stress of 1.5 KG/CM^2, to form cakes about 5 inches high. Next the three cakes were unloaded, removed from the molds, stacked one on top of the other, and the composite sample, measuring 6 inches in diameter and about 15 inches high, was then further consolidated anisotropically under a maximum vertical effective stress of 9.0 KG/CM^2 and a corresponding maximum horizontal effective stress of 5.5 KG/CM^2 (K_c = 0.611). The sample was then rebounded to an isotropic effective stress of 1.0 KG/CM^2, and finally completely unloaded at constant volume from this last isotropic stress state. The three original cakes were then separated, stored under controlled conditions, and from them triaxial specimens were subsequently trimmed with values of the angle β equal to 0° and 90° (for the consolidated undrained tests with pore pressure measurements), and 0°, 45°, and 90° (for the unconsolidated undrained tests). No explanation was given for not conducting consolidated undrained tests with pore pressure measurements on samples with the angle β equal to 45° when the need for such tests became apparent. Data from the unconsolidated undrained tests are tabulated in Table 3.16

and plotted in Figure 3.36. Notice that the slope of the $R_U(\beta)$ curve in Figure 3.36 is not zero at the ends. The cell pressure for these tests was 1.0 KG/CM^2.

Data for the consolidated undrained tests with pore pressure measurements are tabulated in Table 3.17 and plotted in Figure 3.37. Because the samples were not completely saturated when tested, these data may not be entirely accurate. They do, however, indicate three significant trends:

1. All samples exhibited overconsolidated behavior, as would be expected.
2. The effective stress strength line for vertical samples appears to be slightly higher than that for horizontal samples.
3. Excess pore pressures at failure were consistently higher (less negative) for horizontal than for vertical samples. The authors cite this as the most distinctive feature of the tests on ASP-900 kaolinite.

The results of four isotropically consolidated ($\bar{p}_o$ = 1.0 KG/CM^2) drained triaxial tests (with $\bar{\sigma}_3$ = constant = $\bar{p}_o$) gave

strength results consistent with Figure 3.37, but these four drained tests were too few, and the scatter in the undrained test results too great to permit a quantitative estimate of the variation in position of the effective stress strength lines with the angle β.

To study the influence of strain conditions on undrained shear strength anisotropy, Duncan and Seed ran consolidated undrained plane strain, unconsolidated undrained triaxial, and both isotropically and anisotropically consolidated undrained triaxial tests on undisturbed San Francisco Bay Mud from the University of California Field Test Site at Hamilton Air Force Base. Bay Mud is a marine clay deposited in drowned valleys and on drowned sedimentary flats in the San Francisco Bay area. For details concerning the engineering geology of that area, see TRASK AND ROLSTON (1951). At the Hamilton Air Force Base site, Bay Mud is a soft to very soft, grey, slightly organic silty marine clay with isolated silt lenses and a few roots and shells. It has a natural water content of about 90%, a sensitivity of about 8, and the pore water has an electrolyte concentration of about 17 grams per liter total dissolved solids taken as equivalent NaCl. The vertical

effective overburden pressure at the 15 to 25 foot depths from which samples were obtained varies from about 0.4 to 0.6 KG/CM^2, and at these depths the material is approximately normally consolidated. Index properties of Bay Mud which has not been allowed to dry are:

Liquid Limit	88.0%
Plastic Limit	43.0%
Plasticity Index	45.0%
Percent by Weight of Particles Finer than 2 Microns	60.0%
Activity	0.75
Consolidation Coefficient	2.0×10^{-4} CM^2/SEC
Compression Index	1.1
Swelling Index	0.028

Undisturbed samples for all tests were taken by hand sampling with a 5 inch diameter fixed - piston sampler. After transportation to the laboratory the sealed brass sample tubes were stored in a $68^{\circ}F$ humid room. As the material was needed for testing it was extruded from the tube, after which the tube was resealed. The outer 1/2 inch of soil was not used for strength or consolidation tests, due to the possibility of excessive disturbance.

Three types of plane strain tests were conducted, called vertical plane strain (VPS), horizontal plane strain (HPS) and vertical plane strain "perfect sampling" (VPS-UU) tests. In the VPS and VPS-UU tests the material axis coincided with the axial (vertical) direction of the plane strain device. In the HPS tests the material axis coincided with the short lateral (horizontal) direction of the plane strain device. The axial and the short lateral directions are the two directions in which controlled stresses could be applied to the specimen, the trimmed dimensions of which were:

axial dimension (height)	2.80 IN
long lateral dimension (width)	2.80 IN
short lateral dimension (thickness)	1.10 IN

Strain was prevented in the long lateral direction by end plates. The principal features of the three plane strain tests are summarized below:

TEST TYPE	MATERIAL AXIS	CONSOLIDATION $\bar{\sigma}_{1c}$	β_c DEG	FAILURE $\bar{\sigma}_{1f}$	β_f DEG
VPS	axial	axial	0	axial	0
HPS	lateral	lateral	0	axial	90
VPS-UU	axial	axial	0	axial	0

The results of the VPS and HPS plane strain tests are tabulated in Table 3.18 and plotted in Figure 3.38. The VPS and HPS tests were called "in-situ" tests by Duncan and Seed, because they were intended to simulate stress conditions at the head and toe, respectively, of a slope which fails under undrained conditions. The stress path for an HPS test passed through an isotropic (q = 0) point; the stress path for a VPS test did not. In a VPS test the value of q was increased continuously to failure. For comparison with the HPS tests, VPS-UU tests were conducted, differing from VPS tests only in that q was first decreased from q_c to zero, to simulate perfect sampling, then increased to failure. The VPS-UU test results are also shown in Table 3.18 and Figure 3.38. The difference between the HPS and VPS-UU test results is apparently due to characteristics of the plane strain device, as well as the angle β

at failure. The authors recognized that disagreement between K_c values for axial and laterial consolidation shed doubt on the assumption that strain normal to the material axis was completely prevented during consolidation.

Figure 3.38 yields the following parameters:

TEST TYPE	SLOPE OF K_c LINE	SLOPE OF K_f LINE
V	0.34	0.62
H	0.41	0.57

When interpreting the results of soil shear strength tests, it must be remembered that unless the material is proven isotropic with respect to the effective stress shear strength parameters, the slope of the K_f line is not necessarily equal to sin $\bar{\Phi}$. Failure points for both the VPS and VPS-UU tests ($\beta_f = 0^o$) appear to lie on the same line in Figue 3.38, while failure points for the HPS tests ($\beta_f = 90^o$) lie on another. Both failure lines appear to pass through the orgin. Although Figure 3.38 does not contain enough information to permit the determination of $\bar{\Phi}$ for any value of α, it did enable Duncan and Seed to

conclude that anisotropy with respect to $\bar{c}$ and $\bar{\Phi}$ is the least important of the three causes of undrained shear strength anisotropy for Bay Mud.

The results of 27 unconsolidated undrained triaxial tests on undisturbed samples of Bay Mud, trimmed with the angle β equal to 0°, 45°, 60° and 90° are tabulated in Table 3.19 and plotted in Figure 3.39. This data permits a direct comparison of the anisotropic undrained shear strength characteristics of Bay Mud with those of other soils.

As a means of comparing plane strain and triaxial test results, three types of consolidated undrained triaxial tests were conducted on undisturbed Bay Mud. The principal features of the three tests are summarized below.

TEST TYPE	MATERIAL AXIS	CONSOLIDATION $\bar{\sigma}_{1c}$	β_c DEG	FAILURE $\bar{\sigma}_{1f}$	β_f DEG
AC-U-1	vertical	vertical	0	vertical	0
AC-U-2	radial	radial	0	vertical	90
IC-U	vertical	isotropic	0	vertical	0

In test AC-U-1 an attempt was made to prevent radial strain during consolidation. In test AC-U-2 an attempt was made to prevent axial strain during consolidation. Test AC-U-2 was similar in some respects to tests designated $\overline{C(\frac{1}{K_o})URC}$ by LADD AND VARALLYAY (1965), except that the material axis was vertical in the $\overline{C(\frac{1}{K_o})URC}$ tests, so that β_c was equal to 90^o and β_f equal to 0^o. Ladd and Varallyay did not report any triaxial tests in which the angle β_f was equal to 90^o and $\bar{\sigma}_{2f}$ was equal to $\bar{\sigma}_{3f}$, and therefore discussion of their results is contained in Chapter 6, dealing with the influence of the intermediate principal stress. Data from the consolidated undrained triaxial tests are tabulated in Table 3.20 and plotted in Figure 3.40. All failure points appear to lie on the same straight line, but the data are too few to draw firm conclusions. The slope of the K_f line is 0.565, less than the slope of either K_f line obtained in the plane strain "in-situ" tests. The fact that consolidation conditions for the IC-U tests were not ideally isotropic was caused by some of the axial load being resisted by filter paper drains.

The principal observation made by Duncan and Seed was that undrained shear strength anisotropy in both the over-consolidated kaolinite and undisturbed Bay Mud which they

tested was due mainly to anisotropy with respect to excess pore pressure development. Both soils proved to be slightly anisotropic with respect to the effective stress shear strength parameters.

The sinking of a shaft 144 feet deep and 25 feet in diameter at Ashford Common, Middlesex by the London Metropolitan Water Board in 1961 afforded Imperial College of the University of London and the British Building Research Station a rare opportunity for an extensive study of the stress-strain and strength properties of the overconsolidated, fissured London clay; BISHOP, WEBB AND LEWIN (1965); WARD, MARSLAND AND SAMUELS (1965). Work at the Building Research Station was aimed primarily at obtaining a correlation between laboratory and IN-SITU measurements of undrained shear strength and deformation characteristics, and at explaining differences between field and laboratory water content measurements. Work at Imperial College centered around the measurement of effective stress - strain relationships.

The site of the Ashford Common shaft is adjacent to site A of WARD, SAMUELS AND BUTLER (1959). Strength data from this site do not appear in Table 3.5a because the value

of β was not reported by Ward et. al., but they can be found in the original paper. For a geological history of the London Clay in the Thames Valley, see SKEMPTON AND HENKEL (1957).

Average index properties of the London Clay at the Ashford Common site are

Liquid Limit	67%
Plastic Limit	27%
Plasticity Index	40%
Percent by Weight of Particles Finer than 2 Microns	54%
Activity	0.76
Consolidation Coefficient	1.0×10^{-4} CM^2/SEC
Compression Index	0.13
Swelling Index	0.03

Values of index properties at each of six levels at the Ashford Common site, as well as at Bradwell and Waterloo Bridge appear in Tables 1 and 2 of the paper by Bishop et. al. The average water content at Ashford Common is about 3 percent below the plastic limit.

Laboratory triaxial tests were performed at both Imperial College and the Building Research Station, on cylindrical specimens 1 1/2 inches in diameter by 3 inches high, trimmed from 1 foot cube block samples with the angle β equal to either 0° or 90°. Unfortunately lack of time prevented testing specimens with intermediate values of the angle β.

Both undrained and drained specimens exhibited a marked transition from brittle to plastic stress - strain behavior with increase in the value of the minor principal effective stress at failure. This brittle to plastic transition appears to be characteristic of many naturally - formed geologic materials, and has long been associated with rocks such as marble; NADAI (1950, Vol. I, Ch. 17).

Triaxial test data for vertical ($\beta = 0^{\circ}$) and horizontal ($\beta = 90^{\circ}$) samples from level E are tabulated in Tables 3.21 and 3.22 and plotted in Figures 3.41 and 3.42. Data pertinent to samples taken at level E are

depth below present ground level	114 Feet
estimated present vertical effective overburden stress	56 PSI
estimated present coefficient of lateral earth pressure at rest	2.1

Figures 3.41(a) and 3.41(b) show data for isotropically consolidated undrained and drained triaxial compression tests on vertical and horizontal samples, respectively, in which the average of the major and minor principal effective stresses at failure was less than 300 PSI. At these effective stresses the shear strength envelope shows distinct curvature, but there is no significant difference between the results of undrained and drained tests, or between the results of tests on vertical and horizontal samples. Figure 3.42 shows all test data for samples from level E for which the average of the major and minor principal effective stresses at failure fell between 300 and 1300 PSI. Again, there is no significant difference between the results for vertical and horizontal samples, although there appears to be a tendency for horizontal samples to give slightly higher strengths. The maximum past vertical effective stress at level E has been estimated to be about 800 PSI, which, assuming the value of K_o for normally consolidated London clay at that depth to be 0.70, yields a value of $\bar{p}_{MAX} = (800)\left(\frac{1 + 0.70}{2}\right) = 680$ PSI. If the strength line in Figure 3.42 has been drawn correctly, then intact London clay does not exhibit normally consolidated behavior until

the average of the maximum and minimum principal effective stresses at failure exceeds about 130% of the value which existed when the clay was under its estimated maximum past vertical effective stress.

If one interprets Figure 3.42 as indicating the shear strength of intact London clay from level E to be isotropic, in terms of effective stress, then the value of $\bar{\Phi}$ for the normally consolidated material is found to be 16^{o}, which agrees with the result obtained by SKEMPTON (1964) from direct shear tests employing very large displacements. The above data represent primarily the behavior of intact London clay, rather than that of large masses of the fissured clay IN-SITU.

It would be convenient for stability analyses if the variation of undrained shear strength with the angle β were constant throughout a soil mass. However, data from the paper by Ward et. al. show that such is not the case for London Clay at Ashford Common. Table 3.23 contains values of index properties at depths below ground level of 30, 50, 66, 91, 114 and 138 feet, and these values, together with the undrained shear strengths for vertical (V: $\beta = 0^{o}$), diagonal (D: $\beta = 45^{o}$) and horizontal (H: $\beta = 90^{o}$) specimens

are plotted in Figure 3.43. There does not appear to be any strong correlation between the variation of an index property and the variation of the directional strengths. The directional strength data have been tabulated in Table 3.24 and reploted in Figures 3.44 and 3.45.

The decision as to whether a clay exhibits shear strength anisotropy involves determining whether shear strength results for two different value of the angle β differ to a degree which is statistically significant. The decision is difficult to make on a completely rational basis, because rarely do we know what constitutes normal scatter in soil shear strength data. The answer to this question requires more samples of good quality than can generally be afforded. The data presented by Ward et. al. therefore present an unusual opportunity for a probabilistic analysis, which has been performed in Table 3.45 using standard methods; MERKLE (1959). The results are plotted in Figure 3.46. The key assumption in the analysis is that values of $q_u/q_{u,AVG}$ from each of the six levels belong to the sampe population. This assumption is certainly open to question, and therefore the results of the analysis should be interpreted primarily qualitatively. The cumulative distribution curve indicates that 27% of the

test results fell below 80% of the mean, and 19% fell above 120% of the mean. In other words, 46% of the test results differed from the mean by more than ±20%. Ward et. al. attributed the high degree of scatter in their results to the fissured nature of the clay. If this were the cause, one might expect the coefficient of variation to decrease with depth, due to the increase in spacing of fissures with depth. However, this is not the case, as shown below.

LEVEL	DEPTH FT	VARIATION COEFFICIENT
A	30	0.156
B	50	0.264
C	66	0.226
D	91	0.214
E	114	0.338
F	138	0.241
	AVERAGE	0.240

It was, in fact, only because the coefficient of variation shows no consistent trend with depth that it was considered perhaps justifiable to treat the data from all six depths as belonging to the same population.

Ward et. al. noted almost an order of magnitude difference between the secant moduli at $q_u/2$ of standard open-drive borehole and block samples, which would cause some uncertainty in a stress path settlement estimate, depending upon the sample type. Cored samples, however, give results close to those of block samples.

The above data on London clay have been summarized by BISHOP (1966), BISHOP AND LITTLE (1967), and SKEMPTON AND HUTCHINSON (1969), together with a few additional test results obtained by AGARWAL (1967) which are consistent with those obtained previously.

D'APPOLONIA (1968) used undrained shear strength as the criterion for change of element elastic properties in finite element analyses of deformation and progressive yield of saturated clay masses. The undrained shear strength was specified to vary with the angle β, based on results of unconsolidated undrained triaxial tests on both artificially resedimented and undisturbed Boston blue clay. Pore water pressures were measured in all 65 test specimens prior to shear, but in only 9 specimens during shear. The stress history of the UU triaxial samples is shown in Figure 3.47, in which the following stages are identified:

1 - one-dimensional consolidation to the maximum vertical effective stress $\bar{\sigma}_{vm}$.

2 - one-dimensional rebound to the vertical effective stress $\bar{\sigma}_{vc}$.

3 - release of anisotropic stresses without disturbance of soil structure (perfect sampling), resulting in the isotropic effective stress $\bar{\sigma}_{ps}$.

4 - disturbance of the soil structure, resulting in a decrease in capillary pore water tension and consequent decrease in isotropic effective stress to $\bar{\sigma}_{r}$.

5 - increase in isotropic effective stress, due to application of confining cell pressure required to dissolve entrapped air and produce a saturated sample, resulting in the preshear isotropic effective stress $\bar{\sigma}_{s}$.

6 - undrained shear, resulting in the undrained shear strength q_u.

Two overconsolidation ratios were defined, one at the end of one-dimensional rebound, equal to $\bar{\sigma}_{rm}/\bar{\sigma}_{rc} = (OCR)_c$, and the other immediately prior to undrained shear, equal to

$\bar{\sigma}_{vm}/\bar{\sigma}_s = (OCR)_s$. The latter value has been suggested by LADD AND LAMBE (1963) as a means of accounting for the effect of sample disturbance on the results of laboratory shear tests. The artificially resedimented specimens were trimmed from block samples 10 inches in diameter and presumably about 4 inches high, with values of the angle β of 0^o, 30^o, 45^o, 60^o and 90^o. The undisturbed specimens were trimmed from 5 inch diameter thin-walled tube samples, with values of the angle β of 0^o, 45^o and 90^o. Test specimens were 1.41 inches in diameter and 3 inches high, and although frequently referred to by D'Appolonia as unconfined compression specimens, the tests were not conducted as such but rather as unconsolidated undrained triaxial tests with positive cell pressure to insure a pore pressure response of unity. Data for the artificially resedimented samples are tabulated in Tables 3.26, 3.27, 3.28 and 3.29 and plotted in Figures 3.48, 3.49, 3.50 and 3.51. Data for the undisturbed samples are tabulated in Tables 3.30 and 3.31 and plotted in Figures 3.52 and 3.53. The Author prefers an arithemtic plot over a semilogarithmic plot, for relating undrained shear strength to preshear overconsolidation ratio, hence the form of Figures 3.48

and 3.52. Figue 3.51 shows that the artificially resedimented Boston blue clay was essentially isotropic in terms of effective stress, so that any undrained shear strength anisotropy must have been due to anisotropy with respect to pore pressure response. This result is consistent with earlier results obtained by Duncan and Seed and by Bishop et. al., and again underscores Hvorslev's early advice concerning the necessity of obtaining pore pressure measurements in studies of undrained shear strength anisotropy.

SUMMARY

The purpose of this chapter has been to examine the influence of anisotropy with respect to the effective stress shear strength parameters on undrained shear strength anisotropy.

The most important points which have been brought to light are the following:

1. Despite persistent advice from Hvorslev over a period of some 20 years, disappointingly few investigators have obtained pore pressure measurements during shear throughout studies of undrained shear strength anisotropy, and thus been able to report their

results in terms of effective stress. Thus, although the principal intent of this chapter was to examine anisotropy with respect to the effective stress strength parameters, it was not possible to do so, for two reasons:

a. The majority of investigators have not reported their data in terms of effective stress.

b. None of the data which have been reported in terms of effective stress is adequate to determine the variation of effective stress shear strength parameters with failure plane orientation. This is basically because no investigation of which the Author is aware has yet been specifically designed to do so.

2. An investigation designed specifically to measure the variation of effective stress shear strength parameters with failure plane orientation would materially add to existing knowledge of the shear strength behavior of clay. An approach by means of which this might be accomplished has been suggested.

3. Every investigator who has measured pore pressure in a significant number of tests has concluded that anisotropy with respect to pore pressure response is much more important than anisotropy with respect to the effective stress shear strength parameters in producing anisotropy of undrained shear strength.

4. An improved understanding of the fundamental relationship between a general set of applied total stress increments and the resulting excess pore water pressure should therefore be given a high, if not the highest priority in any future study of the shear strength behavior of saturated clay.

5. The three-dimensional failure surface, believed to be shown in Figure 3.11 for the first time, is essential to a clear understanding of undrained shear strength anisotropy. It will be demonstrated in Chapter 5 that the variation of undrained shear strength due to principal stress rotation is defined by the intersection of the above failure surface with a pore pressure surface which will be described in Chapter 4. A simple graphical technique will be

explained for constructing this intersecting curve, using contours of both surfaces.

Additional, more technical points which merit emphasis are as follows.

6. The predominant role played by pore pressure reponse in undrained shear strength anisotropy strengthens the effective stress strength hypothesis. As a matter of interest, there is no necessary conflict between the so-called rheological strength theories and effective stress strength theories, because it is quite possible to incorporate effective stress considerations into a general rheological theory.

7 The assumption that the horizontal plane is the weakest and any vertical plane the strongest leads to the conclusion that failure will never occur on a vertical plane in an unconstrained specimen. The fact that no investigator has reported the occurrence of failure on a vertical plane, even in the highly overconsolidated London clay, lends

support to the above assumed distribution of effective stress shear strength parameters with failure plane orientation.

8. Examination of the more than 30 plots of shear strength variation with principal stress rotation in this chapter shows that they have little in common, except that as the overconsolidation ratio increases the ratio of the strength of a horizontal specimen ($\beta = 90^{\circ}$) to that of a vertical specimen ($\beta = 0^{\circ}$) tends to increase. This appears to be mainly a pore pressure phenomenon. Shear strength is generally not stationary when the angle β is 0° or 90°, and the use of an ellipse to describe the variation of shear strength with principal stress rotation must be considered more a mathematical expedient than an accurate representation of physical behavior. A generally applicable method for describing the variation of shear strength with the angle β would be by a finite Fourier series.

9. When the effective stress shear strength parameters are minimum in a horizontal plane, the shear strength, expressed in terms of effective stress,

will be a minimum when the principal stress rotation is such as to cause failure to occur in a horizontal plane.

10. A general method has been devised, and presented here for the first time, for predicting directly the shear strength and failure plane orientation in a cross anisotropic soil for any desired orientation of the principal stresses, provided:

    a. The intermediate principal stress axis remains perpendicular to the axis of cross-anistropic symmetry, and

    b. The effective stress shear strength parameters increase steadily with increase in the angle between the normal to the failure plane and the axis of cross-anisotropic symmetry. The method accommodates any arbitrary variation of effective stress shear strength parameters, both cohesion and/or friction, subject only to the above restrictions. The method was developed independently by the Author, and does not require a shear strength calculation for any principal stress orientation other than the one desired; c.f. BAKER AND KRIZEK (1970).

11. Soils and artificial graphite appear to have some similar stress-strain characteristics. Both exhibit cross-anisotropy, and both undergo appreciable plastic volume changes.

12. A concise summary has been presented of early theoretical works on shear strength anisotropy by Casagrande and Carrillo, and Hank and McCarty, and the analytical results of both have been shown to be included in more recent work by Jaeger. The results of all three papers have been simplified to the point where they can easily be used for hand or machine calculation. Casagrande and Carrillo's assumptions regarding shear strength variation have been precisely defined.

13. Recent work in the field of geology, not discussed above, has shown that the effective stress shear strength parameters may vary with direction in any given plane; UFF AND NASH (1967).

14. The effect of kinematic restraints is to increase the effective stress shear strength parameters in certain planes.

15. There is no reason why the variation of undrained shear strength with principal stress rotation, obtained from laboratory unconsolidated or isotropically consolidated undrained triaxial tests, should be a good representation of the same behavior IN-SITU, for at least two reasons:

    a. Sample disturbance alters the pore pressure response characteristics of the material.

    b. The influence of the q_o effect is not reflected in any unconsolidated or isotropically consolidated test.

16. The slope and intercept of a plot of $1/2(\bar{\sigma}_1 - \bar{\sigma}_3)$ VERSUS $1/2(\bar{\sigma}_1 + \bar{\sigma}_3)$ at failure are not sufficient, by themselves, to calculate the effective stress shear strength parameters, $\bar{c}$ and $\bar{\Phi}$, unless the material is proven to possess isotropic shear strength characteristics in terms of effective stress. The intercept and slope of such a plot, for an anisotropic material, are sometimes called apparent effective stress shear strength parameters, to indicate that they are not associated with a single failure plane, but rather with a single principal stress orientation.

17. If one takes the Axiomatic Approach and assumes the variation of effective stress shear strength parameters with failure plane orientation, the fact that the parameters defining such variation can be numerically evaluated from test data does not necessarily verify the assumed variation, unless the effective stress shear strength parameters have been measured directly. For example, fitting an hyperbola to plotted points of $1/2(\bar{\sigma}_1 - \bar{\sigma}_3)$ VERSUS $1/2(\bar{\sigma}_1 + \bar{\sigma}_3)$ at failure may enable one to calculate the parameters defining the variation of cohesion assumed by Jaeger. However, this does not, by itself, verify that the material actually obeys Jaeger's hypothesis. On the other hand it may still enable one to make extremely useful predictions, in the same manner as one might make useful predictions of the load-deformation behavior of a nonlinear soil mass by using linear elastic equations and a carefully chosen secant modulus, appropriate to a particular range of loading; see, e.g. D'APPOLONIA (1968).

TABLE 3.1

ANISOTROPIC STRENGTH DATA FROM UNCONFINED COMPRESSION TESTS ON VIENNA AND LITTLE BELT CLAYS

CLAY	β DEG	δ DEG	α DEG	$2q_f/\bar{\sigma}_e$ -	R_u -
Vienna IX	0	(51)	51	0.48	1.00
"	45	53	8	0.44	0.92
"	90	54	-36	0.42	0.88
Little Belt III	0	(47)	47	0.38	0.83
"	45	50	5	0.41	0.89
"	90	(48)	-42	0.46	1.00

Values in parentheses could not be determined accurately; HVORSLEV (1938, E-14).

$\bar{\sigma}_e$ is the equivalent vertical consolidation stress, as defined by Hvorslev, corresponding to the water content at failure.

Data from HVORSLEV (1960).

TABLE 3.2(a)

ANISOTROPIC STRENGTH DATA FROM UNCONFINED COMPRESSION AND SWEDISH CONE TESTS ON VARVED CLAY FROM SURTE, SWEDEN

SAMPLE NUMBER	UNIT WEIGHT T/M^2	β DEG	SHEAR STRENGTH* UNC. COMP. KG/CM^2	SHEAR STRENGTH* CONE KG/CM^2
2649**	1.60	0	0.164	0.145
2443	1.63	0	0.223	0.305
2303	1.63	0	0.211	0.255
3433	1.62	0	0.244	0.345
980	1.63	0	0.219	0.310
3777**	1.63	0	0.164	0.335***
3275	1.63	0	0.234	0.385
2924	1.61	45	0.220	0.320
1978	1.64	45	0.194	0.295
19	1.61	45	0.194	0.255
2480	1.63	45	-	0.320
974	1.63	45	0.179	0.280
259	1.65	45	0.165	0.335
1123	1.64	45	0.164	0.375
3472	1.61	90	0.225	0.310
1863	1.64	90	0.208	0.280
3463	1.62	90	0.228	0.325
1755	1.68	90	0.224	0.335

Continued

TABLE 3.2(a)

ANISOTROPIC STRENGTH DATA FROM UNCONFINED COMPRESSION AND SWEDISH CONE TESTS ON VARVED CLAY FROM SURTE, SWEDEN

SAMPLE NUMBER	UNIT WEIGHT T/M^2	β DEG	SHEAR STRENGTH* UNC. COMP. KG/CM^2	CONE KG/CM^2
2788	1.66	90	0.200	0.310
1028	1.64	90	0.196	0.345
1447	1.67	90	0.196	0.395

Data from JAKOBSON (1952).

* shear strength = $\frac{1}{2}(\sigma_{1f} - \sigma_{3f}) = q_f$

** excluded in calculating average shear strength

*** disturbed

TABLE 3.2(b)

ANISOTROPIC STRENGTH DATA FROM UNCONFINED COMPRESSION AND SWEDISH CONE TESTS ON VARVED CLAY FROM SURTE, SWEDEN

β	TEST	q_f, KG/CM^2		R_u
		MEAN	STD. DEV.	
0	UNC.COMP.	0.226	0.012	1.00
45	"	0.186	0.019	0.82
90	"	0.211	0.013	0.93
0	CONE	0.320	0.043	0.97
45	"	0.311	0.036	0.95
90	"	0.329	0.033	1.00

Data from JAKOBSON (1952).

TABLE 3.3

ANISOTROPIC STRENGTH DATA FROM UNCONFINED COMPRESSION TESTS ON HOMOGENEOUS POST GLACIAL CLAY FROM SALA, SWEDEN

$\beta = 0^\circ$		$\beta = 45^\circ$		$\beta = 90^\circ$	
SAMPLE NUMBER	SHEAR STRENGTH KG/CM^2	SAMPLE NUMBER	SHEAR STRENGTH KG/CM^2	SAMPLE NUMBER	SHEAR STRENGTH KG/CM^2
5515	0.259	4343	0.256	5512	0.218
5542	0.225	5544	0.221	5528	0.255
5556	0.183	5561	0.207	5529	0.227
5557	0.218	5574	0.245	5530	0.209
5572	0.184	5575	0.249	5531	0.265
5759*	0.187	5629	0.273	5532	0.225
5676	0.229	5630	0.261	5533	0.191
5689	0.251	5675	0.260	5546	0.240
5690	0.202	5677	0.263	5560	0.262
5792*	0.294	5691	0.242	5661	0.267
5704	0.208	5721	0.166		
5719	0.243	5543*	0.301		

*These numbers may be misprints in the original paper, since the remaining sample numbers appear in ascending numerical order.

Continued TABLE 3.3

ANISOTROPIC STRENGTH DATA FROM UNCONFINED COMPRESSION TESTS ON HOMOGENEOUS POST GLACIAL CLAY FROM SALA, SWEDEN

β	q_f, KG/CM^2		R_u
	MEAN	STD. DEV.	
0	0.224	0.033	0.92
45	0.245*	0.034	1.00
90	0.236	0.025	0.96

*shown as 0.254 in the original paper

Data from JAKOBSON (1955)

TABLE 3.4

ANISOTROPIC STRENGTH DATA FROM UNCONFINED COMPRESSION TESTS ON VARVED CLAY FROM STEEP ROCK LAKE, ONTARIO

SAMPLE	β	$2\,q_f$	R_u
	DEG	PSI	
2-62	0	19.0	0.85
	10	18.0	0.80
	20	16.7	0.75
	30	14.7	0.66
	40	11.0	0.49
	45	9.6	0.43
	50	9.5	0.42
	60	10.0	0.45
	70	16.2	0.72
	80	20.7	0.92
	90	22.4	1.00
2-68	0	12.3	1.00
	10	12.0	0.98
	20	11.8	0.96
	30	11.7	0.95
	40	11.6	0.94
	45	11.3	0.92
	50	10.6	0.86
	60	9.1	0.74
	70	8.1	0.66
	80	7.3	0.59
	90	6.8	0.55

Data from EDEN (1955)

TABLE 3.5(a)

ANISOTROPIC STRENGTH DATA FROM UNCONSOLIDATED UNDRAINED TRIAXIAL TESTS ON OVERCONSOLIDATED LONDON CLAY

SITE	β	NO. OF TESTS	DEPTH BELOW G.L.	σ_c	q_f	R_u	ϵ_f	δ
	DEG		FT.	PSI	TSF		%	DEG
L	0	11	73	50	5.02	0.74	3.1	57
	90	8		50	6.75	1.00	2.5	58
K1	0	9	64	50	5.76	0.79	3.1	59
	60	4		50	5.70	0.78	1.7	60
	90	8		50	7.34	1.00	2.0	61
K2	0	11	58	50	4.18	0.78	3.1	59
	90	7		50	5.38	1.00	2.0	62
G*	0	10	84	75	3.16	1.00	2.5	59
	90	8		75	2.99	0.95	2.3	59
B1 & B3	0	8	100	50	2.16	0.87	4.4	56
	90	6		50	2.48	1.00	2.8	54
B2	0	9	100	50	2.54	0.72	4.2	50
	90	4		50	3.54	1.00	2.6	60

Continued

TABLE 3.5(a)

ANISOTROPIC STRENGTH DATA FROM UNCONSOLIDATED UNDRAINED TRIAXIAL TESTS ON OVERCONSOLIDATED LONDON CLAY

SITE	β	NO. OF TESTS	DEPTH BELOW G.L.	σ_c	q_f	R_u	ϵ_f	δ
	DEG		FT.	PSI	TSF		%	DEG
P	0	13	160	110	9.95	1.00	1.5	55
O	0	17	55	45	3.23	0.75	2.8	50
	90	9		45	4.33	1.00	2.9	50
T	0	5	137	100	6.35	0.81	1.6	55
	90	3		100	7.85	1.00	1.3	62

*The clay at this site was very fissured.

Data from WARD, SAMUELS AND BUTLER (1959)

TABLE 3.5(b)

ANISOTROPIC STRENGTH DATA FROM UNCONSOLIDATED UNDRAINED TRIAXIAL TESTS ON OVERCONSOLIDATED LONDON CLAY

β	$(R_u)^*_{AVG}$
DEG	
0	0.78
60	0.78
90	1.00

*Sites G and P excluded

Data from WARD, SAMUELS AND BUTLER (1959)

TABLE 3.6

ANISOTROPIC STRENGTH DATA FROM UNCONFINED COMPRESSION TESTS ON SLATE

β DEG	R	β DEG	δ DEG	α DEG
0	1.029	0	61.0	61.0
0	0.971	0	63.0	63.0
15	0.741	15	61.0	46.0
15	0.659	15	61.5	46.5
30	0.535	30	56.0	26.0
30	0.499	30	62.0	32.0
40	0.430	40	61.5	21.5
40	0.351	40	69.0	29.0
45	0.385	45	60.5	15.5
45	0.370	45	64.0	19.0
50	0.342	50	61.0	11.0
50	0.288	50	62.5	12.5
60	0.242	60	69.0	9.0
60	0.197			

Data from JAEGER (1960)

TABLE 3.7(a)

ANISOTROPIC STRENGTH DATA FROM TRIAXIAL COMPRESSION TESTS ON MARTINSBURG SLATE

β	δ_{AVG}	α_{AVG}	μ^{*}(2)	τ_o^{*}(2)
DEG	DEG	DEG		BARS(3)
0	60	60	0.622	630
15	40	25	0.538	420
30	43	13	0.530	240
45	49	4	0.512	120
60	60	0	0.534	40
75(1)	75	0	0.445	150
90(1)	90	0	0.820	300

(1) These data are of questionable reliability, owing to the possible restraining effect of the test device.

(2) The parameters μ^{*} and τ_o^{*} are the slope and intercept of the Mohr envelope. They are not necessarily equal to the Mohr - Coulomb shear strength parameters.

(3) 1 bar equals 14.5 PSI or 1.02 KG/CM^2

Data from DONATH (1961)

TABLE 3.7(b)

ANISOTROPIC STRENGTH DATA FROM TRIAXIAL COMPRESSION TESTS ON MARTINSBURG SLATE

$\bar{p}_f$	β	q_f	R_p
KBARS	DEG	KBARS	
1.0	0	0.98	1.00
	15	0.80	0.82
	30	0.64	0.65
	45	0.51	0.52
	60	0.41	0.42
	75	0.56	0.57
	90	0.87	0.89
2.0	0	1.62	1.00
	15	1.38	0.85
	30	1.07	0.66
	45	0.88	0.54
	60	0.77	0.48
	75	0.97	0.60
	90	1.50	0.93
3.0	0	2.22	1.00
	15	1.86	0.84
	30	1.43	0.64
	45	1.14	0.51
	60	1.05	0.47
	75	1.32	0.59
	90	2.08	0.94

Data from DONATH (1964)

TABLE 3.8(a)

STRESS SYSTEM PARAMETERS AT FAILURE IN $\overline{\text{CIU}}$ HOLLOW CYLINDER TESTS ON COMMERCIAL KAOLINITE

TEST SERIES	TEST NUMBER	TEST LETTER	N	β DEG
I	1	A,B,C	0.500	0
	2	A	0.500	19.0
		B	0.500	23.0
		C	0.500	17.0
	3	A	0.500	30.0
		B	0.500	32.5
		C	0.500	29.5
	4	A,B,C	0.500	45
	5	A	0.500	61.0
		B	0.500	57.0
		C	0.500	61.0
	6	A	0.500	70.0
		B	0.500	71.0
		C	0.500	73.0
	7	A,B,C	0.500	90
II	21	A,B,C	0	0
	22	A	0.254	0
		B	0.210	0
		C	0.250	0
	24	A	0.730	90
		B	0.735	90
		C	0.680	90
	25	A,B,C	1	90

Continued

TABLE 3.8(a)

STRESS SYSTEM PARAMETERS AT FAILURE IN $\overline{\text{CIU}}$ HOLLOW CYLINDER TESTS ON COMMERCIAL KAOLINITE

TEST SERIES	TEST NUMBER	TEST LETTER	N	β DEG
III	32	A	0.240	29.0
		B	0.190	17.0
		C	0.153	23.0
	34	A	0.833	70.0
		B	0.725	58.0
		C	0.900	74.0

Total number of tests: 39

Data from CASBARIAN (1964)

TABLE 3.8(b)

ANISOTROPIC STRENGTH DATA FROM $\overline{\text{CIU}}$ HOLLOW CYLINER TESTS ON COMMERCIAL KAOLINITE

$\bar{\sigma}_c$	TEST	β	$\bar{p}_f$	q_f
PSI		DEG	PSI	PSI
7.0	A(1)	0.0	5.30	4.10
	A(2)	19.0	5.50	3.95
	A(3)	30.0	5.00	3.25
	A(4)	45.0	4.94	3.10
	A(5)	61.0	4.80	3.40
	A(6)	70.0	4.25	4.25
	A(7)	90.0	5.00	3.90
25.0	B(1)	0.0	18.20	12.80
	B(2)	23.0	18.10	11.50
	B(3)	32.5	18.30	9.50
	B(4)	45.0	16.40	10.00
	B(5)	57.0	17.20	9.60
	B(6)	71.0	16.90	10.15
	B(7)	90.0	17.50	12.00
70.0	C(1)	0.0	50.00	31.00
	C(2)	17.0	48.40	27.30
	C(3)	29.5	46.50	24.00
	C(4)	45.0	44.80	20.50
	C(5)	61.0	44.30	23.10
	C(6)	73.0	44.60	26.40
	C(7)	90.0	48.00	30.70

Data from CASBARIAN (1964)

TABLE 3.8(c)

ANISOTROPIC STRENGTH DATA FROM $\overline{\text{CIU}}$ HOLLOW CYLINDER TESTS ON COMMERCIAL KAOLINITE

$\bar{p}_f$	β	$\bar{q}_f$	R_p
PSI	DEG	PSI	
10	0	8.4	1.00
	20	6.8	0.81
	30	6.3	0.75
	45	6.3	0.75
	60	6.3	0.75
	70	6.8	0.81
	90	8.4	1.00
20	0	14.0	1.00
	20	12.7	0.91
	30	11.6	0.83
	45	11.3	0.81
	60	11.6	0.83
	70	12.7	0.91
	90	14.0	1.00
30	0	20.0	1.00
	20	18.3	0.92
	30	16.4	0.82
	45	15.4	0.77
	60	16.4	0.82
	70	18.3	0.92
	90	20.0	1.00

Continued

TABLE 3.8(c)

ANISOTROPIC STRENGTH DATA FROM $\overline{CIU}$ HOLLOW CYLINER TESTS ON COMMERCIAL KAOLINITE

$\bar{p}_f$ PSI	β DEG	$\bar{q}_f$ PSI	R_p
40	0	25.8	1.00
	20	23.7	0.92
	30	20.7	0.80
	45	19.0	0.74
	60	20.7	0.80
	70	23.7	0.92
	90	25.8	1.00
50	0	31.5	1.00
	20	29.0	0.92
	30	24.9	0.79
	45	22.1	0.70
	60	24.9	0.79
	70	29.0	0.92
	90	31.5	1.00

Data from CASBARIAN (1964)

TABLE 3.9(a)

ANISOTROPIC STRENGTH DATA FROM UNCONFINED COMPRESSION TESTS ON HOMOGENEOUS CLAY FROM WELLAND, ONTARIO

BLOCK	β DEG	q_f PSF	BLOCK	β DEG	q_f PSF
D	0	1300	D	60	1050
		1390			1090
		1530			1120
		1570			1170
		1650			1230
	15	1380			1280
		1410		75	1010
	30	1040			1060
		1230		90	1010
		1300			1110
		1390			1150
		1420			1220
		1470			1300
		1540			
	45	1110			
		1160			
		1220			
		1250			
		1290			
		1370			
		1450			

Continued

TABLE 3.9(a)

ANISOTROPIC STRENGTH DATA FROM UNCONFINED COMPRESSION TESTS ON HOMOGENEOUS CLAY FROM WELLAND, ONTARIO

BLOCK	β DEG	q_f PSF
H	0	1595
		1840
	15	1665
		1870
	30	1655
	45	1455
		1605
	60	1370
	75	1350
		1405
	90	1350
		1380

Data from LO(1965a) and LO and MILLIGAN(1967).

TABLE 3.9(b)

ANISOTROPIC STRENGTH DATA FROM UNCONFINED COMPRESSION TESTS ON HOMOGENEOUS CLAY FROM WELLAND, ONTARIO

BLOCK	β	$q_{f,AVG}$	R_u
	DEG	PSF	
D	0	1488	1.00
	15	1395	0.94
	30	1341	0.90
	45	1264	0.85
	60	1156	0.78
	75	1035	0.69
	90	1158	0.78
H	0	1718	0.97
	15	1768	1.00
	30	1655	0.94
	45	1530	0.87
	60	1370	0.78
	75	1378	0.78
	90	1365	0.77

Data from LO(1965a) and LO and MILLIGAN(1967).

TABLE 3.9(c)

ANISOTROPIC STRENGTH DATA FROM UNCONFINED COMPRESSION TESTS ON HOMOGENEOUS CLAY FROM WELLAND, ONTARIO

BLOCK	β DEG	δ DEG	α DEG
D	0	53	53
		55	55
		60	60
	15	60	45
	30	58	28
	45	54	9
		60	15
	60	53	- 7
	75	56	-19
		61	-14
	90	55	-35
		55	-35
		56	-34
		58	-32
H	0	51	51
		64	64
	15	57	42
	30	59	29
	45	48	3
		53	8
	60	51	- 9
		58	- 2

Continued

TABLE 3.9(c)

ANISOTROPIC STRENGTH DATA FROM UNCONFINED COMPRESSION TESTS ON HOMOGENEOUS CLAY FROM WELLAND, ONTARIO

BLOCK	β	δ	α
	DEG	DEG	DEG
H	75	51	-24
		58	-17
	90	62	-28
		68	-22

Data from LO (1965a)

TABLE 3.10(a)

ANISOTROPIC STRENGTH DATA FROM UNCONFINED COMPRESSION TESTS ON STRATIFIED CLAY FROM WELLAND, ONTARIO

BLOCK	β DEG	q_f PSF
F	0	830
		890
		920
		950
		1000
		1040
		1080
	30	550
		710
		750
	45	460
		500
		580
		630
		670
		800
	60	420
		510
		680
	90	780
		820
		910
		960
		1070
		1130

Continued

TABLE 3.10(a)

ANISOTROPIC STRENGTH DATA FROM UNCONFINED COMPRESSION TESTS ON STRATIFIED CLAY FROM WELLAND, ONTARIO

BLOCK	β DEG	q_f PSF	BLOCK	β DEG	q_f PSF
K	0	1110		60	820
		1190			890
		1320			1110
		1420			1310
		1570			1360
	30	710		90	1260
		1020			1300
		1080			1440
		1120			1570
		1200			1610
		1310			
	45	850			
		890			
		980			
		1030			
		1110			

Data from LO AND MILLIGAN (1967)

TABLE 3.10(b)

ANISOTROPIC STRENGTH DATA FROM UNCONFINED COMPRESSION TESTS ON STRATIFIED CLAY FROM WELLAND, ONTARIO

BLOCK	β	$q_{f,\ AVG}$	R_u
	DEG	PSF	
F	0	959	1.00
	30	670	0.70
	45	607	0.63
	60	537	0.56
	90	946	0.99
K	0	1322	0.92
	30	1073	0.75
	45	972	0.68
	60	1098	0.76
	90	1436	1.00

Data from LO AND MILLIGAN (1967)

TABLE 3.10(c)

ANISOTROPIC STRENGTH DATA FROM UNCONFINED COMPRESSION TESTS ON STRATIFIED CLAY FROM WELLAND, ONTARIO

β DEG	NO. TESTS	δ_{AVG} DEG	α_{AVG} DEG
0	13	55	55
30	4	55	25
30	4	30	0
45	13	48	3
60	9	58	-2
90	11	57	-33

Data from LO AND MILLIGAN (1967)

TABLE 3.11

DIMENSIONLESS ANISOTROPIC STRENGTH DATA FROM UNCONFINED COMPRESSION TESTS ON HOMOGENEOUS CLAY FROM WELLAND, ONTARIO

BLOCK	R_u β, DEG						
	0	15	30	45	60	75	90
A	1.00	0.97	0.91	0.87	0.85		0.79
B	1.00		0.82	0.78	0.73		0.64
C	1.00	0.98	0.87	0.82	0.77	0.76	0.74
D	1.00	0.95	0.90	0.85	0.81	0.78	0.75
E	1.00		0.88	0.85	0.83		0.78
G	1.00		0.86	0.81	0.78		0.74
H	1.00	1.00	0.92	0.87	0.84	0.82	0.80
I	1.00	0.94	0.95	0.86	0.83	0.81	0.78
avg.	1.00	0.97	0.89	0.84	0.81	0.79	0.75
theo.	1.00	0.98	0.94	0.88	0.81	0.77	0.75

Data from LO (1965a)

TABLE 3.12

ANISOTROPIC STRENGTH DATA FROM $\overline{\text{CIU}}$ TRIAXIAL TESTS ON HOMOGENEOUS CLAY FROM WELLAND, ONTARIO

		q, PSI			
ϵ	$\Delta\sigma_1$	β, DEG			
PERCENT	PSI	0	30	45	90
0.2	1.50	7.25	5.25	4.50	4.00
0.4	3.00	10.75	9.00	7.00	6.00
0.6	4.30	13.00	11.25	8.75	7.25
0.8	5.60	14.50	13.00	10.00	8.00
1.0	6.80	15.50	14.00	10.75	8.50
1.2	7.60	16.00	14.50	11.25	9.00
1.4	8.30	16.50	15.00	11.75	9.25
1.6	9.00		15.25	12.00	9.40
1.8	9.60			12.25	9.50
2.0	10.10			12.50	9.55
2.2	10.60			12.65	9.60
2.4	11.00			12.70	9.65
2.6	11.40			12.75	9.70
2.8	11.80			12.80	9.75
3.0	12.20				9.80
3.2	12.50				9.85
3.4	12.80				9.90
3.6	13.10				9.95
3.8	13.30				10.00
4.0	13.50				10.05

σ_3 = 30 PSI

Data from LO (1966)

TABLE 3.13

ANISOTROPIC STRENGTH DATA FROM UNCONSOLIDATED UNDRAINED TRIAXIAL TESTS ON HOMOGENEOUS SARNIA GLACIAL LAKE CLAY

BLOCK	β	$q_{f,\ AVG}$	R_u
	DEG	PSF	
1	0	1498	1.00
	90	1300	0.87
2	0	1284	1.00
	45	1283	1.00
	90	1118	0.87

Data from HANNA (1967)

TABLE 3.14

ANISOTROPIC STRENGTH DATA FROM TRIAXIAL TESTS ON A FINNISH VARVED GLACIAL CLAY

β	q_f	R_u
DEG	KG/CM^2	
0	0.232	0.83
22.5	0.280	1.00
45.0	0.160	0.57
67.5	0.177	0.63
90.0	0.220	0.79

Data from SOVERI AND HYYPPA(1967)

TABLE 3.15

ANISOTROPIC STRENGTH DATA FROM CONSOLIDATED UNDRAINED TRIAXIAL TESTS ON HOMOGENEOUS INDIA BLACK COTTON CLAY

β	q_f	R_u
DEG	PSI	
0	12.6	0.80
45	12.5	0.80
50	12.5	0.80
90	15.7	1.00

Data from MATTHAI (1967)

$\bar{\sigma}_c$ = 22.5 PSI

TABLE 3.16

ANISOTROPIC STRENGTH DATA FROM UNCONSOLIDATED UNDRAINED TRIAXIAL TESTS ON ASP-900 KAOLINITE

β	$2\,q_f$	β	$2\,q_{f,\,AVG}$	R_u
DEG	KG/CM^2	DEG	KG/CM^2	
0	2.97	0	2.89	1.00
0	2.80	45	2.14	0.74
45	2.30	90	2.50	0.89
45	1.98			
90	2.55			
90	2.45			

Cell pressure = 1.0 KG/CM^2

Data from DUNCAN AND SEED (1965)

TABLE 3.17

ANISOTROPIC STRENGTH DATA FROM CONSOLIDATED UNDRAINED TRIAXIAL TESTS ON ASP-900 KAOLINITE

β	$\bar{p}_o$	OCR	$\bar{p}_f$	q_f	$\bar{p}_f/p_o$	$q_f/\bar{p}_o$
DEG	KG/CM^2		KG/CM^2	KG/CM^2		
0	0.50	18	2.23	1.08	4.46	2.16
0	0.75	12	2.81	1.34	3.75	1.79
0	1.00	9	2.71	1.28	2.71	1.28
0	1.50	6	3.02	1.35	2.02	0.90
0	3.00	3	4.05	1.84	1.35	0.61
90	0.50	18	1.80	0.85	3.60	1.70
90	0.75	12	2.24	1.16	2.98	1.55
90	1.00	9	2.05	1.03	2.05	1.03
90	1.50	6	2.44	1.22	1.63	0.81
90	3.00	3	3.51	1.61	1.17	0.54

Data from DUNCAN AND SEED (1965)

NOTE: Data have not been corrected for loads carried by filter paper drains and rubber membranes or for piston friction. Data plotted in Figure 3.37 are also uncorrected.

TABLE 3.18

ANISOTROPIC STRENGTH DATA FROM UNDRAINED PLANE STRAIN TESTS ON SAN FRANCISCO BAY MUD FROM HAMILTON AIR FORCE BASE

TEST	β_f	$\bar{p}_c$	q_c	$\bar{p}_f$	q_f	$\bar{p}_s$
	DEG	KG/CM^2	KG/CM^2	KG/CM^2	KG/CM^2	KG/CM^2
VPS-3	0	2.74	0.93	2.26	1.35	
VPS-4	0	0.50	0.14	0.41	0.26	
VPS-5	0	1.04	0.34	0.83	0.52	
VPS-6	0	1.60	0.54	1.28	0.79	
VPS-8	0	2.17	0.73	1.71	1.06	
VPS-9	0	2.74	0.98	2.28	1.38	
HPS-4	90	1.15	0.46	0.72	0.41	0.96
HPS-5	90	2.18	0.98	1.46	0.83	1.76
HPS-6	90	0.58	0.24	0.41	0.21	0.58
HPS-7	90	1.70	0.70	1.08	0.64	1.34
HPS-9	90	2.72	1.26	1.93	1.12	2.31
HPS-11	90	2.83	1.17	1.92	1.12	2.33
HPS-12	90	2.35	0.83	1.55	0.89	1.87
VPS-UU-1	0	0.53	0.14	0.45	0.26	0.50
VPS-UU-2	0	2.84	0.86	2.17	1.33	2.48
VPS-UU-3	0	1.74	0.56	1.27	0.78	1.54
VPS-UU-4	0	2.74	1.13	2.31	1.42	2.31

Data from DUNCAN AND SEED (1965)

TABLE 3.19

ANISOTROPIC STRENGTH DATA FROM UNCONSOLIDATED UNDRAINED TRIAXIAL TESTS ON UNDISTURBED SAMPLES OF SAN FRANCISCO BAY MUD FROM HAMILTON AIR FORCE BASE

β	NO. TESTS	$2\,q_{f,MIN}$	$2\,q_{f,AVG}$	$2\,q_{f,MAX}$	R_u
DEG		KG/CM^2	KG/CM^2	KG/CM^2	
0	3	0.361	0.370	0.400	1.00
45	8	0.288	0.320	0.333	0.86
60	7	0.279	0.292	0.311	0.79
90	9	0.291	0.300	0.305	0.81

$\sigma_3 = 1.0\ KG/CM^2$

Data from DUNCAN AND SEED (1965)

TABLE 3.20

ANISOTROPIC STRENGTH DATA FROM CONSOLIDATED UNDRAINED TRIAXIAL TESTS ON UNDISTURBED SAMPLES OF SAN FRANCISCO BAY MUD FROM HAMILTON AIR FORCE BASE

TEST	β_f	$\bar{p}_c$	q_c	$\bar{p}_f$	q_f
	DEG	KG/CM^2	KG/CM^2	KG/CM^2	KG/CM^2
AC-U-1	0	2.50	0.66	1.81	1.02
AC-U-2	90	2.62	0.56	1.64	0.93
IC-U-1	0	0.94	0.06	0.56	0.33
IC-U-2	0	2.40	0.08	1.44	0.81
IC-U-3	0	3.90	0.08	2.33	1.32

Data from DUNCAN AND SEED (1965)

TABLE 3.21

ANISOTROPIC STRENGTH DATA FROM CONSOLIDATED UNDRAINED TRIAXIAL TESTS ON UNDISTURBED LONDON CLAY

β_f	$\bar{p}_c$	$\bar{p}_f$	q_f
DEG	PSI	PSI	PSI
0	5	26	23
	15	41	33
	40	54	41
	60	69	49
	80	84	58
	110	113	71
	145	155	83
	260	295	138
	370	385	157
	860	745	233
90	5	29	24
	15	44	32
	30	71	46
	45	93	58
	70	122	71
	80	146	81
	110	166	92
	145	216	113
	260	378	168
	370	460	193
	370	470	195
	860	720	253

Data from BISHOP, WEBB AND LEWIN(1965)

TABLE 3.22

ANISOTROPIC STRENGTH DATA FROM CONSOLIDATED DRAINED TRIAXIAL TESTS ON UNDISTURBED LONDON CLAY

β_f	$\bar{p}_f$	q_f	β_f	$\bar{p}_f$	q_f
DEG	PSI	PSI	DEG	PSI	PSI
0	13	13	90	15	15
	15	15		51	40
	16	16		88	48
	35	28		88	58
	64	44		115	70
	104	59		142	81
	126	74		228	119
	158	90		515	205
	180	100		615	230
	195	105		885	245
	224	115		1210	350
	276	128			
	362	159			
	430	177			
	516	199			
	592	212			
	899	261			
	1164	304			
	1172	312			

Data from BISHOP, WEBB AND LEWIN (1965)

TABLE 3.23

INDEX PROPERTIES OF LONDON CLAY AT THE SITE OF THE ASHFORD COMMON SHAFT

LEVEL	DEPTH	LAB. WATER CONTENT	LIQUID LIMIT	PLASTIC LIMIT	ACTIVITY
	FT.	%	%	%	
A	30	22.4	60	24	0.82
B	50	25.8	69	29	0.69
C	66	24.8	71	29	0.79
D	91	22.8	63	26	0.79
E	114	24.2	70	27	0.75
F	138	23.6	69	28	0.68

Data from WARD, MARSLAND AND SAMUELS (1965)

TABLE 3.24

ANISOTROPIC STRENGTH DATA FROM CONFINED UNCONSOLIDATED UNDRAINED TRIAXIAL TESTS ON UNDISTURBED LONDON CLAY AT THE SITE OF THE ASHFORD COMMON SHAFT

LEVEL	β	$q_{u,AVG}$	R_u	δ_{AVG}	α_{AVG}
	DEG	PSI		DEG	DEG
A	0	36.6	0.71	52	52
	45	32.7	0.64	51	6
	90	51.3	1.00	56	-34
B	0	32.9	0.81	55	55
	45	19.6	0.49	59	14
	90	40.4	1.00	58	-32
C	0	44.1	0.62	52	52
	45	33.2	0.47	51	6
	90	70.8	1.00	58	-32
D	0	54.4	0.65	51	51
	45	48.6	0.58	53	8
	90	84.1	1.00	54	-36
E	0	59.9	0.61	53	53
	45	50.4	0.52	53	8
	90	97.8	1.00	58	-32
F	0	81.0	0.75	46	46
	45	52.8	0.49	44	-1
	90	107.4	1.00	59	-31

Data from WARD, MARSLAND AND SAMUELS (1965)

TABLE 3.25

STATISTICAL ANALYSIS OF CONFINED UNCONSOLIDATED UNDRAINED TRIAXIAL TESTS ON VERTICAL SAMPLES OF UNDISTURBED LONDON CLAY

q_u/q_u, AVG	LEVEL						n	r	p
	A	B	C	D	E	F			PERCENT
0.35 - 0.44					1		1	1	0.6
0.45 - 0.54			2		5		7	8	4.8
0.55 - 0.64		1	1		4	2	8	16	9.6
0.65 - 0.74	1	2		3	2	1	9	25	15.1
0.75 - 0.84	3	4	5		4	3	19	44	26.5
0.85 - 0.94	8	7	2	7	3		27	71	42.8
0.95 - 1.04	5	2	8		5	2	22	93	56.0
1.05 - 1.14	5	2	4	3	3	4	21	114	68.6
1.15 - 1.24	4	3	4	1	5	3	20	134	80.7
1.25 - 1.34	2	1	2	4	6	1	16	150	90.4
1.35 - 1.44			1		8	1	10	160	96.4
1.45 - 1.54		2	1		1		4	164	98.8
1.55 - 1.64		1					1	165	99.4
TOTAL	28	25	30	18	47	17	165		

Data from WARD, MARSLAND AND SAMUELS (1965)

TABLE 3.26

ANISOTROPIC STRENGTH DATA FROM UNCONSOLIDATED UNDRAINED TRIAXIAL TESTS ON RESEDIMENTED BOSTON BLUE CLAY

β	$\bar{\sigma}_{vm}$	$\bar{\sigma}_{vm}/\bar{\sigma}_s$	$q_u/\bar{\sigma}_s$	$\bar{\sigma}_s/\bar{\sigma}_{vm}$	$q_u/\bar{\sigma}_{vm}$
DEG	KG/CM^2				
0	3.0	5.2	0.88	0.192	0.169
	3.0	5.7	0.96	0.176	0.168
	3.0	5.0	0.90	0.200	0.180
	3.0	4.4	0.90	0.227	0.204
	3.5	8.8	1.13	0.114	0.128
	3.5	5.4	0.91	0.185	0.169
	3.5	6.5	1.06	0.154	0.163
	3.5	4.7	0.837	0.213	0.178
	8.0	7.8	1.01	0.128	0.129
	8.0	7.5	1.14	0.133	0.152
	8.0	8.1	1.14	0.123	0.141
	8.0	8.3	1.11	0.120	0.134
30	3.0	4.9	0.77	0.204	0.157
	3.0	4.6	0.89	0.218	0.193
	3.5	5.6	0.893	0.179	0.159
	3.5	5.0	0.777	0.200	0.155
	8.0	10.1	1.16	0.099	0.115
	8.0	7.9	1.072	0.127	0.136

(Continued) TABLE 3.26

ANISOTROPIC STRENGTH DATA FROM UNCONSOLIDATED UNDRAINED TRIAXIAL TESTS ON RESEDIMENTED BOSTON BLUE CLAY

β	$\bar{\sigma}_{vm}$	$\bar{\sigma}_{vm}/\bar{\sigma}_s$	$q_u/\bar{\sigma}_s$	$\bar{\sigma}_s/\bar{\sigma}_{vm}$	$q_u/\bar{\sigma}_{vm}$
DEG	KG/CM^2				
45	3.0	6.7	0.74	0.149	0.110
	3.0	4.0	0.63	0.250	0.158
	3.5	9.0	1.241	0.111	0.138
	3.5	3.7	0.69	0.270	0.187
	8.0	13.1	1.30	0.076	0.099
	8.0	9.4	1.029	0.106	0.109
	8.0	11.3	1.17	0.088	0.104
	8.0	10.7	1.165	0.093	0.109
60	3.0	7.0	0.95	0.143	0.136
	3.0	6.7	0.92	0.149	0.137
	3.0	6.3	0.85	0.159	0.135
	3.0	4.5	0.67	0.222	0.149
	3.5	6.2	0.912	0.161	0.147
	3.5	3.5	0.654	0.286	0.187
	8.0	11.0	1.048	0.091	0.095
	8.0	12.9	1.15	0.078	0.089

(Continued) TABLE 3.26

ANISOTROPIC STRENGTH DATA FROM UNCONSOLIDATED UNDRAINED TRIAXIAL TESTS ON RESEDIMENTED BOSTON BLUE CLAY

β	$\bar{\sigma}_{vm}$	$\bar{\sigma}_{vm}/\bar{\sigma}_s$	$q_u/\bar{\sigma}_s$	$\bar{\sigma}_s/\bar{\sigma}_{vm}$	$q_u/\bar{\sigma}_{vm}$
DEG	KG/CM^2				
90	3.0	4.5	0.58	0.222	0.129
	3.0	4.4	0.62	0.227	0.141
	3.0	6.5	0.84	0.154	0.129
	3.0	3.8	0.63	0.263	0.166
	3.5	8.1	0.83	0.123	0.102
	3.5	7.1	0.801	0.141	0.113
	3.5	14.5	1.137	0.069	0.079
	3.5	3.9	0.59	0.256	0.151
	8.0	8.6	0.91	0.116	0.106
	8.0	7.9	0.878	0.127	0.111
	8.0	8.7	0.976	0.115	0.112
	8.0	7.5	1.063	0.133	0.142

Data from D'APPOLONIA (1968)

TABLE 3.27

ANISOTROPIC STRENGTH RATIO FROM UNCONSOLIDATED UNDRAINED TRIAXIAL TESTS ON RESEDIMENTED BOSTON BLUE CLAY

$\bar{\sigma}_s/\bar{\sigma}_{vm}$	β DEG	$q_u/\bar{\sigma}_{vm}$	R_u
0.10	0	0.118	1.00
	30	0.116	0.98
	45	0.113	0.96
	60	0.106	0.90
	90	0.103	0.87
0.15	0	0.152	1.00
	30	0.144	0.95
	45	0.137	0.90
	60	0.136	0.89
	90	0.127	0.84
0.20	0	0.180	1.00
	30	0.168	0.93
	45	0.155	0.86
	60	0.154	0.85
	90	0.142	0.79
0.25	0	0.207	1.00
	30	0.190	0.92
	45	0.170	0.82
	60	0.164	0.79
	90	0.151	0.73

Data from D'APPOLONIA(1968)

TABLE 3.28

VARIATION OF FAILURE PLANE ORIENTATION FOR UU TRIAXIAL TESTS ON RESEDIMENTED BOSTON BLUE CLAY

β DEG	$(OCR)_c$	δ DEG	α DEG	α_{AVG} DEG
0	1.0	58	58	59.1
	1.0	59	59	
	3.5	57	57	
	3.5	57	57	
	10.7	63	63	
	10.7	59	59	
	10.7	61	61	
30	1.0	56	26	23.6
	10.7	54	24	
	10.7	51	21	
45	1.0	53	8	9.1
	3.5	59	14	
	3.5	56	11	
	10.7	50	5	
	10.7	52	7	
	10.7	54	9	
	10.7	55	10	

(Continued) TABLE 3.28

VARIATION OF FAILURE PLANE ORIENTATION FOR UU TRIAXIAL TESTS ON RESEDIMENTED BOSTON BLUE CLAY

β DEG	$(OCR)_c$	δ DEG	α DEG	α_{AVG} DEG
60	1.0	53	-7	-6.5
	3.5	54	-6	
	3.5	54	-6	
	10.7	53	-7	
90	1.0	50	-40	-37.1
	1.0	51	-39	
	3.5	53	-37	
	3.5	53	-37	
	3.5	60	-30	
	3.5	52	-38	
	10.7	52	-38	
	10.7	51	-39	
	10.7	52	-38	
	10.7	55	-35	

Data from D'APPOLONIA (1968)

TABLE 3.29

EFFECTIVE STRESS STRENGTH DATA FROM $\overline{UU}$ TRIAXIAL TESTS ON RESEDIMENTED BOSTON BLUE CLAY

β	$\bar{\sigma}_{vm}/\bar{\sigma}_s$	$\bar{p}_f/\bar{\sigma}_{vm}$	$q_f/\bar{\sigma}_{vm}$	$\bar{p}_f/\bar{\sigma}_s$	$q_f/\bar{\sigma}_s$
DEG					
0	5.2	0.400	0.169	2.08	0.88
	8.8	0.308	0.128	2.71	1.13
	7.8	0.290	0.130	2.26	1.01
45	6.7	0.235	0.111	1.57	0.74
	9.0	0.324	0.138	2.92	1.24
	13.1	0.229	0.099	3.00	1.30
90	4.5	0.283	0.129	1.27	0.58
	8.1	0.233	0.102	1.89	0.83
	8.6	0.248	0.106	2.13	0.91

Data from D'APPOLONIA (1968)

TABLE 3.30

ANISOTROPIC STRENGTH DATA FROM UNCONSOLIDATED UNDRAINED TRIAXIAL TESTS ON UNDISTURBED BOSTON BLUE CLAY

β	SITE	$\bar{\sigma}_{vm}$	$\bar{\sigma}_{vm}/\bar{\sigma}_s$	$q_u/\bar{\sigma}_s$	$\bar{\sigma}_s/\bar{\sigma}_{vm}$	$q_u/\bar{\sigma}_{vm}$
DEG		KG/CM^2				
0	MIT	5.6	6.6	1.00	0.152	0.152
			6.4	1.01	0.156	0.158
			8.4	1.13	0.119	0.134
			5.9	1.01	0.170	0.171
	I95	9.5	19.4	1.647	0.052	0.085
			19.4	1.526	0.052	0.079
			23.8	1.72	0.042	0.072
45	MIT	5.6	12.7	1.26	0.079	0.099
			9.4	1.10	0.106	0.117
	I95	9.5	31.6	1.79	0.032	0.057
			11.7	1.330	0.085	0.114
90	MIT	5.6	8.9	1.12	0.112	0.126
			11.0	1.24	0.091	0.113
			6.9	0.87	0.145	0.126
			7.3	1.09	0.137	0.149
	I95	9.5	25.0	1.85	0.040	0.074
			21.5	1.794	0.047	0.083
			25.6	1.914	0.039	0.075
			18.6	1.793	0.054	0.096

Data from D'APPOLONIA (1968)

TABLE 3.31

VARIATION OF FAILURE PLANE ORIENTATION FOR UU TRIAXIAL TESTS ON UNDISTURBED BOSTON BLUE CLAY

β DEG	SITE	$(OCR)_c$	δ DEG	α DEG	α_{AVG} DEG
0	MIT	3.1	60	60	58.0
		3.1	56	56	
		3.1	56	56	
	I95	17.3	59	59	
		17.3	59	59	
		17.3	58	58	
45	MIT	3.1	57	12	11. 3
		3.1	56	11	
	I95	17.3	56	11	
90	MIT	3.1	55	35	34.8
		3.1	55	35	
		3.1	55	35	
	I95	17.3	56	34	
		17.3	54	36	
		17.3	56	34	

Data from D'APPOLONIA (1968)

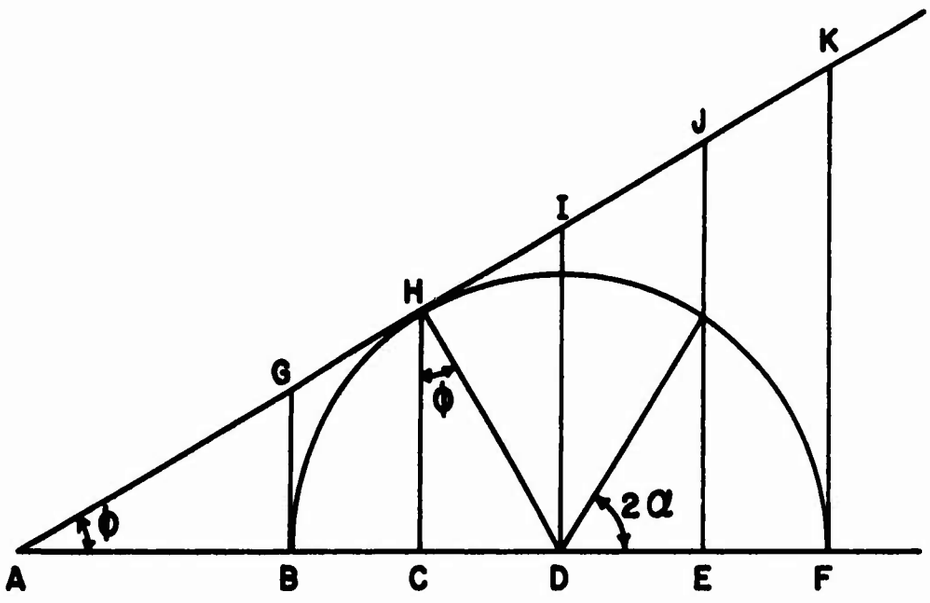

FIGURE 3.1

PRELIMINARY GEOMETRICAL RELATIONSHIPS

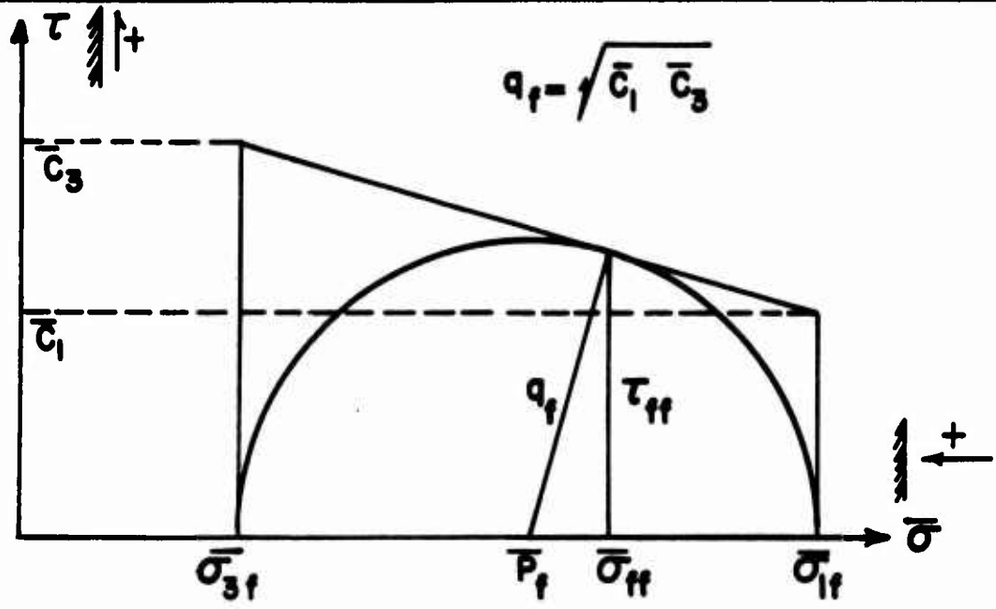

(a) PURELY COHESIVE MATERIAL

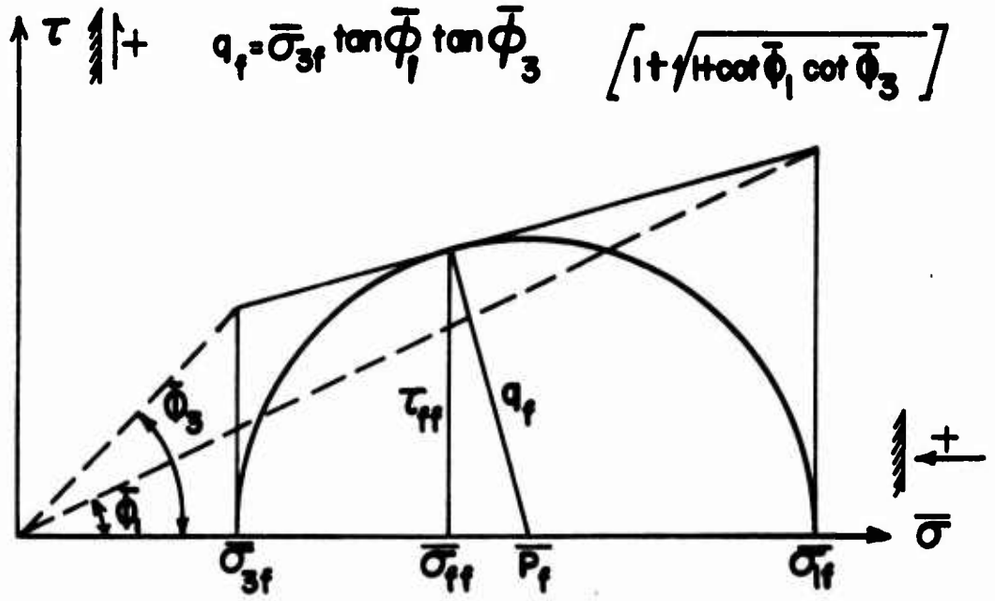

(b) COHESIONLESS MATERIAL

FIGURE 3.2

CASES SOLVED ANALYTICALLY BY CASAGRANDE AND CARRILLO (1944)

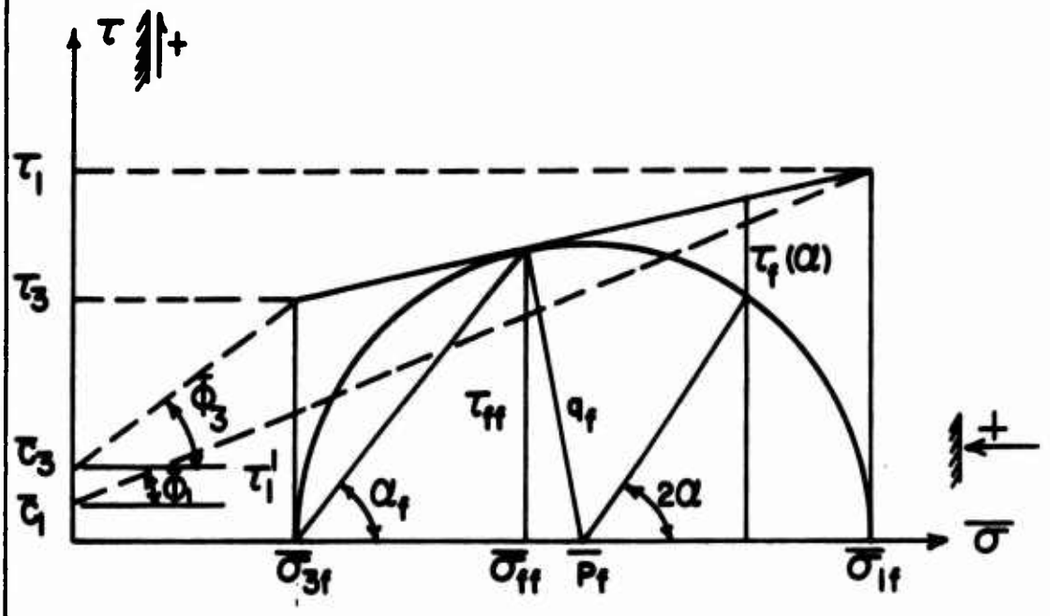

(a) GENERAL PROBLEM

FIGURE 3.3

CASE SOLVED ANALYTICALLY BY
HANK AND McCARTY (1948)

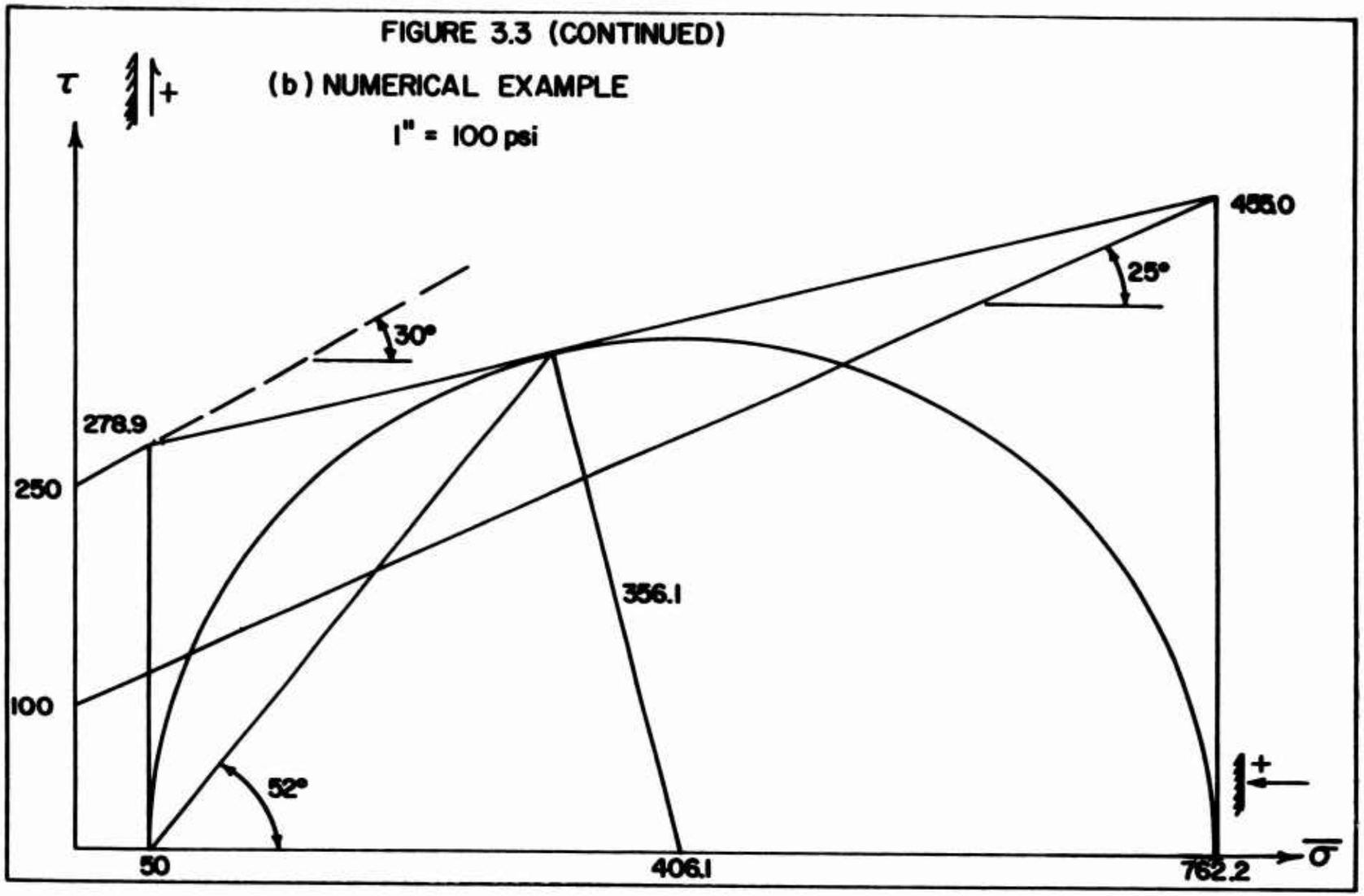
FIGURE 3.3 (CONTINUED)
(b) NUMERICAL EXAMPLE
1" = 100 psi
τ
+
455.0
25°
30°
278.9
250
100
356.1
52°
50
406.1
762.2
σ
+

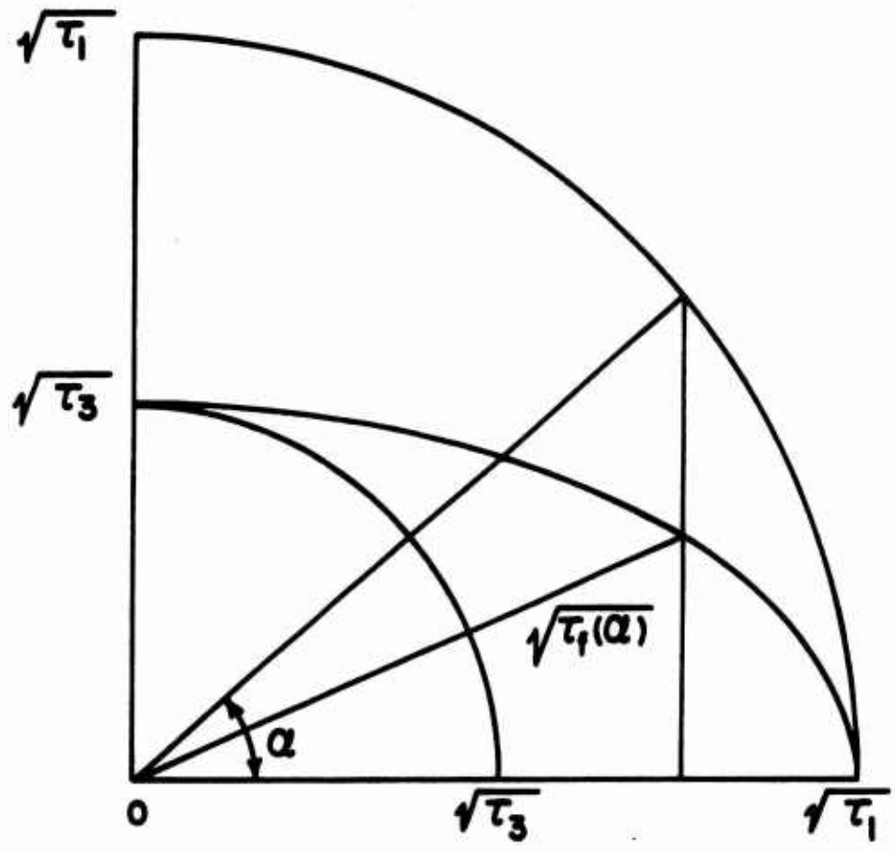

$$x = \sqrt{\tau_1}\cos\alpha$$

$$y = \sqrt{\tau_3}\sin\alpha$$

$$r^2 = x^2 + y^2 = \tau_1\cos^2\alpha + \tau_3\sin^2\alpha = \tau_f(\alpha)$$

$$r = \sqrt{\tau_f(\alpha)}$$

FIGURE 3.4

ELLIPTICAL VARIATION
ASSOCIATED WITH MOHR'S CIRCLE

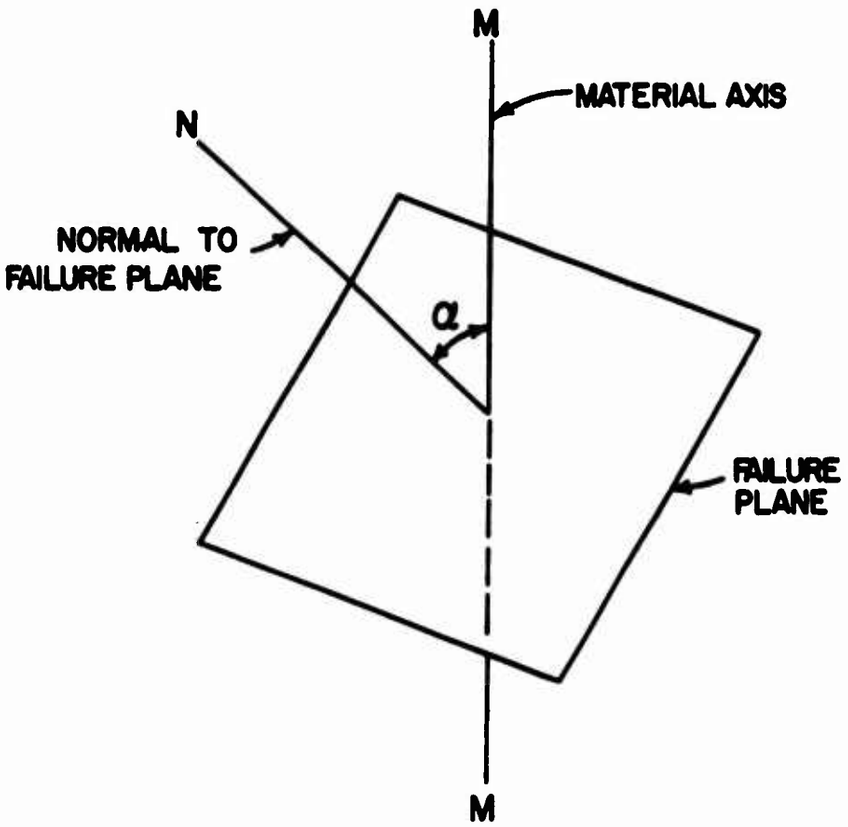

FIGURE 3.5

FAILURE PLANE ORIENTATION

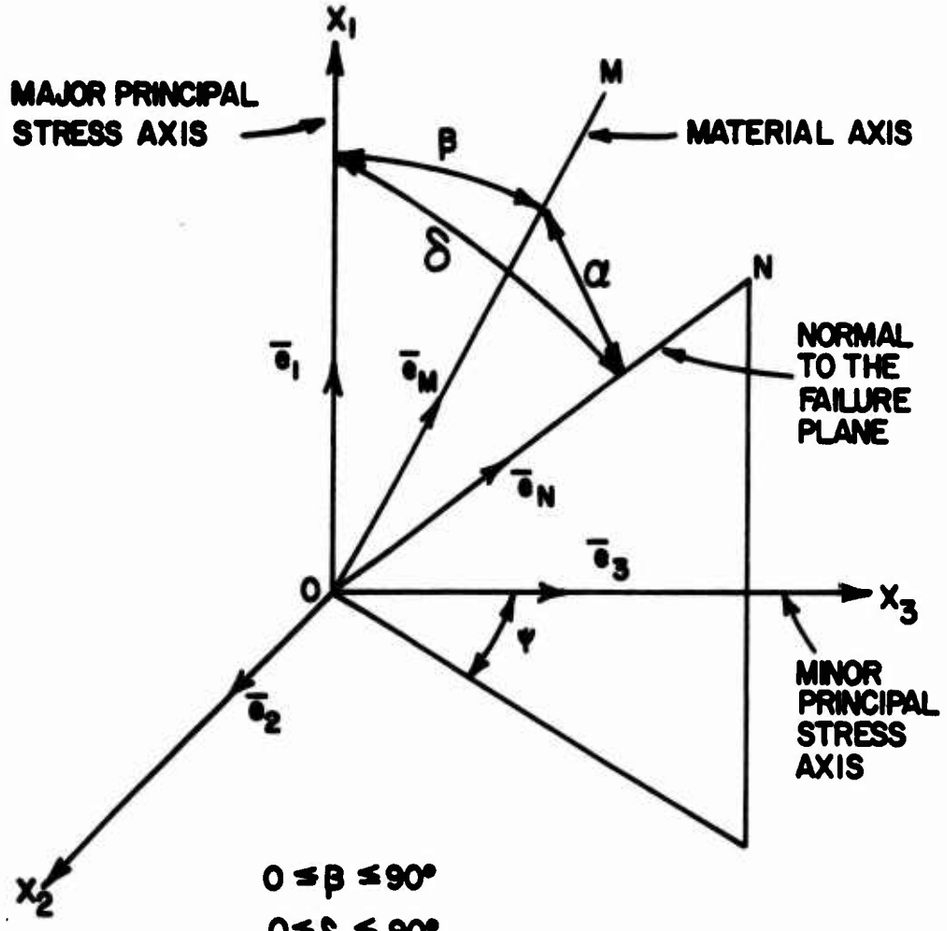

$$0 \le \beta \le 90°$$

$$0 \le \delta \le 90°$$

$$0 \le \psi \le 180°$$

$$\bar{e}_N = \cos\delta\,\bar{e}_1 + \sin\delta\sin\psi\,\bar{e}_2 + \sin\delta\cos\psi\,\bar{e}_3$$

$$\bar{e}_M = \cos\beta\,\bar{e}_1 + \sin\beta\,\bar{e}_3$$

$$\cos\alpha = \bar{e}_N \cdot \bar{e}_M = \cos\beta\cos\delta + \cos\psi\sin\beta\sin\delta$$

FIGURE 3.6

BASIC GEOMETRIC RELATIONS IN A CROSS ANISOTROPIC CLAY AT FAILURE

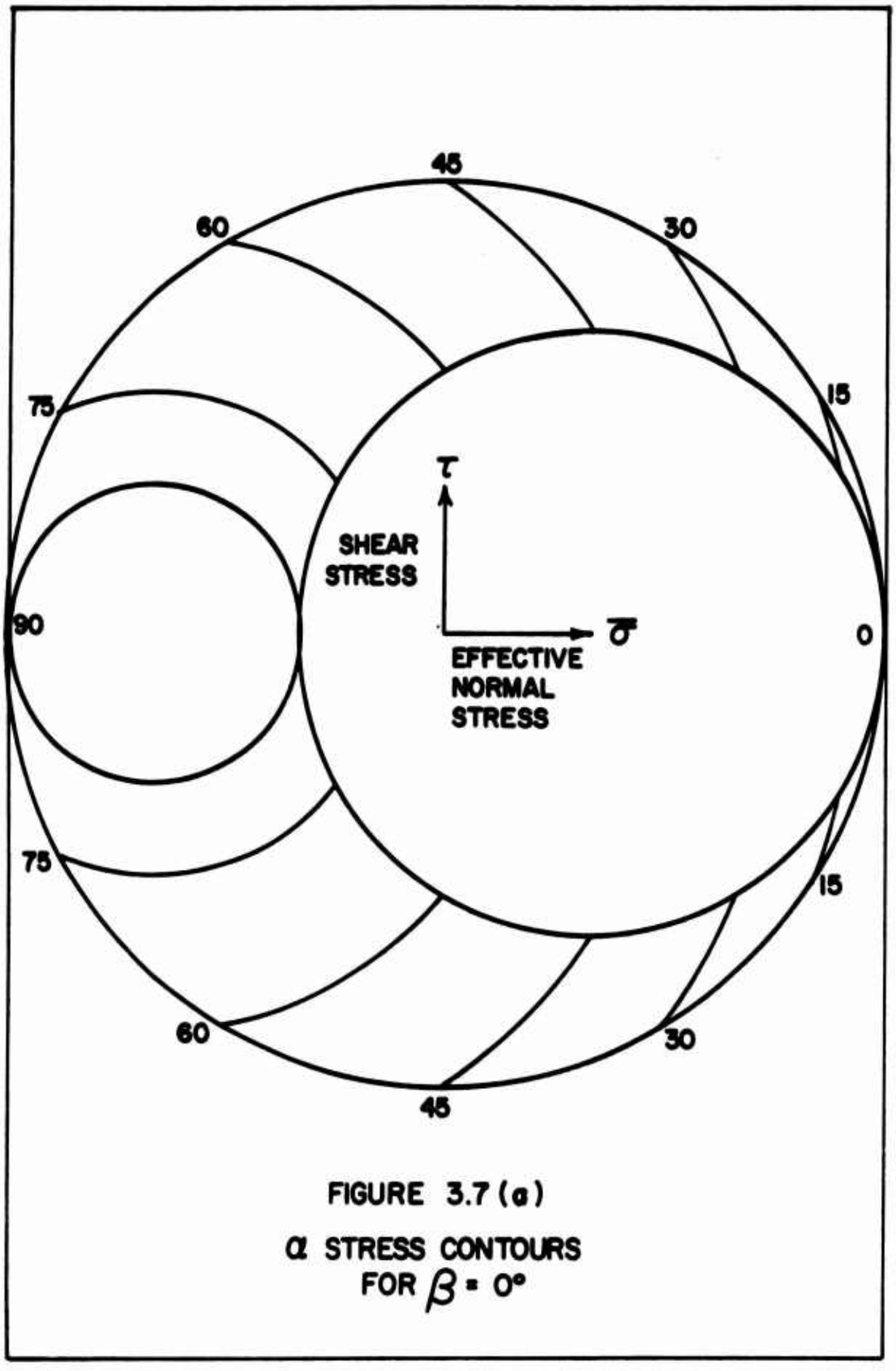

FIGURE 3.7 (a)

α STRESS CONTOURS
FOR $\beta = 0°$

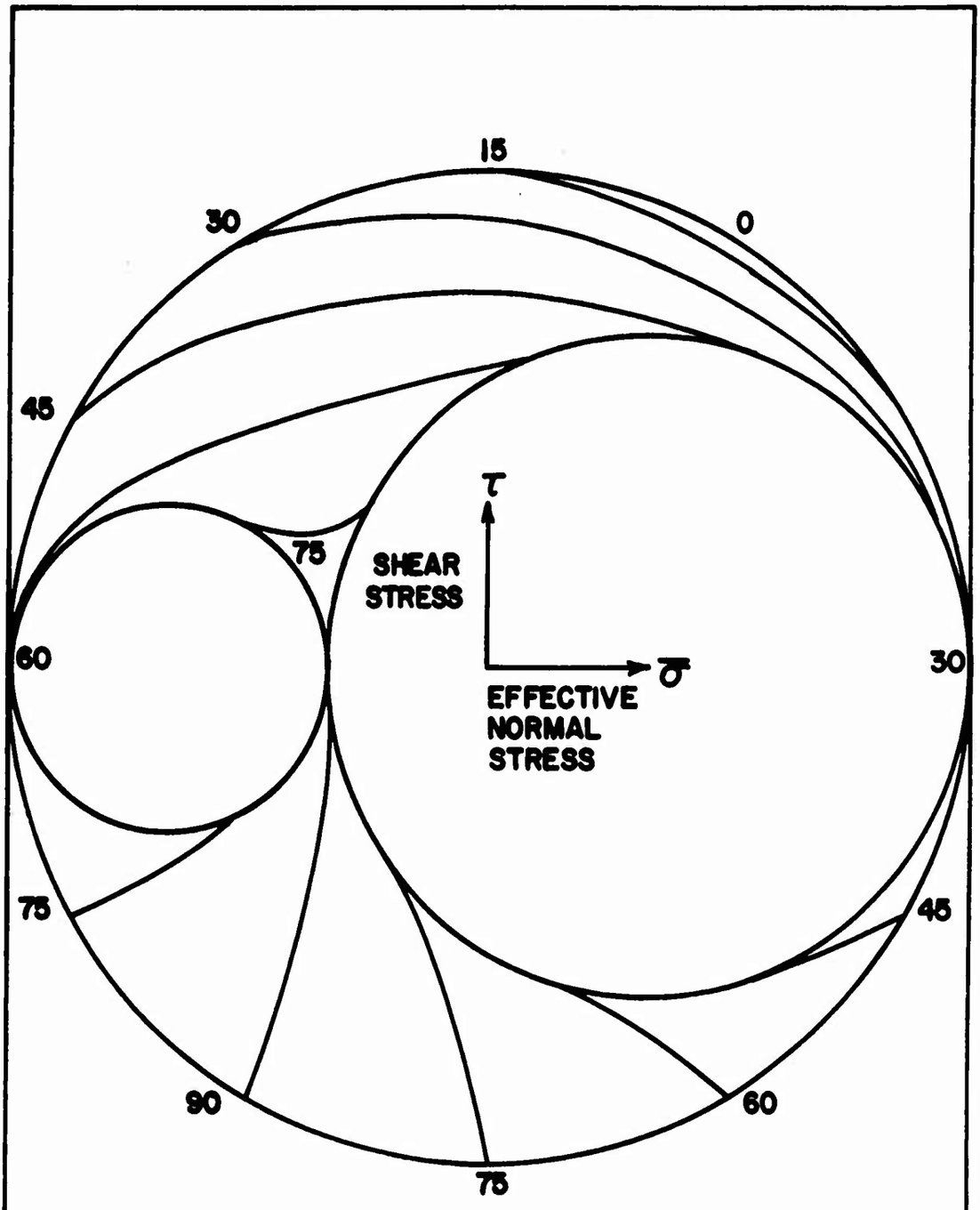

FIGURE 3.7 (b)

α STRESS CONTOURS FOR β = 30°

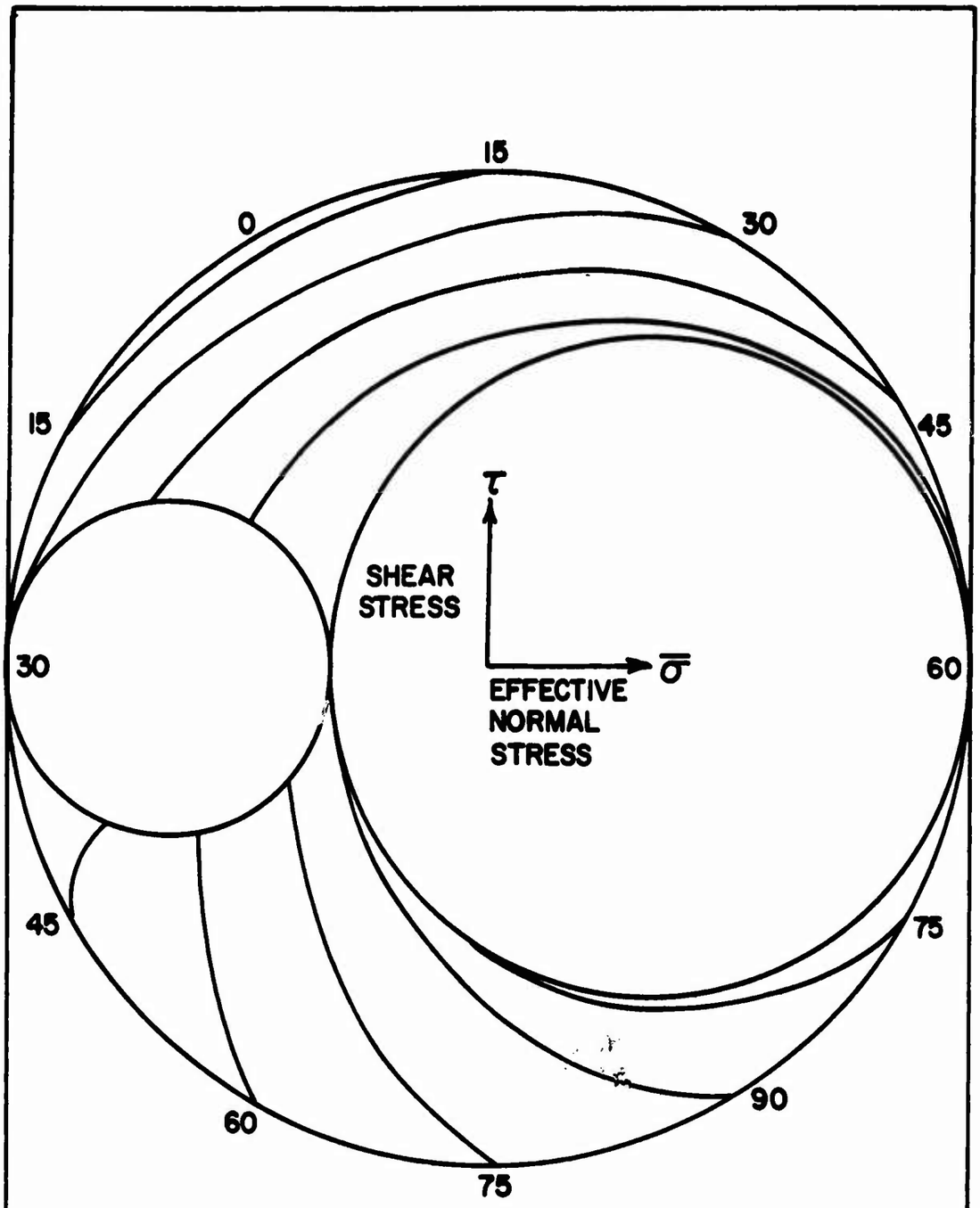

FIGURE 3.7 (c)
α STRESS CONTOURS
FOR $\beta = 60°$

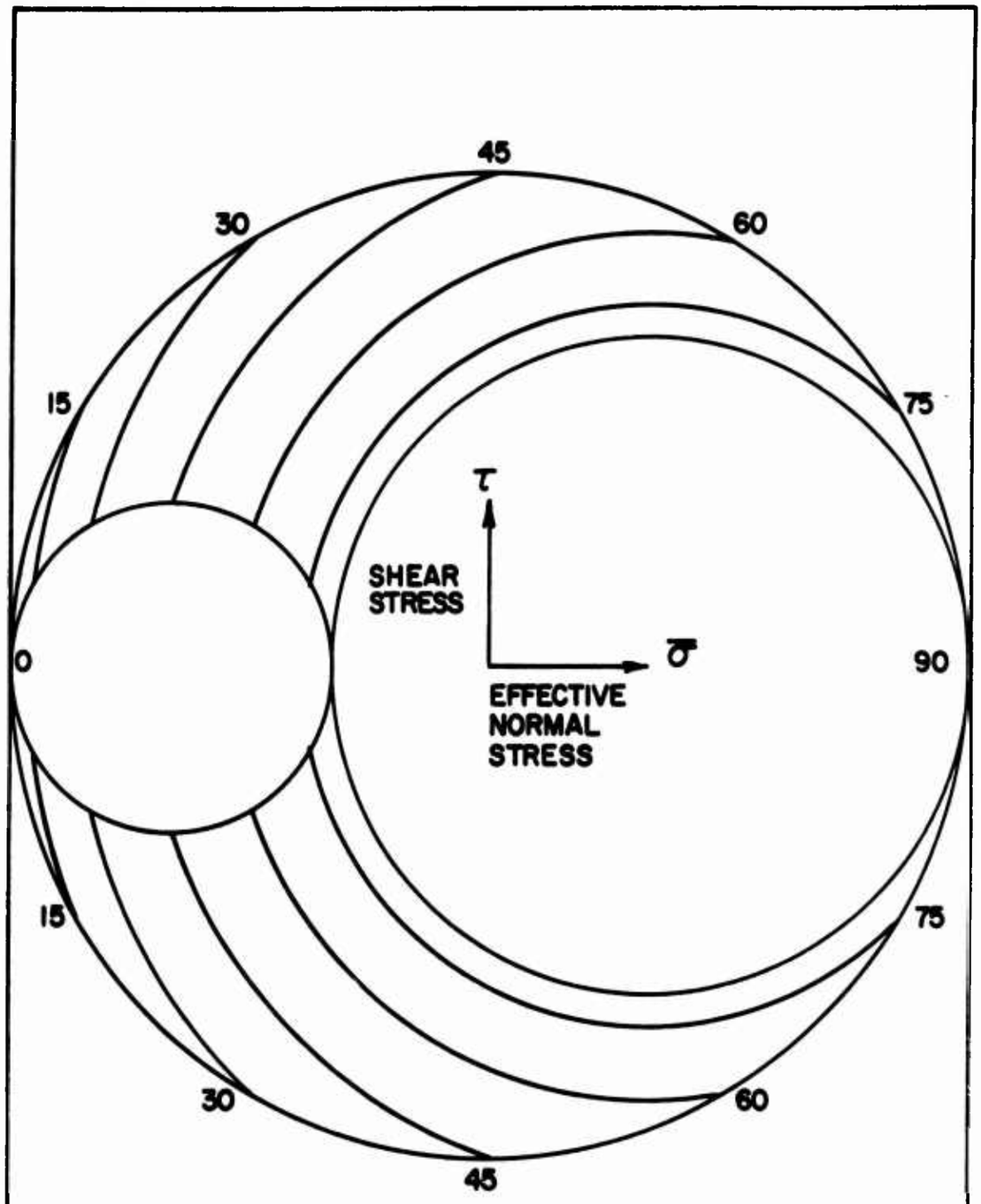

FIGURE 3.7(d)

α STRESS CONTOURS
FOR β = 90°

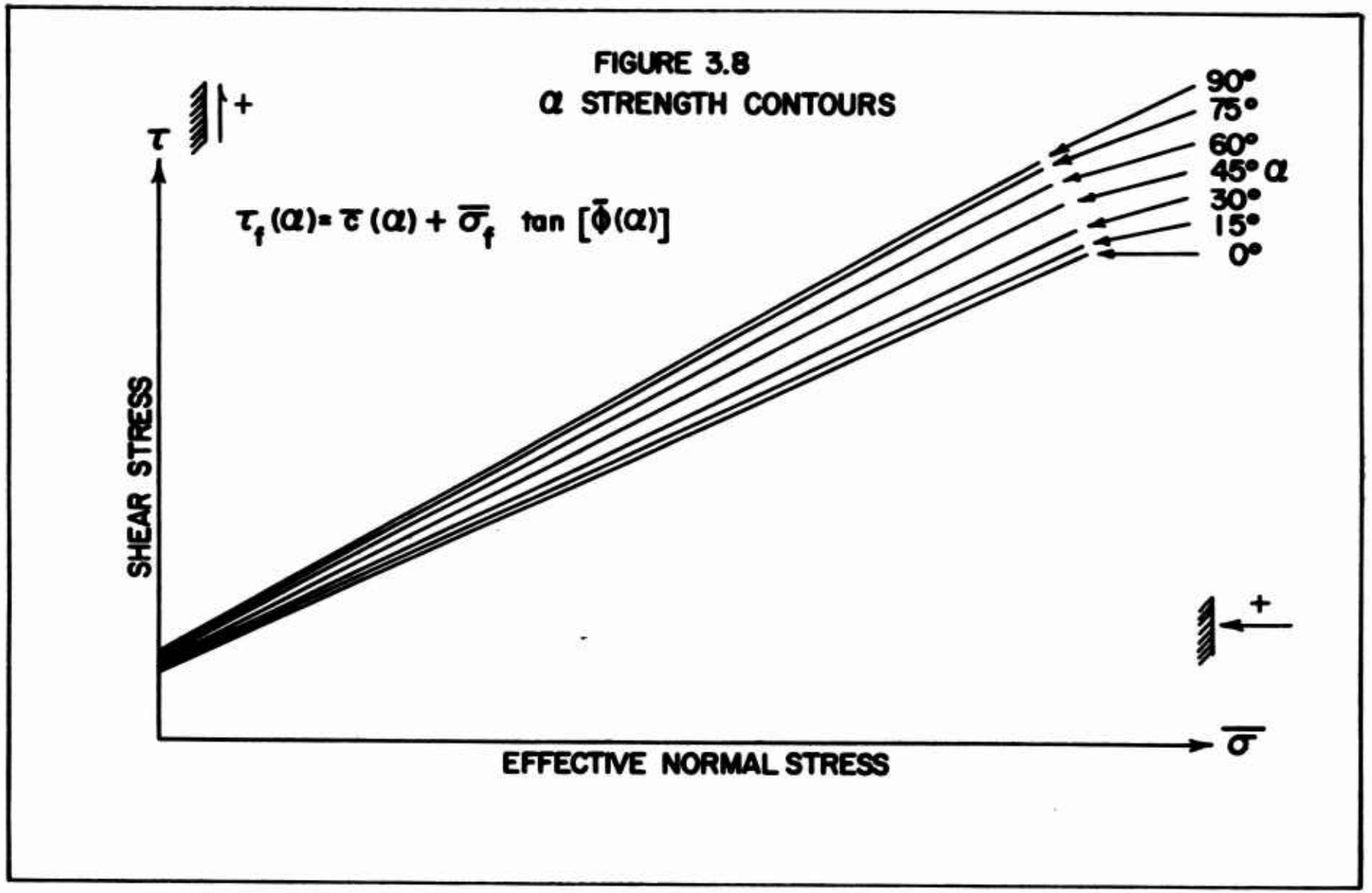
FIGURE 3.8
α STRENGTH CONTOURS
+
τ
$\tau_f(\alpha) = \bar{c}(\alpha) + \bar{\sigma}_f \tan[\bar{\phi}(\alpha)]$
90°
75°
60°
45° α
30°
15°
0°
SHEAR STRESS
+
$\bar{\sigma}$
EFFECTIVE NORMAL STRESS

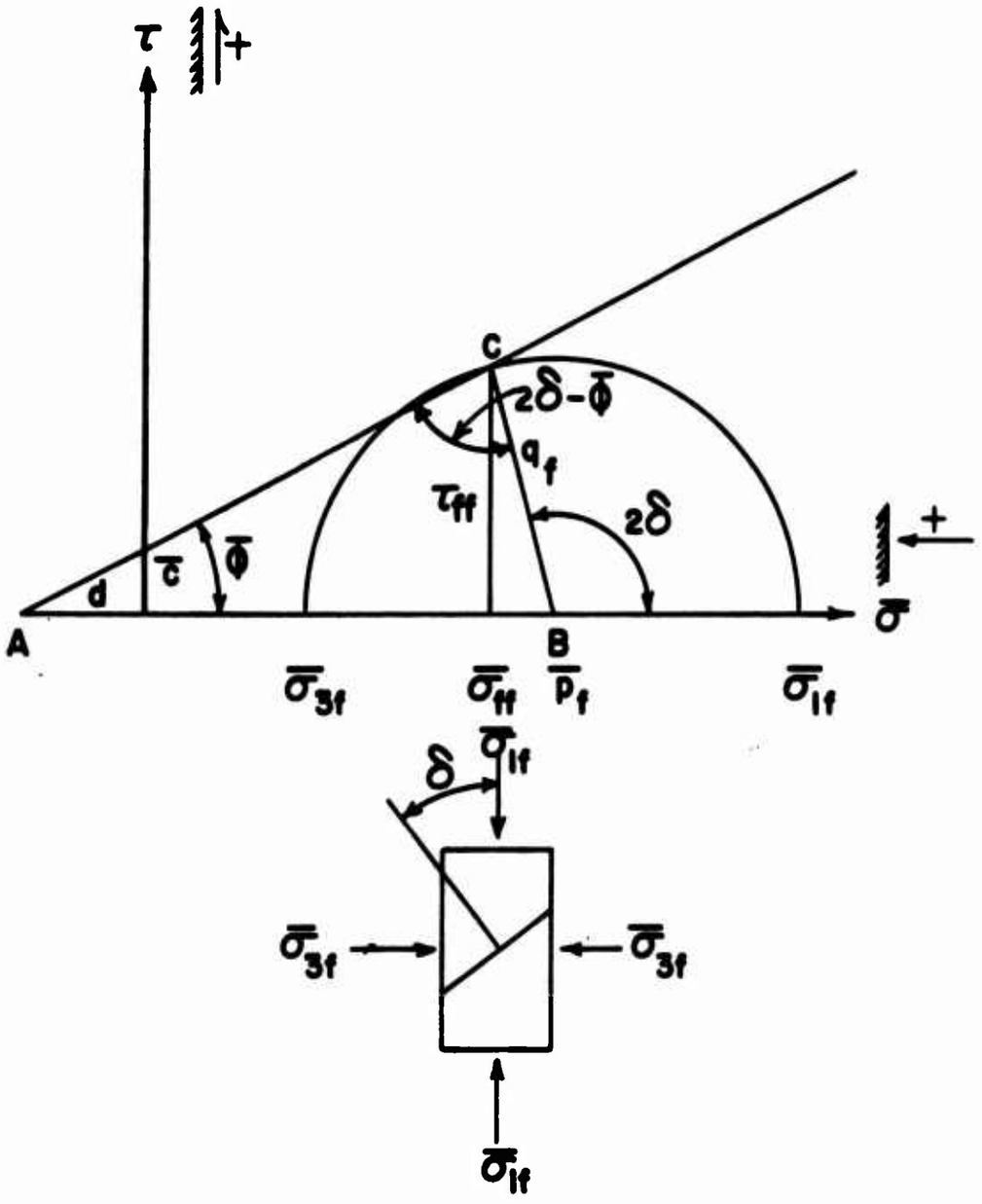

FIGURE 3.9

STATE OF STRESS AT FAILURE IN AN ANISOTROPIC CLAY

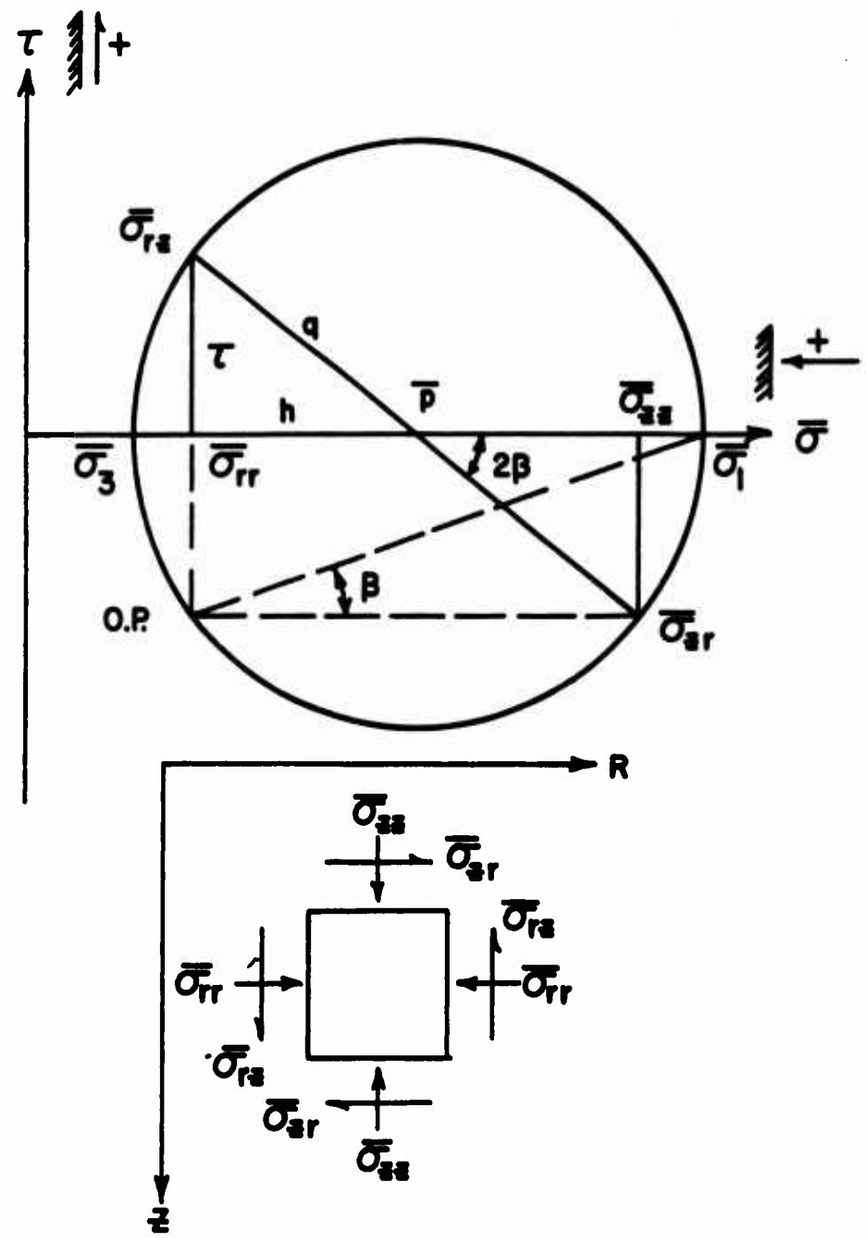

FIGURE 3.10

ROTATION OF PRINCIPAL PLANES

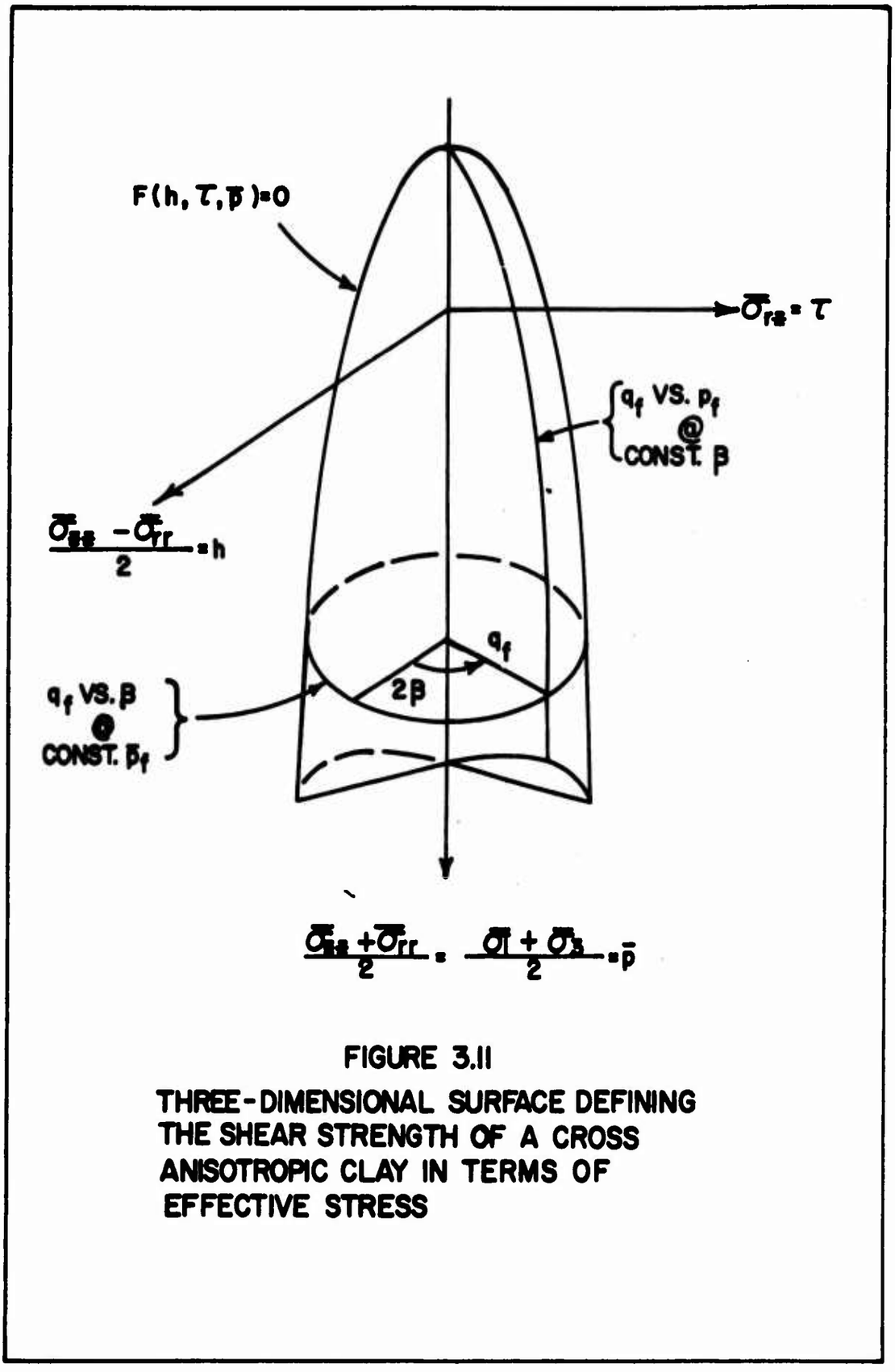

FIGURE 3.11

THREE-DIMENSIONAL SURFACE DEFINING THE SHEAR STRENGTH OF A CROSS ANISOTROPIC CLAY IN TERMS OF EFFECTIVE STRESS

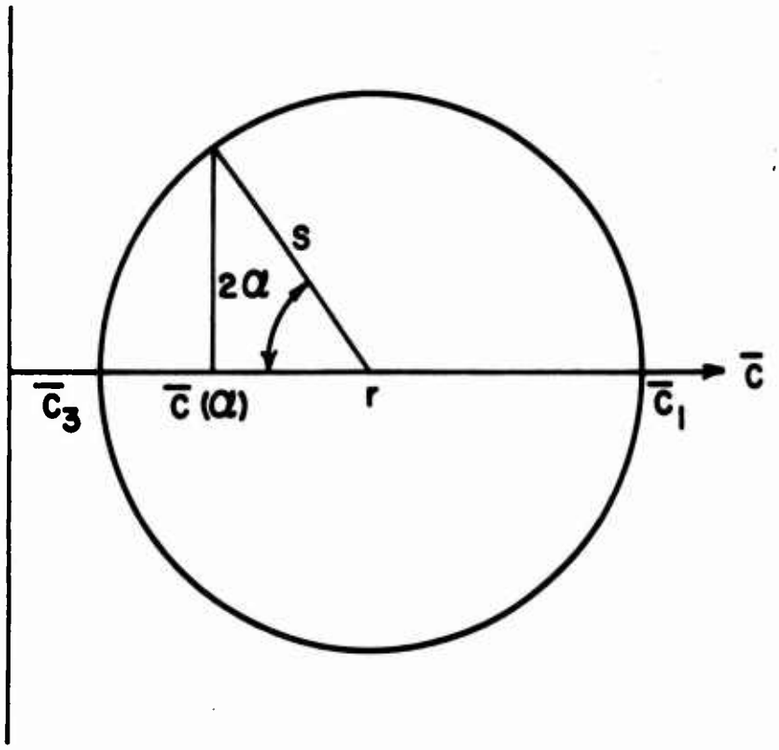

$$\bar{c}(\alpha) = r - S\cos 2\alpha$$

$$r = \frac{\bar{c}_1 + \bar{c}_3}{2}$$

$$S = \frac{\bar{c}_1 - \bar{c}_3}{2}$$

FIGURE 3.12

VARIATION OF $\bar{c}(\alpha)$ ASSUMED BY JAEGER

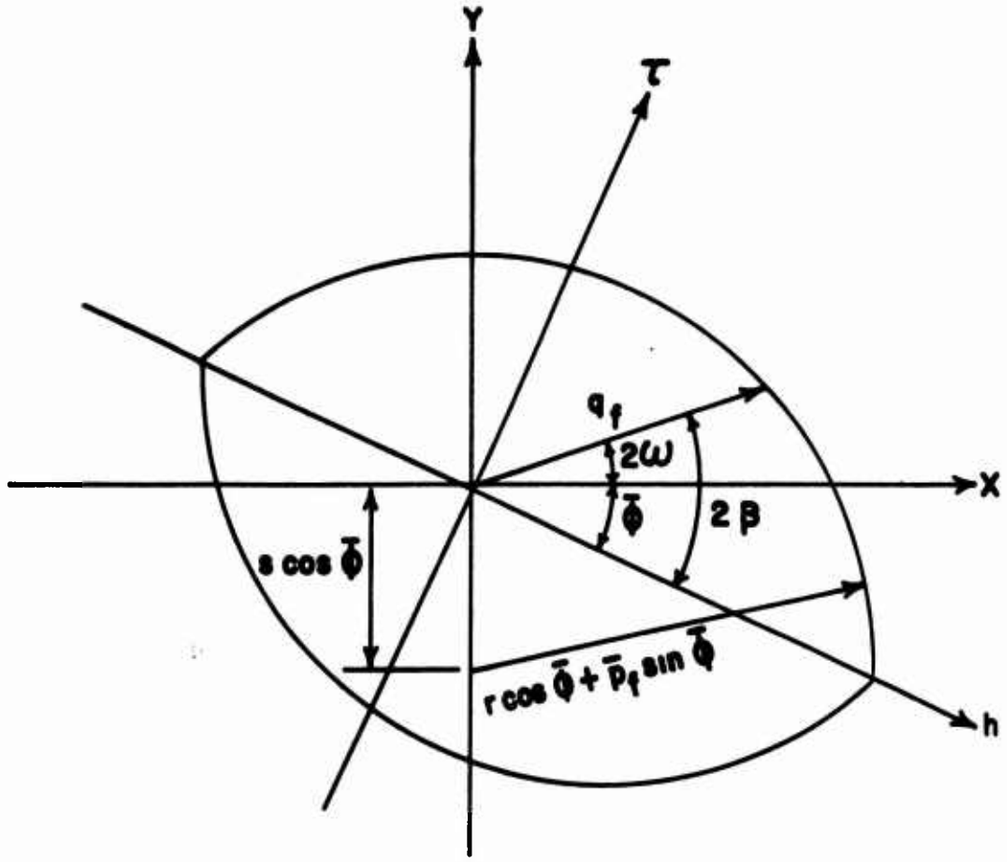

FIGURE 3.13

FOOTBALL SHAPED CONSTANT $\bar{p}_f$
CROSS SECTION OF JAEGER'S
BI-CONICAL FAILURE SURFACE

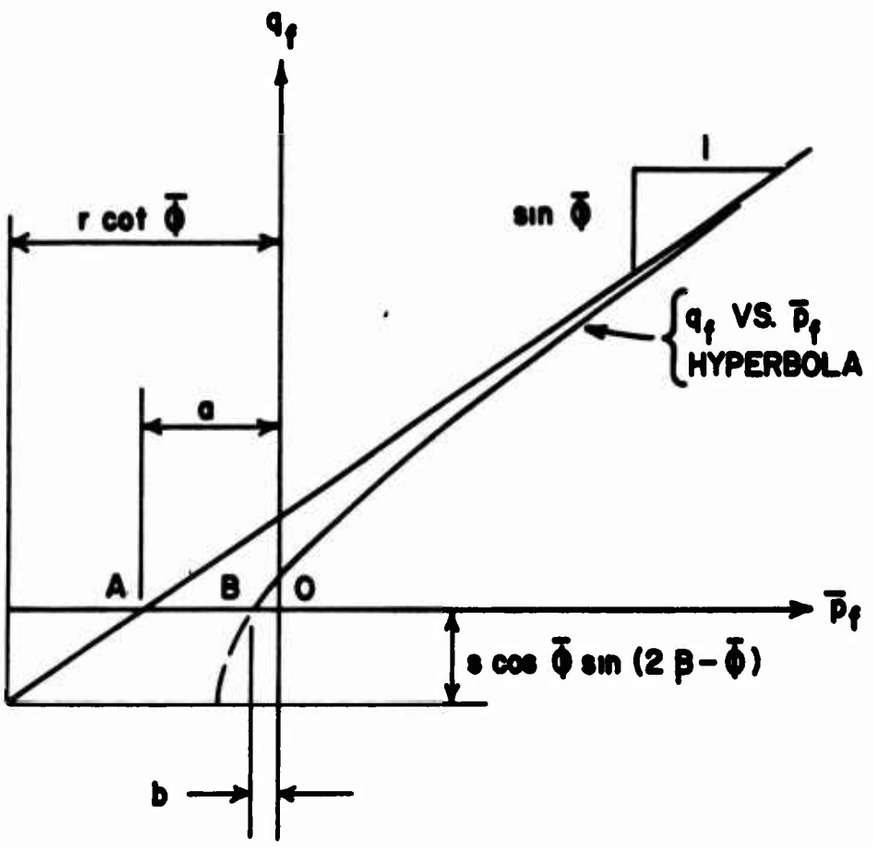

$$a = \left[r - s \sin(2\beta - \bar{\phi}) \right] \cot \bar{\phi}$$

$$b = (r - s) \cot \bar{\phi}$$

FIGURE 3.14

HYPERBOLIC CONSTANT β CROSS SECTION OF JAEGER'S BI-CONICAL FAILURE SURFACE

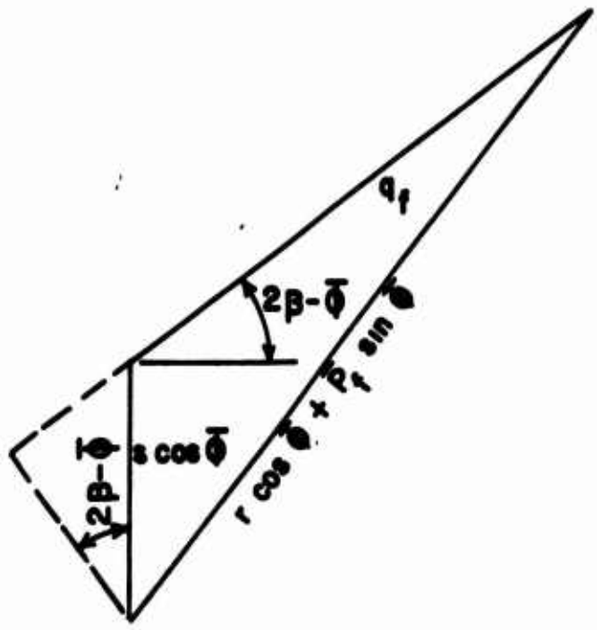

$$q_f = \sqrt{\left[r\cos\bar{\phi}+\bar{P}_f\sin\bar{\phi}\right]^2-\left[s\cos\bar{\phi}\cos(2\beta-\bar{\phi})\right]^2} - s\cos\bar{\phi}\sin(2\beta-\bar{\phi})$$

FIGURE 3.15

DIAGRAM FOR OBTAINING $q_f(\bar{P}_f, \beta)$ FOR JAEGER'S BI-CONICAL FAILURE SURFACE

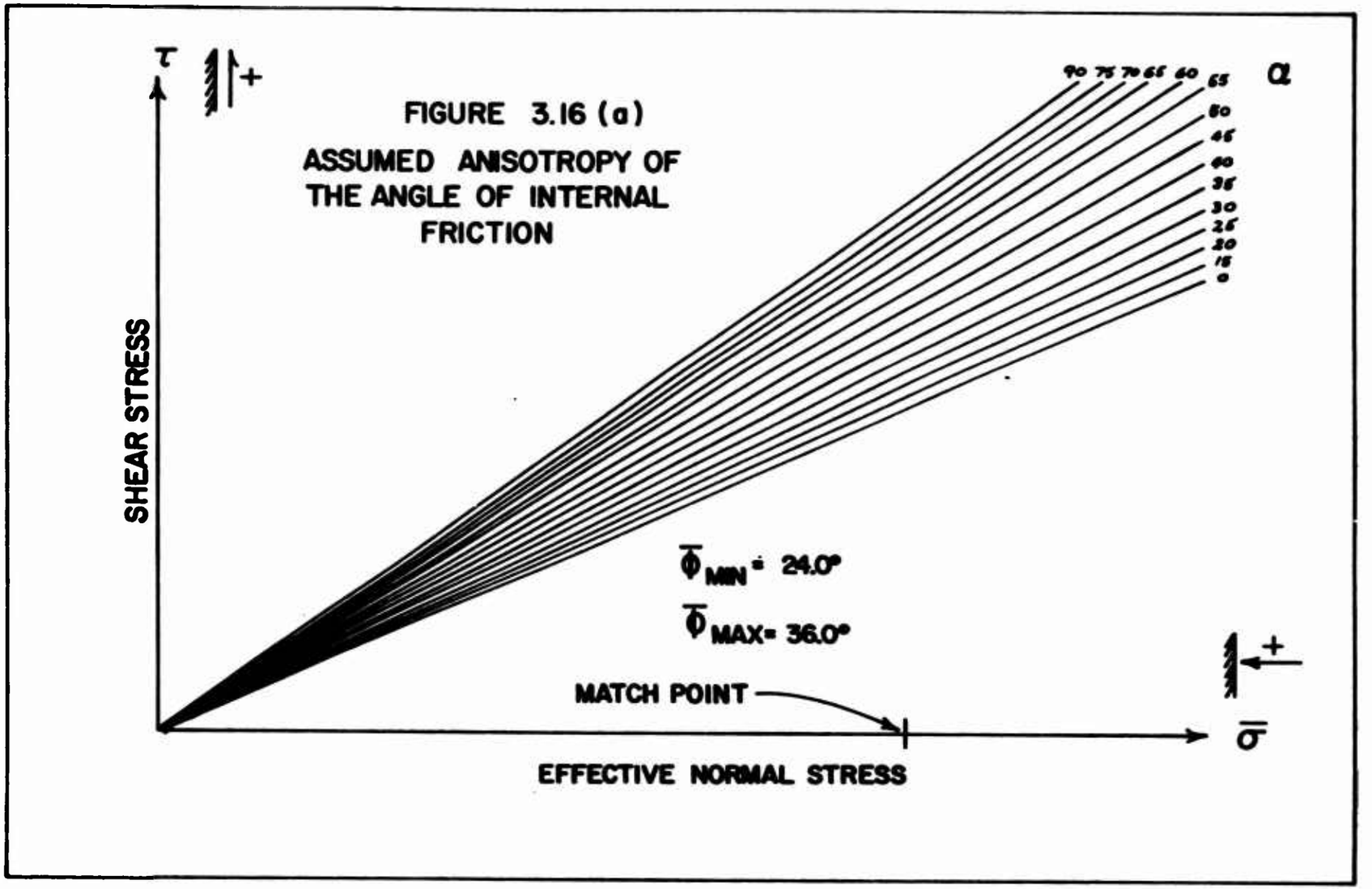

FIGURE 3.16 (a)

ASSUMED ANISOTROPY OF THE ANGLE OF INTERNAL FRICTION

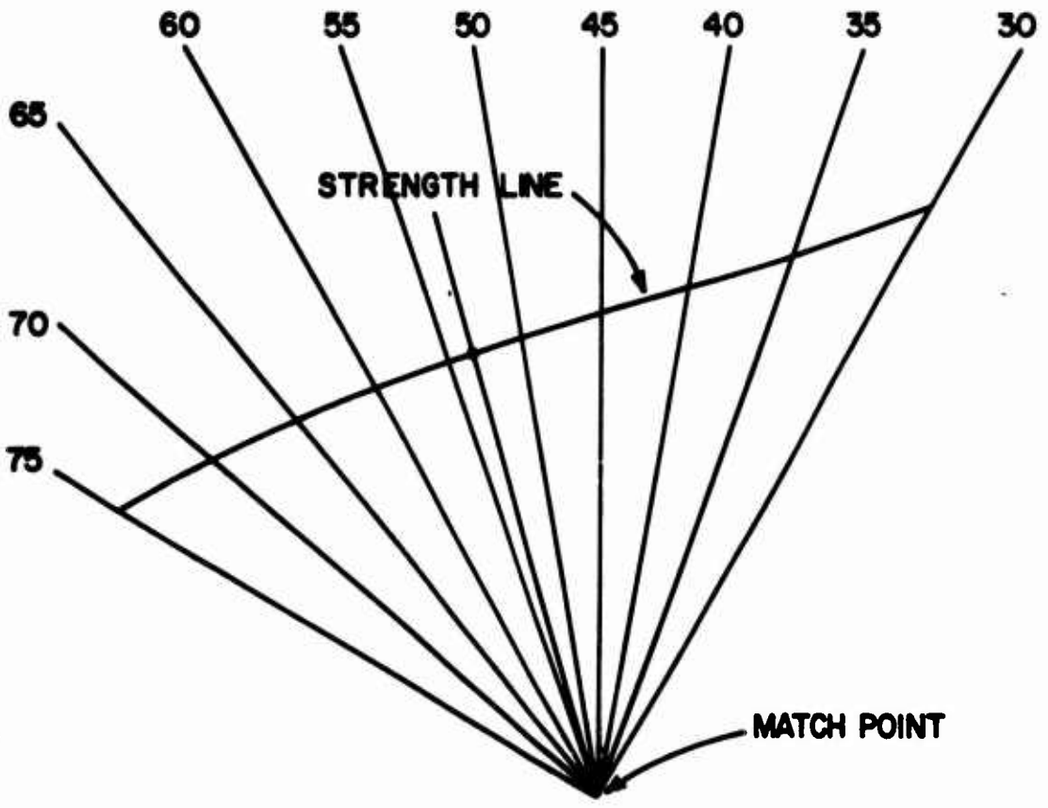

$\beta = 15°$

$2\delta = 106.6°$

$m = 0.495$

FIGURE 3.16 (b)
TYPICAL GRAPHICAL ANISOTROPIC
SHEAR STRENGTH ANALYSIS

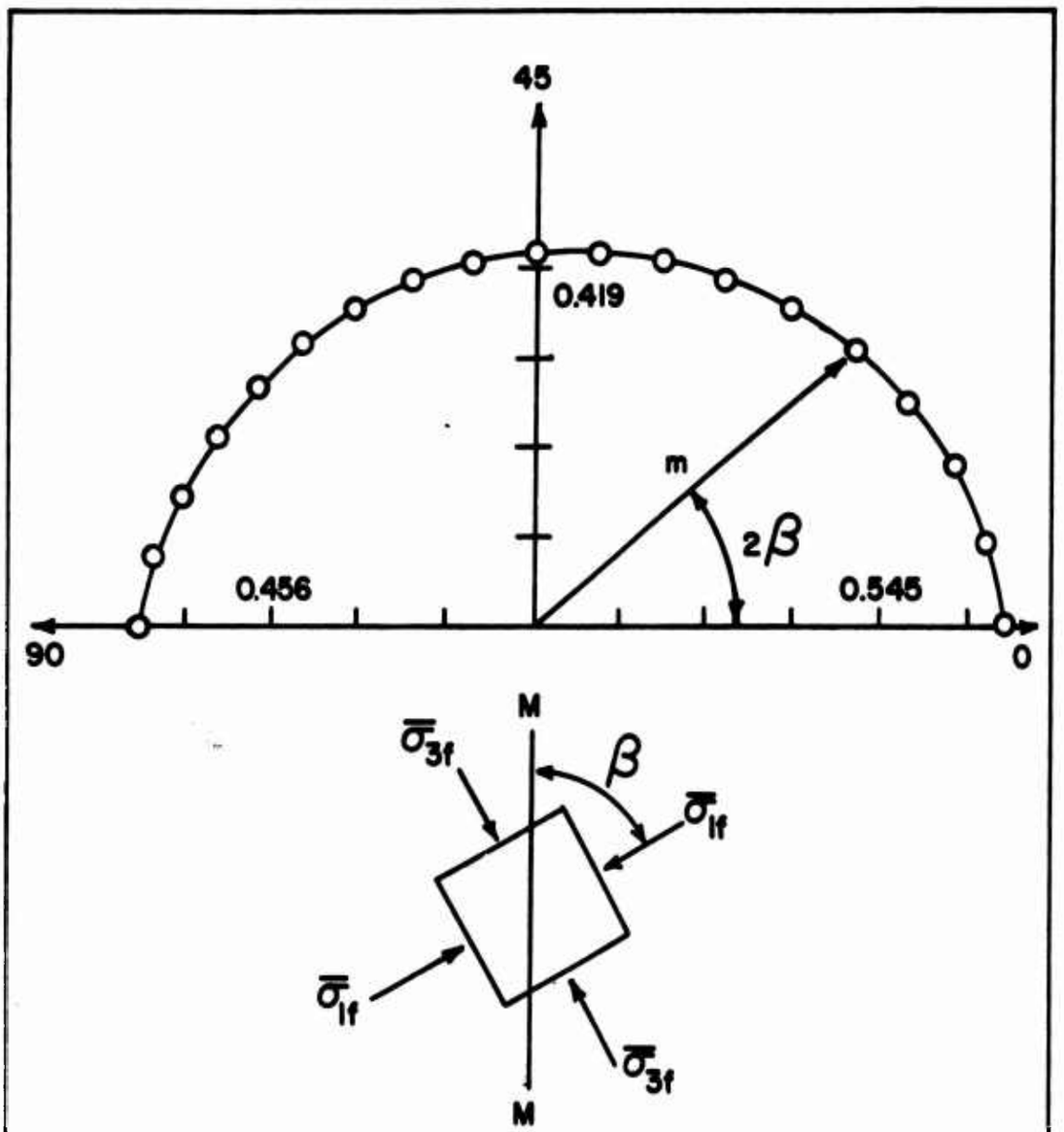

$$m = \frac{\bar{\sigma}_{1f} - \bar{\sigma}_{3f}}{\bar{\sigma}_{1f} + \bar{\sigma}_{3f}}$$

FIGURE 3.16(c)
VARIATION OF SHEAR STRENGTH WITH β FOR CLAY WITH ANISOTROPIC ANGLE OF INTERNAL FRICTION

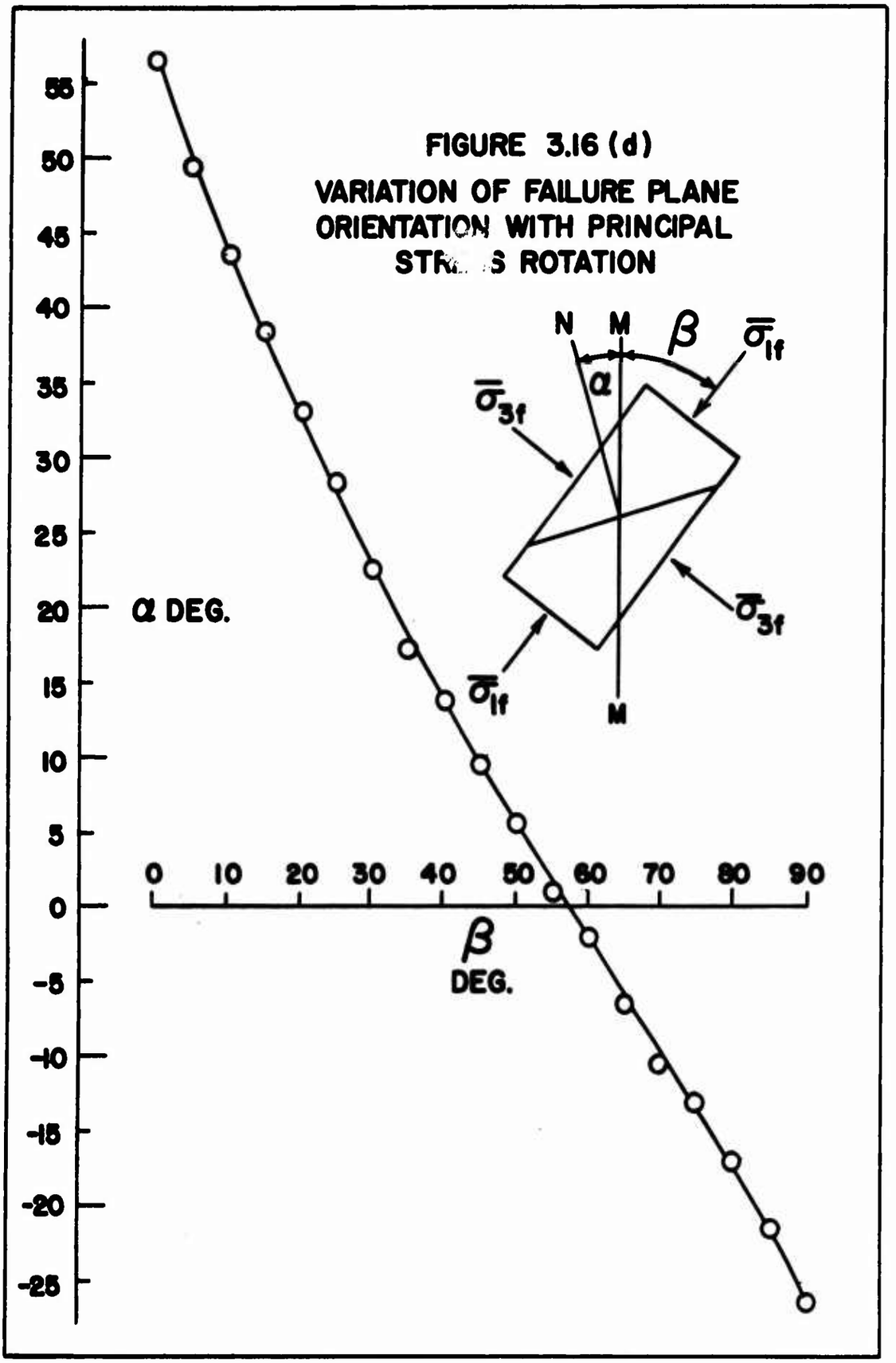

FIGURE 3.16 (d)
VARIATION OF FAILURE PLANE ORIENTATION WITH PRINCIPAL STRESS ROTATION

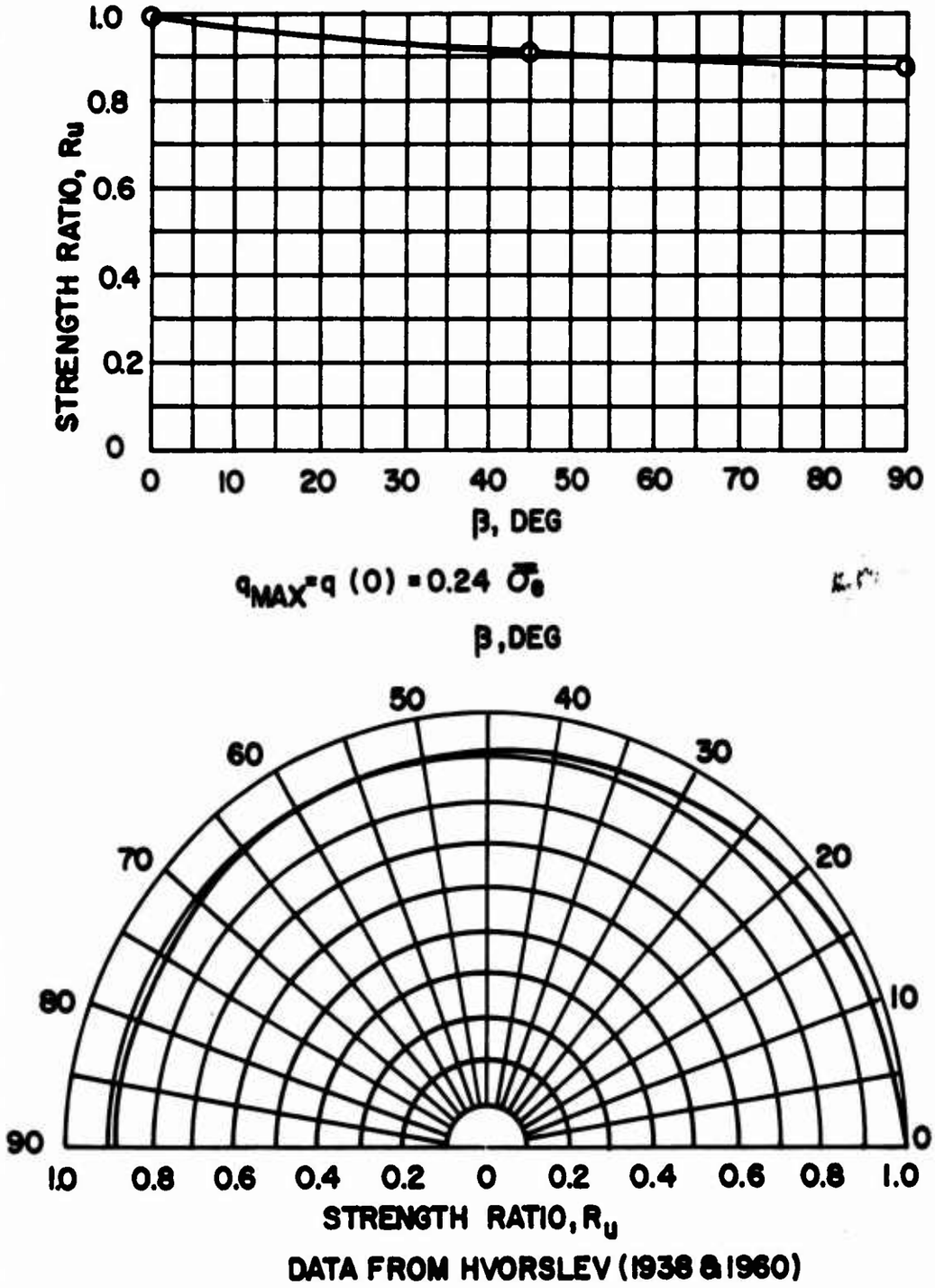

FIGURE 3.17 (a)

ANISOTROPIC STRENGTH RATIO R_u FOR VIENNA CLAY IX

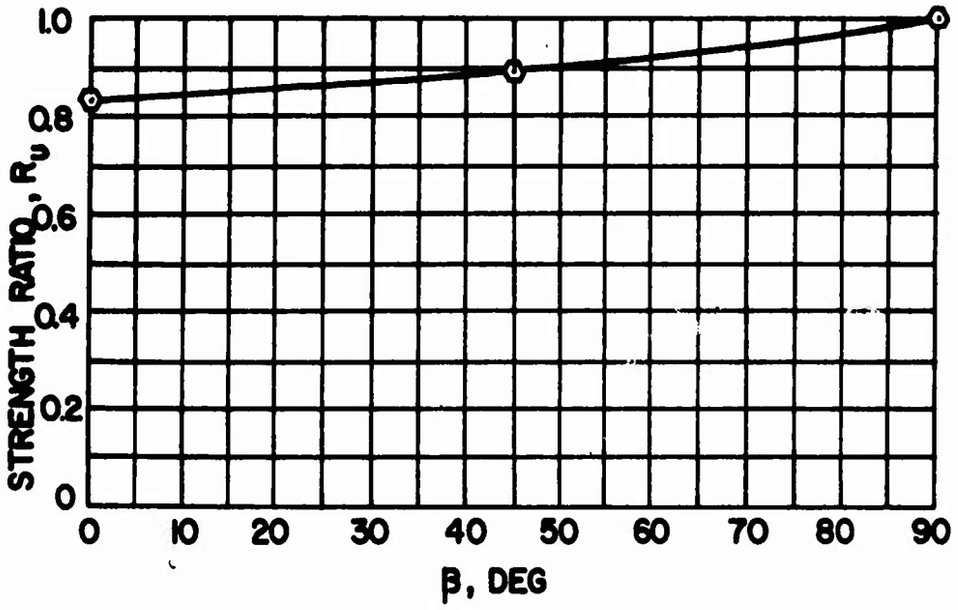

$q_{MAX} = q(90) = 0.23\ \overline{\sigma_e}$

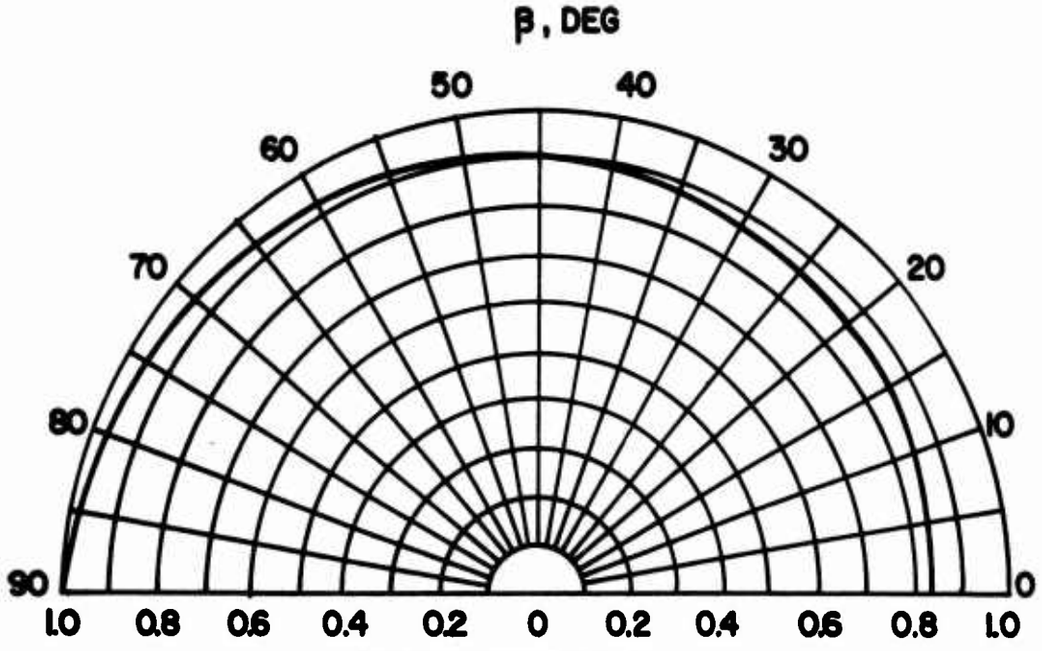

DATA FROM HVORSLEV (1938 & 1960)

FIGURE 3.17 (b)

ANISOTROPIC STRENGTH RATIO R_u FOR LITTLE BELT CLAY III

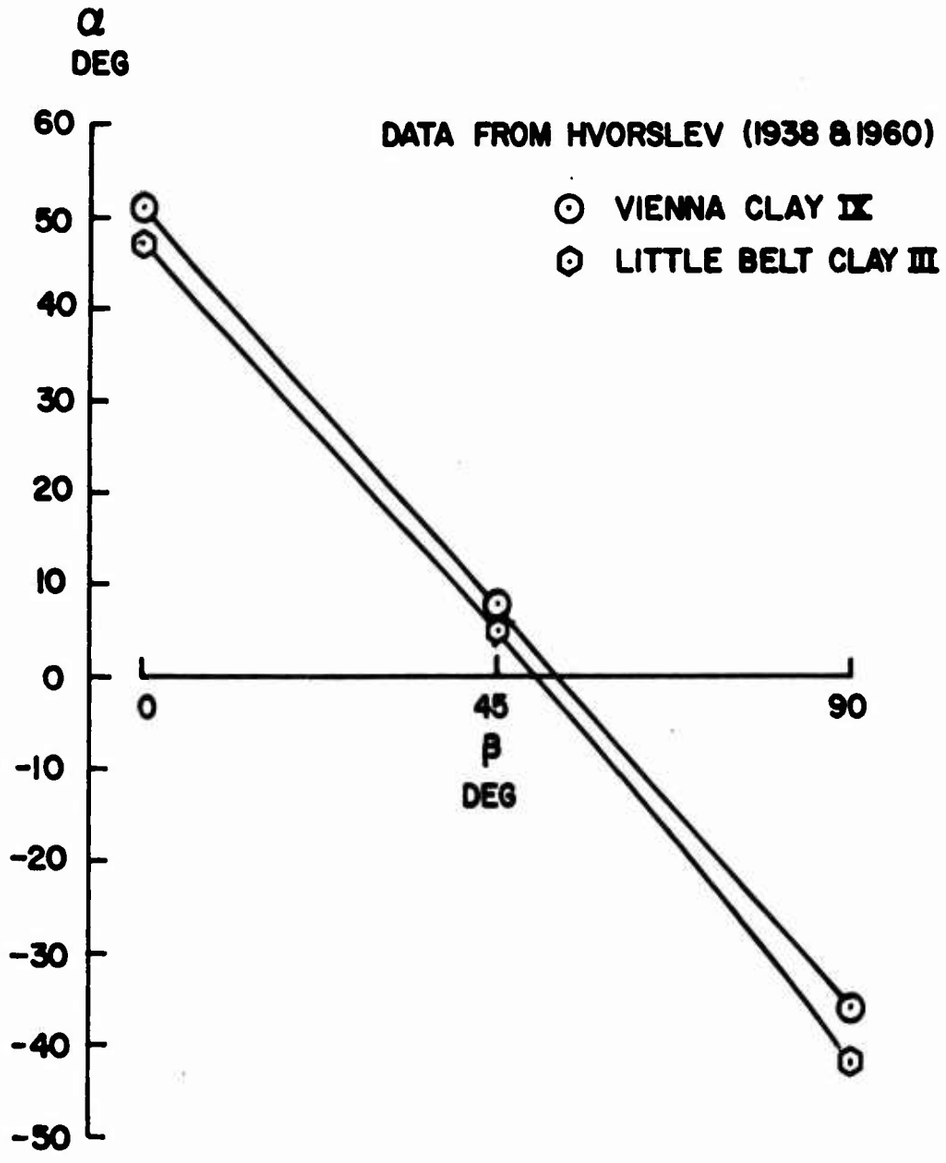

FIGURE 3.17 (c)

VARIATION OF FAILURE PLANE ORIENTATION FOR UNCONFINED COMPRESSION TESTS ON VIENNA AND LITTLE BELT CLAYS

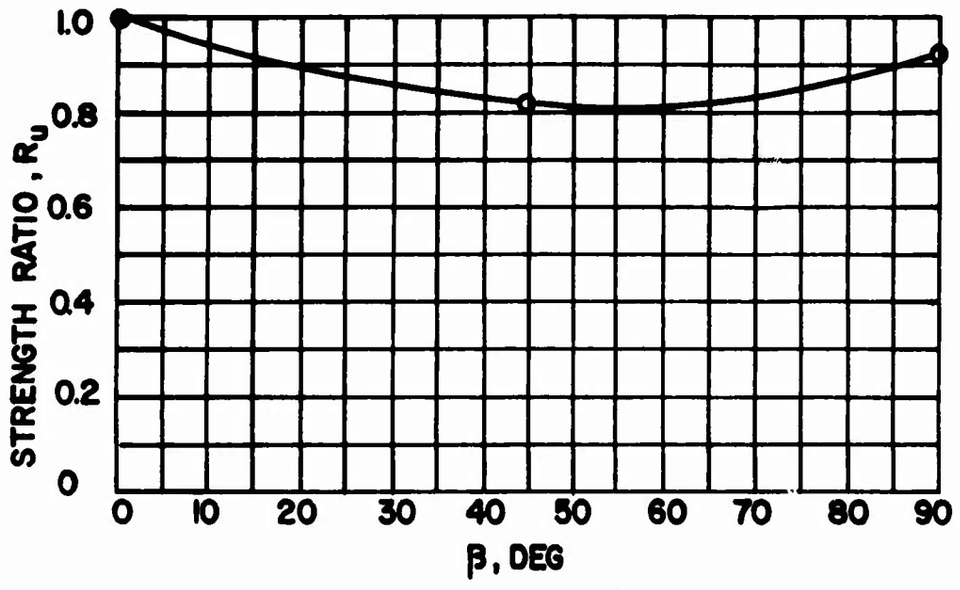

$q_{MAX} = q(0) = 0.226$ KG/CM^2

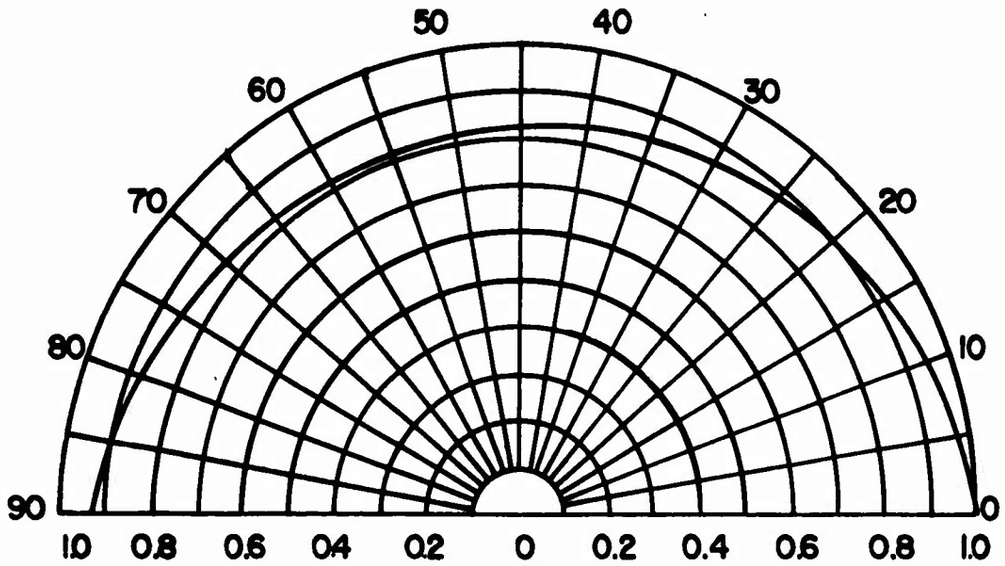

DATA FROM JAKOBSON (1952)

FIGURE 3.18

ANISOTROPIC STRENGTH RATIO R_u FOR VARVED CLAY FROM SURTE, SWEDEN

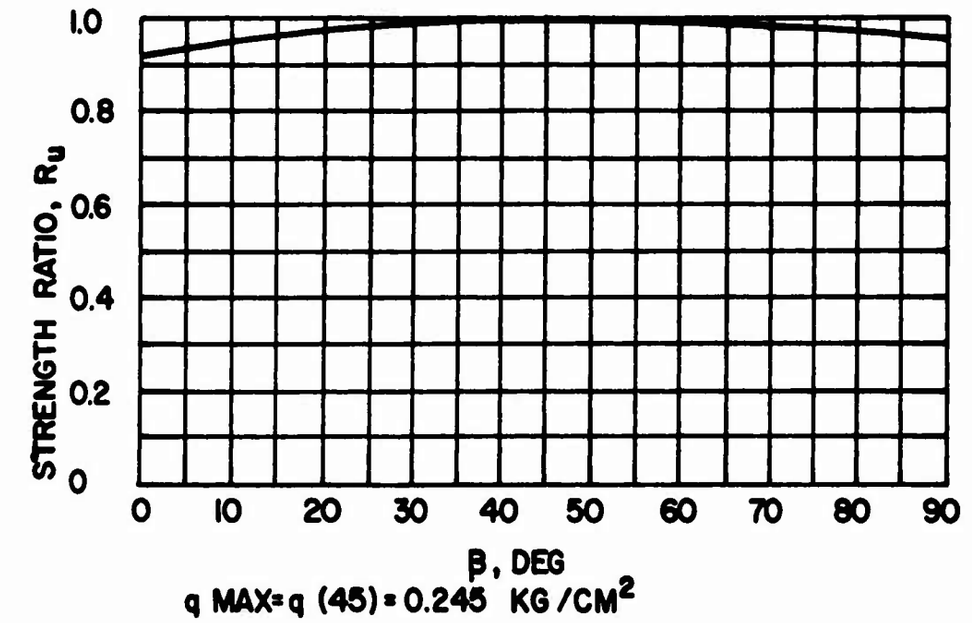

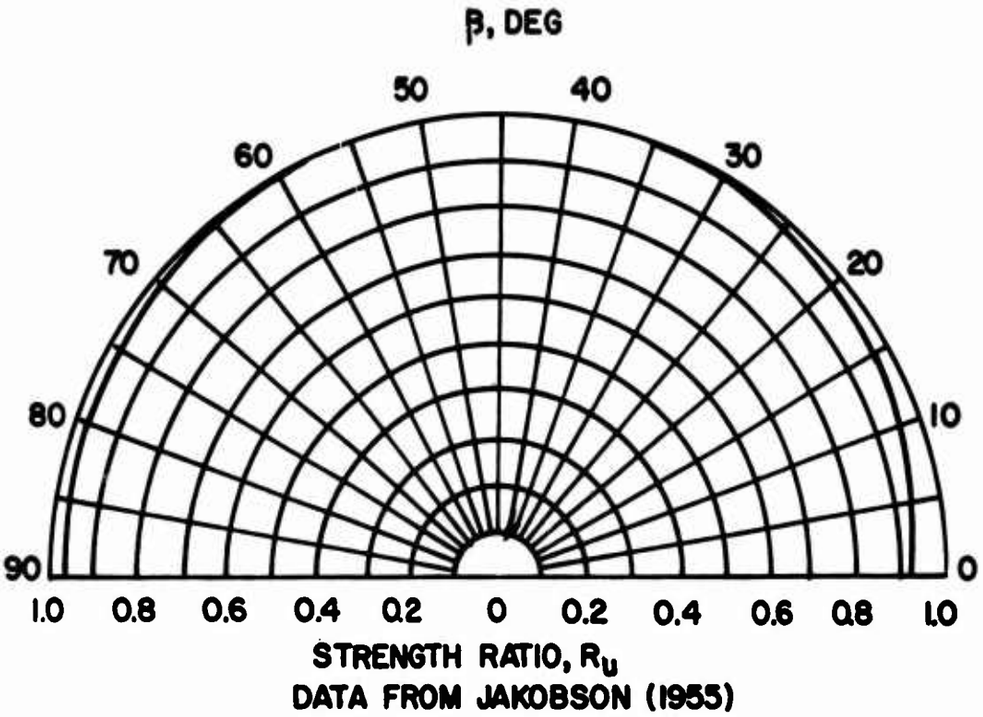

FIGURE 3.19

ANISOTROPIC STRENGTH RATIO R_u FOR HOMOGENEOUS CLAY FROM SALA, SWEDEN

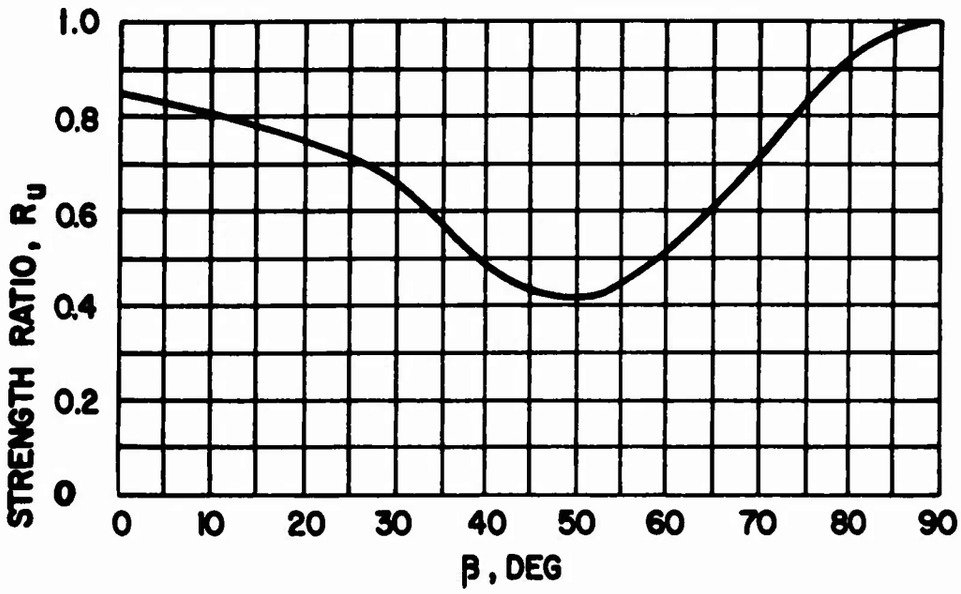

$q_{MAX} = q\ (90) = 11.2$ PSI

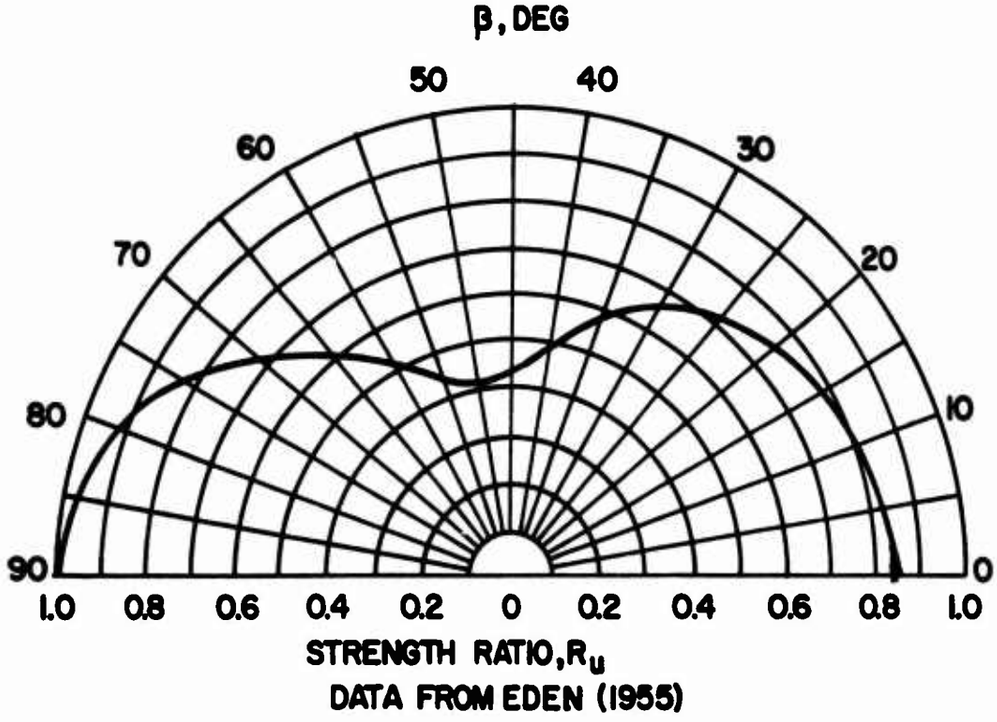

DATA FROM EDEN (1955)

FIGURE 3.20 (a)

ANISOTROPIC STRENGTH RATIO R_u FOR VARVED CLAY FROM STEEP ROCK LAKE, ONTARIO, SAMPLE 2-62

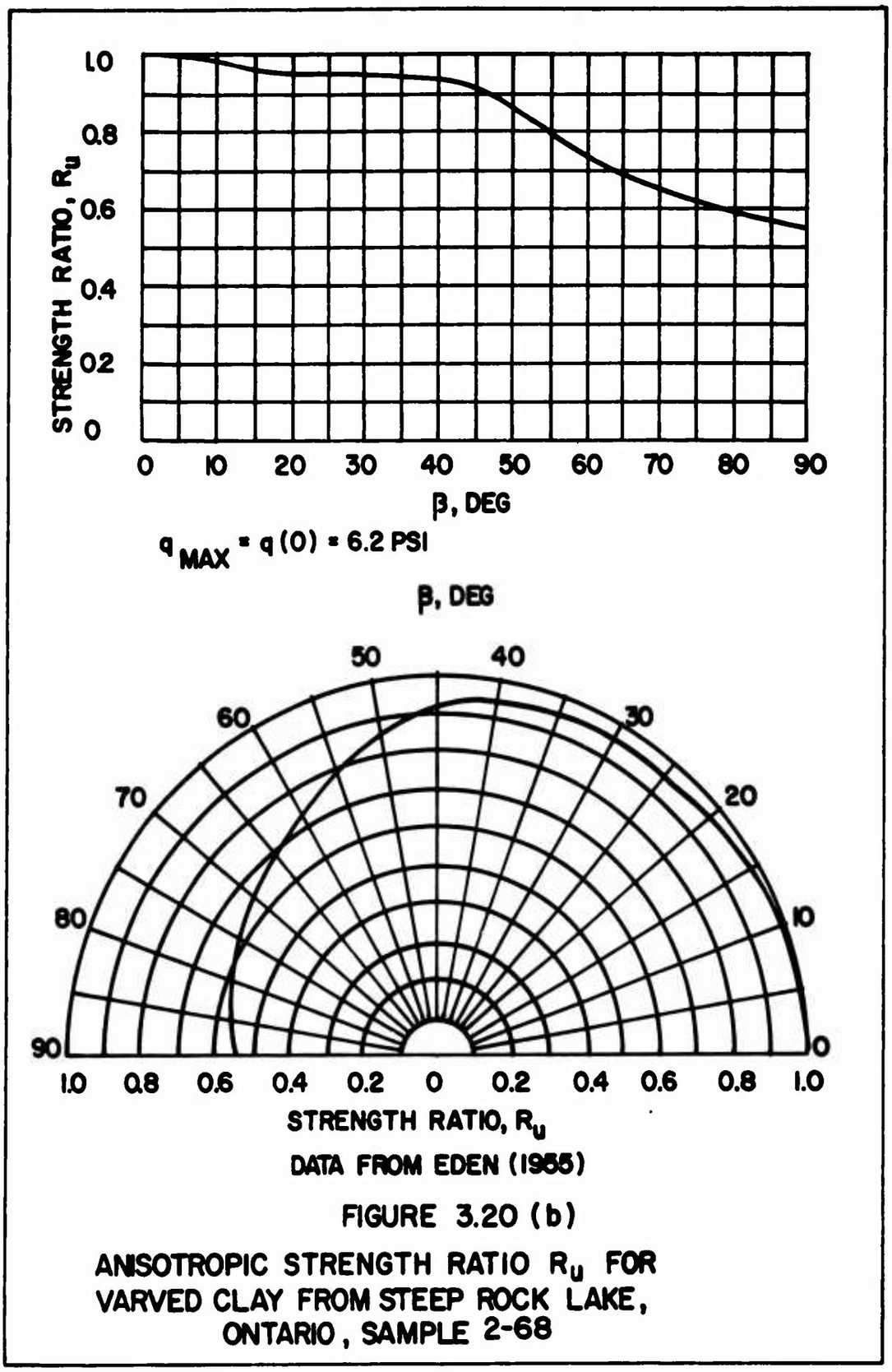

FIGURE 3.20 (b)

ANISOTROPIC STRENGTH RATIO R_u FOR VARVED CLAY FROM STEEP ROCK LAKE, ONTARIO, SAMPLE 2-68

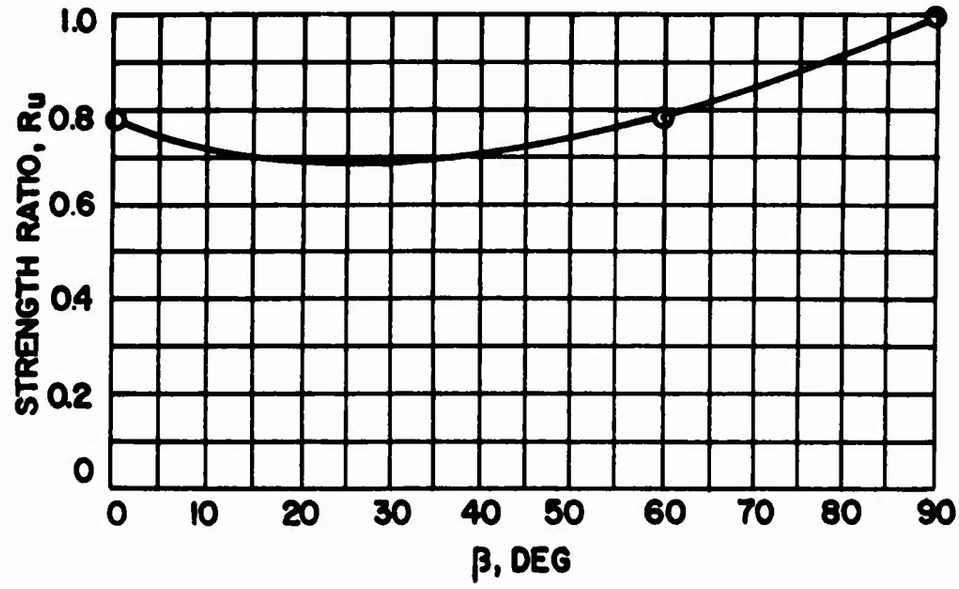

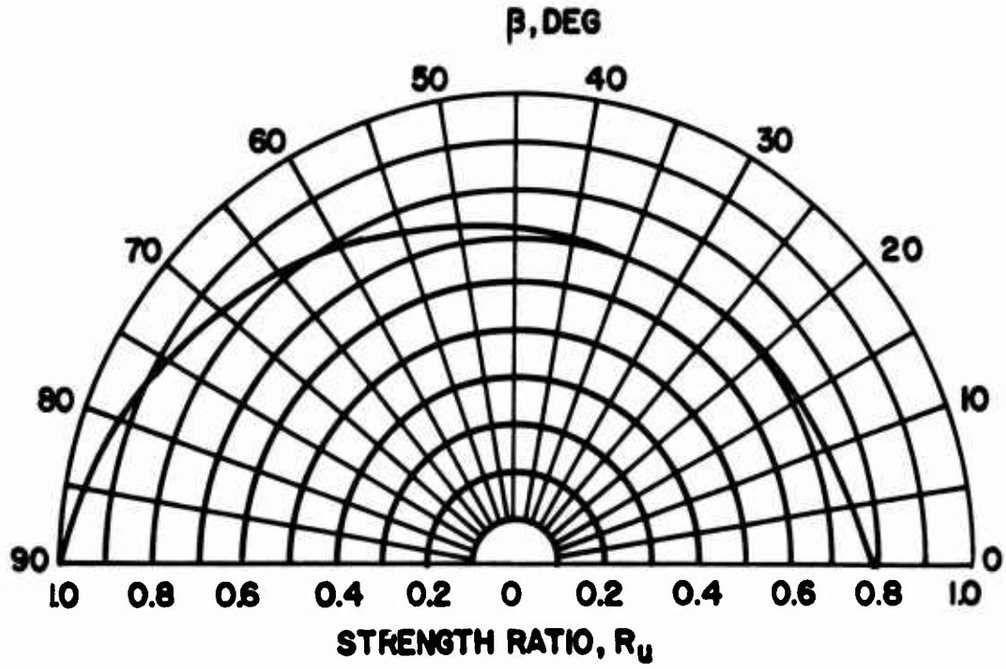

DATA FROM WARD ET. AL. (1959)

FIGURE 3.21

ANISOTROPIC STRENGTH RATIO R_u FOR LONDON CLAY

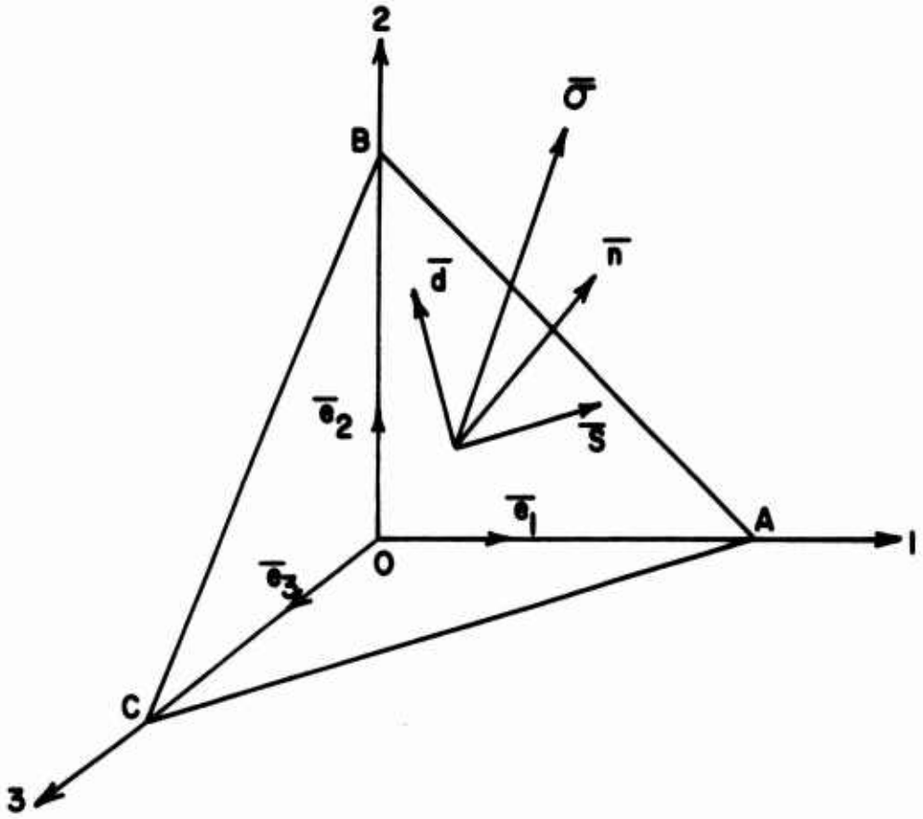

$\bar{n}$ = UNIT NORMAL TO PLANE ABC

$\bar{s}$ = UNIT VECTOR IN PLANE ABC, PARALLEL TO THE 1-3 PLANE

$\bar{d} = \bar{n} \times \bar{s}$, A THIRD UNIT VECTOR, ALSO IN PLANE ABC

$\bar{\sigma}$ = STRESS VECTOR ACTING ON PLANE ABC

FIGURE 3.22

UNIT VECTORS USED TO DEFINE THE ORIENTATION OF THE SHEAR STRESS VECTOR ACTING ON AN ARBITRARY PLANE

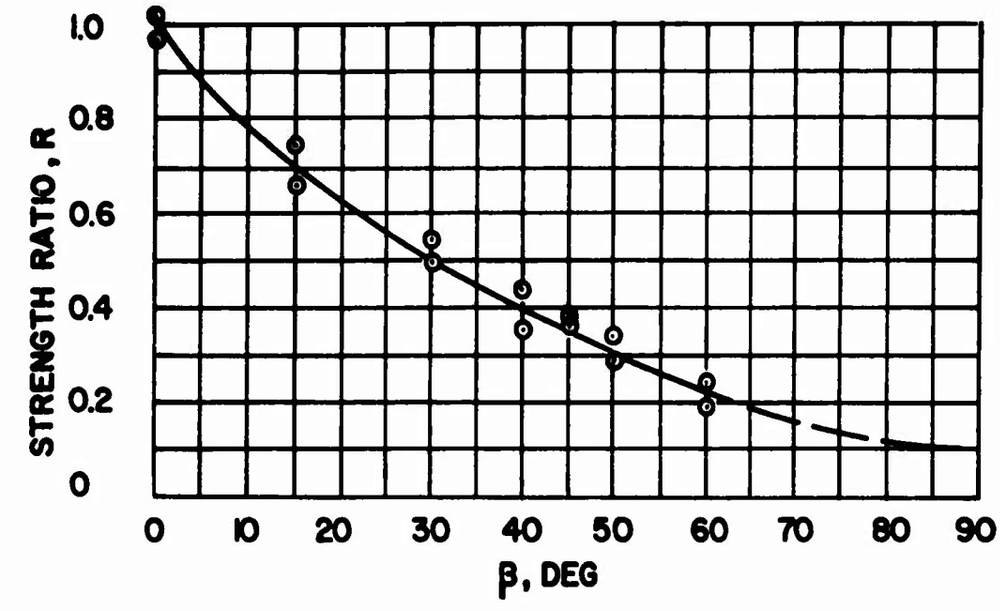

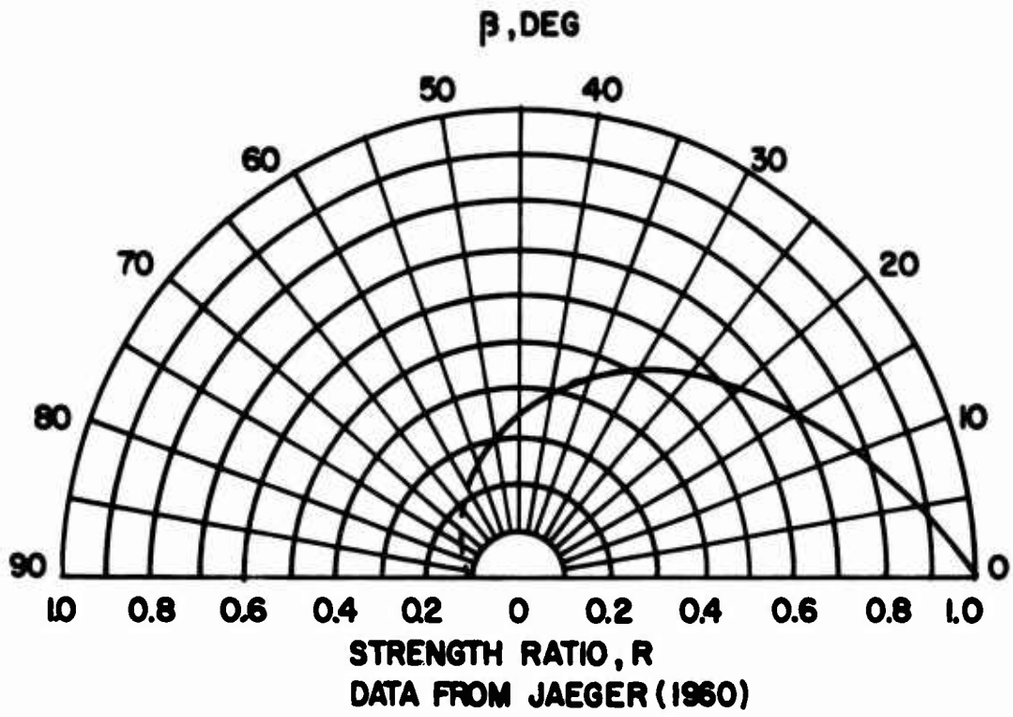

FIGURE 3.23 (a)

ANISOTROPIC STRENGTH RATIO R FOR SLATE

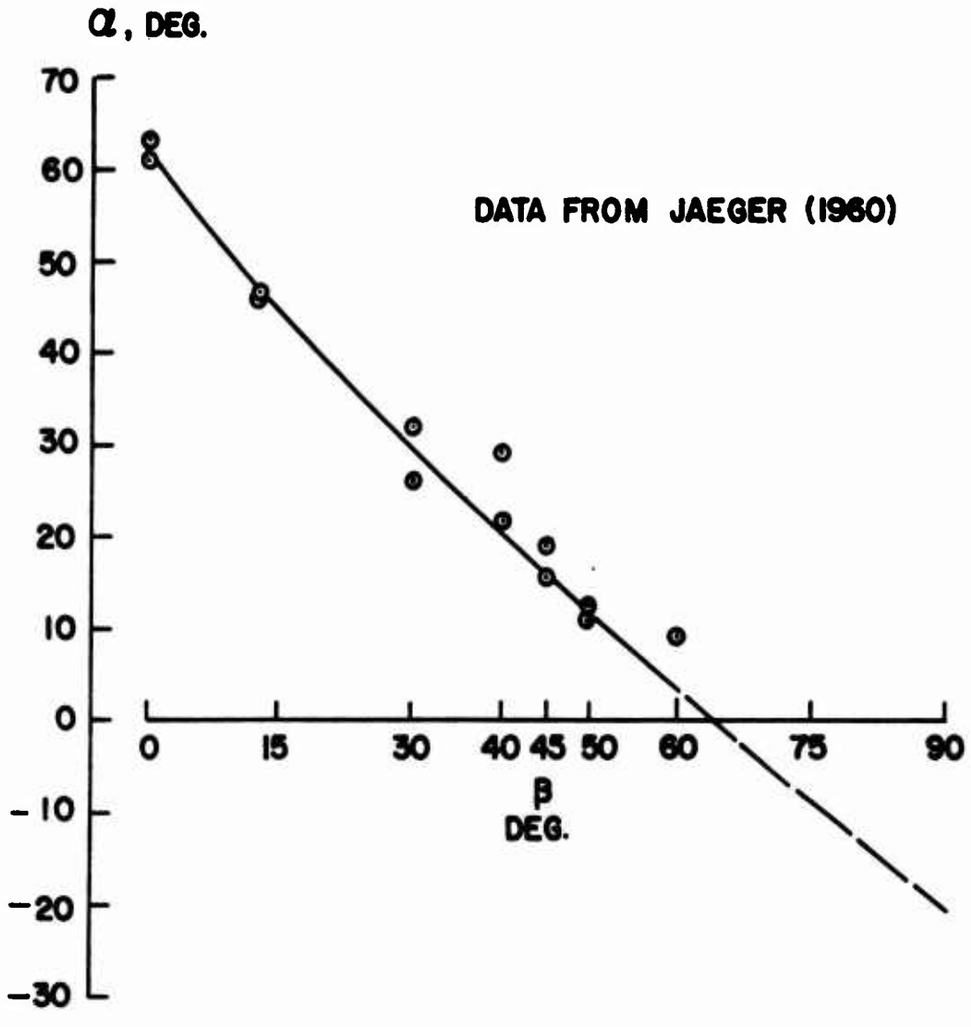

FIGURE 3.23 (b)
VARIATION OF FAILURE PLANE ORIENTATION FOR UNCONFINED COMPRESSIVE TESTS ON SLATE

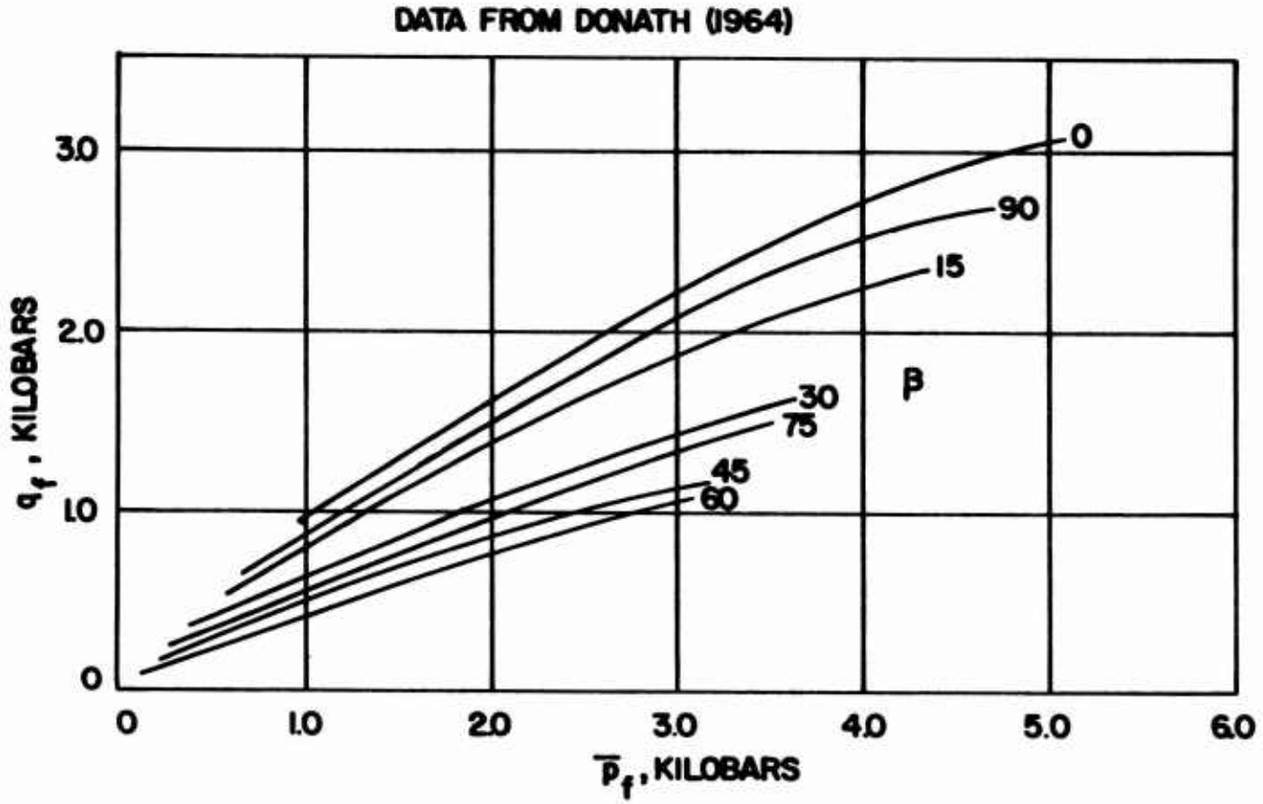

FIGURE 3.24 (a)

ANISOTROPIC STRENGTH DATA FROM TRIAXIAL COMPRESSION TESTS ON MARTINSBURG SLATE

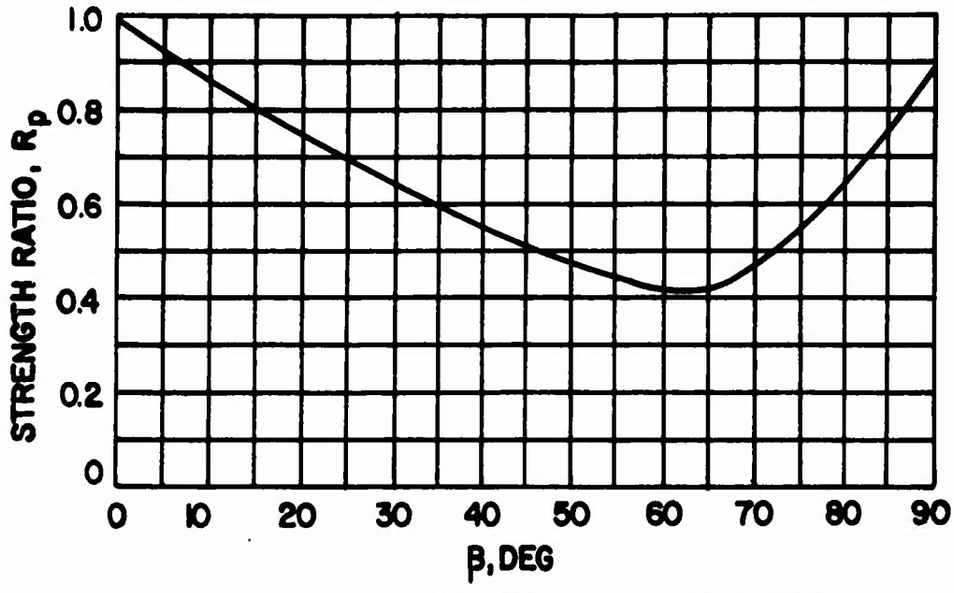

$q_{MAX} = q_f(0) = 0.98$ KBARS $\bar{p}_f = 1.0$ KBARS

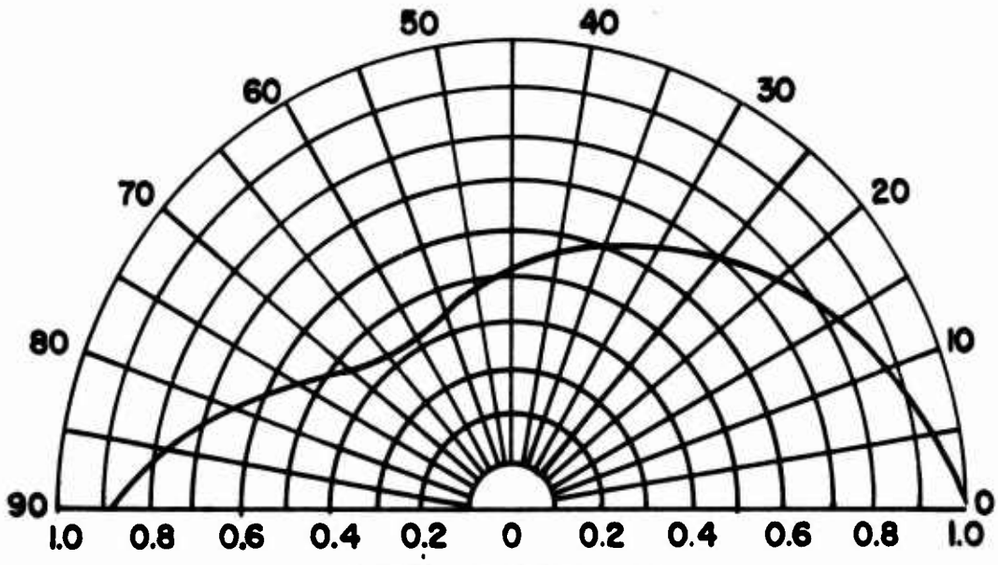

DATA FROM DONATH (1964)

FIGURE 3.24(b)

ANISOTROPIC STRENGTH RATIO R_p FOR MARTINSBURG SLATE

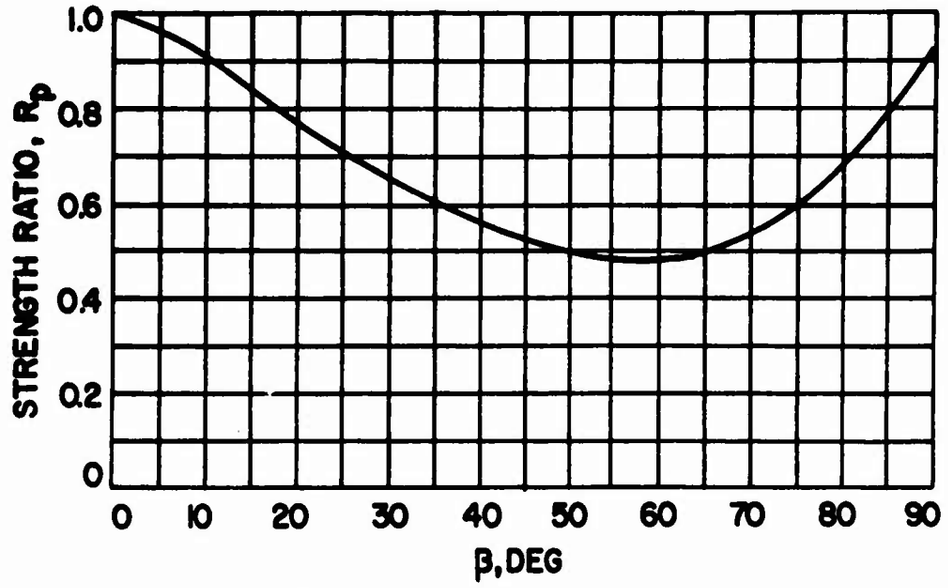

$q_{MAX} = q_f(0) = 1.62$ KBARS $\qquad \bar{p}_f = 2.0$ KBARS

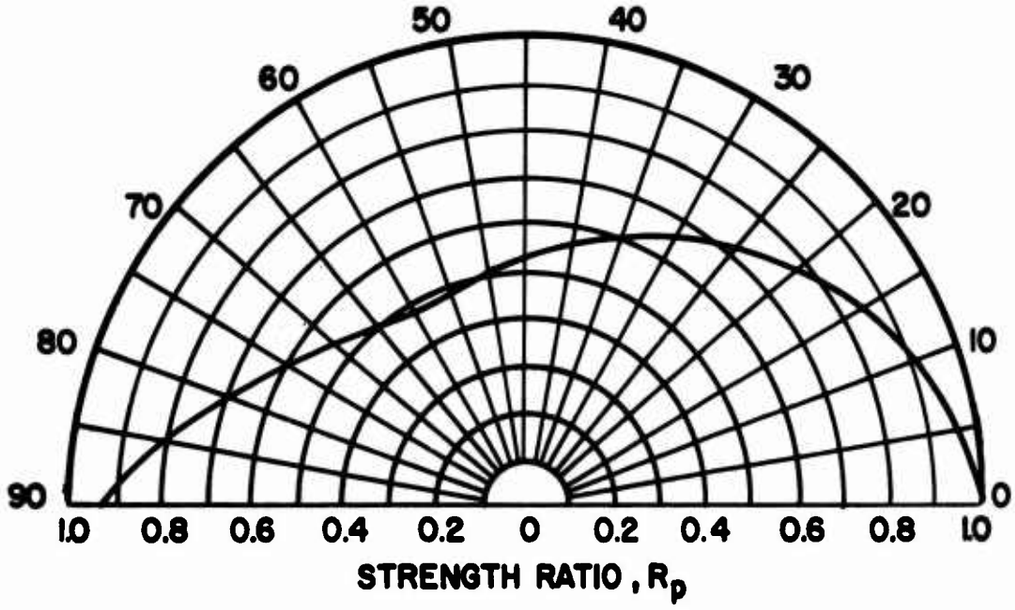

DATA FROM DONATH (1964)

FIGURE 3.24(c)

ANISOTROPIC STRENGTH RATIO R_p FOR MARTINSBURG SLATE

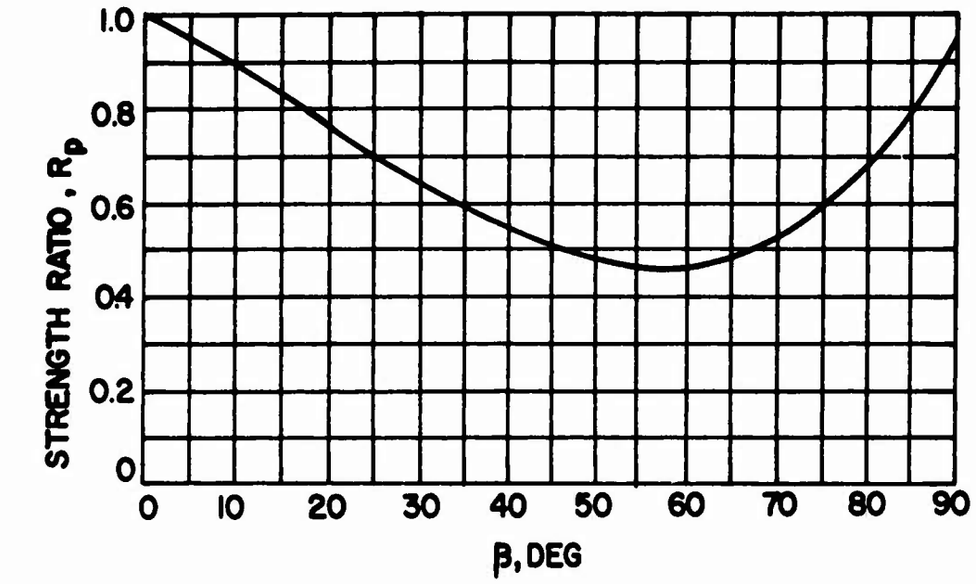

$q_{MAX} = q_f(0) = 2.22$ KBARS $\quad p_f = 3.0$ KBARS

β, DEG

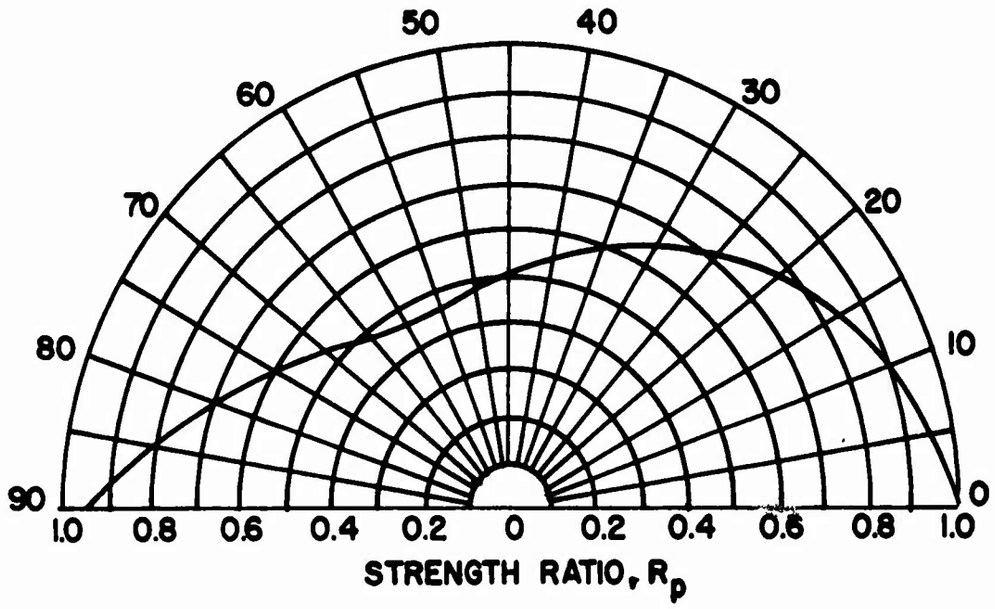

DATA FROM DONATH (1964)

FIGURE 3.24(d)

ANISOTROPIC STRENGTH RATIO R_p FOR MARTINSBURG SLATE

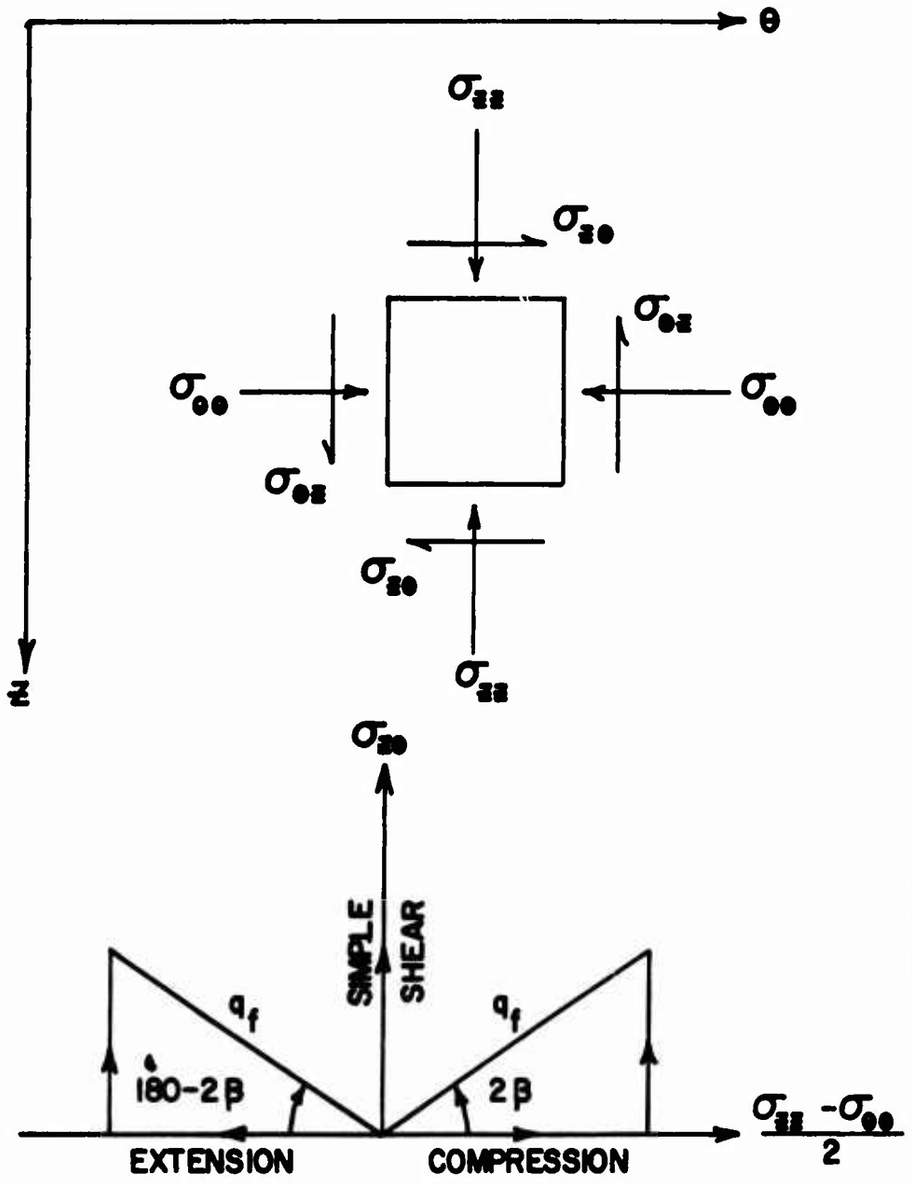

FIGURE 3.25

ROTATION OF PRINCIPAL PLANES IN THE HOLLOW CYLINDER TEST

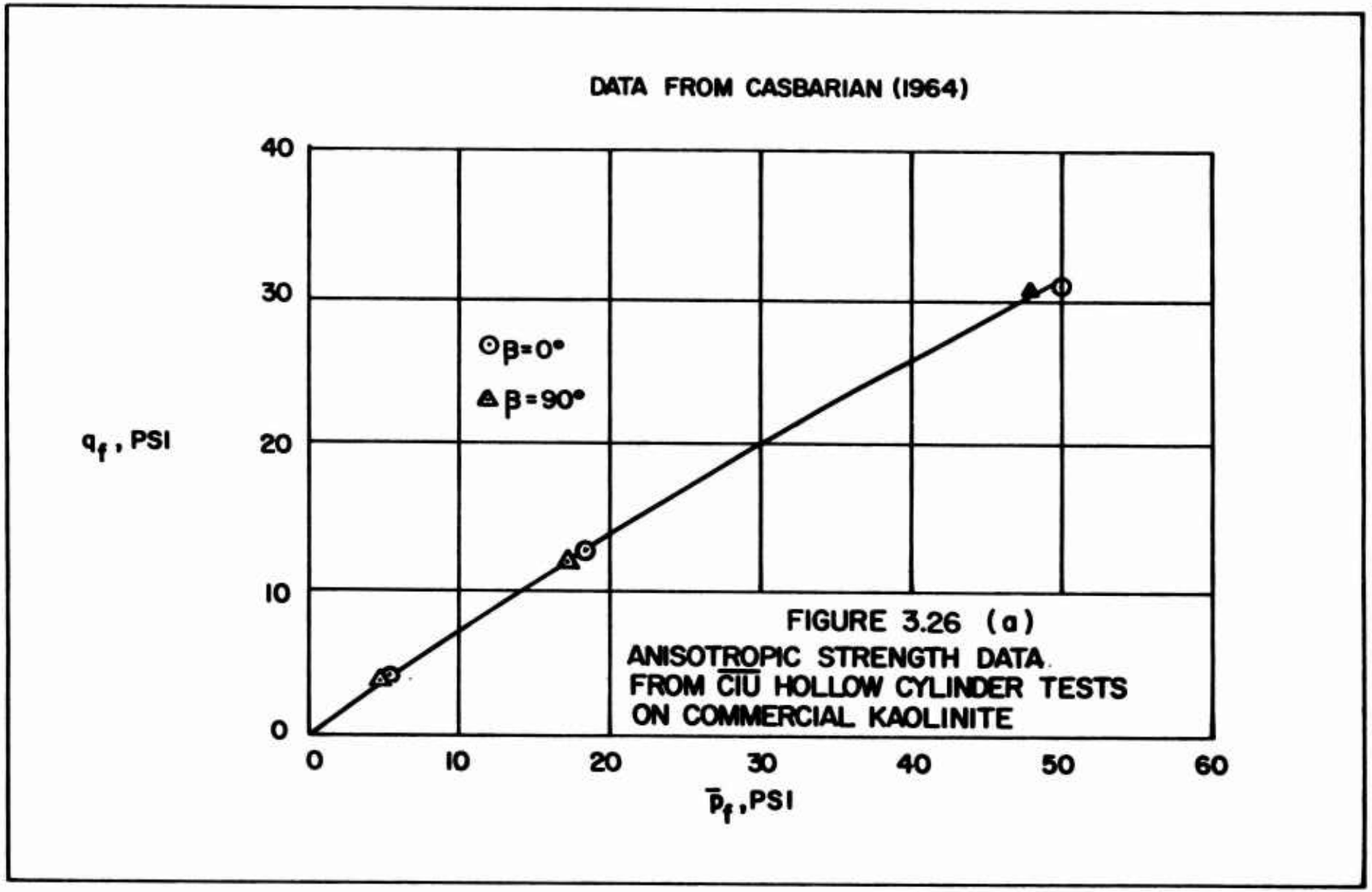

FIGURE 3.26 (a)
ANISOTROPIC STRENGTH DATA FROM $\overline{CIU}$ HOLLOW CYLINDER TESTS ON COMMERCIAL KAOLINITE

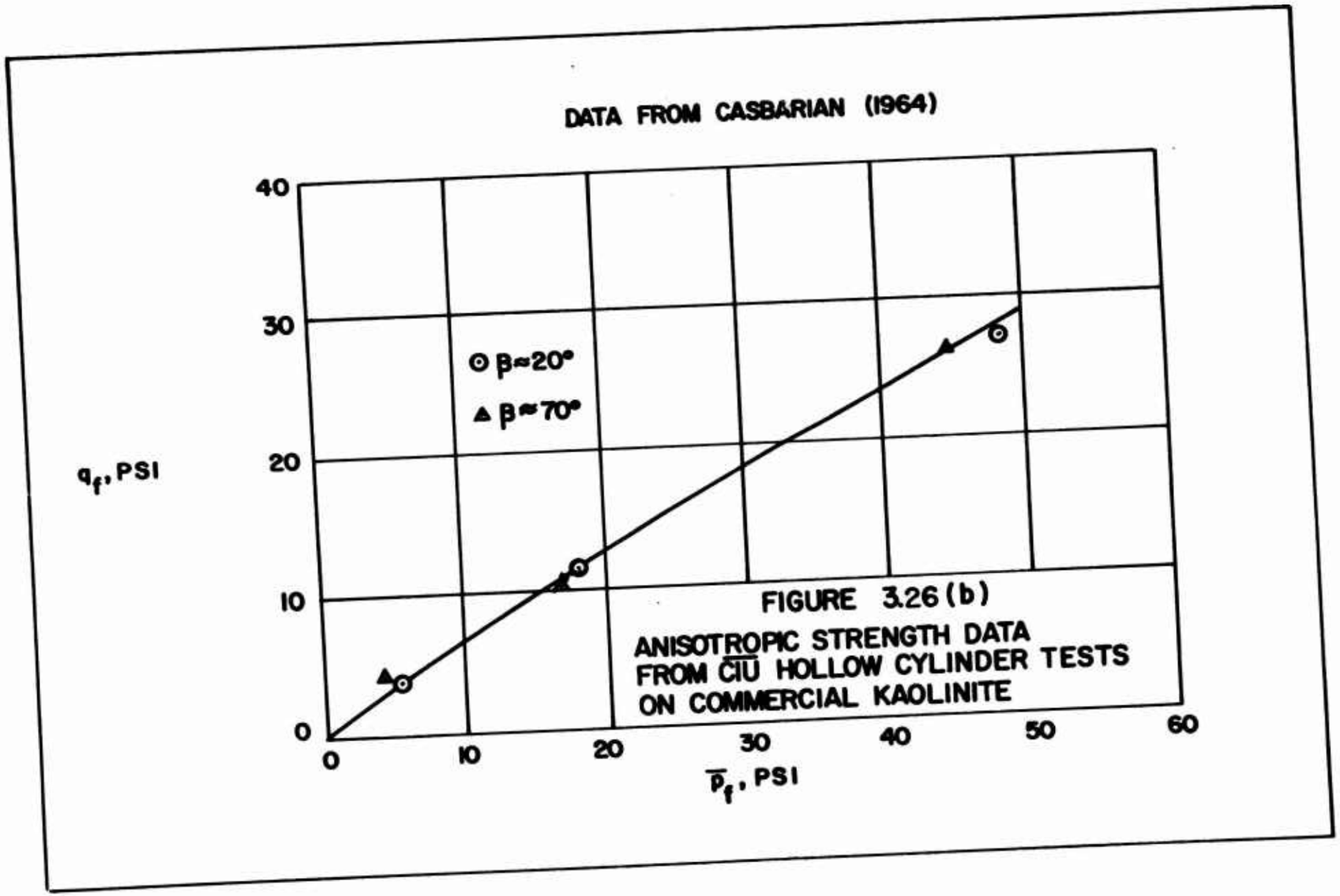

FIGURE 3.26 (b)
ANISOTROPIC STRENGTH DATA FROM $\overline{CIU}$ HOLLOW CYLINDER TESTS ON COMMERCIAL KAOLINITE

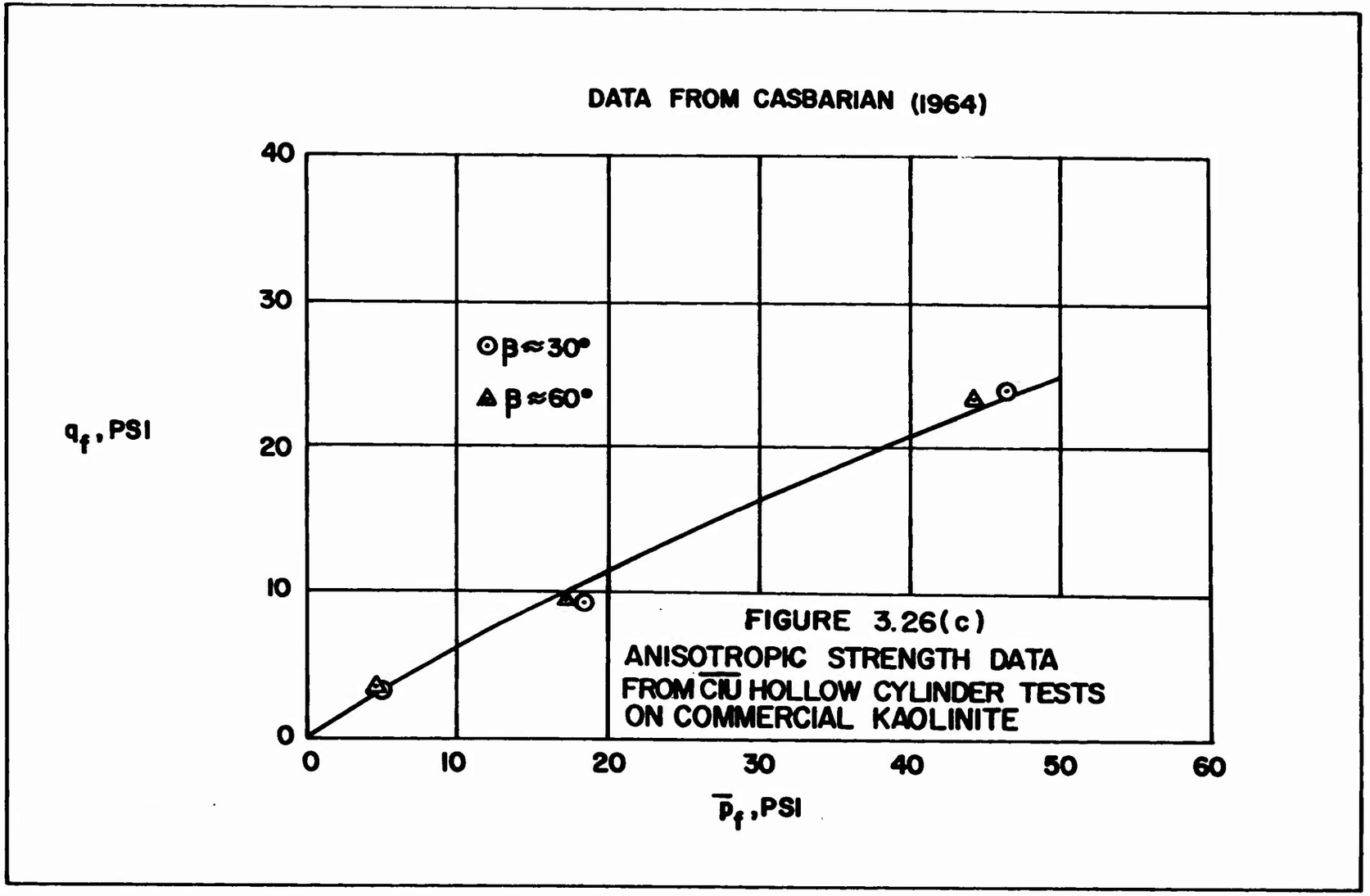
DATA FROM CASBARIAN (1964)
q_f, PSI
40
30
20
10
0
⊙ β≈30°
▲ β≈60°
0
10
20
30
40
50
60
$\bar{p}_f$, PSI
FIGURE 3.26(c)
ANISOTROPIC STRENGTH DATA
FROM $\overline{CIU}$ HOLLOW CYLINDER TESTS
ON COMMERCIAL KAOLINITE

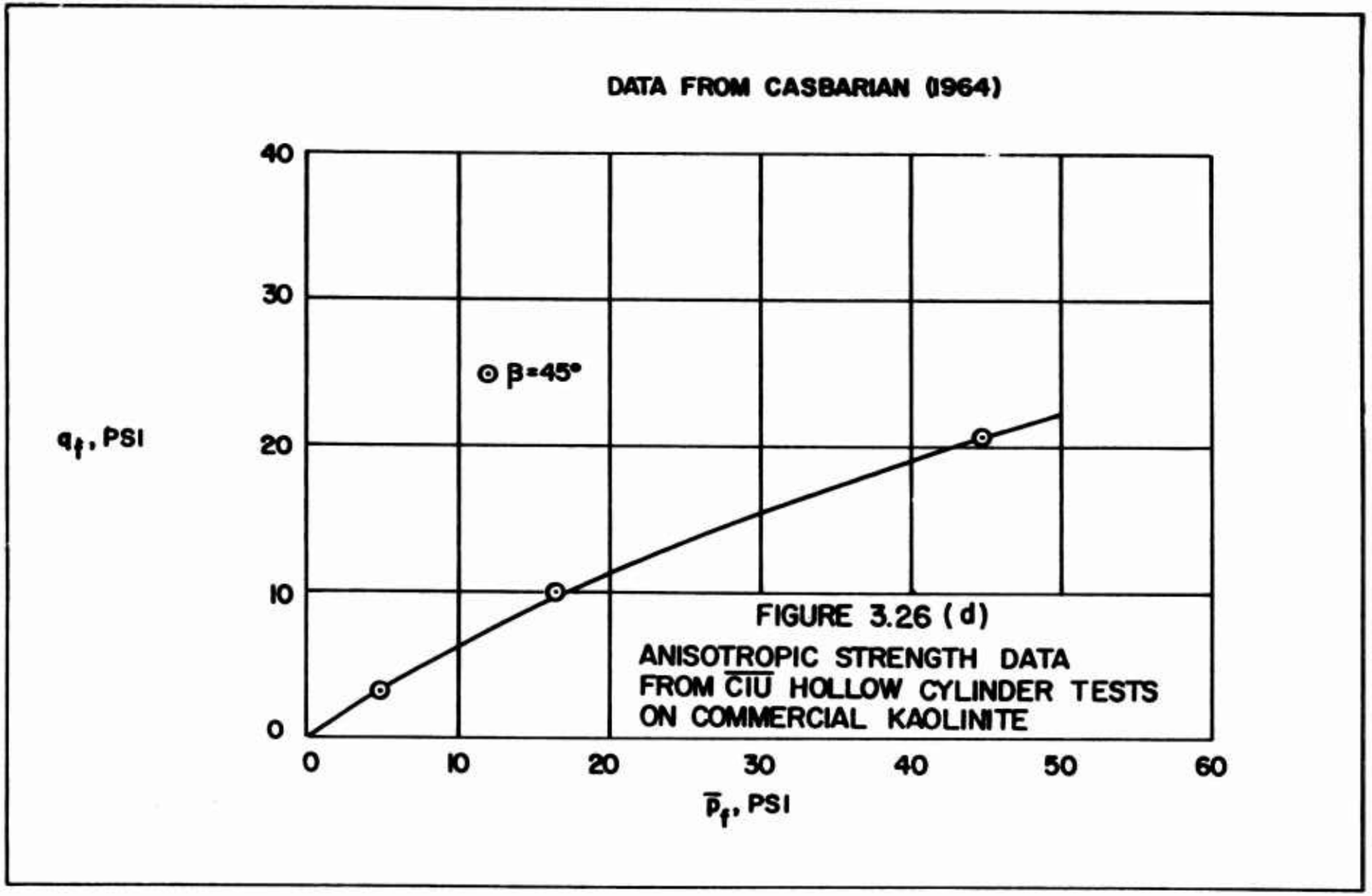

FIGURE 3.26 (d)
ANISOTROPIC STRENGTH DATA FROM $\overline{CIU}$ HOLLOW CYLINDER TESTS ON COMMERCIAL KAOLINITE

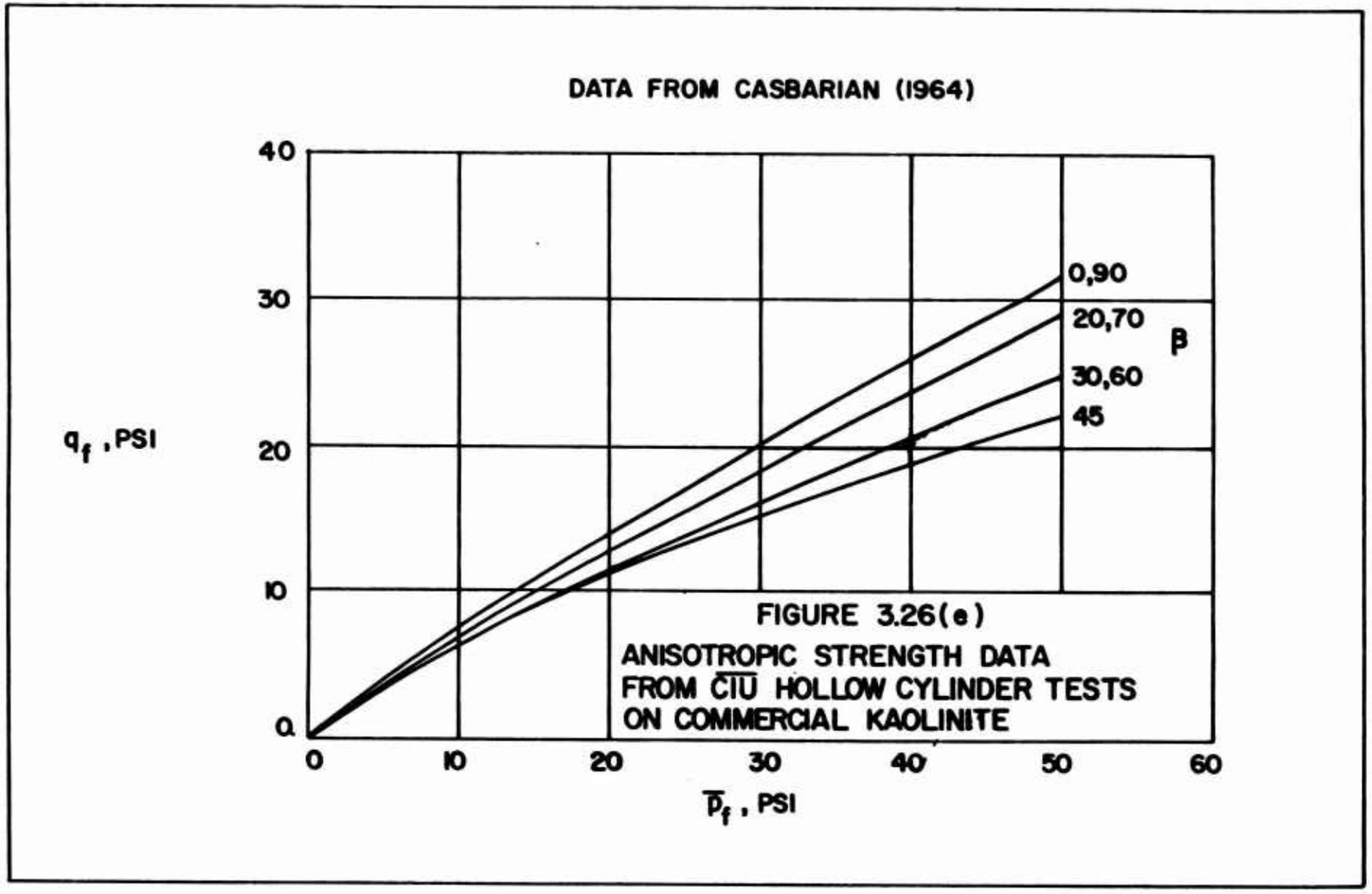

FIGURE 3.26(e)
ANISOTROPIC STRENGTH DATA FROM $\overline{CIU}$ HOLLOW CYLINDER TESTS ON COMMERCIAL KAOLINITE

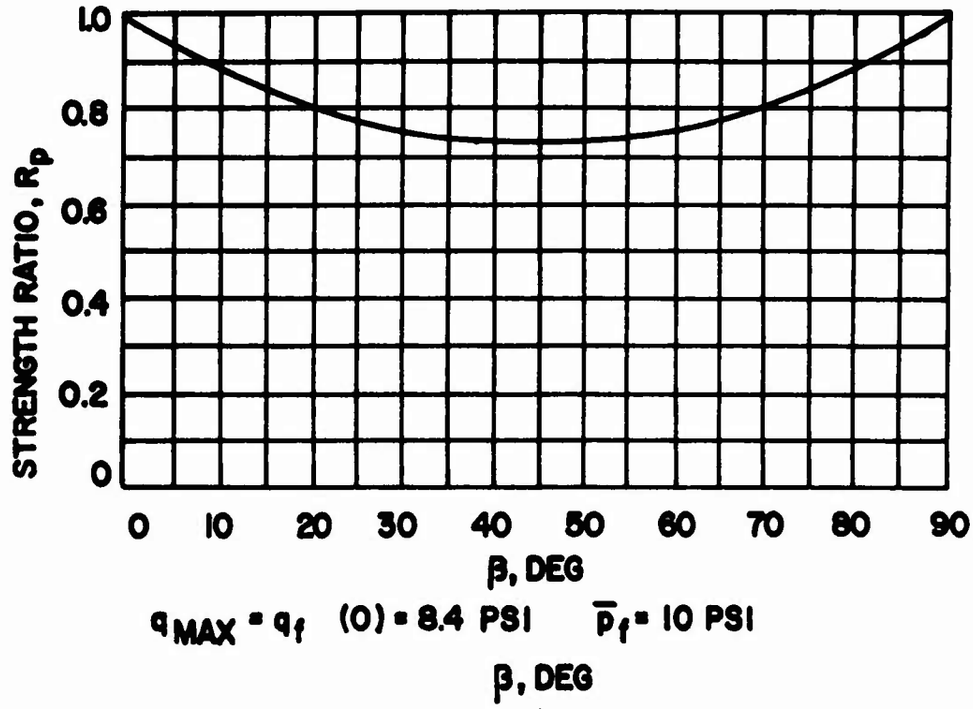

$q_{MAX} = q_f$ (0) = 8.4 PSI $\quad \bar{p}_f$ = 10 PSI

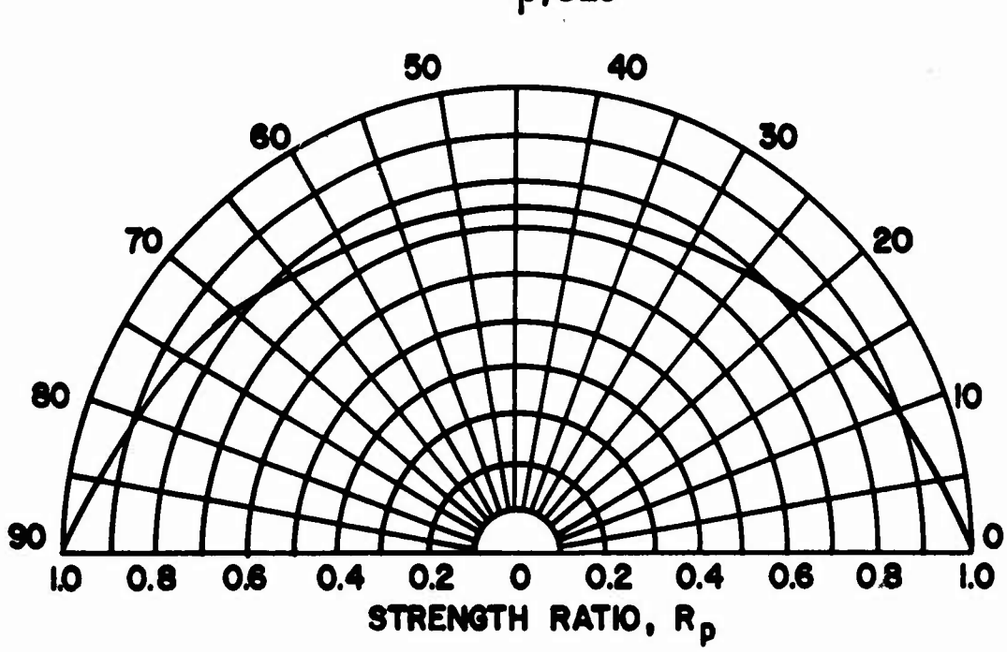

DATA FROM CASBARIAN (1964)

FIGURE 3.27 (a)

ANISOTROPIC STRENGTH RATIO R_p FOR COMMERCIAL KAOLINITE

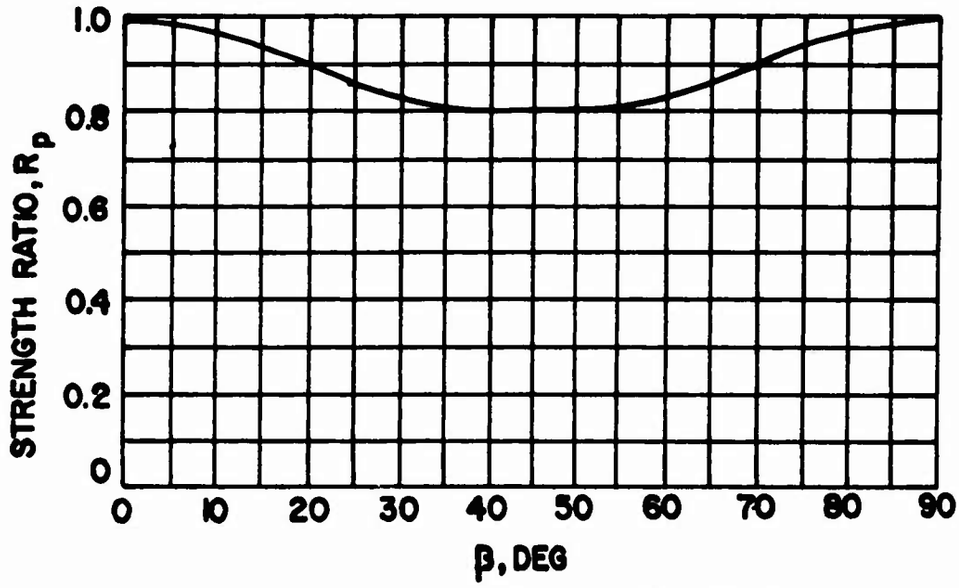

$q_{MAX} = q_f(0) = 14.0$ PSI $\quad \bar{p}_f = 20$ PSI

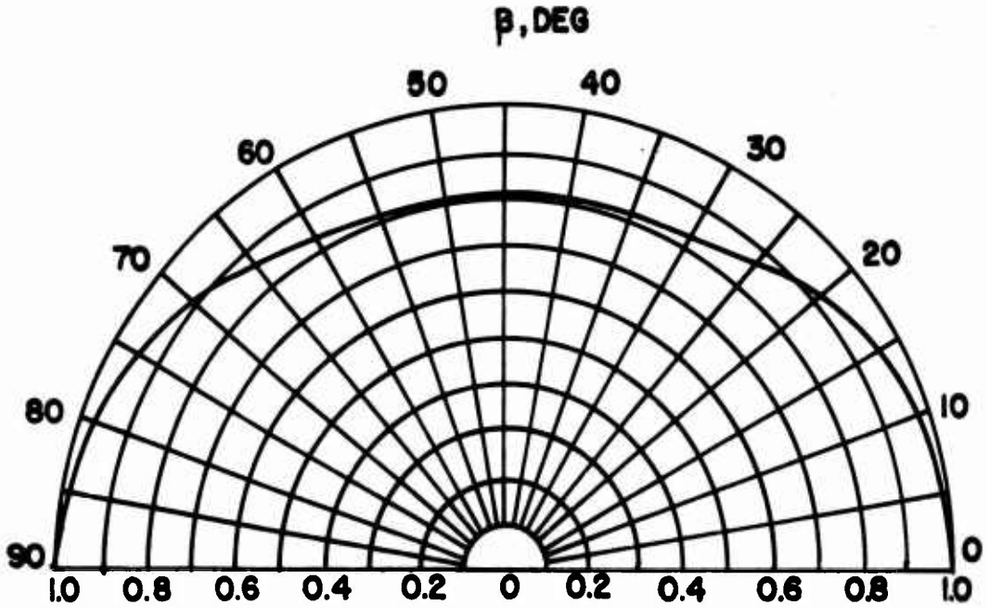

DATA FROM CASBARIAN (1964)

FIGURE 3.27 (b)

ANISOTROPIC STRENGTH RATIO R_p FOR COMMERCIAL KAOLINITE

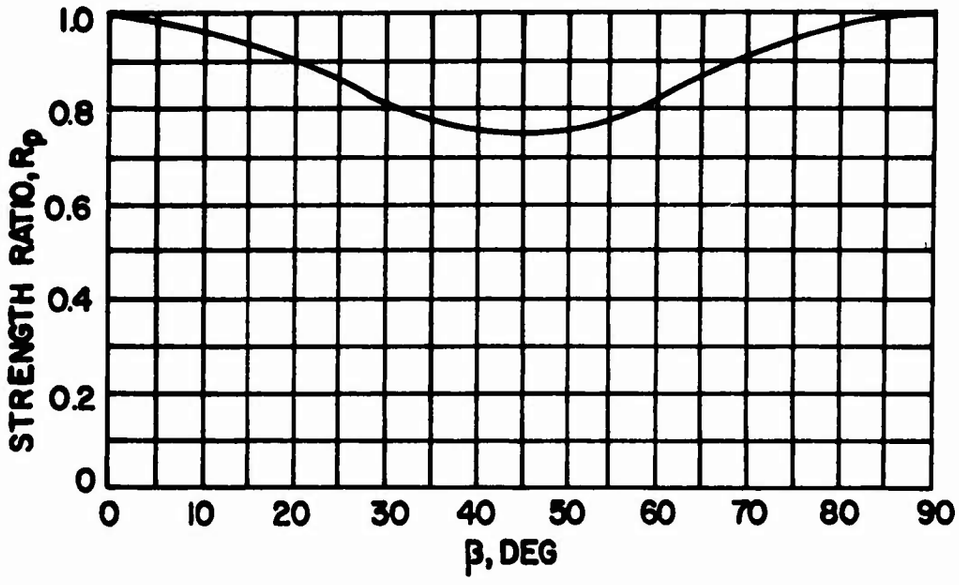

$q_{MAX} = q_f(0) = 20.0$ PSI $\quad \bar{p}_f = 30$ PSI

β, DEG

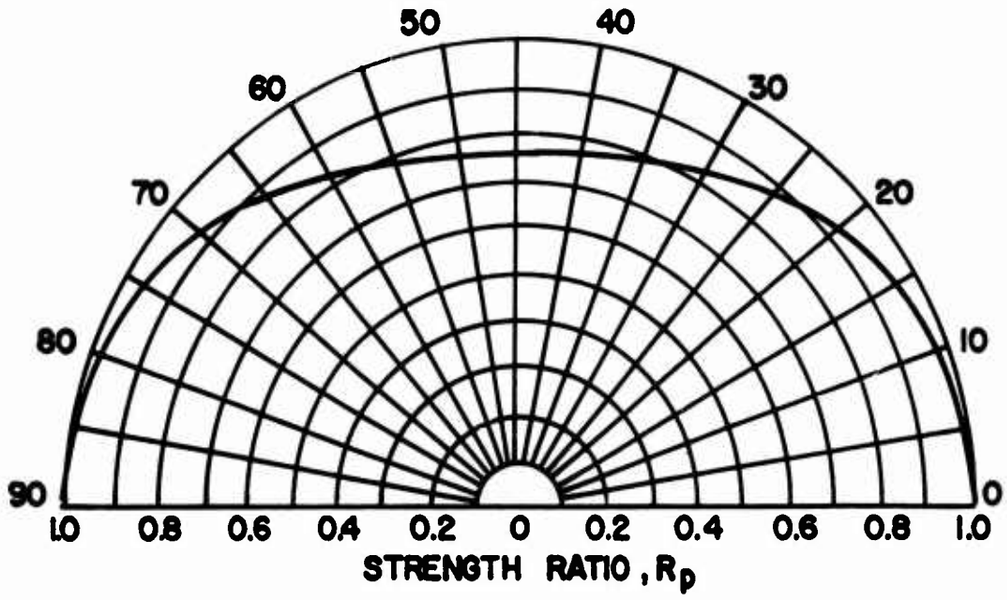

DATA FROM CASBARIAN (1964)

FIGURE 3.27 (c)

ANISOTROPIC STRENGTH RATIO R_β FOR COMMERCIAL KAOLINITE

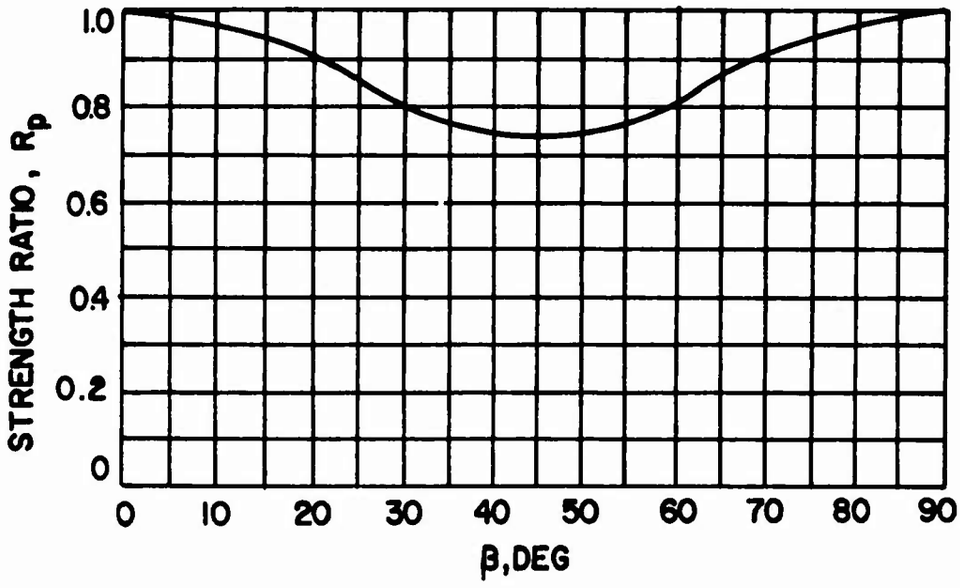

$q_{MAX} = q_f(0) = 25.8$ PSI $\quad \bar{p}_f = 40$ PSI

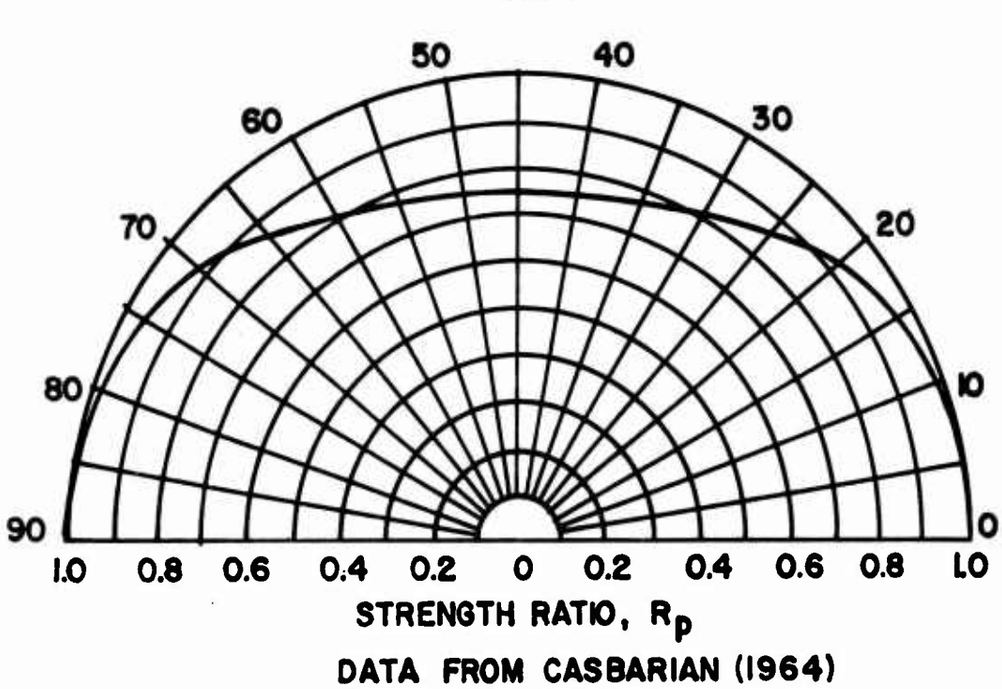

DATA FROM CASBARIAN (1964)

FIGURE 3.27 (d)

ANISOTROPIC STRENGTH RATIO R_p FOR COMMERCIAL KAOLINITE

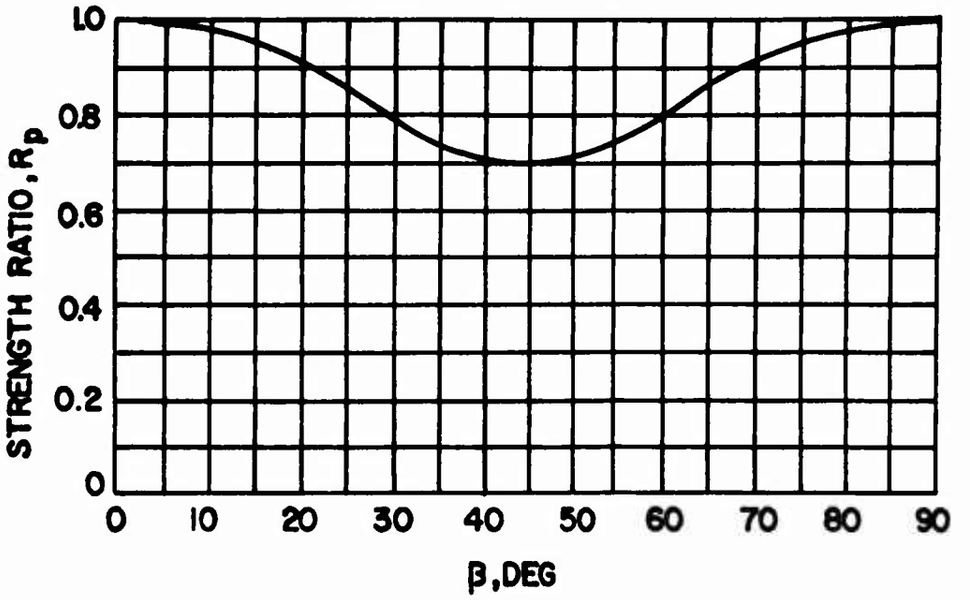

$q_{MAX} = q_f(0) = 31.5$ PSI $\quad \bar{p}_f = 50$ PSI

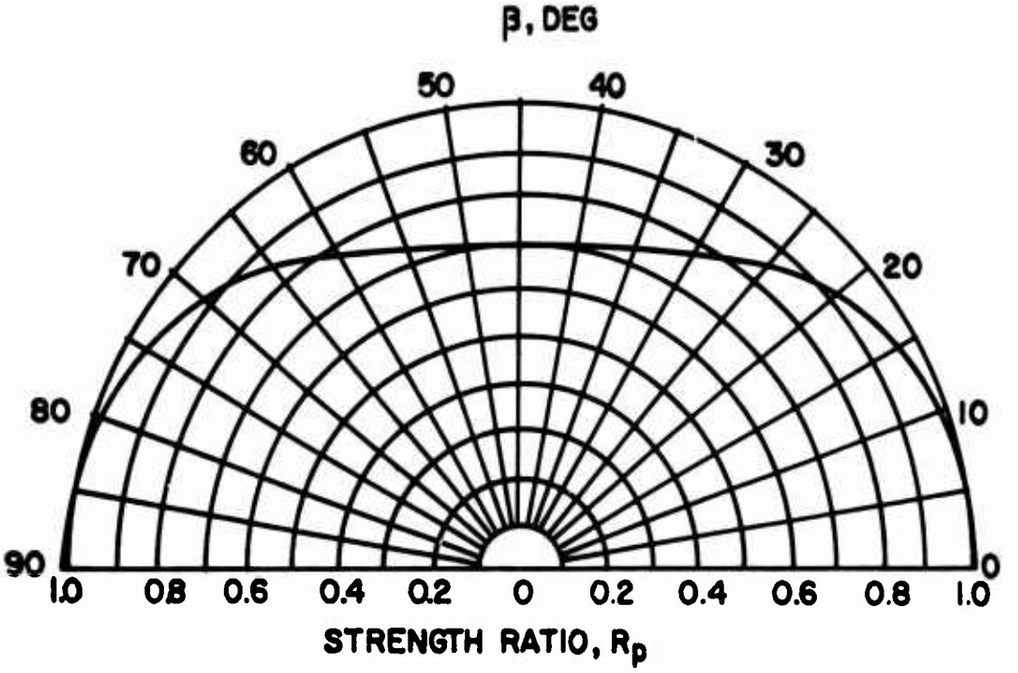

DATA FROM CASBARIAN (1964)

FIGURE 3.27(e)

ANISOTROPIC STRENGTH RATIO R_p FOR COMMERCIAL KAOLINITE

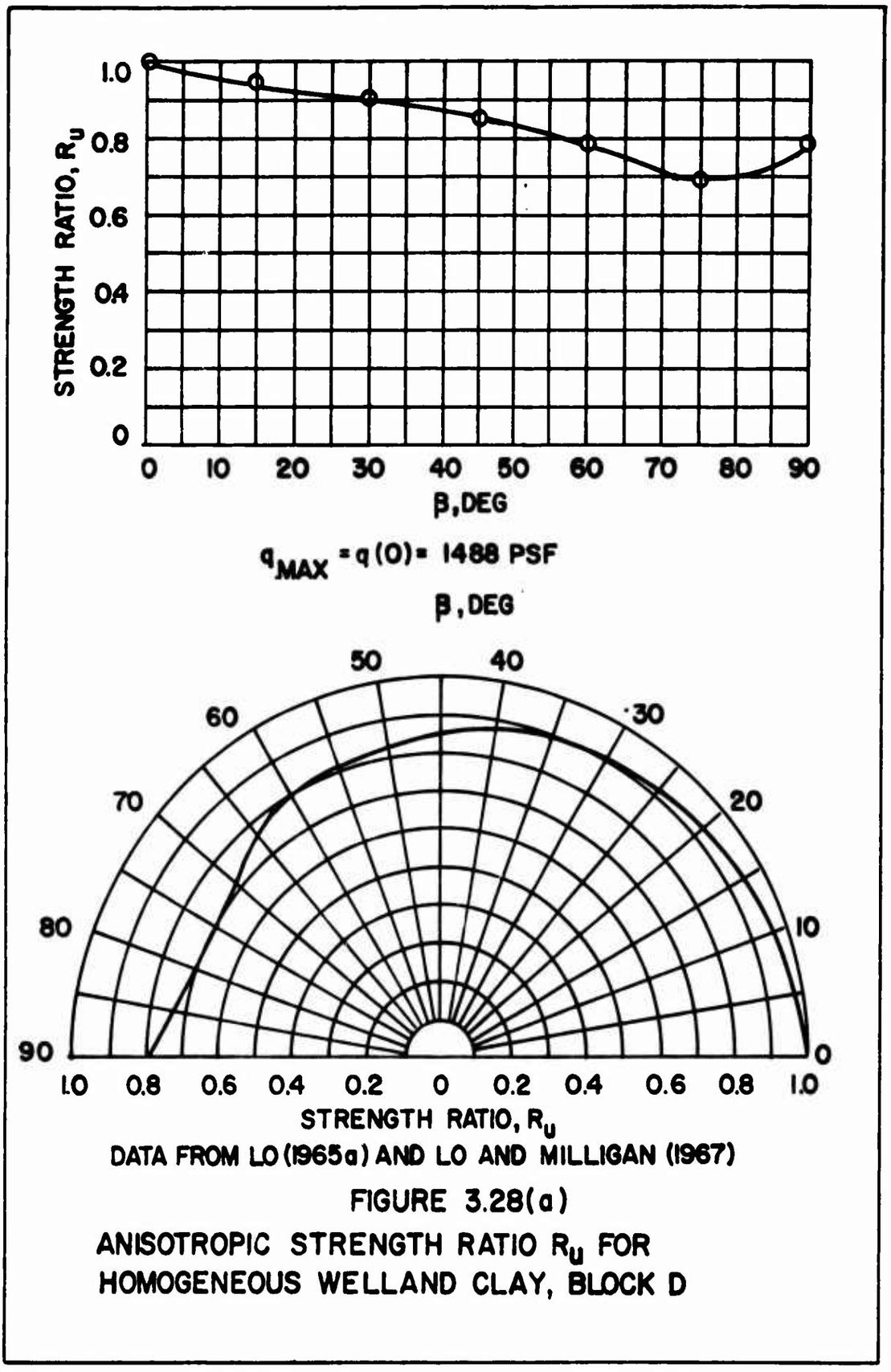

DATA FROM LO (1965a) AND LO AND MILLIGAN (1967)

FIGURE 3.28(a)

ANISOTROPIC STRENGTH RATIO R_u FOR HOMOGENEOUS WELLAND CLAY, BLOCK D

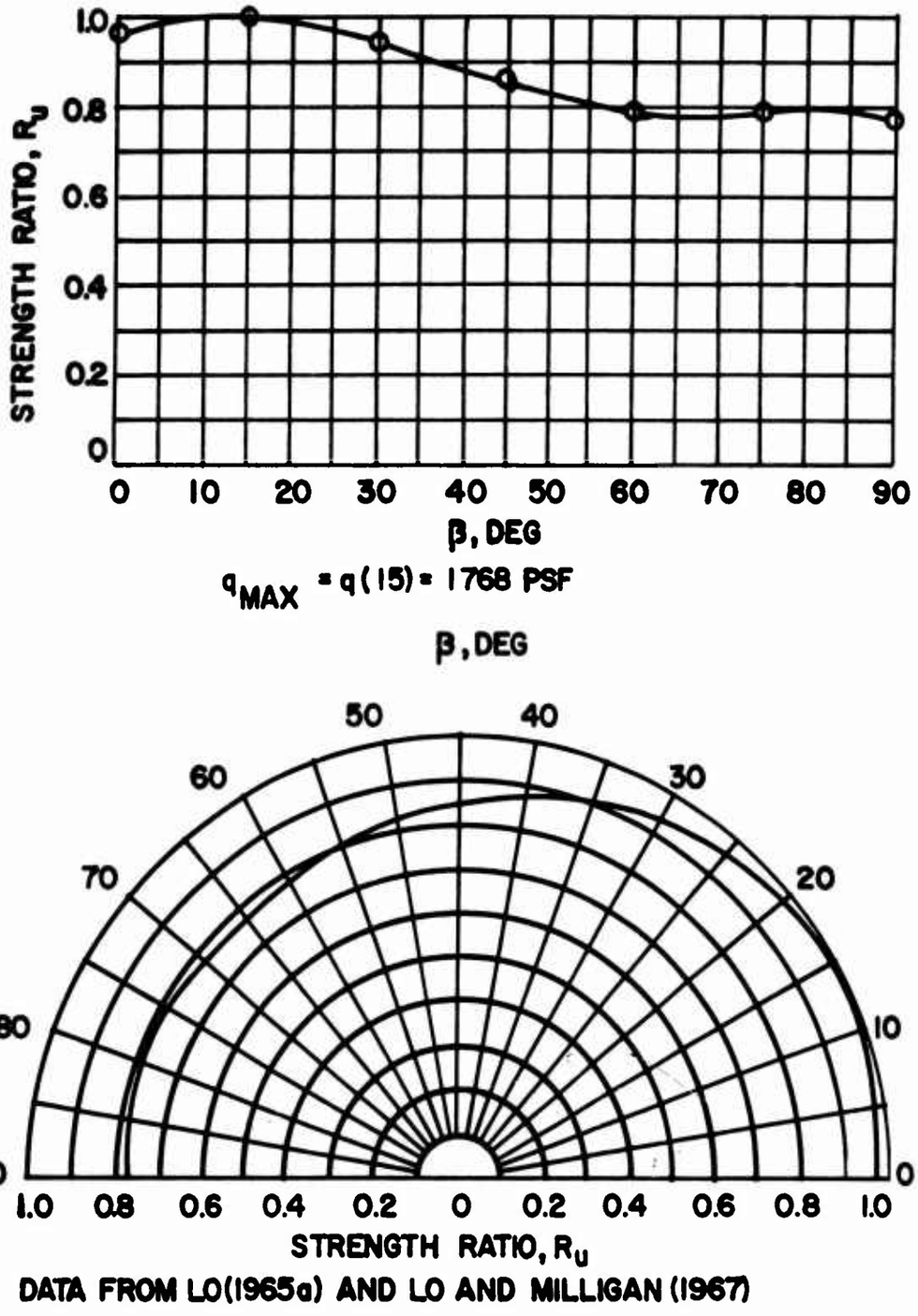

FIGURE 3.28(b)

ANISOTROPIC STRENGTH RATIO R_u FOR HOMOGENEOUS WELLAND CLAY, BLOCK H

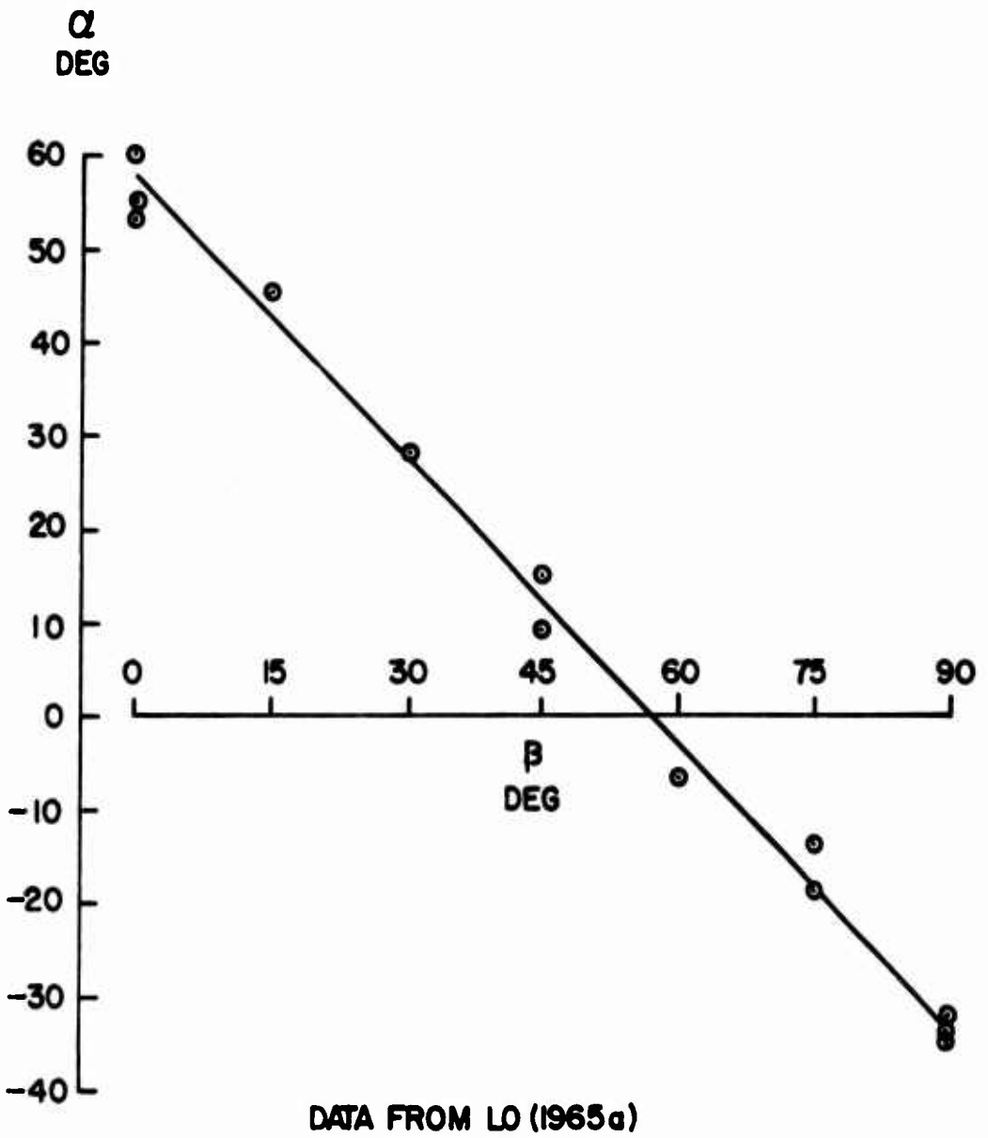

DATA FROM LO (1965a)

FIGURE 3.28 (c)

VARIATION OF FAILURE PLANE ORIENTATION FOR UNCONFINED COMPRESSION TESTS ON HOMOGENEOUS WELLAND CLAY, BLOCK D

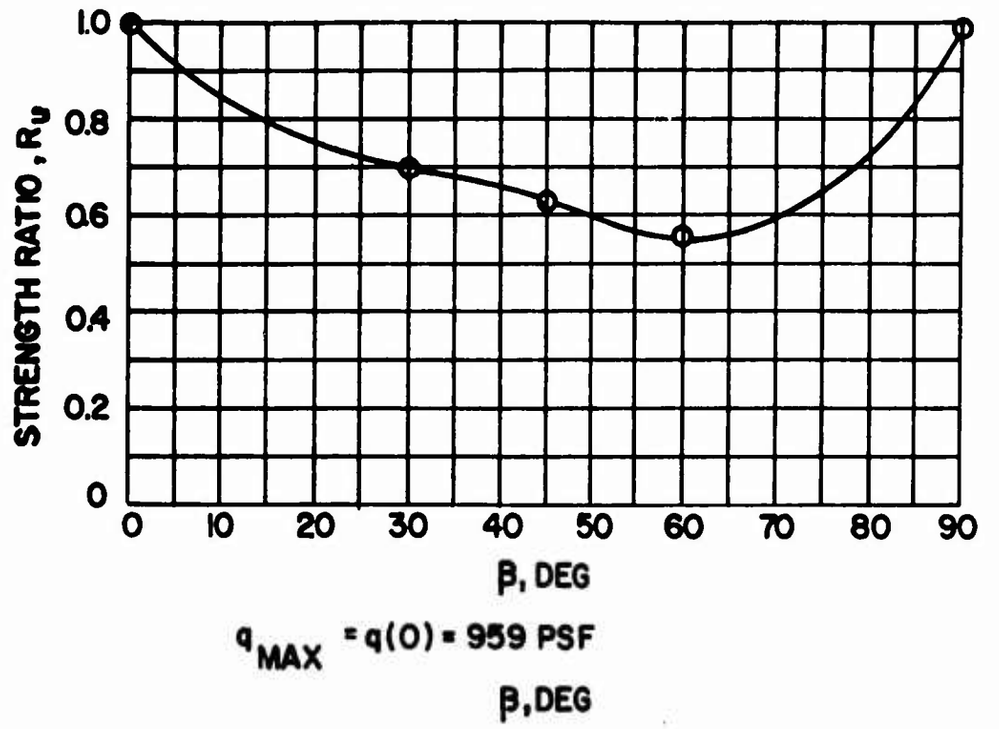

$q_{MAX} = q(0) = 959$ PSF

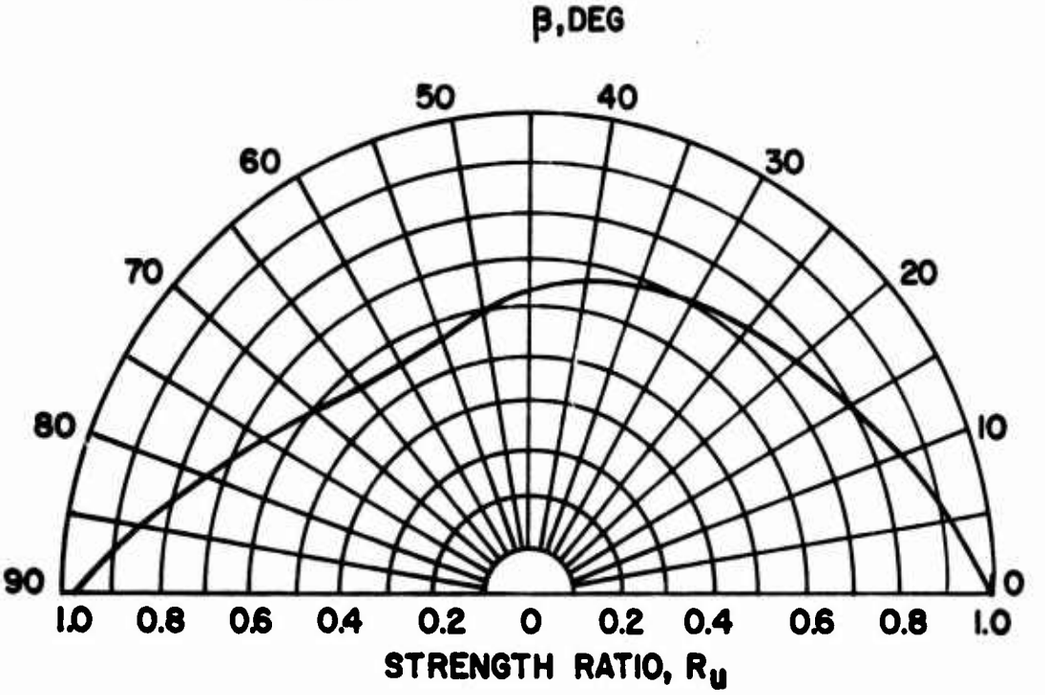

DATA FROM LO AND MILLIGAN (1967)

FIGURE 3.29 (a)

ANISOTROPIC STRENGTH RATIO R_u FOR STRATIFIED WELLAND CLAY, BLOCK F

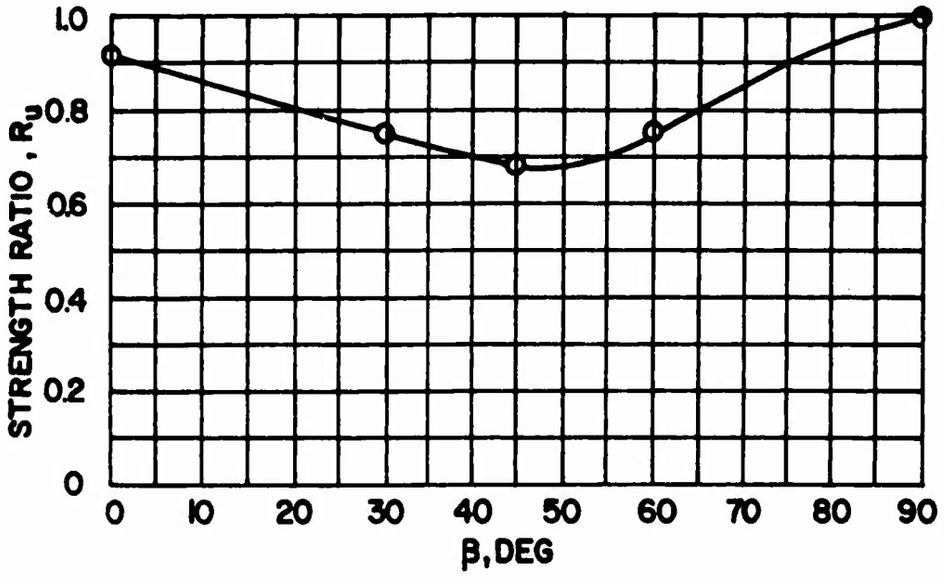

$q_{MAX} = q_f\,(90) = 1436$ PSF

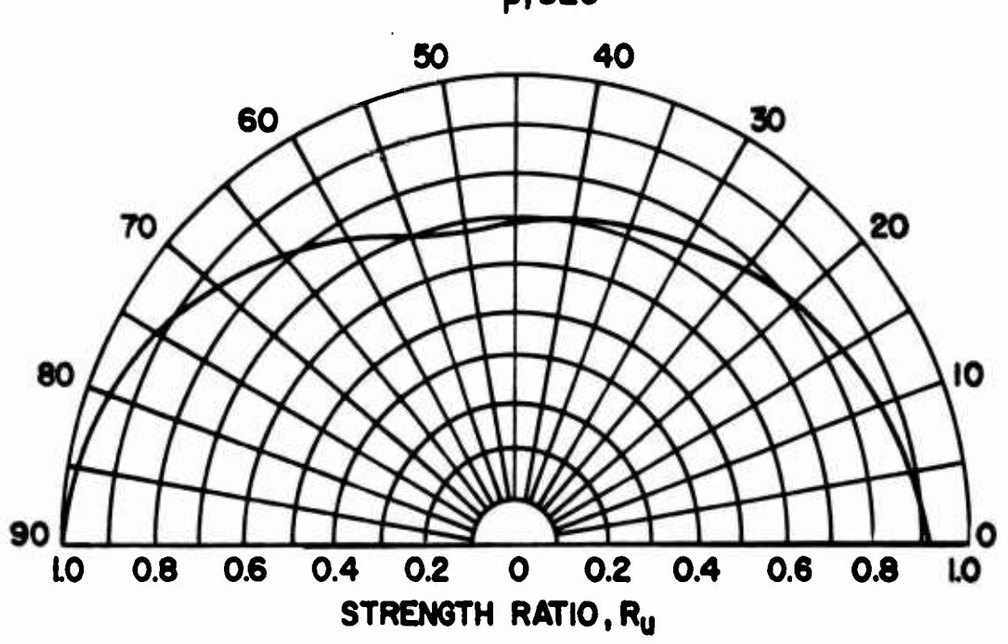

DATA FROM LO AND MILLIGAN (1967)

FIGURE 3.29 (b)

ANISOTROPIC STRENGTH RATIO R_u FOR STRATIFIED WELLAND CLAY, BLOCK K

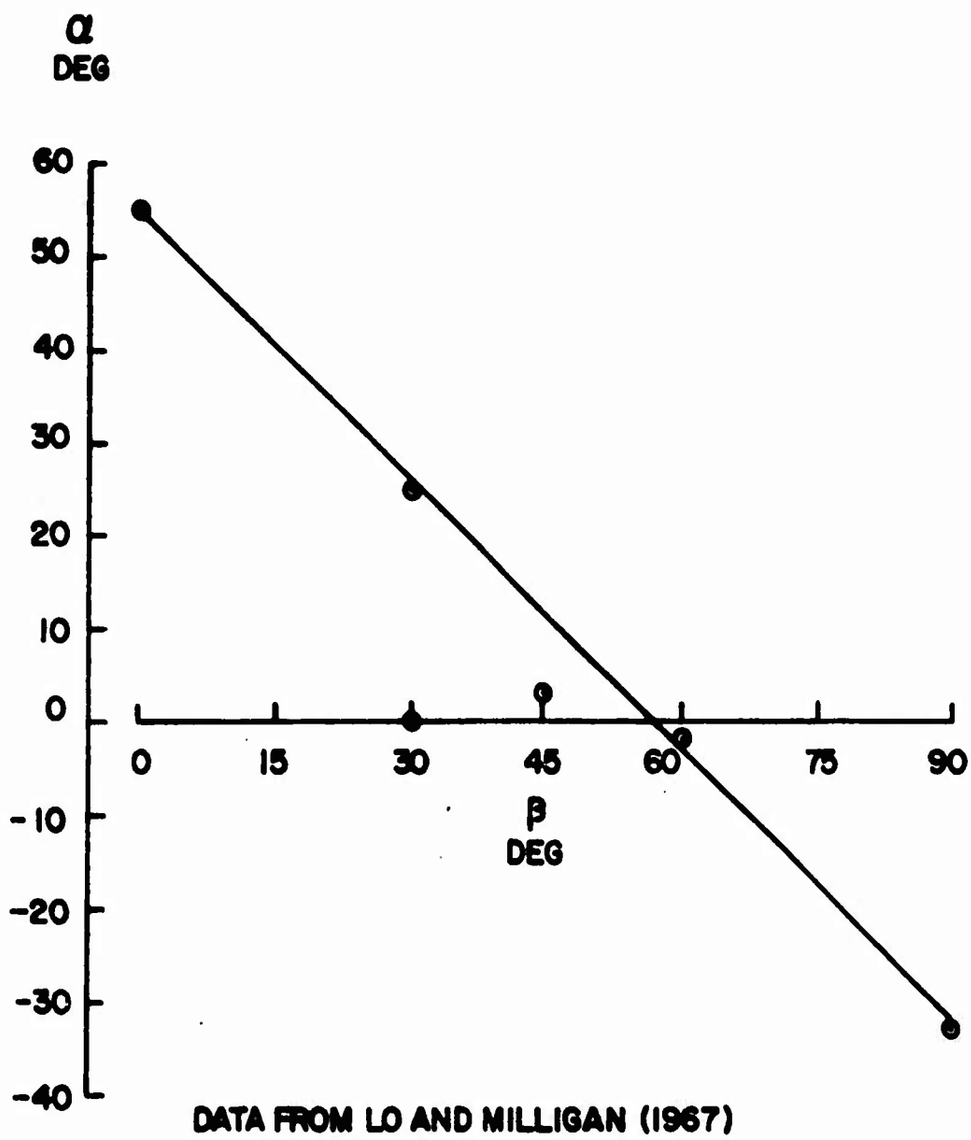

DATA FROM LO AND MILLIGAN (1967)

FIGURE 3.29 (c)

VARIATION OF FAILURE PLANE ORIENTATION FOR UNCONFINED COMPRESSION TESTS ON STRATIFIED WELLAND CLAY, BLOCKS F AND K

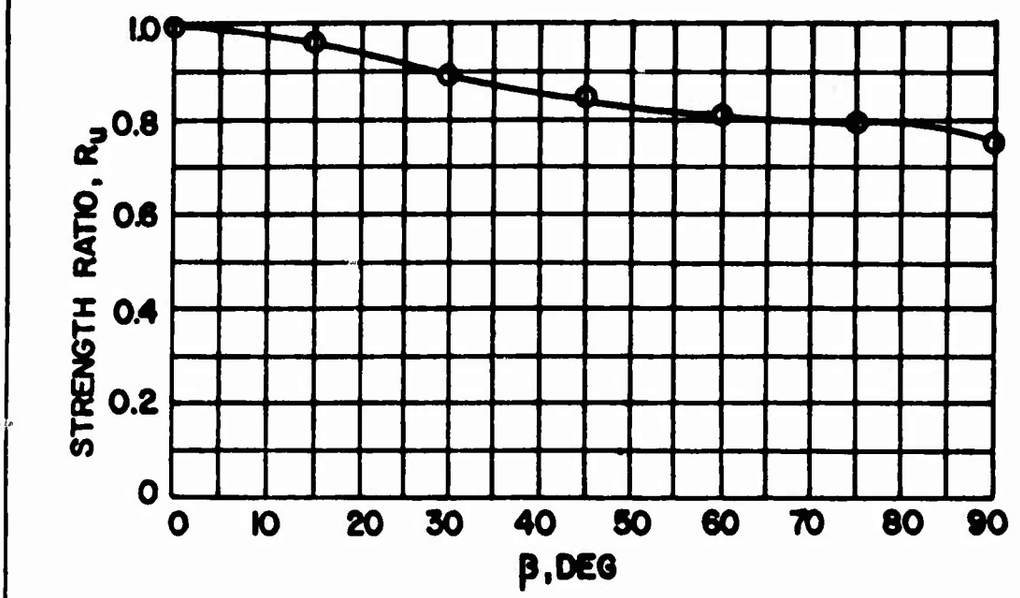

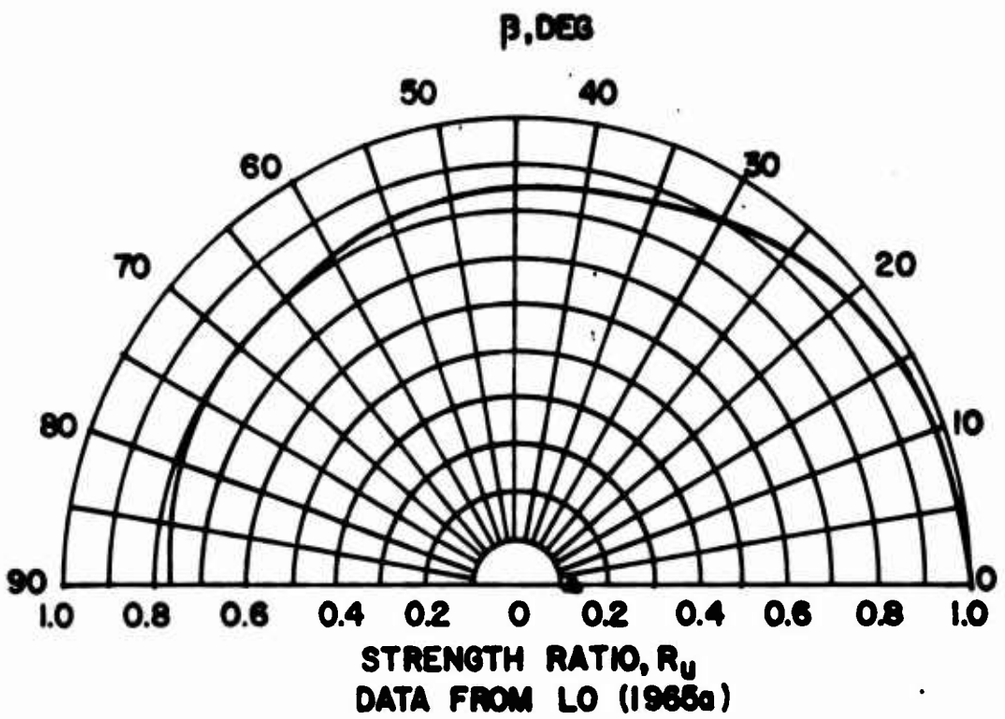

FIGURE 3.30

ANISOTROPIC STRENGTH RATIO R_u FOR HOMOGENEOUS WELLAND CLAY, BLOCKS A, B, C, D, E, G, H & I

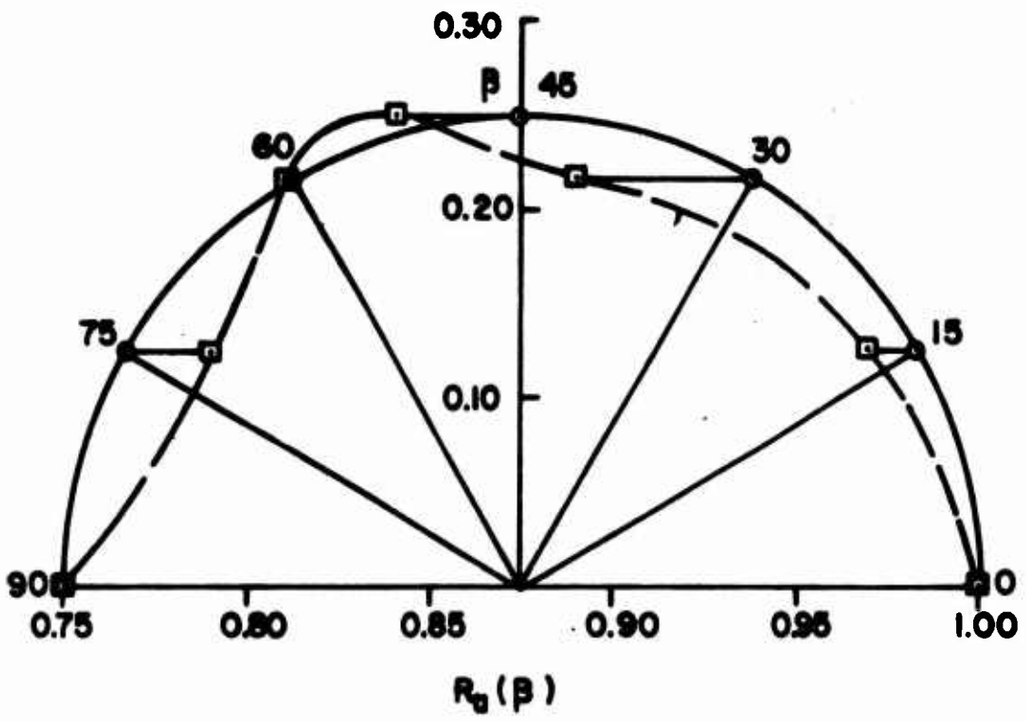

● THEORETICAL POINT

⊡ MEASURED POINT

DATA FROM LO (1965a)

FIGURE 3.31

MOHR CIRCLE PLOT OF ANISOTROPIC STRENGTH RATIO FOR HOMOGENEOUS WELLAND CLAY, BLOCKS A,B,C,D,E,G,H & I

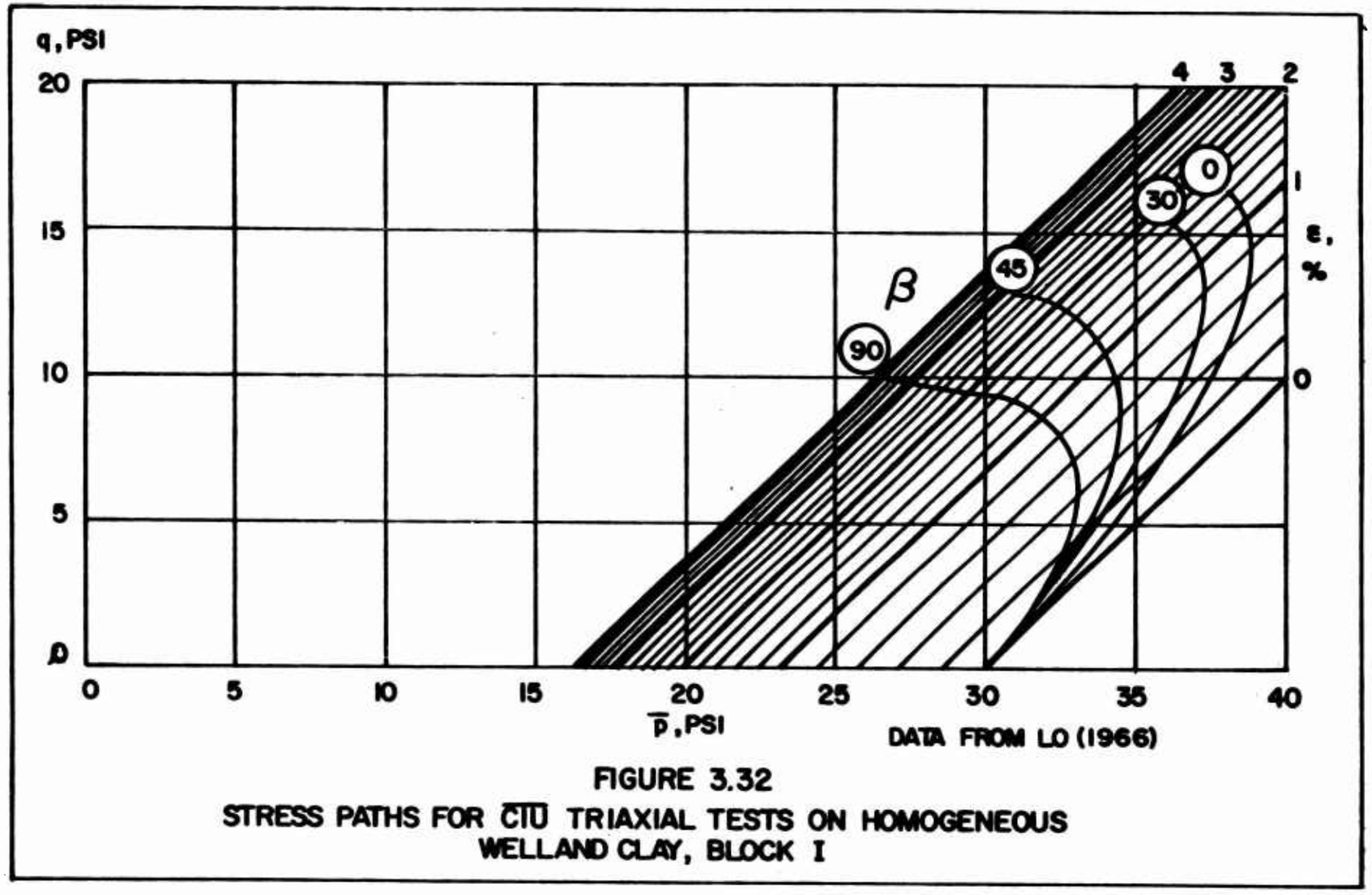

FIGURE 3.32

STRESS PATHS FOR $\overline{CTU}$ TRIAXIAL TESTS ON HOMOGENEOUS WELLAND CLAY, BLOCK I

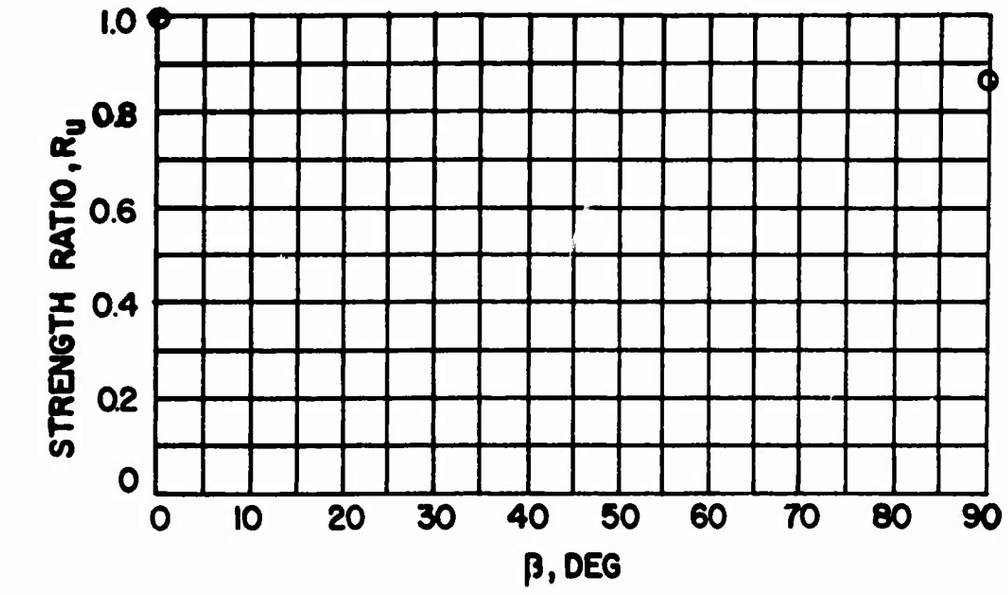

$q_{MAX} = q_f(0) = 1498$ PSF

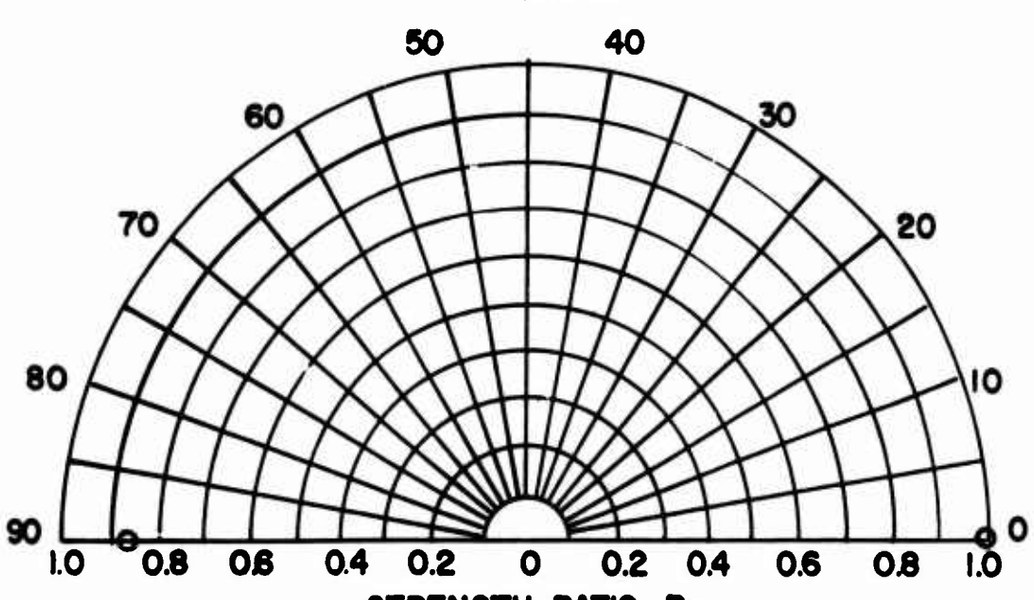

DATA FROM HANNA (1967)

FIGURE 3.33 (a)

ANISOTROPIC STRENGTH RATIO R_u FOR HOMOGENEOUS SARNIA CLAY, BLOCK 1

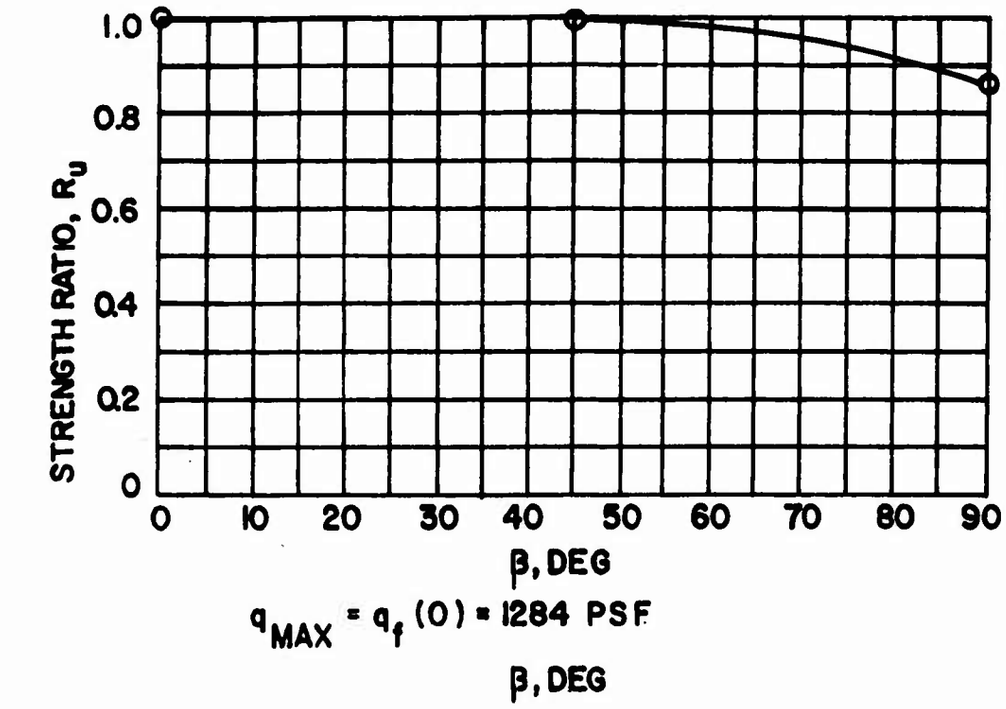

$q_{MAX} = q_f(0) = 1284$ PSF

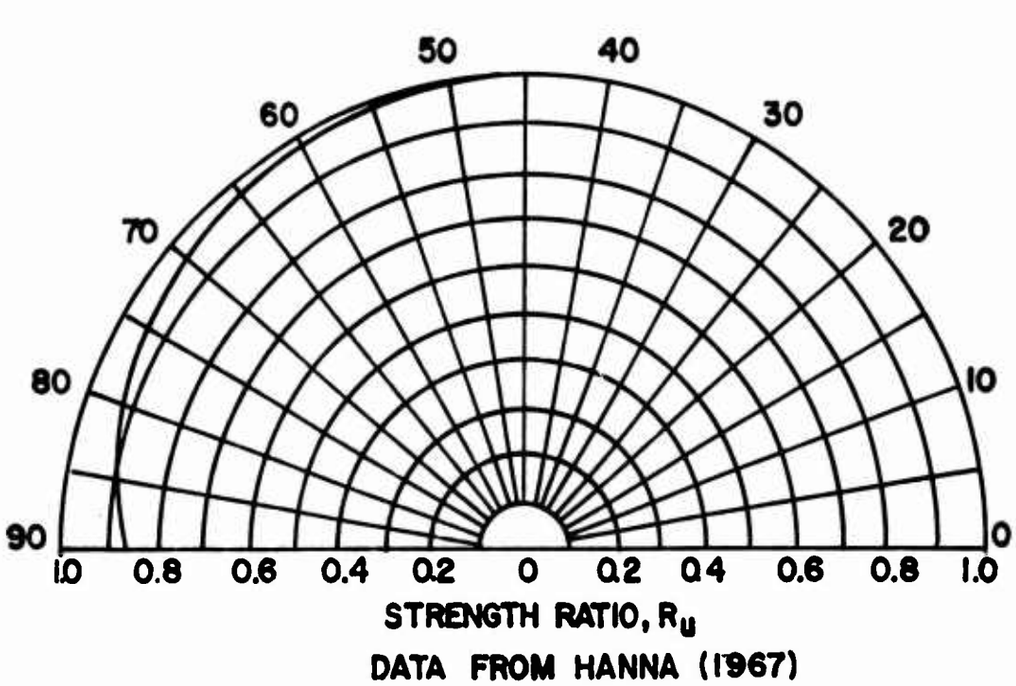

DATA FROM HANNA (1967)

FIGURE 3.33 (b)

ANISOTROPIC STRENGTH RATIO R_u FOR HOMOGENEOUS SARNIA CLAY, BLOCK 2

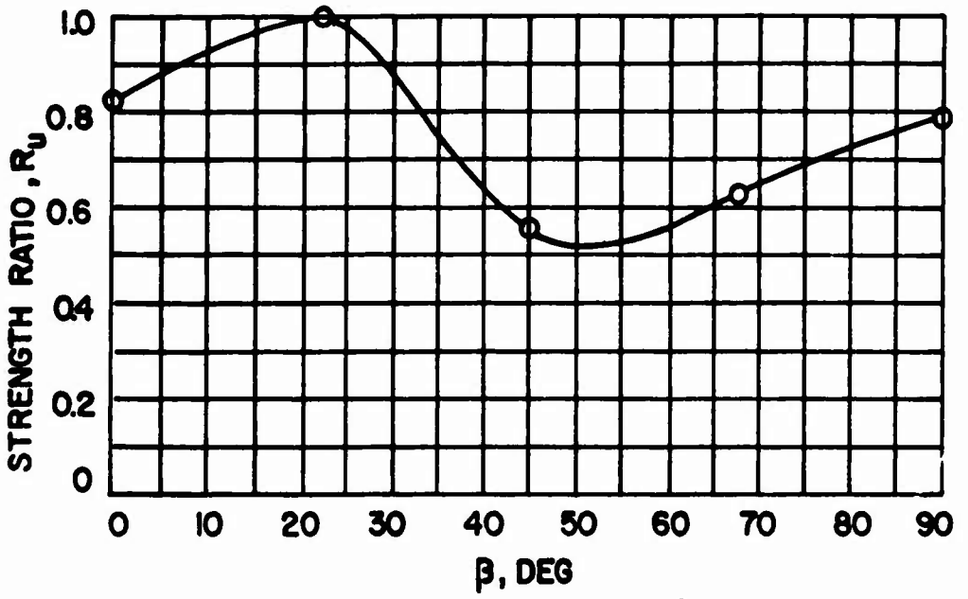

$q_{MAX} = q_f\ (22.5) = 0.280\ KG/CM^2$

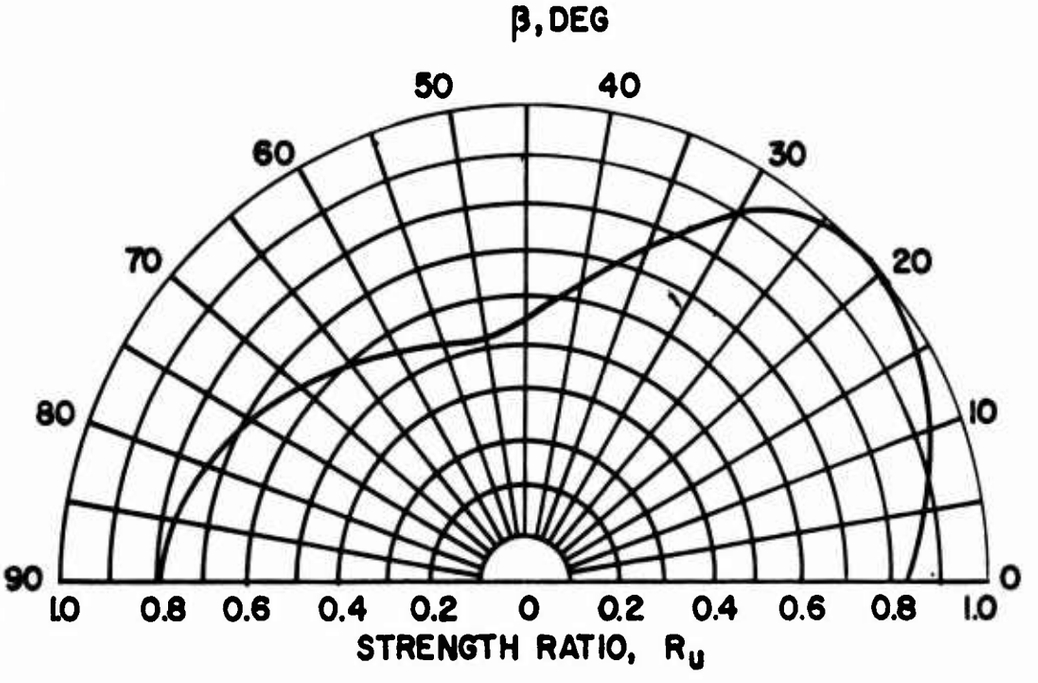

DATA FROM SOVERI AND HYYPPA (1967)

FIGURE 3.34

ANISOTROPIC STRENGTH RATIO R_u FOR A VARVED FINNISH GLACIAL CLAY

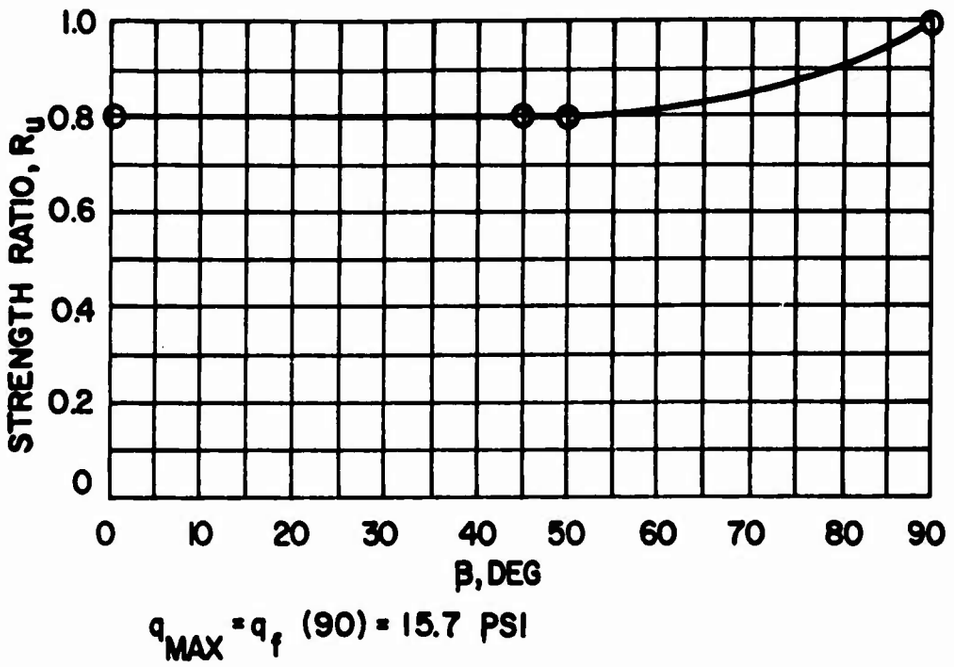

$q_{MAX} = q_f\ (90) = 15.7$ PSI

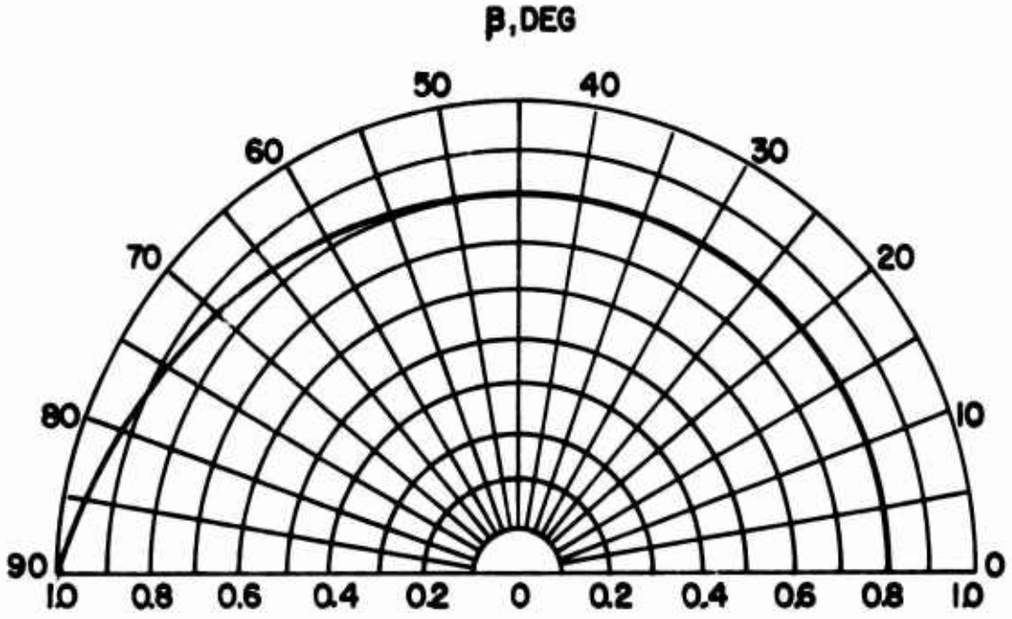

DATA FROM MATTHAI (1967)

FIGURE 3.35

ANISOTROPIC STRENGTH RATIO R_u FOR HOMOGENEOUS INDIA BLACK COTTON CLAY

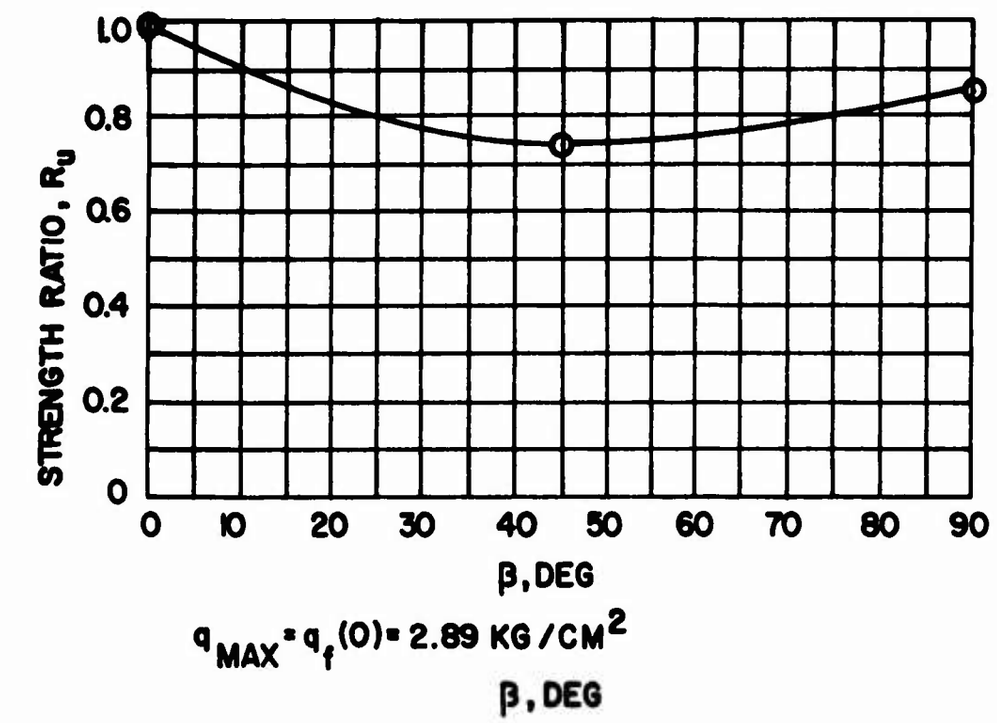

$q_{MAX} = q_f(0) = 2.89\ KG/CM^2$

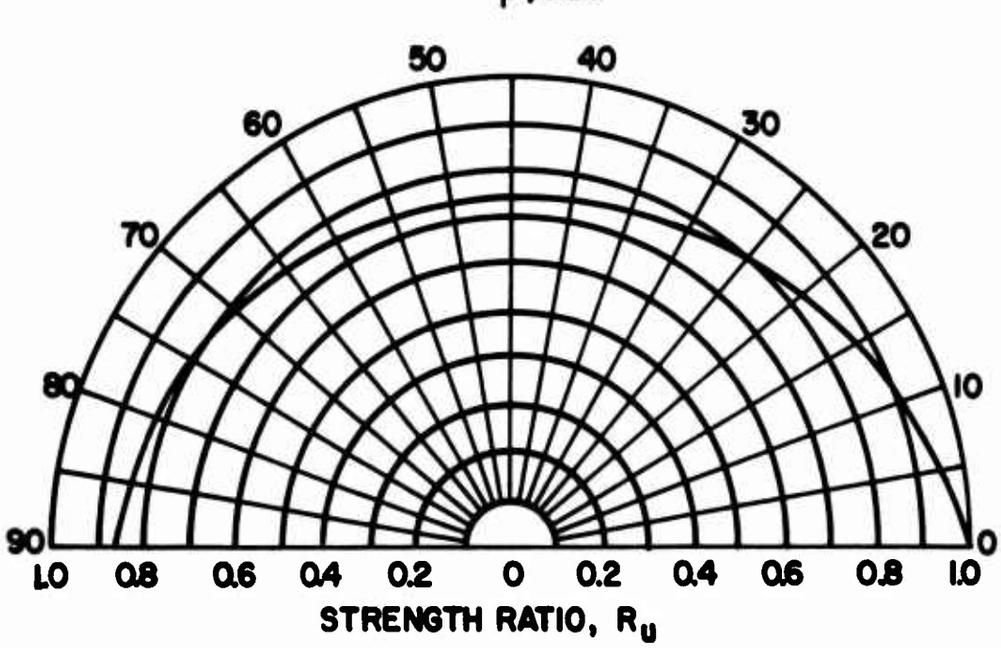

DATA FROM DUNCAN AND SEED (1965)

FIGURE 3.36

ANISOTROPIC STRENGTH RATIO R_u FOR ASP-900 KAOLINITE

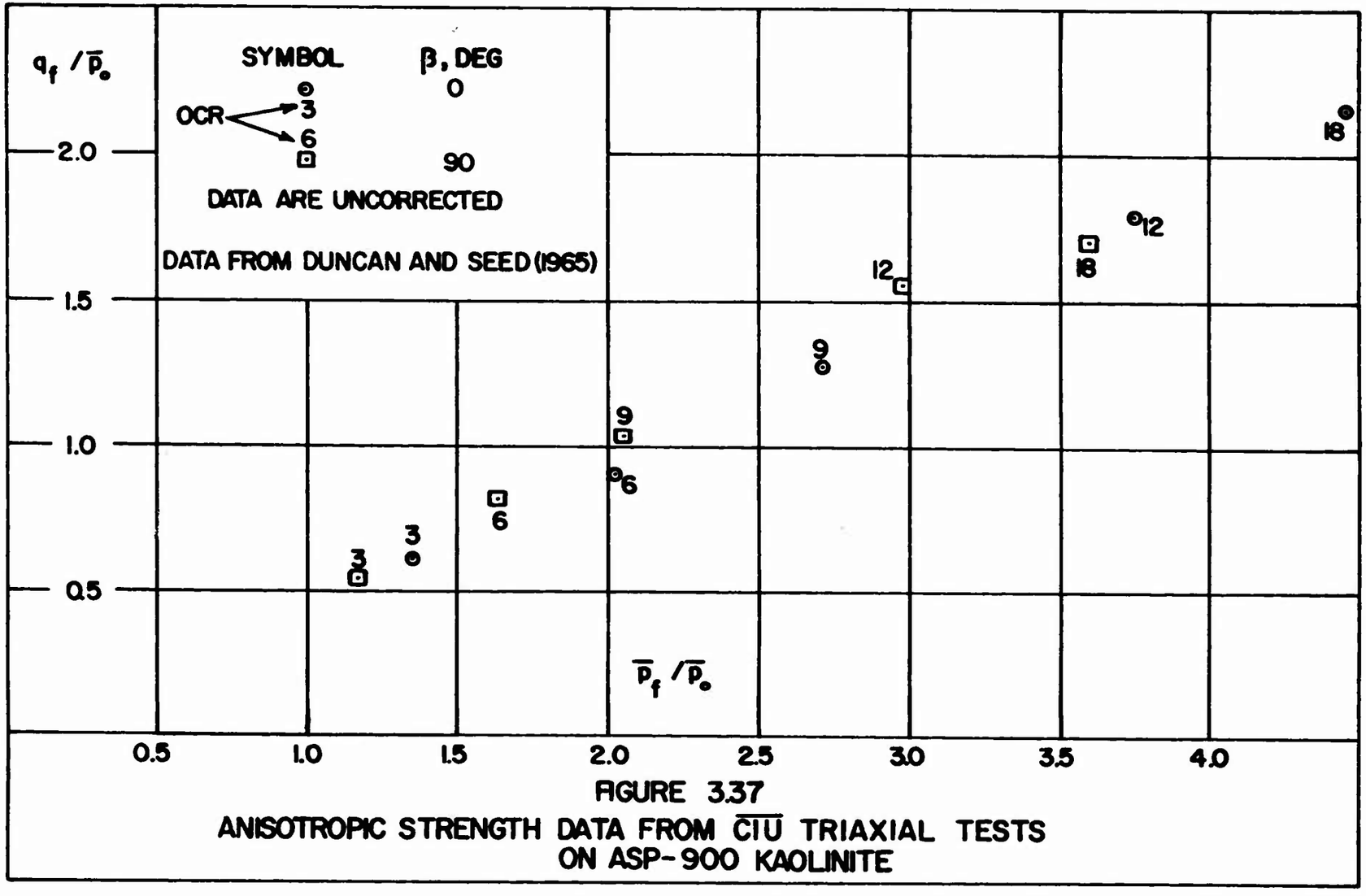

FIGURE 3.37

ANISOTROPIC STRENGTH DATA FROM $\overline{CIU}$ TRIAXIAL TESTS ON ASP-900 KAOLINITE

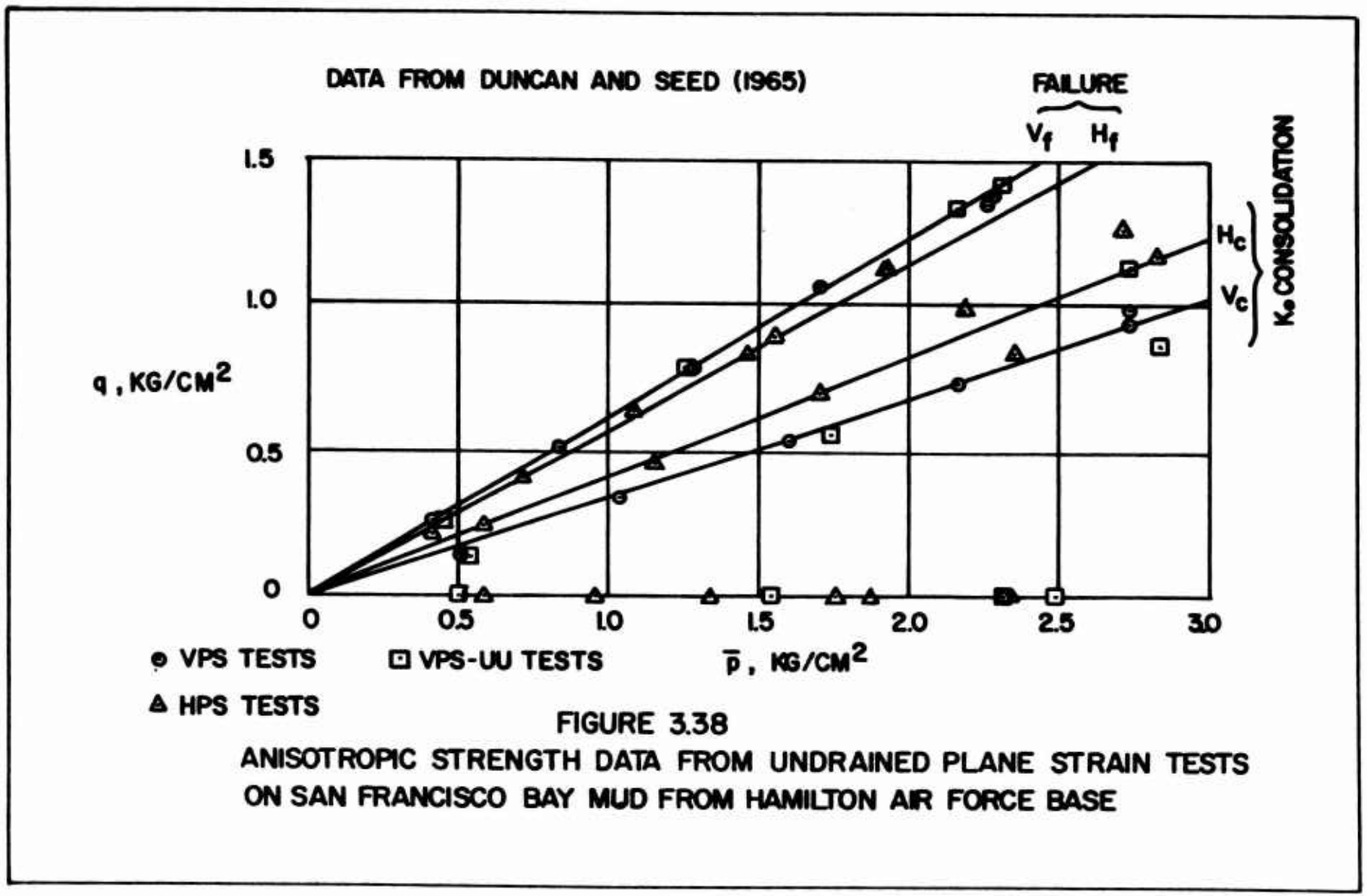

FIGURE 3.38
ANISOTROPIC STRENGTH DATA FROM UNDRAINED PLANE STRAIN TESTS ON SAN FRANCISCO BAY MUD FROM HAMILTON AIR FORCE BASE

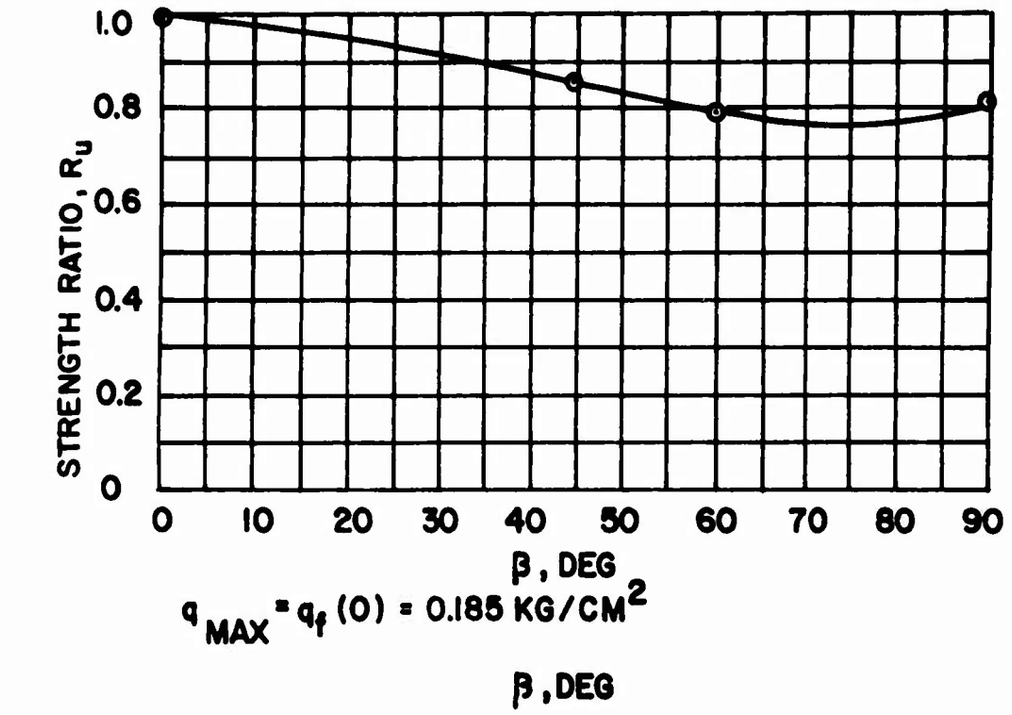

$q_{MAX} = q_f(0) = 0.185\ KG/CM^2$

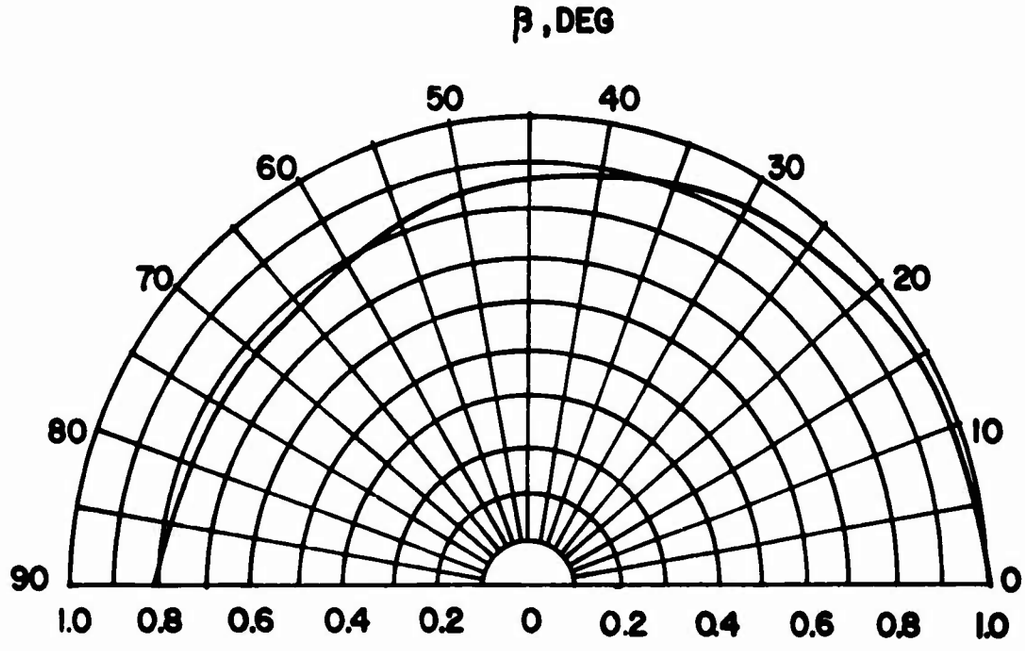

DATA FROM DUNCAN AND SEED (1965)

FIGURE 3.39

ANISOTROPIC STRENGTH RATIO R_u FOR UNDISTURBED SAN FRANCISCO BAY MUD

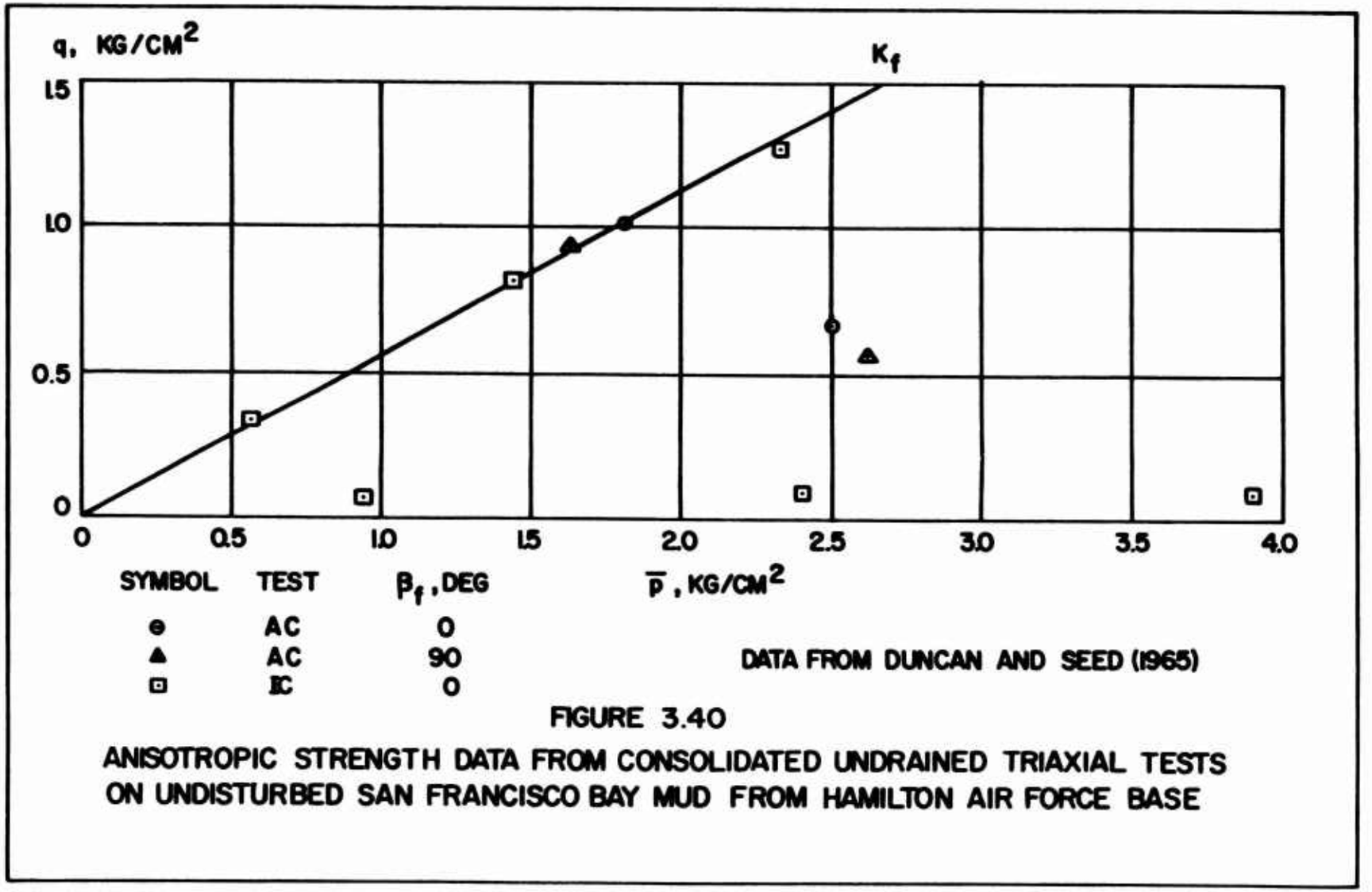

FIGURE 3.40

ANISOTROPIC STRENGTH DATA FROM CONSOLIDATED UNDRAINED TRIAXIAL TESTS ON UNDISTURBED SAN FRANCISCO BAY MUD FROM HAMILTON AIR FORCE BASE

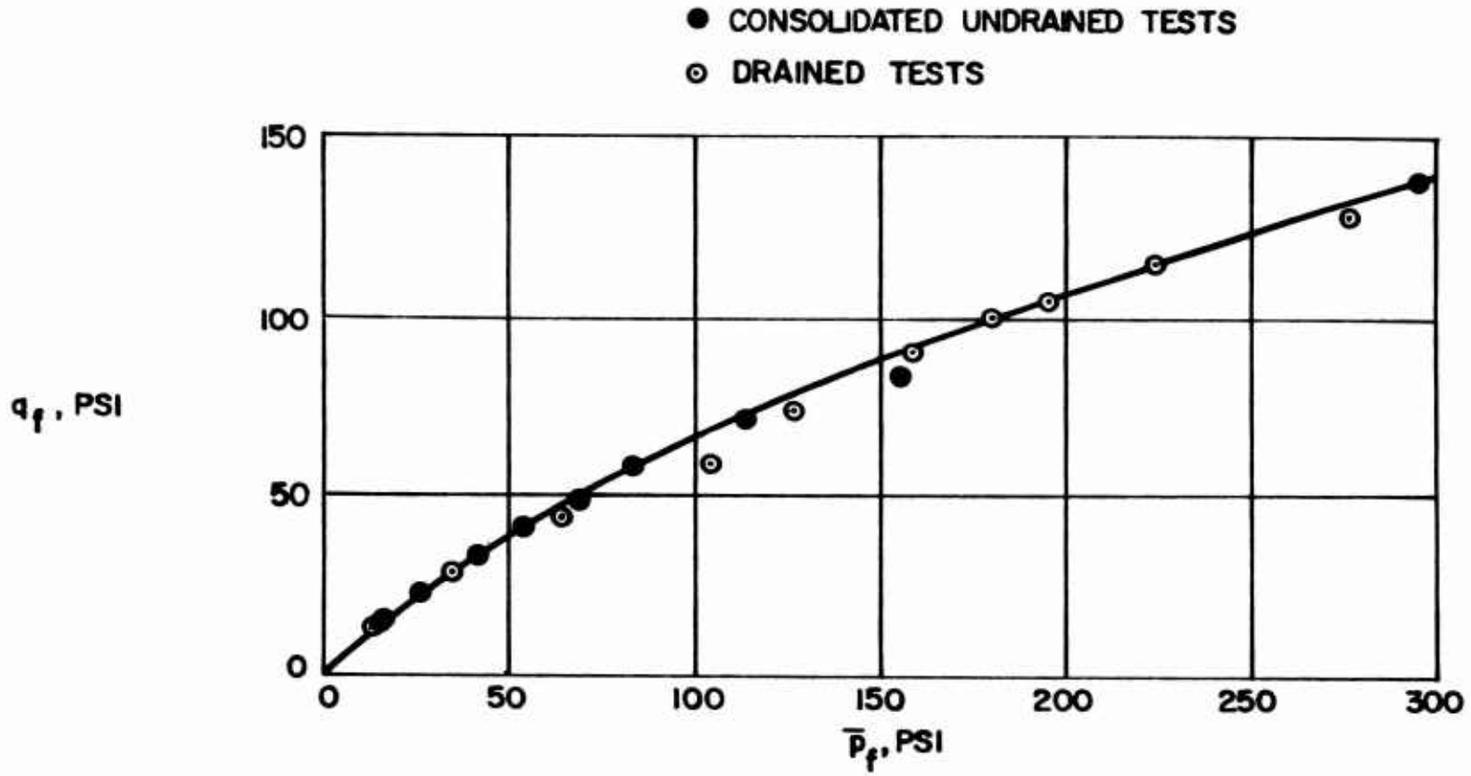

DATA FROM BISHOP, WEBB AND LEWIN (1965)

FIGURE 3.41 (a)

STRENGTH DATA FROM TRIAXIAL TESTS ON VERTICAL ($\beta = 0°$) SPECIMENS OF UNDISTURBED LONDON CLAY, LEVEL E

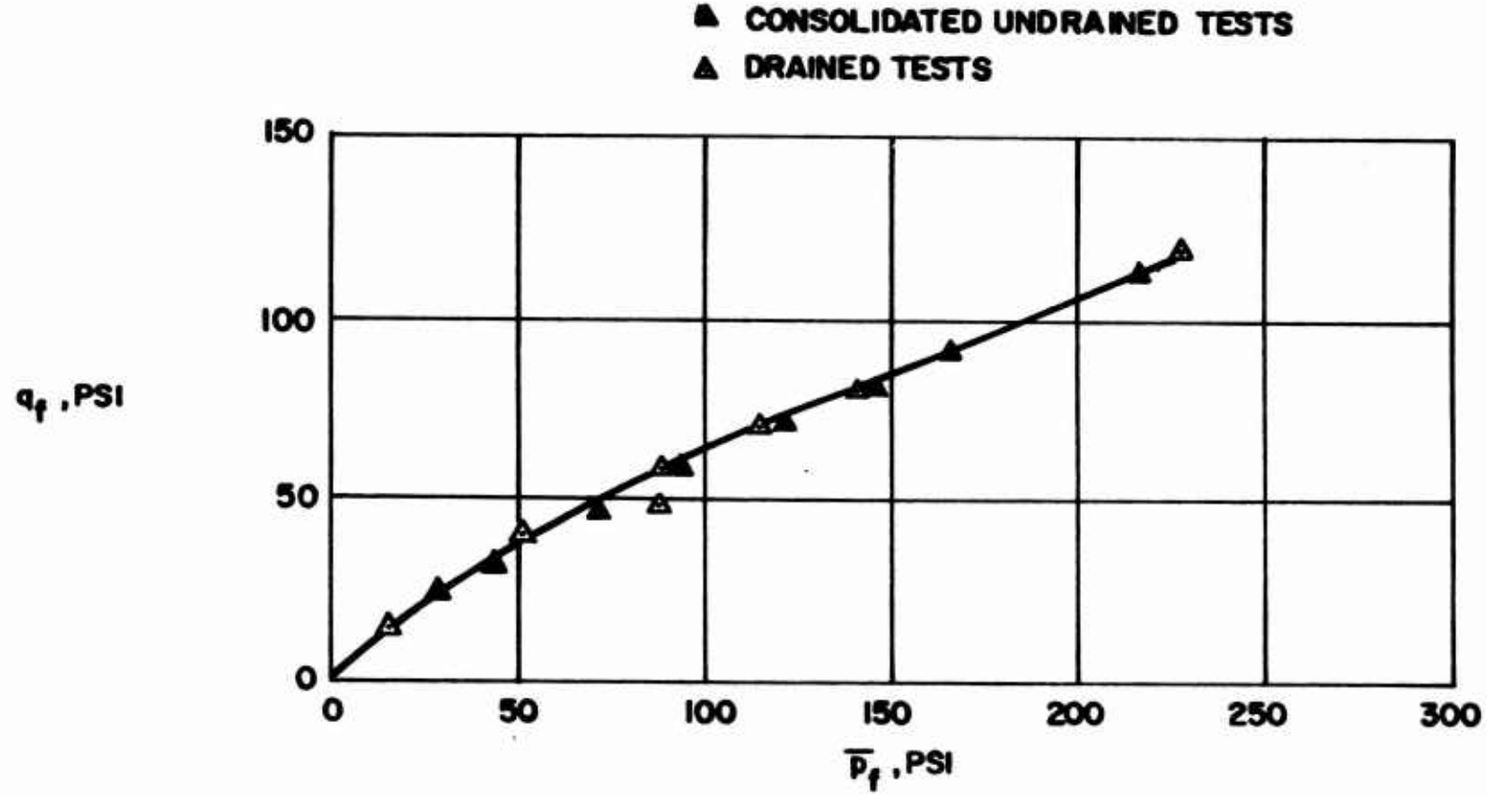

DATA FROM BISHOP, WEBB AND LEWIN (1965)

FIGURE 3.41 (b)

STRENGTH DATA FROM TRIAXIAL TESTS ON HORIZONTAL ($\beta = 90°$)
SPECIMENS OF UNDISTURBED LONDON CLAY, LEVEL E

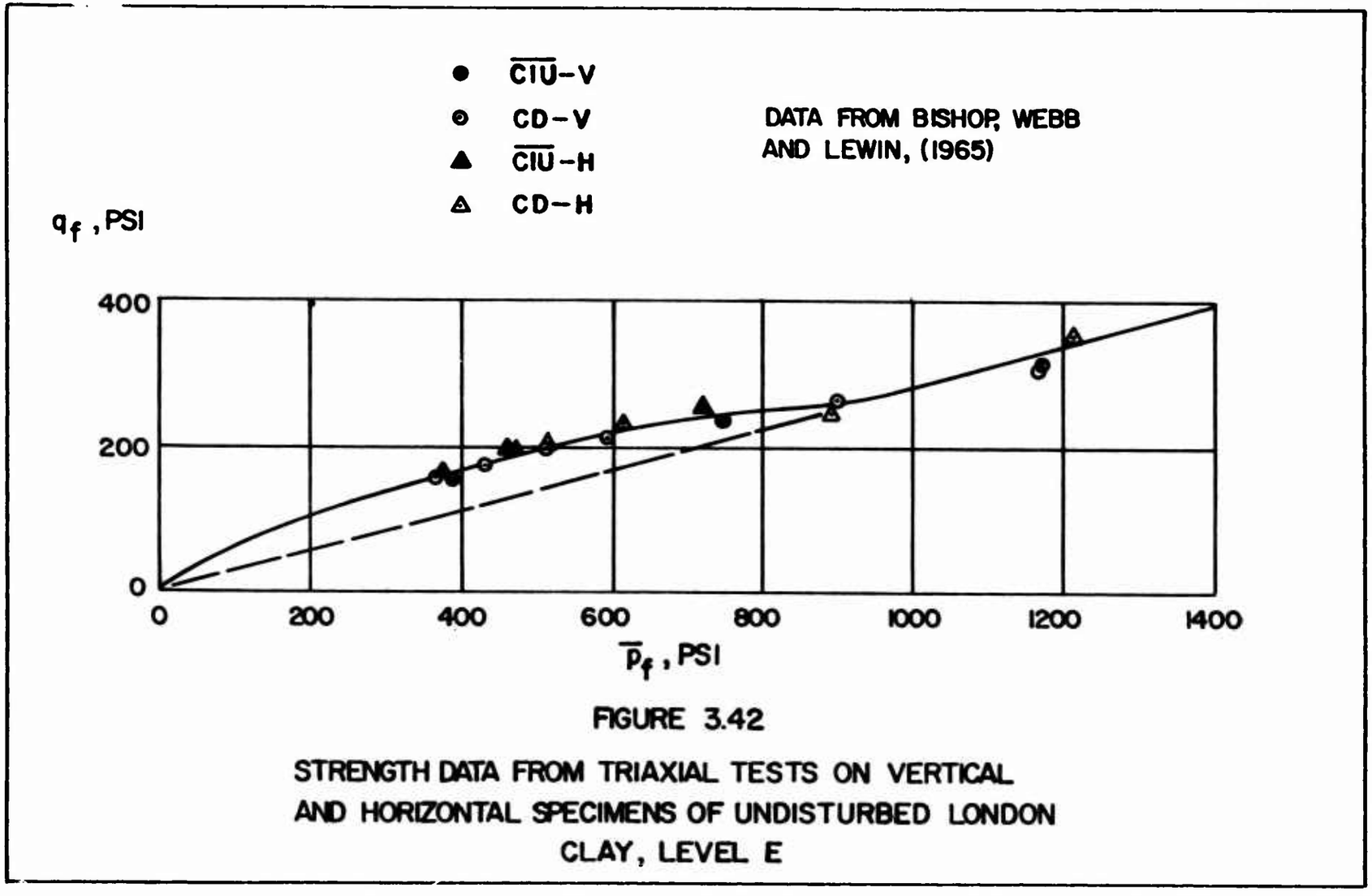

FIGURE 3.42

STRENGTH DATA FROM TRIAXIAL TESTS ON VERTICAL AND HORIZONTAL SPECIMENS OF UNDISTURBED LONDON CLAY, LEVEL E

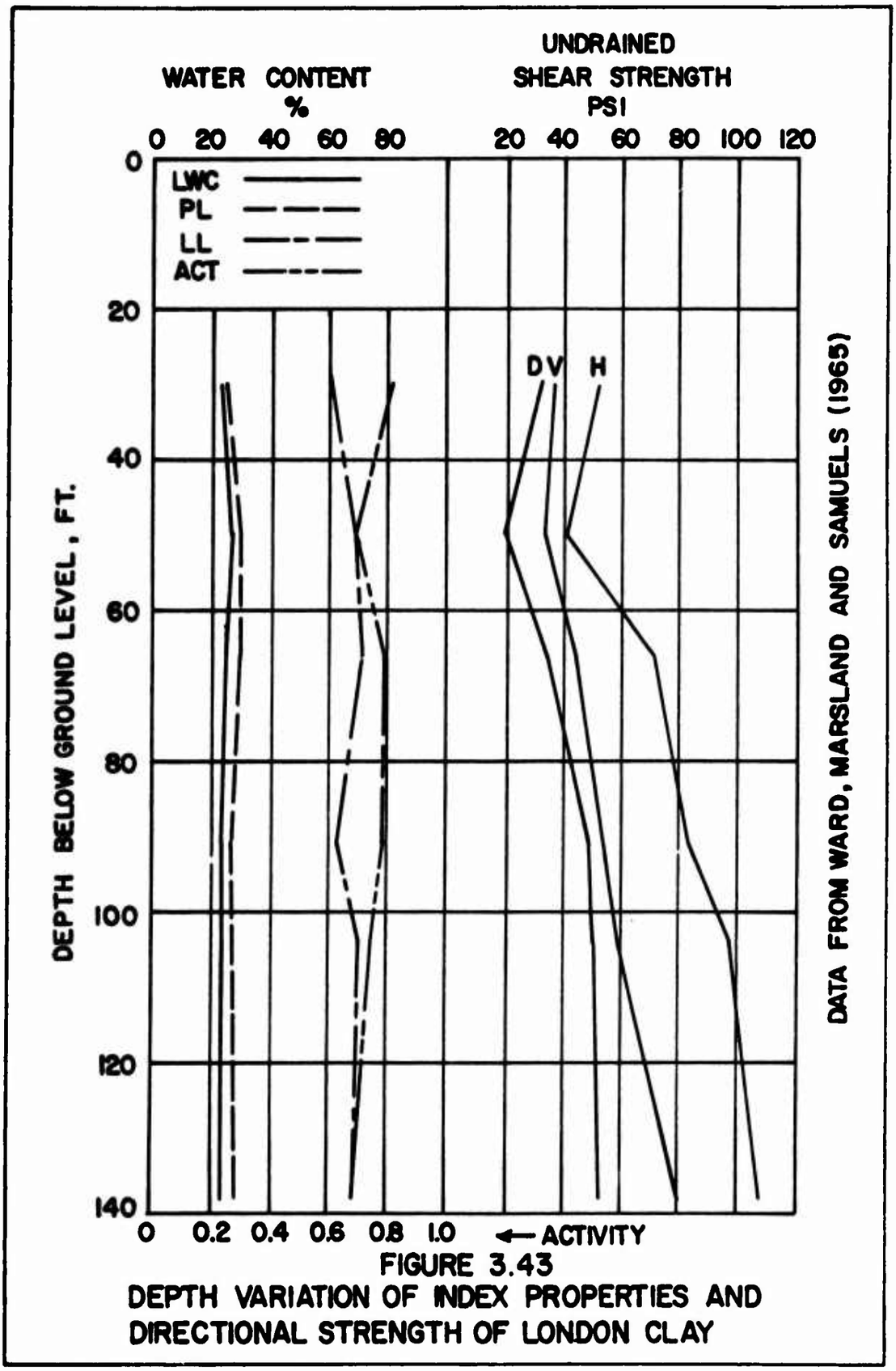

FIGURE 3.43
DEPTH VARIATION OF INDEX PROPERTIES AND DIRECTIONAL STRENGTH OF LONDON CLAY

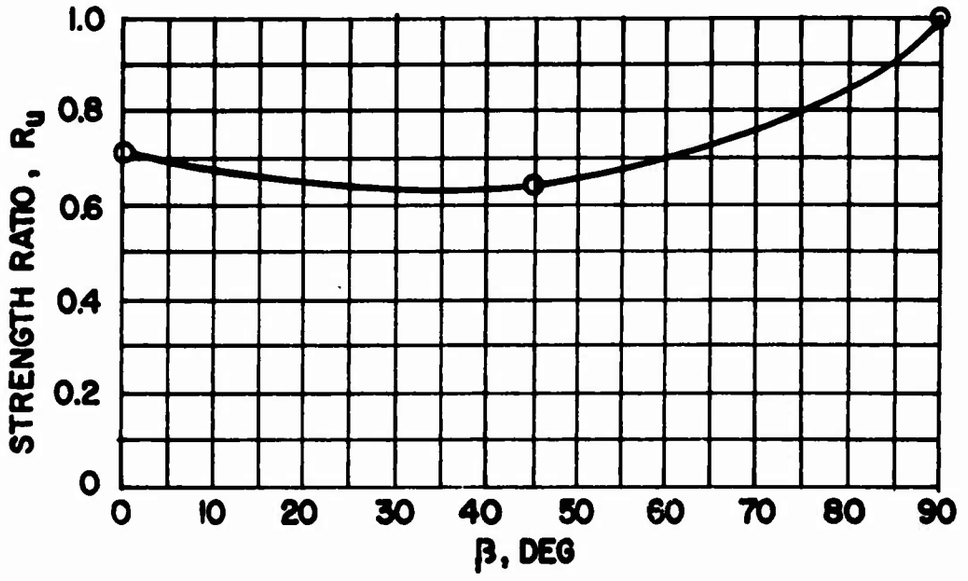

$q_{MAX} = q_f(90) = 51.3$ PSI

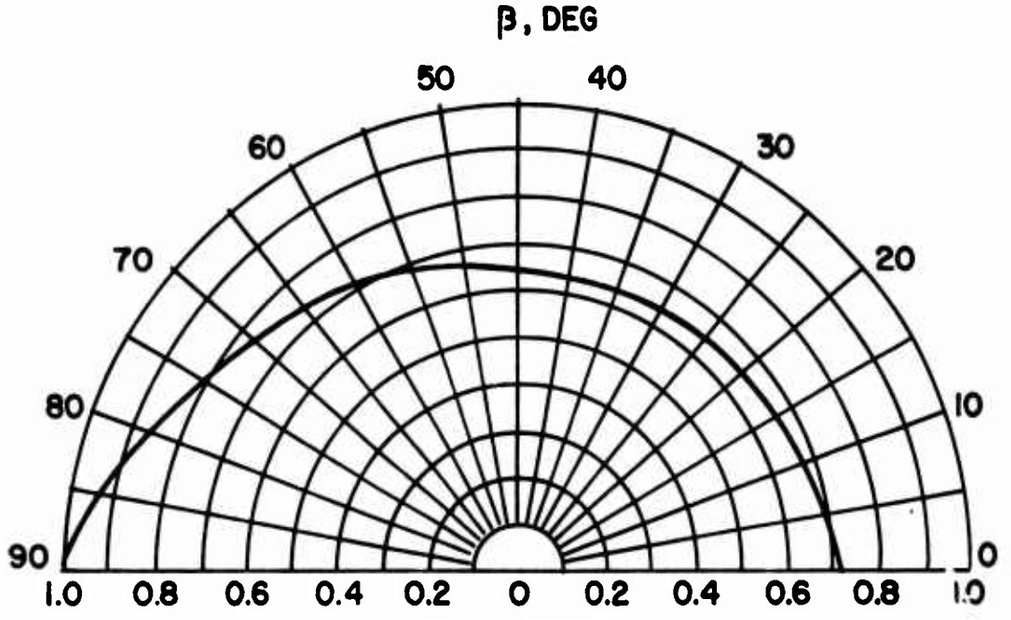

DATA FROM WARD ET. AL. (1965)

FIGURE 3.44 (a)

ANISOTROPIC STRENGTH RATIO R_u FOR LONDON CLAY FROM ASHFORD COMMON, LEVEL A

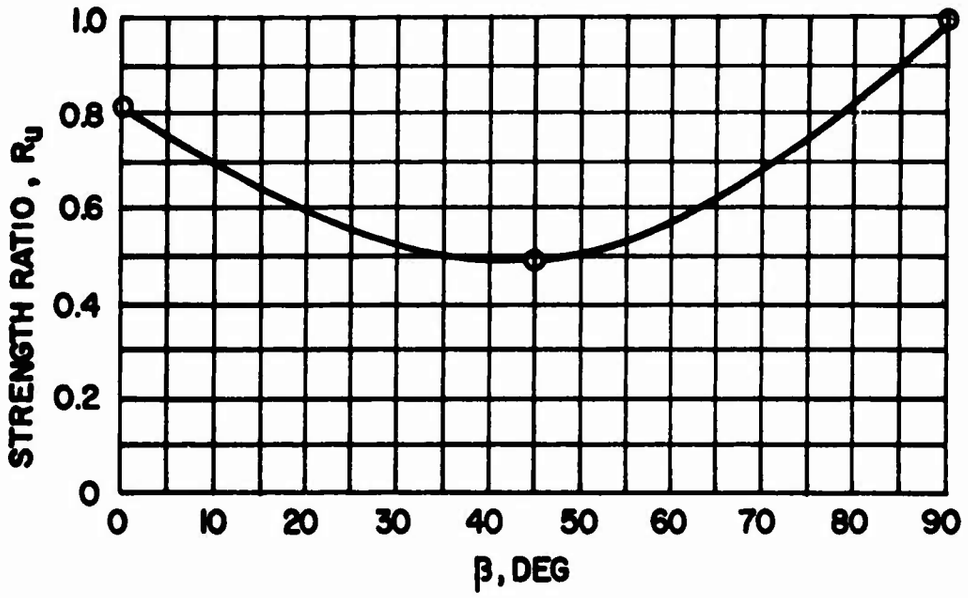

$q_{MAX} = q_f(90) = 40.4$ PSI

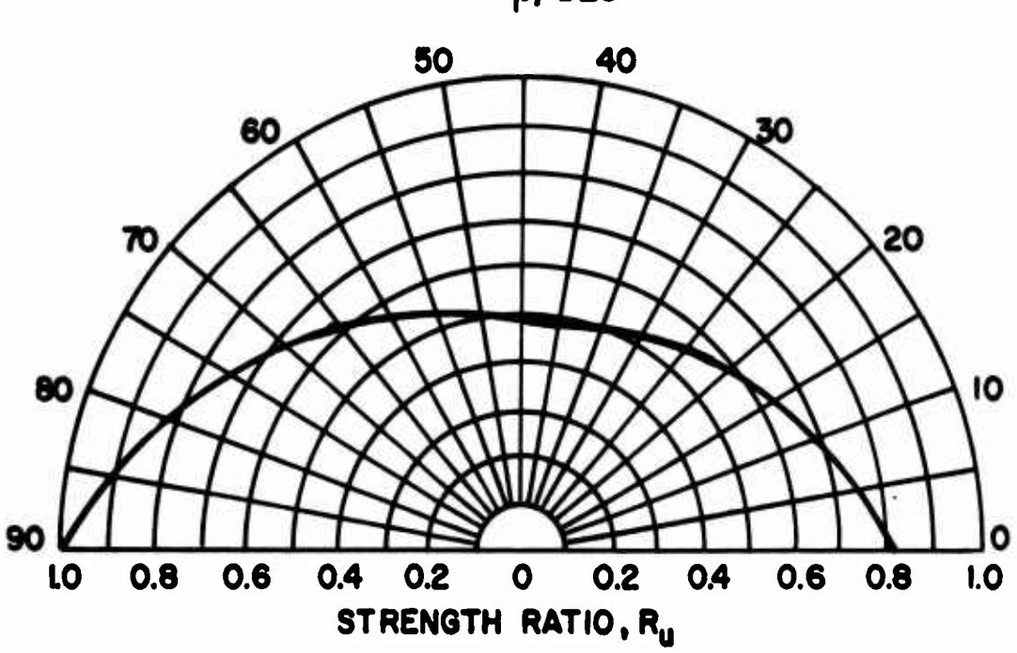

DATA FROM WARD ET. AL. (1965)

FIGURE 3.44 (b)

ANISOTROPIC STRENGTH RATIO R_u FOR LONDON CLAY FROM ASHFORD COMMON, LEVEL B

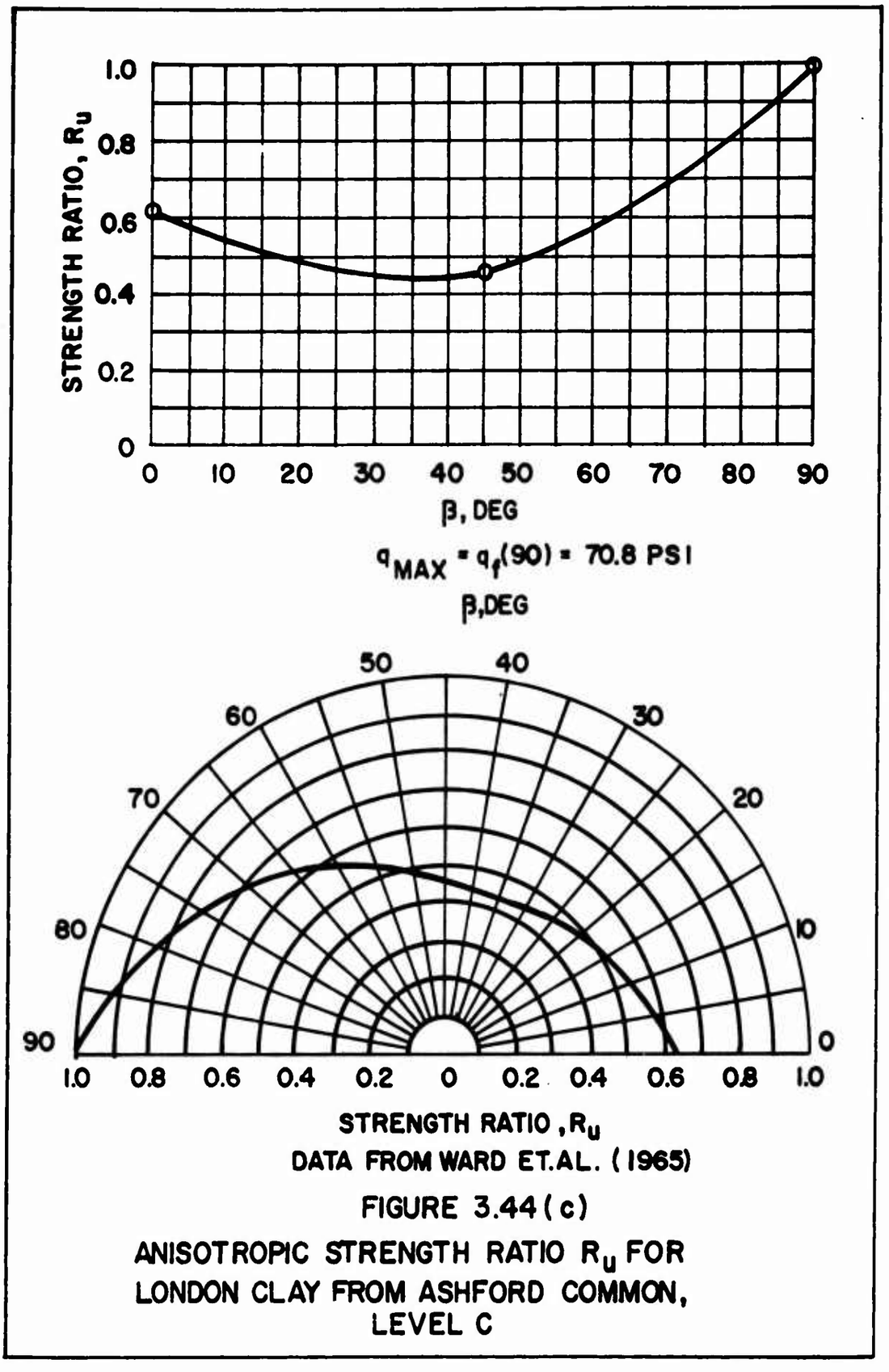

FIGURE 3.44 (c)

ANISOTROPIC STRENGTH RATIO R_u FOR LONDON CLAY FROM ASHFORD COMMON, LEVEL C

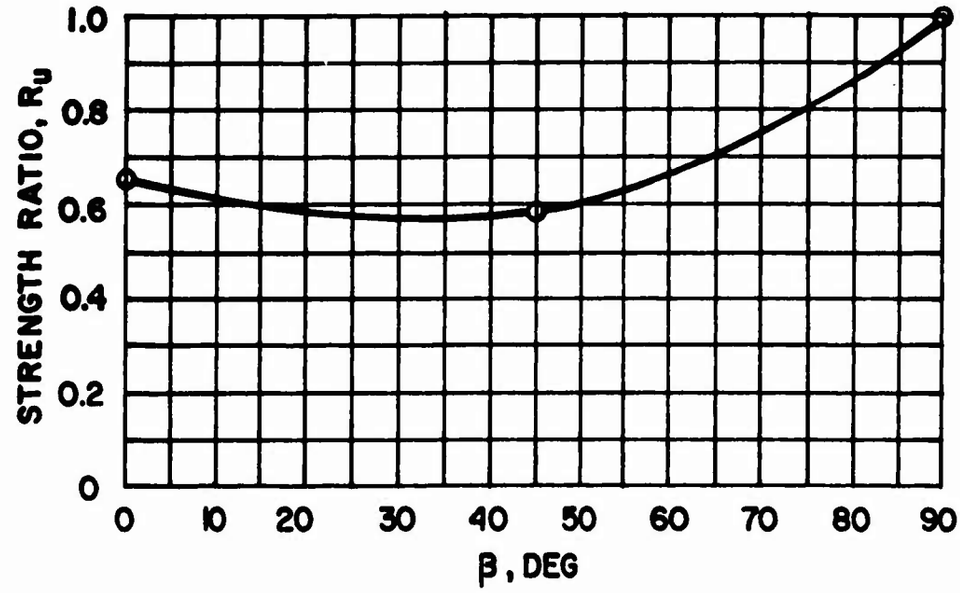

$q_{MAX} = q_f(90) = 84.1$ PSI

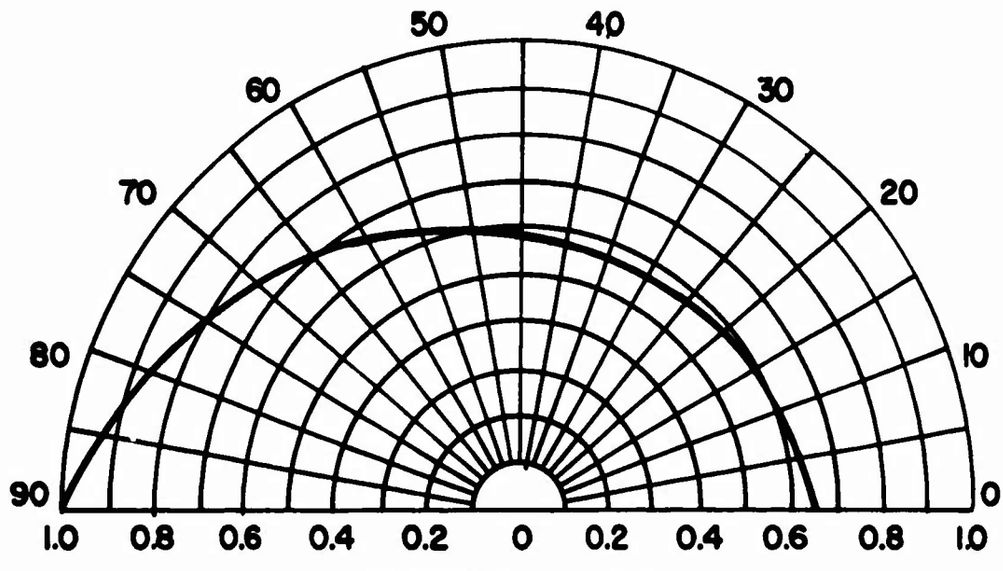

DATA FROM WARD ET. AL. (1965)

FIGURE 3.44 (d)

ANISOTROPIC STRENGTH RATIO R_u FOR LONDON CLAY FROM ASHFORD COMMON, LEVEL D

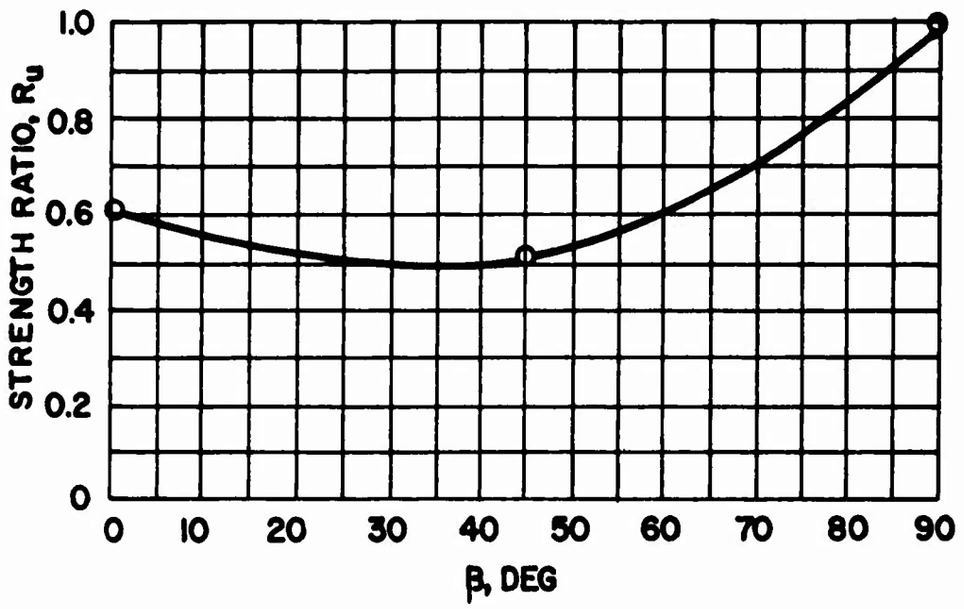

$q_{MAX} = q_f(90) = 97.8$ PSI

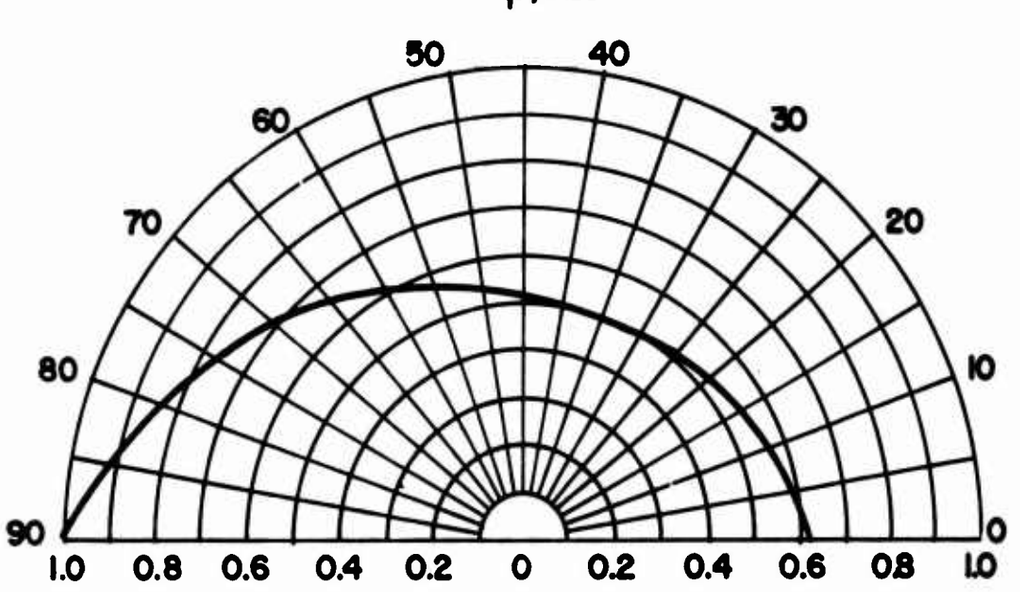

DATA FROM WARD ET. AL. (1965)

FIGURE 3.44 (e)

ANISOTROPIC STRENGTH RATIO R_u FOR LONDON CLAY FROM ASHFORD COMMON, LEVEL E

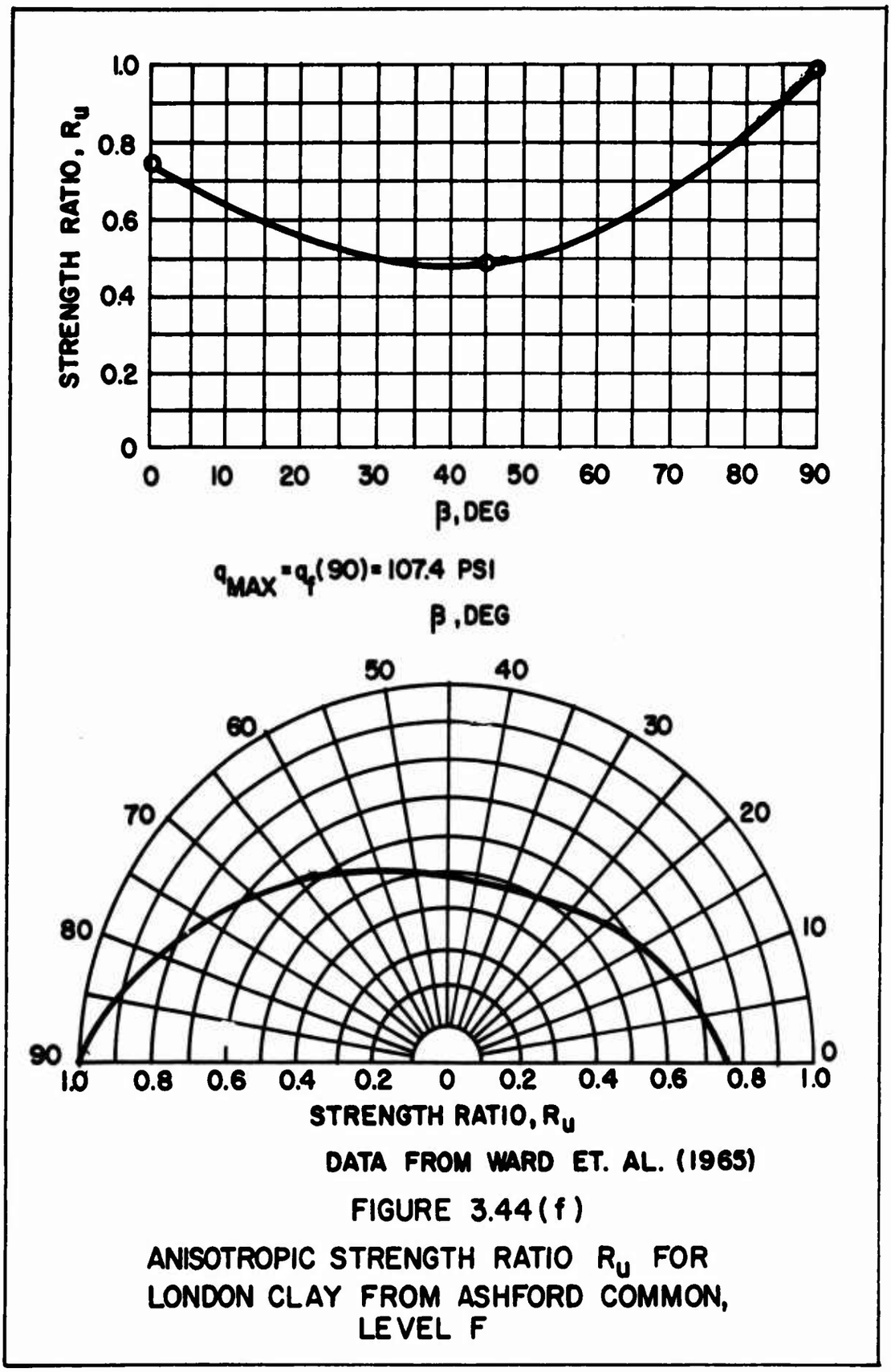

DATA FROM WARD ET. AL. (1965)

FIGURE 3.44(f)

ANISOTROPIC STRENGTH RATIO R_u FOR LONDON CLAY FROM ASHFORD COMMON, LEVEL F

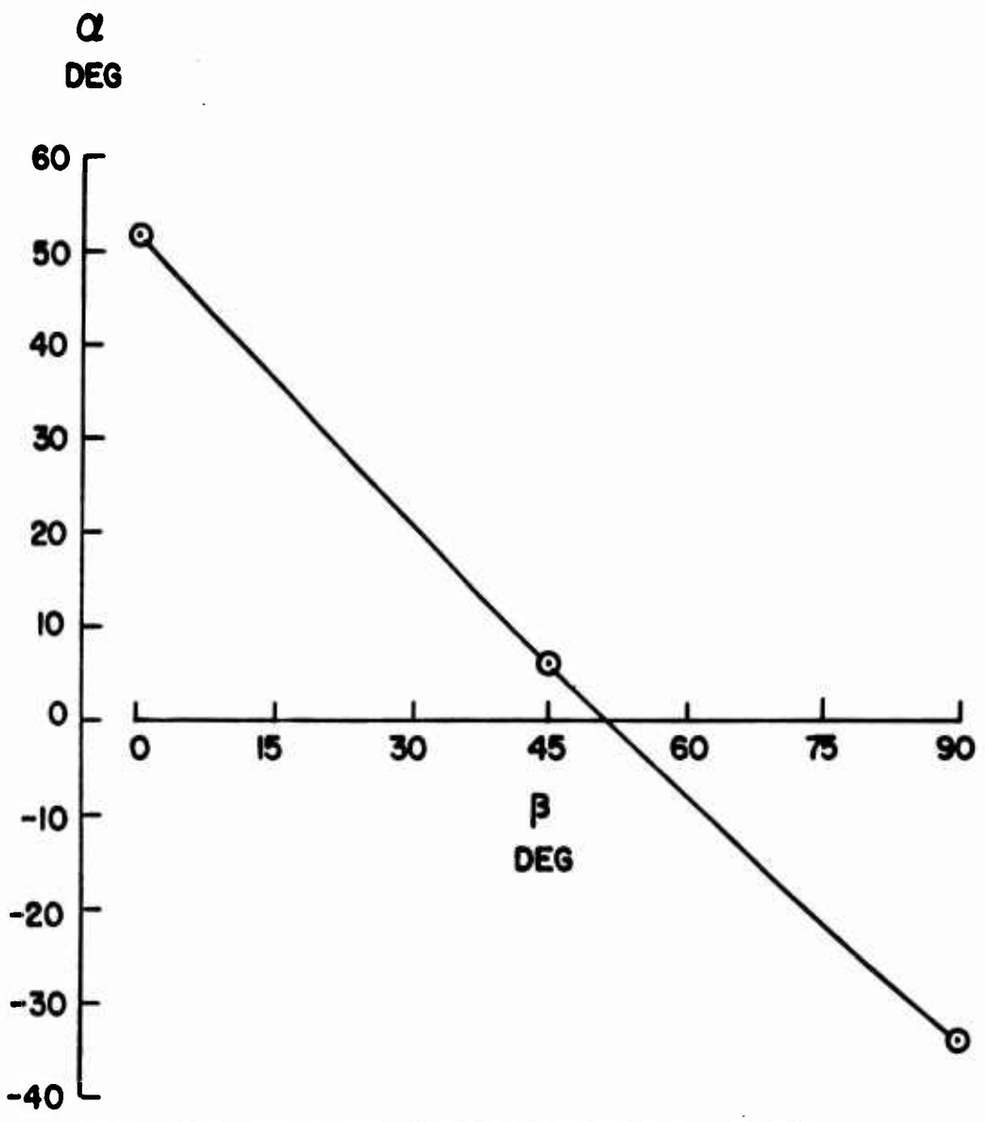

DATA FROM WARD, MARSLAND AND SAMUELS (1965)

FIGURE 3.45 (a)

VARIATION OF FAILURE PLANE ORIENTATION FOR UNCONSOLIDATED UNDRAINED TRIAXIAL TESTS ON LONDON CLAY FROM ASHFORD COMMON, LEVEL A.

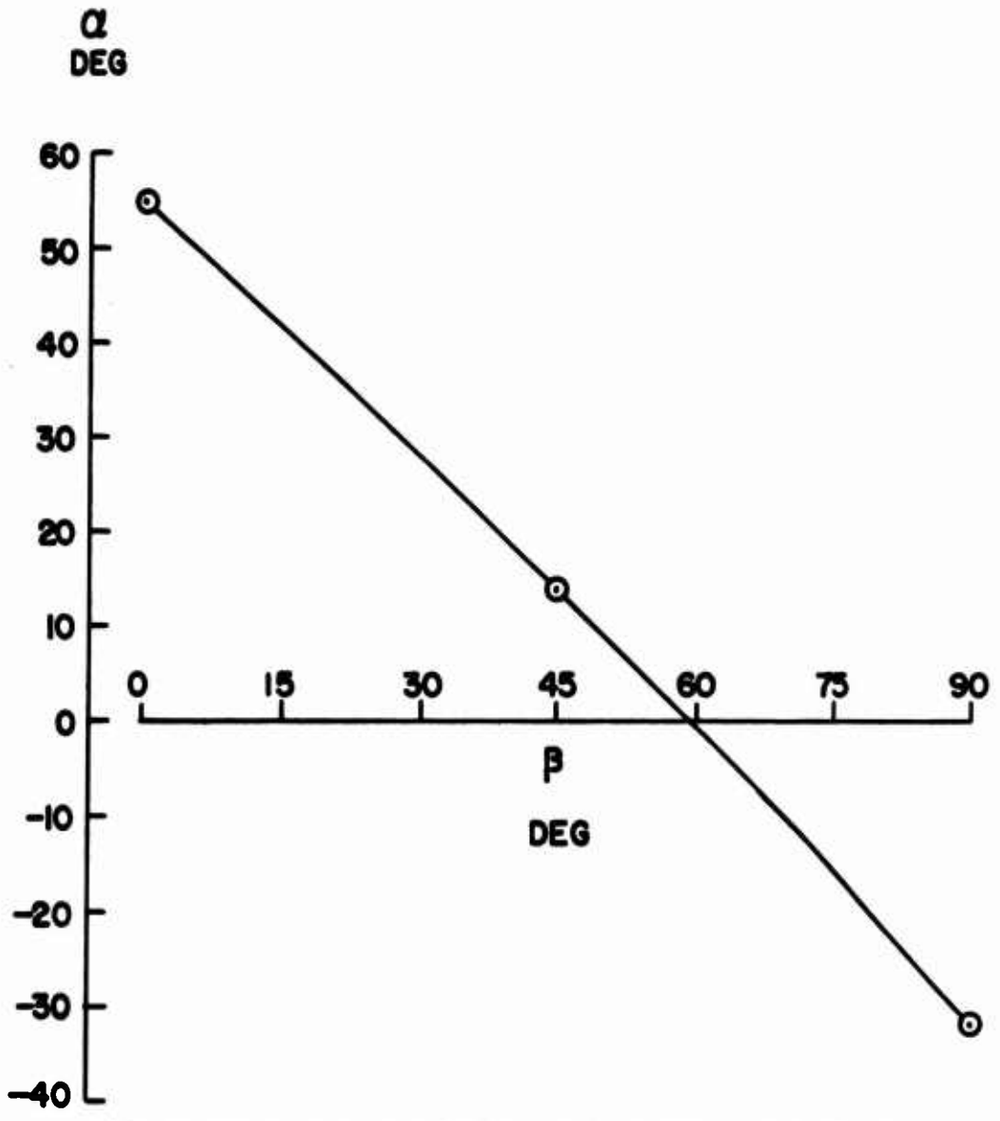

DATA FROM WARD, MARSLAND AND SAMUELS (1965)

FIGURE 3.45 (b)

VARIATION OF FAILURE PLANE ORIENTATION FOR UNCONSOLIDATED UNDRAINED TRIAXIAL TESTS ON LONDON CLAY FROM ASHFORD COMMON, LEVEL B

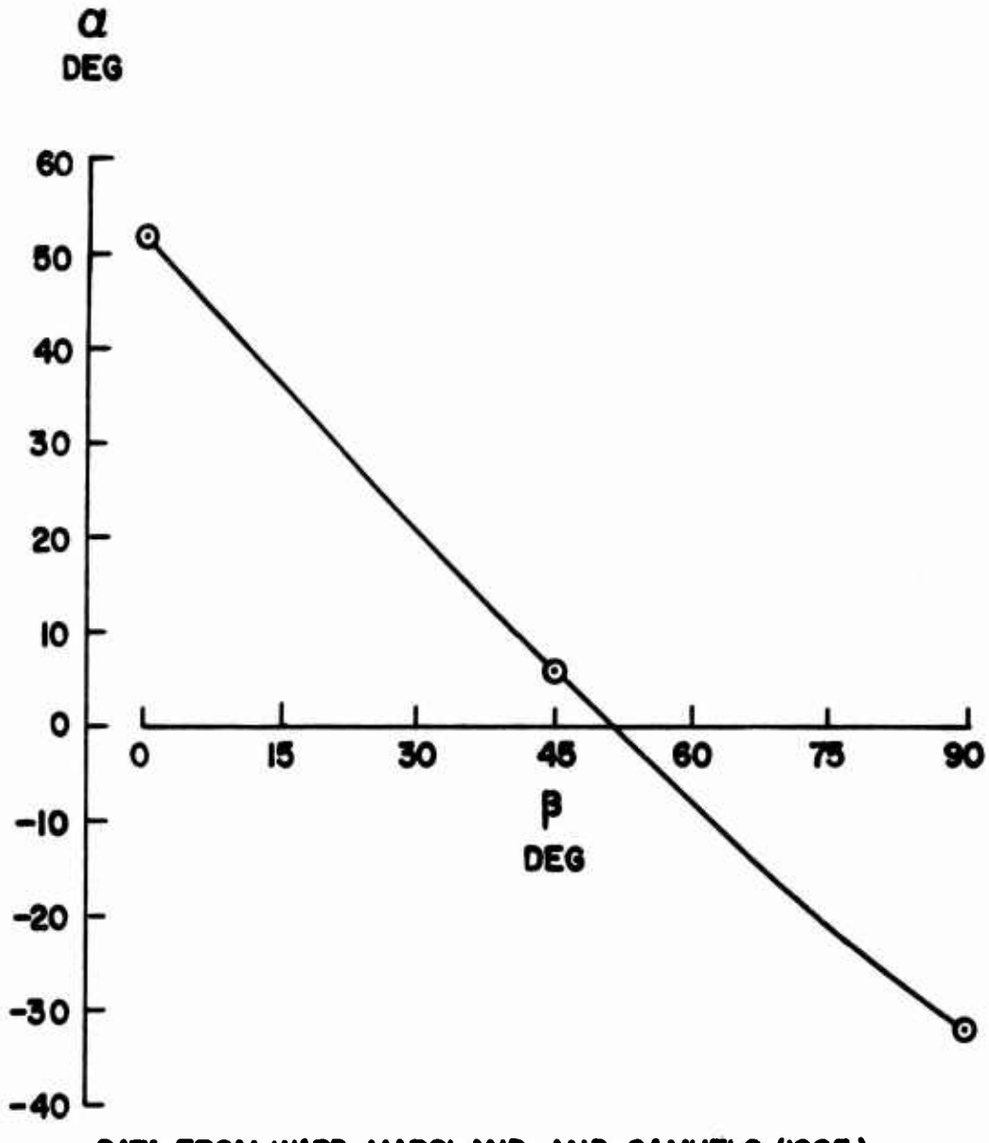

DATA FROM WARD, MARSLAND AND SAMUELS (1965)

FIGURE 3.45 (c)

VARIATION OF FAILURE PLANE ORIENTATION FOR UNCONSOLIDATED UNDRAINED TRIAXIAL TESTS ON LONDON CLAY FROM ASHFORD COMMON, LEVEL C

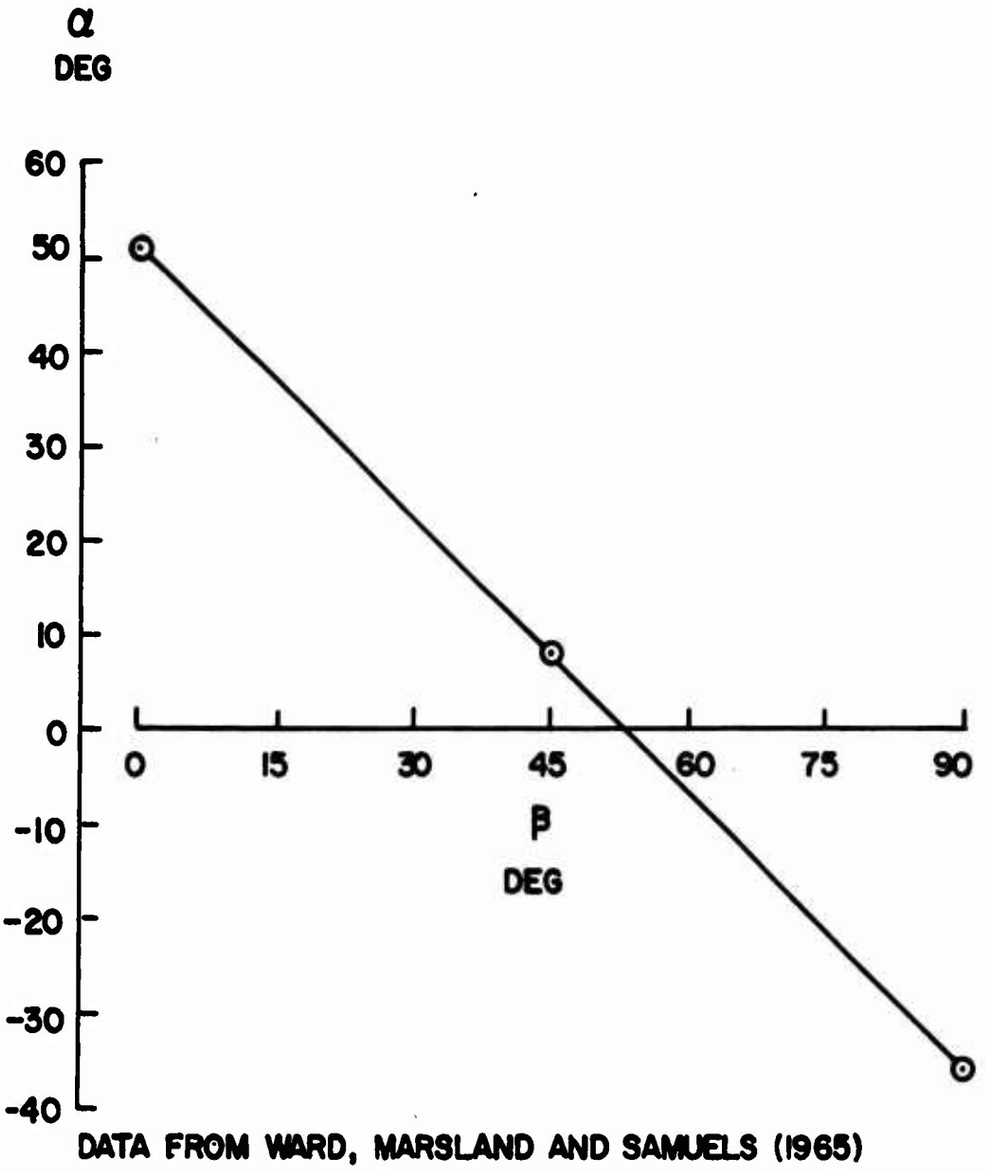

DATA FROM WARD, MARSLAND AND SAMUELS (1965)

FIGURE 3.45 (d)

VARIATION OF FAILURE PLANE ORIENTATION FOR UNCONSOLIDATED UNDRAINED TRIAXIAL TESTS ON LONDON CLAY FROM ASHFORD COMMON, LEVEL D

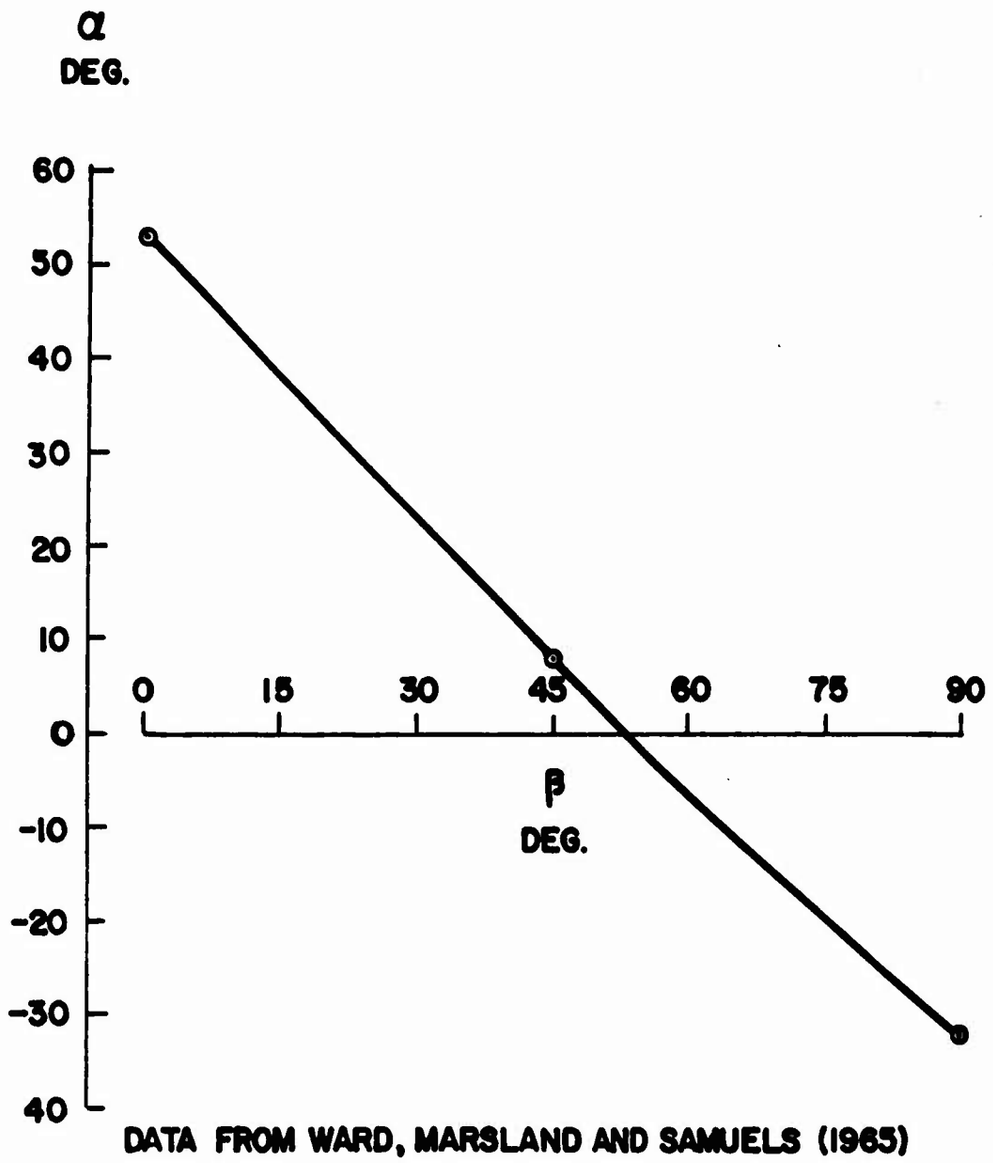

FIGURE 3.45 (e)

VARIATION OF FAILURE PLANE ORIENTATION FOR UNCONSOLIDATED UNDRAINED TRIAXIAL TESTS ON LONDON CLAY FROM ASHFORD COMMON, LEVEL E

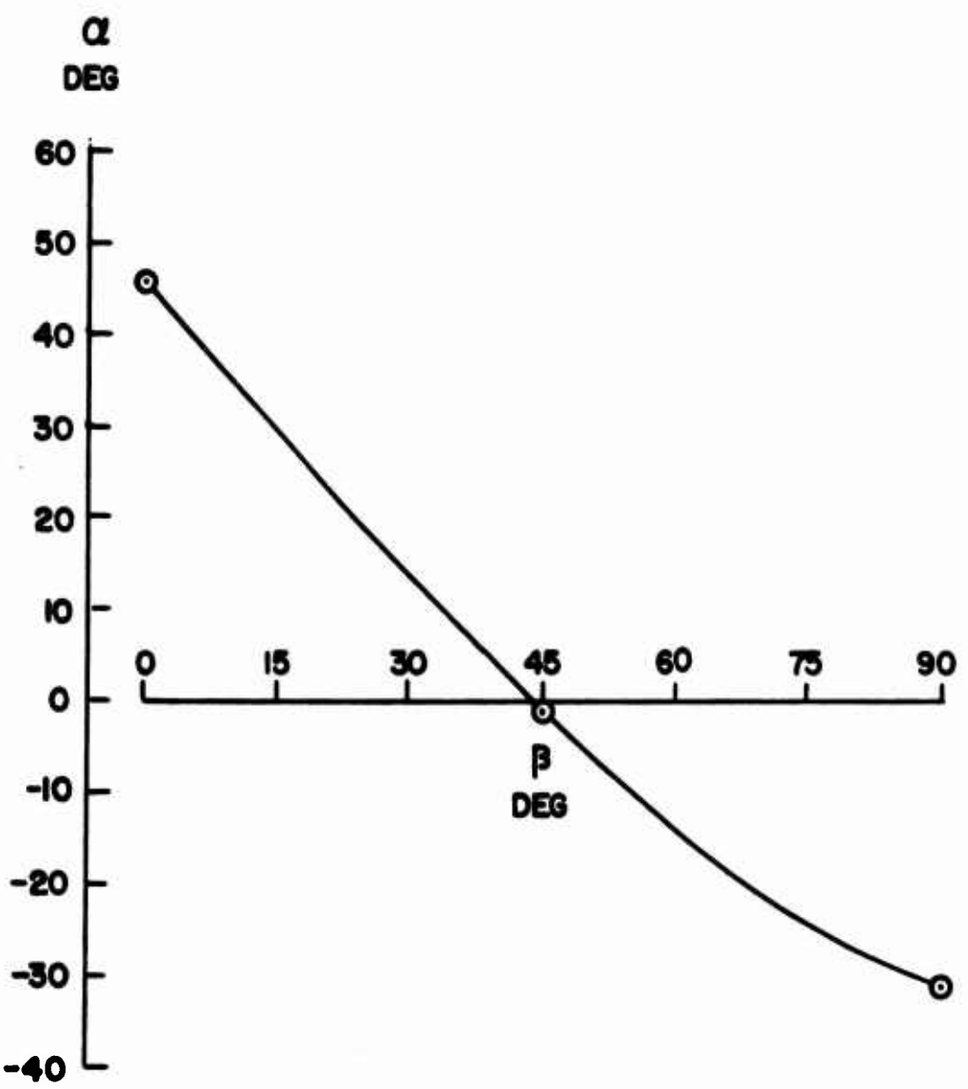

DATA FROM WARD, MARSLAND AND SAMUELS (1965)

FIGURE 3.45 (f)

VARIATION OF FAILURE PLANE ORIENTATION FOR UNCONSOLIDATED UNDRAINED TRIAXIAL TESTS ON LONDON CLAY FROM ASHFORD COMMON, LEVEL F

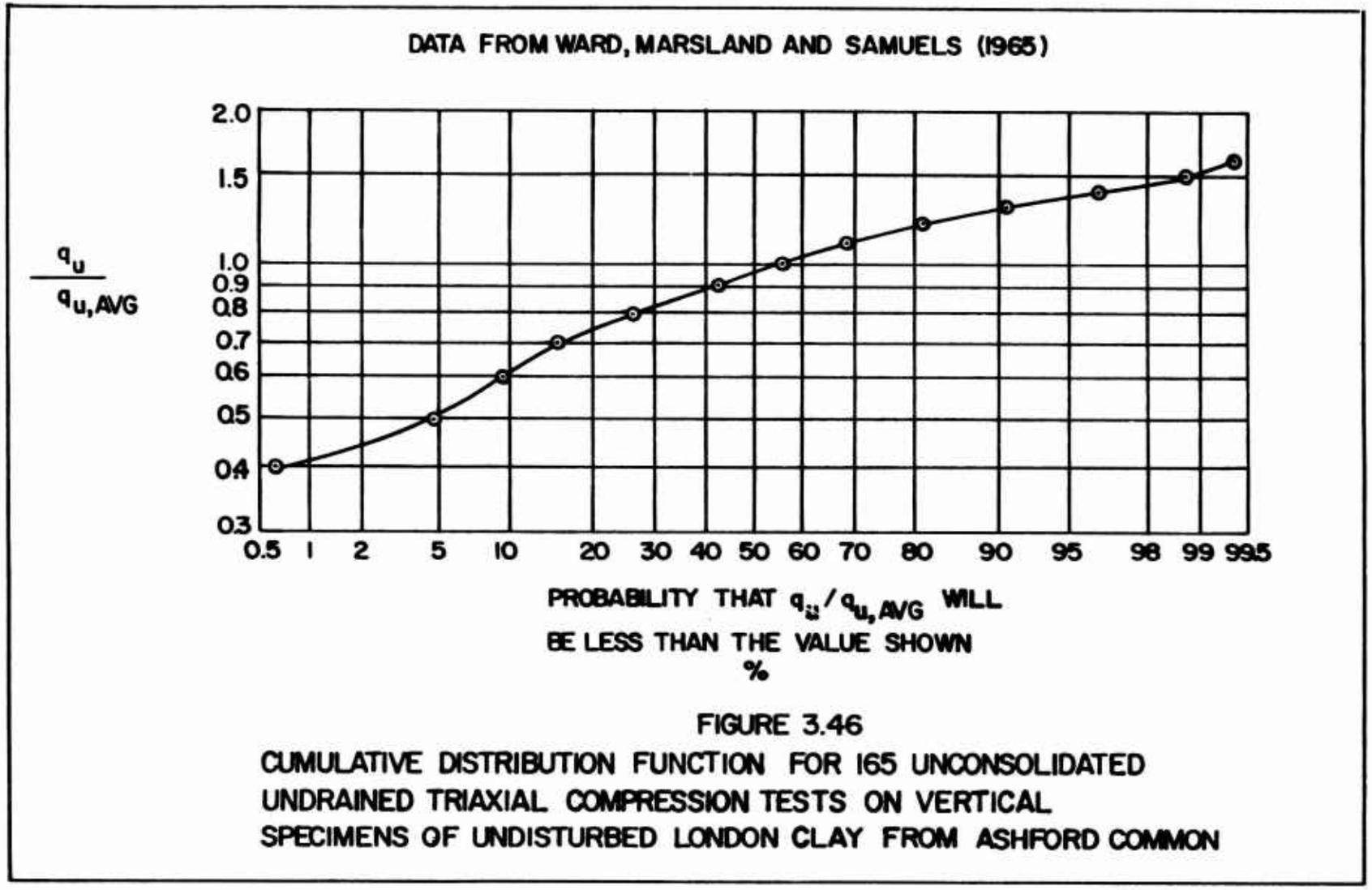

FIGURE 3.46

CUMULATIVE DISTRIBUTION FUNCTION FOR 165 UNCONSOLIDATED UNDRAINED TRIAXIAL COMPRESSION TESTS ON VERTICAL SPECIMENS OF UNDISTURBED LONDON CLAY FROM ASHFORD COMMON

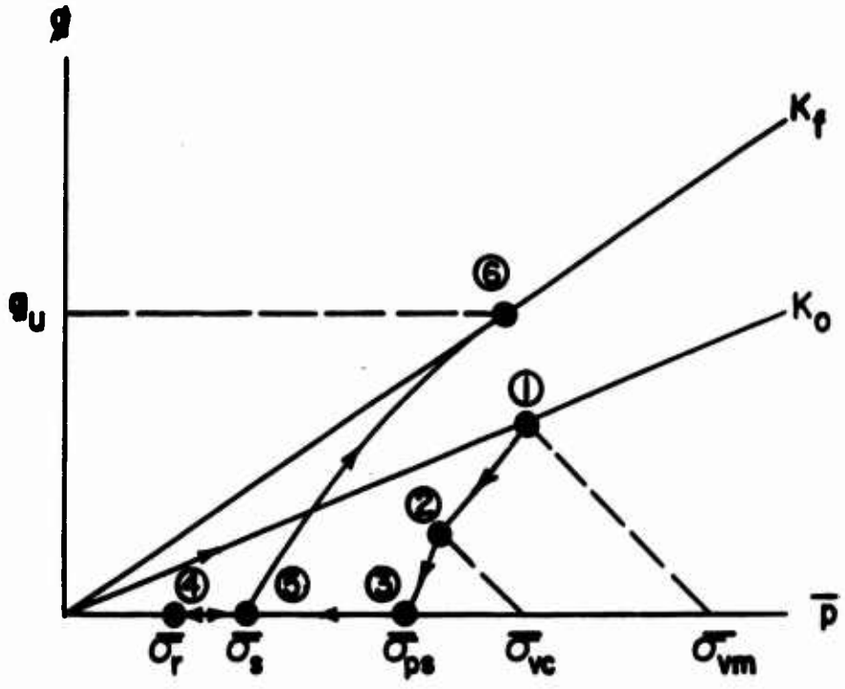

$$(OCR)_c = \frac{\bar{\sigma}_{vm}}{\bar{\sigma}_{vc}}$$

FIGURE 3.47

STRESS HISTORY FOR UU TRIAXIAL TEST ON RESEDIMENTED BOSTON BLUE CLAY

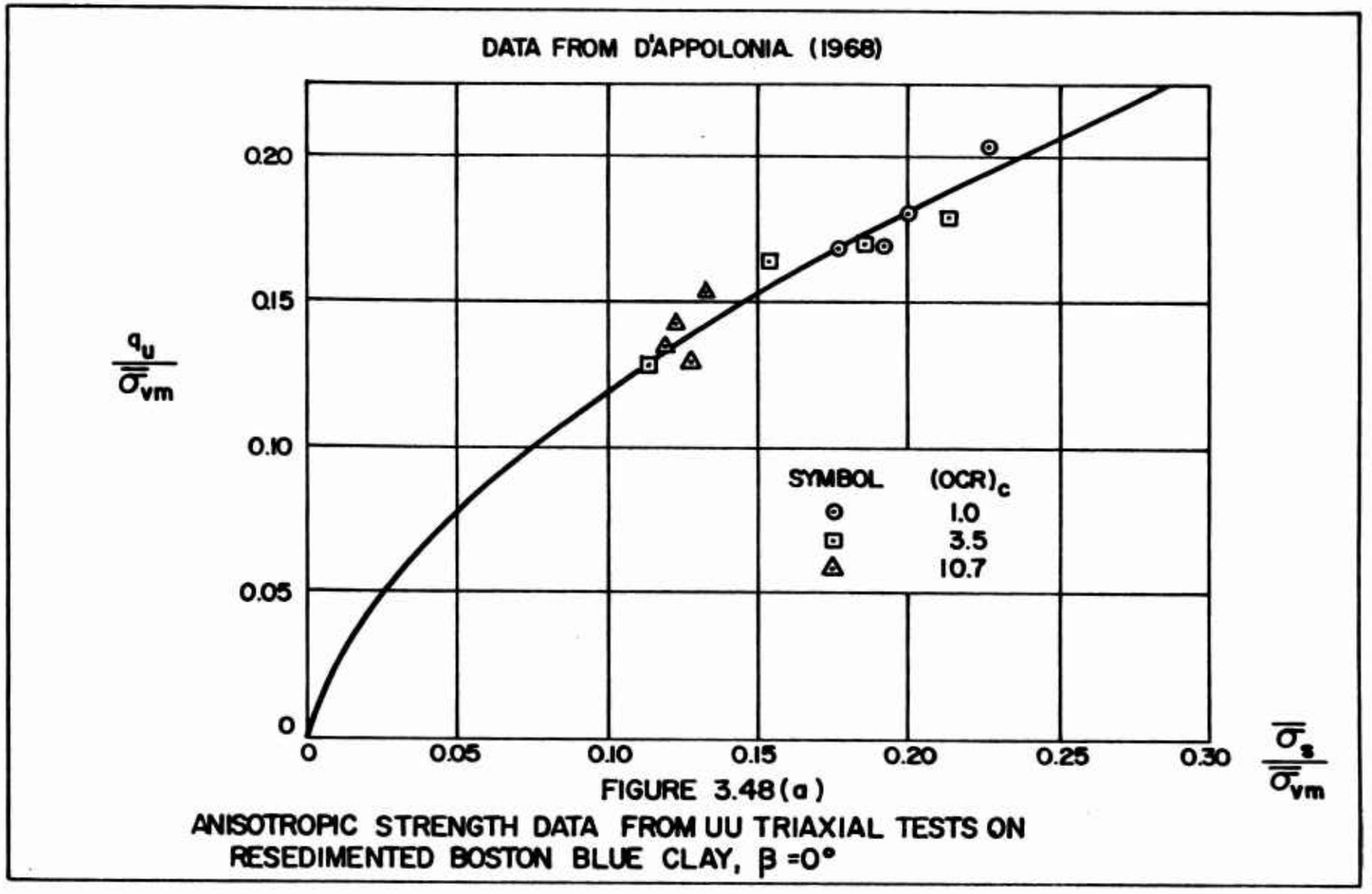

FIGURE 3.48(a)

ANISOTROPIC STRENGTH DATA FROM UU TRIAXIAL TESTS ON RESEDIMENTED BOSTON BLUE CLAY, $\beta = 0°$

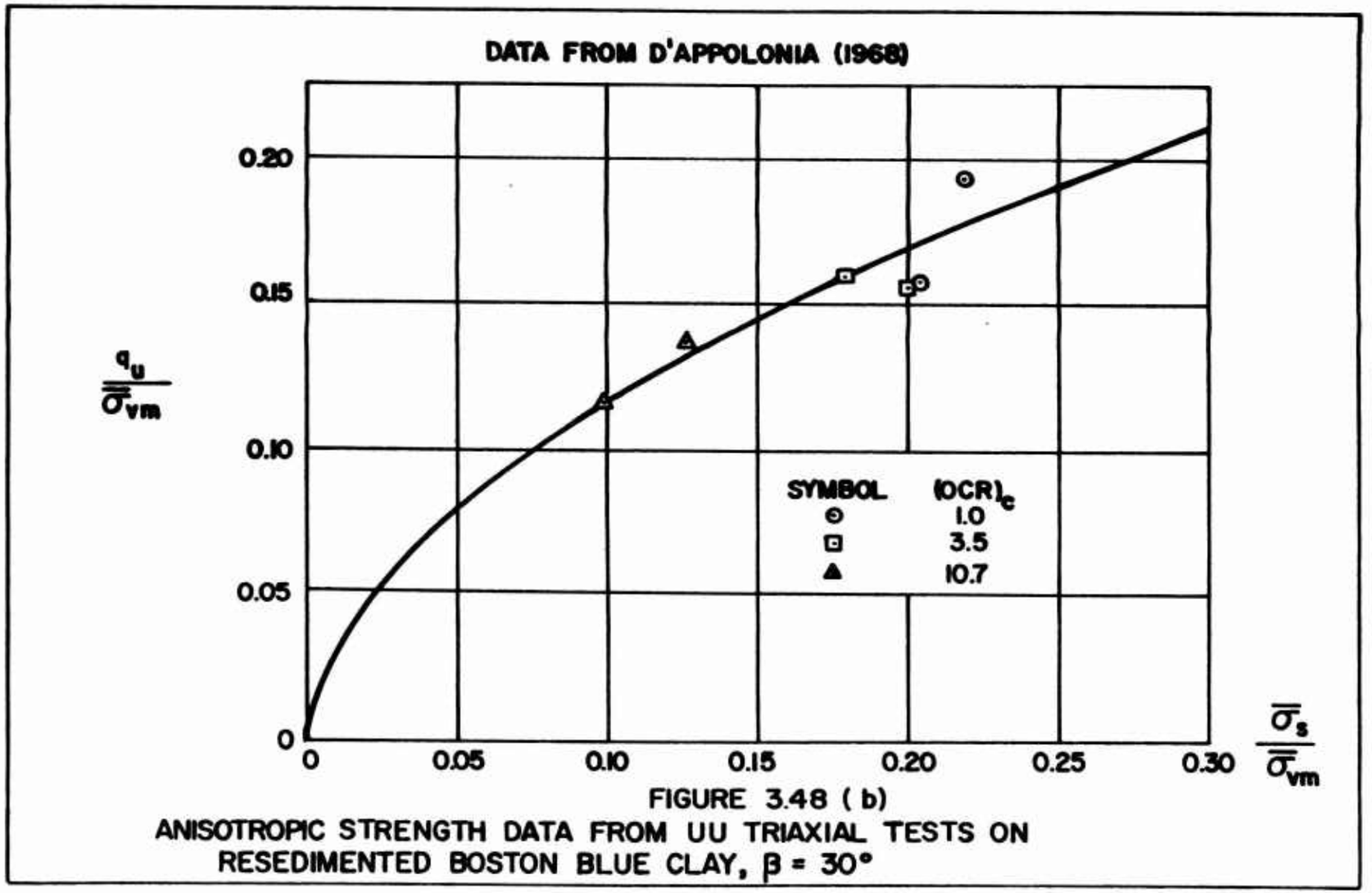

FIGURE 3.48 (b)

ANISOTROPIC STRENGTH DATA FROM UU TRIAXIAL TESTS ON RESEDIMENTED BOSTON BLUE CLAY, $\beta = 30°$

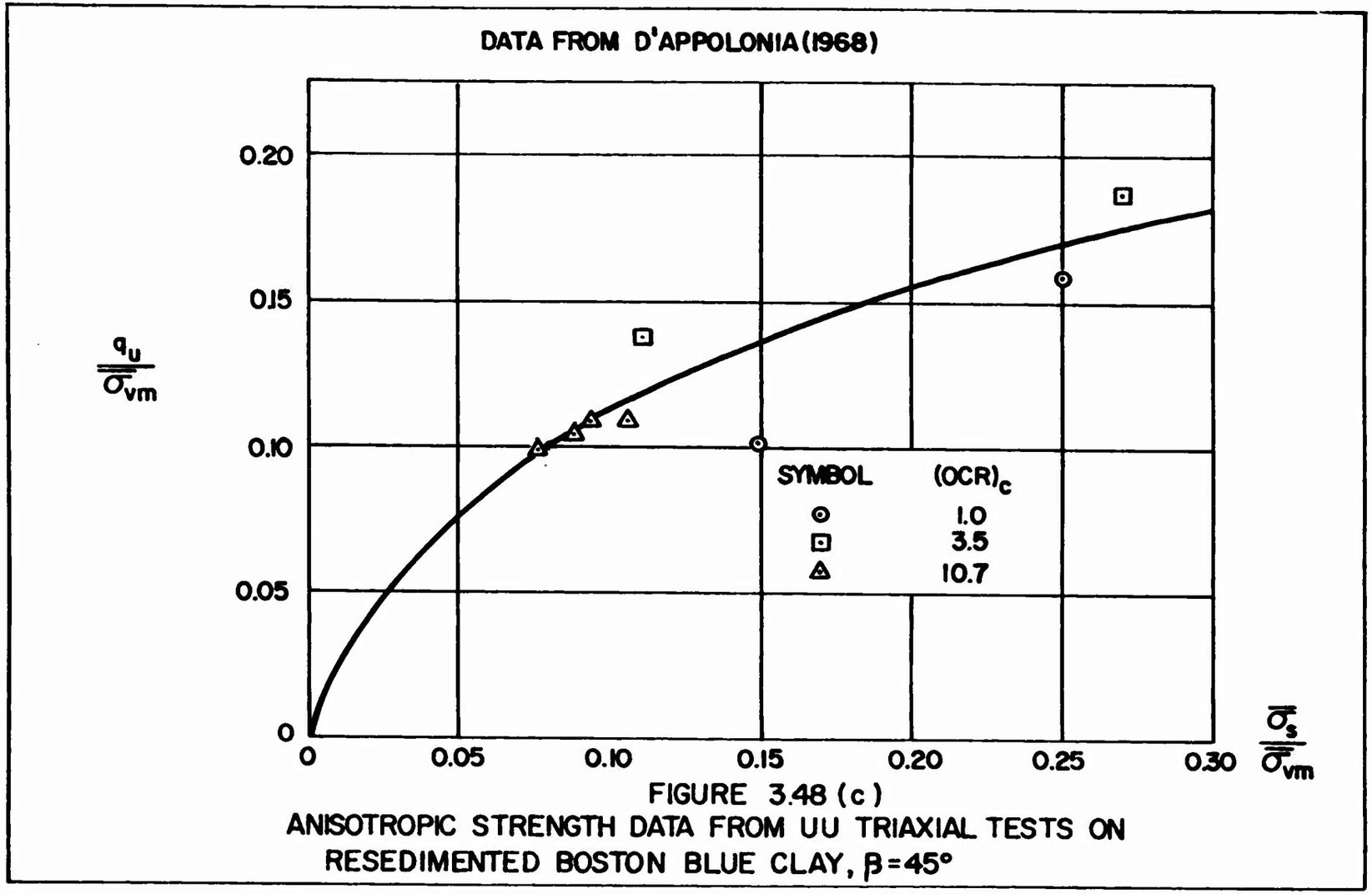

FIGURE 3.48 (c)
ANISOTROPIC STRENGTH DATA FROM UU TRIAXIAL TESTS ON RESEDIMENTED BOSTON BLUE CLAY, $\beta = 45°$

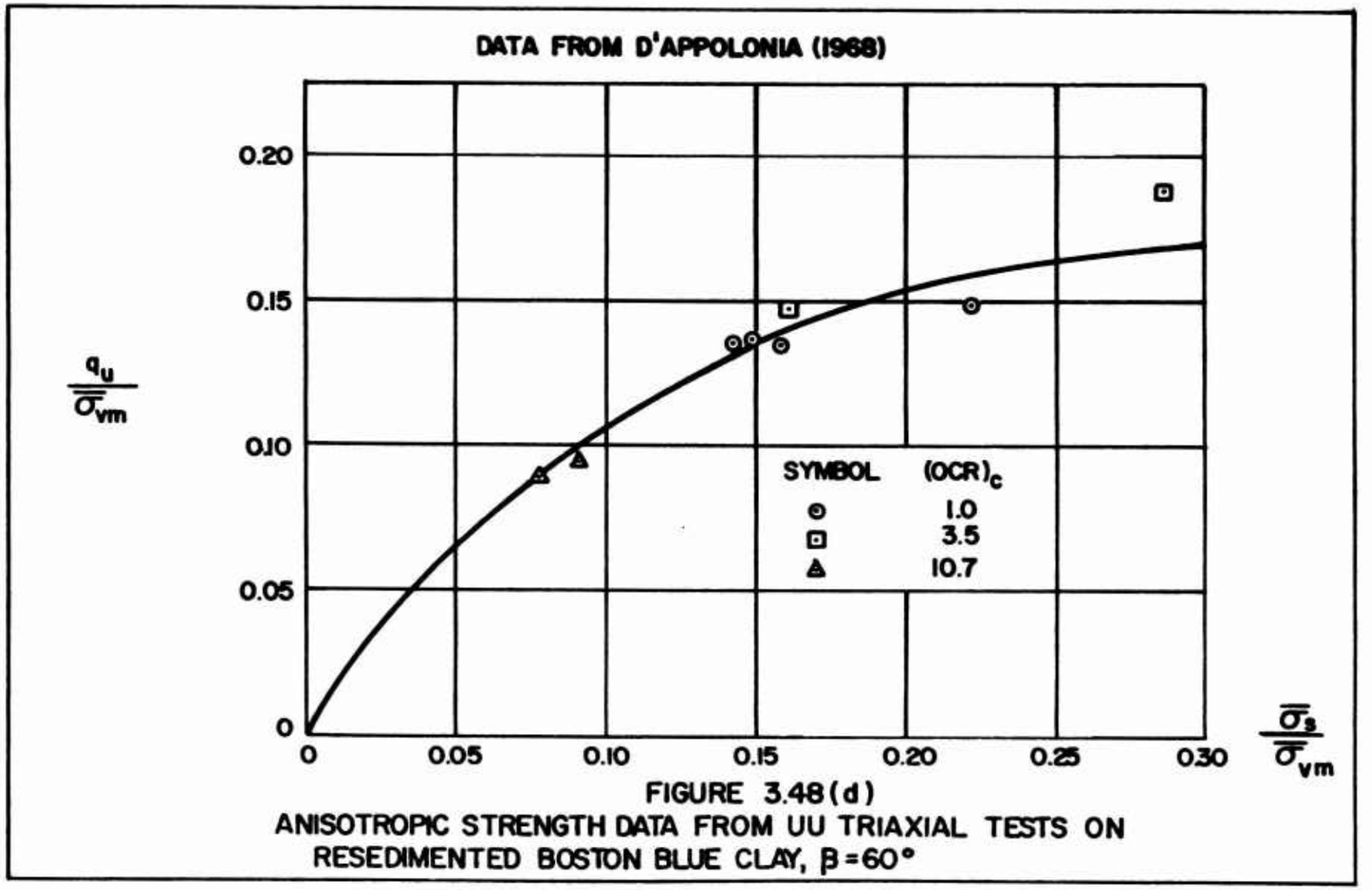

FIGURE 3.48(d)
ANISOTROPIC STRENGTH DATA FROM UU TRIAXIAL TESTS ON RESEDIMENTED BOSTON BLUE CLAY, $\beta = 60°$

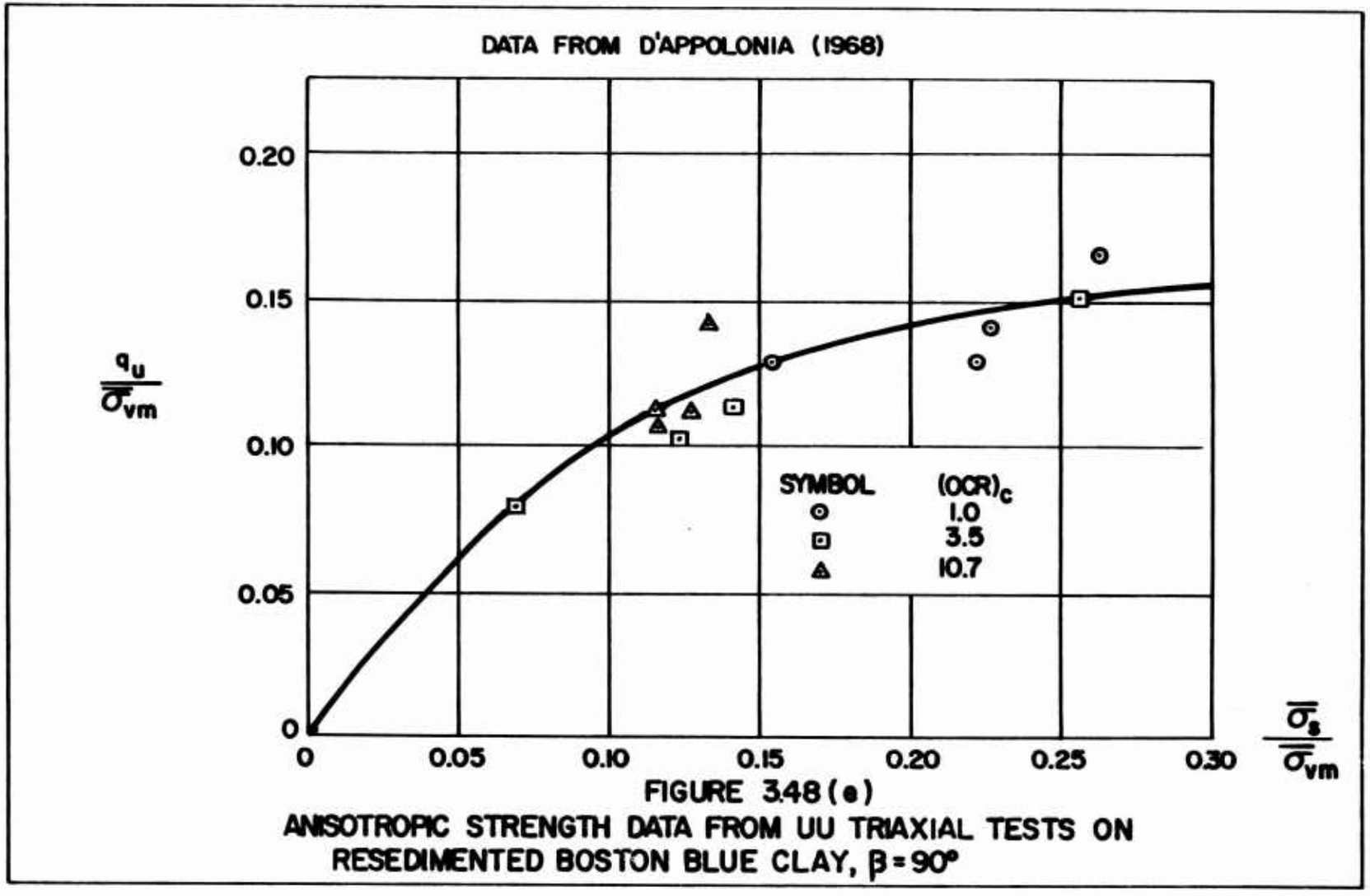

FIGURE 3.48 (e)

ANISOTROPIC STRENGTH DATA FROM UU TRIAXIAL TESTS ON RESEDIMENTED BOSTON BLUE CLAY, $\beta = 90°$

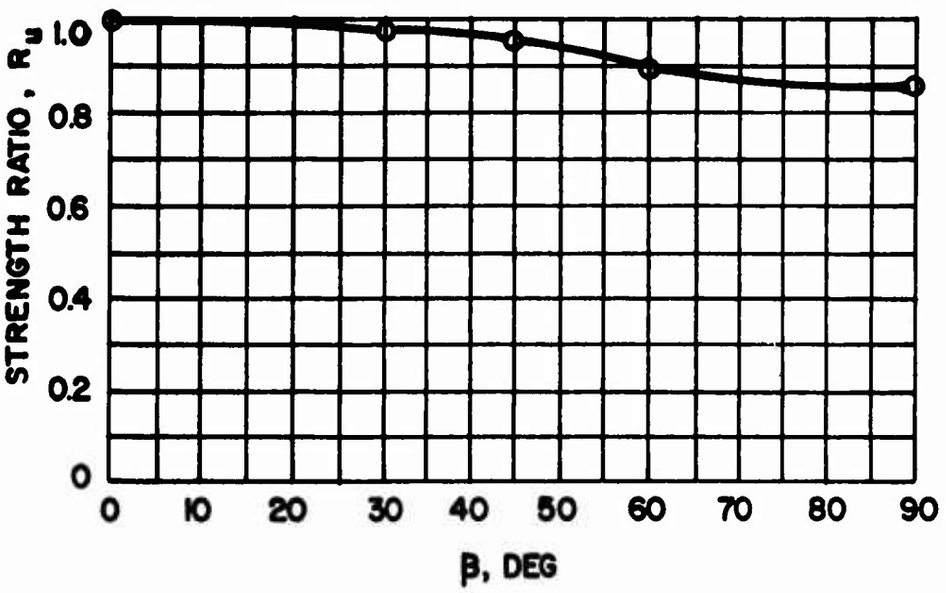

$q_{MAX} = q_f(0) = 0.118\ \overline{\sigma}_{vm}$

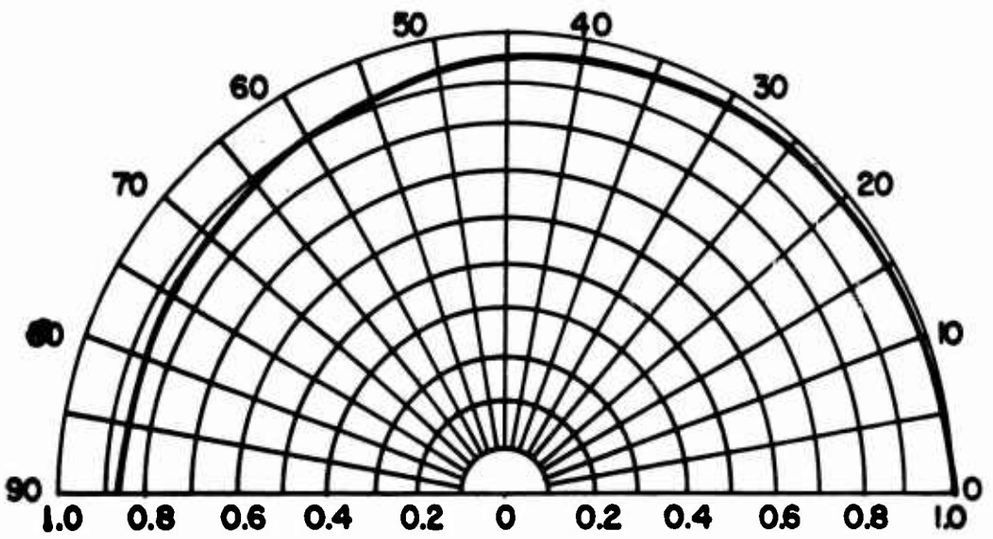

DATA FROM D'APPOLONIA (1968)

FIGURE 3.49 (a)

ANISOTROPIC STRENGTH RATIO R_u FOR RESEDIMENTED BOSTON BLUE CLAY, $\overline{\sigma}_s / \overline{\sigma}_{vm} = 0.10$

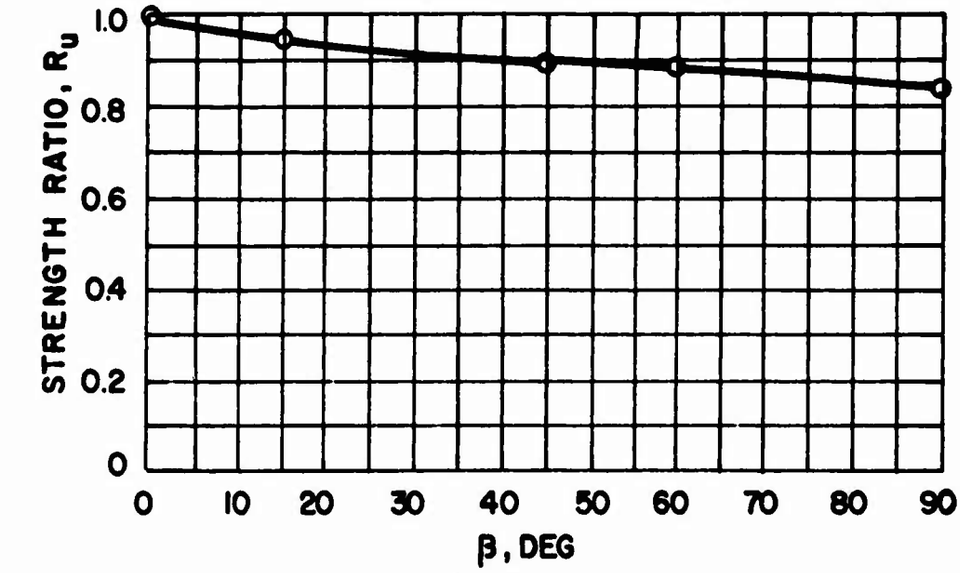

$q_{MAX} = q_f\,(0) = 0.152\,\bar{\sigma}_{vm}$

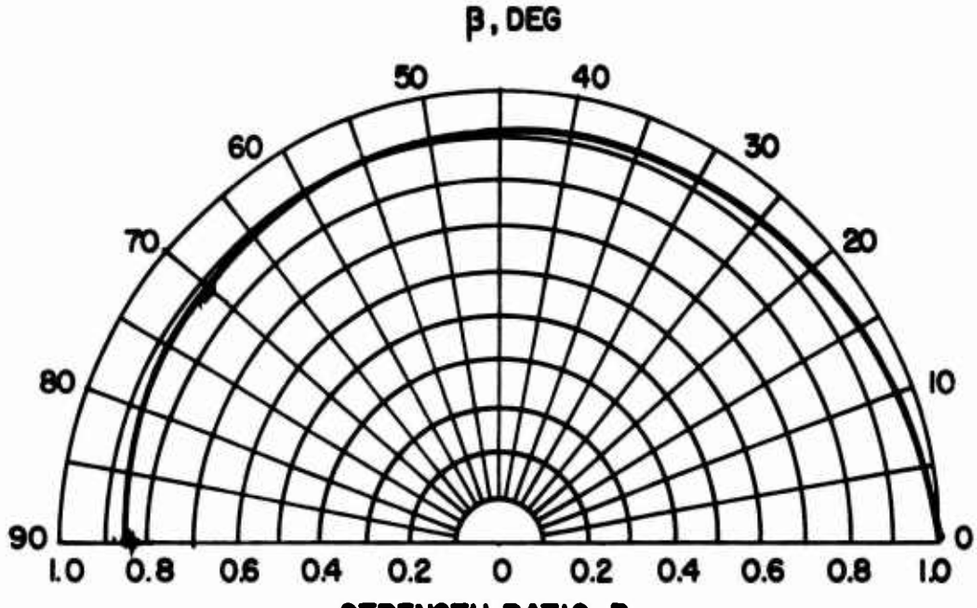

DATA FROM D'APPOLONIA (1968)

FIGURE 3.49 (b)

ANISOTROPIC STRENGTH RATIO R_u FOR RESEDIMENTED BOSTON BLUE CLAY, $\bar{\sigma}_s / \bar{\sigma}_{vm} = 0.15$

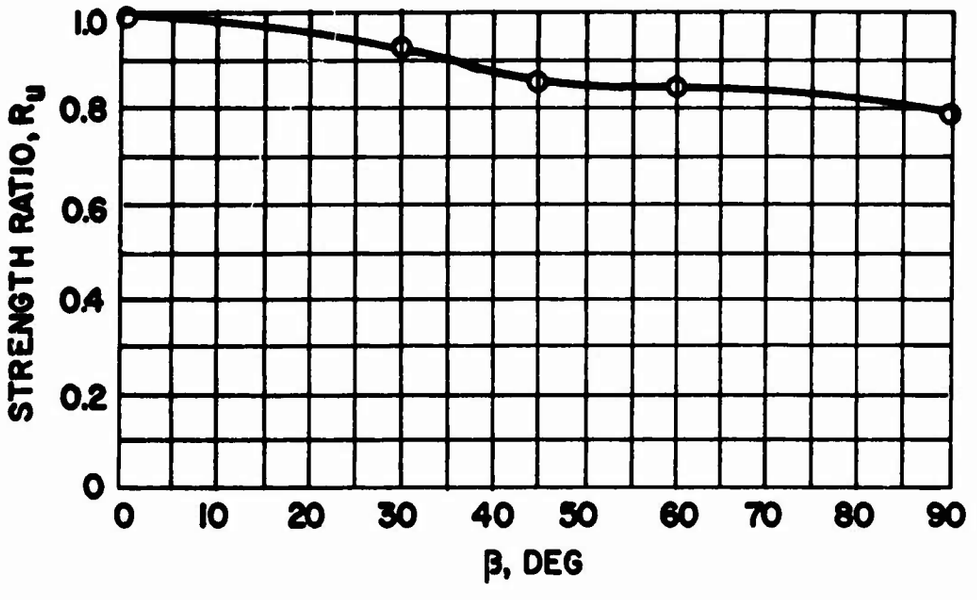

$q_{MAX} = q_f(0) = 0.180\,\overline{\sigma}_{vm}$

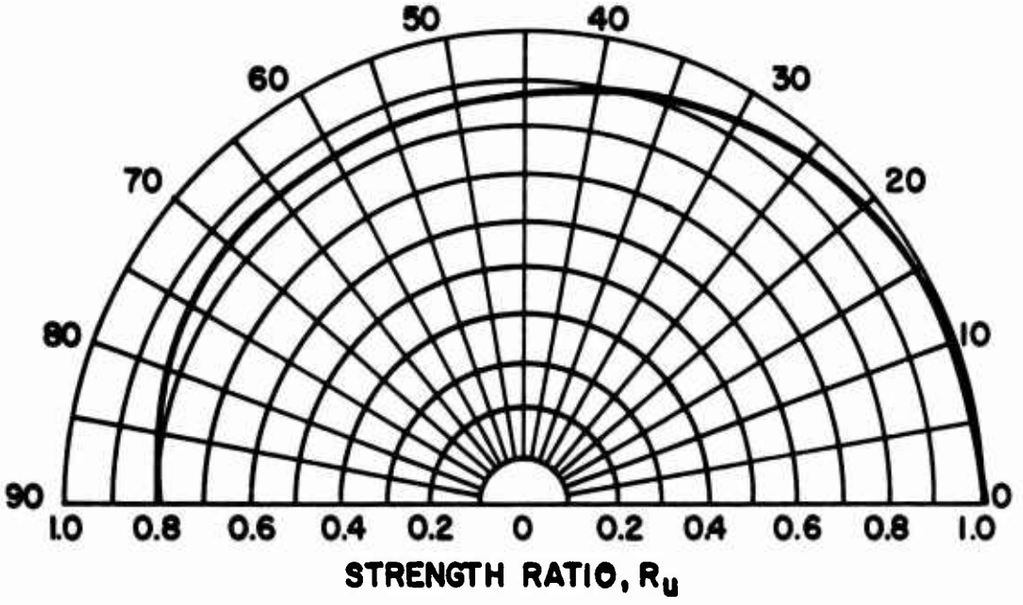

DATA FROM D'APPOLONIA (1968)

FIGURE 3.49 (c)

ANISOTROPIC STRENGTH RATIO R_u FOR RESEDIMENTED BOSTON BLUE CLAY, $\overline{\sigma}_s / \overline{\sigma}_{vm} = 0.20$

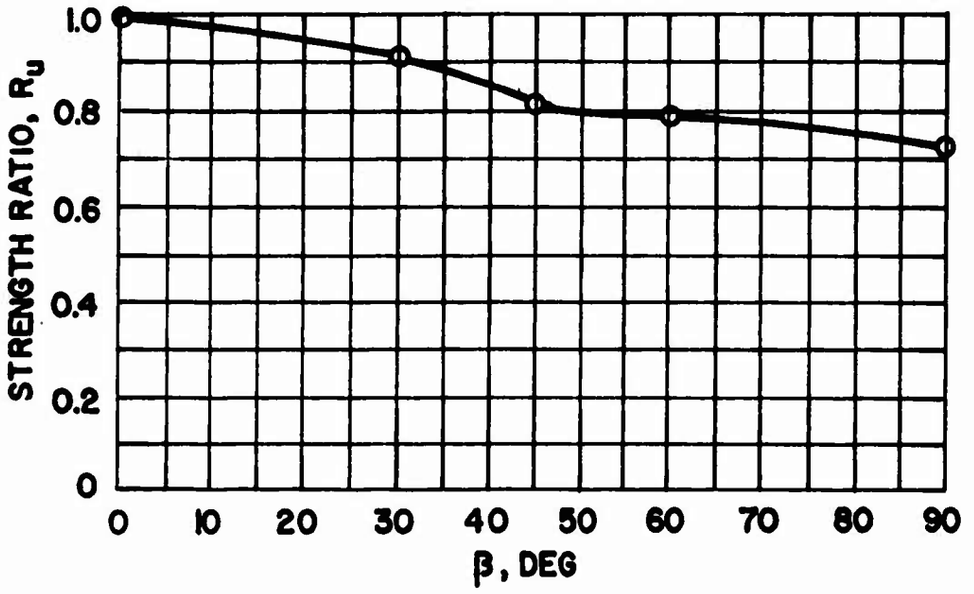

$q_{MAX} = q_f\,(0) = 0.207\,\overline{\sigma}_{vm}$

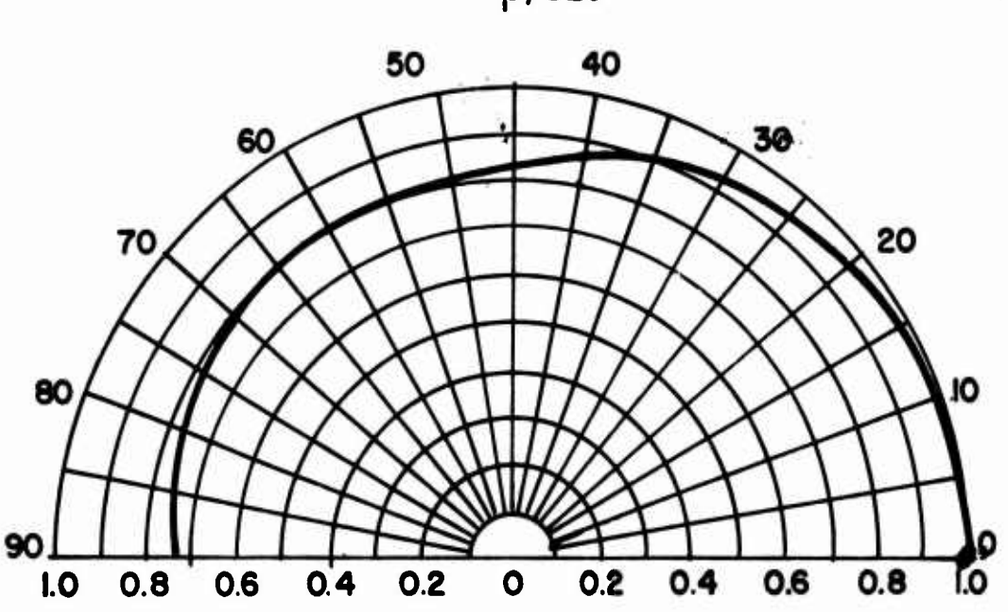

DATA FROM D'APPOLONIA (1968)

FIGURE 3.49 (d)

ANISOTROPIC STRENGTH RATIO R_u FOR RESEDIMENTED BOSTON BLUE CLAY, $\overline{\sigma}_s / \overline{\sigma}_{vm} = 0.25$

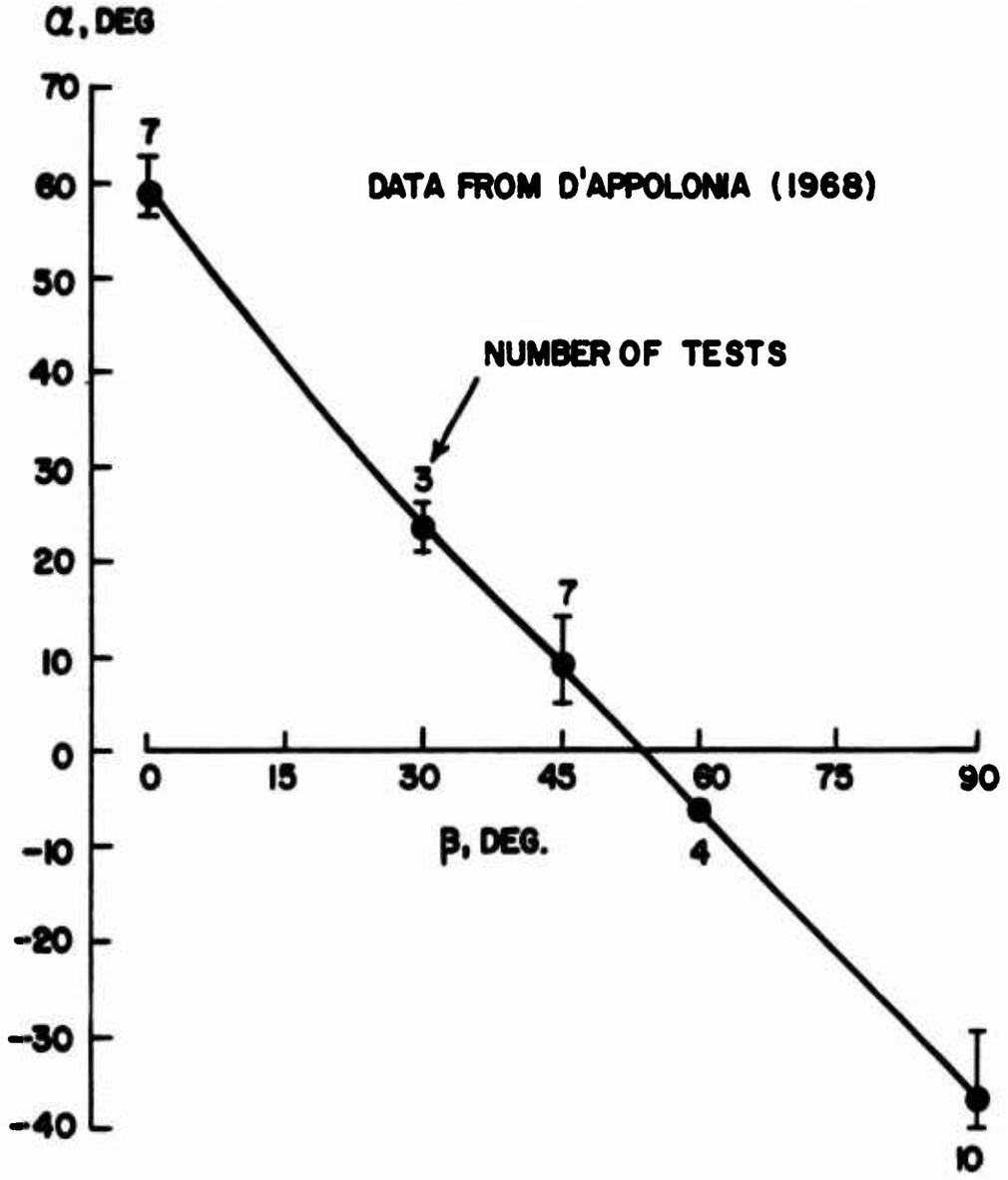

FIGURE 3.50

VARIATION OF FAILURE PLANE ORIENTATION FOR UU TRIAXIAL TESTS ON RESEDIMENTED BOSTON BLUE CLAY.

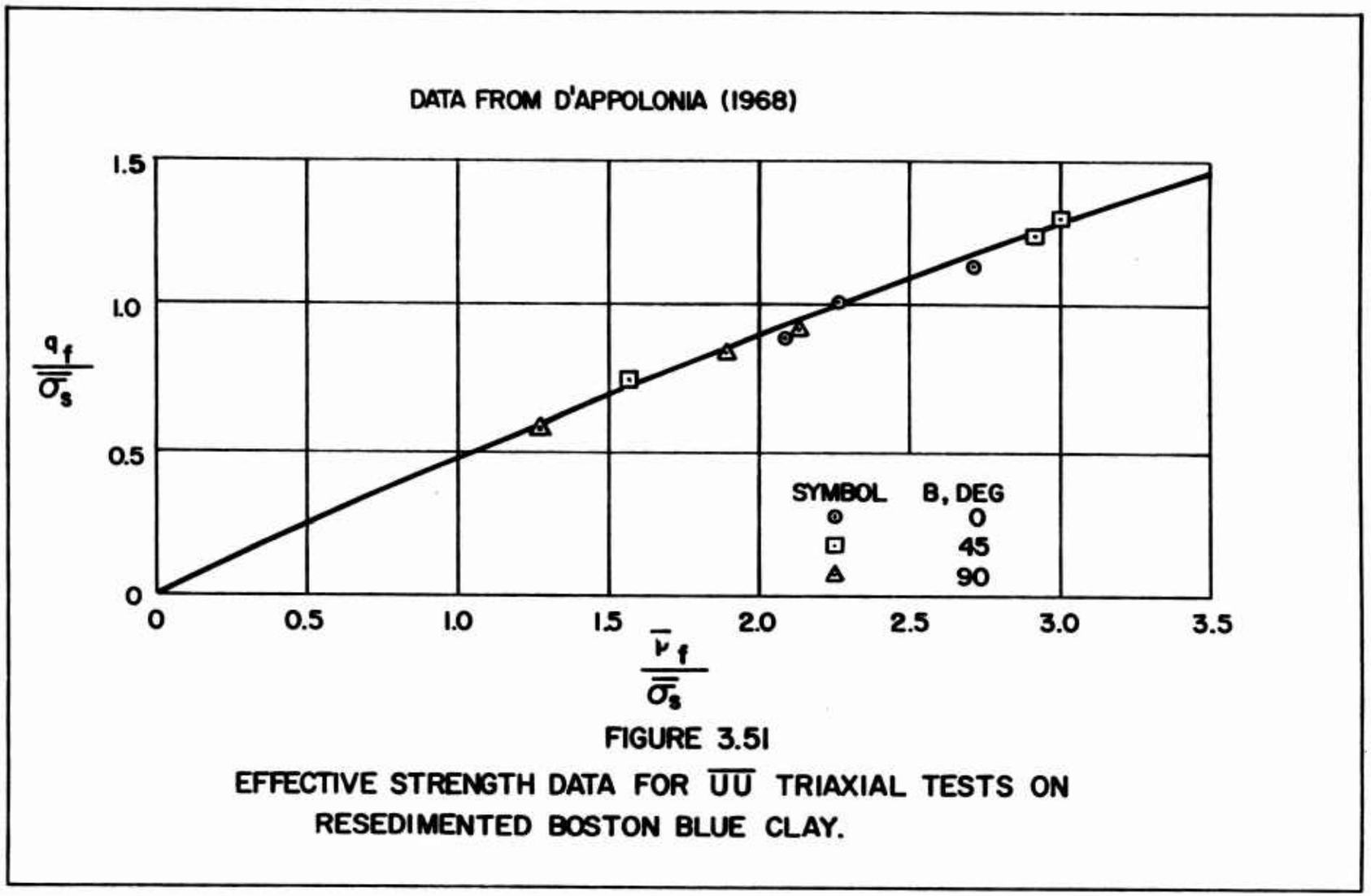

FIGURE 3.51

EFFECTIVE STRENGTH DATA FOR $\overline{UU}$ TRIAXIAL TESTS ON RESEDIMENTED BOSTON BLUE CLAY.

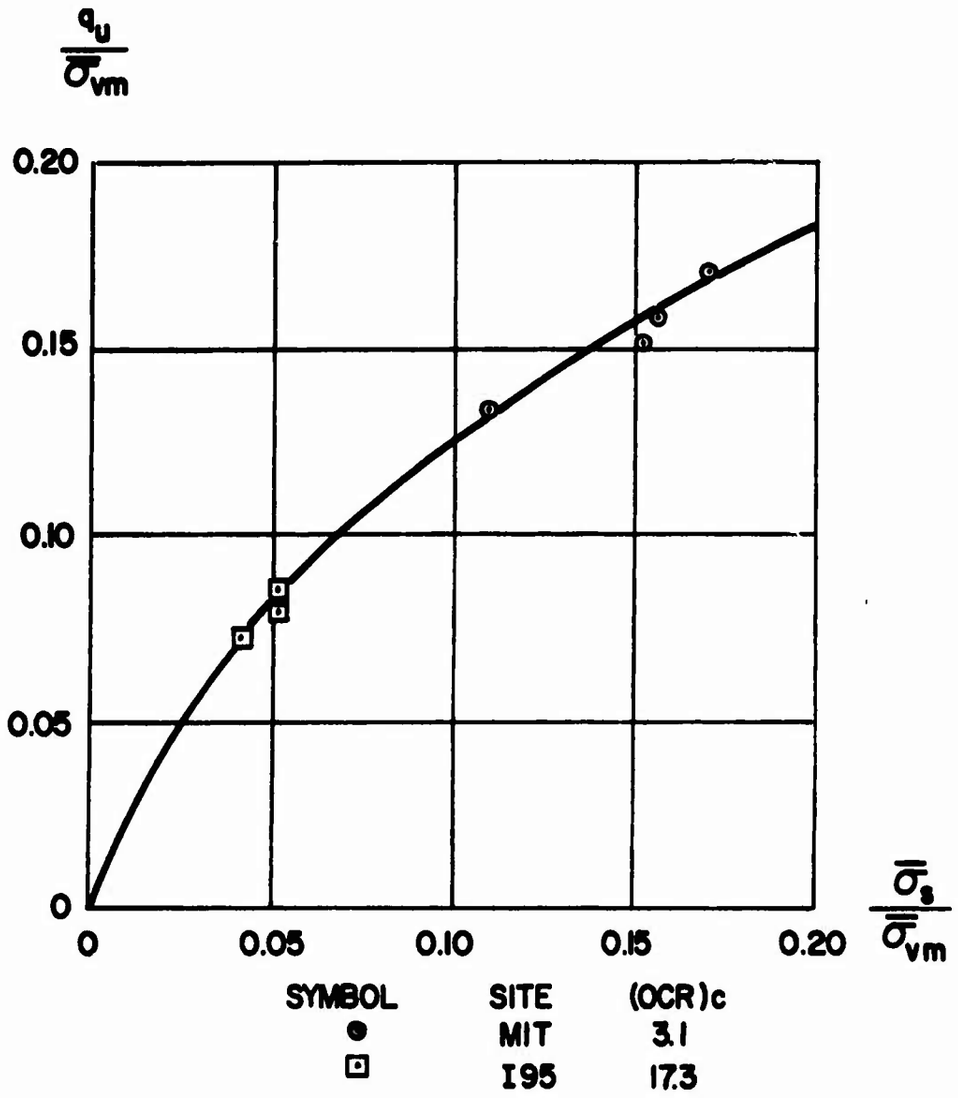

DATA FROM D'APPOLONIA (1968)

FIGURE 3.52(a)

ANISOTROPIC STRENGTH DATA FROM UU TRIAXIAL TESTS ON UNDISTURBED BOSTON BLUE CLAY, $\beta = 0°$

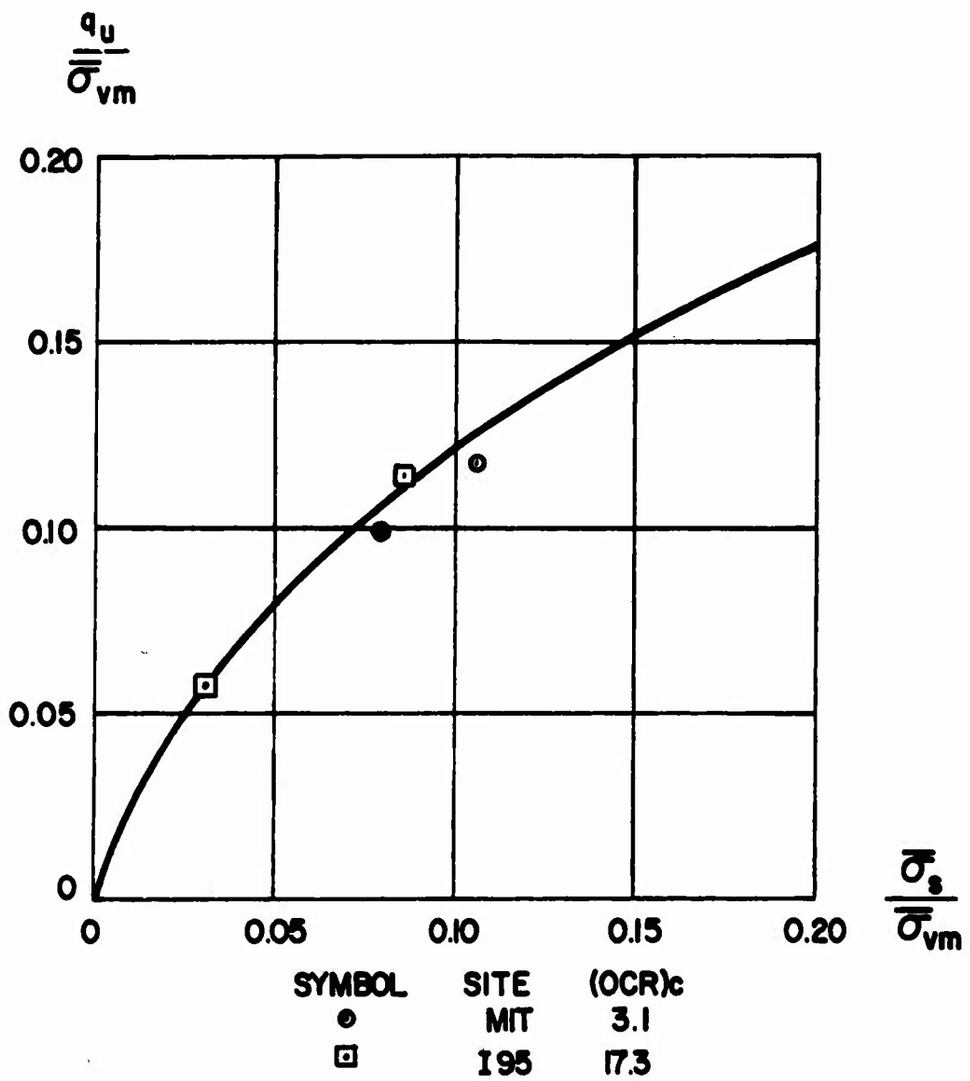

DATA FROM D'APPOLONIA (1968)

FIGURE 3.52(b)

ANISOTROPIC STRENGTH DATA FROM UU TRIAXIAL TESTS ON UNDISTURBED BOSTON BLUE CLAY, $\beta = 45°$

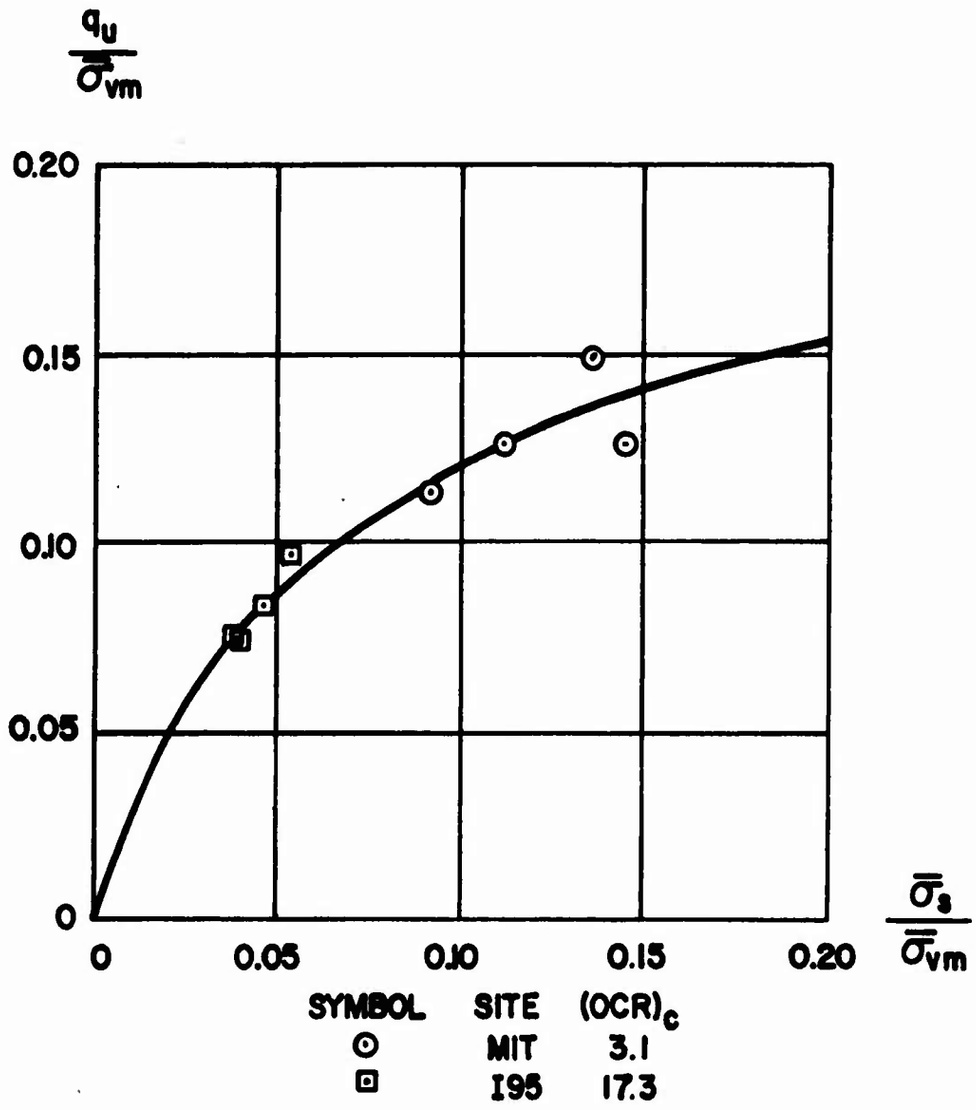

DATA FROM D'APPOLONIA (1968)

FIGURE 3.52(c)

ANISOTROPIC STRENGTH DATA FROM UU TRIAXIAL TESTS ON UNDISTURBED BOSTON BLUE CLAY, $\beta = 90°$

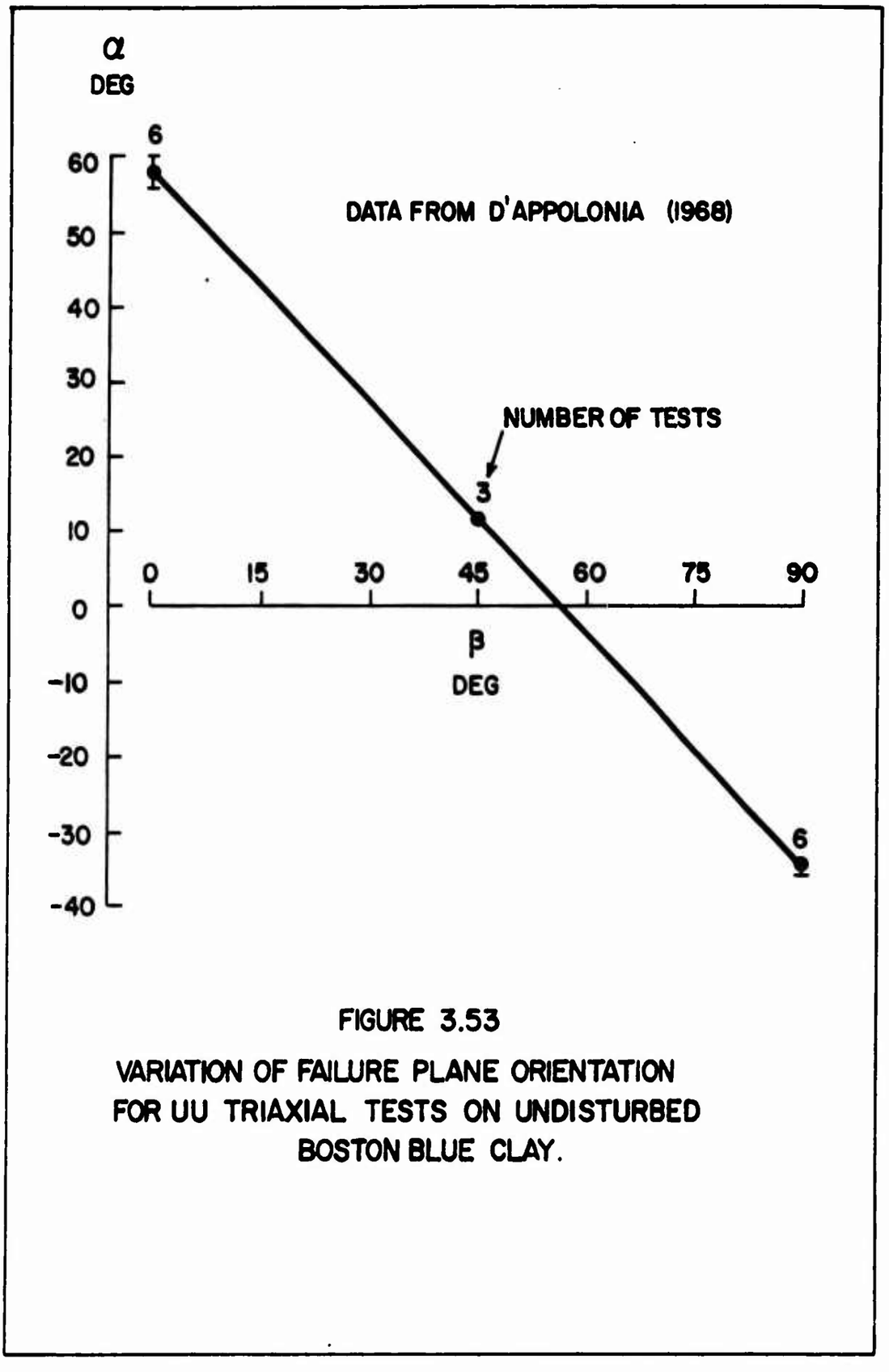

FIGURE 3.53

VARIATION OF FAILURE PLANE ORIENTATION FOR UU TRIAXIAL TESTS ON UNDISTURBED BOSTON BLUE CLAY.

CHAPTER 4

PORE PRESSURE RESPONSE

Purpose

The purpose of this chapter is to briefly review the development of concepts relating applied total stress and the resulting excess pore pressure in saturated clay, and then to propose an empirical pore pressure response relationship which is particularly convenient for treating the problem of rotation of principal planes, to be discussed in the following chapter.

Historical Development

As soon as it was recognized that the shear strength of soils is controlled by effective stress, attempts were made to predict the excess pore pressure induced in saturated clay by the application of given total stresses, under the condition of no pore water flow. The first such attempt known to the Writer was that of CASAGRANDE (1934). Shortly afterward RENDULIC (1936b) developed an empirical approach to excess pore pressure prediction, which is the basis for the method to be presented in this chapter. Subsequent, more theoretical approaches have relied on assumed relationships between a

change in effective stress and the resulting change in volume. The most common assumption of this nature is that a decrease in the minor principal effective stress, $\bar{\sigma}_3$, at constant major principal effective stress, $\bar{\sigma}_1$, always results in a volume increase. However, for normally consolidated and lightly overconsolidated clays this is not what happens. Figure 4.1 shows that at any point on the undrained effective stress path beyond Point B, a decrease in $\bar{\sigma}_3$ at constant $\bar{\sigma}_1$ results in a volume decrease, not an increase. This is because the volume decrease associated with shearing strain more than offsets the volume increase due to the decrease in all-round effective stress.

The reason for approaching the problem of pore pressure prediction analytically is to obtain insight into the meaning and fundamental nature of the pore pressure parameters used in practice; LAMBE (1963, 879). The only reliable method of actually predicting excess pore pressure in the field is to run an undrained test and measure Δu directly; BISHOP (1954), HENKEL (1958, Fig 64), LAMBE (1963, 876). Otherwise, pore pressure parameters are simply useful tools for the exercise of engineering judgement. For example, they emphasize the fact that there are two fundamental causes of excess pore pressure during undrained loading:

1) increase in all-round total stress, and

2) shear

Real progress in understanding the stress-strain and shear strength behavior of saturated cohesive soils was not made until the second cause was recognized; SKEMPTON (1960a, 53).

Pore Pressure Response Prediction

All predictions of stress-strain behavior in engineering materials are empirical, in the sense that tests are required to determine the values of parameters in phenomenological stress-strain equations. In order to independently predict excess pore pressure response, the relation between a change in effective stress and the resulting change in volume must be known. This requires the availability of an incremental plasticity theory which accounts for both strain hardening and substantial plastic volumetric strain. A reliable theory of this type does not exist for soil. Consequently the empirical prediction of pore pressure response in soil really amounts to little more than interpolating or extrapolating observed behavior. Therefore, the question at issue here is really not how to predict pore pressure response, but how to describe it in the most revealing and useful way.

Stress Path Approach

The key to the relation between total stress and pore pressure during undrained loading lies in the Stress Path Method; RENDULIC (1936b), LAMBE (1967). First however, the matter of precisely which total stresses should be used to calculate excess pore pressure must be settled.

Consider the element of soil, shown in Figure 4.2a, currently subjected to a system of total stresses,

$$\left[\sigma_{ij}\right] = \begin{bmatrix} \sigma_{11} & \sigma_{12} & \sigma_{13} \\ \sigma_{21} & \sigma_{22} & \sigma_{23} \\ \sigma_{31} & \sigma_{32} & \sigma_{33} \end{bmatrix}$$

When the system of total stress increments,

$$\left[\Delta\sigma_{ij}\right] = \begin{bmatrix} \Delta\sigma_{11} & \Delta\sigma_{12} & \Delta\sigma_{13} \\ \Delta\sigma_{21} & \Delta\sigma_{22} & \Delta\sigma_{23} \\ \Delta\sigma_{31} & \Delta\sigma_{32} & \Delta\sigma_{33} \end{bmatrix}$$

shown in Figure 4.2b, is applied to the soil element, the resulting total stresses are the sum of $\left[\sigma_{ij}\right]$ and $\left[\Delta\sigma_{ij}\right]$, as shown in Figure 4.2c.

$$\left[\sigma_{ij} + \Delta\sigma_{ij}\right] = \begin{bmatrix} \sigma_{11} + \Delta\sigma_{11} & \sigma_{12} + \Delta\sigma_{12} & \sigma_{13} + \Delta\sigma_{13} \\ \sigma_{21} + \Delta\sigma_{21} & \sigma_{22} + \Delta\sigma_{22} & \sigma_{23} + \Delta\sigma_{23} \\ \sigma_{31} + \Delta\sigma_{31} & \sigma_{32} + \Delta\sigma_{32} & \sigma_{33} + \Delta\sigma_{33} \end{bmatrix}$$

Each of the above total stress tensors $\left[\sigma_{ij}\right]$, $\left[\Delta\sigma_{ij}\right]$ and $\left[\sigma_{ij} + \Delta\sigma_{ij}\right]$ has its own set of principal axes and principal normal stresses. In general, these three sets of principal axes need not coincide. Let the principal values of the three stress tensors be

$$\left.\begin{aligned} (\sigma_1, \sigma_2, \sigma_3) &= P(\sigma_{ij}) \\ (\Delta\sigma_1, \Delta\sigma_2, \Delta\sigma_3) &= P(\Delta\sigma_{ij}) \\ (\sigma_1 + \delta\sigma_1, \sigma_2 + \delta\sigma_2, \sigma_3 + \delta\sigma_3) &= P(\sigma_{ij} + \Delta\sigma_{ij}) \end{aligned}\right\} \quad (4.1)$$

The values $(\Delta\sigma_1, \Delta\sigma_2, \Delta\sigma_3)$ are the applied principal total stress increments, while the value $(\delta\sigma_1, \delta\sigma_2, \delta\sigma_3)$ are the resulting changes in the existing principal total stresses.

Consider the case of ideal passive earth pressure (the plane strain passive case) in a dry soil. The initial principal stresses, shown in Figure 4.3(a) are

$$\left.\begin{aligned} \sigma_1 &= \sigma_z \\ \sigma_2 &= \sigma_y = K_o \sigma_z \\ \sigma_3 &= \sigma_x = K_o \sigma_z \end{aligned}\right\} \qquad (4.2)$$

As loading progresses, the lateral principal stress σ_x increases by the amount $\delta\sigma_x = \Delta\sigma_x$, while the vertical principal stress σ_z remains constant. Parts (b) and (c) of Figure 4.3 show that if the Y direction is to remain the intermediate principal stress direction throughout the loading process, then $\Delta\sigma_y$ must be the major principal stress increment as long as $\Delta\sigma_x$ is less than $(1 - K_o)\sigma_z$, and $\Delta\sigma_y$ must become the intermediate principal stress increment when $\Delta\sigma_x$ exceeds $(1 - K_o)\sigma_z$. On the other hand, if $\Delta\sigma_y$ is always the intermediate principal stress increment, then the Y direction will be the minor principal stress direction until $\Delta\sigma_x$ exceeds $(1 - K_o)\sigma_z$. Both DICKEY (1967) and RIXNER (1967) found that the Y direction did become the minor principal stress direction during the early stages of plane strain passive tests on Boston blue clay. However, when $\Delta\bar{\sigma}_x$ exceeded $(1 - K_o)\bar{\sigma}_z$, the Y direction soon became, and thereafter remained the intermediate principal stress direction. The

point of this discussion is that the assumption that the intermediate principal stress direction remains fixed for a soil element may not be strictly correct in the early stages of loading. even though the axis which originally was the intermediate principal stress axis does remain fixed. However, for purposes of strength analysis the above assumption appears to be satisfactory.

Next consider the case in which the Y axis is initially the intermediate principal stress axis, remains a principal stress axis throughout loading, and the major and minor principal stress increment directions lie in the XZ plane. Then the changes in σ_1 and σ_3, due to the applied total stress increments $\Delta\sigma_1$ and $\Delta\sigma_3$, can be found from the Mohr circle construction shown in Figure 4.4a.

Figure 4.4b shows a situation in which a set of applied total stress increments causes a reorientation of the principal stress axes, but no change in the magnitudes of the principal stresses. The application of the total stress increments shown in Figure 4.4b, under undrained conditions, will generally cause a change in pore pressure, which leads to the following conclusion:

If a relation between total stress and pore pressure during undrained loading is to be formulated, the formulation should be in terms of the applied principal total stress increments, rather than the resulting changes in the principal total stresses.

The above statement applies only to an isotropic soil. If a soil is not isotropic, the above formulation should consider all components of the stress tensor $\Delta\sigma_{ij}$. The above statement also agrees with the way pore pressures are usually calculated in practice; LAMBE (1963, 886).

In order to develop a general relationship between total stress and pore pressure during undrained loading, it is necessary to consider what happens when differential increments of total stress, $d\sigma_1$, $d\sigma_2$ and $d\sigma_3$ are applied.

First, it is necessary to consider what would happen under fully drained conditions. To begin with, consider a sample which has been normally consolidated under a hydrostatic stress,

$$\bar{\sigma}_1 = \bar{\sigma}_2 = \bar{\sigma}_3 = \bar{\sigma}_c$$

If the hydrostatic stress is slowly changed by an amount $d\bar{\sigma}$, and the sample is allowed to drain freely so that no excess pore pressure develops, then the change in void ratio, de, due to the effective stress increment, $d\bar{\sigma}$, will be as shown in Figure 4.5. It is apparent that a discontinuity in slope exists in the relation between $d\bar{\sigma}$ and de, there being one curve for consolidation and another for swelling.

Now consider the general case of a change in e due to applied infinitesimal effective stress increments $d\bar{\sigma}_{ij}$. Based on experience with hydrostatic tests, it seems reasonable to assume that two continuous relationships exist between de and $d\bar{\sigma}_{ij}$, one for all combinations of effective stress increments which cause a decrease in e (consolidation), and another for all combinations of effective stress increments which cause an increase in e (swelling). Thus, it should be possible to write an incremental volume change equation in the form

$$de = c_{11}\, d\bar{\sigma}_{11} + c_{22}\, d\bar{\sigma}_{22} + c_{33}\, d\bar{\sigma}_{33} + c_{12}\, d\sigma_{12} + c_{23}\, d\sigma_{23} + c_{31}\, d\sigma_{31} \qquad (4.3)$$

where

$$c_{11} = \frac{\partial e}{\partial \bar{\sigma}_{11}} \qquad c_{12} = 2\frac{\partial e}{\partial \sigma_{12}}$$

$$c_{22} = \frac{\partial e}{\partial \bar{\sigma}_{22}} \qquad c_{23} = 2\frac{\partial e}{\partial \sigma_{23}} \tag{4.4}$$

$$c_{33} = \frac{\partial e}{\partial \bar{\sigma}_{33}} \qquad c_{31} = 2\frac{\partial e}{\partial \sigma_{31}}$$

The values of the coefficients in Equation (4.3) depend on the previous stress-strain history of the soil and on whether e decreases or increases.

Although a more general treatment is possible, further attention will be restricted to the case in which the 2 axis remains a principal stress axis. During undrained loading of a saturated soil, the pore pressure varies in such a way that the volume of the soil skeleton remains constant. Using the nomenclature of Figure 3.11, Equation (4.3) reduces to

$$de = c_{zz}\, d\bar{\sigma}_{zz} + c_{y}\, d\bar{\sigma}_{y} + c_{rr}\, d\bar{\sigma}_{rr} + c_{rz}\, d\sigma_{rz} = 0 \tag{4.5}$$

Figure 4.6 then shows that if

$$\frac{d\bar{\sigma}_{zz} + d\bar{\sigma}_{rr}}{2} = d\bar{p} \tag{4.6}$$

$$\frac{d\bar{\sigma}_{zz} - d\bar{\sigma}_{rr}}{2} = dh \tag{4.7}$$

$$d\sigma_{rz} = d\tau \tag{4.8}$$

$$\frac{d\tau}{dh} = \tan 2\epsilon \tag{4.9}$$

$$\rho = \frac{d\bar{\sigma}_{y} - d\bar{p}}{dh \cos 2\epsilon + d\tau \sin 2\epsilon} \tag{4.10}$$

then

$$d\bar{\sigma}_{zz} = d\bar{p} + dh \tag{4.11}$$

$$d\bar{\sigma}_{y} = d\bar{p} + \rho\,(dh \cos 2\epsilon + d\tau \, din \, 2\epsilon) \tag{4.12}$$

$$d\bar{\sigma}_{rr} = d\bar{p} - dh \tag{4.13}$$

Equation (4.5), the constant volume equation, can then be written in the form

$$(c_{zz} + c_y + c_{rr})d\bar{p} + (c_{zz} - c_{rr} + \rho c_y \cos 2\epsilon)dh$$

$$+ (c_{rz} + \rho c_y \sin 2\epsilon)d\tau = 0 \qquad (4.14)$$

Equation (4.14) defines the gradient of a constant volume surface (undrained effective stress surface) in the (h, τ, $\bar{p}$) space of Figure 3.11. Provided h, τ and $\bar{p}$ all vary monotonically, integration of Equation (4.14) yields

$$\Delta\bar{p} + b\Delta h + c\Delta\tau = 0 \qquad (4.15)$$

where

$$b\Delta h = \int_0^{\Delta h} \left(\frac{c_{zz} - c_{rr} + \rho c_y \cos 2\epsilon}{c_{zz} + c_y + c_{rr}} \right) dh$$

$$c\Delta\tau = \int_0^{\Delta\tau} \left(\frac{c_{rz} + \rho c_y \sin 2\epsilon}{c_{zz} + c_y + c_{rr}} \right) d\tau \qquad (4.16)$$

Figure 4.7 then shows that if

$$q\Delta = \frac{\Delta\tau_1 - \Delta\tau_3}{2} \tag{4.17}$$

then

$$\Delta h = q\Delta \cos 2\psi \tag{4.18}$$

$$\Delta\tau = q\Delta \sin 2\psi \tag{4.19}$$

so that Equation (4.15) can be written

$$\Delta\bar{p} = -(b \cos 2\psi + c \sin 2\psi)q\Delta \tag{4.20}$$

or simply

$$\Delta\bar{p} = -Fq\Delta \tag{4.21}$$

where

$$F = b \cos 2\psi + c \sin 2\psi \tag{4.22}$$

The quantity F can be interpreted as a pore pressure parameter, since Equation (4.21) can be written in the form

$$\Delta u = \Delta p + Fq\Delta \tag{4.23}$$

Equation (4.22) is not a practical means of calculating the pore pressure parameter F. Its purpose is only to show how F is related to the shape of an undrained effective stress path in (h, τ, $\bar{p}$) space. To evaluate F numerically, use the empirical equation

$$F = 2A - 1 = -\frac{\Delta\bar{p}}{q\Delta} = \frac{\Delta u - \Delta p}{q\Delta} \tag{4.24}$$

The parameter A is a pore pressure parameter defined by SKEMPTON (1948). The pore pressure parameter F and the stress increment parameter ρ are similar to Lode's stress distribution parameter μ, which is defined in Appendix B and used extensively throughout Chapter 6.

Pore Pressure Response Surface

In Chapter 3 the concept of a three-dimensional failure surface was developed, using as rectangular coordinates the variables

$$h = \frac{\bar{\sigma}_{zz} - \bar{\sigma}_{rr}}{2} = \frac{\sigma_{zz} - \sigma_{rr}}{2} \tag{3.23}$$

$$\tau = \bar{\sigma}_{rz} = \sigma_{rz} \tag{3.24}$$

$$\bar{p} = \frac{\bar{\sigma}_{zz} + \bar{\sigma}_{rr}}{2} = \frac{\bar{\sigma}_1 + \bar{\sigma}_3}{2} \tag{3.25}$$

and the associated polar coordinates

$$q = \sqrt{h^2 + \tau^2} \tag{3.26}$$

$$2\beta = \tan^{-1} \frac{\tau}{h} \tag{3.27}$$

The variables h, τ, q and 2β are shown in Figure 3.10. The three dimensional failure surface has the general equation

$$F(h, \tau, \bar{p}) = 0 \tag{3.28}$$

and is shown in Figure 3.11. It is one of the two key elements required to define the variation of undrained shear strength with the angle of rotation of the major principal stress, β.

The second key element is a three-dimensional pore pressure response surface (really a secant effective stress path surface), defined in the same space as that of the three-dimensional failure surface. The equation of the pore pressure response surface shown in Figure 4.8 is Equation (4.21).

$$\Delta\bar{p} = - Fq\Delta \tag{4.21}$$

It has the same general shape as the failure surface defined by Equation (3.28), except that the pore pressure response surface points down instead of up (when the pore pressure parameter F is positive). In general the pore pressure parameter F depends on both $\Delta\bar{p}$ and the angle of inclination of the applied principal total stress increments, Ψ. If the soil remains isotropic throughout loading the pore pressure parameter F will be independent of Ψ and the pore pressure response surface will be a surface of revolution, with the line $\left[h = \left(\frac{1 - K_o}{2} \right) \bar{p}_c \; ; \quad \tau = 0 \right]$ as the axis of revolution. If, in addition, the pore pressure parameter F is independent of $\bar{p}$, i.e. constant, the pore pressure response surface becomes a right circular cone.

Influence of the Intermediate Applied Principal Stress Increment

Theoretical considerations outlined by SKEMPTON (1960b) suggested that the relationship between the applied shear stress and the resulting volume change in an isotropic soil is such that the excess pore pressure is related to the applied principal total stress increments by the equation

$$\Delta u = \frac{\Delta\sigma_1 + \Delta\sigma_2 + \Delta\sigma_3}{3} + \frac{a}{3}\sqrt{(\Delta\sigma_1 - \Delta\sigma_2)^2 + (\Delta\sigma_2 - \Delta\sigma_3)^2 + (\Delta\sigma_3 - \Delta\sigma_1)^2} \qquad (4.25)^*$$

The coefficient of (a) is the octahedral shear component of the applied stress increments. It is generally not equal to the resulting change in the existing octahedral shear stress. The quantity (a) is another pore pressure parameter. An equation of the above form was originally published by HENKEL (1958, 36), and has been discussed since by HENKEL (1960b, 551) JUAREZ - BADILLO (1963, 227), and HENKEL AND WADE (1966, 79). In these discussions, there has not always been a clear distinction between applied principal total stress increments

*c.f. Appendix A.

and resulting changes in the existing principal total stressess. Often this has been because the authors had in mind the tri-axial compression test, in which no rotation of principal planes occurs. As written here, Equation (4.25) is intended to indicate that the excess pore pressure is a linear combination of the octahedral normal and octahedral shear stress components of the applied total stress increments.

The purpose of this section is to assess the influence of the intermediate applied principal total stress increment on the pore pressure response of an isotropic soil, according to the above octahedral theory. To do this, it is convenient to introduce the stress distribution parameter

$$\lambda = \frac{\Delta\sigma_2 - \Delta p}{q\Delta} \tag{4.26}$$

so that Equation (4.25) takes the form

$$\Delta u = \Delta p + \left[\frac{a\sqrt{2(3 + \lambda^2)} + \lambda}{3}\right] q\Delta \tag{4.27}$$

Comparison of Equation (4.27) and (4.23) indicates that the pore pressure parameter F is given by the expression

$$F = \frac{a\sqrt{2(3 + \lambda^2)} + \lambda}{3} \qquad (4.28)$$

For triaxial compression, $\Delta\sigma_2 = \Delta\sigma_3$ and therefore $\lambda = -1$, so that

$$F_C = \frac{2\sqrt{2}\ a - 1}{3}$$

For triaxial extension, $\Delta\sigma_2 = \Delta\sigma_1$, and therefore $\lambda = 1$, so that

$$F_E = \frac{2\sqrt{2}\ a + 1}{3}$$

If pore pressure response is governed by the octahedral theory, then

$$F_E - F_C = \frac{2}{3}$$

or

$$A_E - A_C = \frac{1}{3}$$

According to the octahedral theory, Skempton's pore pressure parameter A should be greater by approximately 1/3 in triaxial extension than in triaxial compression. The results of three

undrained triaxial compression and three extension tests on isotropically normally consolidated specimens of Boston blue clay, reported by LADD AND VARALLYAY (1965, 135) are shown below. Although individual tests do not seem to bear out the 1/3 relationship, the average results do, at least approximately.

TEST	A_f	AVERAGE
$\overline{\text{CIUC-1}}$	1.37	
$\overline{\text{CIUC-2}}$	1.08	1.24
$\overline{\text{CIUC-3}}$	1.27	
$\overline{\text{CIUE-1}}$	1.83	
$\overline{\text{CIUE-2}}$	1.30	1.66
$\overline{\text{CIUE-3}}$	1.85	

Discussion of Test Data

The pore pressure response of a given soil is sensitive to its previous stress history. In particular, sample disturbance can cause the pore pressure response of a clay sample in the laboratory to differ significantly from the response which it would have shown IN SITU. Therefore, extremely careful sampling and testing methods are required to make accurate prediction of IN SITU pore pressure response.

The only laboratory test device, of which the Writer is aware, capable of achieving true rotation of principal planes during shear is the torsional hollow cylinder device used by Hythornthwaite, Casbarian and Saada. (See Chapter 6). Unfortunately, strength data from torsional hollow cylinder tests have so far been inconsistent with data from several other types of carefully conducted strength tests. Consequently it cannot yet be assumed that the torsional hollow cylinder test is free from significant stress inhomogeneity, which renders pore pressure response data from such tests particularly unreliable.

Unconsolidated undrained triaxial tests with pore pressure measurements, on samples trimmed at different angles to the material axis, give pore pressure response data only for the restricted condition

$$\Psi = \beta = \text{constant}$$

At the present time this is the only way of predicting the influence of the angle Ψ on the pore pressure parameter F. Tests of this type were conducted on samples of resedimented Boston blue clay by D'APPOLONIA (1968). He ran nine unconsolidated undrained triaxial tests with pore pressure

measurements on samples trimmed at 0^{o}, 45^{o} and 90^{o} to the material axis. The sequence of one-dimensional consolidation and rebound, sampling, trimming and mounting, application of cell pressure to obtain saturation and finally undrained shear of D'Appolonia's specimens is depicted in Figure 3.47. The motivation for conducting these tests was "to identify the source of anisotropic strength behavior by measuring the effective stress-strength parameters in samples cut at different orientation." However, although three of the samples were normally consolidated prior to shear ($\bar{\sigma}_{vc} = \bar{\sigma}_{vm}$), even the undrained effective stress paths for these samples displayed the characteristics of an overconsolidated material, despite careful precautions to minimize disturbance. This situation merely emphasizes the extreme difficulty of reproducing IN SITU stress-strain behavior in a laboratory test on a sampled specimen, of which D'Appolonia was well aware. Therefore the following calculated pore pressure coefficients probably do not represent the pore pressure response of the material in undrained shear directly from Point 2 in Figure 3.47. For an isotropically consolidated triaxial compression test, Equation (4.24) reduces to

$$F = -\frac{\Delta\bar{p}}{q} = \frac{\bar{p}_o - \bar{p}}{q} \qquad (4.29)$$

Values of the pore pressure parameter F at failure for D'Appolonia's nine tests are tabulated in Table 4.1, in which $\bar{p}_o$ equals $\bar{\sigma}_s$. Unfortunately, the data in Table 4.1 show no consistent trend in F with the angle Ψ, the over-consolidation ratio OCR, or even the ration $\bar{p}_o/\bar{\sigma}_{vm}$.

Summary

The purpose of this chapter has been to examine some of the factors which influence the pore pressure response of a saturated soil during undrained loading, and to propose an empirical pore pressure response relationship which is particularly conveneient for treating the problem of rotation of principal planes, to be discussed in the next chapter.

The concept of a three dimensional pore pressure response surface has been introduced. In the next chapter it will be shown that the intersection of the three dimensional pore pressure response surface with the three dimensional failure surface introduced in the previous chapter defines the variation of undrained shear strength with the angle of orientation of the major principal stress at failure.

TABLE 4.1

ANISOTROPIC PORE PRESSURE RESPONSE DATA FOR RESEDIMENTED BOSTON BLUE CLAY

TEST	$\Psi = \beta$ DEG	OCR	$\bar{p}_o/\bar{\sigma}_{vm}$	$\bar{p}_f/\bar{\sigma}_{vm}$	$\Delta\bar{p}_f/\bar{\sigma}_{vm}$	$q_f/\bar{\sigma}_{vm}$	F
1	0	1.0	0.192	0.400	-0.208	0.169	-1.231
2	45	1.0	0.149	0.235	-0.086	0.111	-0.775
3	90	1.0	0.222	0.283	-0.061	0.129	-0.473
4	0	3.5	0.114	0.308	-0.194	0.128	-1.516
5	45	3.5	0.111	0.324	-0.213	0.138	-1.543
6	90	3.5	0.123	0.233	-0.110	0.102	-1.078
7	0	10.7	0.128	0.290	-0.162	0.130	-1.246
8	45	10.7	0.076	0.229	-0.153	0.099	-1.545
9	90	10.7	0.116	0.248	-0.132	0.106	-1.245

$$OCR = \frac{\bar{\sigma}_{vm}}{\bar{\sigma}_{vc}}$$

Data from D'APPOLONIA (1968)

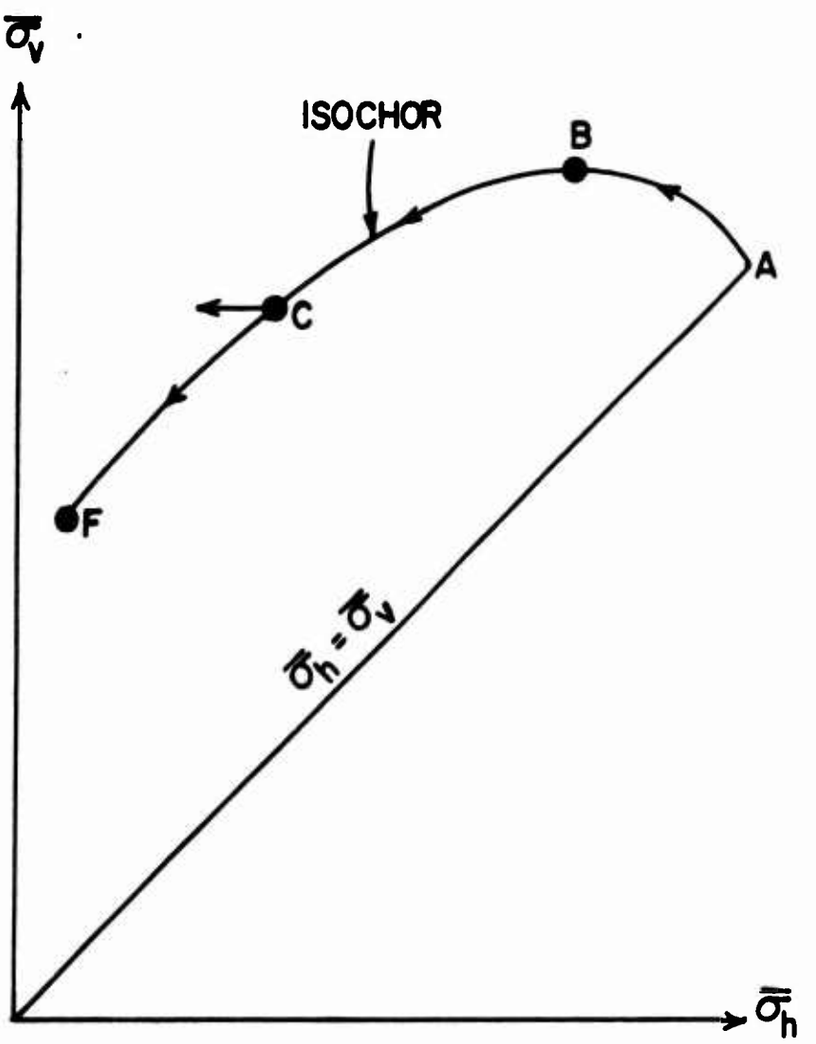

FIGURE 4.1
RELATION BETWEEN EFFECTIVE STRESS
AND VOLUME CHANGE CHARACTERISTICS

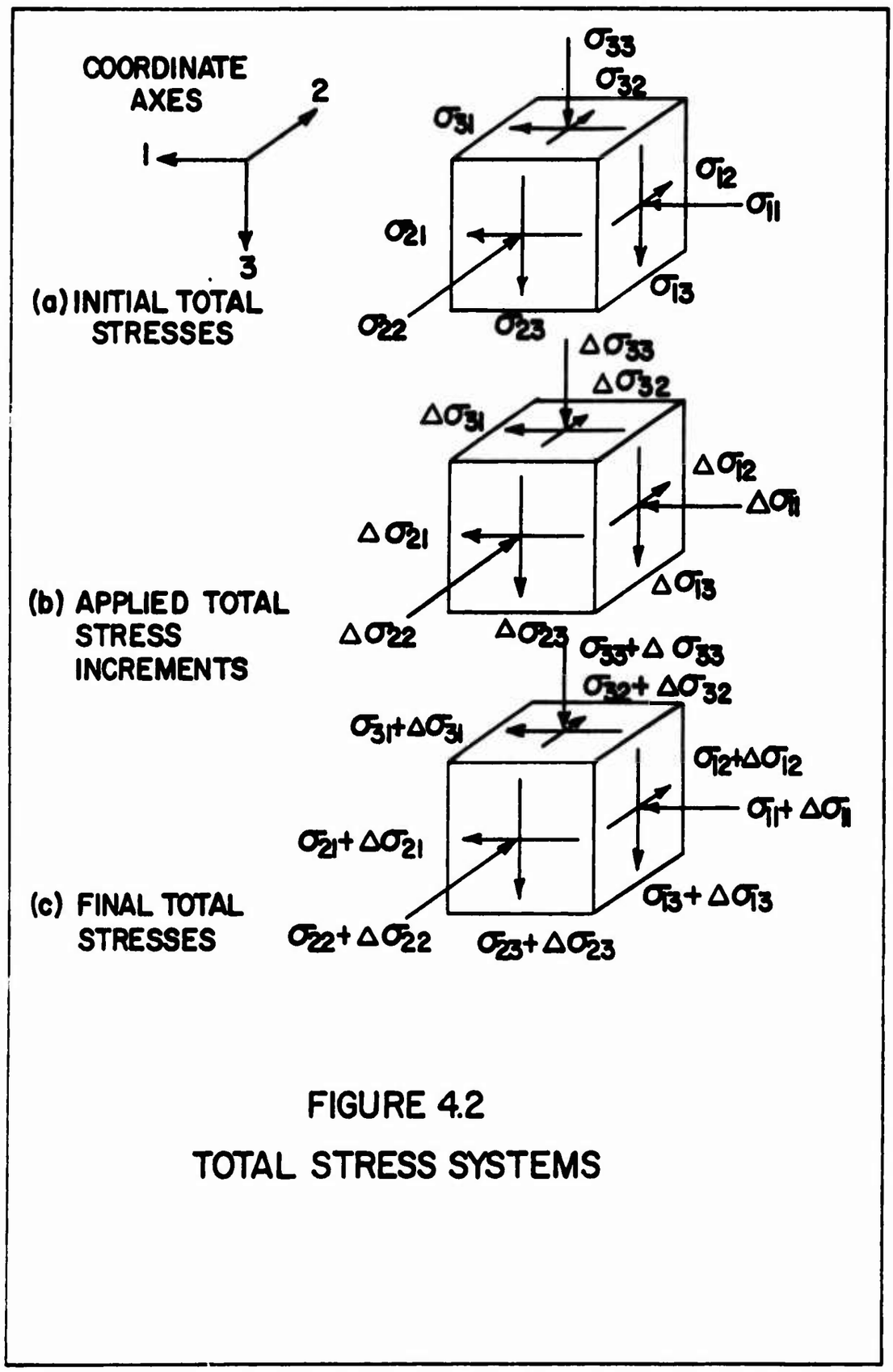

FIGURE 4.2

TOTAL STRESS SYSTEMS

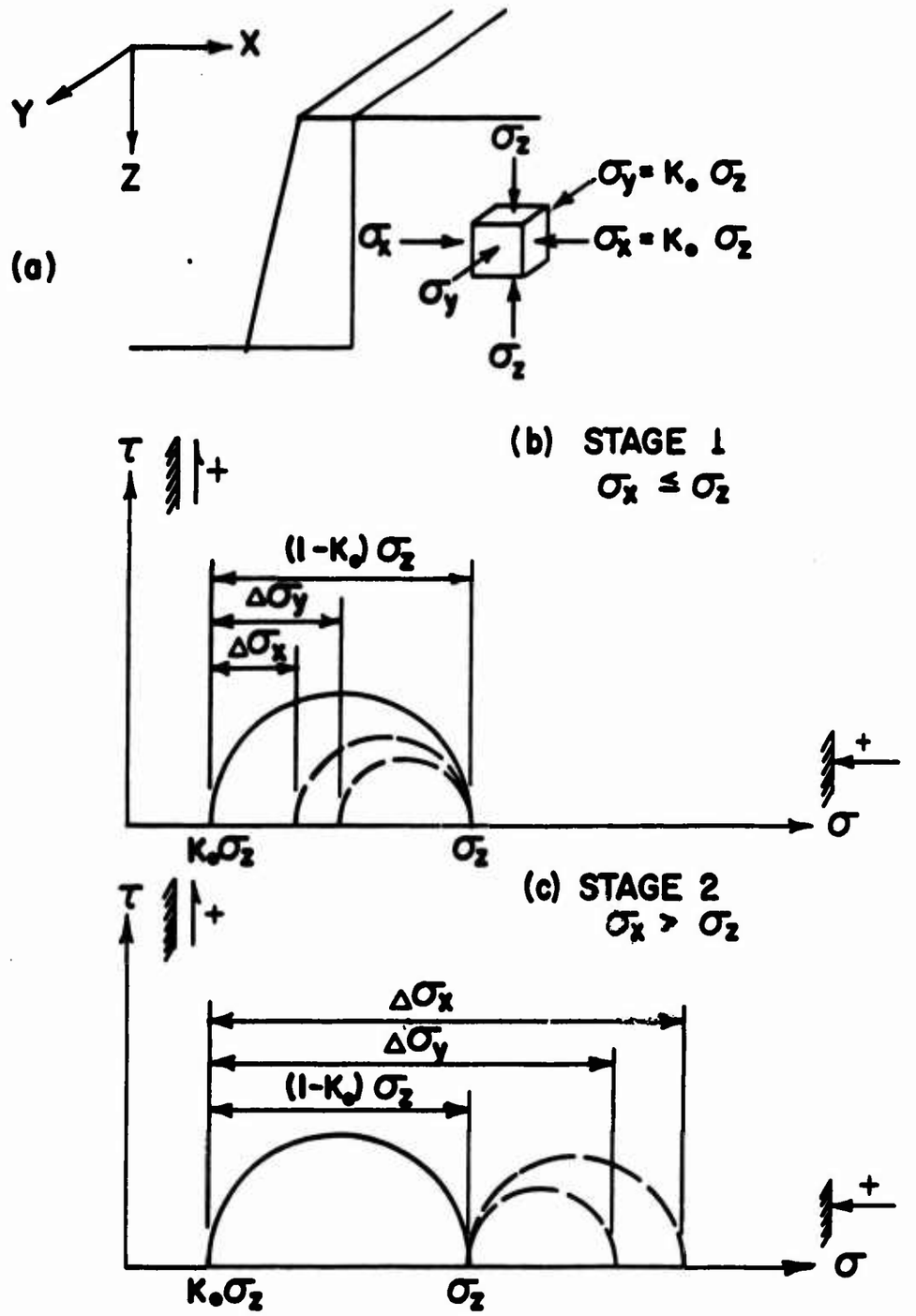

FIGURE 4.3
INTERMEDIATE PRINCIPAL STRESS INCREMENT AND INTERMEDIATE PRINCIPAL STRESS

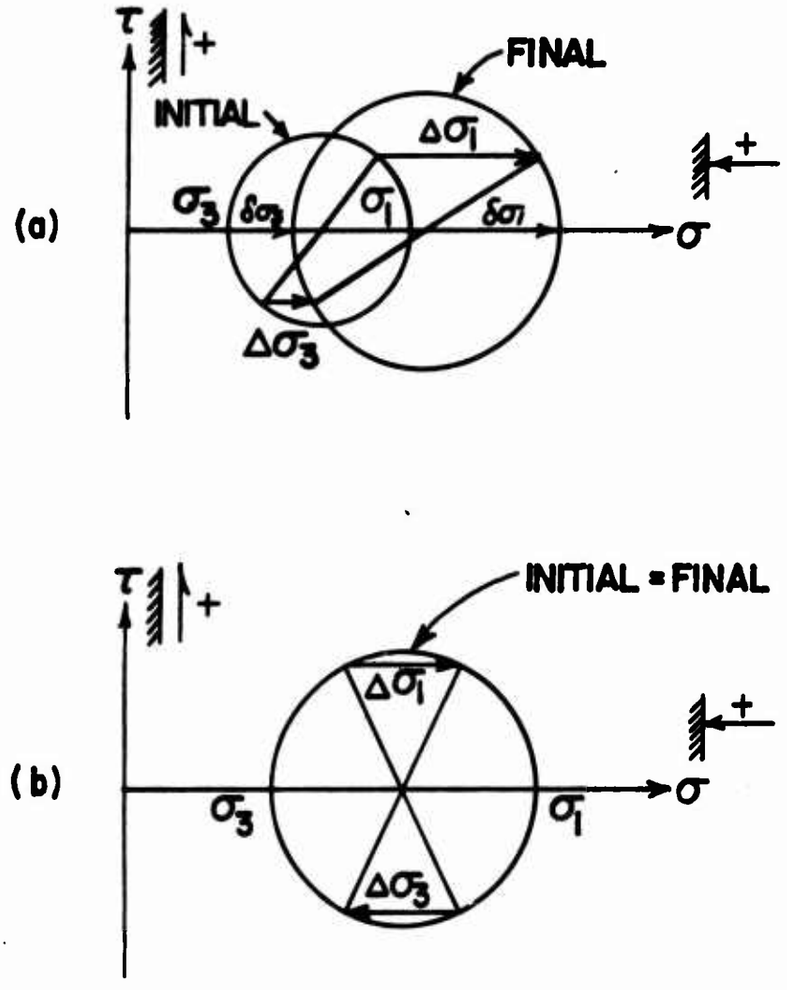

FIGURE 4.4

MOHR CIRCLE CONSTRUCTION FOR TOTAL STRESS

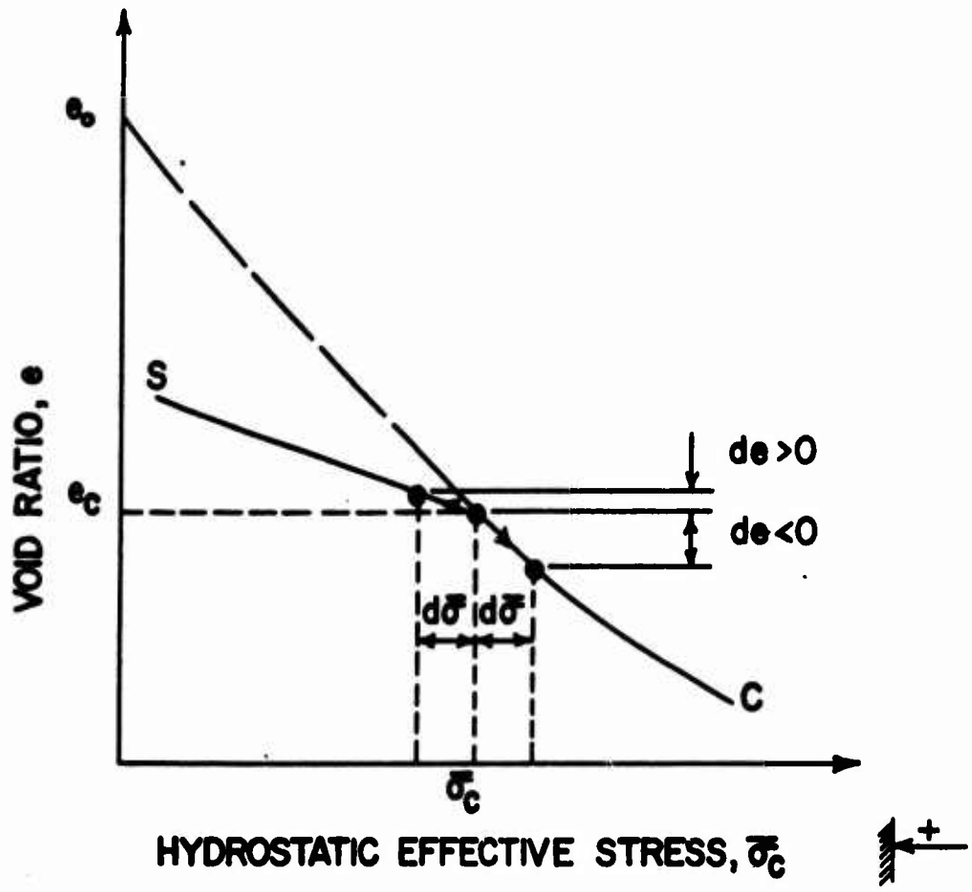

FIGURE 4.5

CHANGE IN VOID RATIO DUE TO A CHANGE IN HYDROSTATIC EFFECTIVE STRESS

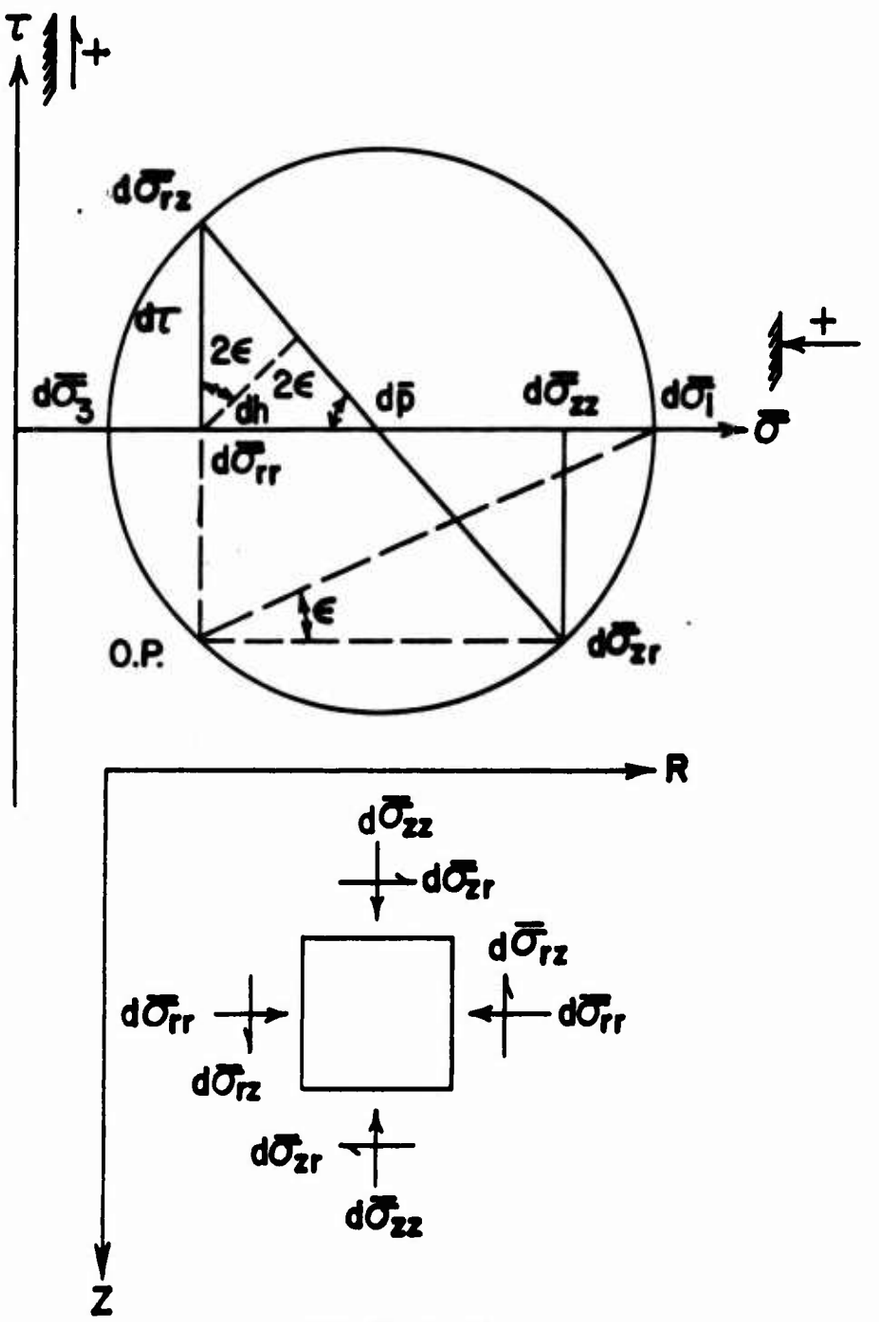

FIGURE 4.6
INFINITESIMAL CHANGES IN EFFECTIVE STRESS

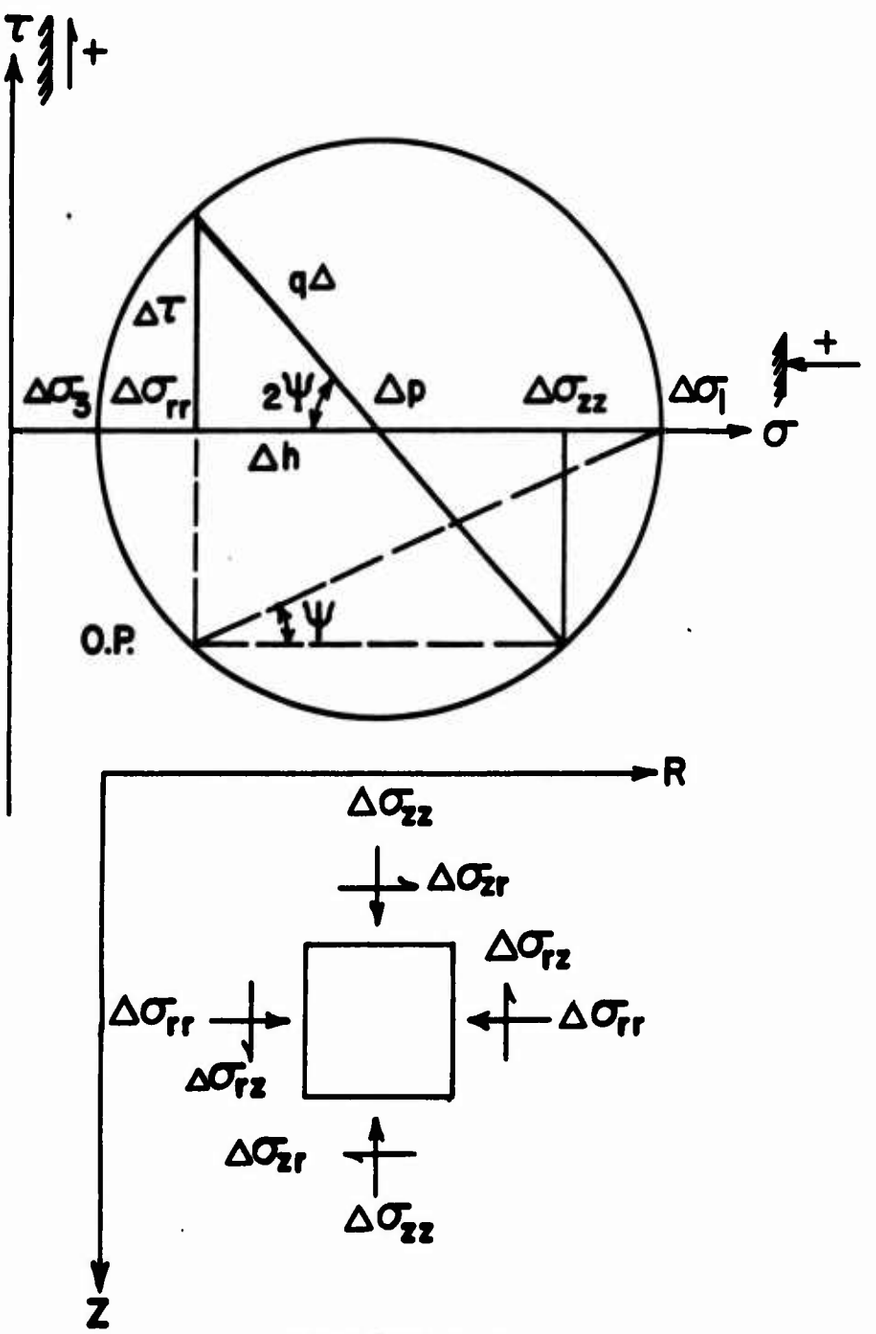

FIGURE 4.7

APPLIED TOTAL STRESS INCREMENTS

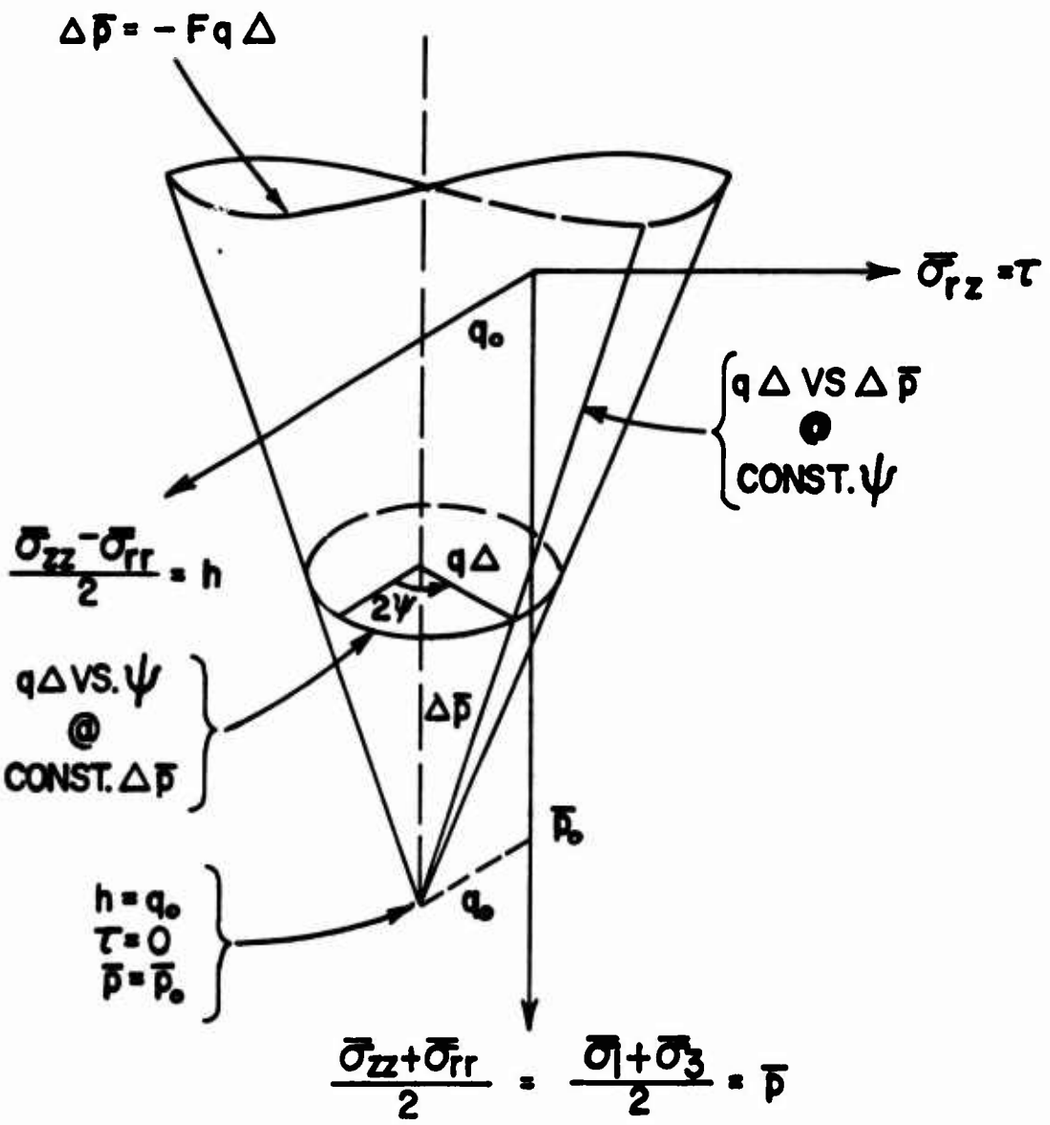

FIGURE 4.8

THREE-DIMENSIONAL PORE PRESSURE RESPONSE SURFACE FOR A CROSS ANISOTROPIC CLAY

CHAPTER 5

ROTATION OF PRINCIPAL PLANES

Purpose

In Chapter 4 a distinction was drawn between four total stress tensors associated with a point in a loaded soil mass:

σ_{ij}, the total stress tensor prior to loading

$d\sigma_{ij}$, a differential increment of applied total stress

$\Delta\sigma_{ij} = \int d\sigma_{ij}$, the accumulated, finite increment of applied total stress

$\sigma_{ij} + \Delta\sigma_{ij}$, the current total stress tensor during loading

Each of these total stress tensors has a set of principal axes and a set of principal normal stresses. In general, no two of the above sets of principal axes coincide, and in most soil deformation problems the principal axes of the last three tensors rotate continuously during loading. Because a failure surface in soil is rarely planar, the influence of anisotropy with respect to the effective stress shear

strength parameters needs to be considered in determining shear strength.

The influence of anisotropy on shear strength in terms of effective stress, for a soil exhibiting transverse isotropy, is analyzed in Chapter 3. There the concept of a three dimensional failure surface is introduced, which describes the variation of shear strength as a function of effective stress and of the angle β between the major principal stress axis at failure and the material axis.

In Chapter 4 some of the factors influencing pore pressure response in a saturated soil during undrained loading are examined, and a new pore pressure parameter is proposed, which is particularly convenient for treating the problem of rotation of principal planes. The concept of a three dimensional pore pressure response surface is also introduced, which describes the variation of effective stress during undrained loading with the applied shear stress and the angle Ψ between the major principal axis of the applied total stress increment and the material axis.

The purpose of this chapter is to explain and illustrate how the three dimensional failure surface and the three dimensional pore pressure response surface combine to give the variation of undrained shear strength with the angle β

between the major principal stress axis at failure and the material axis. The reason why the undrained shear strength will vary with the angle β, even when the soil remains isotropic up to failure, provided the maximum shear stress prior to the beginning of undrained shear, q_o, is not zero will be explained. This last phenomenon is called the q_o or the K_o effect, and it is generally of considerable importance in practical problems.

Variation of Undrained Shear Strength

Determination of the variation of undrained shear strength with the angle β between the major principal stress axis at failure and the material axis is simple, once the three dimensional failure surface and the three dimensional pore pressure response surface have been defined. Consideration is restricted to the case in which the Y axes is initially the intermediate principal stress axis and remains a principal stress axis throughout the loading process, and the applied major and minor principal total stress increments lie in the XZ plane.

The three dimensional failure surface in Figure 3.11 specifies limiting combinations of h and τ for any given value of $\bar{p}$.

The three dimensional pore pressure response surface in Figure 4.7 specifies combinations of h and τ which satisfy a constant volume condition, again as a function of $\bar{p}$.

It follows that the closed space durve, which is the intersection of the failure surface and the pore pressure response surface, specifies limiting values of h and τ, and therefore also of q and β, which also satisfy a constant volume condition. Therefore the projection of this closed curve on the h, τ plane is a polar plot of undrained shear strength, q_f, VERSUS the polar angle 2β, for a given set of consolidation stresses.

When the soil is isotropic with respect to both strength and pore pressure response, and all material parameters involved are constants, then both surfaces are right circular cones. This is the case studied analytically by **BRINCH HANSEN AND** GIBSON (1949). If the preshear consolidation stresses are isotropic ($q_o = 0$; $K_o = 1$), then the axes of both cones coincide with the $\bar{p}$ axis, the intersection of the two cones is a circle and there is no variation of undrained shear strength with the angle β. However, if the preshear consolidation stresses are not isotropic ($q_o \neq 0$; $K_o \neq 1$) then the axis of the pore pressure response cone will not coincide with the $\bar{p}$ axis, and the intersection of the two cones

will indicate a variation of undrained shear strength with the angle β. This phenomenon is called the q_o or the K_o effect.

Numerical Examples

The following numerical examples illustrate the determination of the variation of undrained shear strength with the angle β between the major principal stress axis at failure and the material axis. The method accommodates arbitrary shapes of both the failure surface and the pore pressure response surface.

1. GIVEN:

$$\bar{\Phi} = 35^{o}$$

$$\bar{c} = 0$$

$$K_o = 0.45$$

$$\bar{\sigma}_{vo} = 1.0 \text{ TSF}$$

$$F = 1.20$$

REQUIRED:

Construct a plot showing the variation of undrained shear strength with the angle β.

SOLUTION:

This problem is typical of those to which the analysis of BRINCH, HANSEN AND GIBSON (1949) also applies.

The failure surface has the equation

$$q_f = \bar{p}_f \sin \bar{\Phi} = 0.57358\ \bar{p}_f$$

The initial consolidation stresses are

$$\bar{p}_o = \left(\frac{1 + K_o}{2}\right) \bar{\sigma}_{vo} = 0.725 \text{ TSF}$$

$$q_o = \left(\frac{1 - K_o}{2}\right) \bar{\sigma}_{vo} = 0.275 \text{ TSF}$$

and the equation of the pore pressure response surface is

$$q\Delta = \frac{\bar{p}_o - \bar{p}}{F} = \frac{0.725 - \bar{p}}{1.20}$$

The calculations required to construct constant $\bar{p}$ contours of the failure surface and the pore pressure response surface are tabulated in Table 5.1, and the resulting curve of q_f VS 2β is plotted in Figure 5.1. If the pore pressure parameter F exceeded the ratio $(1 - K_o)/(1 + K_o)$, which could happen in a sensitive clay or a very loose sand, the undrained shear strength curve would not enclose the origin, so that a passive failure could occur before the lateral stress even exceeded the vertical stress.

Since the torsional hollow cylinder test has not yet been refined to the point where the state of stress within the specimen can be considered homogeneous, there is presently no reliable direct means of predicting the variation of undrained shear strength with the angle β IN SITU, when the preshear geostatic stresses are anisotropic. Several recent investigators have assumed that the IN SITU variation of undrained shear strength when $K_o \neq 1$ is the same as that obtained from a series of isotropically ($K_o = 1$) consolidated triaxial tests on samples trimmed at various values of the angle β. They have also concluded that the clays they tested were essentially isotropic with respect to the effective stress shear strength parameters, and therefore that anisotropy with respect to pore pressure response was the major cause of variation of undrained shear strength with the angle β in their isotropically consolidated specimens. It follows that anisotropy with respect to pore pressure response, plus the q_o effect are the two major causes of variation of undrained shear strength with the angle β in anisotropically consolidated specimens. The treatment of this practically important case is illustrated by the following numerical example.

2. GIVEN:

Isotropically consolidated undrained triaxial compression tests with pore pressure measurements, on samples of a silty clay trimmed at seven different values of the angle β, have yielded the results shown below.

β DEG	$\bar{p}_o$ PSI	σ_{1f} PSI	σ_{3f} PSI	Δu_f PSI
0	50.00	81.25	50.00	34.38
15	50.00	80.92	50.00	34.54
30	50.00	79.99	50.00	35.00
45	50.00	78.57	50.00	35.72
60	50.00	76.93	50.00	36.54
75	50.00	75.54	50.00	37.23
90	50.00	75.00	50.00	37.50

REQUIRED:

Compare the variation of undrained shear strength with the angle β obtained from the isotropically consolidated triaxial tests with that to be expected IN SITU, starting from a K_o initial condition.

SOLUTION:

The calculations in Table 5.2(a) show that

$$\sin \bar{\Phi} = 0.500 \text{ (isotropic)}$$

so that

$$K_o = 1 - \sin \bar{\Phi} = 0.500$$

It is assumed that the variation of F with β in the isotropically consolidated tests is the same as the variation of F with Ψ for a K_o initial condition. Data needed to construct contours of the pore pressure response surface are tabulated in Table 5.2(b), using

$$\bar{p}_o = 50.00 \text{ PSI}$$

The initial value of q is

$$q_o = \left(\frac{1 - K_o}{1 + K_o} \right) \bar{p}_o = 16.67 \text{ PSI}$$

The strength curves in Figures 5.2(a) and 5.2(b) have little in common. The q_o effect is by far the most important cause of undrained shear strength variation with the angle β. This effect must be considered in the prediction of undrained shear strength for any important project.

Summary

In this chapter the concept of a three dimensional failure surface, introduced in Chapter 3, and the concept of a three dimensional pore pressure response surface, introduced in Chapter 4, have been combined to yield a simple method for predicting the IN SITU variation of undrained shear strength with the angle β between the major principal stress axis at failure and the material axis. All the calculations required by the method can be based on the results of conventional triaxial tests.

Example 2 illustrates the application of the method to what is believed to be the most common practical field situation:

a) isotropic strength, in terms of effective stress,

b) anisotropic pore pressure response, and

c) anisotropic preshear consolidation stresses.

The application of the method to predicting the behavior of a model footing on resedimented Boston blue clay is discussed in Chapter 7.

TABLE 5.1

VARIATION OF UNDRAINED SHEAR STRENGTH,
EXAMPLE NO. 1

$\bar{p}_f$ TSF	q_f TSF	$\bar{p}_o - \bar{p}_f$ TSF	q_Δ TSF
0.000	0.000	0.725	0.604
0.050	0.029	0.675	0.563
0.100	0.057	0.625	0.521
0.150	0.086	0.575	0.479
0.200	0.115	0.525	0.438
0.250	0.143	0.475	0.396
0.300	0.172	0.425	0.354
0.350	0.201	0.375	0.313
0.400	0.229	0.325	0.271
0.450	0.258	0.275	0.229
0.500	0.287	0.225	0.188
0.550	0.315	0.175	0.146
0.600	0.344	0.125	0.104
0.650	0.373	0.075	0.063
0.700	0.402	0.025	0.021

TABLE 5.2(a)

VARIATION OF UNDRAINED SHEAR STRENGTH, EXAMPLE NO. 2 TEST DATA REDUCTION

β DEG	$\bar{p}_o$ PSI	p_f PSI	Δu_f PSI	$\bar{p}_f$ PSI	q_f PSI	SIN	$\bar{p}_o - \bar{p}_f$ PSI	F
0	50.00	65.62	34.38	31.24	15.62	0.500	18.76	1.20
15		65.46	34.54	30.92	15.46	0.500	19.08	1.23
30		65.00	35.00	30.00	15.00	0.500	20.00	1.33
45		64.28	35.72	28.56	14.28	0.500	21.44	1.50
60		63.46	36.54	26.92	13.46	0.500	23.08	1.71
75		62.77	37.23	25.54	12.77	0.500	24.46	1.92
90		62.50	37.50	25.00	12.50	0.500	25.00	2.00

TABLE 5.2(b)

VARIATION OF UNDRAINED SHEAR STRENGTH, EXAMPLE NO. 2
PORE PRESSURE RESPONSE SURFACE CONTOURS

		Ψ, DEG						
$\bar{P}_f$	$\bar{P}_o - \bar{P}_f$	0	15	30	45	60	75	90
PSI	PSI	$q\Delta$, PSI						
50.00	0.00	0.00	0.00	0.00	0.00	0.00	0.00	0.00
47.50	2.50	2.08	2.03	1.88	1.67	1.46	1.30	1.25
45.00	5.00	4.17	4.06	3.76	3.33	2.92	2.60	2.50
42.50	7.50	6.25	6.10	5.64	5.00	4.39	3.91	3.75
40.00	10.00	8.33	8.13	7.52	6.67	5.85	5.21	5.00
37.50	12.50	10.42	10.16	9.40	8.33	7.31	6.51	6.25
35.00	15.00	12.50	12.20	11.28	10.00	8.77	7.81	7.50
32.50	17.50	14.58	14.23	13.16	11.67	10.23	9.11	8.75
30.00	20.00	16.67	16.26	15.04	13.33	11.70	10.42	10.00
27.50	22.50	18.75	18.29	16.92	15.00	13.16	11.72	11.25
25.00	25.00	20.83	20.33	18.80	16.67	14.62	13.02	12.50
22.50	27.50	22.92	22.36	20.68	18.33	16.08	14.32	13.75
20.00	30.00	25.00	24.39	22.56	20.00	17.54	15.63	15.00
17.50	32.50	27.08	26.42	24.44	21.67	19.00	16.93	16.25
15.00	35.00	29.17	28.46	26.32	23.33	20.47	18.23	17.50
12.50	37.50	31.25	30.49	28.20	25.00	21.93	19.53	18.75
10.00	40.00	33.33	32.52	30.08	26.67	23.39	20.83	20.00
7.50	42.50	35.42	34.55	31.95	28.33	24.85	22.14	21.25

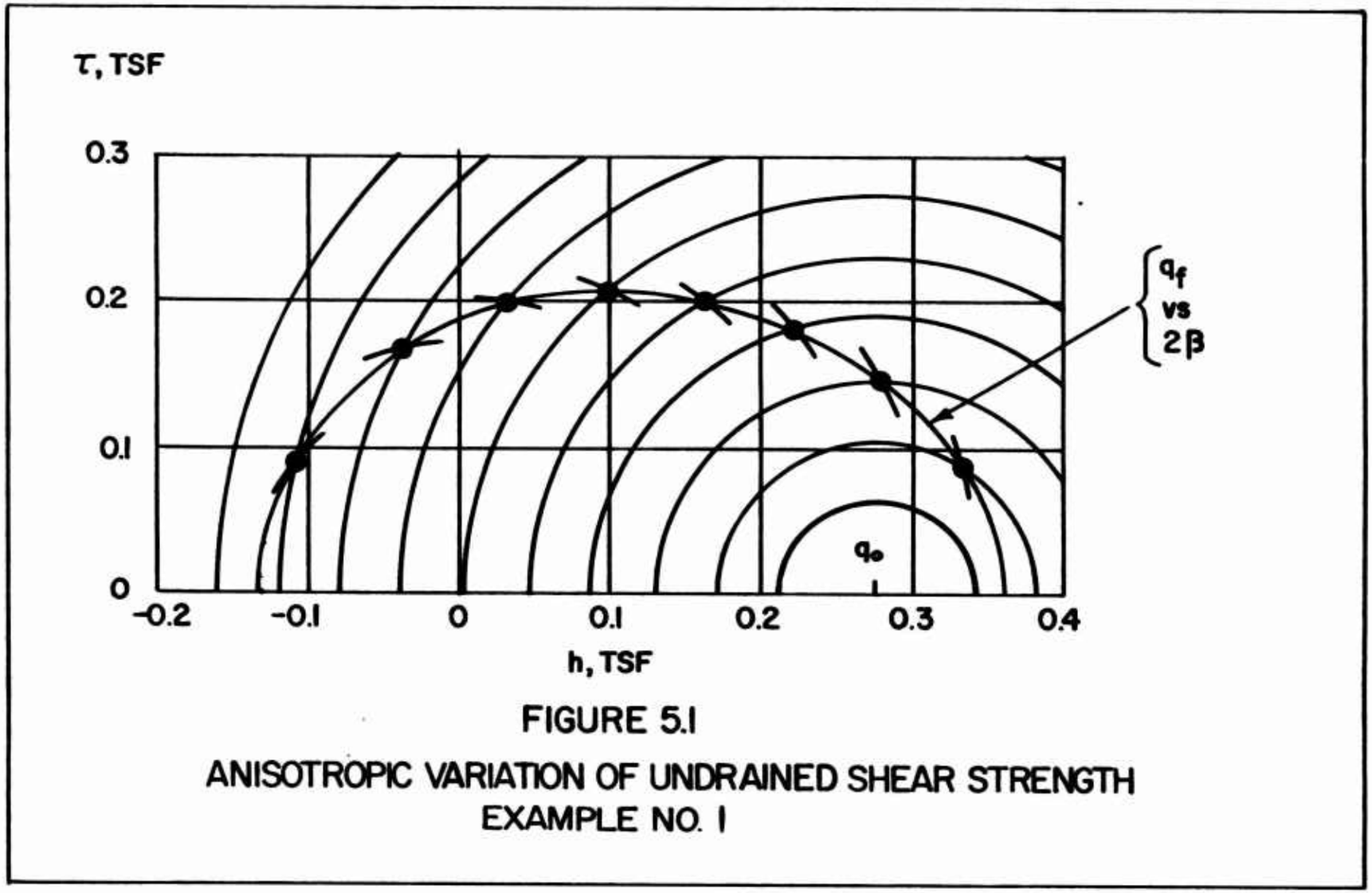

FIGURE 5.1

ANISOTROPIC VARIATION OF UNDRAINED SHEAR STRENGTH
EXAMPLE NO. 1

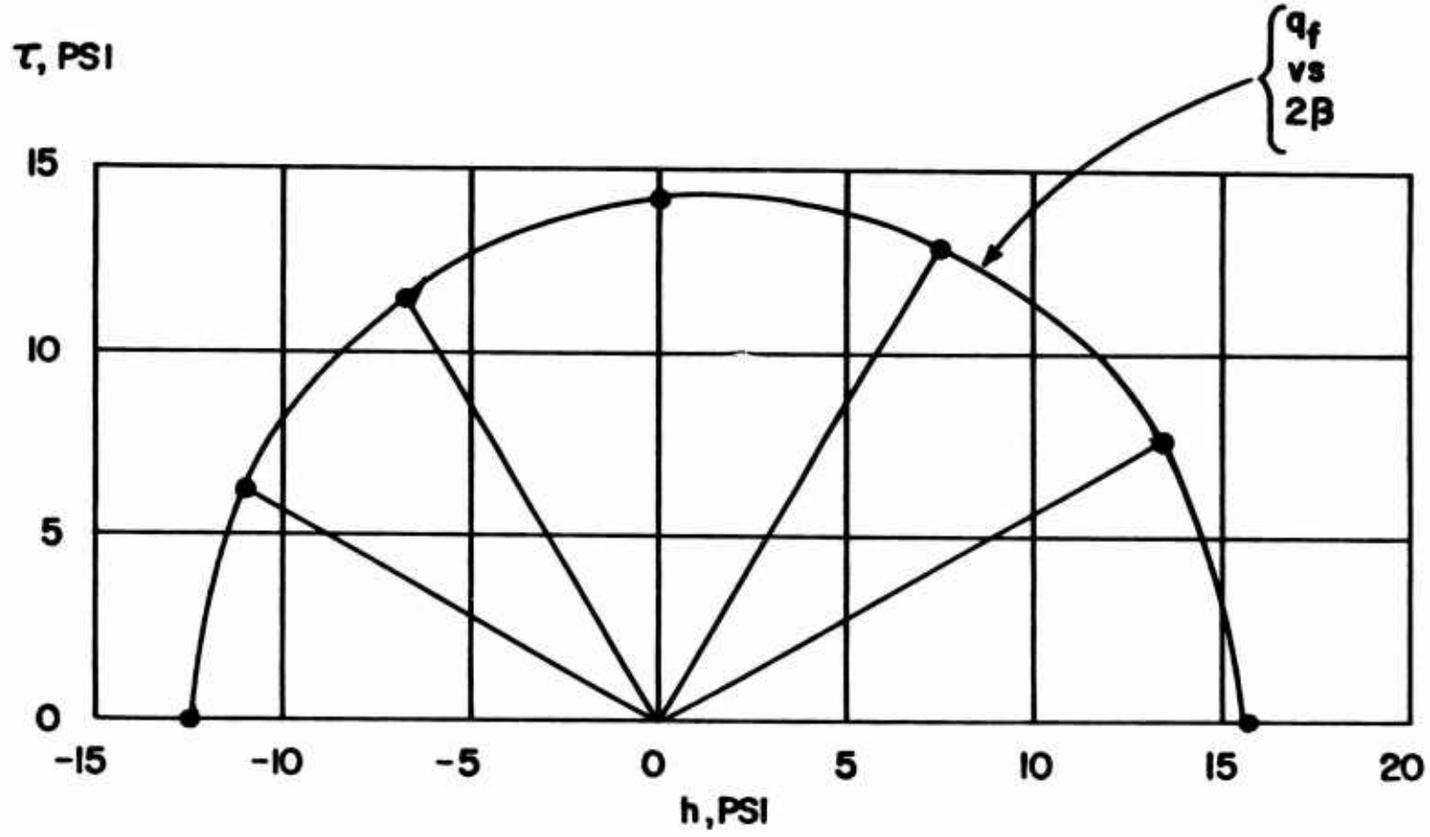

FIGURE 5.2 (a)

ANISOTROPIC VARIATION OF UNDRAINED SHEAR STRENGTH
EXAMPLE NO. 2 - EXCLUDING THE q_o EFFECT

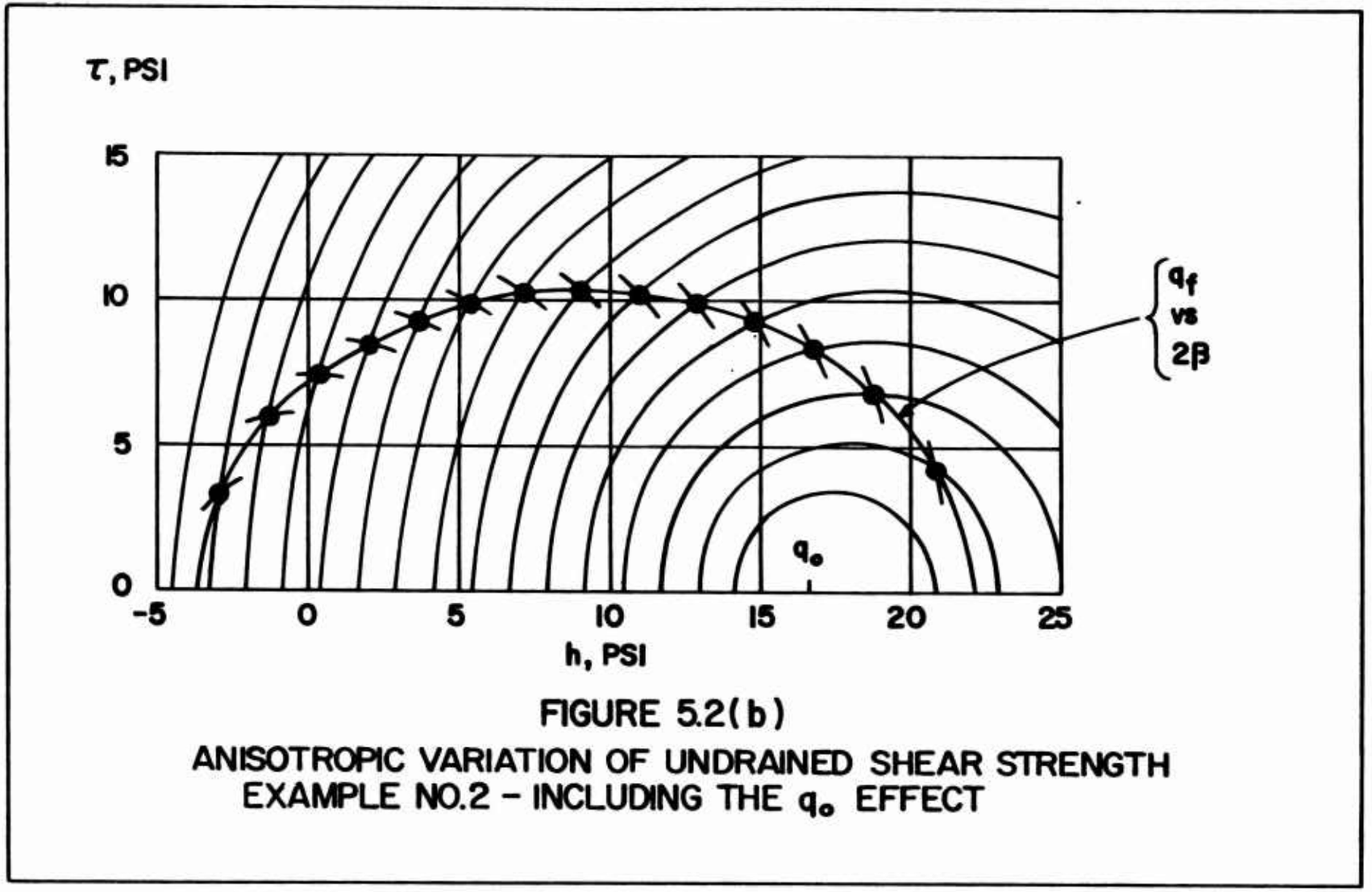

FIGURE 5.2(b)

ANISOTROPIC VARIATION OF UNDRAINED SHEAR STRENGTH
EXAMPLE NO.2 - INCLUDING THE q_o EFFECT

CHAPTER 6

INFLUENCE OF THE INTERMEDIATE PRINCIPAL STRESS

Purpose

The conclusion in Chapter 3 that the intermediate principal stress had no influence on shear strength, expressed in terms of effective stress, was based on four factors:

1. The assumed validity of Equation (3.15),

2. The assumption that the intermediate principal stress axis remains perpendicular to the material axis,

3. The assumption that the effective stress shear strength parameters in Equation (3.15) both increase steadily as the angle α between the normal to the failure plane and the material axis increases, and

4. An analysis of the characteristics of contours of constant α, superimposed on a three dimensional Mohr circle of stress.

In the physical sciences, it is frequently easier to assume a mechanism, such as that described above, which then leads to a correct prediction of specific behavior, than it is to establish the validity of the mechanism. Certainly this is true with the shear strength of soils.

The assumption that the effective stress shear strength parameters do NOT increase steadily as the angle α increases leads to the prediction that the intermediate principal stress will influence shear strength. However, if the intermediate principal stress does influence shear strength, this does not necessarily verify the assumption regarding variation of the effective stress shear strength parameters with failure plane orientation. This is because such a mechanism is not the only one which causes the intermediate principal stress to influence shear strength; many other failure criteria, if satisfied, will also do that.

The purpose of this chapter is therefore only to determine if the influence of the intermediate principal stress on the shear strength of soil is negligible, as is customarily assumed, but no attempt will be made to verify any particular strength mechanism. The assumption of isotropy will be made throughout.

Interpretation of Test Data

The Revised Coulomb Equation defines shear strength in terms of the effective stress shear strength parameters $\bar{c}$ and $\bar{\Phi}$.

$$\tau_{ff} = \bar{c} + \bar{\sigma}_{ff} \tan \bar{\Phi} \qquad (2.5)$$

Equation (2.5) has proved convenient in engineering practice for estimating the strength of earth structures of relatively simple geometry. However, its usefulness is dependent upon the determination of values of $\bar{c}$ and $\bar{\Phi}$, by laboratory or field tests, which accurately reflect field behavior.

SOWERS (1963) reviewed methods of measuring soil strength in both the laboratory and field, and the effects of sample disturbance were assessed by LADD AND LAMBE (1963) in the same volume. BISHOP (1966) reviewed laboratory test techniques, including the plane strain test, and also summarized theoretical considerations, many of which had been concisely treated by NEWMARK (1960) and HVORSLEV (1960), and were recently reviewed again by SCOTT AND KO (1969).

Despite the increasing popularity of the simple shear test and the plane strain test, the triaxial test is still the most popular test for measuring the shear strength properties of soils in the laboratory, for important engineering projects. The mechanics of this test were investigated

by HAYTHORNTHWAITE (1960c), who listed two main reasons for an apparent influence of the intermediate principal stress on values of $\bar{c}$ and $\bar{\Phi}$ measured in axial compression and extension:

1. Nonuniformity of stress distribution in triaxial test specimens which really do obey the Revised Coulomb Equation, and

2. True departure from the Revised Coulomb Equation.

The subject of stress and strain nonuniformity in the triaxial test could well be the subject of an entire thesis, and therefore the following discussion will concentrate entirely on the second item, true departure from the Revised Coulomb Equation.

First, however, other factors which also influence measured values of $\bar{c}$ and $\bar{\Phi}$ deserve mention.

3. There has been a tendency to overlook the difference between a yield criterion and a failure criterion. A sharp distinction between the two was drawn by NADAI (1933), but the desire to treat soil theoretically as a rigid - plastic material (which it is not) has led to the synonymous use of the two terms. Consequently, the Mohr - Coulomb equation has often been used as a yield criterion, and this has, in

turn, led to what may be unjustified criticism of the normality rule of theoretical plasticity. The Mohr - Coulomb Equation is not a yield criterion, but rather a failure criterion. Soil is not a rigid - plastic material, but rather a work - hardening material which undergoes considerable inelastic deformation prior to reaching instability; DRUCKER, GIBSON and HENKEL (1957). The plastic deformation prior to failure should be considered in important stability calculations.

4. Theoretical plasticity analyses have often been done in terms of total, rather than effective stress.

5. Different investigators have not always agreed on a definition of failure.

6. The results of many soil strength tests have yet to be proven independent of the type of test or test device. This is especially true of tests designed to measure the influence of the intermediate principal stress. The writer has come to believe that test results designed to show the influence of the intermediate principal stress should not be considered conclusive until they have been corroborated by at least three different test devices.

7. The determination of internal stresses in a soil test specimen, on the basis or externally applied loads, may not be unique. This is because a stress - strain relation may be needed, but not known. The simple shear test falls in this category.

8. Some investigators use nominal dimensions in performing stress calculations, while others use dimensions corrected on the basis of a few measured deformations. Other corrections employed to account for the restraining effects of rubber membranes, filter paper strips, piston friction, and so forth have not been standardized, and sample calculations are rarely given.

9. In most cases, too few tests are run, so doubt remains about the relative contributions of systematic and random influences. Little information is available on the degree of scatter to be expected in a given soil strength test. There are several reasons for this situation. Identical representative undisturbed samples are hard to come by, as well as being expensive, and skilled technicians who can perform a triaxial stress path test correctly are not always easy to find.

10. The method of displaying results of soil strength tests, designed to show the influence of the intermediate principal stress, is not standard, and some plots reveal more information than others.

Basic Approaches

There are at least two basic approaches to studying the influence of the intermediate principal effective stress on soil shear strength. The first is a general approach, the second a more limited one. The general approach asks:

> Does the intermediate principal effective stress influence shear strength?

The limited approach asks:

> Does the intermediate principal effective stress influence the value of $\bar{\Phi}$ in the Revised Coulomb Equation, assuming the intrinsic pressure to be constant?

Both approaches and their associated methods of data display are discussed below.

The General Approach

A fairly general, time - and strain - independent failure criterion for an isotropic soil is a surface

in principal effective stress space, defined by the equation

$$F(\bar{\sigma}_1, \bar{\sigma}_2, \bar{\sigma}_3) = 0 \tag{6.1}$$

Because the material has been assumed to be isotropic there is no loss of generality in also assuming that $\bar{\sigma}_1$ is the major, $\bar{\sigma}_2$ the intermediate and $\bar{\sigma}_3$ the minor principal effective stress, so that

$$\bar{\sigma}_1 \geq \bar{\sigma}_2 \geq \bar{\sigma}_3 \tag{6.2}$$

There is also no need to assume that the principal stress axes remain fixed in direction. On the other hand, were the material anisotropic, the use of principal stress space would be inadmissable unless the principal stress axes did remain fixed in direction.

If the intermediate principal effective stress is to have no influence on failure, then all contours of the failure surface corresponding to constant values of the intermediate principal effective stress must be portions of a single continuous curve in the 1-3 plane. It is therefore convenient to rewrite Equation (6.1) in the form

$$q_f = f(\bar{p}_f, \bar{\sigma}_{2f}) \tag{6.3}$$

where q_f and $\bar{p}_f$ are defined in Figure 2.1. Then assuming the necessary triaxial testing device were available, one could conduct several series of tests, each at a different value of $\bar{\sigma}_2$. The resulting contours of q_f VERSUS $\bar{p}_f$ at failure, one for each value of $\bar{\sigma}_2$, should combine into a single continuous curve if the failure criterion is to be truly independent of $\bar{\sigma}_2$. A typical constant $\bar{\sigma}_2$ contour is shown in Figure 6.1. Each test series could be conducted by first establishing the end points of a contour, then locating intermediate points. This can be accomplished by varying only one principal effective stress at a time, as indicated in the figure.

For several reasons, it may be convenient to consider intersections of the failure surface, not with planes of constant $\bar{\sigma}_2$, but rather with planes of constant μ, where

$$\mu = \frac{\bar{\sigma}_2 - \bar{p}}{q} \tag{6.4}$$

A few reasons for doing so are:

1. To obtain contours which are not limited in extent,

2. To obtain a direct comparison between data from a genuine triaxial device and that from a conventional triaxial (cylindrical compression/extension)device, and

3. To facilitate plotting octahedral contours of the failure surface.

A plane of constant μ in principal stress space has the equation

$$(1 + \mu)\bar{\sigma}_1 - 2\bar{\sigma}_2 + (1 - \mu)\bar{\sigma}_3 = 0 \qquad (6.5)$$

It therefore contains the origin, and has a normal unit vector defined by the equation

$$\bar{n}_\mu = \frac{(1 + \mu)\bar{e}_1 - 2\bar{e}_2 + (1 - \mu)\bar{e}_3}{\sqrt{2\ (3 + \mu^2)}} \qquad (6.6)$$

If the intermediate principal effective stress is to have no influence on failure, then all contours of constant μ, projected parallel to the 2 axis onto the 1-3 plane, must coincide. It is therefore convenient to rewrite Equation (6.1) once more, this time in the form

$$q_f = g(\bar{p}_f, \mu) \tag{6.7}$$

Then, again assuming the necessary triaxial testing device were available, one could conduct several series of tests, each with a different value of μ. The resulting contours of q_f VERSUS $\bar{p}_f$ at failure, one for each value of μ, should coincide, and furthermore should be identical with the single continuous curve obtained from the constant $\bar{\sigma}_2$ tests, if the failure criterion is to be truly independent of $\bar{\sigma}_2$. A typical constant μ contour is shown in Figure 6.2.

Of course, it is possible to construct constant μ contours from constant $\bar{\sigma}_2$ contours, and to construct constant $\bar{\sigma}_2$ contours from constant μ contours.

Several points on a plot of q_f VERSUS $\bar{p}_f$ at failure, shown in Figure 6.3, have important physical significance. Since

$$\bar{\sigma}_{OCT} = \bar{p} + \frac{\mu}{3} q$$

point A must represent strength under hydrostatic tension. The value d, usually referred to as intrinsic pressure, is really cohesion in the true sense, i.e. hydrostatic tensile strength, as the word implies in the field of Physics. Several ingeneous methods have been devised for creating a state of hydrostatic tension; NADAI (1950, 178) and WILLIAMS (1964). Point B represents strength under pure tension in the 1-3 plane, point C strength under pure shear in the 1-3 plane and point D strength under pure compression in the 1-3 plane, all for some precribed value of $\bar{\sigma}_2$ or μ.

In view of the marked curvature exhibited by shear strength envelopes for natural soils, particularly at high pressure such as those exerted by deep foundations in clay, the general approach to the examination of failure criteria outlined above seems fairly realistic without being too compicated.

The Limited Approach

It is often convenient to assume that within a certain range of $\bar{p}_f$ all constant μ contours are straight lines, meeting

at the same point on the $\bar{p}$ axis. In this case, Equation (6.7) takes the form

$$q_f = (d + \bar{p}_f)\sin \bar{\Phi} \tag{6.8}$$

where d, assumed independent of μ, is now the apparent hydrostatic tensile strength. The slope of a constant μ contour is sin $\bar{\Phi}$, where

$$\bar{\Phi} = \bar{\Phi}(\mu) \tag{6.9}$$

The object of the limited approach is to determine how the angle $\bar{\Phi}$ varies with μ.

In view of the linear relations

$$\bar{\sigma}_{OCT} = \bar{p} + \mu \left(\frac{q}{3}\right)$$

$$\tau_{OCT} = \sqrt{2(3 + \mu^2)} \left(\frac{q}{3}\right)$$

shown in Figure 6.4, Equation (6.8) is tantamount to assuming the failure surface to be a pyramid, with its axis along the octahedral normal. All octahedral cross sections must therefore be geometrically similar.

Equation (6.8), if written in terms of the deviator stress components without the subscript f becomes

$$\frac{s_1 - s_3}{2} = (d + \bar{\sigma}_{OCT} + \frac{s_1 + s_3}{2}) \sin \bar{\Phi}$$

$$= (d + \bar{\sigma}_{OCT} - \frac{s_2}{2}) \sin \bar{\Phi} \qquad (6.10)$$

Referring to Figure B.6, it follows that

$$\left.\begin{aligned} \frac{s_1 - s_3}{2} &= \frac{x}{\sqrt{2}} \\ \frac{s_2}{2} &= \frac{y}{\sqrt{6}} \end{aligned}\right\} \qquad (6.11)$$

and therefore Equation (6.10) assumes the form

$$\frac{x}{\sqrt{2}} = (d + \bar{\sigma}_{OCT}) \sin \bar{\Phi} - y \frac{\sin \bar{\Phi}}{\sqrt{6}}$$

or

$$y = \sqrt{6}\ (d + \bar{\sigma}_{OCT}) - \frac{\sqrt{3}}{\sin \bar{\Phi}}\, x \tag{6.12}$$

It is convenient to normalize Equation (6.12) by dividing by $d + \bar{\sigma}_{OCT}$, to obtain

$$\frac{y}{d + \bar{\sigma}_{OCT}} = \sqrt{6} - \frac{\sqrt{3}}{\sin \bar{\Phi}}\ \frac{x}{d + \bar{\sigma}_{OCT}} \tag{6.13}$$

A plot of Equation (6.13) is shown in Figure 6.5, from which it is seen that a stress point can quickly be plotted in the octahedral plane, using the coordinates

$$\sqrt{6} \tan \theta_2 = \frac{\sqrt{2}\, q}{d + \bar{p}} \tag{6.14}$$

$$\mu = \frac{\bar{\sigma}_2 - \bar{p}}{q} = \sqrt{3} \cot \omega_2 \tag{6.15}$$

As long as $\bar{\sigma}_1 \geq \bar{\sigma}_2 \geq \bar{\sigma}_3 \geq 0$, the parameters in Figure 6.5 will satisfy the relationships

$$0 \leq \theta_2 \leq 30^\circ$$

$$-1 \leq \mu \leq 1 \qquad (6.16)$$

$$60^\circ \leq \omega_2 \leq 120^\circ$$

so that all points lie within a 30-60-90 right triangle, the hypotenuse of which is equal to $\sqrt{6} \approx 2.45$, and which forms the lower half of triangle O'AB in Figure B.6. Such a plot will have the following properties:

1. The radial distance from the origin O' to any point P is equal to the ratio $\sqrt{3}\,\tau_{OCT}/(d + \bar{\sigma}_{OCT})$ for that point.
2. The cotangent of the angle ω_2 between a radius from the origin O' to any point P and the vertical is equal to the ratio $\mu/\sqrt{3}$ for that point.
3. The horizontal distance from the origin O' to a line drawn from B through any point P is equal to the ratio $\sqrt{2}(\bar{\sigma}_1 - \bar{\sigma}_3)/(\bar{\sigma}_1 + \bar{\sigma}_3)$ for that point.

The Mohr - Coulomb failure criterion can be concisely expressed in terms of octahedral stress invariants by applying the Law of Sines to triangle O'BP in Figure 6.5, in the form

$$\frac{O'P}{O'B} = \frac{\sqrt{3}\,\tau_{OCT}/(d + \bar{\sigma}_{OCT})}{\sqrt{6}} = \frac{\sin\theta_2}{\sin(\omega_2 + \theta_2)}$$

which can be written in the form

$$\frac{\tau_{OCT}}{d + \bar{\sigma}_{OCT}} - \frac{\sqrt{2}\sin\theta_2}{\sin(\omega_2 + \theta_2)} = 0 \qquad (6.17)$$

Equation (6.17) is an expression for the so-called partial Mohr - Coulomb failure criterion, in terms of stress invariants. The complete Mohr - Coulomb failure criterion is obtained by considering all possible relative magnitude permutations of $\bar{\sigma}_1$, $\bar{\sigma}_2$ and $\bar{\sigma}_3$, and can be concisely written in the form

$$C_1\,C_2\,C_3 = 0 \qquad (6.18)$$

The functions C_1, C_2 and C_3 are the Mohr - Coulomb octahedral stress invariant functions, defined by the equations

$$C_j = \frac{\tau_{OCT}}{d + \bar{\sigma}_{OCT}} - \frac{\sqrt{2} \sin \theta_j}{\sin(\omega_j + \theta_j)} \tag{6.19}$$

$$\tan \theta_j = \epsilon_{ijk} \frac{1}{\sqrt{3}} \left(\frac{\bar{\sigma}_i - \bar{\sigma}_k}{\bar{\sigma}_i + \bar{\sigma}_k} \right) \tag{6.20}$$

$$\cot \omega_j = \epsilon_{ijk} \frac{1}{\sqrt{3}} \frac{2\sigma_j - (\bar{\sigma}_i + \bar{\sigma}_k)}{\bar{\sigma}_i - \bar{\sigma}_k} \tag{6.21}$$

where ϵ_{ijk} is the permutation tensor, equal to +1 when i, j and k form a clockwise permutation of 1, 2 and 3, equal to -1 when the permutation is counterclockwise, and zero otherwise. Figure 6.6 shows an octahedral plane stress plot of the complete Mohr - Coulomb failure surface. It is symmetric about each stress axis, as Equation (6.19) indicates, since θ_j and ω_j change sign simultaneously. The conciseness of Equations (6.18) and (6.19) should encourage their use in treatments of failure under general states of stress. They can be easily programmed for computer application.

Similar expressions can be written for other failure criteria. For example, the Tresca (maximum shear stress) failure criterion has the equation

$$\frac{\bar{\sigma}_1 - \bar{\sigma}_3}{2} = \frac{s_1 - s_3}{2} = \frac{x}{\sqrt{2}} = \bar{c} \tag{6.22}$$

which means that

$$\frac{x}{\sqrt{2}} = \bar{c} = \sqrt{\frac{3}{2}}\ \tau_{OCT} \sin \omega_2 \tag{6.23}$$

Therefore by defining the Tresca octahedral stress invariant functions by the equation

$$T_j = \sqrt{\frac{3}{2}}\ \tau_{OCT} \left| \sin \omega_j \right| - \bar{c} \tag{6.24}$$

the Tresca failure criterion can be concisely expressed in terms of stress invariants by the equation

$$T_1\ T_2\ T_3 = 0 \tag{6.25}$$

Discussion of Test Data

As early as 1900 Foppl investigated the fracture strength of rock cubes by loading them in plane stress; JAEGER AND COOK (1969, 149), NADAI (1950, 239). The fact that the minor principal stress in Foppl's tests was always zero does not detract from the fact that the three principal stresses at failure were unequal, and therefore that Foppl's tests were capable of yielding some information concerning the influence of the intermediate principal stress on fracture strength.

HANDIN AND HAGER (1957) and SOWERS (1963) cite several investigations by F.D. Adams and his collaborators, starting in 1901, in which the minor (radial) principal compressive stress was applied to a rock cylinder under axial compression by a heavy steel jacket which resisted the radial expansion of the rock cylinder. Handin and Hager also state that the first triaxial tests in which a truly hydrostatic confining pressure of more than a few atmospheres could be applied were those of VON KARMAN (1911), and that the first triaxial extension tests on rock were conducted by von Karman's student, BOKER (1915). According to ROSCOE (1969) the first use of the triaxial test for soil testing was by WESTERBERG (1921). TSCHEBOTARIOFF (1951, 130) and SOWERS (1963) cite

other early triaxial soil test references. The triaxial test was employed at the University of Illinois in the study of concrete strength by RICHART, BRANDTZAEG AND BROWN (1928).

Triaxial strength data from tests on jacketed cylinders of Carrara marble by von Karman and Boker are tabulated in Table 6.1 and plotted in Figures 6.7 and 6.8. The data were obtained from a paper by RUTLEDGE (1939). The two strength contours in Figure 6.7 have been approximated by straight lines over the range 10 KSI < $\bar{p}_f$ < 30 KSI, using the value d = 11.0 KSI, thus yielding the following values of $\bar{\Phi}$:

μ	$\bar{\Phi}$ DEG	$\sqrt{2}$ SIN $\bar{\Phi}$
-1	30.1	0.710
9	33.0	0.770

Values of $\sqrt{2}$ SIN $\bar{\Phi}$ for individual tests within the range 10 KSI < $\bar{p}_f$ < 40 KSI are tabulated in Table 6.1. Only the average values appear in Figure 6.8.

The most notable feature of von Karman's tests was the transition from brittle to ductile behavior as the

confining pressure increased. His plots of $\bar{\sigma}_1 - \bar{\sigma}_3$ VERSUS axial strain, ϵ_1, had shapes similar to those for dense sand, at confining pressures below about 10.5 KSI, and at higher confining pressures had shapes similar to those for loose sand. There is no mention in the literature of von Karman having made volume change measurements during shear. As the confining pressure increased beyond 10.5 KSI the failure mode changed from fracture to flow. At confining pressures in the neighborhood of 20 KSI the flow limit appeared to level off at a q_f value of about 29 KSI for $\mu = -1$ and 31 KSI for $\mu = 1$.

Boker also subjected solid marble cylinders to combined hydrostatic fluid pressure, axial compression and torsion. Some of these specimens are shown by NADAI (1950, 243).

KJELLMAN (1936) reported the design of a device capable of applying three independent principal normal stresses, up to a maximum value of 13 KG/CM^2, to the faces of a 62 x 62 x 62 CM soil cube. Pressure was transmitted to each face by the flat ends of 100 square brass bars, 62 x 62 MM in cross section. The spacing between bars, which was initially 0.2 MM, was intended to compensate for specimen deformation and friction between the specimen and the bar ends. Speciman deformation in each of the three principal directions was measured to the nearest

0.001 MM by means of dial gages. To demonstrate the possibilities of his apparatus, Kjellman reported results of tests on a dry German quartz sand, having a grain size of about 1 MM and an initial void ratio of 0.67. He performed the following types of tests: hydrostatic compression, one-dimensional compression, plain strain compression ($\sigma_1 = \sigma_2$; $\epsilon_3 = 0$), axially symmetric compression ($\mu = -1$) and genuine triaxial compression.

One-dimensional compression tests were carried out in both the new device and an oedometer, and differences between the two compression curves were attributed to friction in the oedometer. A continuous plot of axial VERSUS lateral pressure in the new device was almost perfectly linear during loading, with a slope (K_o) of about 0.52. During unloading the relationship became nonlinear, and at an overconsolidation ratio of 3 the ratio of lateral to axial stress was slightly less than unity.

Kjellman displayed the results of three genuine triaxial tests by plots of σ_x, σ_y, σ_z, ϵ_x, ϵ_y and ϵ_z VERSUS a parameter t, defined as

$$t = 6.00 - \sigma_x, \text{ KG/CM}^2$$

The failure stresses were found by extrapolating the stress curves to the value of t at which two or all three of the extrapolated strain curves had vertical tangents. Failure data for the three tests are tabulated in Table 6.2 and plotted in Figure 6.9. A series of direct shear tests yielded $\bar{\Phi} = 34^{\circ}$, which is considerably lower than two of the triaxial strength results but agrees well with the one axially symmetric test.

Comparison of Kjellman's results with those obtained within the last few years indicates his data to be of excellent quality.

RENDULIC (1936a, 1937) conducted both drained and "undrained," isotropically consolidated triaxial compression and extension tests on a blue, silty Tertiary clay from Vienna, having the following index properties:

Liquid Limit	47.6%
Plastic Limit	22.8%
Plasticity Index	24.8%
Percent by Weigth Finer Than 0.002 MM	20.0%
Activity	1.24
Specific Gravity of Solids	2.76

His test specimens were hollow cylinders, having a height of 8 CM, an outside diameter of 5 CM and an inside diameter of 0.8 CM. The inner core was filled with a sand-mica mixture, at Terzaghi's suggestion, for the purpose of obtaining pore pressure measurements. Therefore the term "undrained", as applied to Rendulic's tests, must be qualified to account for possible pore water migration between the cylindrical clay specimen and the sand-mica core. Although Rendulic made no mention of how he designed the sand-mica core, he probably used the results of tests at the Massachusetts Institute of Technology in attempting to match the compressibilities of clay and core; GILBOY (1928). However, it seems unlikely that the effective stress - void ratio characteristics of the core exactly matched those of the clay, so some internal pore water migration must have taken place.

The results of Rendulic's isotropically consolidated "undrained" triaxial compression and extension tests are tabulated in Tables 6.3 and 6.4, and plotted in Figures 6.10 and 6.11. He made no correction to the recorded principal stress difference to account for deformation. Figure 6.11 therefore illustrates the influence of the area correction

on measured effective stresses in the compression tests. Strains were not reported for the extension tests. The influence of the area correction is by no means negligible, but neither is it certain. This is because the magnitude of the area correction depends on the deformed configuration, which is usually not measured. The influence of sample deformation on the magnitude of the required area correction was mentioned briefly by ROSCOE, SCHOFIELD AND WROTH (1959) and was later studied in detail by ROSCOE, SCHOFIELD AND THURAIRAJAH (1963). It is not known whether Rendulic made any corrections for friction or rubber membrane resistance. None has been attempted here.

Rendulic's samples were remolded at a liquidity index of 0.189 (w_o = 27.5%). He was well aware that his samples were therefore overconsolidated, and suggested that tests similar to his be conducted on normally consolidated clay; RENDULIC (1936a, 51). The stress paths in Figure 6.11 exhibit the features of a lightly overconsolidated clay, including an apparently large hydrostatic tensile strength, d. However, d is not consistent for compression and extension tests (even when no area correction is applied to the compression test results). These tests are therefore

primarily of historical interest. Rendulic concluded that void ratio isochors were surfaces of revolution, with the hydrostatic stress axis as the axis of revolution. Thus he was later led to the generalized von Mises failure criterion.

HABIB (1953) reported the results of tests on Fontainebleau sand, similar in nature to those Boker had conducted on marble in 1915. Habib referred to his test as a Confined Torsion Test. It was a drained triaxial test with a provision for applying an axial torque, and he assumed the torsional shear stress acting on a horizontal plane at failure to be uniform. Under this assumption, he calculated the torsional shear stress, t, from the expression

$$t = \frac{C}{2\pi \int_0^R r^2 \, dr} = \frac{C}{\frac{2\pi R^3}{3}}$$

where C = applied couple

R = specimen radius

Habib also conducted tests on clay samples, but did not obtain pore pressure measurements. His confined torsion results for sand, corrected for sample deformation (necking) by YONG AND WARKENTIN (1966, 339) plus other triaxial test results from his original paper are tabulated in Table 6.5 and plotted in Figures 6.12 and 6.13. All the confined torsion tests on sand were conducted at the same intermediate principal effective stress. Habib stated that strength lines for constant μ were linear, but exhibited cohesion, which he attributed entirely to the "parasitic shear" of the rubber membrane.

BISHOP AND ELDIN (1953) conducted conventional triaxial tests along 10 different effective stress paths using 1.5 inch diameter by 3.5 inch long specimens of the medium-to-fine fraction of a well graded sand obtained next to the River Darent near Brasted, England. Their objective was to study the effect of stress history and mode of failure on the apparent angle of internal friction, and the effect of anisotropic consolidation on the shear strength, in consolidated undrained tests. Figure 6.14 shows the 10 effective stress paths employed, the determining features of which are also tabulated in Table 6.6. The effect of anisotropic consolidation on undrained shear strength can be explained by examining

the effective stress paths in Figure 6.14.

Four angles of internal friction, with respect to effective stress, were measured in the various tests, as indicated below.

$\bar{\Phi}_{rm}$: undrained, at maximum obliquity

$\bar{\Phi}_{rf}$: undrained, at maximum principal stress difference

$\bar{\Phi}_{d}$: drained, without energy correction

$\bar{\Phi}_{dr}$: drained, with energy correction

To compensate for the volume change which occurred during drained tests, an energy correction was applied, similar to the one originally used by TAYLOR (1948, 346) for the direct shear test. A portion of the work done by the piston force was equated to the work done by the sample against the cell pressure, as a result of sample volume change. However, the work so calculated was not equal to volumetric strain energy, and so the true distortional stress-strain curve was not obtained. In fact, it is questionable whether any correction needs to be applied to the measured principal stress difference to eliminate the influence of volume change, and this is borne out by the fact that values of

$\bar{\Phi}_d$, plotted as a function of initial porosity for $\mu = -1$ (compression) and $\mu = 1$ (extension) agreed fairly well, while values of $\bar{\Phi}_{dr}$ did not. The values of $\bar{\Phi}_{dr}$ for $\mu = -1$ increased with decreasing initial porosity, while those for $\mu = 1$ were reported to have decreased rapidly with decreasing initial porosity, although no data were presented for the latter case. Neither was there any information presented relating effective stresses at the end of consolidation to initial porosity, so a more detailed analysis of what data were published does not appear possible.

JAKOBSON (1957) used Kjellman's device to study the stress - strain properties of two sands. He plotted incremental elastic constants, E(Young's modulus) and 2 (Poisson's ratio) as functions of the angle of maximum stress obliquity, i.e. the angle whose sine equals $(\bar{\sigma}_1 - \bar{\sigma}_3)/(\bar{\sigma}_1 + \bar{\sigma}_3)$. The plane of maximum stress obliquity of course changes during loading, which makes it difficult to interpret the results of shear strength mobilization studies such as Jakobson's. He obtained many values of 2 in excess of 0.5 (which indicated a negative bulk modulus), but made no comment about it. Neither did he comment on the possibility of coupling between shear and volumentric

strains. Jakobson's tests were conducted using values of both 1 and -1 for μ, and he found the measured elastic constants to be quite sensitive to the value of Lode's parameter.

KIRKPATRICK (1957) conducted drained tests on hollow cylindrical specimens of Loch Aline sand, using unequal interior and exterior hydrostatic pressures. Conventional triaxial compression and extension tests were also conducted. The initial dimensions of the hollow cylinder specimens were:

height	h_o = 6.00 inches
inside radius	a_o = 1.25 inches
outside radius	b_o = 2.00 inches

The internal and external hydrostatic pressures were P_a and P_b, and because the ends of the specimens were sealed in such a way that the pressure differential created an axial compressive stress, the three average principal effective stresses were

$$\bar{\sigma}_1 = \bar{\sigma}_{r,AVG} = \frac{P_b + P_a}{2}$$

$$\bar{\sigma}_2 = \bar{\sigma}_{z,AVG} = \frac{b^2P_b - a^2P_a}{b^2 - a^2}$$

$$\bar{\sigma}_3 = \bar{\sigma}_{t,AVG} = \frac{bP_b - aP_a}{b - a}$$

where a and b were the instantaneous inside and outside radii, which were measured at failure. The tests were conducted by maintaining P_b constant and increasing P_a until failure occurred. The average of the major and monor principal effective stresses was

$$\bar{p} = \bar{\sigma}_2 + \frac{b - a}{4(b + a)} (P_a - P_b)$$

and one-half the difference between the major and minor principal effective stresses was

$$q = \frac{b + a}{4(b + a)} (P_a - P_b)$$

Lode's parameter was therefore

$$\mu = -\left(\frac{\frac{b}{a} - 1}{\frac{b}{a} + 1}\right)^2$$

For b/a equal to 1.6, the value of μ was -0.05. Lode's parameter is dependent only on the ratio b/a and is not influenced by the sand strength.

Data for the conventional triaxial tests (average initial porosity 0.351) and the hollow cylinder tests (average initial porosity of 0.356) are tabulated in Table 6.7 and plotted in Figures 6.15 and 6.16. Figure 6.15 shows that the three different types of tests were conducted over different ranges of effective stress, with not very much overlap. A single straight line through the origin fits all the data fairly well and yields the result

$$\sin \bar{\Phi} = 0.63$$

$$\bar{\Phi} = 39^{\circ}$$

The value of Φ for the hollow cylinder data alone is slightly higher (about 42°) but there is no way of telling whether this difference would be maintained at larger values of $\bar{p}$. An octahedral plane stress plot is shown in Figure 6.16.

PELTIER (1957) found that the results of direct shear tests on each of three sands, with controlled intermediate principal stress could be described by the expression

$$\tau_{ff} = A\bar{\sigma}_{ff} + B\bar{\sigma}_{2f} \qquad (6.26)$$

where

τ_{ff} = shear stress acting on the failure plane at failure.

$\bar{\sigma}_{ff}$ = effective normal stress acting on the failure plane at failure.

$\bar{\sigma}_{2f}$ = intermediate principal effective stress at failure.

Examination of Equations (2.5) and (2.14) shows that the Revised Coulomb Equation, together with the assumption that the major Mohr stress circle at failure is tangent to the shear strength line, yields a failure criterion which is linear in $\bar{\sigma}_{1f}$ and $\bar{\sigma}_{3f}$. Equation (2.14) is a straight line in $(\bar{\sigma}_1, \bar{\sigma}_3)$ space. Peltier's Equation (6.26) suggests the possibility of generalizing the Revised Coulomb Equation to obtain a failure criterion which is linear in $\bar{\sigma}_{1f}$, $\bar{\sigma}_{2f}$ and $\bar{\sigma}_{3f}$. Such a failure criterion can be defined by two statements:

1. The equation

$$\tau_{ff} = A\bar{\sigma}_{ff} + B\bar{\sigma}_{2f} + \bar{c} \tag{6.27}$$

2. The assumption that the major Mohr stress circle at failure is tangent to the strength line having slope A and shear stress intercept $\bar{c} + B\bar{\sigma}_{2f}$, as shown in Figure 6.17.

It is convenient to let

$$A = \tan \bar{\Phi} \tag{6.28}$$

and

$$\frac{1 + \sin \bar{\Phi}}{1 - \sin \bar{\Phi}} = N_{\bar{\Phi}} \tag{6.29}$$

Equation (6.27) can then be written in the form

$$\bar{\sigma}_{1f} = N_{\Phi}\bar{\sigma}_{3f} + 2\sqrt{N_{\Phi}}\,(B\bar{\sigma}_{2f} + \bar{c}) \qquad (6.30)^*$$

which is the equation of a plane in $(\bar{\sigma}_1, \bar{\sigma}_2, \bar{\sigma}_3)$ space. The hydrostatic tensile strength is most easily obtained by setting $\bar{\sigma}_{ff} = \bar{\sigma}_{2f} = -d$ and $\tau_{ff} = 0$ in Equation (6.27), which yield

$$d = \frac{\bar{c}}{A + B} = \frac{\bar{c}\cot\bar{\Phi}}{1 + D} \qquad (6.31)$$

where

$$D = \frac{B}{A} \qquad (6.32)$$

In order to determine the value of d experimentally, it is convenient to write Equation (6.27) in the form

$$q_f \cos\bar{\Phi} = (\bar{p}_f - q_f \sin\bar{\Phi})\tan\bar{\Phi} + B(\bar{p}_f + \mu q_f) + \bar{c}$$

After collecting terms and multiplying through by $\cos\bar{\Phi}$ the above expression becomes

---

*A failure criterion of this same form has since been proposed by TOPPING (1955) and MALYSHEV (1967a).

$$q_f = (\bar{p}_f + d)\sin \bar{\varphi} \tag{6.33}$$

where $\bar{\varphi}$, the apparent angle of internal friction is defined as a function of $\bar{\Phi}$, B and μ by the relation

$$\sin \bar{\varphi} = \frac{\sin \bar{\Phi} + B \cos \bar{\Phi}}{1 - \mu B \cos \bar{\Phi}} \tag{6.34}$$

For a conventional triaxial compression test

$$(\mu = -1) \quad \sin \bar{\varphi}_c = \frac{\sin \bar{\Phi} + B \cos \bar{\Phi}}{1 + B \cos \bar{\Phi}} \tag{6.35a}$$

and for a conventional triaxial extension test

$$(\mu = 1) \quad \sin \bar{\varphi}_E = \frac{\sin \bar{\Phi} + B \cos \bar{\Phi}}{1 - B \cos \bar{\Phi}} \tag{6.35b}$$

which means that the apparent friction angles for compression and extension are related by the expression

$$\frac{\sin \bar{\varphi}_E}{\sin \bar{\varphi}_C} = \frac{1 + B \cos \bar{\Phi}}{1 - B \cos \bar{\Phi}} \tag{6.36}$$

Plots of q_f VERSUS $\bar{p}_f$ for different values of μ should yield a consistent value of the apparent hydrostatic tensile strength, d. If this is the case, and the plots are also linear (or if fitted straight lines with a single value of d can be determined) then an octahedral plane stress plot is justified.

Under the above conditions the octahedral plane stress plot should be a straight line, because it is the intersection of two planes. The equation of the straight line is obtained by writing Equation (6.27) in the form

$$q_f = \left[(B\bar{\sigma}_{2f} + \bar{c}) \cot \bar{\Phi} + \bar{p}_f \right] \sin \bar{\Phi}$$

Then, proceeding in the same manner as was used to obtain Equations (6.10), one obtains

$$\begin{aligned} \frac{s_1 - s_3}{2} &= \left[\frac{B}{A} (\bar{\sigma}_{OCT} + s_2) + \frac{\bar{c}}{A} + \bar{\sigma}_{OCT} + \frac{s_1 + s_3}{2} \right] \sin \bar{\Phi} \\ &= \left[(1 + \frac{B}{A})(d + \bar{\sigma}_{OCT}) - (1 - 2\frac{B}{A}) \frac{s_2}{2} \right] \sin \bar{\Phi} \\ &= \left[\left(\frac{1 + D}{1 - 2D} \right) (d + \bar{\sigma}_{OCT}) - \frac{s_2}{2} \right] (1 - 2D) \sin \bar{\Phi} \end{aligned} \qquad (6.37)$$

Comparison of Equation (6.37) with Equation (6.10) indicates that the equation of the octahedral plane stress plot is

$$\frac{y}{d + \bar{\sigma}_{OCT}} = \left(\frac{1 + D}{1 - 2D}\right)\sqrt{6} - \frac{\sqrt{3}}{(1 - 2D)\sin \bar{\Phi}}\left(\frac{x}{d + \bar{\sigma}_{OCT}}\right) \tag{6.38}$$

The intercept on the horizontal axis must therefore be $(1 + D)\sqrt{2} \sin \bar{\Phi}$.

Peltier tested three sands in direct shear, with a controlled value of the intermediate principal stress:

a) Leucate sand (1.6 to 2.0 MM)

b) Sienne sand (0.5 to 1.0 MM)

c) Leucate sand (0.5 to 1.0 MM)

He indicated that d was zero for all three and listed the following values of A, B, $\bar{\varphi}_c$ and $\bar{\varphi}_E$:

SAND	A	B	$\bar{\varphi}_c$	$\bar{\varphi}_E$	$\sin \bar{\varphi}_c$	$\sin \bar{\varphi}_E$
a	0.540	0.093	31°	38°	0.515	0.616
b	0.600	0.095	$33^\circ 30'$	$41^\circ 20'$	0.552	0.660
c	0.600	0.120	$34^\circ 05'$	$45^\circ 25'$	0.560	0.712

Octahedral plane stress plots for each of the above sands are plotted in Figure 6.18, although there is no way of knowing whether these plots are justified because Peltier published neither test data nor references.

His comparison of the apparent friction angles for conventional triaxial compression and extension tests conflicted with earlier results obtained by M. Habib, M. Brice and the Laboratorie Central des Ponts et Chaussees (L.P.C.C.), which Peltier quotes as having indicated that

$$\bar{\varphi}_C - \bar{\varphi}_E \approx 7^o$$

Peltier's data showed the opposite trend, i.e. $\bar{\varphi}_E$ greater than $\bar{\varphi}_C$ by 7 to 11 degrees for the three different sands he tested.

In his contribution to the discussion of Soil Properties and Their Measurement, BISHOP (1957) listed several points which can serve as a summary of then current thinking concerning the influence of the intermediate principal effective stress on soil shear strength.

1. Shear strength is generally measured in the laboratory under conditions of axial symmetry, while conditions occurring in many field situations are much nearer to plane strain than axial symmetry.

2. There are two general ways of studying the influence of the intermediate principal effective stress on soil shear strength:

   a) Compare field data obtained under plane strain conditions with laboratory data obtained under axially symmetric conditions.

   b) Conduct both axially symmetric and plane strain tests in the laboratory, where many extraneous and complicating conditions which occur in the field can be eliminated, or at least controlled.

3. It is not clear whether the horizontal plane in a shear box (direct shear device) is a plane of rupture or a plane of maximum shear stress, so that the direct shear test (used by Peltier) may not be the best device to use in studying the influence of the intermediate principal effective stress. Also, the stress distribution in the shear box test is unknown.

4. Failure in plane strain occurs at much smaller major principal strains than in the usual triaxial test.

PARRY (1956; 1960) reported the results of a considerable number of triaxial tests on remolded Weald and London clay, conducted by GILBERT (1954), PLANT (1955) and himself.

The most comprehensive data were obtained for Weald clay, the London clay being used mainly to check the general validity of conclusions drawn from the data on Weald clay. Index properties of the two clays were as follows:

	Weald Clay	London Clay
Liquid Limit	43%	78%
Plastic Limit	18%	26%
Plasticity Index	25%	52%
Percent by Weight Finer than 0.002MM	40%	50%
Activity	0.6	1.0
Specific Gravity of Solids	2.74	2.75

All tests reported by Parry employed isotropic consolidation from an initially high water content, corresponding to an undrained shear strength of about 0.6 PSI, to a maximum all-round stress $\bar{p}_m$, followed by rebound under an all-round stress

$\bar{p}_c$, followed by either undrained or drained shear in either compression or extension. The initial water contents were: Weald clay 34% (L.I. = 0.64); London clay 56% (L.I. = 0.58). Althogether, 10 different tests were employed, as shown below:

1. Undrained compression

   UC1: σ_r constant, σ_v increased

   UC2: σ_r decreased, σ_v constant

2. Drained compression

   DC1: $\bar{\sigma}_r$ constant, $\bar{\sigma}_v$ increased

   DC2: $\bar{\sigma}_r$ decreased, $\bar{\sigma}_v$ constant

   DC3: $(\bar{\sigma}_v + 2\bar{\sigma}_r)$ constant

3. Undrained extension

   UE1: σ_r constant, σ_v decreased

   UE2: σ_r increased, σ_v constant

4. Drained extension

   DE1: $\bar{\sigma}_r$ constant, $\bar{\sigma}_v$ decreased

   DE2: $\bar{\sigma}_r$ increased, $\bar{\sigma}_v$ constant

   DE3: $(\bar{\sigma}_v + 2\bar{\sigma}_r)$ constant

Stress conditions at failure, as given by Parry, are tabulated in Tables 6.9 and 6.10 and plotted in Figures 6.19 and 6.20.

Figure 6.19 indicates that the effective stress strength envelopes for remolded Weald clay are essentially independent of test type, and also identical in compression and extension, for a given value of $\bar{p}_m$. No extension tests were reported for London clay.

In plotting Figures 6.19 and 6.20, use was made of the fact that both these remolded clays appear to exhibit what has come to be called normalized behavior, i.e. an almost exclusive dependence of effective stress - deformation characteristics on the overconsolidation ratio prior to shear. This dependence was noted by HENKEL (1956), who further documented it by plotting contours of constant water content in $(\bar{\sigma}_1, \bar{\sigma}_3)$ space for both undrained and drained tests, using the data on Weald and London clay obtained by Gilbert, Plant and Parry under his direction; HENKEL (1958; 1959; 1960a, 1960b). Henkel's results can be concisely stated as follows:

1. If

   $\bar{p}_c$ = isotropic effective stress corresponding to a given void ratio

then for a given initial void ratio at the start of consolidation, contours of constant void ratio in $(\bar{\sigma}_1, \bar{\sigma}_3)$ space obtained

from isotropically consolidated triaxial tests and corresponding to the same value of $\bar{p}_c/\bar{p}_m$ are geometrically similar and independent of the type of triaxial test employed; and the scale of any contour is proportional to the value of $\bar{p}_m$.

2. The void ratio increase which occurs during rebound under isotropic effective stress depends only on the ratio $\bar{p}_c/\bar{p}_m$.

The four independent state variables ($\bar{\sigma}_1$, $\bar{\sigma}_3$, Δu and e) for a remolded clay exhibiting normalized axially-symmetric effective stress-deformation characteristics can therefore be determined from four independent pieces of information:

1. the isotropic virgin consolidation curve, which is a plot of e_c VERSUS $\log_{10}\bar{p}_m$,

2. the isotropic swell curve, which is a plot of $e_s - e_c$ VERSUS $\log_{10}\bar{p}_c/\bar{p}_m$,

3. the family of void ratio contours covering all admissable combinations of normalized effective stress, and

4. the failure curve, which is a plot of $\bar{\sigma}_{1f}/\bar{p}_m$ VERSUS $\bar{\sigma}_{3f}/\bar{p}_m$.

If a fifth state variable, the axial strain ϵ, is added, a fifth independent piece of information is required. This could be the family of axial strain contours covering all admissable combinations of normalized effective stress, sometimes referred to as strength mobilization contours.

WOOD (1958) conducted both plane strain compression and conventional triaxial compression tests on the minus 3/8 INCH fraction of a well graded sandy gravel (17% gravel, 55% sand, 26% silt and 2% clay) used in the construction of the Glen Shira earth dam in Scotland. He compacted the soil at a water content about 3% above the Proctor optimum of 10.5% (molding water content between 12.6% and 14.2%), which yielded dry unit weights between about 117 and 123 PCF and corresponded to field placement conditions for the actual earth dam. Dimensions of the plane strain samples in the three principal directions are shown below.

PRINCIPAL DIRECTION	DIMENSION, IN.
1	4
2	2
3	16

Although Wood was aware that his samples were not fully saturated, he still presented his results in terms of what he called effective stress. However, he gave no indication of how he computed effective stress, and so his results may need to be treated with a certain degree of caution. BISHOP (1957, 103) indicated that the value of the molding water content was chosen "to avoid any ambiguity in the measurement of pore pressure", but did not elaborate. Perhaps he felt that at such a high molding water content the air phase would be discontinuous, i.e. would consists of bubbles in a continuous liquid phase, so that the measured pore pressure would be the pressure in a statistically homogeneous, even if compressible liquid pore fluid.

Following compaction, all samples were loaded in two stages, each under a controlled rate of major principal compressive strain and without permitting exterior drainage. The tests were called undrained tests, but because the samples were not saturated they were not constant volume tests. Volume changes were recorded by measuring the volume of water passing into or out of the cell (not the sample),

and presumably these volume changes represented compression of the air phase prior to its being driven into solution. During Stage 1 the intermediate and minor principal effective stresses were equal and were manually adjusted by varying the cell pressure in order to prevent lateral strain, using values of K_o measured earlier for the same soil by FRASER (1957). During Stage 2 the cell pressure, i.e. the minor principal total stress, was held constant. In the plane strain test the intermediate principal effective stress then adjusted itself to the condition of zero intermediate principal strain, enforced by end plates held a fixed distance apart by a null displacement hydraulic system, which also allowed the intermediate principal total stress to be measured. Pore pressure measurements were taken throughout both stages.

Although the values of effective stress reported by Wood may be subject to debate, the following qualitative observations are still significant:

1. Plane strain samples attained both maximum obliquity and maximum principal stress difference at lower major principal strains then did conventional triaxial compression samples.

2. Plane strain samples showed a smaller volume increase, hence higher positive pore pressure and lower effective stress at any given value of the major principal strain than did cylindrical compression samples loaded to the same point during Stage 1. The lesser dilation of plane strain samples was apparently due to a lesser degree of particle mobility, and undoubtedly was a major cause of the earlier shear strength mobilization which characterized the plane strain samples.

3. Each plane strain sample failed by sliding along a plane which was continuous along the length of the specimen and could be seen in the end faces. The inclination of the plane with the horizontal was $60^{\circ} \pm 5^{\circ}$.

Keeping in mind the questions of the physical meaning of measured pore pressure and the definition of effective stress in partly saturated soil, Wood's strength data for both plane strain compression and conventional triaxial compression have been tabulated in Table 6.11 and plotted in Figures 6.21 and 6.22. There were a few apparent minor internal inconsistencies in Wood's tabulated data, which had to be resolved more or less arbitrarily in order to construct Table 6.11. However, none of them had an appreciable affect

on the apparent effective stress shear strength parameters. The definition of failure chosen for the presentation here is that of maximum principal stress difference, because strength values obtained by this definition can be compared with strength values obtained in tests without pore pressure measurements. Wood's thesis also contains data obtained at maximum obliquity, however, and a comparison of the apparent effective stress shear strength parameters obtained by him, using the method of least squares, is shown below.

APPARENT EFFECTIVE STRESS SHEAR STRENGTH PARAMETERS

FAILURE CRITERION	PLANE STRAIN		CYLINDRICAL COMPRESSION	
	$\bar{c}$	$\bar{\Phi}$	$\bar{c}$	$\bar{\Phi}$
	PSI	DEG	PSI	DEG
$(\bar{\sigma}_1 - \bar{\sigma}_3)_{MAX}$	1.9	36.9	0.2	35.1
$(\bar{\sigma}_1/\bar{\sigma}_3)_{MAX}$	1.7	41.9	0.9	37.2

The strength lines in Figure 6.21 were drawn by eye, assuming zero cohesion.

Table 6.11 reveals what could be considered a drawback of the plane strain test, insofar as the determination of a failure criterion in terms of effective stress is concerned,

and that is the fact that Lode's parameter μ is not constant. If plane strain tests 28, 21 and 26 are ignored in Figure 6.21, one obtains a strength line for $\mu \approx -0.58$, which is essentially parallel to the one for cylindrical compression, but exhibits cohesion. Variation in both density and water content could be the cause of this apparent inconsistency.

A notable feature of Wood's thesis is his use of stress paths plotted in q VERSUS $\bar{p}$ space (his Figure 44). Both plane strain and cylindrical compression test specimens exhibited overconsolidated behavior, and therefore reached maximum obliquity prior to reaching maximum principal stress difference.

Another interesting feature is his observation that

$$\bar{\sigma}_2 \approx K_o \bar{\sigma}_1$$

throughout Stage 2 of the plane strain tests. Of course, the reliability of this result can only be judged along with the reliability of pore pressure measurements and effective stress calculations. If true, his observation, when combined with the empirical relation

$$K_o = 1 - \sin \bar{\Phi}$$

leads to the result

$$\mu = \frac{\bar{\sigma}_2 - \bar{p}}{q} = \frac{K_o \bar{\sigma}_1 - \bar{p}}{q} = \frac{(1 - \sin \bar{\Phi})(1 + \sin \bar{\Phi}) - 1}{\sin \bar{\Phi}}$$

$$= - \sin \bar{\Phi} = K_o - 1 \qquad (6.40)$$

HAYTHORNTHWAITE (1960a, 1960b) presented results of fully drained* tests on hollow cylinders of a clayey silt, in which a triaxial state of stress was achieved by combining equal inside and outside cell pressures, axial load and a torque about the vertical axis. His main interest was in establishing an experimental basis for the formulation of an incremental theory of plasticity for soils. The samples were prepared by tamping thee layers of a mixture of 30% by weight Boston blue clay and 70% quartz flour between two cylindrical molds, which were then removed after a vacuum had been applied to the sample. The sample was then consolidated

---

*According to HAYTHORNTHWAITE (1960b, 991) and (1963, 120). However, in analyzing the test data, he assumed the volume of the samples remained constant during shear, even though both axial and volumetric strains were measured.

under a hydrostatic pressure of 100 PSI for 14 hours prior to testing, which resulted in an average pre-shear water content of 24% and a porosity of 34%. The grain size distribution curve for the sample mixture yielded the following values:

$$D_{60} = 0.032 \text{ MM}$$

$$D_{30} = 0.013 \text{ MM}$$

$$D_{10} = 0.0015 \text{ MM} = \text{effective size}$$

Coefficient of Uniformity, $C_U = \frac{D_{60}}{D_{10}} = 21.3$

Coefficient of Curvature, $C_C = \frac{(D_{30})^2}{D_{10}D_{60}} = 3.52$

Two types of tests were conducted, in order to see whether the failure criterion was stress path independent. No definition of failure was stated, but since these were fully drained tests the maximum principal stress difference and the maximum principal effective stress ratio occurred simultaneously, so that both could have and probably did serve to define the occurrence of failure. The two test series were conducted as follows:

Series A: cell pressure reduced from 100 PSI to 40 PSI then excess axial force and torque increased in constant ratio to failure.

Series B: particular values of excess axial force and torque applied, then held constant while cell pressure reduced from 100 PSI to failure.

In order to see whether strain hardening was isotropic* Haythornthwaite reported the results of the Series B tests by interpolating between results of tests which failed at cell pressures above and below 40 PSI. From the values of excess axial load, W, and torque, T, at failure which he reported, the stresses at failure have been calculated and tabulated in Table 6.12, using initial sample dimensions also calculated from his reported data:

inside diameter, D_i = 2.5 IN

outside diameter, D_o = 4.5 IN

---

*See, e.g. JOHNSON AND MELLOR (1962, 53).

The following formulae used to calculate stresses in Table 6.12 assume a homogeneous state of stress throughout the cylinder at failure.

$$\bar{\sigma}_2 = \bar{\sigma}_{rr} = \bar{\sigma}_{\theta\theta} = \sigma_c = \text{cell pressure}$$

$$\frac{\bar{\sigma}_{zz} - \bar{\sigma}_{\theta\theta}}{2} = \frac{2W}{\pi(D_o^2 - D_i^2)} = \frac{W}{21.991}$$

$$\tau_{z\theta} = \frac{12T}{\pi(D_o^3 - D_i^3)} = \frac{T}{19.776}$$

$$\bar{p} = \frac{\bar{\sigma}_{zz} + \bar{\sigma}_{\theta\theta}}{2} = \bar{\sigma}_{\theta\theta} + \frac{\bar{\sigma}_{zz} - \bar{\sigma}_{\theta\theta}}{2} = \bar{\sigma}_2 + q \cos 2\beta$$

$$q = \sqrt{\left(\frac{\bar{\sigma}_{zz} - \bar{\sigma}_{rr}}{2}\right)^2 + \tau_{z\theta}^2}$$

$$\bar{\sigma}_1 = \bar{p} + q$$

$$\bar{\sigma}_3 = \bar{p} - q$$

$$\mu = \frac{\bar{\sigma}_2 - \bar{p}}{q} = -\cos 2\beta$$

$$\bar{\sigma}_{zz} \geq \bar{\sigma}_{\theta\theta} \rightarrow 0 \leq \beta \leq 45^\circ$$

$$\bar{\sigma}_{zz} < \bar{\sigma}_{\theta\theta} \rightarrow 45^\circ \leq \beta \leq 90^\circ$$

Haythornthwaite indicated that a series of tests without torsion, corresponding to the standard triaxial test (presumably drained compression tests with constant cell pressure) had yielded the following angle of shearing resistance and cohesion intercept:

$$\bar{\Phi} = 35^{o}$$
$$\bar{c} = 4.8 \text{ PSI}$$

No details concerning this test series were given, so there is no way of telling whether the pre-shear effective stress history was the same for the conventional triaxial compression tests as for the tests with torsion. Consequently the constant μ failure lines have been assumed linear, but the material has been assumed cohesionless in order to construct the octahedral plane stress plot in Figure 6.23. It is quite likely that had sample deformation been taken into account in calculating the stresses in Table 6.12, agreement with the Revised Coulomb failure criterion would have been somewhat better. The rapid increase in the angle of shearing resistance, as Lode's parameter increases from -1 to about

-0.7, has been observed by several investigators since Haythornthwaite. Some possible reasons for it are:

1. stress inhomogeneity in the test specimen,

2. progressive failure, caused by (1) and also by an increase in area and consequent strengthening of the samples at the location where a compression failure begins,

3. differences in void ratio at failure,

4. rapid decrease in particle mobility accompanying a relatively small increase in the intermediate principal effective stress, and

5. true sudden deviation from the Revised Coulomb criterion, as determined by triaxial compression ($\mu = -1$) and triaxial extension ($\mu = 1$) tests.

After slightly modifying the plane strain apparatus designed by Bishop and built by Wood, CONFORTH (1961, 1964) used it to conduct both drained and undrained plane strain compression tests on saturated Brasted sand. He also conducted conventional triaxial compression and extension tests on the same material, with the object of comparing the strength-density relationships yielded by the three

types of tests. Conforth's plane strain specimens had the same nominal dimensions as did Wood's, viz 16 inches long, 4 inches high and 2 inches wide. His triaxial specimens had a diameter of 4 inches and a height of 8 inches. Brasted sand was selected for the investigation because it had already been studied by KOLBUSZEWSKI (1948), HAFIZ (1950), ELDIN (1951) and FRASER (1957). It is a medium to fine uniform quartz sand with angular grains, containing a slight trace of mica but no organic matter. Prior to testing, the grain size distribution curve yielded the following values:

$$D_{60} = 0.32 \text{ MM}$$

$$D_{30} = 0.22 \text{ MM}$$

$$D_{10} = 0.14 \text{ MM} = \text{effective size}$$

Coefficient of Uniformity, $C_U = \frac{D_{60}}{D_{10}} = 2.28$

Coefficient of Curvature, $C_C = \frac{(D_{30})^2}{D_{10}D_{60}} = 1.08$

Near the end of the test program the gain size distribution curve showed slight evidence of grain crushing. The average value for specific gravity of solids was 2.684, and the limiting values of porosity, as defined by KOLBUSZEWSKI (1948), were

$n_{MAX} = 44.2\%$

$n_{MIN} = 32.2\%$

Both plane strain and conventional triaxial compression tests began with a K_o consolidation phase. Tests details are summarized below.

TEST SERIES	NO. OF TESTS	DESCRIPTION
A	13	drained plane strain compression with increasing axial stress and constant cell pressure
B	4	drained plane strain compression with constant axial stress and decreasing cell pressure
C	5	same as Series A, but without plane strain control device
D	8	undrained plane strain compression with increasing axial total stress and constant cell pressure
E	16	drained cylindrical compression with increasing axial stress and constant cell pressure
F	5	drained cylindrical compression with constant axial stress and decreasing cell pressure
G*	6	drained cylindrical extension with decreasing axial stress and constant cell pressure
H	4	undrained cylindrical compression with increasing axial total stress and constant cell pressure
J*	2	undrained cylindrical extension with decreasing axial total stress and constant cell pressure

*These tests were among, if not the first conventional triaxial extension tests on 4 inch diameter specimens of cohesionless soil.

The number of tests of each type were:

plane strain:	30
cylindrical compression:	25
cylindrical extension:	8
TOTAL:	63

Conforth used the maximum principal stress ratio as the failure criterion for his undrained tests, because some of his denser Series D specimens and all of his Series H specimens could not be made to exhibit a maximum principal stress difference. Most of the tests were not stopped at failure, but rather continued until the ultimate condition was reached. The ultimate condition is that in which the sample shows no further tendency to change volume, as reflected either by actual volume change in a drained test or by excess pore water pressure change in an undrained test. The conventional triaxial extension tests were stopped as soon as the maximum principal stress difference was reached. Because of necking, the stresses acting on the failure plane of an extension sample had to be calculated by estimating the dimensions of the failure

plane from closely spaced measurements of the sample diameter in the necked region, also taking account of changes in specimen size during stress release after the test.

Conforth concentrated on the relationship between strength and initial porosity, i.e. the porosity immediately after placement but prior to both K_o consolidation and shear. He assumed the material to be cohesionless. In view of Hvorslev's work relating the true cohesion of clay to the void ratio in the failure plane at the time of failure, it is of interest to reexamine Conforth's data, and to concentrate instead on the relationship between strength and average porosity at failure. The data are tabulated in Table 6.13. In order to be sure the material really is cohesionless at all densities, failure data were plotted in Figure 6.24 for seven different narrow ranges of porosity at failure, n_f: 35.0 - 35.9, 36.0 - 36.9, 37.0 - 37.9, 38.0 - 38.9, 39.0 - 39.9, 40.0 - 40.9 and 41.0 - 41.9%. The most reasonable interpretation of the seven plots is that the material is cohesionless, but that the angle of shearing resistance varies with both porosity at failure and the intermediate

principal stress. Consequently the failure data were reploted in Figure 6.25 for each of the three types of tests: plane strain, cylindrical compression and cylindrical extension. These three plots of sin $\bar{\Phi}$ VERSUS n_f showed enough scatter that it was decided to fit straight lines to the data using the Method of Least Squares, whereupon an interesting result was observed: the slopes of the three strength - density lines varied at most by only 9.5%. The equations of the three lines are given below.

PLANE STRAIN: $(\sin \bar{\Phi} - 0.6284) = -0.0199(n_f - 38.2566)$

CYLINDRICAL COMPRESSION: $(\sin \bar{\Phi} - 0.5985) = -0.0180(n_f - 38.6680)$

CYLINDRICAL EXTENSION : $(\sin \bar{\Phi} - 0.5896) = -0.0184(n_f - 38.0625)$

An even more surprising result was observed when the value of Lode's parameter for the plane strain tests was plotted against the porosity at failure in Figure 6.26. The slope of that line was found to be equal in magnitude to that of the strength - density line for cylindrical compression in Figure 6.25(b), the equation being

$$(\mu + 0.5670) = 0.0180\ (n_f - 38.1833)$$

Since the material was cohesionless and the data gave no indication of curvature in the strength lines, and since there existed (statistically) unique relations between n_f, $\bar{\Phi}$ and μ, it was possible to construct a family of octahedral plane strength contours in Figure 6.27. The line labeled "plane strain line" enables one to predict the values of both $\bar{\Phi}$ and μ in a plane strain test, for any value of n_f between 34% and 42%. These plots show that for any value of n_f the shear strength of Brasted sand is slightly higher in plane strain and slightly lower in cylindrical extension than in cylindrical compression. It must be noted, however, that n_f is the average porosity of the entire sample at failure, and therefore lower than the porosity in the failure zone at failure, due to nonuniform volume changes during shear. Although not tabulated or plotted here, Conforth observed the initial tangent modulus of plane strain specimens to be somewhat lower, and the axial strain at failure to be considerably lower (by a factor of about 3) than for cylindrical compression tests.

RATNAM (1962) conducted hollow cylinder tests on a commerical kaolinite, in which Lode's parameter at failure was either -1.00 (triaxial compression) or else about -0.25. However, his main interest was in the influence of Lode's parameter during consolidation on the effective stress shear strength parameters and pore pressure response. Consequently his results do not all pertain to the same preshear soil structure. See also BROMS AND RATNAM (1963).

WU, LOH AND MALVERN (1963) conducted hollow cylinder tests on remolded Sault Ste. Marie clay and on the fraction of standard Ottawa sand passing a number 30 sieve (0.590 MM) and retained on a number 50 sieve (0.297 MM). In effect they did what Kirkpatrick originally intended to do but decided not to: apply an axial load to the hollow cylinder in order to vary Lode's parameter. Six different isotropically consolidated undrained test series were conducted, each with pore pressure measurements, as shown below.

TEST	SPECIMEN	STRESS CONDITIONS AT FAILURE
C1	solid cylinder	$\bar{\sigma}_z > \bar{\sigma}_r = \bar{\sigma}_\theta$
C1a	hollow cylinder	$\bar{\sigma}_z > \bar{\sigma}_r = \bar{\sigma}_\theta$
E1	solid cylinder	$\bar{\sigma}_r = \bar{\sigma}_\theta > \bar{\sigma}_z$
I1	hollow cylinder	$\bar{\sigma}_\theta > \bar{\sigma}_z > \bar{\sigma}_r$
I2	hollow cylinder	$\bar{\sigma}_z > \bar{\sigma}_\theta > \bar{\sigma}_r$
I3	hollow cylinder	$\bar{\sigma}_\theta > \bar{\sigma}_z > \bar{\sigma}_r$

The conventional triaxial tests were strain-controlled, while the hollow cylinder tests were stress-controlled. The hollow cylinder specimens had the following initial dimensions:

outside radius: $r_o = 2.0$ IN

inside radius: $r_i = 1.5$ IN

height: $h = 5.0$ IN

Index properties of the two batches of Sault Ste, Marie clay used are shown below.

	BATCH NO. 1	BATCH NO. 2
Liquid Limit	52%	56%
Plastic Limit	28%	27%
Plasticity Index	24%	29%
Percent by Weight Finer than 0.002MM	65%	
Activity	0.2	

Unfortunately, the failure criterion for the tests on clay was not stated, i.e. whether maximum principal stress difference or maximum principal effective stress ratio. The test data have been tabulated in Table 6.14, assuming the average radial effective stress to be the mean of the effective radial stresses at the outside and inside walls, and calculating the average tangential stress from horizontal equilibrium, assuming uniform radial strain. These values generally differ only slightly from corresponding values appearing in the original paper, which were calculated on the basis of plasticity theory, using assumed values of the effective stress shear strength parameters. Triaxial compression and extension data for both batches of remolded Sault Ste. Marie clay, plotted in Figures 6.28 and 6.29, indicate the

material to be cohesionless. An octahedral plane stress plot has therefore been constructed in Figure 6.30, assuming the material to be both isotropic and cohesionless. Although there is a fair amount of scatter, the material appears to obey a cohesionless revised Coulomb failure criterion, with an average effective angle of internal friction of about 31° ($\sin \bar{\Phi} = 0.515$).

As with Conforth's tests on Brasted sand, the strength results for Ottawa sand were influenced by void ratio. However, since 13 out of 23 specimens had void ratios between 0.47 ($n = 32.0\%$) and 0.52 ($n = 34.2\%$), these 13 tests will be analyzed as though they had the same void ratio, and the other 10 tests will be excluded from consideration. Data for all 23 tests, at maximum principal effective stress ratio, are tabulated in Table 6.15, to which the previous comments regarding stress calculations also apply. Triaxial compression and extension data, plotted in Figure 6.31 indicate the material to be cohesionless. Again assuming isotropy and zero cohesion, an octahedral plane stress plot has been constructed in Figure 6.32, and indicates that standard Ottawa sand also obeys a cohesionless revised Coulomb failure

criterion, with about the same scatter as for Sault Ste. Marie clay. The average effective angle of internal friction appears to be about 38° ($\sin \bar{\Phi} = 0.616$).

LIAM FINN AND MITTAL (1963) presented stress - strain data for triaxial compression and plane strain tests on a compacted clay. No indication was given of whether the intermediate principal stress was measured in the plane strain tests. The plane strain tests yielded higher maximum principal effective stress ratios and considerably smaller failure strains than did the triaxial compression tests. The authors also presented a theoretical discussion of the effect of the intermediate principal stress on the strength of a cohesionless material, originally developed by LIAM FINN (1963). It is interesting to examine their presentation, to see what the resulting failure criterion looks like in an octahedral plane stress plot. Liam Finn and Mittal suggested that the plot of principal effective stress ratio $\bar{\sigma}_1/\bar{\sigma}_3$ VERSUS axial (maximum principal) strain ϵ_1 be idealized as an elastic - perfectly plastic curve, and that the material be considered linearly elastic up to the point of failure. Under the above assumption, the axial strain at failure (initial yield) will be

$$\epsilon_{1f} = \frac{1}{E}\left[\bar{\sigma}_{1f} - \nu\,(\bar{\sigma}_{2f} + \bar{\sigma}_{3f})\right]$$

They then obtained what they claimed to be an upper bound for the shear strength under a general stress system, by assuming ϵ_{1f} to be the same under any stress system. Although they did not write the general expression which results from their assumption regarding ϵ_{1f}, it is

$$\bar{\sigma}_{1f} = \nu\bar{\sigma}_{3f} + \nu\bar{\sigma}_{2f} + C$$

where

$$C = E\,\epsilon_{1f} = \text{constant}$$

The above expression for $\bar{\sigma}_{1f}$ is a special form of Equation (6.30), and therefore Liam Finn and Mittal's proposed strength relationship is basically the same as Peltier's. It yields a linear octahedral plane stress plot.

LEUSSINK AND WITTKE (1963) summarized the results of theoretical analyses of the shear strength of various regular packings of uniform spheres under conditions of cylindrical compression and plane strain. They also performed triaxial compression and plane strain tests on regular packings of steel and glass balls, but did not report values of the intermediate principal stress for the plane strain tests.

ROSCOE, SCHOFIELD AND THURAIRAJAH (1963), after reviewing conflicting conclusions drawn by earlier investigators, offered the opinion that "Much of the uncertainty [in the definition of a general failure criterion] has been caused by different authors' concepts of 'failure', but the most important source of error is probably the lack of uniformity of the deformation within the specimen and the variation in the pattern of deformation under different triaxial test conditions." In fact, they went so far as to suggest "that the nonuniformity of deformation within triaxial specimens is such that data from triaxial tests cannot be used to establish the correctness of either the Mohr - Coulomb or any other criterion of failure." They based their indictment against the triaxial test on the results of drained triaxial compression and extension tests on rounded Leighton Buzzard sand, in which local as well as over-all deformation measurements were obtained. When analyzed by conventional methods, using measured over-all deformations, the results appeared to favor the Mohr - Coulomb failure criterion. But when stresses were calculated (presumably more accurately) on the basis of measured local deformation, the results appeared

to favor the extended von Mises criterion. It should be noted that when stresses are calculated using measured local deformations, the definition of failure is more difficult than when the conventional (cylindrical) area correction is employed. When the conventional area correction was employed, the stress-strain curve in extension reached a definite maximum (point of instability), whereas when measured local deformations were used to calculate the area of the necked region the stress-strain curve never did become unstable but displayed two plateaus. The first plateau, which was quite short, essentially coincided with the point of instability of the conventionally calculated curve. The second plateau was longer and higher, and the contention that the data supported the extended von Mises rather than the Mohr Coulomb failure criterion was based upon the selection of this second plateau as the definition of failure. Starting with the work of ROSCOE, SCHOFIELD AND WROTH (1958), the Cambridge Group has consistently taken as state variables the effective octahedral normal stress, the octahedral shear stress and the void ratio, which is equivalent to assuming the validity of the extended von Mises failure criterion. The main difficulty lies in the fact that most soil strength data do not support the extended von Mises failure criterion.

WADE (1963) and SOWA (1963) wrote companion theses at the University of London's Imperial College, designed to assess the influence of K_o consolidation and plane strain deformation on the shear behavior of remolded Weald clay. The Weald clay used in both investigations was obtained in May, 1960 from the excavated pits of the London Brick Works in Dorking, Surrey, by Dr. D.J. Henkel and Dr. Wade. Three samples were taken at depths below the original ground surface ranging from ten to twenty feet, and two of these were found to have an average liquid limit of about 46%. These two samples were selected for both test programs because of their similarity to the Weald clay previously tested at Imperial College. Index properties of the Weald clay used by Wade and Sowa are shown below.

Liquid Limit	46%
Plastic Limit	20%
Plasticity Index	26%
Percent by Weight Finer Than 0.002 MM	38%
Activity	0.68
Compression Index	0.20
Specific Gravity of Solids	2.72

Sowa conducted several different types of isotropically consolidated and one-dimensionally (K_o) consolidated triaxial tests, for which symbols are defined below.

ISOTROPICALLY CONSOLIDATED TESTS

NUC: normally consolidated, then failed in undrained compression with pore pressure measurements.

NDC: normally consolidated, then failed in drained compression with constant cell pressure.

OUC: overconsolidated, then failed in undrained compression with pore pressure measurements.

NUE: normally consolidated, then failed in undrained extension with pore pressure measurements.

K_o CONSOLIDATED TESTS

NUC: normally consolidated, then failed in undrained compression with pore pressure measurements.

NPSUC: normally consolidated, deviator stress released undrained, then failed in undrained compression, with pore pressure measurements during both undrained phases.

NPSIUC: normally consolidated, deviator stress released undrained, then isotropically consolidated to an all-round effective stress equal to the previous maximum vertical effective stress attained during K_o consolidation, then failed in undrained compression, with pore pressure measurements during both undrained phases.

OUC: overconsolidated, then failed in undrained compression with pore pressure measurements.

OPSUC: overconsolidated, deviator stress released undrained, then failed in undrained compression, with pore pressure measurements during both undrained phases.

NUE: normally consolidated, then failed in undrained extension with pore pressure measurements.

NSUC: normally consolidated in a large oedometer, consolidation stresses released and triaxial sample trimmed undrained, then failed in undrained compression with pore pressure measurements.

RUC: previously tested NSUC sample completely remolded by hand undrained, then failed in undrained compression with pore pressure measurements.

The effective stress paths corresponding to each of the above tests are shown in Figures 6.33 and 6.34. By comparing Wade's plane strain test results with his own K_o consolidated and isotropically consolidated triaxial test results, Sowa hoped to determine whether the effects of plane strain deformation during consolidation and shear were significant enough to warrant modification of current design procedures based on the more conventional triaxial tests.

Stress histories for Sowa's isotropically consolidated and K_o consolidated triaxial tests are tabulated in Tables 6.16 and 6.17. The strength results (at maximum principal stress difference) are tabulated in Tables 6.18 and 6.19 and plotted in Figures 6.35 and 6.36. In addition to initial water content, the other major test variables were axial strain rate and whether or not a special rotating bushing was used to eliminate ram friction. Neither of these last two variables appeared to have a significant influence on strength, expressed in terms of effective stress, and the influence of initial water content was inconsistent. Specimens with an initial water content of

33.4% were hand molded with a spatula in a brass tube, while specimens with initial water contents of 49% and 227% were trimmed from cakes consolidated in a large oedometer. Of all the undrained compression tests on isotropically, normally consolidated specimens, only the four with an initial water content of 49% gave strengths, in terms of effective stress, which were significantly and consistently higher than the rest. All the undrained compression tests on K_o normally consolidated specimens were consistent. Sowa fit straight lines to various sets of data obtained under similar test conditions, using the Method of Least Squares, and in several cases obtained a small cohesion intercept. It is clear from Figures 6.35 and 6.36, however, that the strength lines actually pass through the origin, and that the cohesion intercepts are the result of a slight downward curvature of the strength lines. There is good reason to doubt whether Sowa's K_o consolidated triaxial tests were consolidated exactly one-dimensionally, because the plots of measured VERSUS calculated volume decrease during consolidation did not have slopes of unity. However, the influence of this discrepancy on strength was probably

negligible. The principal feature of Figures 6.35 and 6.36 is that the strength lines for compression tests on both isotropically and K_o normally consolidated specimens seem, for practical engineering purposes, to be identical. The same is true in extension. Also, an interesting observation made by Sowa, which is not reflected by Figures 6.35 and 6.36, is that the pore pressure response during sampling of K_o consolidated specimens tended toward that of an elastic material ($F = -\frac{1}{3}$ for triaxial compression) as the overconsolidation ratio increased. This could be an indication that the applicability of elastic theory to problems of load-deformation behavior of soil masses increases with their degree of overconsolidation. See also SKEMPTON AND SOWA (1963) and HENKEL AND SOWA (1963).

Wade's plane strain tests on saturated, remolded Weald clay are the first successful plane strain tests on saturated clay known to the Writer. In 1958 Conforth attempted tests on Supreme Kaolin, similar to those conducted later by Sowa and Wade. However, he encountered difficulties with Bishop's triaxial K_o device, as well as a tendency for specimens consolidated in a large oedometer to suck water back out of the porous stones during release of the consolidation stress,

and also an unacceptably high degree of scatter of measured shear strength characteristics. Although his test series on kaolin had to be abandoned after a long but unsuccessful effort, Conforth clearly did pioneer work on plane strain testing of saturated remolded clays.

Wade's plane strain specimens had the same nominal overall dimensions as Wood's and Conforth's: 16 inches long, 4 inches high and 2 inches thick. Consolidation stress histories for all Wade's plane strain tests on saturated remolded Weald clay are tabulated in Table 6.20. All were undrained compression tests with pore pressure measurements, on K_o normally consolidated specimens, using a slightly modified version of the plane strain device employed by Wood and Conforth. Of Wade's 15 plane strain tests on Weald clay, 12 involved some sort of irregularity or deviation from "standard" test procedure, as shown in Table 6.21. There is no way of assessing the influence of these irregularities on his test results. Most of the samples failed by general overall distortion, rather than by sliding along a distinct failure plane. The strength results (at maximum principal stress difference) are tabulated in Table 6.22, and plotted in Figure 6.37.

An octahedral plane stress plot, summarizing both Sowa's and Wade's results, is shown in Figure 6.38. The average values of sin $\bar{\Phi}$ for Sowa's triaxial tests are shown below.

CONSOLIDATION	FAILURE	SIN $\bar{\Phi}$
isotropic	compression	0.446
isotropic	extension	0.505
K_o	compression	0.440

Figure 6.38 indicates that on the basis of Sowa's and Wade's tests, the best failure criterion for remolded Weald clay is a cohesionless Mohr-Coulomb criterion with sin $\bar{\Phi}$ equal to about 0.450 ($\bar{\Phi} = 26.8^{o}$)*. Wade noted that his plane strain specimens reached maximum principal stress difference at a lower axial strain (2-3%) than was required to mobilize the maximum principal stress difference in Sowa's K_o consolidated triaxial compression tests (5-6%). He also noted a higher ratio of maximum principal stress difference to average principal stress at the end of consolidation for the plane strain tests than for the triaxial compression tests. These two strength effects appeared to be closely

*Wade did not reach this conclusion, because he assumed a value of $\bar{\Phi}$ in order to construct an octahedral plane stress plot.

related to lack of particle mobility (i.e. motion restraint) in the $\bar{\sigma}_2$ direction, because samples tested in the plane strain device without end restraint exhibited stress ratios within the limits of values obtained for the triaxial tests, but at axial strains of only 2-4%. The above comparative results are consistent with earlier comparisons by WOOD (1958) and CONFORTH (1961). However, the failure strain comparison may be significantly dependent upon the initial molding water content, because more recent tests at the Massachusetts Institute of Technology on triaxial and plane strain specimens of Boston blue clay, initially consolidated from a dilute slurry, have shown higher strains at failure in plane strain than in triaxial compression; DICKEY, LADD AND RIXNER (1968).

For the 10 plane strain tests in which Wade obtained intermediate principal stress measurements, the following average values of sin $\bar{\Phi}$ and μ resulted:

$$(\sin \bar{\Phi})_{AVG} = 0.445$$

$$(\mu)_{AVG} = -0.441$$

Thus for remolded Weald clay Bishop's suggested plane strain relation

$$\mu = - \sin \bar{\Phi} \qquad (6.40)$$

appears to be quite accurate, on the average. However, inspection of Table 6.22 shows that the scatter of individual test results from the above average is considerable.

In a discussion of the paper by HENKEL AND WADE (1966), LADANYI (1967) suggested that stress-strain curves for triaxial and plane strain tests on remolded Weald clay might better be compared by plotting octahedral shear stress VERSUS octahedral shear strain, rather than maximum principal stress difference VERSUS maximum principal (axial) strain. If the major principal strains and maximum principal stress differences for the two cases are ϵ_{1a}, ϵ_{1ps}, $(\sigma_1 - \sigma_3)a$ and $(\sigma_1 - \sigma_3)ps$, then the octahedral shear strains and stresses for undrained loading are:

$$\gamma_{OCT,a} = \sqrt{2}\ \epsilon_{1a}$$

$$\gamma_{OCT,ps} = \frac{2\sqrt{2}}{\sqrt{3}}\ \epsilon_{1ps}$$

$$\tau_{OCT,a} = \frac{\sqrt{2}}{3} (\sigma_1 - \sigma_3)_a$$

$$\tau_{OCT,ps} = \frac{\sqrt{6 + 2\mu^2}}{6} (\sigma_1 - \sigma_3)_{ps}$$

Ladanyi did not compute Lodes' parameter for plane strain loading, but in effect assumed it to be zero (by using an elasticity equation for the intermediate principal stress and assuming Poisson's ratio to be one half). This resulted in equivalent stress-strain curves for plane strain which fell off much more rapidly after their peak than did those for axial symmetry. This in turn led Ladanyi to suggest that perhaps Wade's plane strain specimens had failed by sliding along a distinct failure plane, whereas Sowa's tri-axial specimens had failed by overall distortion. However, as noted previously, WADE (1963, 83) was rarely able to detect a distinct failure plane, so that Ladanyi's suggestion that two different failure mechanisms may have been operating in the two tests is not supported by Wade's own direct observations. Also, the test data (Wade's Figures A3-34 and A3-37) show that Lode's parameter was well below zero

for the tests Ladanyi considered, and that μ increased after the maximum principal stress difference was reached. This would make the plane strain curves fall off less rapidly after their peak.

In order to compare the effects of plane strain deformation on clay with those on sand, Wade also conducted plane strain, as well as both triaxial compression and extension tests, all of them drained, on a fine, uniform, quartzite sand which he called Belgium sand. The same material had been tested previously by LADANYI (1960). The grain size distribution curve for this material yielded the following values:

$$D_{60} = 0.192 \text{ MM}$$

$$D_{30} = 0.158 \text{ MM}$$

$$D_{10} = 0.125 \text{ MM} = \text{effective size}$$

Coefficient of Uniformity, $C_U = \frac{D_{60}}{D_{10}} = 1.54$

Coefficient of Curvature, $C_C = \frac{(D_{30})^2}{D_{10}D_{60}} = 1.04$

The average value for specific gravity of solids was 2.65, and the limiting values of porosity, as defined by KOLBUSZEWSKI (1948), were

$$n_{MAX} = 47\%$$

$$n_{MIN} = 36\%$$

Wade plotted his test results against initial porosity, n_i, i.e. the average porosity prior to K_o consolidation. Here the results have been related to the average porosity at failure, n_f, which has been calculated using the formula

$$n_f = \frac{n_c + \epsilon_{vf}}{1 + \epsilon_{vf}/100}$$

where n_c is the porosity at the end of K_o consolidation, and ϵ_{vf} is the volumetric strain at failure (expansion considered positive). Values of n_c, ϵ_{vf} and n_f for both plane strain and triaxial tests are tabulated in Table 6.23. In Figure 6.39 are shown plots of ϵ_{vf} VERSUS n_c for each of the three test series. In each case, the relation between ϵ_{vf} and n_c is comparatively smooth. Figure 6.39 was used to estimate two values of ϵ_{vf} which were not recorded (Tests PS12 and T9).

The most important reason for relating test results to average porosity at failure, rather than to average initial porosity, is that apparent differences between plane strain and triaxial compression behavior essentially disappear. WADE (1963, 106) reported that, "The relative values of $(\bar{\sigma}_1/\bar{\sigma}_3)$ are higher for conditions of plane strain [than in the standard triaxial test] in the range of [initial] porosities used." On the other hand, when tabulated against average porosity at failure in Tables 6.24 and 6.25 and plotted in Figure 6.40, the relations between sin Φ and n_f for plane strain and triaxial compression are essentially identical. Too few triaxial extension tests were run for their results to be conclusive. Straight lines fit to the three sets of data by the Method of Least Squares have the following equations:

PLANE STRAIN: $(\sin \bar{\Phi} - 0.6213) = - 0.0202 \ (n_f - 40.1722)$

CYLINDRICAL COMPRESSION: $(\sin \bar{\Phi} - 0.5918) = - 0.0195 \ (n_f - 41.4187)$

CYLINDRICAL EXTENSION : $(\sin \bar{\Phi} - 0.6015) = - 0.0116 \ (n_f - 39.8750)$

However, Lode's parameter at failure did not follow Bishop's proposed equation

$$\mu = - \sin \bar{\Phi}$$

nearly as well in Wade's plane strain tests on Belgium sand as was the case for Conforth's plane strain tests on Brasted sand. See Figure 6.41. The Least Squares equation for Wade's plane strain data is

$$(\mu + 0.5938) = 0.00355 \ (n_f + 40.1722)$$

Figures 6.40 and 6.41 were used to construct the octahedral plane stress plots in Figure 6.42, which show the influence of density on the failure criterion for Belgium sand. Comparison of Figures 6.41 and 6.27 shows that both Belgium sand and Brasted sand have similar shaped failure criteria. Both can be reasonably approximated by a Mohr-Coulomb failure criterion for any given porosity at failure and both failure criteria are affected in the same way by a change in porosity at failure.

CASBARIAN (1964) modified Ratnam's test equipment, and conducted additional hollow cylinder tests on the same commercial kaolinite used by Ratnam. (See Chapter 3 of this thesis.) Casbarian's test results appeared to indicate that the compacted, isotropically consolidated kaolinite was anisotropic with respect to the effective stress shear strength parameters. However, the strength anisotropy appeared to be symmetric with respect to the value $45^{\circ} - \beta$. Therefore, because all of Casbarian's Series II tests, which were designed to show the influence of the intermediate principal stress, were conducted without torsion, so that the angle β was either 0° or 90°, octahedral plane stress plots have been constructed. However, they apply only to these two values of the angle β, and do not imply isotropic behavior. The Series II data are tabulated in Table 6.26 and plotted in Figure 6.43. The nonlinearity of the effective stress strength envelope, which is apparent in Figure 3.27a, is also apparent in Figure 6.43. As the isotropic prehsear consolidation stress increases (see Table 3.8b), the apparent failure criterion transitions from beyond the extended Tresca criterion, through the extended Von Mises criterion,

towards a cohesionless Revised Coulomb criterion. This apparent transition raises an interesting question: To what extent is the failure criterion for soils influenced by over-consolidation ratio, for a given value of Lode's parameter during consolidation? To the Writer's knowledge, this question has never been investigated.

SHIBATA AND KARUBE (1965) conducted undrained tests with pore pressure measurements on remolded, normally consolidated Osaka alluvial clay, in a modified triaxial device which permitted independent control of all three principal stresses. The test specimens were 6 CM long, 2 CM thick and 3.5 CM wide, having been trimmed from a 25 CM diameter block of clay, reconsolidated one dimensionally under a maximum vertical effective stress of 0.45 KG/CM^2. Conventional triaxial compression and extension tests were also conducted. Index properties of the reconsolidated Osaka alluvial clay are shown below.

Liquid Limit	69%
Plastic Limit	20%
Plasticity Index	49%
Percent by Weight Finer Than 0.002 MM	10%
Activity	2.0

In the $\sigma_1 > \sigma_2 > \sigma_3$ tests, the testing sequence was as follows:

1. Further consolidate the specimen isotropically to the desired value of $\sigma_3 = \bar{\sigma}_c$.

2. Increase σ_1 and σ_2 simultaneously until $\sigma_1 - \sigma_3 = \sigma_2 - \sigma_3 =$ a desired value, keeping σ_3 constant, under undrained conditions with pore pressure measurements.

3. Increase σ_1 until failure occurs, keepting σ_2 and σ_3 constant, under undrained conditions with pore pressure measurements.

In reporting their results, Shibata and Karube elected to project effective stress paths for the plane $\sigma_2 - \sigma_3 =$ constant onto the plane $\sigma_2 = \sigma_3$, along rays normal to both planes, rather than along rays parallel to the σ_2 axis. Using the latter method, values at failure (both maximum principal effective stress ratio and maximum principal stress difference) have been calculated and tabulated along with other failure data in Tables 6.27 and 6.28. Results of the conventional triaxial compression and extension tests are plotted in Figures 6.44 and 6.45. They indicate that remolded normally consolidated Osaka alluvial clay is

cohesionless, and that the failure lines for constant μ are probably linear. Consequently octahedral plane stress plots have been constructed in Figures 6.46 and 6.47, and show the Revised Coulomb failure criterion to be the best, slightly conservative theoretical failure criterion for this material. The definition of failure has little influence on the failure locus for normally consolidated material.

Shibata and Karube observed a family of decreasing linear relationships between the strain at maximum principal stress difference $(\sigma_1 - \sigma_3)_{MAX}$ and the intermediate principal stress difference $(\sigma_2 - \sigma_3)$, each for a constant value of $\bar{\sigma}_c$. However, when the strain at maximum principal stress difference is plotted against Lode's parameter, a unique relationship results, as shown in Figure 6.48. The influence of the intermediate principal stress at failure on the axial strain at failure displayed in Figure 6.48 is consistent with similar observations by WOOD (1958) and CONFORTH (1961). See also SHIBATA AND KARUBE (1967) for further data from plane strain tests on Osaka alluvial clay with slightly different index properties.

In his opening address to the ASCE Research Conference on Shear Strength of Cohesive Soils, NEWMARK (1960) suggested that consideration be given to the possibility of defining a relationship between stress and strain in cohesive soils by use of relationships, even in the non-linear range, of the form

$$J_i = \sum_{j=1}^{3} f_{ij} (I_j) \qquad (i = 1,2,3)$$

where the J_i are independent strain invariants, the I_j are independent stress invarients and the f_{ij} are arbitrary functions. BELL (1965) was apparently the first to attempt such a formulation for soil, but instead of using a cohesive soil he used standard Ottawa sand having the following grain size distribution characteristics:

D_{60} = 0.66 MM

D_{30} = 0.52 MM

D_{10} = 0.39 MM = effective size

Coefficient of Uniformity, $C_U = \frac{D_{60}}{D_{10}} = 1.69$

Coefficient of Curvature, $C_U = \frac{(D_{30})^2}{D_{10}D_{60}} = 1.05$

The specific gravity of solids was determined to be 2.65, and the maximum and minimum porosities, determined by simple tests devised by Bell, were 43% and 34% respectively.

Using a device which he designed, Bell conducted drained, stress-controlled tests on plate-shaped samples 15.5 inches square by 1.9 inches thick, in which each of the principal stresses was controlled independently. The major and minor principal stresses were applied to the sides of the sample, and the intermediate principal stress was applied to the top and bottom faces, i.e. the faces which measured 15.5 inches by 15.5 inches. The principal stress directions remained fixed throughout the tests. Three types of stress paths were employed to obtain stress-strain data for formulating an invariant deformation-type stress-strain relation, as shown below.

STRESS PATH	STRESS INVARIANT I_1	I_2*	I_3*
S.C.	V	F	F
radial	F	V	F
circular	F	F	V

S.C. = spherical compression
F = fixed
V = varied

Bell's stress invariants are related to the invariants shown in Figure 6.5 as follows:

$$I_1 = 3\,\sigma_{OCT}$$

$$I_2^* = \left(\frac{r}{3}\right)^2$$

$$I_3^* = \cos 3\omega$$

The invariants define a set of three mutually orthogonal curvilinear coordinates in principal stress space.

Bell's circular stress path tests were the first of their type known to the Writer. Strength data were obtained by running radial stress path tests on samples previously subjected only to several spherical (hydrostatic) stress cycles. For all the radial strength tests the values of porosity and octahedral normal effective stress were

$$n \approx 34\%$$

$$\bar{\sigma}_{OCT} = \sigma_{OCT} \approx 18 \text{ PSI}$$

Because these were stress-controlled tests, it was not possible to define failure as the occurence of the peak of the $(\sigma_1 - \sigma_3)$ VERSUS ϵ_1 curve. Instead, when the rate

of volume change, as recorded by a burette, did not decrease with time after the application of a deviatoric stress increment, it was assumed that first yield had taken place, Thus, it was possible to identify states of stress before and after, but generally not precisely at initial yield. Stress data before and after initial yield are tabulated in Table 6.29 and plotted in an octahedral plane stress plot in Figure 6.49. It must be assumed that $\bar{p}$ VERSUS q plots for any particular value of μ would be linear. Although the rate of strain at initial yield undoubtedly varied with μ, it probably had only a minor influence on the results.

Bell fit the following curve to his initial yield data:

$$I_2^* = 0.116 + 0.016\ (1 + I_3^*)^2$$

Referring to Figure 6.5, Bell's failure criterion can be used to calculate sin Φ as a function of μ by means of the following relationships:

$$\omega = \cos^{-1} \frac{\mu}{\sqrt{3 + \mu^2}}$$

$$r = \sqrt{1.044 + 0.144 \ (1 + \cos 3\omega)^2}$$

$$\sin \Phi = \frac{\sqrt{3}\, r \sin \omega}{\sqrt{6} - r \cos \omega}$$

The results are plotted in Figure 6.50.

Bell's failure criterion is simply a truncated Fourier cosine series in the angle 3ω, because

$$I_2^* = 0.140 + 0.032 \cos 3\omega + 0.008 \cos 6\omega$$

The criterion is similar to one which NEWMARK (1960) labeled a "Possible" Failure Theory, and which had previously been suggested by TOPPING (1955), who proposed the Mohr-circle type relationship

$$r = \frac{r_C + r_E}{2} + \left(\frac{r_C - r_E}{2} \right) \cos 3\omega$$

where

r_C = value of r for triaxial compression

r_E = value of r for triaxial extension

In order to construct an octahedral plane stress plot of Topping's failure criterion, based on data from triaxial compression and extension tests, the following relations can be used:

$$r = \frac{\sqrt{6}\sin\bar{\Phi}}{\sqrt{3}\sin\omega + \sin\bar{\Phi}\cos\omega}$$

$$\omega_C = 120^\circ$$

$$\omega_E = 60^\circ$$

$$r_C = \frac{2\sqrt{6}\sin\bar{\Phi}_C}{3 - \sin\bar{\Phi}_C}$$

$$r_E = \frac{2\sqrt{6}\sin\bar{\Phi}_E}{3 + \sin\bar{\Phi}_E}$$

Figure 6.51 shows Topping's failure criterion, corresponding to the values

$$\sin \bar{\Phi}_C = 0.6187$$

$$\sin \bar{\Phi}_E = 0.7906$$

calculated according to Bell's formula. Comparison of Topping's curve in Figure 6.51 with Bell's original data in Figure 6.49 shows good agreement, which could be made even better by reducing the value of $\sin \bar{\Phi}_C$ to about 0.60. It appears that Topping's failure criterion offers a fairly simple means of representing the influence of the intermediate principal effective stress on the shear strength of soil.

Even though Bell's samples were about as dense as he could get them, failure along a distinct plane was observed in only one test. He therefore rejected the Mohr-Coulomb failure criterion.

Contours of equal octahedral shear strain and equal volumetric strain for the radial stress path tests, which Bell plotted in the octahedral plane, were approximately geometrically similar to his initial yield curve. See his Figures 8.5 and 8.9. Thus, initial yield occurred at about

the same volumetric strain in all tests (roughly 0.8 percent). As with the initial yield criterion, Bell noted a substantial break in the volumetric strain contours, in the range $-1.0 < \mu < -0.8$, and he judged this to be a true material characteristic, not just the result of testing error. These results are extremely significant, and are the basis of a proposed stress-strain relationship in Chapter 7.

Bell has continued his study of the triaxial shear strength of sand at Colorado State University, under sponsorship of the National Science Foundation. He has taken considerable pains to achieve a homogeneous state of stress in a 4 inch cube sample, using hydraulic load actuators capable of either load or displacement control.

LENOE (1966) tested silty sand specimens, rectangular in cross-section (dimensions not stated), in a device similar in principle to the one employed by Shibata and Karube. However, in Lenoe's device the sand was in a perfectly dry state, and the minor principal stress was applied by lowering the pore air pressure inside the sample with a vacuum pump. The grain size distribution curve for the sand yielded the following values:

D_{60} = 0.58 MM

D_{30} = 0.22 MM

D_{10} = 0.065 MM = effective size

Coefficient of Uniformity, $C_U = \frac{D_{60}}{D_{10}} = 8.93$

Coefficient of Curvature, $C_C = \frac{(D_{30})^2}{D_{10}D_{60}} = 1.29$

The average initial density of the samples was 110 PCF. No information was reported concerning failure densities or the influence of density on strength. The strength values tabulated in Table 6.30 are based on initial specimen geometry. Lenoe stated that the change in mid-height area of the specimens at failure amounted to no more than 6 percent. Failure consistently occurred at an exial strain of about 3.5 percent. Application of corrections for specimen deformation causes the calculated value of $\bar{\Phi}$ to decrease slightly and the calculated value of μ to increase slightly, due mainly to a decrease in the calculated value of $\bar{\sigma}_1$. For example, assuming an axial strain at failure of 3.5 percent (compression) and a radial strain at failure of 3.0 percent (expansion), the corrected values for Test 6 would be

$$\bar{\sigma}_1 = \frac{33.60}{1.060} = 31.70 \text{ PSI (vs. } 33.60)$$

$$\bar{\sigma}_3 = 3.50 \text{ PSI (unchanged)}$$

$$\bar{\sigma}_2 = 3.50 + \frac{3.00}{0.995} = 6.52 \text{ PSI (vs. } 6.50)$$

$$\bar{p} = 17.60 \text{ PSI (vs. } 18.55)$$

$$q = 14.10 \text{ PSI (vs. } 15.05)$$

$$\mu = -0.786 \text{ (vs. } -0.801)$$

$$\sin \bar{\Phi} = 0.800 \text{ (vs. } 0.811)$$

The triaxial compression strength data in Figure 6.52 indicate that the material is cohesionless and the failure line linear, but the octahedral plane stress plot in Figure 6.53 reveals a strong possibility of experimental error, as well as an unfortunately small range of Lode's parameter.

Using a pneumatic analog computer to achieve a controlled rate of applied total stress, SAADA AND BAAH (1966) tested conventional triaxial and torsional hollow cylinder specimens of commercial kaolinite in undrained shear with pore pressure measurements. Unfortunately, their results are difficult to interpret, because they allowed three important variables to change simultaneously:

1. the angle of principal stress rotation, β
2. Lode's parameter, μ
3. the rate of applied stress, $R = \frac{d}{dt}[(\sigma_1 - \sigma_3)\cos 2\beta]$

Because the inside and outside cell pressures were always equal in their torsional hollow cylinder tests, their values of β and μ were related by the expression

$$\mu = -\cos 2\beta$$

Also, assuming that soil deformation is controlled by effective stress, they failed in their attempt to have shear strains in the cross-anisotropic clay be caused entirely by the significant stress deviator, because they maintained a constant value of the mean total normal stress, instead of the mean effective normal stress. Although they measured the pore water pressure, their pneumatic analog computer was not designed to respond to it. For an account of the rheological theory of soil behavior developed at Princeton University and used at Case Institute by Saada see SCHMID (1960), KLAUSNER (1960), SCHMID, KLAUSNER AND WHITMORE (1960) and SAADA (1962). It has been stated here previously, but

perhaps bears repeating, that there appears to be no reason why rheological concepts cannot be applied without abandoning the concept of effective stress. Rheology and effective stress are compatible.

The commercial kaolinite used by Saada and Baah had the following index properties.

Liquid Limit	62.5%
Plastic Limit	39.0%
Plasticity Index	23.5%
Percent by Weight Finer Than 0.002 MM	73.0%
Activity	0.32
Specific Gravity of Solids	2.61

Conventional triaxial specimens 1.46 IN in diameter and 3.56 IN high were subjected only to hydrostatic consolidation prior to undrained shear, and were therefore presumably isotropic. Hollow cylinder specimens approximately 5.95 IN high, with inside and outside radii of approximately 1.00 IN and 1.38 IN were trimmed from material initially consolidated one-dimensionally, and were therefore presumably cross-

anisotropic, with the material axis parallel to the cylinder axis. Both specimens were prepared by mixing dry clay powder with distilled, deaired water at a high water content, then consolidating blocks of clay either hydrostatically or one-dimensionally, and finally trimming the test specimens from these blocks. The conventional triaxial specimens had an average water content of 36.3%; the water content of the hollow cylinder specimens was 40.4%. All specimens were finally isotropically consolidated under a cell pressure of 78 PSI with a backpressure of 18 PSI, for about 3 days immediately prior to undrained shear. Test results for both the isotropic (Series A) and cross-anisotropic (Series B through H) specimens are tabulated in Table 6.31 and plotted in Figure 6.54. Because the tests were stress-controlled, failure was defined as the occurrence of a very large rate of distortion, i.e. by a vertical tangent to the recorded distortion-time curve. For an analysis of the isotropic (Series A) results see SAADA (1967), in which he obtains a linear relation between the octahedral shear stress at failure and the logarithm of the time rate of increase of the applied principal stress difference. The octahedral plane stress

plot in Figure 6.55 has been constructed using average values of sin $\bar{\Phi}$ from Table 6.31. The large increase in sin $\bar{\Phi}$ as Lode's parameter increases from -1 to about -0.87 is apparently due mainly to a difference in the type of test used, as Figure 6.54 indicates even more clearly.

KO (1966) attempted to improve upon Bell's triaxial test device. Although Ko's device was easier to operate than Bell's, questions have been raised by several investigators concerning Ko's claim that he achieved a homogeneous state of stress in his 4 inch cubic samples of Ottawa sand. The following data must therefore be considered to be somewhat controversial. The grain size characteristics of the Ottawa sand tested by Ko were similar, but not identical to those of the Ottawa sand tested by Bell:

D_{60} = 0.61 MM

D_{30} = 0.58 MM

D_{10} = 0.50 MM = effective size

Coefficient of Uniformity, $C_U = \frac{D_{60}}{D_{10}} = 1.22$

Coefficient of Curvature, $C_U = \frac{(D_{30})^2}{D_{10}D_{60}} = 1.10$

Most of Ko's attention was focused on stress-strain behavior prior to failure. Since his tests were stress-controlled, none of his stress-strain curves exhibited peaks which could be used to define failure. Instead, Ko defined failure as a point of slope discontinuity on a semilogarithmic plot of octahedral shear stress VERSUS the logarithm of the major principal strain. This definition has a precendent in the practice of defining bearing capacity in a load-controlled plate bearing test as the point of slope discontinuity of the load-settlement curve; SOWERS (1962, 538).

Ko's strength data are tabulated in Table 6.32. The strength tests were conducted at constant effective octahedral normal stress (15 PSI for Tests TCa-6 and TEa-5 and 20 PSI for the rest) and at a constant value of Lode's parameter. Thus the stress paths in principal stress space were radial, according to the definition given by BELL (1965). In order to achieve a continuous, proportional variation of the three principal stresses during a test, Ko made ingenious use of the well known formula for calculating loads on piles in an eccentrically loaded pile group; TENG (1962, 223); WESTERGAARD (1952, 71). It is easily shown that if a vertical load P

acts at a distance R from the centroid of a group of three piles, which are arranged in an equilateral triangle and spaced a distance S apart, that the loads on the three piles, W_1, W_2 and W_3 will be

$$W_1 = \frac{P}{3}\left[1 + \frac{2R}{S}\cos\ (\omega - 120^o)\right]$$

$$W_2 = \frac{P}{3}\left[1 + \frac{2R}{S}\cos\ \omega\right]$$

$$W_3 = \frac{P}{3}\left[1 + \frac{2R}{S}\cos\ (\omega + 120^o)\right]$$

The angle ω is the angle subtended at the centroid of the pile group by pile 2 and the load P, and the distances $S\cos(\omega - 120)$, $S\cos\omega$ and $S\cos(\omega + 120)$ are the moment arms of piles 1, 2 and 3 with respect to the axis of the resultant moment of P about the pile group centroid. The above expressions for the three pile loads are identical in form to formulas for the three principal stresses; see Equations (B.52) and (B.32). In Ko's stress control device, hydraulic cylinders took the place of the loads P, W_1, W_2 and W_3. The pressures in cylinders 1, 2 and 3 were transmitted to the cubic soil specimen by water-filled rubber

membranes as principal stresses σ_1, σ_2 and σ_3, with the angle ω being the same as that shown in Figure B.6 as ω_2.

Ko, like Bell, was only able to bracket "failure", and therefore average values of sin $\bar{\Phi}$ have been calculated in Table 6.33, in order to construct plots of sin $\bar{\Phi}$ VERSUS initial porosity, n_i, in Figure 6.56. In Ko's tests the volumetric strains at failure were so small (less than 0.4%) that initial and failure porosities were nearly equal. Using data from Figure 6.56, octahedral plane stress plots have been constructed in Figure 6.57 for several values of initial porosity. The shape of the curves in Figure 6.57 is dictated by the location of strength lines in Figure 6.56. In particular, the pointed shape of the curves in the neighborhood of $\mu = -1$ in Figure 6.57, which is in accordance with the Mohr-Coulomb equation but not with most other test data (including Bell's), is a consequence of the Writer's arbitrary location of the strength line for $\mu = -0.464$ in Figure 6.56. Too few tests were run to reliably define the shape of the failure surfaces for $-1 < \mu < 1$. The curves in Figure 6.57 differ from

similar curves drawn by Ko, because his values of $\bar{\Phi}$ were shown about 2^{o} lower for triaxial compression and 2^{o} higher for triaxial extension, even though his plots of $\bar{\Phi}$ VERSUS initial void ratio were consistent with the strength lines shown in Figure 6.56. See also KO AND SCOTT (1967a), (1967b) and (1968).

The strength of Boston blue clay resedimented from a slurry, when tested under various stress systems has been studied recently by LADD AND VARALLYAY (1965), MERKLE (1967), DICKEY (1967), RIXNER (1967) and DICKEY, LADD AND RIXNER (1968). Index properties of resedimented Boston blue clay, as measured by several investigators, are tabulated below.

	LADD & VARALLYAY (1965)	MERKLE (1967)	DICKEY (1967)	RIXNER (1967)
Liquid Limit, %	33	43	44	39
Plastic Limit, %	20	23	24	21
Plasticity Index, %	13	20	20	18
Percent by Weight Finer Than 0.002 MM, %	35	49	33	52
Activity	0.47	0.41	0.60	0.35
Specific Gravity of Solids	2.78	2.79		

The strength data tabulated in Table 6.34 were obtained from four types of consolidated undrained tests with pore pressure measurements, performed on samples normally consolidated one-dimensionally, from a slurry with an initial water content approximately twice the liquid limit. In each case, failure was defined as the occurrence of the maximum principal stress difference. Test symbols used in Table 6.34 are defined below.

CC: conventional triaxial (cylindrical) compression

CE: conventional triaxial (cylindrical) extension

PSA: plane strain "active" ($\bar{\sigma}_{1f}$ in same direction as $\bar{\sigma}_{1c}$)

PSP: plane strain "passive" ($\bar{\sigma}_{1f}$ perpendicular to direction of $\bar{\sigma}_{1c}$)

The triaxial compression and extension data plotted in Figure 6.58 indicate that resedimented Boston blue clay is cohesionless, but has a somewhat higher effective angle of shearing resistance in extension than in compression. There appears to be a relation between Lode's parameter and water content at failure for active plane strain tests, as shown in Figure 6.59. However, inspection of Table 6.34 reveals no consistent

relationship between the effective angle of shearing resistance and water content at failure, such as was disclosed in Figure 6.25(a) for Brasted sand. This could be because Dickey's and Rixner's early plane strain tests were hampered by the type of mechanical difficulties which often accompany the development of a new piece of equipment, of which they were well aware. Refer to their theses for details. These mechanical difficulties were of such a nature that they would have had a stronger influence on the measured angle of shearing resistance than on Lode's parameter. They are believed to have been corrected by the time the active plane strain test PSA4 was run. An octahedral plane stress plot has been constructed in Figure 6.60, with a possible failure criterion shown by the dashed curve. Considerably more data are required to determine if the apparent sudden increase in strength as Lode's parameter increases from -1.00 to -0.483 is a true material property or is due to mechanical characteristics of the plane strain device.

LOMIZE AND KRYZHANOVSKY (1967) tested 71 MM cubes of air dried quartz sand from the Volga region in a device somewhat like Ko's, except that the edges of their six membranes were fixed. The grain size characteristics of the Volga sand were:

$$D_{60} = 0.116 \text{ MM}$$

$$D_{30} = 0.095 \text{ MM}$$

$$D_{10} = 0.078 \text{ MM} = \text{effective size}$$

Coefficient of Uniformity, $C_U = \frac{D_{60}}{D_{10}} = 1.49$

Coefficient of Curvature, $C_U = \frac{(D_{30})^2}{D_{10}D_{60}} = 1.00$

The specific gravity of solids was 2.65, and the maximum and minimum porosities were

$$n_{MAX} = 1 - \frac{\gamma_{MIN}}{G_s \gamma_w} = 1 - \frac{1.43}{2.65} = 46.0\%$$

$$n_{MIN} = 1 - \frac{\gamma_{MAX}}{G_s \gamma_w} = 1 - \frac{1.79}{2.65} = 32.5\%$$

The initial density for the special triaxial shear tests was 1.61 KG/CM^3 ($n_i = 39.3\%$). A [direct?] shear test yielded a friction angle of $39^{o}20'$.

In describing the results of their tests Lomize and Kryzhanovsky used the following stress invarients:

$$U_1 = \bar{\sigma}_1 + \bar{\sigma}_2 + \bar{\sigma}_3 = 3\,\bar{\sigma}_{OCT}$$

$$U_2 = \sqrt{\frac{1}{6}\left[(\bar{\sigma}_1 - \bar{\sigma}_2)^2 + (\bar{\sigma}_2 - \bar{\sigma}_3)^2 + (\bar{\sigma}_3 - \bar{\sigma}_1)\right]}$$

$$= \sqrt{\frac{3}{2}}\ \tau_{OCT}$$

$$U_3 = \bar{\sigma}_1\,\bar{\sigma}_2\,\bar{\sigma}_3 = \frac{\tau_{OCT}^3 \cos 3\omega}{\sqrt{2}} - \frac{3}{2}\,\tau_{OCT}^2\,\bar{\sigma}_{OCT} + \bar{\sigma}_{OCT}^3$$

and the following strain invariants:

$$I_1 = \epsilon_1 + \epsilon_2 + \epsilon_3 = 3\,\epsilon_{OCT}$$

$$I_2 = \sqrt{\frac{2}{3}\left[(\epsilon_1 - \epsilon_2)^2 + (\epsilon_2 - \epsilon_3)^2 + (\epsilon_3 - \epsilon_1)^2\right]}$$

$$= \sqrt{\frac{3}{2}}\ \gamma_{OCT}$$

They conducted tests at three values of Lode's parameter, μ: -1.0, 0.0 and 1.0, using the following constant values of effective octahedral normal stress, $\bar{\sigma}_{OCT}$: 1.5, 2.0, 3.0 and 3.5 KG/CM^2. Other more complex stress paths were also used, but it is not clear from their paper precisely which if any of these other test results formed the basis of the conclusions to follow.

Having defined the normalized second stress invariant,

$$D_K = \frac{U_2}{U_1} = \frac{\tau_{OCT}}{\sqrt{6}\,\sigma_{OCT}} ,$$

which is proportional to the radius r = O'P in Figure 6.5, Lomize and Kryzhanovsky apparently found, as had Bell, that contours of I_1 and I_2 in the octahedral plane were essentially geometrically similar. In order to study the influence of the intermediate principal stress on the shape of the strain invariant contours, they expressed the contour radius, in terms of D_K, as a function of the normalized third stress invariant, which is

$$\frac{U_3}{U_1^3} = \frac{6\sqrt{3}\cos 3\omega\, D_K^3 - 9D_K^2 + 1}{27}$$

If plotted on log log paper, the relation between D_K and $\frac{U_3}{U_1^3}$ along any contour was approximately a straight line, having the equation

$$\log D_K = \log \pi^* + \alpha \log \frac{U_3}{U_1^3}$$

The intercept π^* depended upon the value of strain (i.e. which strain contour was being studied) but the value of α was constant for all strain contours because they were geometrically similar. For the Volga sand α was 1.73. Thus it was possible to obtain unique relationships between both I_2 and I_1 and the stress invariant function

$$\pi^* = \frac{D_K}{\left(\frac{U_3}{U_1^3}\right)^{1.73}} ,$$

these relationships being simply an expression of the geometric similarity of both the I_1 and I_2 contours in the octahedral plane. For small values of I_2 the relation between I_2 and π^* was approximately linear, with the equation

$$\pi^* = 15 + 2500\ I_2 \quad (0 \leq I_2 \leq 0.09)$$

However, as failure was approached the spacing between the I_2 contours decreased, so that the relation between π^* and

I_2 suddenly became nonlinear, much like the moment-curvature relation for a steel beam as the plastic moment capacity is approached, reaching the maximum value

$$\pi^*_{MAX} = \pi^*_0 = 260,$$

which Lomize and Kryzhanovsky defined as failure.

At this point it should be noted that the relation between D_K and $\frac{U_3}{U_1}_3$ proposed by Lomize and Kryzhanovsky is the same kind of relation as Topping's Mohr-circle type relation between r and ω. Moreover, Topping's appears to be the more convenient, because it expresses r directly in terms of ω, whereas the expression proposed by Lomize and Kryzhanovsky does not give D_K directly in terms of ω. However, by writing their failure criterion for Volga sand in the form

$$6\sqrt{3}\cos 3\omega\, D_K^3 - 9\, D_K^2 - 1.0858\, D_K^{0.578} + 1 = 0$$

the value of D_K at failure can be calculated numerically for any given value of ω (or μ). The results of these calculations are tabulated in Table 6.35 and plotted in Figure 6.61. The shape of the octahedral plane stress plot in Figure 6.61 closely resembles those of Bell and Topping in Figures 6.51 and 6.52, the most striking feature being a rapid increase in Φ as μ increases from -1 to about -0.6.

It is interesting to note that COLEMAN (1960) proposed a similar failure criterion in the form

$$9\left(\frac{\tau_{OCT}}{\sigma_{OCT}}\right)^2 = \left[2\sqrt{2} + \left(\frac{\tau_{OCT}}{\sigma_{OCT}}\right)(\cos 3\omega)^{1/3}\right]^2 \sin^2 \Phi_C$$

but, like Topping, did not attempt to relate this function to strains prior to failure.

MAYLSHEV (1967a) proposed a generalization of the Mohr-Coulomb strength criterion, and of a criterion previously proposed by JOHANSEN (1958), in the form

$$a_{11}\bar{\sigma}_1^2 + a_{22}\bar{\sigma}_2^2 + a_{33}\bar{\sigma}_3^2 + a_{12}\bar{\sigma}_1\bar{\sigma}_2 + a_{23}\bar{\sigma}_2\bar{\sigma}_3$$

$$+ a_{31}\bar{\sigma}_3\bar{\sigma}_1 = C(a_1\bar{\sigma}_1 + a_2\bar{\sigma}_2 + a_3\bar{\sigma}_3) + C^2$$

The coefficients in the above expression are obtained by writing the Mohr-Coulomb strength criterion in terms of average stresses $\tau_{n,av}$ and $\bar{\sigma}_{nn,av}$ i.e.

$$(\tau_{n,av})^2 = (C + \bar{\sigma}_{nn,av} \tan \bar{\Phi})^2$$

where

$$(\tau_{n,av})^2 = \frac{\int_S \tau_n^2 \, ds}{\int_S ds}$$

and

$$\bar{\sigma}_{nn,av} = \frac{\int_S \bar{\sigma}_{nn} \, ds}{\int_S ds}$$

The Stress quantities τ_n^2 and $\bar{\sigma}_{nn}$ are given by Equations (B.89). All the above integrals are surface integrals, and the region of integration, S, surrounds the point

$$\left[\alpha_{n1} = \cos\left(\frac{\pi}{4} + \frac{\bar{\Phi}}{2}\right);\ \alpha_{n2} = 0;\ \alpha_{n3} = \sin\left(\frac{\pi}{4} + \frac{\bar{\Phi}}{2}\right)\right] .$$

Unfortunately, Malyshev's method of surface integration admits impossible combinations of the direction cosines in Equation (B.89),

so that the expressions given in his paper for the coefficients of the principal effective stresses in his generalized quadratic failure criterion are questionable. Mathematically correct expressions for the coefficients can be derived, using Novozhilov's method of surface integration, but they are too complex to be given here. J.G. MERKLE (1970) has proposed a similar expression, with C = 0, as a yield function for graphite. Graphite, like many soils, exhibits both anisotropic plastic stress-strain behavior and significant plastic volumetric strain. If only the linear terms in Malyshev's generalized quadratic failure criterion are retained, the resulting linear function of the three principal effective stresses is similar to that used by Peltier; MALYSHEV (1967a). Another simplified form of his own generalized quadratic failure criterion was derived by MALYSHEV (1967b), by expressing the average shear stress

$$\tau_{n,av} = \sqrt{\tau^2_{n,av}}$$

in a truncated power series. He then obtained an expression for $\bar{\Phi}$ which can be written in the form

$$\sin \Phi = \frac{A}{B\left[1 - (1 - B)\left(\frac{1 - \mu^2}{4}\right)\right]}$$

Since this expression predicts equal values of Φ in triaxial compression and extension, it is not in agreement with most test data, except that of MALYSHEV AND FRALIS (1968) and SUTHERLAND AND MESDARY (1969).

GREEN (1969) constructed an independent stress control (ISC) apparatus, the operation of which has been briefly described by BISHOP (1967). It appears to be similar to the device used by SHIBATA AND KARUBE (1965). Green's apparatus is contained within a pressurized cell, the minor principal total stress, σ_3, being the cell pressure. The difference between the major and minor principal stresses, $(\sigma_1 - \sigma_3)$, is applied through a pair of rigid platens by a screw-operated testing machine, the applied load being measured by a load cell. The difference between the intermediate and minor principal stresses, $(\sigma_2 - \sigma_3)$, is also applied through a pair of rigid platens, by a hydraulic ram. In order to avoid interferrence between the two sets of rigid platens when

the intermediate principal strain is compressive, the lateral ($\sigma_2 - \sigma_3$) plattens are not quite as wide as the sample. Whether this really does avoid interferrence between the two sets of platens is not certain; MESDARY AND SUTHERLAND (1970). Green conducted drained ISC tests on cuboidal samples of dense Ham River sand, using values of $\bar{\sigma}_3$ between 30 and 40 PSI. The edge dimensions of the samples in the three principal directions were 3.3 IN, 3.2 IN and 2.1 IN. Strength data for an initial porosity of 39.0%, taken from the note by GREEN AND BISHOP (1969), are plotted in an octahedral plane stress plot in Figure 6.62. The agreement of the data with the Mohr-Coulomb failure criterion in the range $-0.7 < \mu < 1$ is striking.

HAMBLY (1969) described the operation of a true triaxial apparatus, in which all three principal stresses are applied through rigid platens, each of which covers an entire sample face. Provided friction can be minimized, this device appears to hold great promise for the triaxial testing of a wide variety of construction materials.

PROCTER AND BARDEN (1969) performed triaxial tests on dense River Welland sand, using a device modeled after Green's. Their results are also similar to Green's, and are plotted in Figure 6.63.

MESDARY AND SUTHERLAND (1970) discussed the problem of platen interference in the ISC apparatus, pointing out that its influence should increase as $\bar{\sigma}_2$ increases beyond the value required to maintain plane strain. They compared results of several series of tests on cubical samples of sand, including their own, to show the possible influence of test technique on strength results. Of the strength curves which they showed, the three which have not already been discussed here are shown in Figure 6.64. Two come from the paper by SUTHERLAND AND MESDARY (1969) and the third comes from a paper by MALYSHEV and FRALIS (1968).

An Idealized Strength Model

So many of the octahedral plane stress plots presented in this chapter indicate a rapid increase in the effective angle of shearing resistance, as the value of Lode's parameter increases from -1 to about -0.7, that this is probably a true

soil characteristic and not entirely a result of test errors. One simple mechanical model which behaves in the same fashion is a dense packing of rough, rigid spheres, for which an original strength analysis is presented in Appendix C. This analysis, which is a variation of one by Parkin, is simpler yet more revealing than previous similar analyses. It predicts that the failure (slip) criterion will be an ellipse in the octahedral plane, with its major axis coinciding with the s_1 axis. It also predits that slip strains will obey the normality rule of classical plasticity. Thus it provides a link between the mechanics of particulate and continuous media.

Summary

The purpose of this chapter has been to examine the influence of the intermediate principal effective stress on the shear strength of soil, and to determine whether this influence is in fact negligible, as is customarily assumed in soils engineering practice.

The most important points which have been brought to light are the following:

1. For research purposes, the influence of the intermediate principal effective stress on soil shear strength is not negligible. However, from the standpoint of soils engineering practice, it will generally be possible to determine a value of the apparent angle of internal friction which will yield slightly conservative, but still economical values of shear strength, no matter what the value of the intermediate principal effective stress.

2. The apparent angle of internal friction is almost always a minimum for triaxial compression ($\bar{\sigma}_1 > \bar{\sigma}_2 = \bar{\sigma}_3$).

3. For the purpose of computer analyses of the deformation and stability of soil masses, it is possible to express soil stress-strain and strength relations in simple invariant form. This conclusion is based on the work of TOPPING (1955), NEWMARK (1960), BELL (1965), and LOMIZE AND KRYZHANOVSKY (1967), and is descussed further in Chapter 7.

4. The time has come to begin routinely reporting the results of soil shear strength tests in invariant form, in order for them to be of maximum usefulness in the design and performance evaluation of foundations and earth structures, and in comparisons of the shear strength behavior of different soils. The invariant parameters most useful in this respect are:

$$\bar{p} = \frac{\bar{\sigma}_1 + \bar{\sigma}_3}{2}$$

$$q = \frac{\bar{\sigma}_1 - \bar{\sigma}_3}{2}$$

$$\mu = \frac{\bar{\sigma}_2 - \bar{p}}{q}$$

The so-called octahedral stress invariants are easily expressable in terms of the above invariants.

5. By using Figure 6.5, an octahedral plane stress plot of soil shear strength data can be constructed in just a few minutes. This plot is as easy to construct, and more informative, than any other strength plot now in use. It permits a rapid and consistent analysis of any strength data, provided only that the three principal effective stresses at failure are known.

6. One of the more pressing needs in soil shear strength research today is to reconcile conflicting results from different test devices. At present, it is extremely difficult to assess the reliability of any one set of test results.

Additional, more technical points which merit emphasis are the following.

7. The rapid increase in the apparent angle of internal friction, as Lode's parameter increases from -1 to about -0.7, which is exhibited by many of the soils discussed in this chapter is probably a true soil characteristic. A theoretical analysis of a dense packing of rough rigid spheres, presented in Appendix C, predicts exactly this type of strength behavior.

8. Any failure criterion for an isotropic material can be expressed as a simple function of the octahedral invariants. This of course includes the Revised Coulomb failure criterion.

9. As shear strength tests have become more sophisticated, there has been a tendency for different investigators to adopt different definitions of failure. Often the definition of failure has not been clearly stated. This fact alone seriously weakens a detailed comparison of their results.

10. In order to use a normalized octahedral plane stress plot, of the type shown in Figure 6.5, it is necessary to either:

a) establish the fact that $\bar{p}$ - q plots at constant μ are all linear, with a common origin, or

b) recognize that the plot applies only within a limited range of $\bar{\sigma}_{OCT}$.

11. Thus far, there appears to have been no serious attempt to investigate the shape of a yield surface for soil as a surface of constant plastic work.

12. The extended von Mises failure criterion, which is the basis of the Cambridge hypothesis, is not supported by most available test data.

13. The torsional hollow cylinder test, although appealing from a theoretical viewpoint, appears to be disadvantageous, at its present state of development, from the standpoint of stress inhomogeneity.

14. The test device designed at Cambridge University by Hambly appears to hold considerable promise. In principle it is extremely simple, and can be made strong enough to test almost any construction material.

15. The degree of applicability of elastic theory to the prediction of deformation and pore pressure response in a loaded soil mass appears to increase with the degree of overconsolidation. The assumption that the nonlinear portion of stress-strain response (i.e. the departure from that predicted by the initial tangent to the stress-strain curve) is also the plastic (irrecoverable) portion appears to be a fairly accurate one for Ottawa sand, and perhaps for other soils.

TABLE 6.1

TRIAXIAL STRENGTH DATA FOR CARRARA MARBLE

TEST	$\bar{\sigma}_1$ KSI	$\bar{\sigma}_2$ KSI	$\bar{\sigma}_3$ KSI	$\bar{p}$ KSI	q KSI	μ	$d + \bar{p}$ KSI	SIN $\bar{\Phi}$
1	19.990	0	0	9.995	9.995	-1.000	20.995	0.476
2	34.325	3.455	3.455	18.890	15.435	-1.000	29.890	0.516
3	46.300	7.350	7.350	26.825	19.475	-1.000	37.825	0.515
4	52.400	10.070	10.070	31.235	21.165	-1.000	42.235	0.501
5	59.610	12.420	12.420	36.015	23.595	-1.000	47.015	0.502
6	81.580	24.250	24.250	52.915	28.665	-1.000	63.915	0.448
7	35.570	35.570	2.220	18.885	16.685	1.000	29.885	0.558
8	56.590	56.590	8.740	32.665	23.925	1.000	43.665	0.548
9	58.140	58.140	9.770	33.955	24.185	1.000	44.955	0.538
10	66.300	66.300	12.500	39.400	26.900	1.000	50.400	0.534
11	73.800	73.800	15.880	44.840	28.960	1.000	55.840	0.519
12	80.560	80.560	19.400	49.980	30.580	1.000	60.980	0.501

μ = -1 tests by VON KARMAN (1911)

μ = 1 tests by BOKER (1915)

Data from RUTLEDGE (1939)

TABLE 6.2

TRIAXIAL STRENGTH DATA FOR DRY GERMAN QUARTZ SAND

TEST	$\bar{\sigma}_1$ KG/CM^2	$\bar{\sigma}_2$ KG/CM^2	$\bar{\sigma}_3$ KG/CM^2	$\bar{p}$ KG/CM^2	q KG/CM^2	μ	SIN $\bar{\Phi}$
1	12.00	6.00	2.27	7.14	4.86	-0.233	0.682
2	10.13	6.00	1.87	6.00	4.13	0	0.688
3	9.70	2.65	2.65	6.18	3.52	-1.000	0.571

$\bar{\Phi}$ from direct shear test was 34°

(sin 34° = 0.559)

Data from KJELLMAN (1936)

TABLE 6.3

TRIAXIAL COMPRESSION DATA FOR VIENNA BLUE CLAY

				AREA CORRECTION					
				NONE		CYLINDRICAL		PARABOLIC	
TEST	μ	σ_3	ϵ	$\bar{p}$	q	$\bar{p}$	q	$\bar{p}$	q
		KG/CM^2	%	KG/CM^2	KG/CM^2	KG/CM^2	KG/CM^2	KG/CM^2	KG/CM^2
8	-1.00	1.00	0.0	1.00	0.00	1.00	0.00	1.00	0.00
			1.1	0.85	0.23	0.85	0.23	0.85	0.23
			1.5	0.82	0.28	0.82	0.28	0.82	0.28
			1.8	0.83	0.32	0.82	0.31	0.82	0.31
			2.6	0.83	0.38	0.82	0.37	0.81	0.36
			7.2	0.99	0.53	0.95	0.49	0.94	0.48
			13.2	1.20	0.66	1.11	0.57	1.08	0.54
			17.8	1.33	0.75	1.20	0.62	1.15	0.57
			24.6	1.59	0.88	1.37	0.66	1.30	0.59
			31.2	1.72	1.00	1.41	0.69	1.31	0.59

(Continued)

TABLE 6.3

TRIAXIAL COMPRESSION DATA FOR VIENNA BLUE CLAY

TEST	μ	σ_3	ϵ	AREA CORRECTION: NONE		CYLINDRICAL		PARABOLIC	
				$\bar{p}$	q	$\bar{p}$	q	$\bar{p}$	q
		KG/CM^2	%	KG/CM^2	KG/CM^2	KG/CM^2	KG/CM^2	KG/CM^2	KG/CM^2
9	-1.00	2.00	0.0	2.00	0.00	2.00	0.00	2.00	0.00
			0.3	1.97	0.25	1.97	0.25	1.97	0.25
			0.5	1.83	0.38	1.83	0.38	1.82	0.37
			1.1	1.62	0.50	1.62	0.50	1.61	0.49
			2.2	1.58	0.63	1.56	0.61	1.56	0.61
			4.2	1.60	0.75	1.57	0.72	1.56	0.71
			7.6	1.73	0.88	1.66	0.81	1.63	0.78
			13.0	1.96	1.00	1.83	0.87	1.78	0.82
			20.0	2.22	1.13	1.99	0.90	1.91	0.82
			23.4	2.32	1.19	2.04	0.91	1.94	0.81

(Continued)

TABLE 6.3

TRIAXIAL COMPRESSION DATA FOR VIENNA BLUE CLAY

TEST	μ	σ_3	ϵ	AREA CORRECTION: NONE		CYLINDRICAL		PARABOLIC	
				$\bar{p}$	q	$\bar{p}$	q	$\bar{p}$	q
		KG/CM^2	%	KG/CM^2	KG/CM^2	KG/CM^2	KG/CM^2	KG/CM^2	KG/CM^2
10	-1.00	2.50	0.0	2.50	0.00	2.50	0.00	2.50	0.00
			0.5	2.40	0.32	2.40	0.32	2.39	0.31
			0.8	2.25	0.47	2.25	0.47	2.25	0.47
			1.5	2.00	0.63	1.99	0.62	1.98	0.61
			3.2	1.77	0.78	1.75	0.76	1.74	0.75
			4.4	1.82	0.86	1.78	0.82	1.76	0.80
			5.8	1.96	0.94	1.90	0.88	1.88	0.86
			7.6	2.09	1.02	2.01	0.94	1.98	0.91
			9.6	2.20	1.10	2.09	0.99	2.05	0.95
			12.4	2.31	1.17	2.17	1.03	2.11	0.97

(Continued)

TABLE 6.3

TRIAXIAL COMPRESSION DATA FOR VIENNA BLUE CLAY

TEST	μ	σ_3	ϵ	AREA CORRECTION: NONE		CYLINDRICAL		PARABOLIC	
				$\bar{p}$	q	$\bar{p}$	q	$\bar{p}$	q
		KG/CM^2	%	KG/CM^2	KG/CM^2	KG/CM^2	KG/CM^2	KG/CM^2	KG/CM^2
11	-1.00	3.00	0.0	3.00	0.00	3.00	0.00	3.00	0.00
			0.3	2.68	0.38	2.68	0.38	2.68	0.38
			0.8	2.43	0.57	2.42	0.56	2.42	0.56
			1.9	2.20	0.75	2.19	0.74	2.18	0.73
			3.8	2.19	0.94	2.16	0.91	2.14	0.89
			6.4	2.33	1.13	2.26	1.06	2.22	1.02
			10.0	2.61	1.32	2.48	1.19	2.42	1.13
			16.2	2.92	1.50	2.68	1.26	2.58	1.16
			19.6	3.05	1.60	2.73	1.28	2.62	1.17
			23.8	3.29	1.69	2.89	1.29	2.75	1.15

(Contined)

TABLE 6.3

TRIAXIAL COMPRESSION DATA FOR VIENNA BLUE CLAY

TEST	μ	σ_3	ϵ	AREA CORRECTION: NONE $\bar{p}$	NONE q	CYLINDRICAL $\bar{p}$	CYLINDRICAL q	PARABOLIC $\bar{p}$	PARABOLIC q
		KG/CM^2	%	KG/CM^2	KG/CM^2	KG/CM^2	KG/CM^2	KG/CM^2	KG/CM^2
12	-1.00	4.00	0.0	4.00	0.00	4.00	0.00	4.00	0.00
			0.2	4.00	0.25	4.00	0.25	4.00	0.25
			0.6	3.74	0.50	3.74	0.50	3.74	0.50
			1.0	3.55	0.75	3.55	0.75	3.54	0.74
			1.6	3.27	1.00	3.26	0.99	3.25	0.98
			3.8	2.95	1.25	2.91	1.21	2.88	1.18
			8.0	3.12	1.50	3.00	1.38	2.95	1.33
			12.9	3.55	1.75	3.33	1.53	3.23	1.43
			15.5	3.80	1.88	3.51	1.59	3.39	1.47
			18.4	4.00	2.00	3.63	1.63	3.49	1.49

(Continued)

TABLE 6.3

TRIAXIAL COMPRESSION DATA FOR VIENNA BLUE CLAY

TEST	μ	σ_3 KG/CM^2	ϵ %	AREA CORRECTION: NONE $\bar{p}$ KG/CM^2	NONE q KG/CM^2	CYLINDRICAL $\bar{p}$ KG/CM^2	CYLINDRICAL q KG/CM^2	PARABOLIC $\bar{p}$ KG/CM^2	PARABOLIC q KG/CM^2
13	-1.00	5.00	0.0	5.00	0.00	5.00	0.00	5.00	0.00
			0.6	4.81	0.50	4.81	0.50	4.81	0.50
			0.9	4.55	0.75	4.55	0.75	4.54	0.74
			1.4	4.03	1.00	4.02	0.99	4.01	0.98
			2.0	3.59	1.25	3.57	1.23	3.56	1.22
			3.6	3.60	1.50	3.55	1.45	3.52	1.42
			6.5	3.80	1.75	3.69	1.64	3.64	1.59
			10.8	4.37	2.05	4.15	1.83	4.06	1.74
			14.2	5.47	2.25	5.15	1.93	5.02	1.80
			18.0	5.76	2.45	5.32	2.01	5.15	1.84

(Continued)

TABLE 6.3

TRIAXIAL COMPRESSION DATA FOR VIENNA BLUE CLAY

TEST	μ	σ_3 KG/CM^2	ϵ %	AREA CORRECTION: NONE $\bar{p}$ KG/CM^2	NONE q KG/CM^2	CYLINDRICAL $\bar{p}$ KG/CM^2	CYLINDRICAL q KG/CM^2	PARABOLIC $\bar{p}$ KG/CM^2	PARABOLIC q KG/CM^2
14	-1.00	3.00	0.0	3.00	0.00	3.00	0.00	3.00	0.00
			0.2	2.90	0.30	2.90	0.30	2.90	0.30
			0.6	2.70	0.50	2.70	0.50	2.70	0.50
			1.5	2.50	0.70	2.49	0.69	2.49	0.69
			3.3	2.15	0.90	2.12	0.87	2.11	0.86
			5.9	2.30	1.10	2.24	1.04	2.21	1.01
			8.6	2.51	1.25	2.41	1.15	2.36	1.10
			12.5	2.77	1.40	2.60	1.23	2.52	1.15
			18.0	3.01	1.55	2.73	1.27	2.62	1.16

Uncorrected data from RENDULIC (1937)

TABLE 6.4

TRIAXIAL EXTENSION DATA FOR VIENNA BLUE CLAY

TEST	μ	σ_3 KG/CM^2	$\bar{p}$ KG/CM^2	q KG/CM^2
15	1.00	1.00	1.00	0.00
			0.80	0.20
			0.77	0.25
			0.71	0.30
			0.65	0.35
16	1.00	1.50	1.50	0.00
			1.27	0.30
			1.08	0.45
			1.01	0.50
			0.96	0.55
			0.85	0.70
			0.84	0.75
			0.87	0.80
17	1.00	2.00	2.00	0.00
			1.88	0.20
			1.79	0.30
			1.60	0.40
			1.50	0.50
			1.37	0.60
			1.11	0.70
			1.03	0.80
			1.07	0.90

(Continued) TABLE 6.4

TRIAXIAL EXTENSION DATA FOR VIENNA BLUE CLAY

TEST	μ	σ_3 KG/CM^2	$\bar{p}$ KG/CM^2	q KG/CM^2
18	1.00	3.00	3.00	0.00
			2.86	0.30
			2.73	0.45
			2.61	0.60
			2.28	0.75
			2.10	0.90
			2.04	0.95
			1.82	1.05
			1.82	1.20
			1.90	1.25
19	1.00	4.00	4.00	0.00
			3.55	0.40
			3.28	0.60
			3.25	0.70
			3.03	0.80
			2.89	0.90
			2.52	1.00
			2.32	1.10
			2.28	1.20
			2.35	1.30

(Continued) TABLE 6.4

TRIAXIAL EXTENSION DATA FOR VIENNA BLUE CLAY

TEST	μ	σ_3 KG/CM^2	$\bar{p}$ KG/CM^2	q KG/CM^2
20	1.00	2.00	2.00	0.00
			1.82	0.20
			1.75	0.30
			1.65	0.40
			1.52	0.50
			1.32	0.60
			1.09	0.70
			1.00	0.80
			1.02	0.85
			1.11	0.90

Data from RENDULIC (1937)

TABLE 6.5

TRIAXIAL STRENGTH DATA FOR FONTAINEBLEAU SAND

TEST	$\bar{\sigma}_1$ KG/CM^2	$\bar{\sigma}_2$ KG/CM^2	$\bar{\sigma}_3$ KG/CM^2	$\bar{p}$ KG/CM^2	q KG/CM^2	μ	SIN $\bar{\Phi}$
C1	3.33	1.02	1.02	2.18	1.16	-1.000	0.531
C2	6.11	1.94	1.94	4.02	2.08	-1.000	0.518
C3	11.10	3.70	3.70	7.40	3.70	-1.000	0.500
C4	25.00	8.24	8.24	16.62	8.38	-1.000	0.504
E1	3.89	3.89	1.85	2.87	1.02	1.000	0.355
E2	8.24	8.24	3.70	5.97	2.27	1.000	0.380
T1	16.00	5.00	5.00	10.50	5.50	-1.000	0.524
T2	13.92	5.00	4.08	9.00	4.92	-0.813	0.547
T3	11.93	5.00	3.07	7.50	4.43	-0.564	0.591
T4	7.56	5.00	2.44	5.00	2.56	0.000	0.512
T5	6.58	5.00	2.42	4.50	2.08	0.240	0.462
T6	5.71	5.00	2.29	4.00	1.71	0.585	0.428
T7	5.00	5.00	2.00	3.50	1.50	1.000	0.429

Data from HABIB (1953) and YONG AND WARKENTIN (1966, 339)

TABLE 6.6

EFFECTIVE STRESS PATHS USED BY BISHOP AND ELDIN (1953) FOR TRIAXIAL TESTS ON BRASTED SAND

STRESS PATH	CONSOLIDATION K_o	CONSOLIDATION OCR	DRAINAGE	CONSTANT STRESS	μ	DEGREE OF SATURATION
1	1	1	$\bar{U}$	σ_r	-1	100%
2	<1	1	$\bar{U}$	σ_r	-1	100%
3	1	1	D	$\bar{\sigma}_r$	-1	100%
4	<1	1	D	$\bar{\sigma}_r$	-1	100%
5	1	>1	D	$\bar{\sigma}_r$	-1	100%
6	1	1	D	$\bar{\sigma}_v$	-1	100%
7	1	1	D	$\bar{\sigma}_r$	-1	0%
8	1	1	D	$\bar{\sigma}_v$	1	100%
9	1	1	D	$\bar{\sigma}_r$	1	100%
10	1	1	$\bar{U}$	σ_r	1	100%

See also Figure 6.13.

TABLE 6.7(a)

HOLLOW CYLINDER DATA FOR LOCH ALINE SAND

TEST	P_a PSI	P_b PSI	P_a/P_b	b/a
H1	21.21	14.40	1.473	1.620
H2	27.18	18.70	1.453	1.603
H3	44.08	30.60	1.441	1.594
H4	55.68	38.50	1.446	1.600
H5	65.75	45.80	1.436	1.565
H6	68.63	47.92	1.432	1.565
H7	72.88	50.30	1.449	1.604
H8	77.16	54.02	1.428	1.578
H9	78.43	54.80	1.431	1.563

Data from KIRKPATRICK (1957)

TABLE 6.7(b)

TRIAXIAL STRENGTH DATA FOR LOCH ALINE SAND

TEST	$\bar{\sigma}_1$ PSI	$\bar{\sigma}_2$ PSI	$\bar{\sigma}_3$ PSI	$\bar{p}$ PSI	q PSI	μ	SIN $\bar{\Phi}$
C1	87.75	20.00	20.00	53.88	33.88	-1.000	0.629
C2	89.75	20.00	20.00	54.88	34.88	-1.000	0.636
C3	134.25	30.00	30.00	82.13	52.13	-1.000	0.635
C4	175.00	40.00	40.00	107.50	67.50	-1.000	0.628
C5	210.00	50.00	50.00	130.00	80.00	-1.000	0.615
C6	218.00	50.00	50.00	134.00	84.00	-1.000	0.627
C7	260.00	60.00	60.00	160.00	100.00	-1.000	0.625
C8	295.00	67.50	67.50	181.25	113.75	-1.000	0.628
E1	58.75	58.75	14.50	36.62	22.12	1.000	0.604
E2	100.00	100.00	23.25	61.62	38.38	1.000	0.623
E3	120.00	120.00	27.50	73.75	46.25	1.000	0.627
E4	130.00	130.00	30.00	80.00	50.00	1.000	0.625
E5	140.00	140.00	32.00	86.00	54.00	1.000	0.628
H1	17.81	10.50	3.49	10.65	7.16	-0.021	0.672
H2	22.94	13.30	4.77	13.86	9.08	-0.061	0.656
H3	37.34	22.30	8.07	22.70	14.64	-0.028	0.645
H4	47.09	27.95	10.12	28.60	18.48	-0.035	0.646

(Continued)

TABLE 6.7(b)

TRIAXIAL STRENGTH DATA FOR LOCH ALINE SAND

TEST	$\bar{\sigma}_1$ PSI	$\bar{\sigma}_2$ PSI	$\bar{\sigma}_3$ PSI	$\bar{p}$ PSI	q PSI	μ	SIN $\bar{\Phi}$
H5	55.78	32.30	10.71	33.24	22.54	-0.042	0.678
H6	58.28	34.05	11.54	34.91	23.37	-0.037	0.669
H7	61.59	35.90	13.22	37.40	24.18	-0.062	0.647
H8	65.59	38.90	14.37	39.98	25.61	-0.042	0.641
H9	66.62	38.20	13.10	39.86	25.76	-0.062	0.671

Data from KIRKPATRICK (1957)

TABLE 6.8

TRIAXIAL STRENGTH CRITERIA FOR THREE SANDS

SAND	A	B	D	2D	1-2D	sin $\bar{\Phi}$	INTERCEPT	SLOPE
a	0.540	0.093	0.172	0.344	0.656	0.475	0.789	-5.56
b	0.600	0.095	0.158	0.316	0.684	0.515	0.842	-4.92
c	0.600	0.120	0.200	0.400	0.600	0.515	0.874	-5.61

Data from PELTIER (1957)

TEST 6.9(a)

TRIAXIAL STRENGTH DATA FOR REMOLDED WEALD CLAY

TEST	$\bar{p}_m$ PSI	$\bar{p}_c$ PSI	OCR	$\bar{\sigma}_1$ PSI	$\bar{\sigma}_2$ PSI	$\bar{\sigma}_3$ PSI	$\bar{p}$ PSI	q PSI	μ
UC1-1	15.00	15.00	1.00	17.60	7.70	7.70	12.65	4.95	-1.00
UC1-2	30.00	30.00	1.00	30.80	13.50	13.50	22.15	8.65	-1.00
UC1-3	45.00	45.00	1.00	45.10	20.10	20.10	32.60	12.50	-1.00
UC1-4	60.00	60.00	1.00	59.60	27.00	27.00	43.30	16.30	-1.00
UC1-5	120.00	120.00	1.00	121.50	53.50	53.50	87.50	34.00	-1.00
UC1-6	30.00	15.00	2.00	24.10	10.80	10.80	17.45	6.65	-1.00
UC1-7	30.00	7.50	4.00	18.60	8.50	8.50	13.55	5.05	-1.00
UC1-8	30.00	5.00	6.00	14.80	6.60	6.60	10.70	4.10	-1.00
UC1-9	30.00	2.00	15.00	9.60	4.30	4.30	6.95	2.65	-1.00
UC1-10	60.00	46.00	13.04	57.10	25.40	25.40	41.25	15.85	-1.00
UC1-11	60.30	30.00	2.01	50.60	21.60	21.60	36.10	14.50	-1.00
UC1-12	60.00	22.20	2.70	42.30	18.60	18.60	30.45	11.85	-1.00
UC1-13	60.00	15.00	4.00	34.90	14.90	14.90	24.90	10.00	-1.00
UC1-14	60.00	9.80	6.12	29.60	13.10	13.10	21.35	8.25	-1.00
UC1-15	60.00	5.00	12.00	20.60	9.30	9.30	14.95	5.65	-1.00

(Continued)

TABLE 6.9(a)

TRIAXIAL STRENGTH DATA FOR REMOLDED WEALD CLAY

TEST	$\bar{p}_m$ PSI	$\bar{p}_c$ PSI	OCR	$\bar{\sigma}_1$ PSI	$\bar{\sigma}_2$ PSI	$\bar{\sigma}_3$ PSI	$\bar{p}$ PSI	q PSI	μ
UC1-16	120.00	70.50	1.70	107.50	48.90	48.90	78.20	29.30	-1.00
UC1-17	120.00	60.00	2.00	100.20	45.50	45.50	72.85	27.35	-1.00
UC1-18	120.00	44.50	2.70	83.20	37.20	37.20	60.20	23.00	-1.00
UC1-19	120.00	30.00	4.00	69.90	30.70	30.70	50.30	19.60	-1.00
UC1-20	120.00	15.00	8.00	48.70	20.90	20.90	34.80	13.90	-1.00
UC1-21	120.00	10.00	12.00	36.00	16.00	16.00	26.00	10.00	-1.00
UC1-22	120.00	4.90	2.45	22.90	9.50	9.50	16.20	6.70	-1.00
UC2-1	30.00	30.00	1.00	28.90	13.50	13.50	21.20	7.70	-1.00
UC2-2	120.00	30.00	4.00	68.80	30.10	30.10	49.45	19.35	-1.00
DC1-1	15.00	15.00	1.00	31.60	15.00	15.00	23.30	8.30	-1.00
DC1-2	30.00	30.00	1.00	65.50	30.00	30.00	47.75	17.75	-1.00
DC1-3	45.00	45.00	1.00	95.50	45.00	45.00	70.25	25.25	-1.00
DC1-4	60.00	60.00	1.00	129.80	60.00	60.00	94.90	34.90	-1.00
DC1-5	120.00	120.00	1.00	255.00	120.00	120.00	187.50	67.50	-1.00
DC1-6	30.00	15.00	2.00	33.20	15.00	15.00	24.10	9.10	-1.00
DC1-7	30.00	7.50	4.00	16.40	7.50	7.50	11.95	4.45	-1.00

(Continued)

TABLE 6.9(a)

TRIAXIAL STRENGTH DATA FOR REMOLDED WEALD CLAY

TEST	$\bar{p}_m$ PSI	$\bar{p}_c$ PSI	OCR	$\bar{\sigma}_1$ PSI	$\bar{\sigma}_2$ PSI	$\bar{\sigma}_3$ PSI	$\bar{p}$ PSI	q PSI	μ
DC1-8	30.00	5.10	5.88	12.30	5.10	5.10	8.70	3.60	-1.00
DC1-9	60.00	30.00	2.00	65.40	30.00	30.00	47.70	17.70	-1.00
DC1-10	60.00	22.10	2.72	48.80	22.10	22.10	35.45	13.35	-1.00
DC1-11	60.00	15.00	4.00	33.60	15.00	15.00	24.30	9.30	-1.00
DC1-12	60.00	7.50	8.00	17.40	7.50	7.50	12.45	4.95	-1.00
DC1-13	60.00	5.00	12.00	13.20	5.00	5.00	9.10	4.10	-1.00
DC1-14	120.00	70.10	1.71	153.40	70.10	70.10	111.75	41.65	-1.00
DC1-15	120.00	60.00	2.00	131.00	60.00	60.00	95.50	35.50	-1.00
DC1-16	120.00	44.70	2.68	97.50	44.70	44.70	71.10	26.40	-1.00
DC1-17	120.00	30.00	4.00	68.80	30.00	30.00	49.40	19.40	-1.00
DC1-18	120.00	15.00	8.00	36.00	15.00	15.00	25.50	10.50	-1.00
DC1-19	120.00	10.00	12.00	24.80	10.00	10.00	17.40	7.40	-1.00
DC1-20	120.00	5.00	24.00	13.10	5.00	5.00	9.05	4.05	-1.00
DC2-1	30.00	30.00	1.00	28.10	13.30	13.30	20.70	7.40	-1.00
DC2-2	60.00	60.00	1.00	58.10	26.20	26.20	42.15	15.95	-1.00
DC2-3	120.00	120.00	1.00	117.90	55.00	55.00	86.45	31.45	-1.00
DC2-4	60.00	30.00	2.00	28.30	12.10	12.10	20.20	8.10	-1.00

(Continued)

TABLE 6.9(a)

TRIAXIAL STRENGTH DATA FOR REMOLDED WEALD CLAY

TEST	$\bar{p}_m$ PSI	$\bar{p}_c$ PSI	OCR	$\bar{\sigma}_1$ PSI	$\bar{\sigma}_2$ PSI	$\bar{\sigma}_3$ PSI	$\bar{p}$ PSI	q PSI	μ
DC2-5	60.00	15.00	4.00	13.30	5.10	5.10	9.20	4.10	-1.00
DC2-6	60.00	5.00	12.00	4.30	1.30	1.30	2.80	1.50	-1.00
DC2-7	120.00	70.50	1.70	68.20	31.30	31.30	49.75	18.45	-1.00
DC2-8	120.00	60.00	2.00	58.20	26.20	26.20	42.20	16.00	-1.00
DC2-9	120.00	30.00	4.00	28.30	11.30	11.30	19.80	8.50	-1.00
DC2-10	120.00	15.00	8.00	13.20	4.80	4.80	9.00	4.20	-1.00
DC2-11	120.00	10.00	12.00	8.60	3.00	3.00	5.80	2.80	-1.00
DC2-12	120.00	5.00	24.00	4.20	1.20	1.20	2.70	1.50	-1.00
DC3-1	30.00	30.00	1.00	46.70	21.40	21.40	34.05	12.65	-1.00
DC3-2	120.00	30.00	4.00	48.00	20.80	20.80	34.40	13.60	-1.00
DC3-3	120.00	10.00	12.00	17.40	6.50	6.50	11.95	5.45	-1.00
UE1-1	30.00	30.00	1.00	26.00	26.00	11.80	18.90	7.10	1.00
UE1-2	60.00	60.00	1.00	52.20	52.20	23.90	38.05	14.15	1.00
UE1-3	120.00	120.00	1.00	104.00	104.00	48.30	76.15	27.85	1.00
UE1-4	60.00	30.00	2.00	42.00	42.00	19.00	30.50	11.50	1.00
UE1-5	60.00	15.00	4.00	29.20	29.20	13.40	21.30	7.90	1.00
UE1-6	60.00	5.00	12.00	16.50	16.50	6.40	11.45	5.05	1.00
UE1-7	120.00	70.50	1.70	88.90	88.90	39.80	64.35	24.55	1.00

(Continued)

TABLE 6.9(a)

TRIAXIAL STRENGTH DATA FOR REMOLDED WEALD CLAY

TEST	$\bar{p}_m$ PSI	$\bar{p}_c$ PSI	OCR	$\bar{\sigma}_1$ PSI	$\bar{\sigma}_2$ PSI	$\bar{\sigma}_3$ PSI	$\bar{p}$ PSI	q PSI	μ
UE1-8	120.00	60.00	2.00	83.70	83.70	38.50	61.10	22.60	1.00
UE1-9	120.00	30.00	4.00	58.20	58.20	23.80	41.00	17.20	1.00
UE1-10	120.00	15.00	8.00	37.50	37.50	15.10	26.30	11.20	1.00
UE1-11	120.00	10.00	12.00	29.80	29.80	10.90	20.35	9.45	1.00
UE1-12	120.00	5.00	24.00	19.10	19.10	6.60	12.85	6.25	1.00
UE2-1	30.00	30.00	1.00	26.10	26.10	11.30	18.70	7.40	1.00
UE2-2	60.00	5.00	12.00	16.90	16.90	6.60	11.75	5.15	1.00
UE2-3	120.00	30.00	4.00	59.90	59.90	26.40	43.15	16.75	1.00
UE2-4	120.00	15.00	8.00	40.50	40.50	16.80	28.65	11.85	1.00
UE2-5	120.00	10.00	12.00	30.70	30.70	11.90	21.30	9.40	1.00
UE2-6	120.00	5.00	24.00	18.40	18.40	6.80	12.60	5.80	1.00
DE1-1	30.00	30.00	1.00	30.00	30.00	13.40	21.70	8.30	1.00
DE1-2	60.00	60.00	1.00	60.00	60.00	27.50	43.75	16.25	1.00
DE1-3	120.00	120.00	1.00	120.00	120.00	53.70	86.85	33.15	1.00
DE1-4	60.00	30.00	2.00	30.00	30.00	12.80	21.40	8.60	1.00
DE1-5	60.00	15.00	4.00	15.00	15.00	6.50	10.75	4.25	1.00
DE1-6	60.00	5.00	12.00	5.00	5.00	1.40	3.20	1.80	1.00
DE1-7	120.00	70.50	1.70	70.50	70.05	31.00	50.75	19.75	1.00

(Continued)

TABLE 6.9(a)

TRIAXIAL STRENGTH DATA FOR REMOLDED WEALD CLAY

TEST	$\bar{p}_m$	$\bar{p}_c$	OCR	$\bar{\sigma}_1$	$\bar{\sigma}_2$	$\bar{\sigma}_3$	$\bar{p}$	q	μ
	PSI	PSI		PSI	PSI	PSI	PSI	PSI	
DE1-8	120.00	60.00	2.00	60.00	60.00	25.20	42.60	17.40	1.00
DE1-9	120.00	30.00	4.00	30.00	30.00	11.80	20.90	9.10	1.00
DE1-10	120.00	15.00	8.00	15.00	15.00	5.00	10.00	5.00	1.00
DE1-11	120.00	10.00	12.00	10.00	10.00	3.10	6.55	3.45	1.00
DE1-12	120.00	5.00	24.00	5.00	5.00	1.30	3.15	1.85	1.00
DE2-1	30.00	30.00	1.00	66.00	66.00	30.50*	48.25	17.75	1.00
DE2-2	60.00	60.00	1.00	131.00	131.00	61.50	96.25	34.75	1.00
DE2-3	60.00	30.00	2.00	67.00	67.00	30.40	48.70	18.30	1.00
DE2-4	60.00	15.00	4.00	33.30	33.30	15.30	24.30	9.00	1.00
DE2-5	60.00	5.00	12.00	14.00	14.00	5.30	9.65	4.35	1.00
DE2-6	120.00	60.00	2.00	131.50	131.50	60.40	95.95	35.55	1.00
DE2-7	120.00	30.00	4.00	68.00	68.00	30.10	49.05	18.95	1.00
DE2-8	120.00	15.00	8.00	38.00	38.00	15.20	26.60	11.40	1.00
DE2-9	120.00	10.00	12.00	27.10	27.10	10.10	18.60	8.50	1.00
DE2-10	120.00	5.00	24.00	15.30	15.30	5.20	10.25	5.05	1.00
DE3-1	30.00	30.00	1.00	36.50	36.50	16.50	26.50	10.00	1.00
DE3-2	120.00	30.00	4.00	37.40	37.40	14.80	26.10	11.30	1.00
DE3-3	120.00	10.00	12.00	12.90	12.90	4.50	8.70	4.20	1.00

Data from PARRY(1956;1960)

*The original paper gives $\bar{\sigma}_1-\bar{\sigma}_3 = 35.5$; $\bar{\sigma}_1 = 66.0$; $\bar{\sigma}_3 = 30.0$

TABLE 6.9(b)

NORMALIZED TRIAXIAL STRENGTH DATA FOR REMOLDED WEALD CLAY

TEST	$\bar{p}/\bar{p}_m$	$q/\bar{p}_m$	TEST	$\bar{p}/\bar{p}_m$	$q/\bar{p}_m$
UC1-1	0.843	0.330	DC1-1	1.553	0.553
UC1-2	0.738	0.283	DC1-2	1.592	0.592
UC1-3	0.724	0.278	DC1-3	1.561	0.561
UC1-4	0.722	0.272	DC1-4	1.582	0.582
UC1-5	0.729	0.283	DC1-5	1.563	0.563
UC1-6	0.582	0.222	DC1-6	0.803	0.303
UC1-7	0.452	0.168	DC1-7	0.398	0.148
UC1-8	0.357	0.137	DC1-8	0.290	0.120
UC1-9	0.232	0.088	DC1-9	0.795	0.295
UC1-10	0.688	0.264	DC1-10	0.591	0.223
UC1-11	0.599	0.240	DC1-11	0.405	0.155
UC1-12	0.508	0.197	DC1-12	0.208	0.083
UC1-13	0.415	0.167	DC1-13	0.152	0.068
UC1-14	0.356	0.138	DC1-14	0.931	0.347
UC1-15	0.249	0.094	DC1-15	0.796	0.296
UC1-16	0.652	0.244	DC1-16	0.593	0.220
UC1-17	0.607	0.228	DC1-17	0.412	0.162
UC1-18	0.502	0.192	DC1-18	0.213	0.088
UC1-19	0.419	0.163	DC1-19	0.145	0.062
UC1-20	0.290	0.116	DC1-20	0.075	0.034
UC1-21	0.217	0.083			
UC1-22	0.135	0.056	DC2-1	0.690	0.247
			DC2-2	0.703	0.266
UC2-1	0.707	0.257	DC2-3	0.720	0.262
UC2-2	0.412	0.161	DC2-4	0.337	0.135

(Continued) TABLE 6.9(b)

NORMALIZED TRIAXIAL STRENGTH DATA FOR REMOLDED WEALD CLAY

TEST	$\bar{p}/\bar{p}_m$	$q/\bar{p}_m$	TEST	$\bar{p}/\bar{p}_m$	$q/\bar{p}_m$
DC2-5	0.153	0.068	UE2-1	0.623	0.247
DC2-6	0.047	0.025	UE2-2	0.196	0.086
DC2-7	0.415	0.154	UE2-3	0.360	0.140
DC2-8	0.352	0.133	UE2-4	0.239	0.099
DC2-9	0.165	0.071	UE2-5	0.178	0.078
DC2-10	0.075	0.035	UE2-6	0.105	0.048
DC2-11	0.048	0.023			
DC2-12	0.023	0.013	DE1-1	0.723	0.277
			DE1-2	0.729	0.271
DC3-1	1.135	0.422	DE1-3	0.724	0.276
DC3-2	0.287	0.113	DE1-4	0.357	0.143
DC3-3	0.100	0.045	DE1-5	0.179	0.071
			DE1-6	0.053	0.030
UE1-1	0.630	0.237	DE1-7	0.423	0.165
UE1-2	0.634	0.236	DE1-8	0.355	0.145
UE1-3	0.635	0.232	DE1-9	0.174	0.076
UE1-4	0.508	0.192	DE1-10	0.083	0.042
UE1-5	0.355	0.132	DE1-11	0.055	0.029
UE1-6	0.191	0.084	DE1-12	0.026	0.015
UE1-7	0.536	0.205			
UE1-8	0.509	0.188	DE2-1	1.610	0.610
UE1-9	0.342	0.143	DE2-2	1.604	0.579
UE1-10	0.219	0.093	DE2-3	0.812	0.305
UE1-11	0.170	0.079	DE2-4	0.405	0.150
UE1-12	0.107	0.052	DE2-5	0.161	0.073

(Continued) TABLE 6.9(b)

NORMALIZED TRIAXIAL STRENGTH DATA FOR REMOLDED WEALD CLAY

TEST	$\bar{p}/\bar{p}_m$	$q/\bar{p}_m$
DE2-6	0.800	0.296
DE2-7	0.409	0.158
DE2-8	0.222	0.095
DE2-9	0.155	0.071
DE2-10	0.085	0.042
DE3-1	0.883	0.333
DE3-2	0.218	0.094
DE3-3	0.073	0.035

Data from PARRY (1956;1960)

TABLE 6.10(a)

TRIAXIAL STRENGTH DATA FOR REMOLDED LONDON CLAY

TEST	$\bar{p}_m$	$\bar{p}_c$	OCR	$\bar{\sigma}_1$	$\bar{\sigma}_2$	$\bar{\sigma}_3$	$\bar{p}$	q	μ
	PSI	PSI		PSI	PSI	PSI	PSI	PSI	
UC1-1	14.70	14.70	1.00	14.50	7.20	7.20	10.85	3.65	-1.00
UC1-2	30.00	30.00	1.00	28.80	14.60	14.60	21.70	7.10	-1.00
UC1-3	60.00	60.00	1.00	62.00	31.80	31.80	46.90	15.10	-1.00
UC1-4	120.00	120.00	1.00	126.20	66.50	66.50	96.35	29.85	-1.00
UC1-5	30.00	15.00	2.00	22.00	10.10	10.10	16.05	5.95	-1.00
UC1-6	30.00	7.50	4.00	15.10	7.20	7.20	11.15	3.95	-1.00
UC1-7	30.00	3.75	8.00	10.20	4.30	4.30	7.25	2.95	-1.00
UC1-8	60.00	30.00	2.00	43.80	21.70	21.70	32.75	11.05	-1.00
UC1-9	60.00	15.00	4.00	30.80	14.40	14.40	22.60	8.20	-1.00
UC1-10	60.00	7.50	8.00	18.50	8.20	8.20	13.35	5.15	-1.00
UC1-11	60.00	3.75	16.00	12.10	5.20	5.20	8.65	3.45	-1.00
UC1-12	120.00	60.00	2.00	93.90	48.00	48.00	70.95	22.95	-1.00
UC1-13	120.00	30.00	4.00	60.10	29.40	29.40	44.75	15.35	-1.00
UC1-14	120.00	15.00	8.00	37.40	17.10	17.10	27.25	10.15	-1.00
UC1-15	120.00	7.40	16.20	21.00	9.20	9.20	15.10	5.90	-1.00
UC1-16	120.00	3.75	32.00	12.75	4.90	4.90	8.83	3.93	-1.00

(Continued)

TABLE 6.10(a)

TRIAXIAL STRENGTH DATA FOR REMOLDED LONDON CLAY

TEST	$\bar{p}_m$ PSI	$\bar{p}_c$ PSI	OCR	$\bar{\sigma}_1$ PSI	$\bar{\sigma}_2$ PSI	$\bar{\sigma}_3$ PSI	$\bar{p}$ PSI	q PSI	μ
DC1-1	15.00	15.00	1.00	30.30	15.00	15.00	22.65	7.65	-1.00
DC1-2	30.00	30.00	1.00	58.90	30.00	30.00	44.45	14.45	-1.00
DC1-3	60.00	60.00	1.00	114.00	60.00	60.00	87.00	27.00	-1.00
DC1-4	120.00	120.00	1.00	225.20	120.00	120.00	172.60	52.60	-1.00
DC1-5	30.00	22.50	1.33	45.50	22.50	22.50	34.00	11.50	-1.00
DC1-6	30.00	15.00	2.00	31.20	15.00	15.00	23.10	8.10	-1.00
DC1-7	30.00	7.50	4.00	16.70	7.50	7.50	12.10	4.60	-1.00
DC1-8	30.00	3.75	8.00	9.25	3.75	3.75	6.50	2.75	-1.00
DC1-9	60.00	30.00	2.00	59.50	30.00	30.00	44.75	14.75	-1.00
DC1-10	60.00	15.00	4.00	32.50	15.00	15.00	23.75	8.75	-1.00
DC1-11	60.00	7.50	8.00	18.10	7.50	7.50	12.80	5.30	-1.00
DC1-12	120.00	60.00	2.00	113.80	60.00	60.00	86.90	26.90	-1.00
DC1-13	120.00	30.00	4.00	61.50	30.00	30.00	45.75	15.75	-1.00
DC1-14	120.00	15.00	8.00	34.00	15.00	15.00	24.50	9.50	-1.00
DC1-15	120.00	7.50	16.00	19.10	7.50	7.50	13.30	5.80	-1.00
DC1-16	120.00	3.75	32.00	10.25	3.75	3.75	7.00	3.25	-1.00

(Continued)

TABLE 6.10(a)

TRIAXIAL STRENGTH DATA FOR REMOLDED LONDON CLAY

TEST	$\bar{p}_m$ PSI	$\bar{p}_c$ PSI	OCR	$\bar{\sigma}_1$ PSI	$\bar{\sigma}_2$ PSI	$\bar{\sigma}_3$ PSI	$\bar{p}$ PSI	q PSI	μ
DC2-1	30.00	30.00	1.00	28.40	14.00	14.00	21.20	7.20	-1.00
DC2-2	60.00	60.00	1.00	57.40	28.60	28.60	43.00	14.40	-1.00
DC2-3	120.00	120.00	1.00	115.60	60.30	60.30	87.95	27.65	-1.00
DC2-4	120.00	60.00	2.00	57.80	27.50	27.50	42.65	15.15	-1.00
DC2-5	120.00	30.00	4.00	28.20	11.40	11.40	19.80	8.40	-1.00
DC2-6	120.00	15.00	8.00	13.50	4.60	4.60	9.05	4.45	-1.00
DC2-7	120.00	7.50	16.00	6.40	1.80	1.80	4.10	2.30	-1.00

Data from PARRY (1956)

TABLE 6.10(b)

NORMALIZED TRIAXIAL STRENGTH DATA FOR REMOLDED LONDON CLAY

TEST	$\bar{p}/\bar{p}_m$	$q/\bar{p}_m$
UC1-1	0.738	0.248
UC1-2	0.723	0.237
UC1-3	0.782	0.252
UC1-4	0.803	0.249
UC1-5	0.535	0.198
UC1-6	0.372	0.132
UC1-7	0.242	0.098
UC1-8	0.546	0.184
UC1-9	0.377	0.137
UC1-10	0.223	0.086
UC1-11	0.144	0.057
UC1-12	0.591	0.191
UC1-13	0.373	0.128
UC1-14	0.227	0.085
UC1-15	0.126	0.049
UC1-16	0.074	0.033
DC1-1	1.510	0.510
DC1-2	1.482	0.482
DC1-3	1.450	0.450
DC1-4	1.438	0.438
DC1-5	1.133	0.383
DC1-6	0.770	0.270
DC1-7	0.403	0.153
DC1-8	0.217	0.092

TEST	$\bar{p}/p_m$	$q/\bar{p}_m$
DC1-9	0.746	0.246
DC1-10	0.396	0.146
DC1-11	0.213	0.088
DC1-12	0.724	0.224
DC1-13	0.381	0.131
DC1-14	0.204	0.079
DC1-15	0.111	0.048
DC1-16	0.058	0.027
DC2-1	0.707	0.240
DC2-2	0.717	0.240
DC2-3	0.733	0.230
DC2-4	0.355	0.126
DC2-5	0.165	0.070
DC2-6	0.075	0.037
DC2-7	0.034	0.019

Data from PARRY (1956)

TABLE 6.11

TRIAXIAL STRENGTH DATA FOR GLEN SHIRA DAM MATERIAL

TEST	$\bar{\sigma}_1$ PSI	$\bar{\sigma}_2$ PSI	$\bar{\sigma}_3$ PSI	$\bar{p}$ PSI	q PSI	μ	SIN $\bar{\Phi}$
27	36.00	12.90	6.50	21.25	14.75	-0.566	0.694
22	65.50	-	14.00	39.75	25.75	-	-
28	105.00	35.30	24.00	64.50	40.50	-0.721	0.628
21	18.00	8.70	2.50	10.25	7.75	-0.200	0.756
25	47.50	18.90	11.00	29.25	18.25	-0.567	0.624
26	109.50	45.90	24.00	66.75	42.75	-0.488	0.640
19	56.30	21.20	12.20	34.25	22.05	-0.592	0.644
29	118.20	46.50	28.20	73.20	45.00	-0.593	0.615
14	168.50	45.00	45.00	106.75	61.75	-1.000	0.578
15	94.50	25.00	25.00	59.75	34.75	-1.000	0.582
16	62.40	16.20	16.20	39.30	23.10	-1.000	0.588
30	83.00	20.00	20.00	51.50	31.50	-1.000	0.612
33	187.00	50.00	50.00	118.50	68.50	-1.000	0.578
31	41.50	10.00	10.00	25.75	15.75	-1.000	0.612
35	68.50	18.00	18.00	43.25	25.25	-1.000	0.584
39	43.00	12.00	12.00	27.50	15.50	-1.000	0.564
36	109.00	29.50	29.50	69.25	39.75	-1.000	0.574
37	82.50	22.00	22.00	52.25	30.25	-1.000	0.579
38	51.30	14.30	14.30	32.80	18.50	-1.000	0.564

Data from WOOD (1958)

TABLE 6.12

TRIAXIAL STRENGTH DATA FOR A CLAYEY SILT

TEST	β DEG	$\bar{\sigma}_1$ PSI	$\bar{\sigma}_2$ PSI	$\bar{\sigma}_3$ PSI	$\bar{p}$ PSI	q PSI	μ	SIN $\bar{\Phi}$
A1	0.00	161.42	40.00	40.00	100.71	60.71	-1.000	0.603
A2	5.75	170.01	40.00	38.67	104.34	65.67	-0.980	0.629
A3	14.50	162.31	40.00	31.83	97.07	65.24	-0.875	0.672
A4	19.70	157.89	40.00	24.87	91.38	66.51	-0.773	0.728
A5	23.80	147.26	40.00	19.14	83.20	64.06	-0.674	0.770
A6	28.60	119.68	40.00	16.24	67.96	51.72	-0.541	0.761
A7	34.15	90.64	40.00	16.64	53.64	37.00	-0.369	0.690
A8	45.00	66.31	40.00	13.69	40.00	26.31	0	0.658
A9	55.40	53.61	40.00	11.39	32.50	21.11	0.355	0.650
A10	73.30	42.43	40.00	13.01	27.72	14.71	0.835	0.531
A11	90.00	40.00	40.00	9.08	24.54	15.46	1.000	0.630
B1	0.00	166.88	40.00	40.00	103.44	63.44	-1.000	0.613
B2	7.90	158.25	40.00	37.71	97.98	60.27	-0.962	0.615
B3	49.70	58.67	40.00	14.05	36.36	22.31	0.163	0.614
B4	90.00	40.00	40.00	8.16	24.08	15.92	1.000	0.661
B5	24.10	158.82	44.00	21.04	89.93	68.89	-0.667	0.766

Data from HAYTHORNETHWAITE (1960c)

TABLE 6.13

TRIAXIAL STRENGTH DATA FOR BRASTED SAND

TEST	n_f	$\bar{\sigma}_1$	$\bar{\sigma}_2$	$\bar{\sigma}_3$	$\bar{p}$	q	μ	SIN $\bar{\Phi}$
	%	PSI	PSI	PSI	PSI	PSI		
AP-5	35.2	224.70	71.50	40.00	132.35	92.35	-0.659	0.698
AP-6	40.6	155.60	65.00	40.00	97.80	57.80	-0.567	0.591
AP-8	39.4	174.00	69.50	40.00	107.00	67.00	-0.560	0.626
AP-9	41.1	142.40	64.10	40.00	91.20	51.20	-0.529	0.561
AP-10	41.8	147.40	74.30	40.00	93.70	53.70	-0.361	0.573
AP-16	35.3	214.80	68.80	40.00	127.40	87.40	-0.670	0.686
AP-17	34.2	235.60	80.40	40.00	137.80	97.80	-0.587	0.710
AP-18	38.8	167.90	71.70	40.00	103.95	63.95	-0.504	0.615
AP-19	37.6	180.90	68.00	40.00	110.45	70.45	-0.603	0.638
AP-20	40.6	145.30	62.80	40.00	92.65	52.65	-0.567	0.568
AP-21	40.6	151.90	66.70	40.00	95.95	55.95	-0.523	0.583
AP-23	36.0	217.60	73.00	40.00	128.80	88.80	-0.628	0.689
AP-24	38.1	171.30	66.30	40.00	105.65	65.65	-0.599	0.621
BP-22	41.3	145.00	66.50	40.30	92.65	52.35	-0.500	0.565
BP-25	39.3	163.90	71.90	41.50	102.70	61.20	-0.503	0.596
BP-26	37.5	185.70	74.30	41.00	113.35	72.35	-0.540	0.638
BP-27	35.8	214.60	76.80	40.00	127.30	87.30	-0.578	0.686

(Continued)

TABLE 6.13

TRIAXIAL STRENGTH DATA FOR BRASTED SAND

TEST	n_f	$\bar{\sigma}_1$	$\bar{\sigma}_2$	$\bar{\sigma}_3$	$\bar{p}$	q	μ	SIN $\bar{\Phi}$
	%	PSI	PSI	PSI	PSI	PSI		
CP-11	37.8	177.80	N/M	40.00	108.90	68.90	-	0.633
CP-12	35.3	227.80	N/M	40.00	133.90	93.90	-	0.701
CP-13	39.0	164.20	N/M	40.00	102.10	62.10	-	0.608
CP-14	41.2	146.00	N/M	40.00	93.00	53.00	-	0.570
CP-15	36.2	200.80	N/M	40.00	120.40	80.40	-	0.668
DP-28	40.4	116.40	52.10	31.20	73.80	42.60	-0.509	0.577
DP-29	39.0	179.10	75.70	44.00	111.55	67.55	-0.531	0.606
DP-30	37.9	209.00	81.90	47.60	128.30	80.70	-0.575	0.629
DP-31	34.6	199.70	65.90	37.90	118.80	80.90	-0.654	0.681
DP-32	39.2	34.10	14.00	8.00	21.05	13.05	-0.540	0.620
DP-33	40.9	88.20	39.00	23.10	55.65	32.55	-0.512	0.585
DP-34	37.8	79.50	31.10	17.20	48.35	31.15	-0.554	0.644
DP-35	35.2	236.40	81.10	44.10	140.25	96.15	-0.615	0.686

(Continued)

TABLE 6.13

TRIAXIAL STRENGTH DATA FOR BRASTED SAND

TEST	n_f	$\bar{\sigma}_1$	$\bar{\sigma}_2$	$\bar{\sigma}_3$	$\bar{p}$	q	μ	SIN $\bar{\Phi}$
	%	PSI	PSI	PSI	PSI	PSI		
EC-7	36.6	266.80	60.00	60.00	163.40	103.40	-1.000	0.633
EC-8	40.1	220.60	60.00	60.00	140.30	80.30	-1.000	0.572
EC-9	36.3	283.00	60.00	60.00	171.50	111.50	-1.000	0.650
EC-10	40.6	215.90	60.00	60.00	137.95	77.95	-1.000	0.565
EC-12	41.9	205.30	60.00	60.00	132.65	72.65	-1.000	0.548
EC-13	38.5	236.20	60.00	60.00	148.10	88.10	-1.000	0.595
EC-15	38.2	247.50	60.00	60.00	153.75	93.75	-1.000	0.610
EC-16	36.2	273.00	60.00	60.00	166.50	106.50	-1.000	0.640
EC-21	41.8	136.90	40.00	40.00	88.45	48.45	-1.000	0.548
EC-25	40.1	151.40	40.00	40.00	95.70	55.70	-1.000	0.583
EC-27	37.8	170.20	40.00	40.00	105.10	65.10	-1.000	0.619
EC-29	35.3	195.70	40.00	40.00	117.85	77.85	-1.000	0.661
EC-32	37.5	177.60	40.00	40.00	108.80	68.80	-1.000	0.632
EC-33	38.7	162.40	40.00	40.00	101.20	61.20	-1.000	0.605
EC-34	37.0	176.00	40.00	40.00	108.00	68.00	-1.000	0.630
EC-36	38.6	161.00	40.00	40.00	100.50	60.50	-1.000	0.602

(Continued)

TABLE 6.13

TRIAXIAL STRENGTH DATA FOR BRASTED SAND

TEST	n_f	$\bar{\sigma}_1$	$\bar{\sigma}_2$	$\bar{\sigma}_3$	$\bar{p}$	q	μ	SIN $\bar{\Phi}$
	%	PSI	PSI	PSI	PSI	PSI		
FC-23	42.0	139.50	41.00	41.00	90.25	49.25	-1.000	0.546
FC-26	39.6	152.10	40.00	40.00	96.05	56.05	-1.000	0.584
FC-28	38.1	166.90	38.50	38.50	102.70	64.20	-1.000	0.625
FC-31	35.3	198.80	40.50	40.50	119.65	79.15	-1.000	0.662
FC-40	38.2	164.40	39.80	39.80	102.10	62.30	-1.000	0.610
GC-43	39.7	130.00	130.00	37.70	83.85	46.15	1.000	0.550
GC-44	35.8	130.00	130.00	28.19	79.09	50.90	1.000	0.644
GC-45	39.3	130.00	130.00	36.00	83.00	47.00	1.000	0.566
GC-46	37.4	130.00	130.00	33.03	81.51	48.48	1.000	0.595
GC-47	35.7	130.10	130.10	27.32	78.71	51.39	1.000	0.653
GC-48	37.1	139.80	139.80	34.65	87.22	52.57	1.000	0.603
HC-22	41.5	158.20	46.80	46.80	102.50	55.70	-1.000	0.543
HC-37	38.7	68.10	18.50	18.50	43.30	24.80	-1.000	0.573
HC-38	38.1	72.90	19.50	19.50	46.20	26.70	-1.000	0.578
HC-39	40.0	181.60	52.80	52.80	117.20	64.40	-1.000	0.549
JC-49	41.2	8.20	8.20	2.30	5.25	2.95	1.000	0.562
JC-50	38.3	125.70	125.70	37.10	81.40	44.30	1.000	0.544

Data from CONFORTH (1961)

TABLE 6.14a

TRIAXIAL STRENGTH DATA FOR REMOLDED SAULT STE MARIE CLAY - BATCH 1

TEST	$\bar{\sigma}_1$ KG/CM^2	$\bar{\sigma}_2$ KG/CM^2	$\bar{\sigma}_3$ KG/CM^2	$\bar{p}$ KG/CM^2	q KG/CM^2	μ	SIN $\bar{\Phi}$
C1-27D	1.52	0.42	0.42	0.97	0.55	-1.000	0.567
C1-28D	5.45	1.60	1.60	3.52	1.92	-1.000	0.546
C1-36D	3.17	0.92	0.92	2.04	1.12	-1.000	0.550
C1a-5	4.54	1.31	1.31	2.92	1.62	-1.000	0.552
C1a-6	3.53	1.03	1.03	2.28	1.25	-1.000	0.548
C1a-7	2.43	0.81	0.81	1.62	0.81	-1.000	0.500
E1-20	3.60	3.60	1.07	2.34	1.26	1.000	0.542
E1-21	2.58	2.58	0.75	1.66	0.92	1.000	0.550
E1-22	1.80	1.80	0.52	1.16	0.64	1.000	0.552
I1-8	3.16	2.98	1.06	2.11	1.05	0.829	0.498
I1-17	4.99	4.80	1.82	3.40	1.58	0.880	0.466
I2-9	3.48	1.46	0.94	2.21	1.27	-0.591	0.575
I2-10	3.45	1.86	0.98	2.22	1.24	-0.287	0.558
I2-11	4.55	2.28	1.40	2.98	1.58	-0.441	0.529

(Continued)

TABLE 6.14a

TRIAXIAL STRENGTH DATA FOR REMOLDED SAULT STE MARIE CLAY - BATCH 1

TEST	$\bar{\sigma}_1$ KG/CM^2	$\bar{\sigma}_2$ KG/CM^2	$\bar{\sigma}_3$ KG/CM^2	$\bar{p}$ KG/CM^2	q KG/CM^2	μ	SIN $\bar{\Phi}$
I3-12	4.51	3.69	1.71	3.11	1.40	0.414	0.450
I3-14	3.82	2.51	1.37	2.60	1.22	-0.069	0.472

Data from WU, LOH AND MALVERN (1963)

TABLE 6.14b

TRIAXIAL STRENGTH DATA FOR REMOLDED SAULT STE MARIE CLAY - BATCH 2

TEST	$\bar{\sigma}_1$ KG/CM^2	$\bar{\sigma}_2$ KG/CM^2	$\bar{\sigma}_3$ KG/CM^2	$\bar{p}$ KG/CM^2	q KG/CM^2	μ	SIN $\bar{\Phi}$
C1-41	2.84	0.90	0.90	1.87	0.97	-1.000	0.519
C1-42	3.56	1.15	1.15	2.36	1.20	-1.000	0.512
C1-43	5.12	1.60	1.60	3.36	1.76	-1.000	0.524
I1-25	3.42	2.76	1.32	2.37	1.05	0.371	0.443
I1-32	4.14	3.30	1.41	2.78	1.36	0.385	0.492
I2-31	3.52	1.50	1.15	2.34	1.18	-0.705	0.507
I2-26	4.96	1.68	1.33	3.14	1.82	-0.807	0.577
I2-29	3.75	2.40	1.18	2.46	1.28	-0.051	0.521
I2-30	3.79	2.28	1.06	2.42	1.36	-0.106	0.563
I2-24	3.43	2.68	1.10	2.26	1.16	0.356	0.514

Data from WU, LOH AND MALVERN (1963)

TABLE 6.15

TRIAXIAL STRENGTH DATA FOR THE 30-50 FRACTION OF OTTAWA SAND

TEST	e	$\bar{\sigma}_1$ KG/CM^2	$\bar{\sigma}_2$ KG/CM^2	$\bar{\sigma}_3$ KG/CM^2	$\bar{p}$ KG/CM^2	q KG/CM^2	μ	SIN $\bar{\Phi}$
C1-51	0.52	12.92	3.16	3.16	8.04	4.88	-1.000	0.607
C1-52	0.57	23.17	5.97	5.97	14.57	8.60	-1.000	0.590
C1-53	0.50	21.43	5.38	5.38	13.40	8.02	-1.000	0.599
E1-101	0.76	2.91	2.91	0.81	1.86	1.05	1.000	0.565
E1-103	0.75	4.48	4.48	1.22	2.85	1.63	1.000	0.572
E1-110	0.58	2.11	2.11	0.50	1.30	0.80	1.000	0.617
E1-111	0.59	4.01	4.01	1.11	2.56	1.45	1.000	0.566
E1-113	0.49	5.59	5.59	1.35	3.47	2.12	1.000	0.611
E1-114	0.50	4.29	4.29	1.11	2.70	1.59	1.000	0.589
E1-116	0.49	6.39	6.39	1.58	3.98	2.40	1.000	0.604
E1-117	0.44	3.30	3.30	0.78	2.04	1.26	1.000	0.618
I1-213	0.44	18.72	12.22	4.37	11.54	7.18	0.094	0.621
I1-214	0.47	8.36	5.36	1.71	5.04	3.32	0.098	0.660
I1-215	0.47	10.18	6.46	2.13	6.16	4.02	0.076	0.654
I1-216	0.42	4.94	3.33	1.09	3.02	1.92	0.164	0.638

(Continued)

TABLE 6.15

TRIAXIAL STRENGTH DATA FOR THE 30-50 FRACTION OF OTTAWA SAND

TEST	e	$\bar{\sigma}_1$ KG/CM^2	$\bar{\sigma}_2$ KG/CM^2	$\bar{\sigma}_3$ KG/CM^2	$\bar{p}$ KG/CM^2	q KG/CM^2	μ	SIN $\bar{\Phi}$
I2-203	0.49	7.86	3.34	2.12	4.99	2.87	-0.575	0.575
I2-205	0.47	10.12	4.35	2.60	6.36	3.76	-0.535	0.591
I2-212	0.47	12.10	4.65	2.90	7.50	4.60	-0.620	0.613
I2-210	0.49	15.17	6.17	3.37	9.27	5.90	-0.525	0.636
I2-209	0.51	14.95	6.55	3.05	9.00	5.95	-0.412	0.661
I2-211	0.49	18.73	12.63	3.88	11.30	7.42	0.178	0.657
I2-207	0.43	13.18	5.02	3.80	8.49	4.69	-0.740	0.552
I2-206	0.43	13.01	5.21	3.46	8.24	4.78	-0.634	0.580

Data from WU, LOH AND MALVERN (1963)

TABLE 6.16

CONSOLIDATION STRESS HISTORIES FOR ISOTROPICALLY CONSOLIDATED TRIAXIAL TESTS ON REMOLDED WEALD CLAY

SERIES	TEST	w_i	$\bar{p}_m$	$\bar{p}_o$	w_f
		%	PSI	PSI	%
NUC1	1	33.4	30.50		24.0
	2	33.6	60.60		21.6
	5	33.2	90.40		20.3
	30	33.2	120.40		19.2
	32	33.2	120.00		-
	40	33.5	90.00		20.8
	90	33.6	110.00		19.0
NUC1(b)	15	33.5	30.00		23.7
	16	33.8	30.00		23.8
	18	33.1	30.00		23.7
	21	33.5	30.00		23.8
NUC2	116	33.3	30.00		-
	113	33.6	50.00		22.3
	68	33.4	66.00		21.0
	62	33.4	90.00		20.3
	58	33.5	105.00		19.9
NUC3	70	33.0	45.00		22.2
	72	33.5	64.00		21.2
	76	33.5	61.80		20.8
	95	33.1	74.00		20.1
	96	33.5	44.80		21.9
	97	33.4	30.00		23.6
	107	33.3	69.00		20.5
	112	33.5	50.00		22.1
	115	33.2	50.00		21.8

(Continued) TABLE 6.16

CONSOLIDATION STRESS HISTORIES FOR ISOTROPICALLY CONSOLIDATED TRIAXIAL TESTS ON REMOLDED WEALD CLAY

SERIES	TEST	w_i	$\bar{p}_m$	$\bar{p}_o$	w_f
		%	PSI	PSI	%
NUC4	100	49.0	30.00		24.7
	102	49.0	110.00		19.4
	103	49.0	60.00		22.0
	104	49.0	90.00		20.0
NUC5	109	227.0	50.00		25.3
	110	227.0	100.40		21.6
	108	227.0	100.00		22.4
NDC	42	33.4	30.00		21.2
	43	33.3	90.00		17.7
	46	33.0	60.00		19.0
	47	33.2	120.00		16.8
	49	32.8	30.00		21.2
	69	33.3	15.00		23.2
	71	33.5	53.50		19.2
	75	33.6	62.00		18.2
OUC	4	33.3	120.40	60.60	19.9
	6	33.3	120.40	30.50	20.5
	33	33.9	120.00	30.00	20.6
	34	33.7	120.00	59.90	20.1
	82	32.9	120.00	15.00	21.3
NUE1	41	33.3	30.00		24.2
	45	32.4	90.00		20.5
	54	33.7	60.00		22.3
	57	33.4	60.00		22.0
	67	33.2	120.00		19.6
	87	33.8	30.00		23.7

(Continued) TABLE 6.16

CONSOLIDATION STRESS HISTORIES FOR ISOTROPICALLY CONSOLIDATED TRIAXIAL TESTS ON REMOLDED WEALD CLAY

SERIES	TEST	w_i %	$\bar{p}_m$ PSI	$\bar{p}_o$ PSI	w_f %
NUE2	101	33.6	30.00		24.1
	105	33.7	60.00		21.3
	106	33.1	90.00		20.2

Date from SOWA (1963)

TABLE 6.17

STRESS HISTORIES FOR K_o CONSOLIDATED TRIAXIAL TESTS ON REMOLDED WEALD CLAY

SERIES	TEST	w_i %	$\bar{\sigma}_{vm}$ PSI	$\bar{\sigma}_{hm}$ PSI	$\bar{\sigma}_{vo}$ PSI	$\bar{\sigma}_{ho}$ PSI	w_f %	$\bar{p}_k$* PSI
NUC	35	33.4	28.20	18.00			24.6	
	64	33.4	90.10	53.50			21.4	
	88	33.4	127.20	75.00			20.0	
	85	33.5	167.20	100.00			19.3	
	98	49.0	92.20	53.50			21.7	
	39	32.6	34.40	20.60			23.8	
	48	32.2	52.10	30.70			22.9	
	44	33.1	61.90	37.70			22.6	
	77	34.0	171.70	100.00			19.2	
	80	33.8	164.80	100.00			19.3	
NPSUC	28	33.3	28.00	18.00			25.1	17.00
	63	33.6	90.10	53.50			21.4	51.40
	89	33.3	127.20	75.00			20.1	73.20
	86	33.5	166.80	100.00			19.3	98.10
	99	49.0	92.20	53.50			21.4	52.60
NPSIUC	65	33.8	90.00	53.50			20.2	51.50
OUC	92	33.6	162.60	100.00	78.70	63.00	19.6	
	84	33.6	171.00	100.00	39.00	39.00	20.1	39.00
	83	33.8	174.00	100.00	12.60	17.00	21.3	14.95

(Continued)

TABLE 6.17

STRESS HISTORIES FOR K_o CONSOLIDATED TRIAXIAL TESTS ON REMOLDED WEALD CLAY

SERIES	TEST	w_i %	$\bar{\sigma}_{vm}$ PSI	$\bar{\sigma}_{hm}$ PSI	$\bar{\sigma}_{vo}$ PSI	$\bar{\sigma}_{ho}$ PSI	w_f %	$\bar{p}_k^*$ PSI
OPSUC	91	33.6	166.70	100.00	78.80	63.00	19.6	68.00
	79	33.6	169.40	100.00	13.50	17.00	21.1	15.90
NUE	66	33.4	90.00	53.50			21.2	51.70
NSUC	LO4-3	34.5	10.00	-			28.6	4.10
	LO6-3	33.5	24.90	-			25.3	10.40
	LO3-1	32.9	51.10	-			23.2	22.50
	LO3-5	32.9	51.10	-			22.4	23.00
RUC	LO3-1						23.2	1.10
	LO3-5	32.9					22.4	1.10

Data from SOWA (1963) and SKEMPTON AND SOWA (1963)

*$\bar{p}_k$ = isotropic effective stress after sampling

TABLE 6.18

STRENGTH DATA FOR ISOTROPICALLY CONSOLIDATED TRIAXIAL TESTS ON REMOLDED WEALD CLAY

SERIES	TEST	$\bar{\sigma}_1$ PSI	$\bar{\sigma}_2$ PSI	$\bar{\sigma}_3$ PSI	$\bar{p}$ PSI	q PSI	μ	SIN $\bar{\Phi}$
NUC1	1	32.80	12.00	12.00	22.40	10.40	-1.000	0.464
	2	62.00	23.60	23.60	42.80	19.20	-1.000	0.449
	5	91.80	35.50	35.50	63.65	28.15	-1.000	0.442
	30	129.20	49.20	49.20	89.20	40.00	-1.000	0.448
	32	126.60	49.30	49.30	87.95	38.65	-1.000	0.439
	40	90.00	35.00	35.00	62.50	27.50	-1.000	0.440
	90	114.30	44.40	44.40	79.35	34.95	-1.000	0.440
NUC1(b)	15	31.60	12.10	12.10	21.85	9.75	-1.000	0.446
	16	30.40	11.70	11.70	21.05	9.35	-1.000	0.444
	18	31.20	11.70	11.70	21.45	9.75	-1.000	0.455
	21	31.40	12.10	12.10	21.75	9.65	-1.000	0.444
NUC2	116	31.80	12.70	12.70	22.25	9.55	-1.000	0.429
	113	53.50	20.90	20.90	37.20	16.30	-1.000	0.438
	68	68.50	26.80	26.80	47.65	20.85	-1.000	0.438
	62	93.30	36.70	36.70	65.00	28.30	-1.000	0.435
	58	110.60	42.50	42.50	76.55	34.05	-1.000	0.445

(Continued)

TABLE 6.18

STRENGTH DATA FOR ISOTROPICALLY CONSOLIDATED TRIAXIAL TESTS ON REMOLDED WEALD CLAY

SERIES	TEST	$\bar{\sigma}_1$ PSI	$\bar{\sigma}_2$ PSI	$\bar{\sigma}_3$ PSI	$\bar{p}$ PSI	q PSI	μ	SIN $\bar{\Phi}$
NUC3	70	51.90	19.60	19.60	35.75	16.15	-1.000	0.452
	72	72.40	27.10	27.10	49.75	22.65	-1.000	0.455
	76	71.60	27.90	27.90	49.75	21.85	-1.000	0.439
	95	86.30	34.00	34.00	60.15	26.15	-1.000	0.435
	96	54.10	20.40	20.40	37.25	16.85	-1.000	0.452
	97	34.80	13.30	13.30	24.05	10.75	-1.000	0.447
	107	78.60	30.40	30.40	54.50	24.10	-1.000	0.442
	112	57.60	22.00	22.00	39.80	17.80	-1.000	0.447
	115	55.00	21.90	21.90	38.45	16.55	-1.000	0.430
NUC4	100	29.40	10.20	10.20	19.80	9.60	-1.000	0.485
	102	112.10	40.80	40.80	76.45	35.65	-1.000	0.466
	103	58.90	20.90	20.90	39.90	19.00	-1.000	0.476
	104	92.80	33.20	33.20	63.00	29.80	-1.000	0.473
NUC5	109	43.00	15.80	15.80	29.40	13.60	-1.000	0.463
	110	92.40	34.70	34.70	63.55	28.85	-1.000	0.454
	108	92.10	34.50	34.50	63.30	28.80	-1.000	0.455

(Continued)

TABLE 6.18

STRENGTH DATA FOR ISOTROPICALLY CONSOLIDATED TRIAXIAL TESTS ON REMOLDED WEALD CLAY

SERIES	TEST	$\bar{\sigma}_1$ PSI	$\bar{\sigma}_2$ PSI	$\bar{\sigma}_3$ PSI	$\bar{p}$ PSI	q PSI	μ	SIN $\bar{\Phi}$
NDC	42	79.00	30.00	30.00	54.50	24.50	-1.000	0.450
	43	223.20	90.00	90.00	156.60	66.60	-1.000	0.425
	46	150.00	60.00	60.00	105.00	45.00	-1.000	0.429
	47	299.80	120.00	120.00	209.90	89.90	-1.000	0.428
	49	77.80	30.00	30.00	53.90	23.90	-1.000	0.443
	69	39.30	15.00	15.00	27.15	12.15	-1.000	0.448
	71	134.80	53.50	53.50	94.15	40.65	-1.000	0.432
	75	154.00	62.00	62.00	108.00	46.00	-1.000	0.426
OUC	4	104.80	40.20	40.20	72.50	32.30	-1.000	0.446
	6	83.10	32.10	32.10	57.60	25.50	-1.000	0.443
	33	82.40	30.90	30.90	56.65	25.75	-1.000	0.455
	34	105.20	40.90	40.90	73.05	32.15	-1.000	0.440
	82	65.40	25.20	25.20	45.30	20.10	-1.000	0.444
NUE1	41	23.80	23.80	6.90	15.35	8.45	1.000	0.550
	45	75.30	75.30	27.60	51.45	23.85	1.000	0.464
	54	50.70	50.70	15.00	32.85	17.85	1.000	0.543
	57	50.20	50.20	16.20	33.20	17.00	1.000	0.512
	67	100.30	100.30	35.70	68.00	32.30	1.000	0.475
	87	29.60	29.60	9.40	19.50	10.10	1.000	0.518

(Continued) TABLE 6.18

STRENGTH DATA FOR ISOTROPICALLY CONSOLIDATED TRIAXIAL TESTS ON REMOLDED WEALD CLAY

SERIES	TEST	$\bar{\sigma}_1$ PSI	$\bar{\sigma}_2$ PSI	$\bar{\sigma}_3$ PSI	$\bar{p}$ PSI	q PSI	μ	SIN $\bar{\Phi}$
NUE2	101	27.40	27.40	8.40	17.90	9.50	1.000	0.531
	105	52.80	52.80	18.40	35.60	17.20	1.000	0.483
	106	77.50	77.50	27.70	52.60	24.90	1.000	0.473

Data from SOWA (1963)

TABLE 6.19

STRENGTH DATA FOR K_o CONSOLIDATED TRIAXIAL TESTS ON REMOLDED WEALD CLAY

SERIES	TEST	$\bar{\sigma}_1$ PSI	$\bar{\sigma}_2$ PSI	$\bar{\sigma}_3$ PSI	$\bar{p}$ PSI	q PSI	μ	SIN $\bar{\Phi}$
NUC	35	25.10	9.90	9.90	17.50	7.60	-1.000	0.434
	64	80.50	31.70	31.70	56.10	24.40	-1.000	0.435
	88	111.90	45.70	45.70	78.80	33.10	-1.000	0.420
	85	114.70	59.30	59.30	102.00	42.70	-1.000	0.419
	98	82.30	33.80	33.80	58.05	24.25	-1.000	0.418
	39	30.50	11.80	11.80	21.15	9.35	-1.000	0.442
	48	47.00	18.40	18.40	32.70	14.30	-1.000	0.437
	44	53.80	21.40	21.40	37.60	16.20	-1.000	0.431
	77	144.70	58.80	58.80	101.75	42.95	-1.000	0.422
	80	140.70	57.30	57.30	99.00	41.70	-1.000	0.421
NPSUC	28	24.10	8.90	8.90	16.50	7.60	-1.000	0.461
	63	77.30	29.90	29.90	53.60	23.70	-1.000	0.442
	89	109.80	43.80	43.80	76.80	33.00	-1.000	0.430
	86	141.30	57.70	57.70	99.50	41.80	-1.000	0.420
	99	78.10	30.40	30.40	54.25	23.85	-1.000	0.440
NPSIUC	65	108.00	43.00	43.00	75.50	32.50	-1.000	0.430

(Continued)

TABLE 6.19

STRENGTH DATA FOR K_o CONSOLIDATED TRIAXIAL TESTS ON REMOLDED WEALD CLAY

SERIES	TEST	$\bar{\sigma}_1$	$\bar{\sigma}_2$	$\bar{\sigma}_3$	$\bar{p}$	q	μ	SIN $\bar{\Phi}$
		PSI	PSI	PSI	PSI	PSI		
OUC	92	120.50	49.00	49.00	84.75	35.75	-1.000	0.422
	84	101.40	39.80	39.80	70.60	30.80	-1.000	0.436
	83	64.60	25.80	25.80	45.20	19.40	-1.000	0.429
OPSUC	91	123.30	49.80	49.80	86.55	36.75	-1.000	0.425
	79	69.10	27.10	27.10	48.10	21.00	-1.000	0.437
NUE	66	49.30	49.30	15.40	32.35	16.95	1.000	0.524
NSUC	LO4-3	10.00	3.80	3.80	6.90	3.10	-1.000	0.449
	LO6-3	22.10	8.10	8.10	15.10	7.00	-1.000	0.464
	LO3-1	35.80	13.30	13.30	24.55	11.25	-1.000	0.458
	LO3-5	36.40	12.80	12.80	24.60	11.80	-1.000	0.480
RUC	LO3-1	20.70	7.90	7.90	14.30	6.40	-1.000	0.448
	LO3-5	20.40	7.70	7.70	14.05	6.35	-1.000	0.452

Data from SOWA (1963) and SKEMPTON AND SOWA (1963)

TABLE 6.20

CONSOLIDATION STRESS HISTORIES FOR PLANE STRAIN TESTS ON REMOLDED WEALD CLAY

TEST*	ω_i %	ω_f %	$\bar{\sigma}_{1C}$ PSI	$\bar{\sigma}_{2C}$ PSI	$\bar{\sigma}_{3C}$ PSI	$K_{o,AVG}$+
WC4	32.8	22.3	68.90	39.10	39.10	0.57
WC6	33.0	23.1	54.60	31.40	31.10	0.58
WC7	33.8	23.0	75.90	48.00	47.30	0.62
WC8	32.2	23.2	44.50	25.50	25.00	0.57
WC9	31.0	22.6	48.80	27.80	26.80	0.55
WC10	34.3	20.5	117.40	69.60	69.60	0.595
WC11	33.1	22.5	59.40	37.10	34.20	0.57
WC12	34.4	23.6	43.10	-	27.60	0.64
WC13(0)	60±	20.9	110.00	69.40	60.40	0.545
WC14(0)	106±	25.0	81.10	48.10	48.10	0.595
WC15(0)	35.1	21.0	104.60	62.00	61.10	0.59
WC16(0)	33.9	19.5	157.40	-	96.70	0.62
WC17(0)	32.7	20.4	110.70	-	68.50	0.62
WC18(0)	33.8	21.2	87.50	-	53.40	0.62
WC19(0)	34.3	21.3	65.60	-	65.20	-

*The suffix (0) indicates that the sample was initially consolidated under a small load in a 9 IN diam. x 6 IN deep oedometer. Most of the oedometer specimens were consolidated under a vertical effective stress of 7.7 PSI. Plane strain samples initially consolidated in this manner were formed by placing two 2 IN x 2 IN x 8 IN blocks end to end, so that each of the last 7 samples had a vertical plane of weakness at mid-length. The remaining samples were formed by placing clay in a mold with a spatula.

+The average value of K_o was determined as the slope of a straight line fit to a plot of σ_3 VERSUS σ_1 during consolidation.

Data from WADE (1963).

TABLE 6.21

REMARKS CONCERNING PLANE STRAIN TESTS ON REMOLDED WEALD CLAY

TEST	REMARKS
WC4	Apparatus breakdown caused several false starts, and resulted in a slightly overconsolidated condition at the start of the consolidation stage.
WC7	There was a probable leak in the rubber membrane enclosing the sample.
WC10	Excessive cell leakage caused the consolidation cell pressure to drop from 86 to 50 PSI overnight.
WC11	The intermediate principal stress was controlled automatically, resulting in a higher than average value of $\bar{\sigma}_2$ at the end of consolidation.
WC12	Intermediate principal stress measurements were invalid, due to interference of the loading head with the end clamp.
WC13(0)	The initial water content was high (60±%). Oedometer consolidation to 15 PSI produced an overconsolidation effect. Large temperature flucuations at the end of consolidation caused a large variation in excess pore pressure from that expected.
WC14(0)	The initial water content was high (106±%). The volume change device was not properly de-aired during the assembly process.
WC15(0)	The intermediate principal stress was not measured during consolidation due to a ruptured pressure line.
WC16(0)	There was no end restraint ($\epsilon_{2f} \approx 1.0\%$). Apparatus breakdown caused several false starts, and resulted in a slightly overconsolidated condition at the start of the consolidation stage. During consolidation, the volume change device burst, causing the back pressure to drop from 35 to 22 PSI.

(Continued) TABLE 6.21

REMARKS CONCERNING PLANE STRAIN TESTS ON REMOLDED WEALD CLAY

TEST	REMARKS
WC17(0)	There was no end restraint.
WC18(0)	There was no end restraint (ϵ_{2f} = 1.4%).
WC19(0)	The initial oedometer consolidation phase was one-dimensional, but the final consolidation phase in the plane strain device was isotropic. There was therefore no end restraint.

Information from WADE (1963).

TABLE 6.22

STRENGTH DATA FOR PLANE STRAIN TESTS ON REMOLDED WEALD CLAY

TEST	$\bar{\sigma}_1$ PSI	$\bar{\sigma}_2$ PSI	$\bar{\sigma}_3$ PSI	$\bar{p}$ PSI	q PSI	μ	SIN $\bar{\Phi}$
WC4	61.00	31.70	22.90	41.95	19.05	-0.538	0.454
WC6	50.70	29.50	19.50	35.10	15.60	-0.359	0.444
WC7	66.20	39.00	26.20	46.20	20.00	-0.360	0.433
WC8	41.10	22.90	15.10	28.10	13.00	-0.400	0.463
WC9	45.80	25.90	17.20	31.50	14.30	-0.392	0.454
WC10	108.30	59.10	43.20	75.75	32.55	-0.512	0.430
WC11	56.80	33.50	23.30	40.05	16.75	-0.391	0.418
WC12	39.60	-	14.90	27.25	12.35	-	0.453
WC13(0)	104.60	51.70	38.60	71.60	33.00	-0.603	0.461
WC14(0)	71.70	40.80	28.70	50.20	21.50	-0.437	0.428
WC15(0)	93.40	51.60	34.50	63.95	29.45	-0.419	0.461
WC16(0)	141.80	-	56.70	99.25	42.55	-	0.429
WC17(0)	101.50	-	40.00	70.75	30.75	-	0.435
WC18(0)	76.90	-	29.90	53.40	23.50	-	0.440
WC19(0)	64.50	-	23.90	44.20	20.30	-	0.459

Data from WADE (1963)

TABLE 6.23

AVERAGE POROSITY AT FAILURE FOR PLANE STRAIN AND TRIAXIAL TESTS ON BELGIUM SAND

TEST	n_c %	ϵ_{vf} %	n_f %	TEST	n_c %	ϵ_{vf} %	n_f %
PS1	39.20	0.37	39.42	T2	37.35	2.52	38.89
PS2	37.24	0.42	37.50	T3	39.27	1.80	40.34
PS3	37.93	0.35	38.15	T4	39.76	1.60	40.71
PS4	37.83	0.44	38.10	T5	40.06	1.81	41.13
PS5	40.69	0.06	40.73	T6	42.99	0.60	43.33
PS6	41.78	-0.13	41.70	T7	38.20	2.22	39.54
PS7	41.53	-0.13	41.45	T8	38.16	2.48	39.66
PS8	41.40	0.05	41.43	T9	38.31	2.28*	39.69
PS9	41.53	-0.01	41.52	T10	42.73	0.89	43.24
PS10	31.02	0.33	39.22	T11	42.03	1.07	42.64
PS11	38.71	0.28	38.88	T12	43.18	0.65	43.55
PS12	40.44	0.14*	40.52	T13	38.21	2.25	39.57
PS14	41.72	-0.11	41.66	T14	43.81	0.18	43.91
PS15	41.57	-0.14	41.49	T15	39.40	2.02	40.60
PS16	41.88	-0.18	41.78	T16	42.54	0.57	42.87
PS18	39.39	0.18	39.50	T17	42.58	0.89	43.09
PS19	40.54	0.07	40.58	T15E	42.21	-0.38	41.99
PS20	39.30	0.28	39.47	T27E	38.73	0.78	39.20
				T28E	38.66	0.78	39.13
				T29E	38.98	0.30	39.16

*Estimated from Figure 6.39

n_o and ϵ_{vf} data from WADE (1963)

TABLE 6.24

STRENGTH DATA FROM PLANE STRAIN TESTS ON BELGIUM SAND

TEST	n_f %	$\bar{\sigma}_1$ PSI	$\bar{\sigma}_2$ PSI	$\bar{\sigma}_3$ PSI	$\bar{p}$ PSI	q PSI	μ	SIN $\bar{\Phi}$
PS1	39.4	191.80	72.10	40.40	116.10	75.70	-0.581	0.652
PS2	37.5	203.00	73.90	40.20	121.60	81.40	-0.586	0.669
PS3	38.2	200.70	70.00	40.20	120.45	80.25	-0.629	0.666
PS4	38.1	196.50	67.80	40.20	118.35	78.15	-0.647	0.660
PS5	40.7	165.40	68.00	40.20	102.80	62.60	-0.556	0.609
PS6	41.7	156.50	58.20	40.20	98.35	58.15	-0.690	0.591
PS7	41.4	158.40	62.50	40.20	99.30	59.10	-0.623	0.595
PS8	41.4	163.40	66.40	40.20	101.80	61.60	-0.575	0.605
PS9	41.5	157.90	66.00	40.20	99.05	58.85	-0.562	0.594
PS10	39.2	189.20	69.90	40.20	114.70	74.50	-0.601	0.650
PS11	38.9	187.20	66.30	40.20	113.70	73.50	-0.645	0.646
PS12	40.5*	163.10	67.50	40.20	101.65	61.45	-0.556	0.605
PS14	41.7	157.90	66.00	40.20	99.05	58.85	-0.562	0.594
PS15	41.5	158.10	65.20	40.20	99.15	58.95	-0.576	0.595
PS16	41.8	150.90	61.70	40.20	95.55	55.35	-0.612	0.579
PS18	39.5	176.50	68.40	40.20	108.35	68.15	-0.586	0.629
PS19	40.6	167.80	66.40	40.20	104.00	63.80	-0.589	0.613
PS20	39.5	178.00	73.80	40.20	109.10	68.90	-0.512	0.632

*Estimated from Figure 6.39

Strength data from WADE (1963)

TABLE 6.25

STRENGTH DATA FROM TRIAXIAL TESTS ON BELGIUM SAND

TEST	n_f %	$\bar{\sigma}_1$ PSI	$\bar{\sigma}_2$ PSI	$\bar{\sigma}_3$ PSI	$\bar{p}$ PSI	q PSI	μ	SIN $\bar{\Phi}$
T2	38.9	189.80	40.20	40.20	115.00	74.80	-1.000	0.650
T3	40.3	167.00	40.20	40.20	103.60	63.40	-1.000	0.612
T4	40.7	163.30	40.20	40.20	101.75	61.55	-1.000	0.605
T5	41.1	161.60	40.20	40.20	100.90	60.70	-1.000	0.602
T6	43.3	141.30	40.20	40.20	90.75	50.55	-1.000	0.557
T7	39.5	175.10	40.20	40.20	107.65	67.45	-1.000	0.627
T8	39.7	169.60	40.20	40.20	104.90	64.70	-1.000	0.617
T9	39.7*	169.70	40.20	40.20	104.95	64.75	-1.000	0.617
T10	43.2	141.10	40.20	40.20	90.65	50.45	-1.000	0.557
T11	42.6	145.40	40.20	40.20	92.80	52.60	-1.000	0.567
T12	43.6	139.80	40.20	40.20	90.00	49.80	-1.000	0.553
T13	39.6	181.30	40.20	40.20	110.75	70.55	-1.000	0.637
T14	43.9	136.40	40.20	40.20	88.30	48.10	-1.000	0.545
T15	40.6	164.50	40.20	40.20	102.35	62.15	-1.000	0.607
T16	42.9	140.40	40.20	40.20	90.30	50.10	-1.000	0.555
T17	43.1	142.50	40.20	40.20	91.35	51.15	-1.000	0.560
T15E	42.0	40.30	40.30	10.80	25.55	14.75	1.000	0.577
T27E	39.2	139.80	139.80	32.50	86.15	53.65	1.000	0.623
T28E	39.1	139.80	139.80	33.20	86.50	53.30	1.000	0.616
T29E	39.2	139.80	139.80	36.00	87.90	51.90	1.000	0.590

*Estimated from Figure 6.39

Strength data from WADE (1963)

TABLE 6.26

TRIAXIAL STRENGTH DATA FOR COMMERCIAL KAOLINITE

TEST	β DEG	$\bar{p}$ PSI	q PSI	μ	SIN $\bar{\Phi}$
I-A(1)	0	5.30	4.10	0.000	0.774
I-B(1)	0	18.20	12.80	0.000	0.703
I-C(1)	0	50.00	31.00	0.000	0.620
I-A(7)	90	5.00	3.90	0.000	0.780
I-B(7)	90	17.50	12.00	0.000	0.686
I-C(7)	90	48.00	30.70	0.000	0.640
II-A(21)	0	7.55	4.05	-1.000	0.536
II-A(22)	0	5.78	3.93	-0.492	0.680
II-A(24)	90	4.25	3.85	0.460	0.906
II-A(25)	90	3.35	3.35	1.000	1.000
II-B(21)	0	24.10	12.30	-1.000	0.510
II-B(22)	0	22.45	14.20	-0.580	0.633
II-B(24)	90	14.98	11.42	0.470	0.762
II-B(25)	90	13.25	9.25	1.000	0.698
II-C(21)	0	59.50	30.00	-1.000	0.504
II-C(22)	0	52.60	31.50	-0.500	0.599
II-C(24)	90	46.50	25.00	0.360	0.538
II-C(25)	90	37.75	23.75	1.000	0.629

SERIES	$\bar{\sigma}_C$ PSI
A	7
B	25
C	70

Data from CASBARIAN (1964)

TABLE 6.27

TRIAXIAL STRENGTH DATA FOR REMOLDED OSAKA ALLUVIAL CLAY AT MAXIMUM PRINCIPAL EFFECTIVE STRESS RATIO

TEST	w_f %	$\bar{\sigma}_1$ KG/CM^2	$\bar{\sigma}_2$ KG/CM^2	$\bar{\sigma}_3$ KG/CM^2	$\bar{p}$ KG/CM^2	q KG/CM^2	μ	SIN $\bar{\Phi}$
1	52.5	0.66	0.17	0.17	0.42	0.24	-1.000	0.590
2	47.0	1.13	0.30	0.30	0.72	0.42	-1.000	0.580
3		0.93	0.93	0.25	0.59	0.34	1.000	0.576
4		1.23	0.50	0.30	0.76	0.46	-0.570	0.608
5		1.28	0.69	0.29	0.78	0.50	-0.192	0.631
6		1.24	0.84	0.24	0.74	0.50	0.200	0.676
7	40.2	2.12	0.58	0.58	1.35	0.77	-1.000	0.570
8		1.85	1.85	0.51	1.18	0.67	1.000	0.568
9		2.20	0.78	0.58	1.39	0.81	-0.753	0.583
10		2.22	0.95	0.55	1.38	0.84	-0.521	0.603
11		2.27	1.16	0.56	1.42	0.86	-0.298	0.604
12		2.28	1.38	0.58	1.43	0.85	-0.059	0.594
13		2.22	1.58	0.58	1.40	0.82	0.220	0.586
14	36.0	3.41	0.93	0.93	2.17	1.24	-1.000	0.571
15		2.83	2.83	0.82	1.82	1.00	1.000	0.551
16		3.59	1.27	0.97	2.28	1.31	-0.771	0.575
17		3.63	1.50	0.90	2.26	1.36	-0.560	0.603
18		3.51	1.82	0.82	2.16	1.34	-0.257	0.621

Data from SHIBATA AND KARUBE (1965)

TABLE 6.28

TRIAXIAL STRENGTH DATA FOR REMOLDED OSAKA ALLUVIAL CLAY AT MAXIMUM PRINCIPAL STRESS DIFFERENCE

TEST	ϵ_f %	$\bar{\sigma}_1$ KG/CM^2	$\bar{\sigma}_2$ KG/CM^2	$\bar{\sigma}_3$ KG/CM^2	$\bar{P}$ KG/CM^2	q KG/CM^2	μ	SIN $\bar{\Phi}$
1		0.70	0.20	0.20	0.45	0.25	-1.000	0.556
2	9.00	1.18	0.34	0.34	0.75	0.42	-1.000	0.553
3		0.93	0.93	0.25	0.59	0.34	1.000	0.576
4	5.80	1.34	0.57	0.37	0.86	0.48	-0.588	0.567
5	5.50	1.28	0.69	0.29	0.78	0.50	-0.192	0.631
6	4.50	1.24	0.84	0.24	0.74	0.50	0.200	0.676
7	8.75	2.24	0.64	0.64	1.44	0.80	-1.000	0.556
8		1.85	1.85	0.51	1.18	0.67	1.000	0.568
9	7.85	2.32	0.84	0.64	1.48	0.84	-0.762	0.568
10	7.50	2.32	1.02	0.62	1.47	0.85	-0.529	0.578
11	6.40	2.44	1.22	0.62	1.53	0.91	-0.341	0.595
12	5.50	2.38	1.42	0.62	1.50	0.88	-0.091	0.587
13	4.60	2.36	1.65	0.65	1.50	0.86	0.170	0.568
14	9.80	3.52	1.00	1.00	2.26	1.26	-1.000	0.558
15		2.83	2.83	0.82	1.82	1.00	1.000	0.551
16	8.30	3.69	1.32	1.02	2.36	1.34	-0.775	0.567
17	7.75	3.68	1.54	0.94	2.31	1.37	-0.562	0.593
18	6.60	3.62	1.91	0.91	2.26	1.36	-0.262	0.598

Data from SHIBATA AND KARUBE (1965)

TABLE 6.29

TRIAXIAL STRENGTH DATA FOR STANDARD OTTAWA SAND

TEST	n_f %	$\bar{\sigma}_1$ PSI	$\bar{\sigma}_2$ PSI	$\bar{\sigma}_3$ PSI	$\bar{p}$ PSI	q PSI	μ	SIN $\bar{\Phi}$
			JUST BEFORE YIELD					
4-4	34.3	34.77	9.18	8.70	21.74	13.04	-0.963	0.600
8-5	33.9	34.32	12.63	5.60	19.96	14.36	-0.510	0.719
13-5	34.0	33.28	14.37	4.84	19.06	14.22	-0.330	0.746
12-5	34.1	32.24	15.74	4.41	18.32	13.92	-0.186	0.759
11-5	34.1	31.18	16.93	4.18	17.68	13.50	-0.056	0.764
10-4	34.3	29.51	19.02	3.57	16.54	12.97	0.191	0.784
15-5	33.9	28.35	20.00	3.64	16.00	12.36	0.324	0.772
14-5	34.2	27.59	21.11	3.25	15.42	12.17	0.468	0.789
9-4	34.4	26.57	22.45	3.11	14.84	11.73	0.649	0.790
5-6	34.2	24.97	23.59	3.03	14.00	10.97	0.874	0.784
			JUST AFTER YIELD					
4-4	34.3	35.64	8.65	8.25	21.94	13.70	-0.971	0.624
8-5	33.9	35.32	12.31	5.02	20.17	15.15	-0.519	0.751
13-5	34.0	33.74	14.25	4.68	19.21	14.53	-0.341	0.756
12-5	34.1	32.69	15.66	4.21	18.45	14.24	-0.196	0.772
11-5	34.1	31.68	16.89	3.95	17.82	13.86	-0.067	0.778
10-4	34.3	29.96	19.07	3.26	16.61	13.35	0.184	0.804
15-5	33.9	28.83	20.09	3.31	16.07	12.76	0.315	0.794

(Continued)

TABLE 6.29

TRIAXIAL STRENGTH DATA FOR STANDARD OTTAWA SAND

TEST	n_f	$\bar{\sigma}_1$	$\bar{\sigma}_2$	$\bar{\sigma}_3$	$\bar{p}$	q	μ	SIN $\bar{\Phi}$
	%	PSI	PSI	PSI	PSI	PSI		
14-5	34.2	28.03	21.25	2.90	15.46	12.56	0.460	0.812
9-4	34.4	27.03	22.65	2.69	14.86	12.17	0.640	0.819
5-6	34.2	24.31	23.94	2.51	13.41	10.90	0.966	0.813

$\sigma_{OCT,f} \approx$ 18 PSI for all tests.

Data from Bell (1965)

TABLE 6.30

TRIAXIAL STRENGTH DATA FOR A SILTY SAND

TEST	$\bar{\sigma}_1$ PSI	$\bar{\sigma}_2$ PSI	$\bar{\sigma}_3$ PSI	$\bar{p}$ PSI	q PSI	μ	SIN $\bar{\Phi}$
1	12.60	1.74	1.74	7.17	5.43	-1.000	0.757
2	21.90	3.50	3.50	12.70	9.20	-1.000	0.724
3	24.10	4.50	3.50	13.80	10.30	-0.903	0.746
4	29.50	5.50	3.50	16.50	13.00	-0.846	0.788
5	32.20	6.50	3.50	17.85	14.35	-0.791	0.804
6	33.60	6.50	3.50	18.55	15.05	-0.801	0.811
7	30.12	5.22	5.22	17.67	12.45	-1.000	0.705
8	37.02	6.22	5.22	21.12	15.90	-0.937	0.753
9	39.72	7.22	5.22	22.47	17.25	-0.884	0.768
10	44.72	8.22	5.22	24.97	19.75	-0.848	0.791
11	39.85	6.95	6.95	23.40	16.45	-1.000	0.703
12	47.85	7.95	6.95	27.40	20.45	-0.951	0.746
13	49.25	8.95	6.95	28.10	21.15	-0.905	0.753
14	53.75	9.95	6.95	30.35	23.40	-0.872	0.771
15	52.00	8.70	8.70	30.35	21.65	-1.000	0.713

Data from LENOE (1966)

TABLE 6.31

TRIAXIAL STRENGTH DATA FOR COMMERCIAL KAOLINITE

TEST	β	$\bar{\sigma}_1$	$\bar{\sigma}_2$	$\bar{\sigma}_3$	$\bar{p}$	q	μ	R
	DEG	PSI	PSI	PSI	PSI	PSI		PSI/HR
A1	0	76.78	27.46	27.46	52.12	24.66	-1.000	67.05
A2	0	75.16	26.02	26.02	50.59	24.57	-1.000	27.54
A3	0	77.46	29.52	29.52	53.49	23.97	-1.000	13.50
A4	0	74.80	28.90	28.90	51.85	22.95	-1.000	2.70
A5	0	71.70	29.40	29.40	50.55	21.15	-1.000	1.35
B1	0	70.30	22.60	22.60	46.45	23.85	-1.000	12.70
B2	0	69.26	22.37	22.37	45.82	23.44	-1.000	8.16
C1	15	70.25	22.10	18.65	44.45	25.80	-0.866	12.70
D1	31.75	66.31	28.65	14.24	40.28	26.04	-0.447	6.35
D2	31.75	64.99	29.62	16.09	40.54	24.45	-0.447	4.30
D3	31.75	62.39	27.52	14.19	38.29	24.10	-0.447	2.14
D4	31.75	63.81	28.79	15.40	39.60	24.20	-0.447	1.06
D5	31.75	58.71	28.23	16.56	37.64	21.08	-0.446	0.455
E1	45	62.55	38.60	14.65	38.60	23.95	0	6.685
E2	45	64.48	40.80	17.12	40.80	23.68	0	4.318
E3	45	59.54	36.80	14.06	36.80	22.74	0	2.519
E4	45	59.53	38.00	16.47	38.00	21.53	0	1.127
E5	45	NO PORE PRESSURE MEASUREMENT					0	0.577
F1	58.25	59.90	47.49	15.01	37.46	22.44	0.447	6.674
F2	58.25	59.40	46.99	14.51	36.96	22.44	0.447	4.22
F3	58.25	58.05	45.86	13.99	36.02	22.03	0.447	2.183

(Continued)

TABLE 6.31

TRIAXIAL STRENGTH DATA FOR COMMERCIAL KAOLINITE

TEST	β DEG	$\bar{\sigma}_1$ PSI	$\bar{\sigma}_2$ PSI	$\bar{\sigma}_3$ PSI	$\bar{p}$ PSI	q PSI	μ	R PSI/HR
F4	58.25	59.30	46.89	14.41	36.86	22.44	0.447	1.112
F5	58.25	58.60	46.19	13.71	36.16	22.44	0.447	0.558
G1	75	57.80	54.90	13.30	35.55	22.25	0.870	13.33
H1	90	55.80	55.80	10.80	33.30	22.50	1.000	13.33

Data from SAADA AND BAAH (1966)

TABLE 6.32

TRIAXIAL STRENGTH DATA FOR STANDARD OTTAWA SAND

TEST	n_i %	$\bar{\sigma}_1$ PSI	$\bar{\sigma}_2$ PSI	$\bar{\sigma}_3$ PSI	$\bar{p}$ PSI	q PSI	μ	SIN $\bar{\Phi}$
				BEFORE YIELD				
TCa-1	33.8	44.25	7.88	7.88	26.06	18.18	-1.000	0.698
TCa-2	35.1	40.78	9.61	9.61	25.20	15.58	-1.000	0.619
TCa-3	37.9	39.63	10.19	10.19	24.91	14.72	-1.000	0.591
TCa-4	38.9	38.48	10.76	10.76	24.62	13.86	-1.000	0.563
TCa-5	40.1	37.32	11.34	11.34	24.33	12.99	-1.000	0.534
TCa-6	34.9	30.59	7.21	7.21	18.90	11.69	-1.000	0.619
RS75-1	34.7	39.18	14.86	5.96	22.57	16.61	-0.464	0.736
RS75-2	37.8	35.84	15.76	8.41	22.12	13.72	-0.464	0.620
RS60-1	34.2	35.00	20.00	5.00	20.00	15.00	0.000	0.750
RS60-2	38.0	33.00	20.00	7.00	20.00	13.00	0.000	0.650
RS45-1	34.5	31.43	24.18	4.39	17.91	13.52	0.464	0.755
RS45-2	37.9	30.21	23.74	6.06	18.14	12.08	0.464	0.666
TEa-1	33.4	27.91	27.91	4.18	16.04	11.86	1.000	0.739
TEa-2	35.0	27.62	27.62	4.76	16.19	11.43	1.000	0.706
TEa-3	39.0	26.76	26.76	6.49	16.62	10.14	1.000	0.610
TEa-4	40.1	26.47	26.47	7.07	16.77	9.70	1.000	0.578
TEa-5	34.7	20.50	20.50	4.00	12.25	8.25	1.000	0.673
A-1	34.2	40.79	9.61	9.61	25.20	15.59	-1.000	0.619
A-2	38.0	32.50	20.00	7.50	20.00	12.50	0.000	0.625

(Continued)

TABLE 6.32

TRIAXIAL STRENGTH DATA FOR STANDARD OTTAWA SAND

TEST	n_i %	$\bar{\sigma}_1$ PSI	$\bar{\sigma}_2$ PSI	$\bar{\sigma}_3$ PSI	$\bar{p}$ PSI	q PSI	μ	SIN $\bar{\Phi}$
				AFTER YIELD				
TCa-1	33.8	45.40	7.30	7.30	26.35	19.05	-1.000	0.723
TCa-2	35.1	43.09	8.45	8.45	25.77	17.32	-1.000	0.672
TCa-3	37.9	40.78	9.61	9.61	25.20	15.58	-1.000	0.619
TCa-4	38.9	39.63	10.19	10.19	24.91	14.72	-1.000	0.591
TCa-5	40.1	38.48	10.76	10.76	24.62	13.86	-1.000	0.563
TCa-6	34.9	32.32	6.34	6.34	19.33	12.99	-1.000	0.672
RS75-1	34.7	40.30	14.56	5.14	22.72	17.58	-0.464	0.774
RS75-2	37.8	36.95	15.46	7.59	22.27	14.68	-0.464	0.659
RS60-1	34.2	35.50	20.00	4.50	20.00	15.50	0.000	0.775
RS60-2	38.0	33.50	20.00	6.50	20.00	13.50	0.000	0.675
RS45-1	34.5	31.84	24.33	3.83	17.84	14.00	0.464	0.785
RS45-2	37.9	30.61	23.89	5.50	18.06	12.56	0.464	0.695
TEa-1	33.4	28.20	28.20	3.60	15.90	12.30	1.000	0.774
TEa-2	35.0	27.91	27.91	4.18	16.04	11.86	1.000	0.739
TEa-3	39.0	27.04	27.04	5.91	16.48	10.56	1.000	0.641
TEa-4	40.1	26.76	26.76	6.49	16.62	10.14	1.000	0.610
TEa-5	34.7	20.72	20.72	3.57	12.14	8.58	1.000	0.706
A-1	34.2	43.09	8.45	8.45	25.77	17.32	-1.000	0.672
A-2	38.0	33.00	20.00	7.00	20.00	13.00	0.000	0.650

Data from KO (1966)

TABLE 6.33

AVERAGE TRIAXIAL STRENGTH DATA FOR STANDARD OTTAWA SAND

TEST	μ	n_i %	SIN $\bar{\Phi}_{(-)}$	SIN $\bar{\Phi}_{(+)}$	SIN $\bar{\Phi}$
TCa-1	-1.000	33.8	0.698	0.723	0.710
TCa-2		35.1	0.619	0.672	0.646
TCa-3		37.9	0.591	0.619	0.605
TCa-4		38.9	0.563	0.591	0.577
TCa-5		40.1	0.534	0.563	0.548
TCa-6		34.9	0.619	0.672	0.646
RS75-1	-0.464	34.7	0.736	0.774	0.755
RS75-2		37.8	0.620	0.659	0.640
RS60-1	0.000	34.2	0.750	0.775	0.762
RS60-2		38.0	0.650	0.675	0.662
RS45-1	0.464	34.5	0.755	0.785	0.770
RS45-2		37.9	0.666	0.695	0.680
TEa-1	1.000	33.4	0.739	0.774	0.756
TEa-2		35.0	0.706	0.739	0.722
TEa-3		39.0	0.610	0.641	0.626
TEa-4		40.1	0.578	0.610	0.594
TEa-5		34.7	0.673	0.706	0.690

Data from KO (1966)

TABLE 6.34

TRIAXIAL STRENGTH DATA FOR RESEDIMENTED BOSTON BLUE CLAY

TEST	$\bar{\sigma}_{1c}$ KG/CM^2	w_f %	$\bar{\sigma}_1$ KG/CM^2	$\bar{\sigma}_2$ KG/CM^2	$\bar{\sigma}_3$ KG/CM^2	$\bar{p}$ KG/CM^2	q KG/CM^2	μ	SIN $\bar{\Phi}$
CC1	4.10	25.9	4.39	1.69	1.69	3.04	1.35	-1.000	0.444
CC2	6.10	23.3	6.64	2.64	2.64	4.64	2.00	-1.000	0.431
CC114.2	3.96	30.8	4.09	1.60	1.60	2.84	1.24	-1.000	0.438
CE1	4.04	26.1	1.12	1.12	0.05	0.58	0.54	1.000	0.915
CE2	4.03	26.5	1.33	1.33	0.32	0.82	0.50	1.000	0.612
CE4	4.00	26.0	1.70	1.70	0.38	1.04	0.66	1.000	0.635
CE5	6.00	23.1	2.31	2.31	0.60	1.46	0.86	1.000	0.588
PSA1	1.91	31.4	1.87	0.78	0.40	1.14	0.74	-0.483	0.648
PSA2	3.86	30.1	3.48	1.54	1.05	2.26	1.22	-0.597	0.536
PSA3	3.82	29.2	3.71	1.49	0.98	2.34	1.36	-0.626	0.582
PSA4	3.88	28.1	4.14	1.87	1.43	2.78	1.36	-0.675	0.487
PSP1	4.63	27.1	2.71	1.43	0.48	1.60	1.12	-0.148	0.699
PSP2	3.85	27.8	2.47	1.57	0.42	1.44	1.02	0.122	0.709

Data from LADD AND VARALLYAY (1965), MERKLE (1967), DICKEY (1967), RIXNER (1967) and DICKEY, LADD AND RIXNER (1968)

TABLE 6.35

INFLUENCE OF THE INTERMEDIATE PRINCIPAL STRESS ON THE STRENGTH OF VOLGA SAND

μ	D_K	r	SIN $\bar{\Phi}$
-1.0	0.28062	1.19057	0.58653
-0.9	0.28007	1.18824	0.60929
-0.8	0.27837	1.18102	0.63065
-0.7	0.27551	1.16889	0.65008
-0.6	0.27164	1.15247	0.66726
-0.5	0.26699	1.13274	0.68207
-0.4	0.26182	1.11081	0.69445
-0.3	0.25642	1.08790	0.70457
-0.2	0.25103	1.06503	0.71258
-0.1	0.24586	1.04310	0.71872
0	0.24104	1.02265	0.72312
0.1	0.23669	1.00419	0.72605
0.2	0.23285	0.98790	0.72760
0.3	0.22956	0.97394	0.72797
0.4	0.22682	0.96232	0.72731
0.5	0.22461	0.95294	0.72570
0.6	0.22290	0.94568	0.72326
0.7	0.22164	0.94034	0.72005
0.8	0.22080	0.93678	0.71621
0.9	0.22033	0.93478	0.71178
1.0	0.22018	0.93414	0.70682

$$r = 3\sqrt{2}\, D_K$$

Data for LOMIZE AND KRYZHANOVSKY (1967)

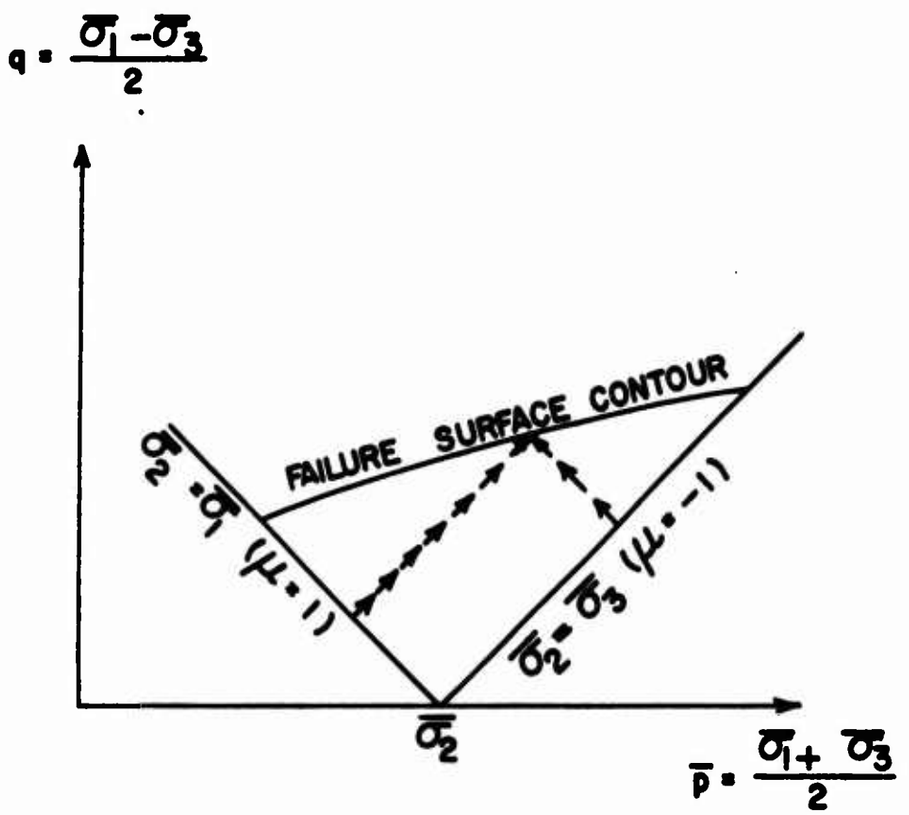

FIGURE 6.1

CONSTANT $\bar{\sigma}_2$ CONTOUR OF ASSUMED FAILURE SURFACE

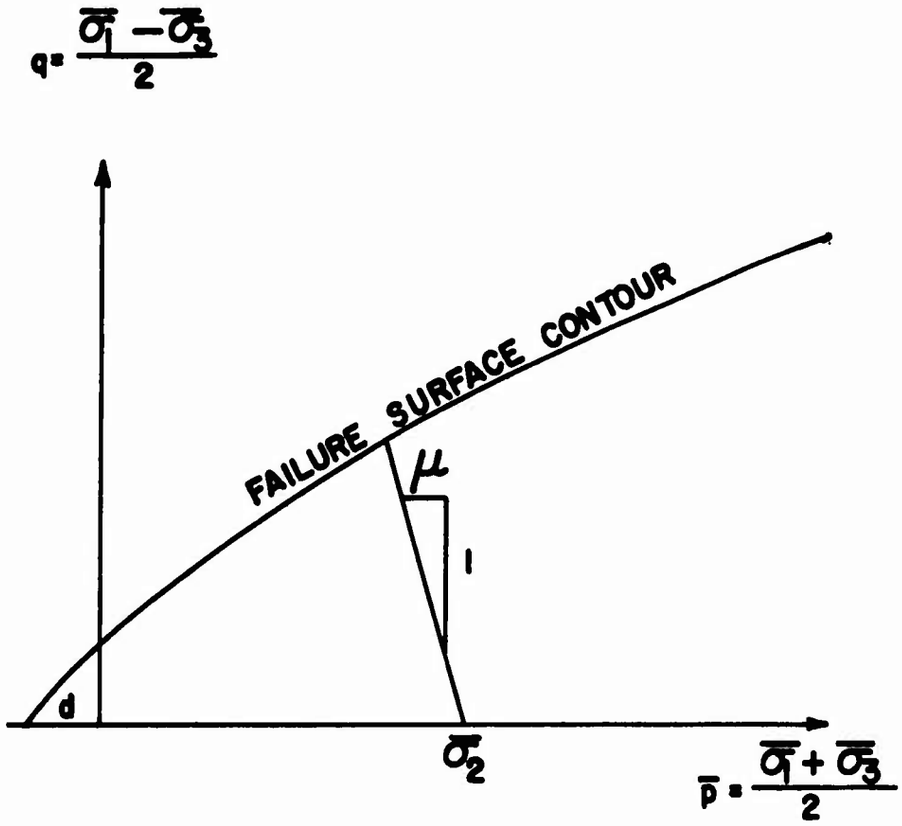

FIGURE 6.2

CONSTANT μ CONTOUR OF ASSUMED FAILURE SURFACE

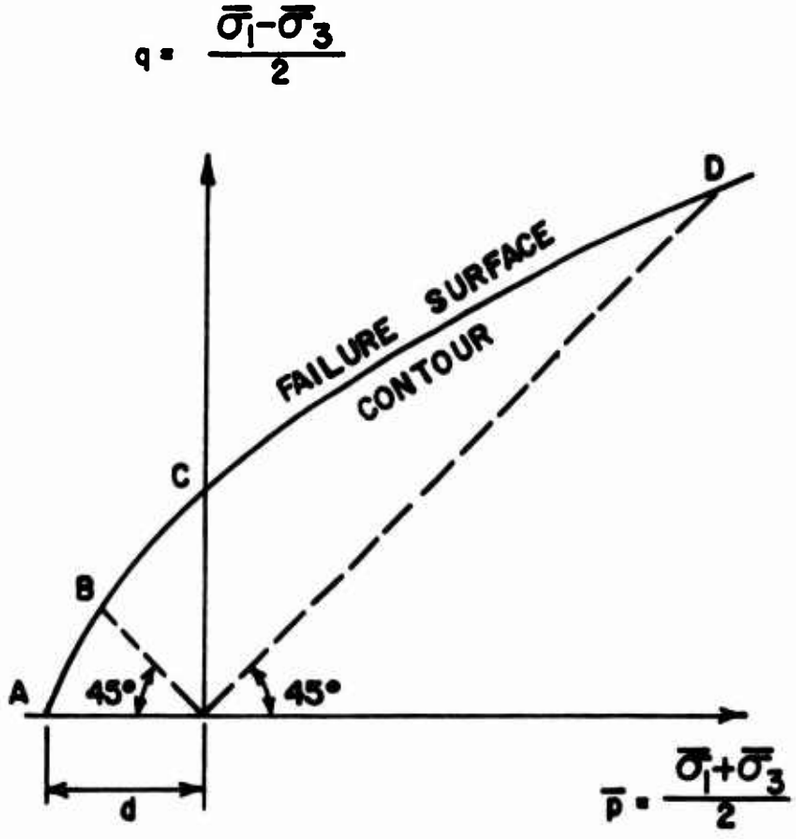

POINT	PHYSICAL SIGNIFICANCE	
A	HYDROSTATIC TENSION	
B	PURE TENSION	} IN 1-3 PLANE
C	PURE SHEAR	
D	PURE COMPRESSION	

FIGURE 6.3

PHYSICAL SIGNIFICANCE OF POINTS ON A FAILURE SURFACE CONTOUR

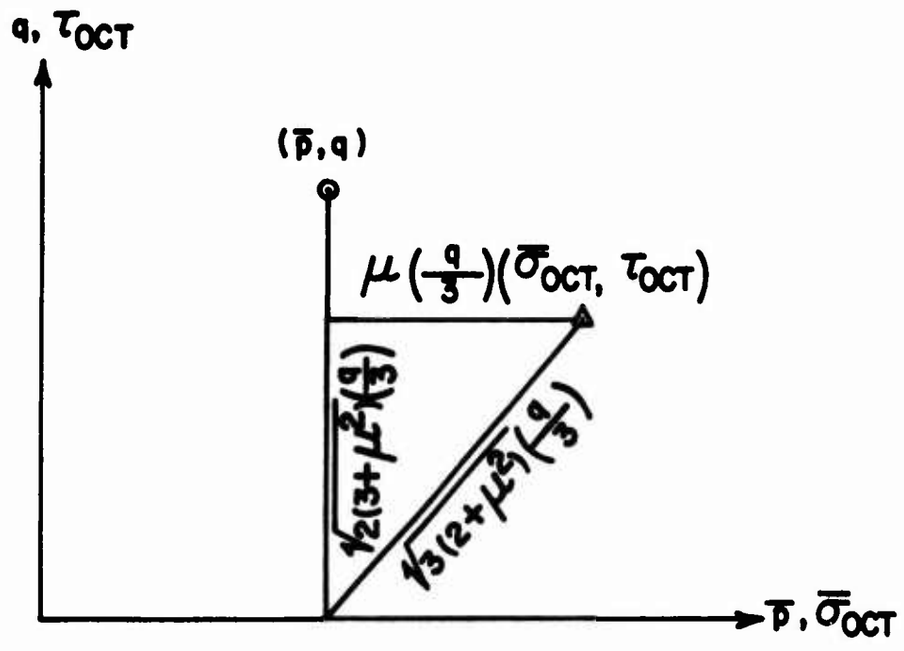

FIGURE 6.4
RELATION BETWEEN THE
PARAMETERS $\bar{p}, q, \mu, \bar{\sigma}_{OCT}$ AND τ_{OCT}

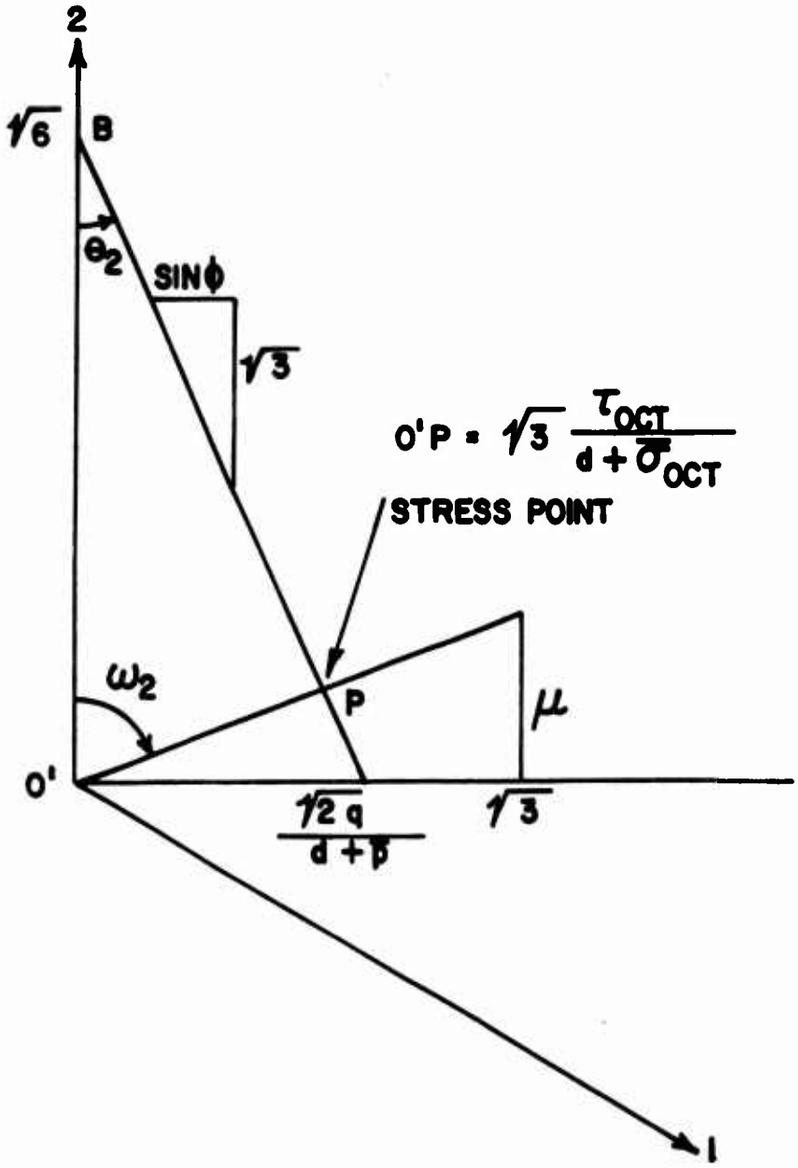

FIGURE 6.5
LOCATION OF A STRESS POINT IN
THE OCTAHEDRAL PLANE

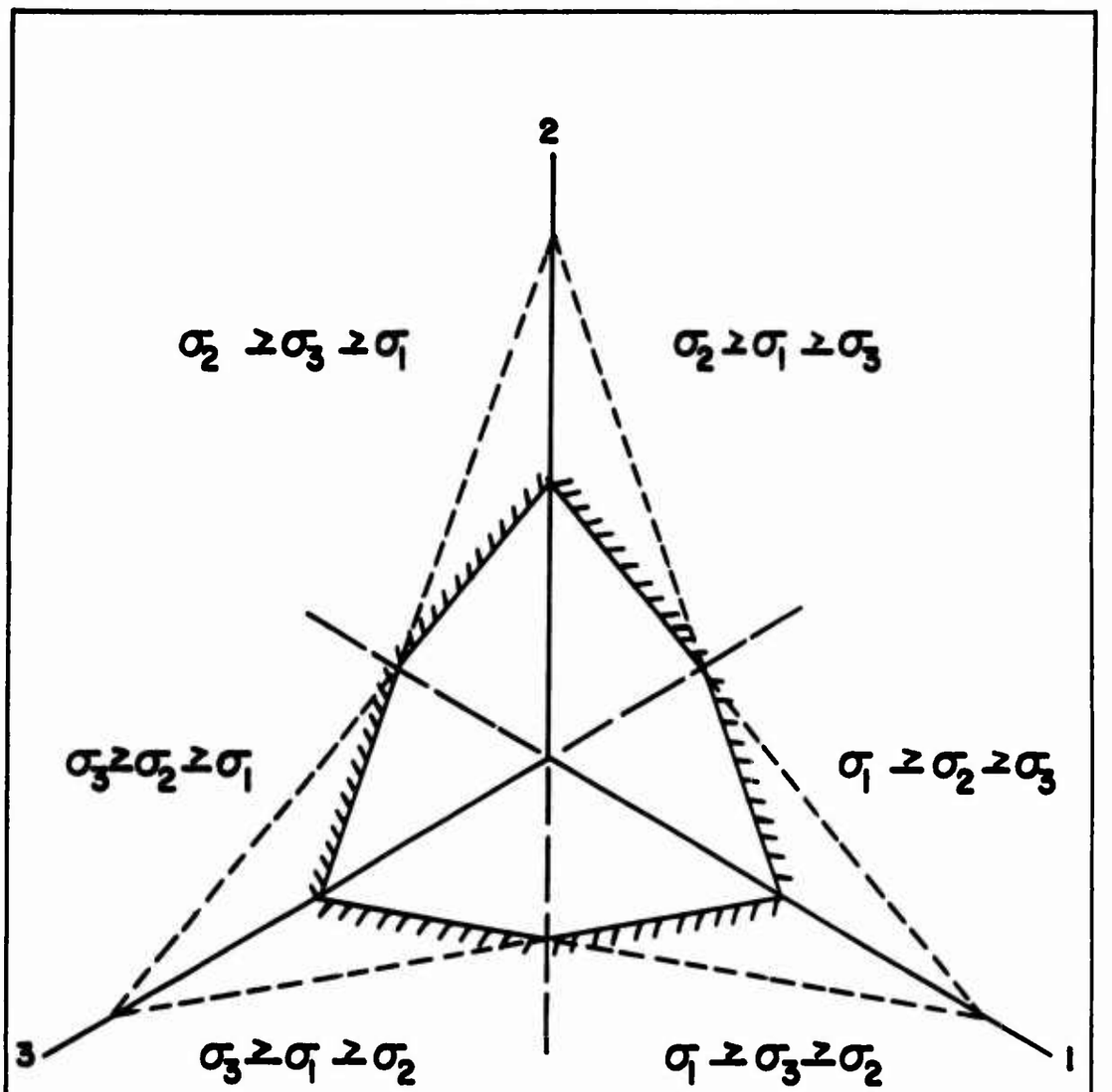

FIGURE 6.6

OCTAHEDRAL PLANE PLOT OF THE COMPLETE MOHR–COULOMB FAILURE CRITERION

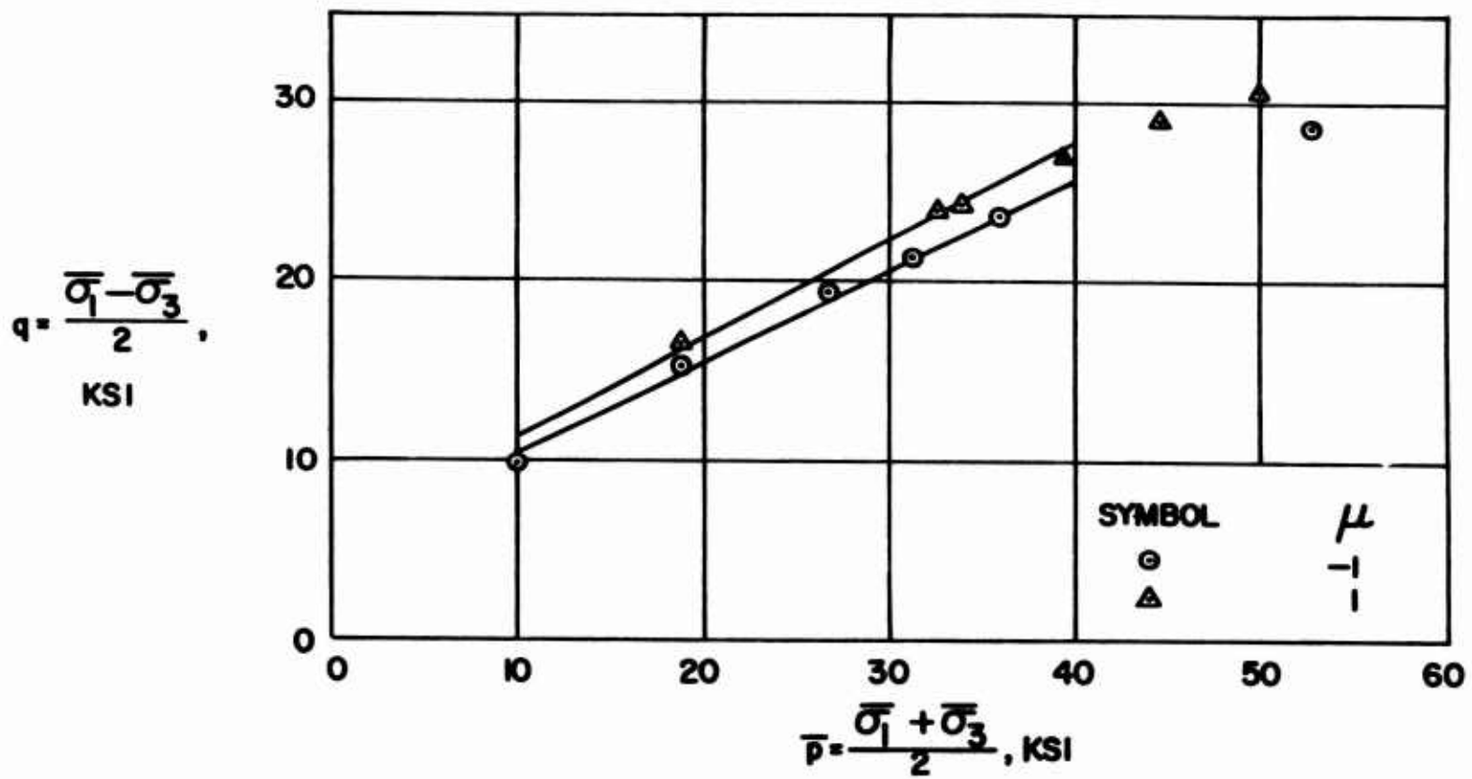

TESTS BY VON KARMAN (1911) AND BOKER (1915)
DATA FROM RUTLEDGE (1939)

FIGURE 6.7

TRIAXIAL STRENGTH DATA FOR CARRARA MARBLE

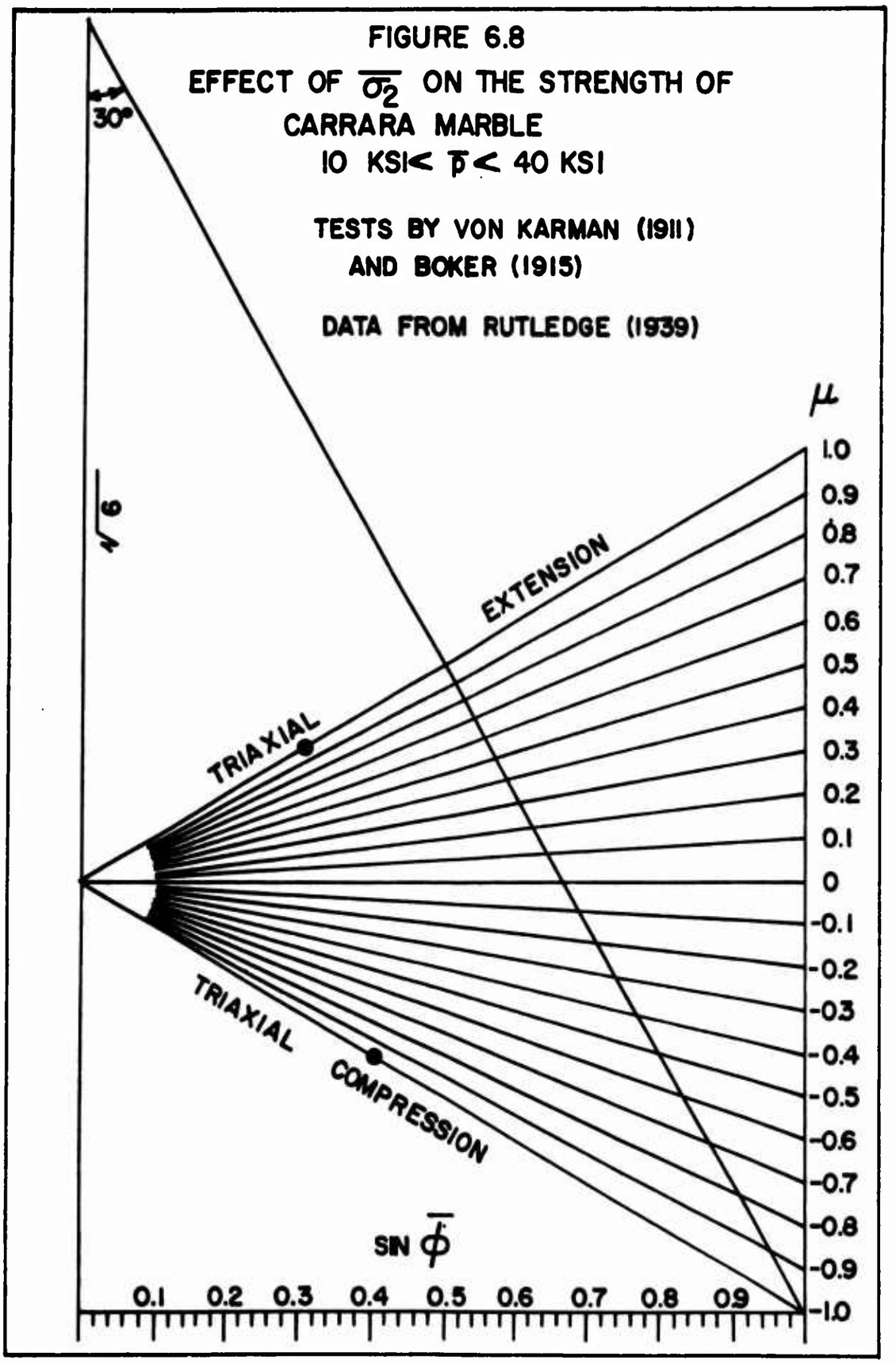

FIGURE 6.8

EFFECT OF $\overline{\sigma_2}$ ON THE STRENGTH OF CARRARA MARBLE

10 KSI $< \bar{p} <$ 40 KSI

TESTS BY VON KARMAN (1911) AND BOKER (1915)

DATA FROM RUTLEDGE (1939)

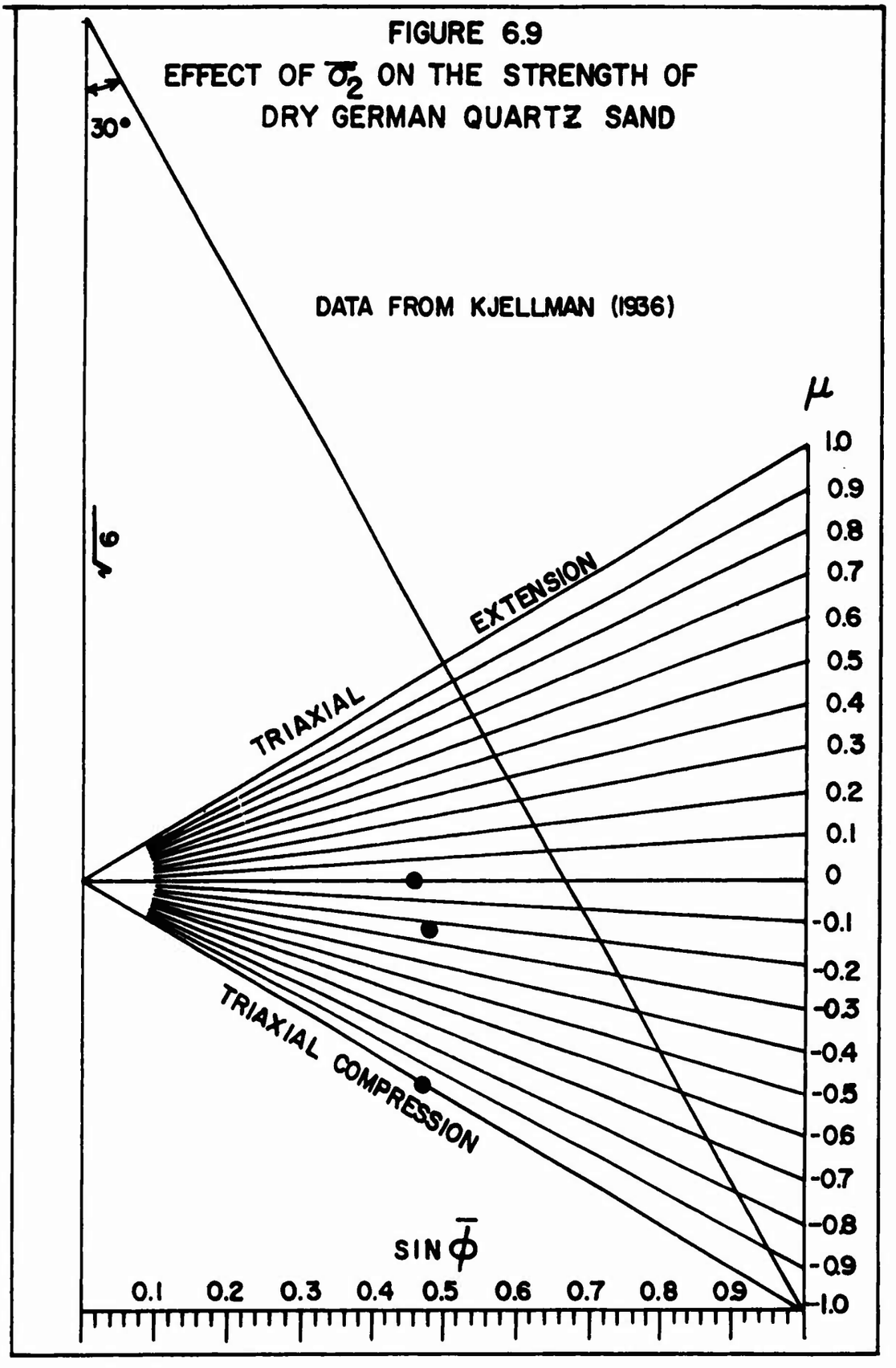
FIGURE 6.9
EFFECT OF $\bar{\sigma}_2$ ON THE STRENGTH OF
DRY GERMAN QUARTZ SAND
DATA FROM KJELLMAN (1936)
30°
$\sqrt{6}$
μ
1.0
0.9
0.8
0.7
0.6
0.5
0.4
0.3
0.2
0.1
0
-0.1
-0.2
-0.3
-0.4
-0.5
-0.6
-0.7
-0.8
-0.9
-1.0
EXTENSION
TRIAXIAL
TRIAXIAL COMPRESSION
SIN $\bar{\phi}$
0.1 0.2 0.3 0.4 0.5 0.6 0.7 0.8 0.9

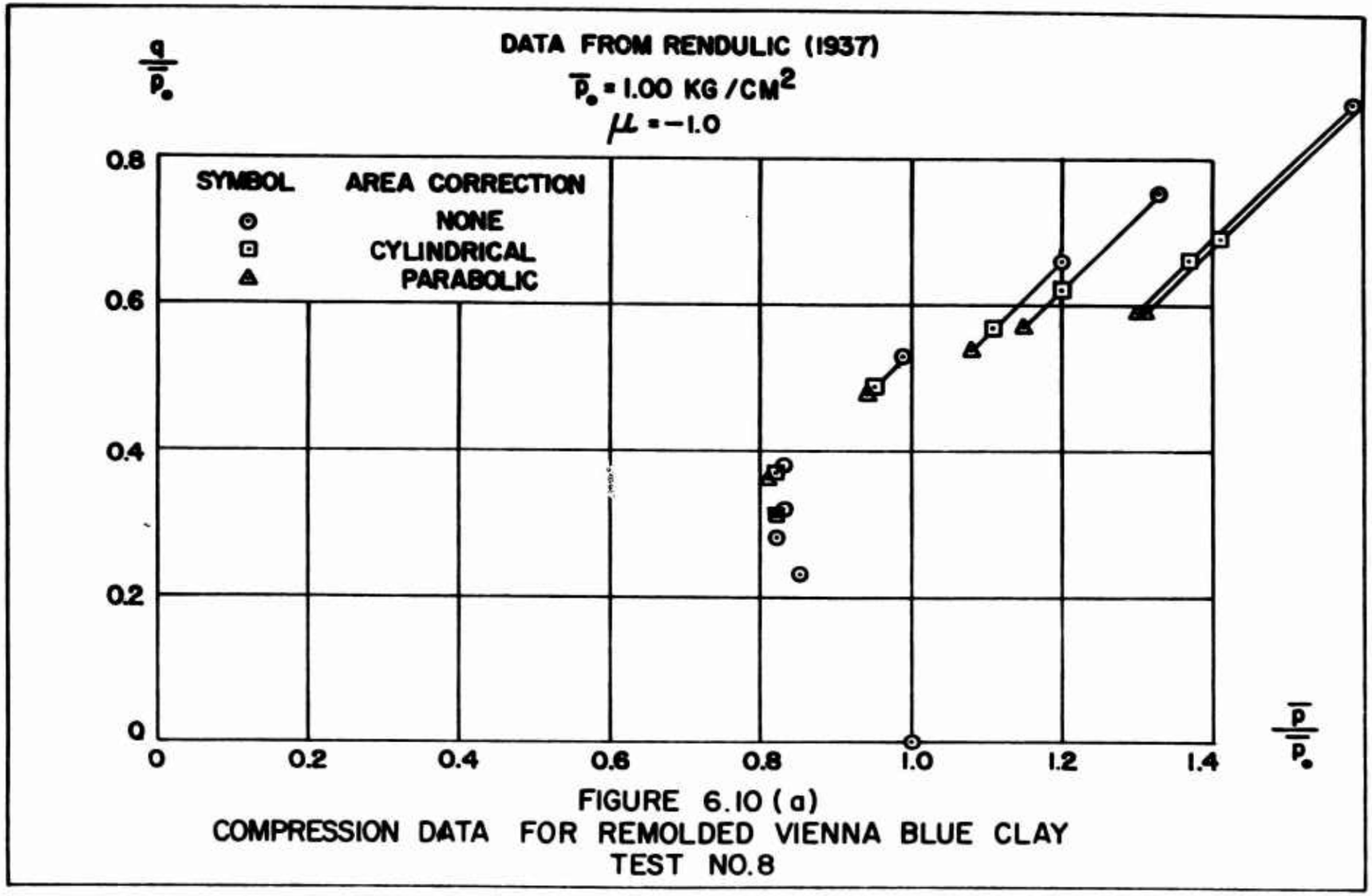

FIGURE 6.10 (a)
COMPRESSION DATA FOR REMOLDED VIENNA BLUE CLAY
TEST NO.8

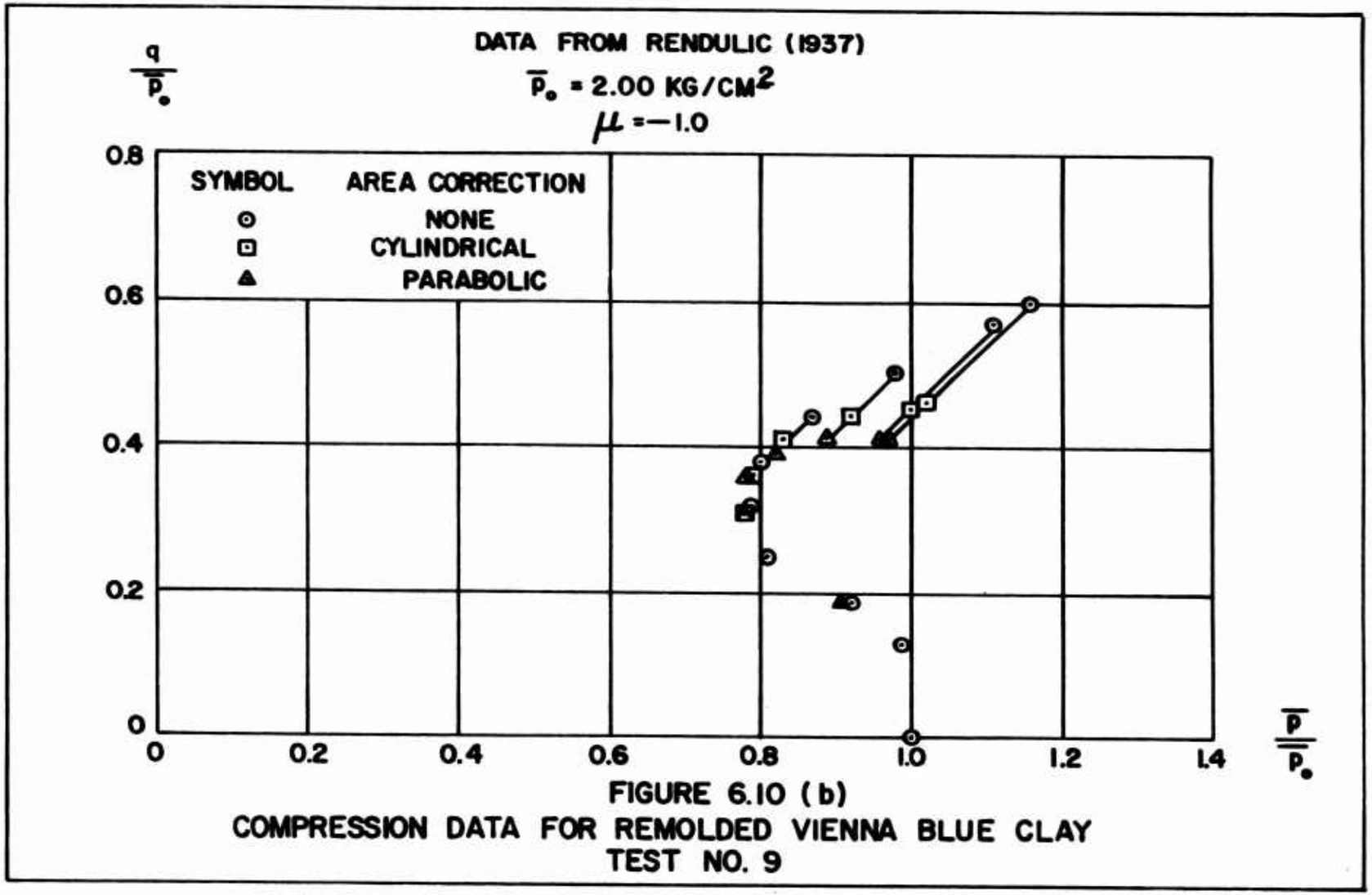

FIGURE 6.10 (b)
COMPRESSION DATA FOR REMOLDED VIENNA BLUE CLAY
TEST NO. 9

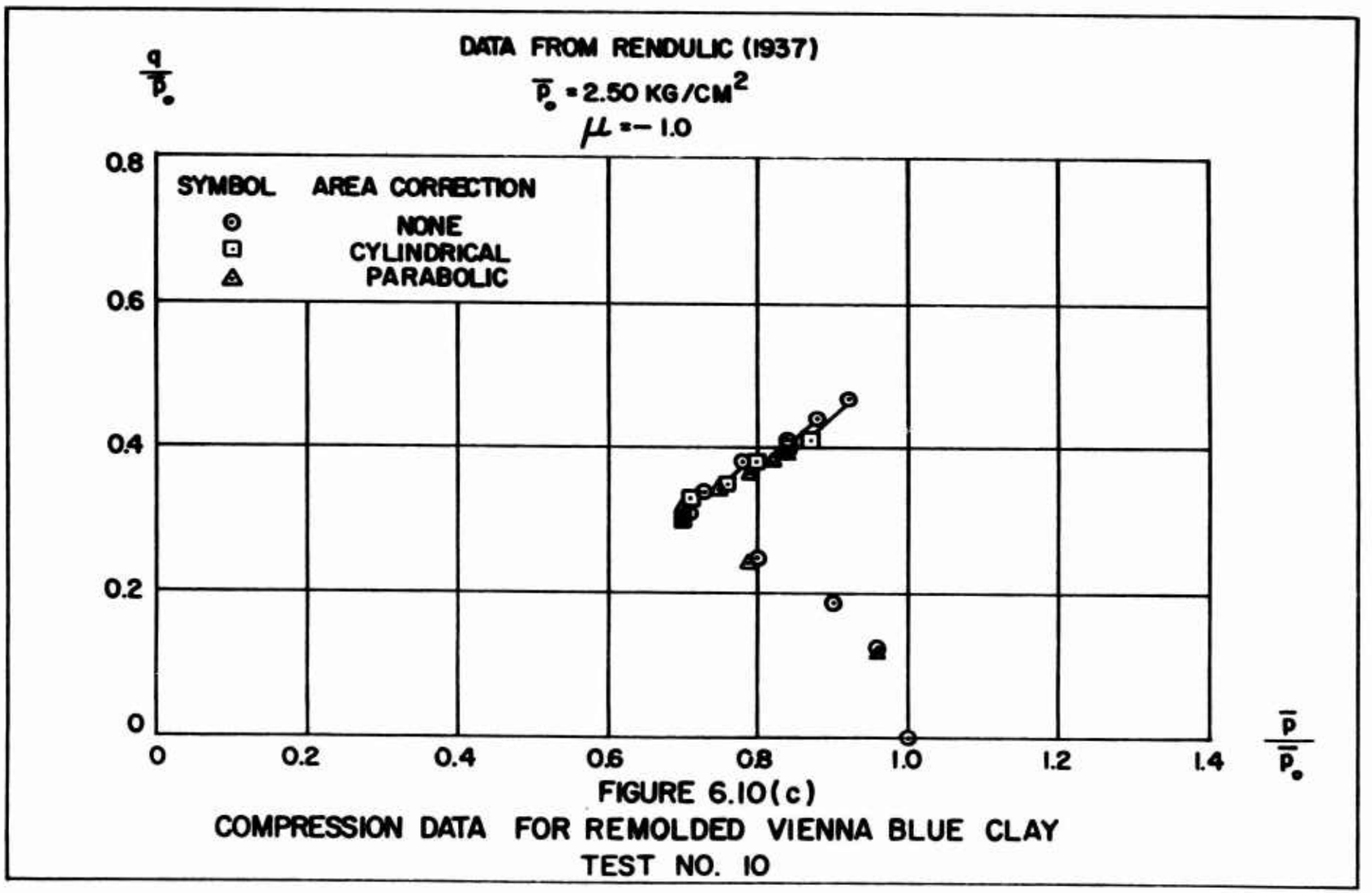

FIGURE 6.10(c)

COMPRESSION DATA FOR REMOLDED VIENNA BLUE CLAY

TEST NO. 10

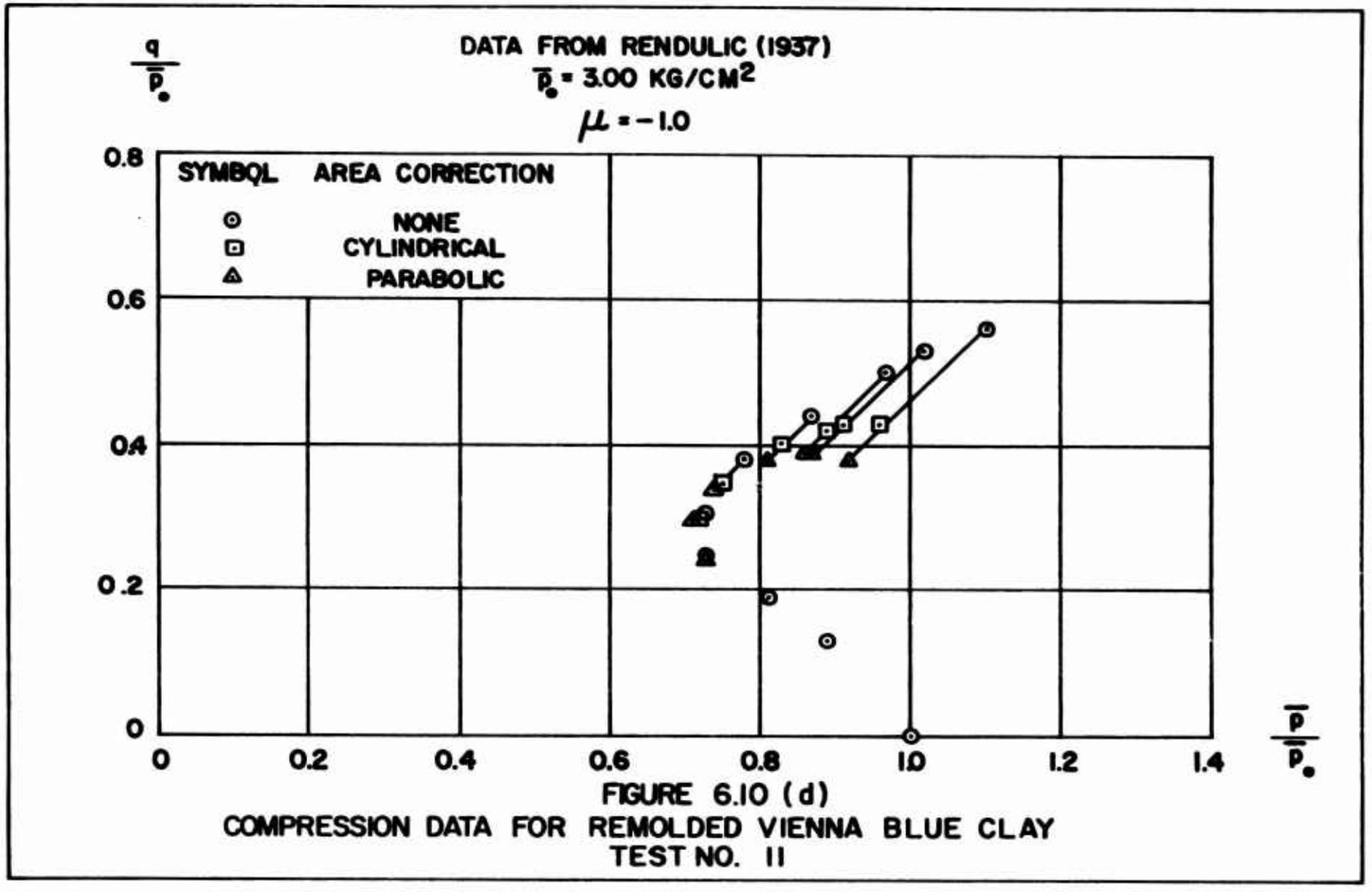

FIGURE 6.10 (d)
COMPRESSION DATA FOR REMOLDED VIENNA BLUE CLAY
TEST NO. 11

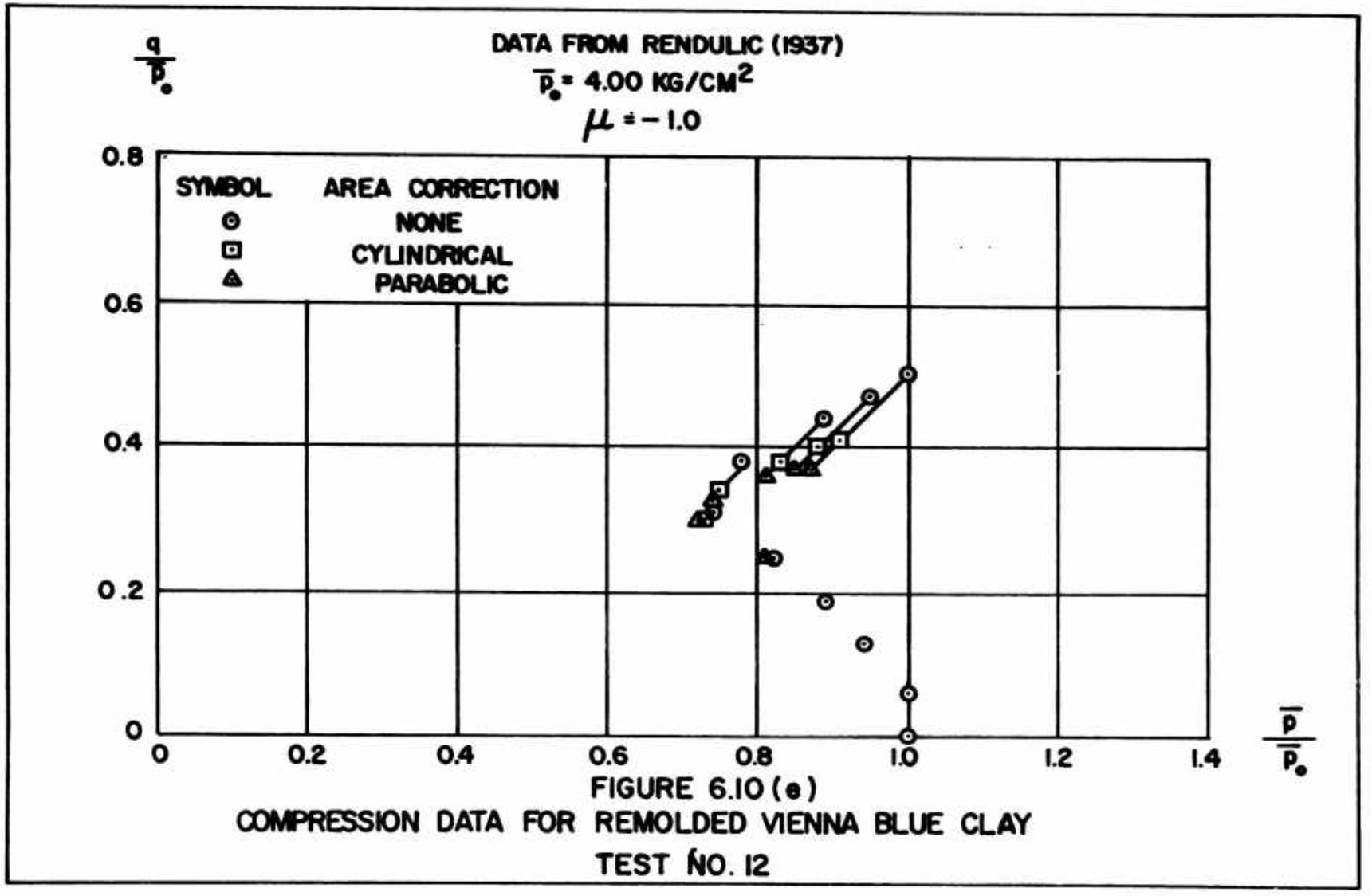

FIGURE 6.10 (e)
COMPRESSION DATA FOR REMOLDED VIENNA BLUE CLAY
TEST NO. 12

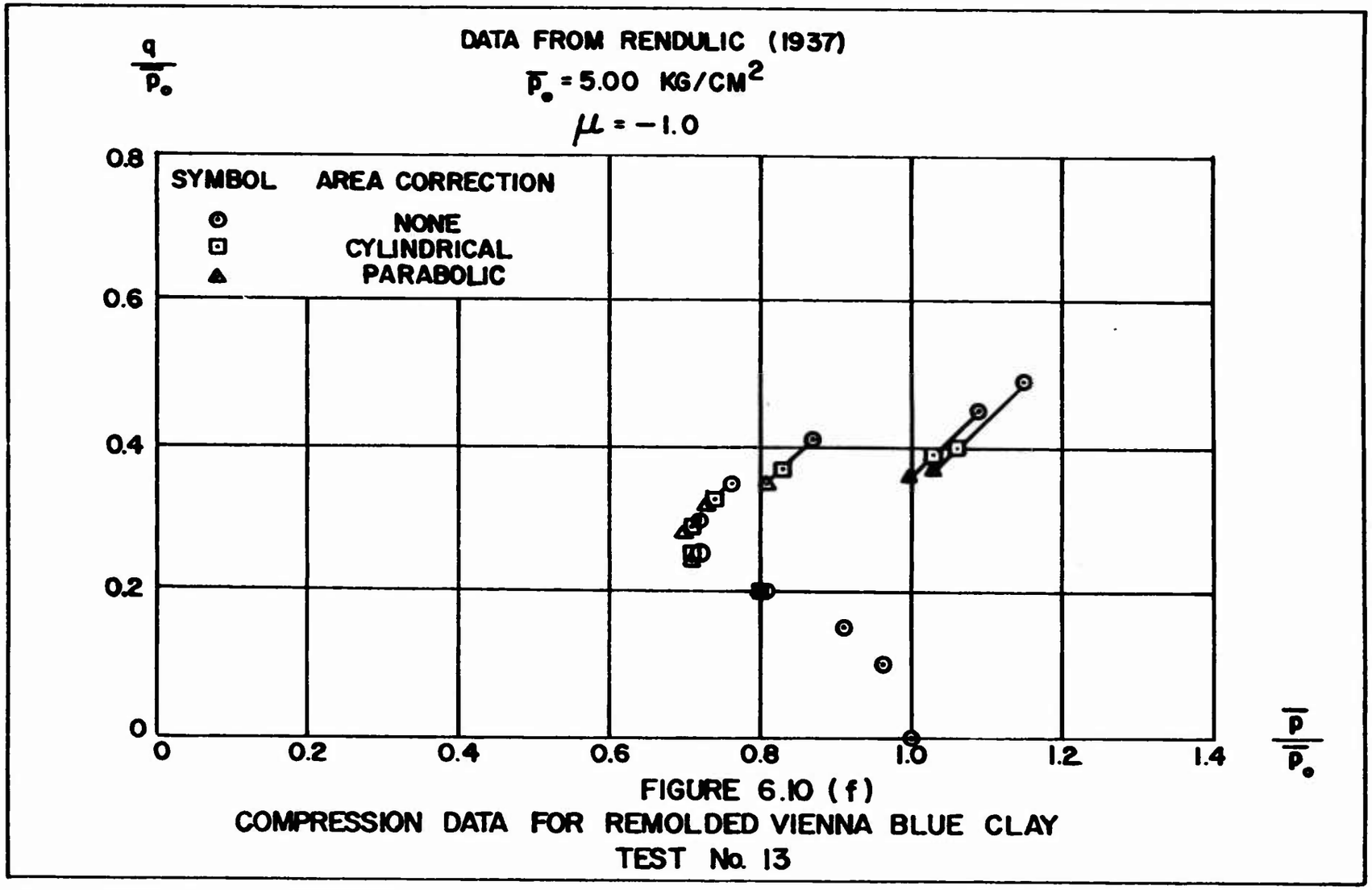

FIGURE 6.10 (f)
COMPRESSION DATA FOR REMOLDED VIENNA BLUE CLAY
TEST No. 13

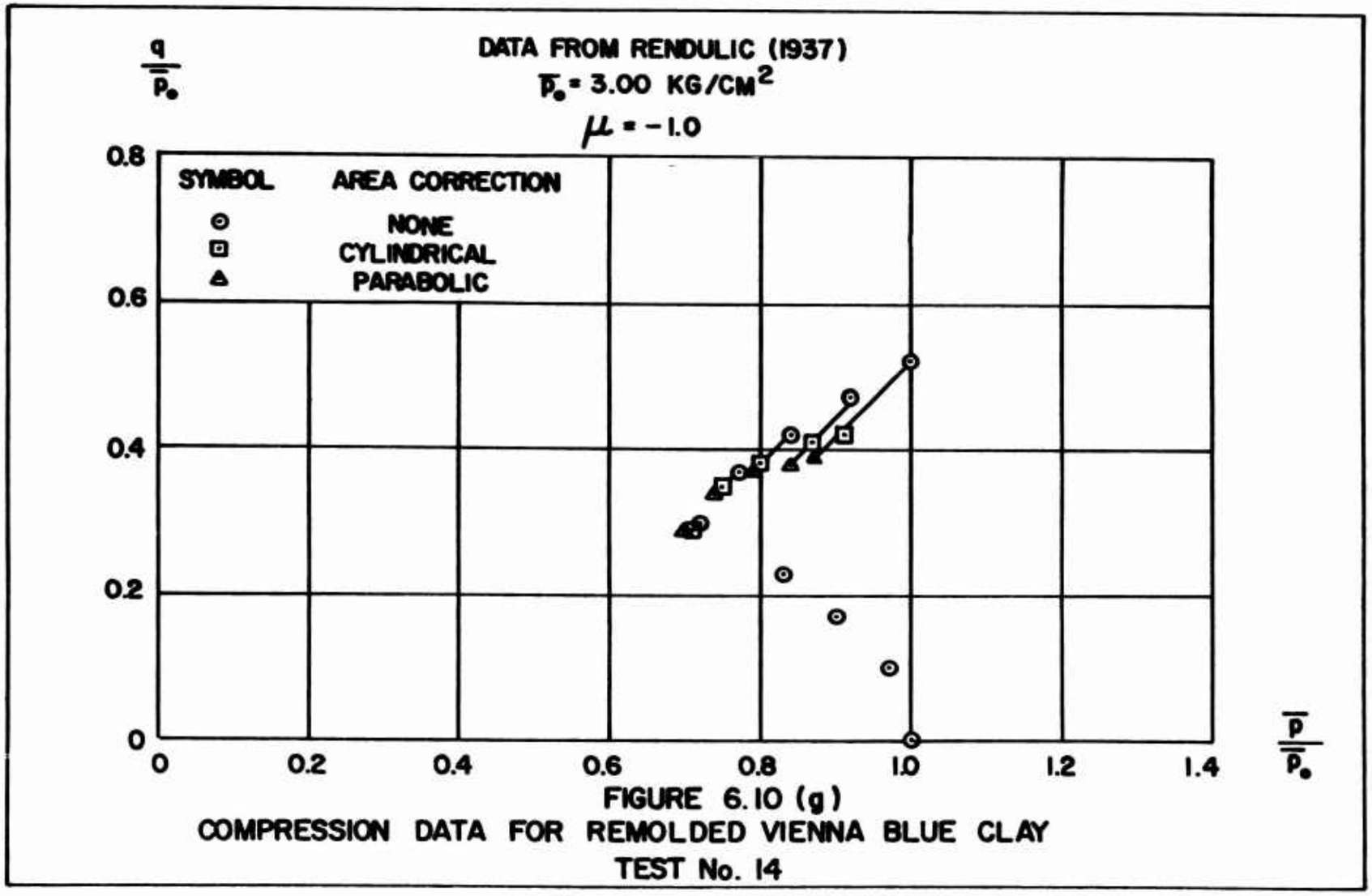

FIGURE 6.10 (g)
COMPRESSION DATA FOR REMOLDED VIENNA BLUE CLAY
TEST No. 14

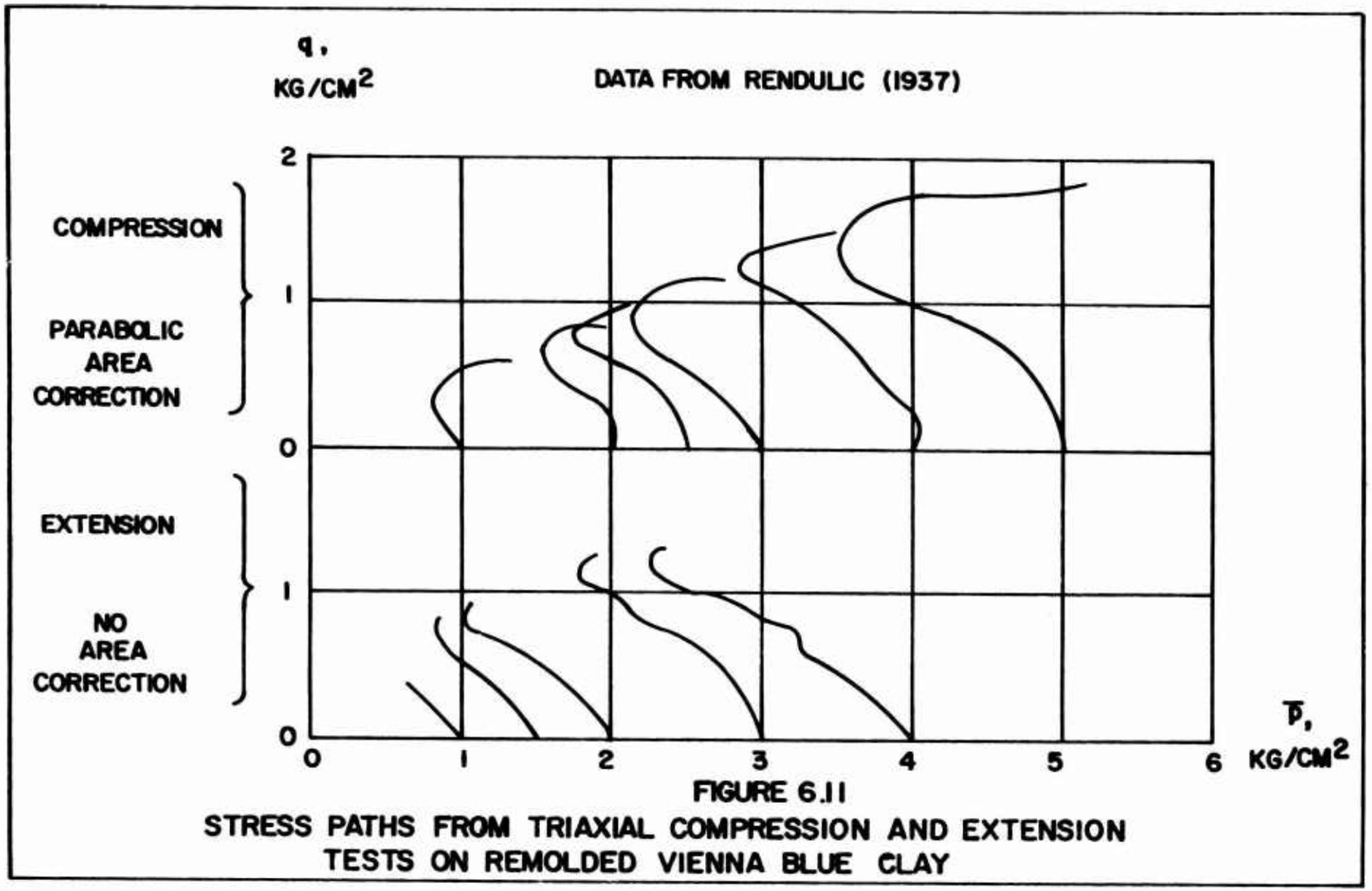

FIGURE 6.11

STRESS PATHS FROM TRIAXIAL COMPRESSION AND EXTENSION TESTS ON REMOLDED VIENNA BLUE CLAY

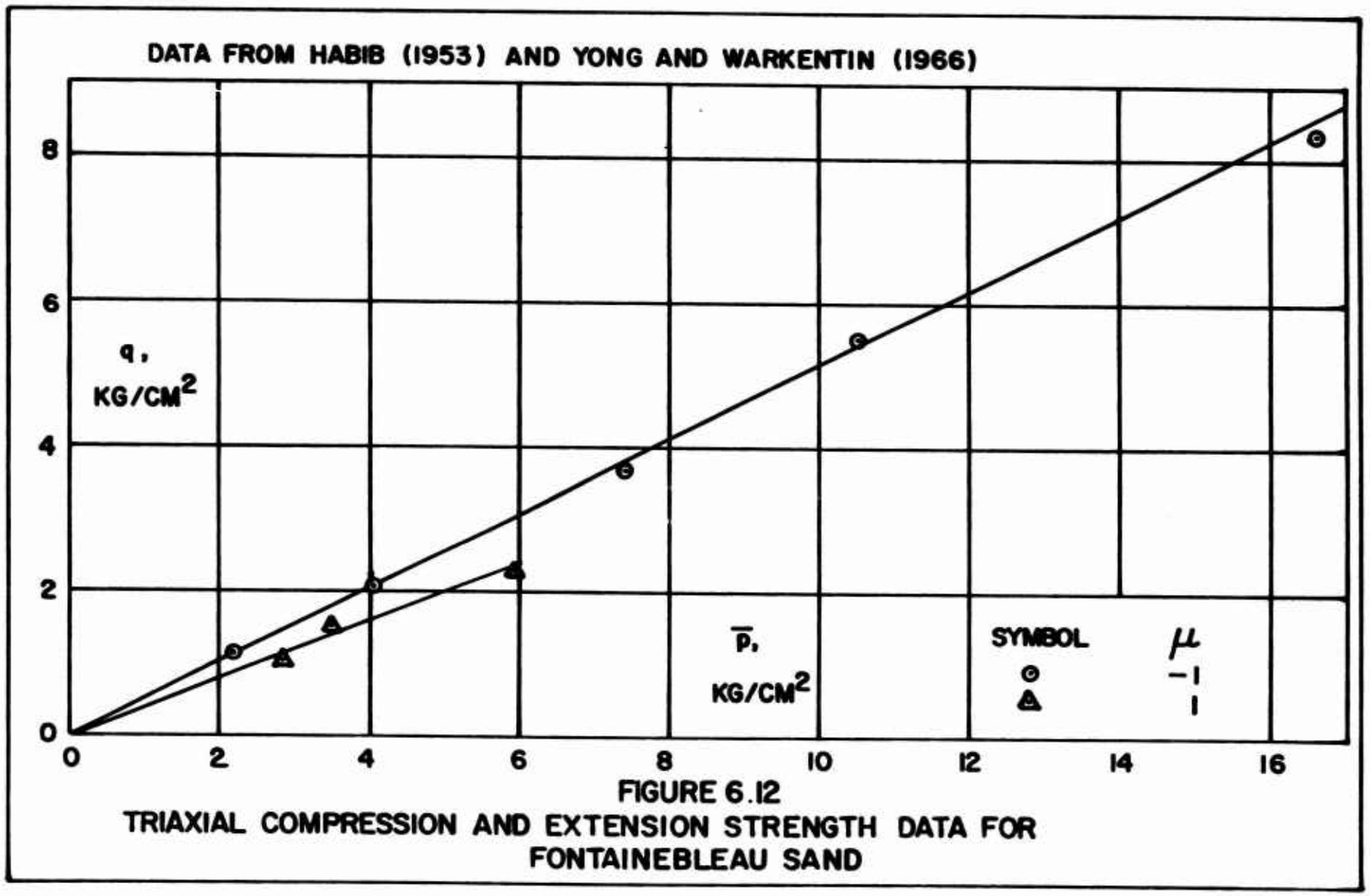

FIGURE 6.12
TRIAXIAL COMPRESSION AND EXTENSION STRENGTH DATA FOR FONTAINEBLEAU SAND

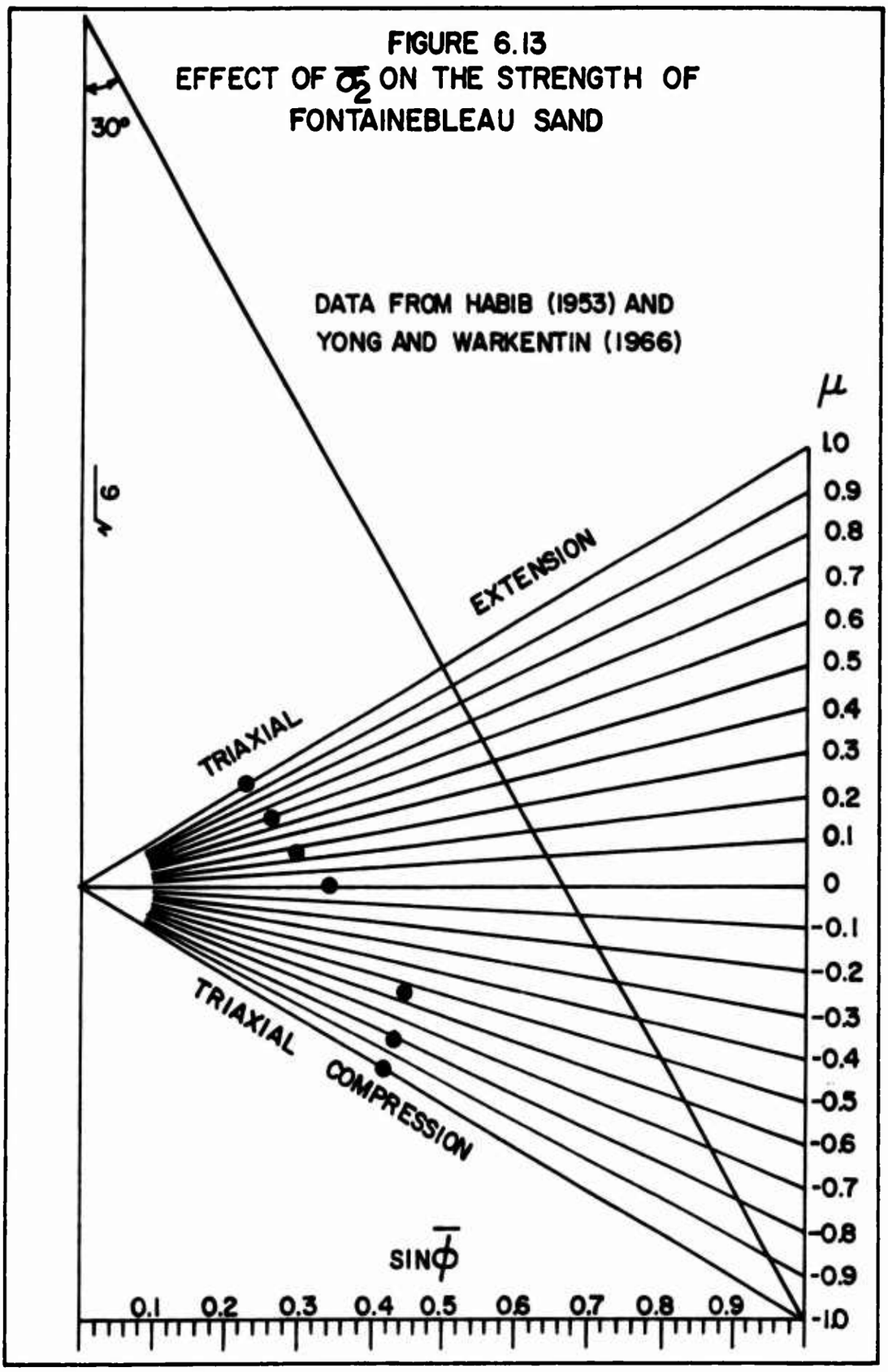

FIGURE 6.13
EFFECT OF $\bar{\sigma}_2$ ON THE STRENGTH OF
FONTAINEBLEAU SAND

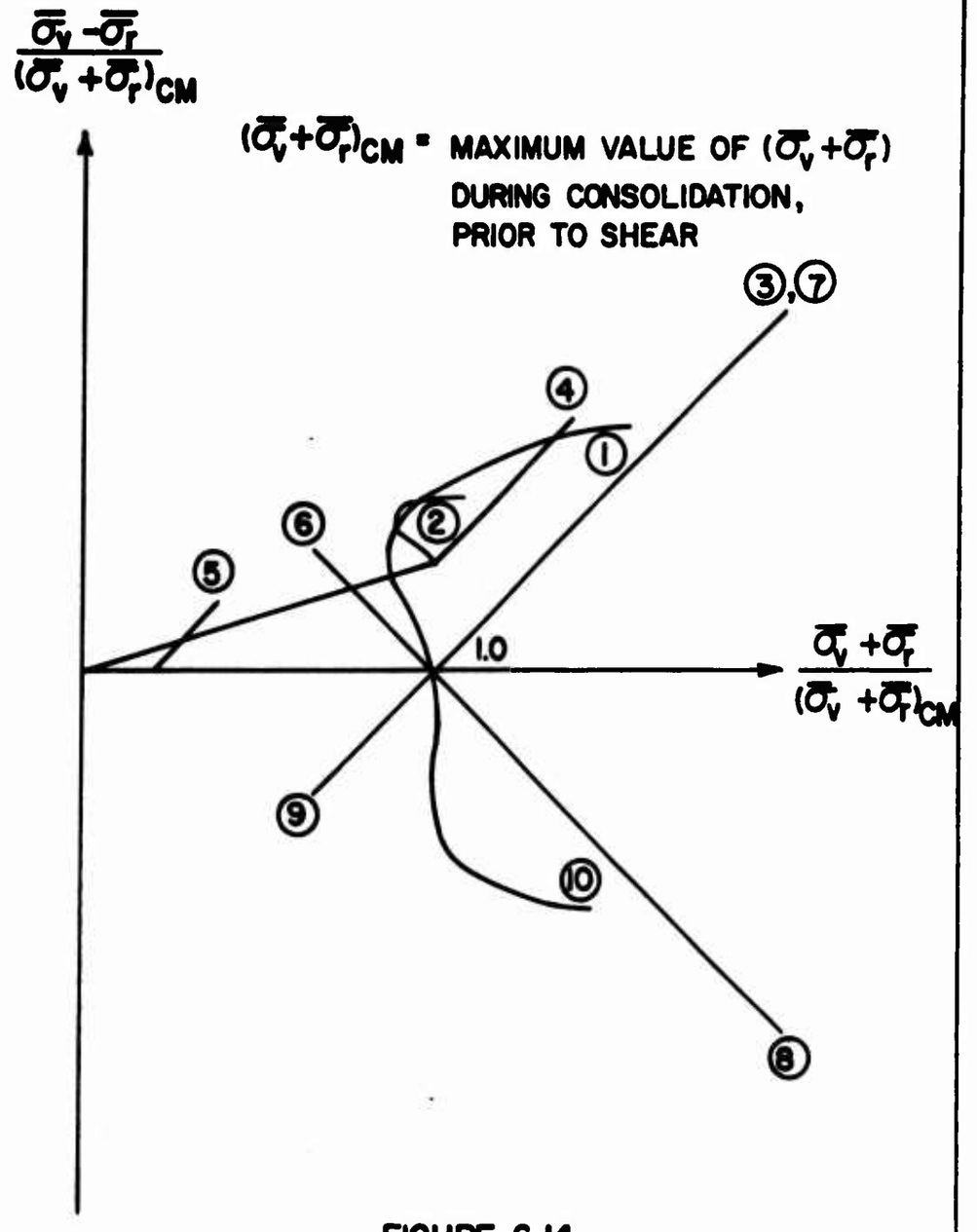

FIGURE 6.14

EFFECTIVE STRESS PATHS USED BY BISHOP AND ELDIN (1953) FOR TRIAXIAL TESTS ON BRASTED SAND

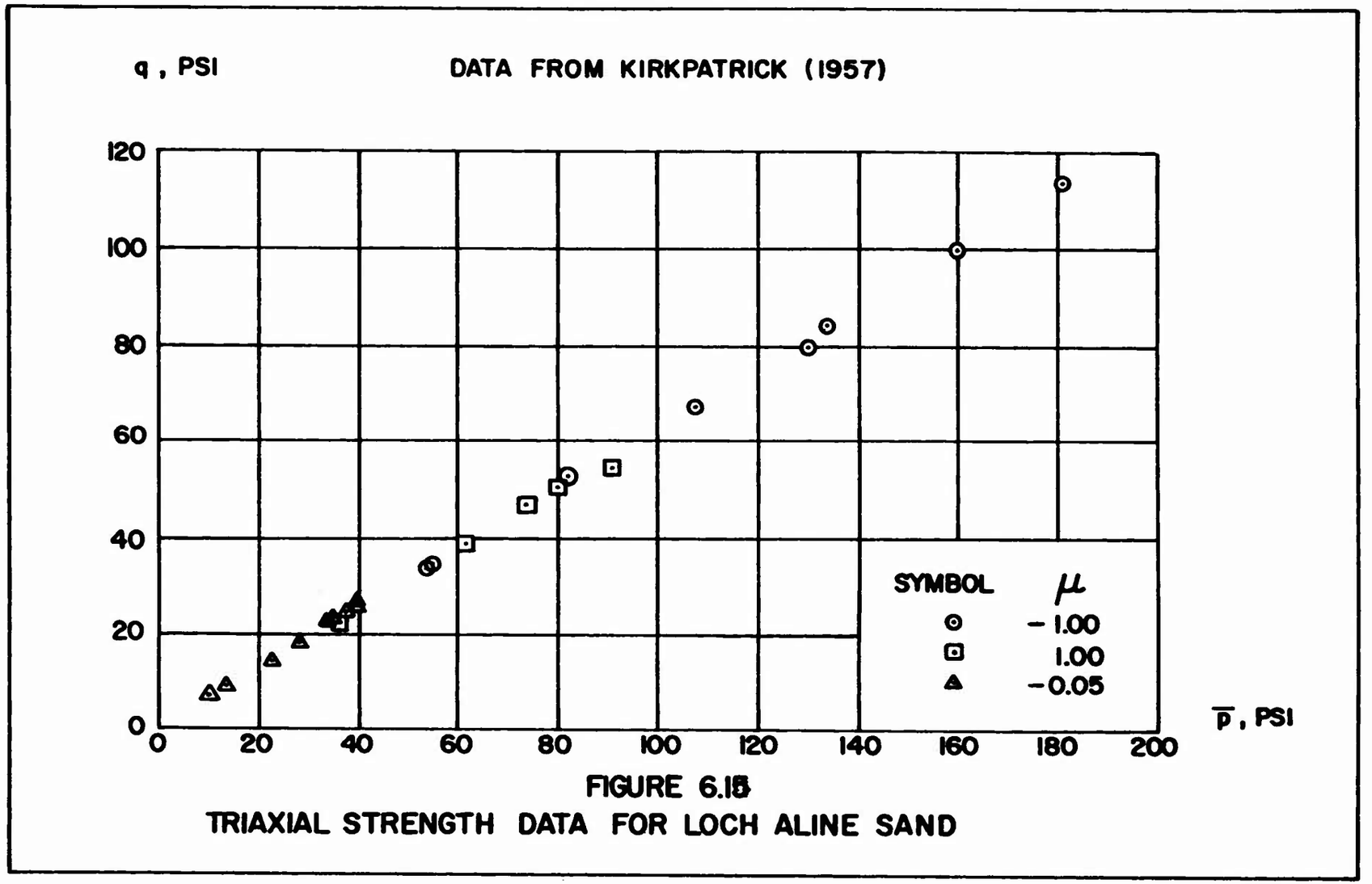

FIGURE 6.15
TRIAXIAL STRENGTH DATA FOR LOCH ALINE SAND

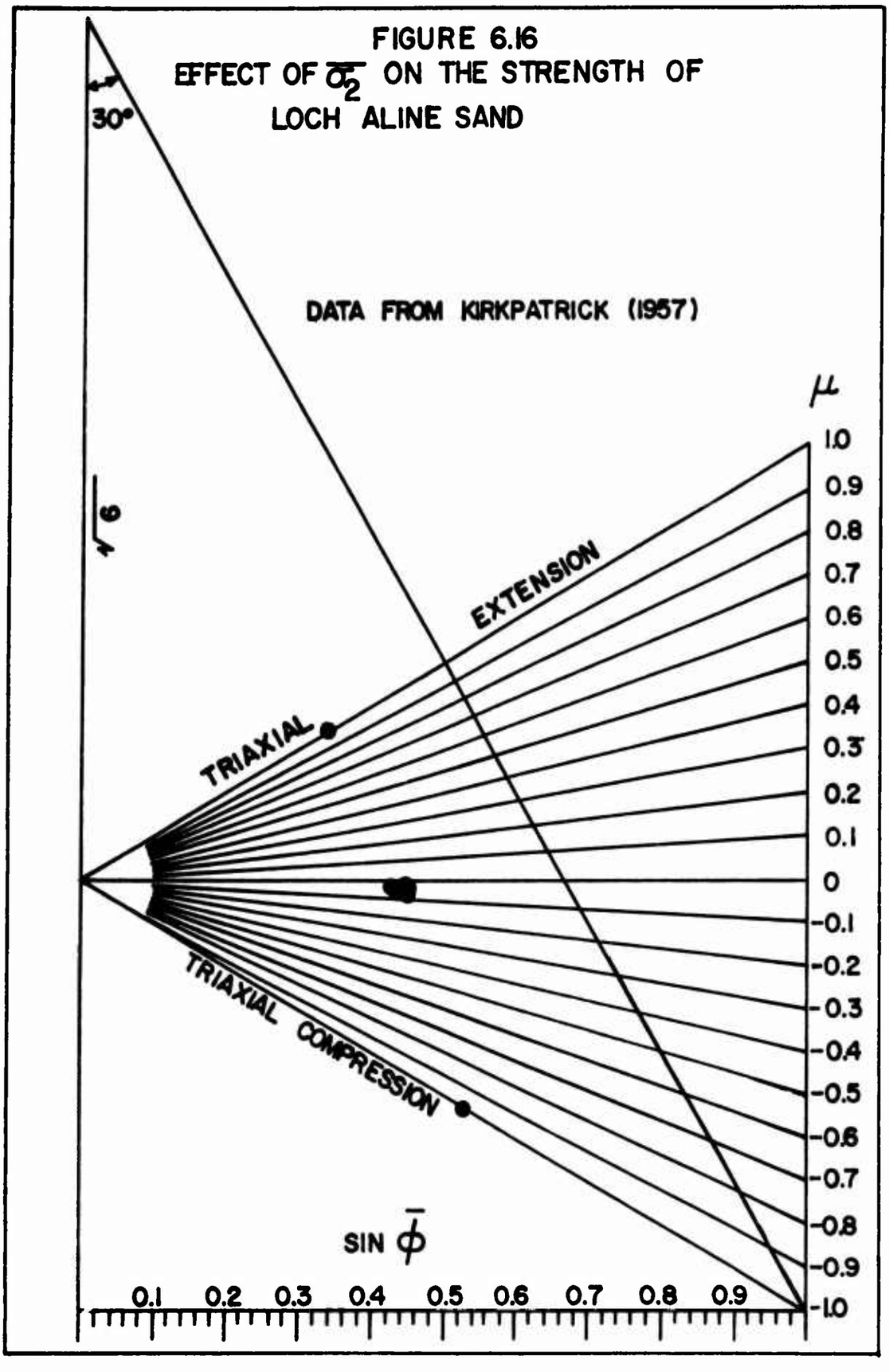

FIGURE 6.16
EFFECT OF $\bar{\sigma}_2$ ON THE STRENGTH OF LOCH ALINE SAND

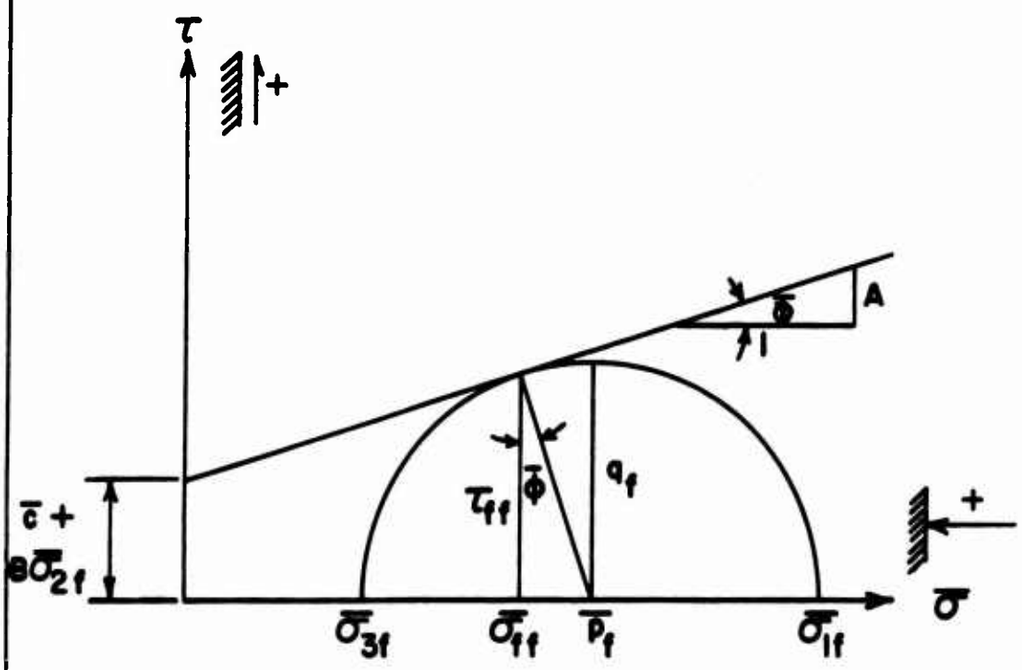

FIGURE 6.17

A GENERALIZED LINEAR FAILURE HYPOTHESIS FOR SOIL

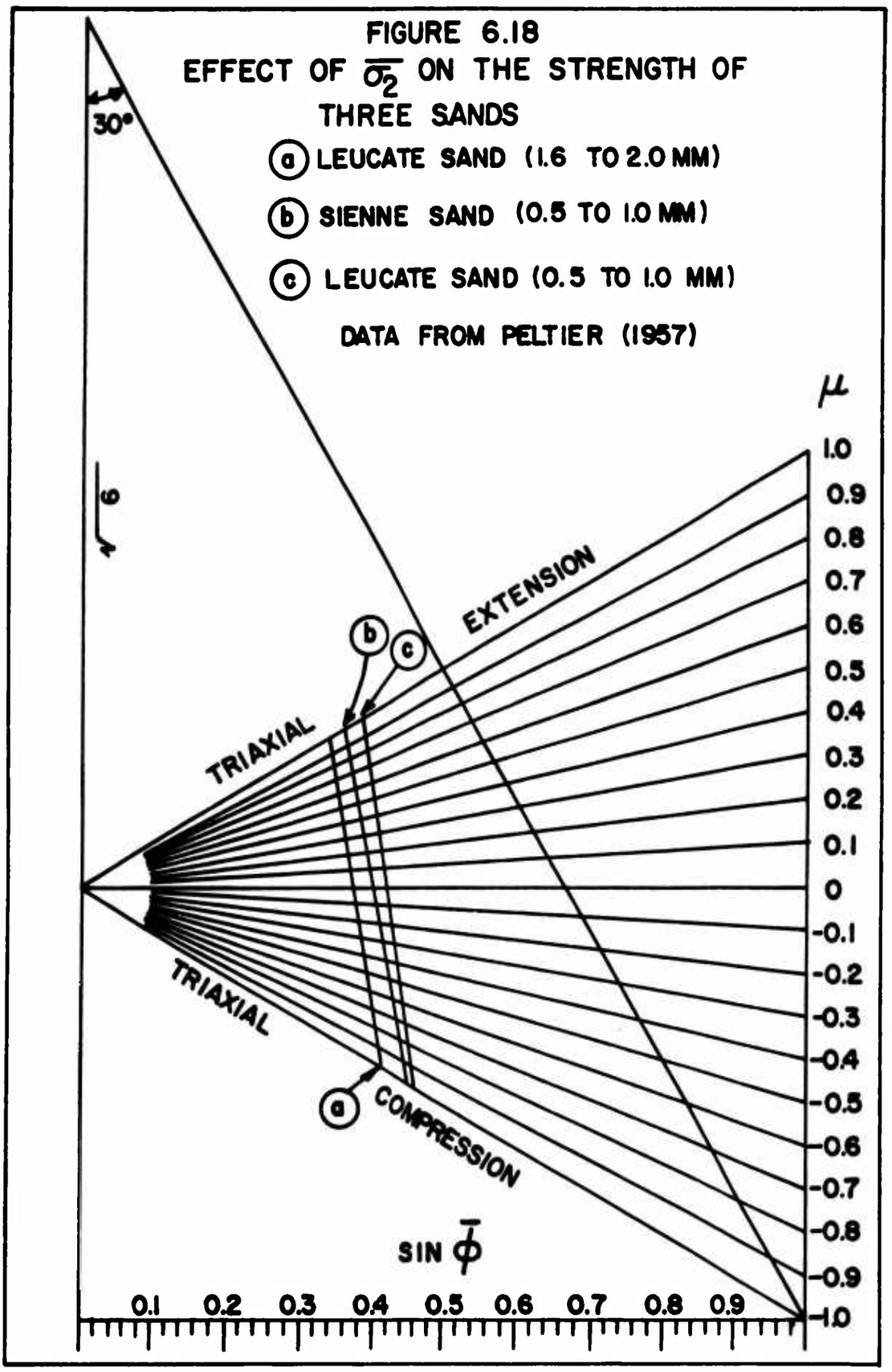

FIGURE 6.18
EFFECT OF $\overline{\sigma_2}$ ON THE STRENGTH OF THREE SANDS

(a) LEUCATE SAND (1.6 TO 2.0 MM)

(b) SIENNE SAND (0.5 TO 1.0 MM)

(c) LEUCATE SAND (0.5 TO 1.0 MM)

DATA FROM PELTIER (1957)

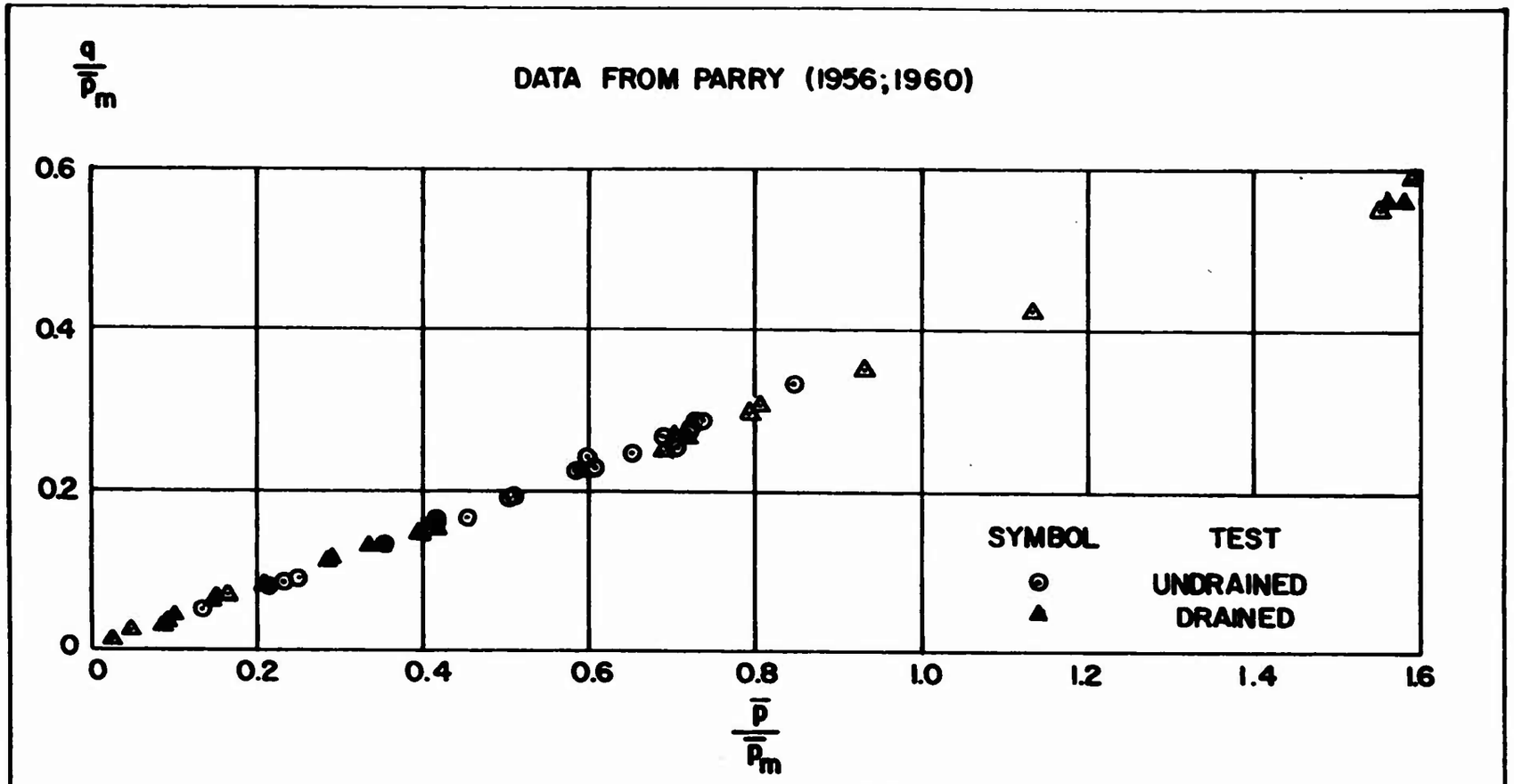

FIGURE 6.19 (a)

NORMALIZED STRENGTH DATA FROM TRIAXIAL COMPRESSION TESTS ON REMOLDED WEALD CLAY

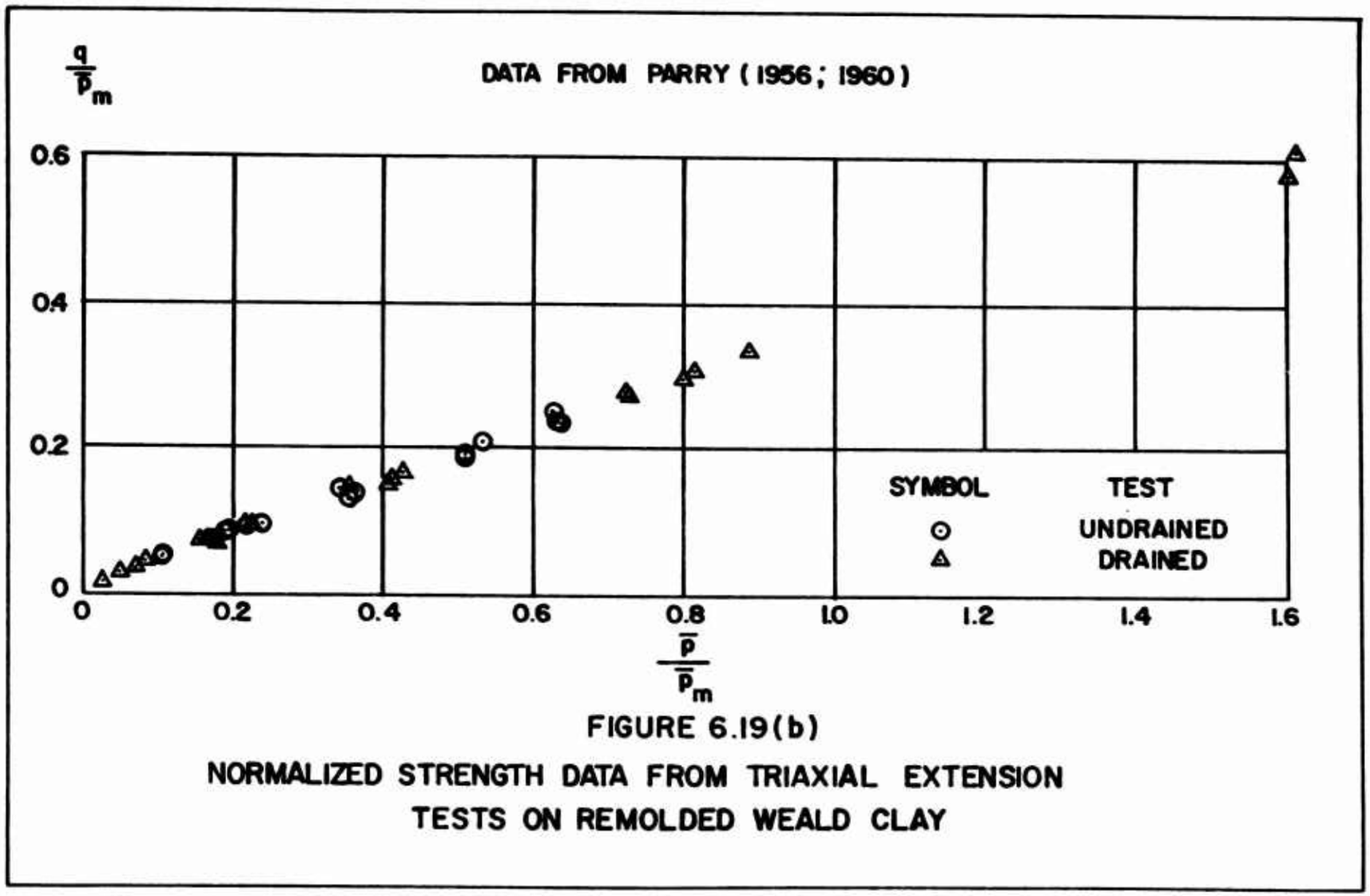

FIGURE 6.19(b)

NORMALIZED STRENGTH DATA FROM TRIAXIAL EXTENSION TESTS ON REMOLDED WEALD CLAY

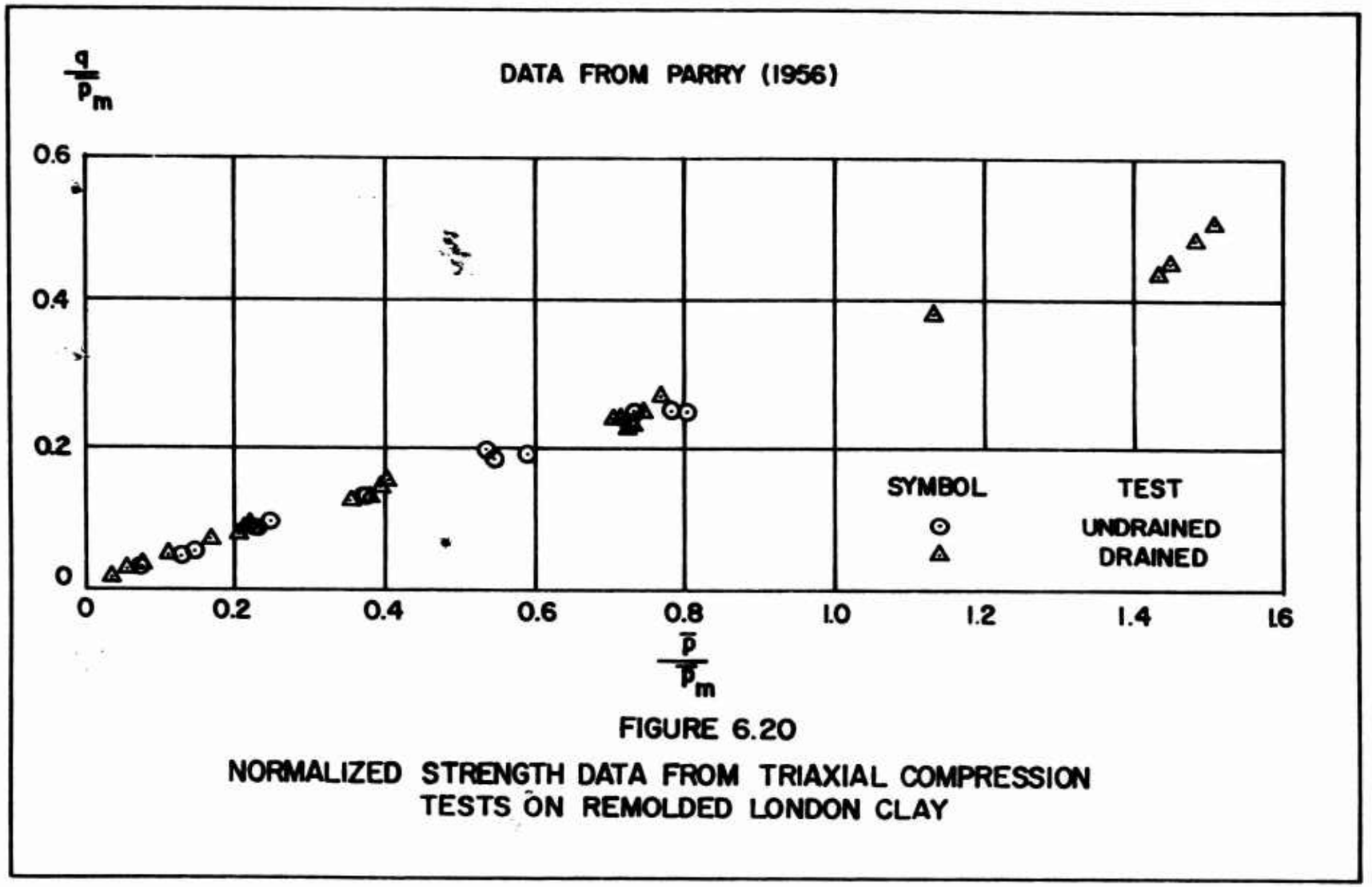

FIGURE 6.20

NORMALIZED STRENGTH DATA FROM TRIAXIAL COMPRESSION TESTS ON REMOLDED LONDON CLAY

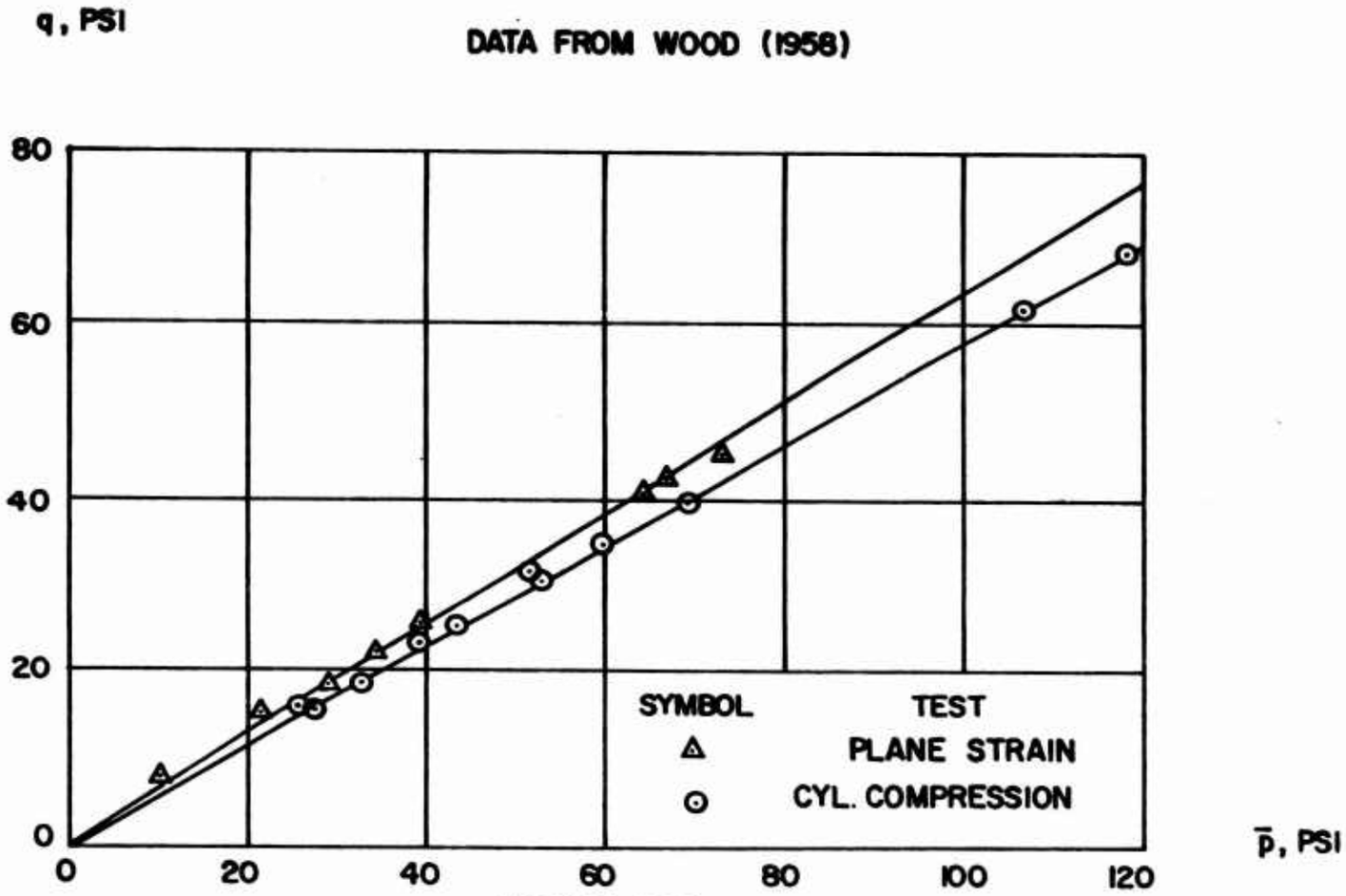

FIGURE 6.21
TRIAXIAL STRENGTH DATA FOR GLEN SHIRA DAM MATERIAL

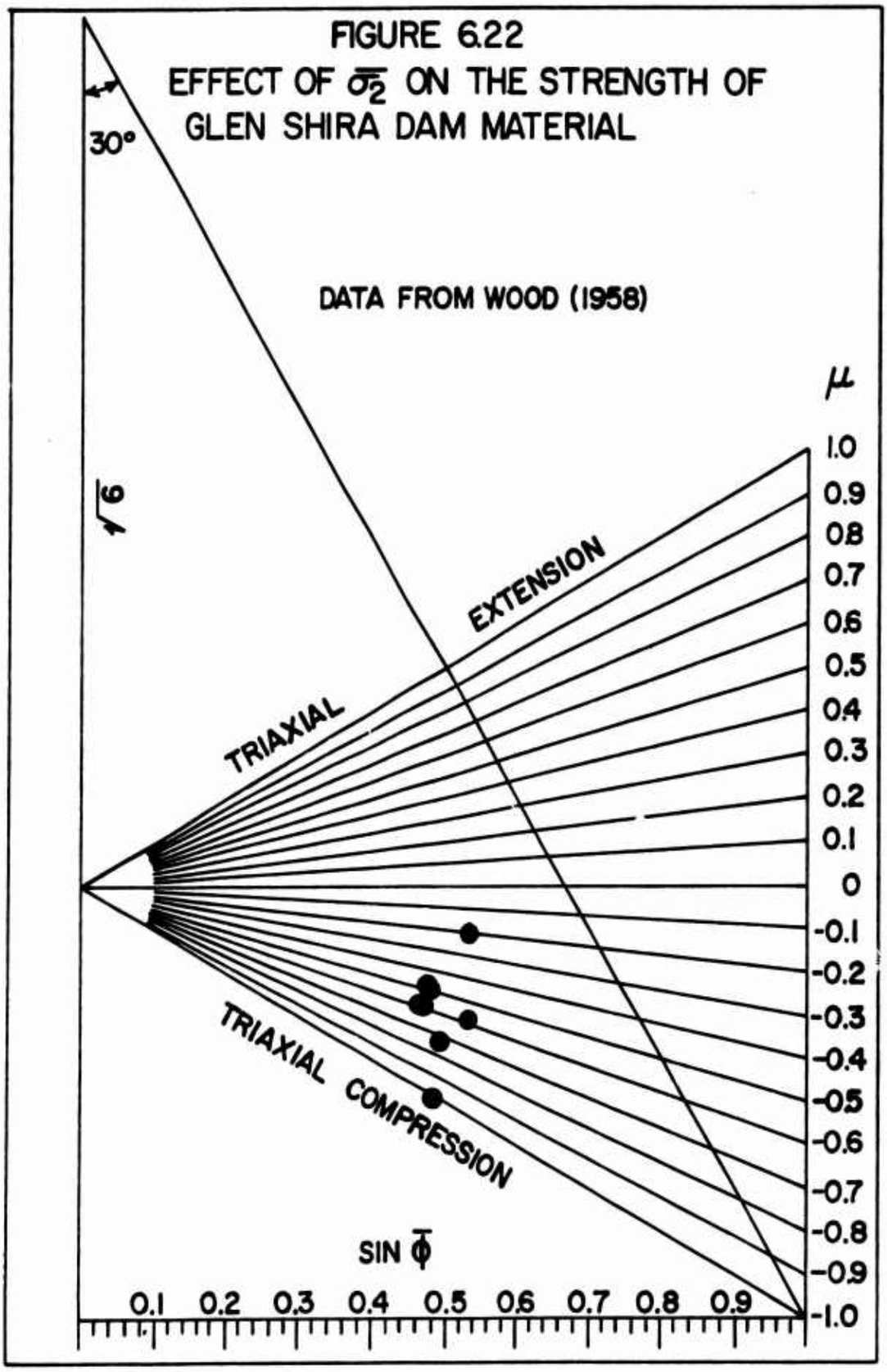
FIGURE 6.22
EFFECT OF $\overline{\sigma_2}$ ON THE STRENGTH OF
GLEN SHIRA DAM MATERIAL
30°
DATA FROM WOOD (1958)
μ
1.0
0.9
0.8
0.7
0.6
0.5
0.4
0.3
0.2
0.1
0
-0.1
-0.2
-0.3
-0.4
-0.5
-0.6
-0.7
-0.8
-0.9
-1.0
$\sqrt{6}$
EXTENSION
TRIAXIAL
TRIAXIAL COMPRESSION
SIN $\overline{\phi}$
0.1 0.2 0.3 0.4 0.5 0.6 0.7 0.8 0.9

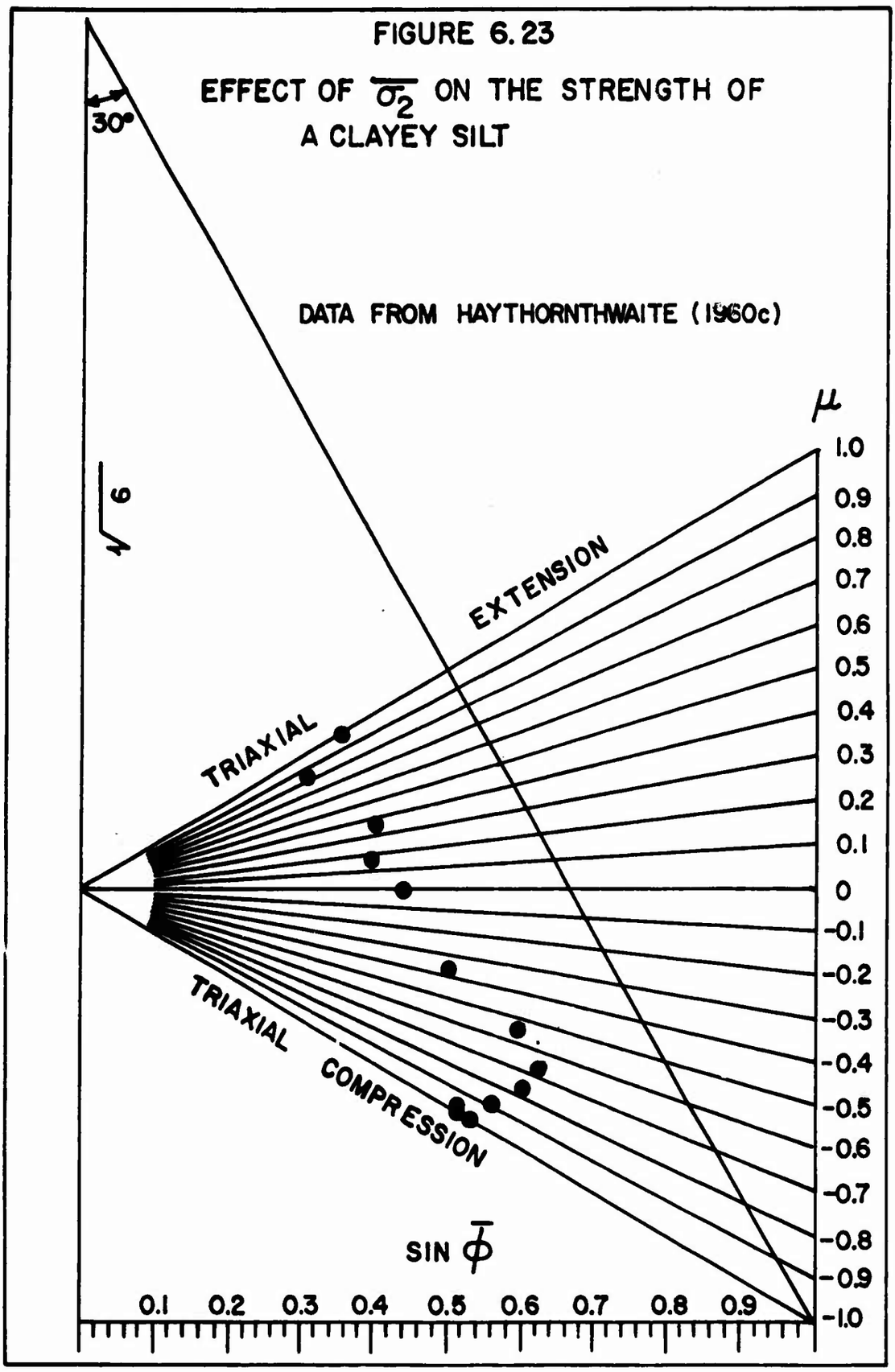
FIGURE 6.23
EFFECT OF $\overline{\sigma_2}$ ON THE STRENGTH OF A CLAYEY SILT
DATA FROM HAYTHORNTHWAITE (1960c)
30°
$\sqrt{6}$
μ
1.0
0.9
0.8
0.7
0.6
0.5
0.4
0.3
0.2
0.1
0
-0.1
-0.2
-0.3
-0.4
-0.5
-0.6
-0.7
-0.8
-0.9
-1.0
EXTENSION
TRIAXIAL
TRIAXIAL COMPRESSION
SIN $\overline{\Phi}$
0.1 0.2 0.3 0.4 0.5 0.6 0.7 0.8 0.9

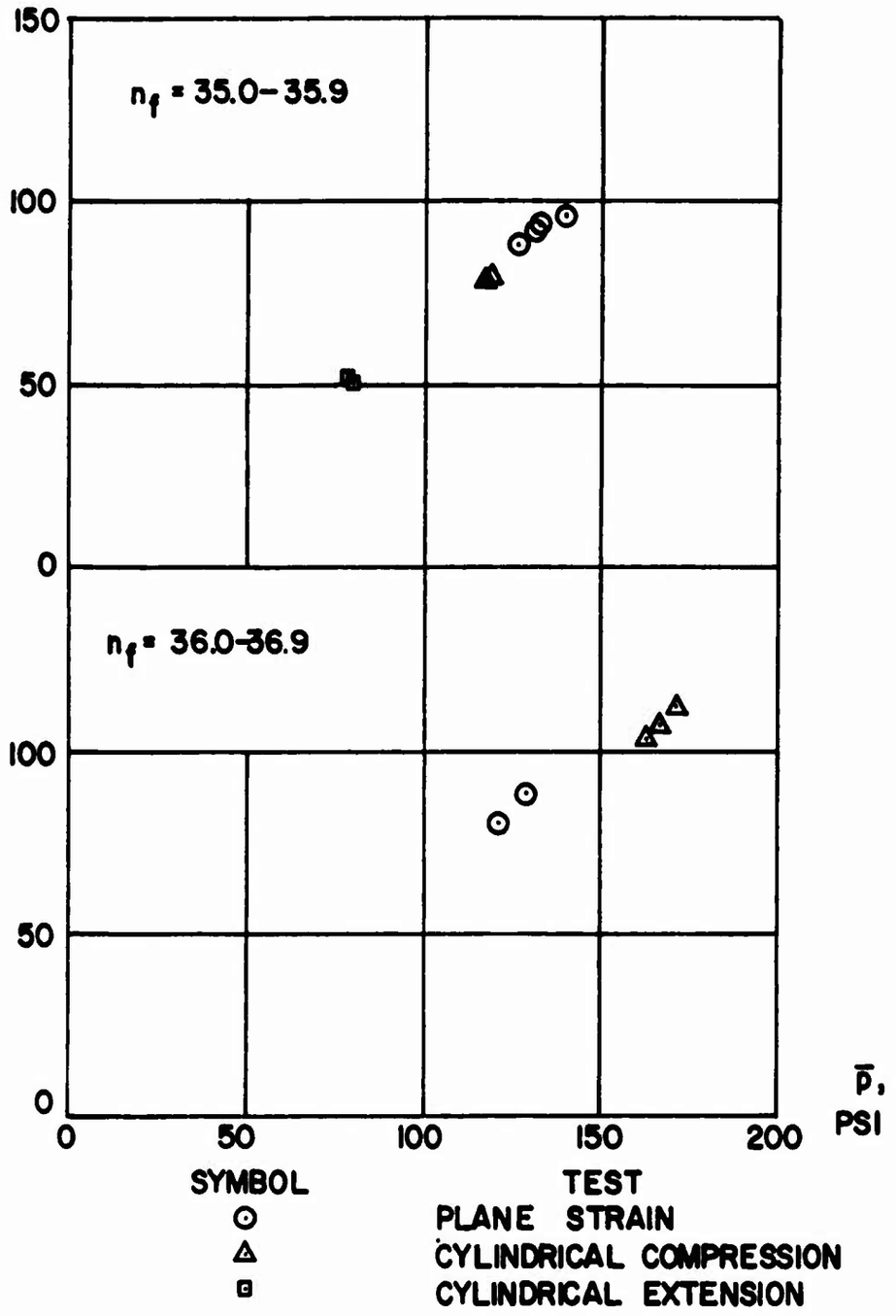

FIGURE 6.24(a)
TRIAXIAL STRENGTH DATA FOR
BRASTED SAND

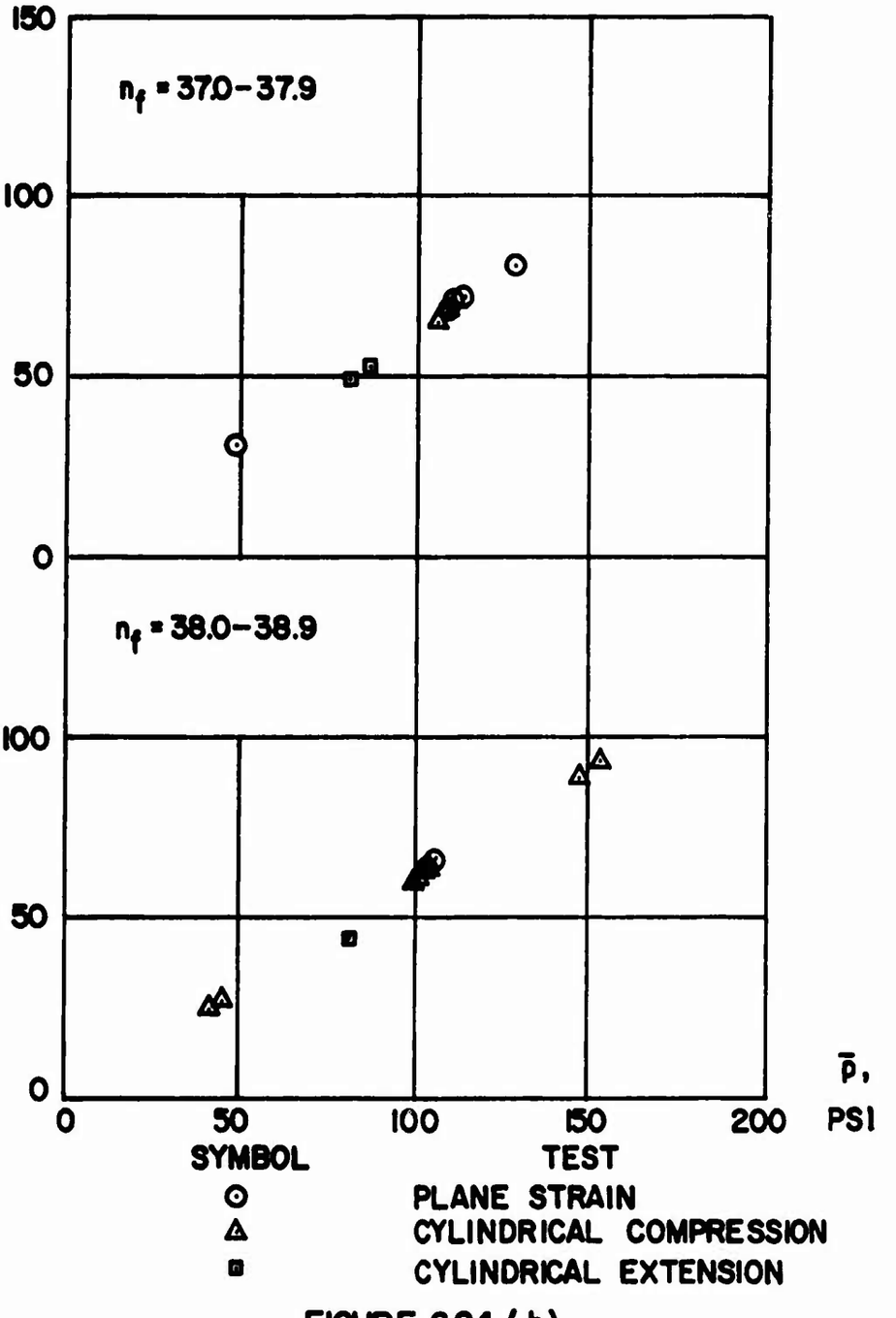

FIGURE 6.24 (b)

TRIAXIAL STRENGTH DATA FOR BRASTED SAND

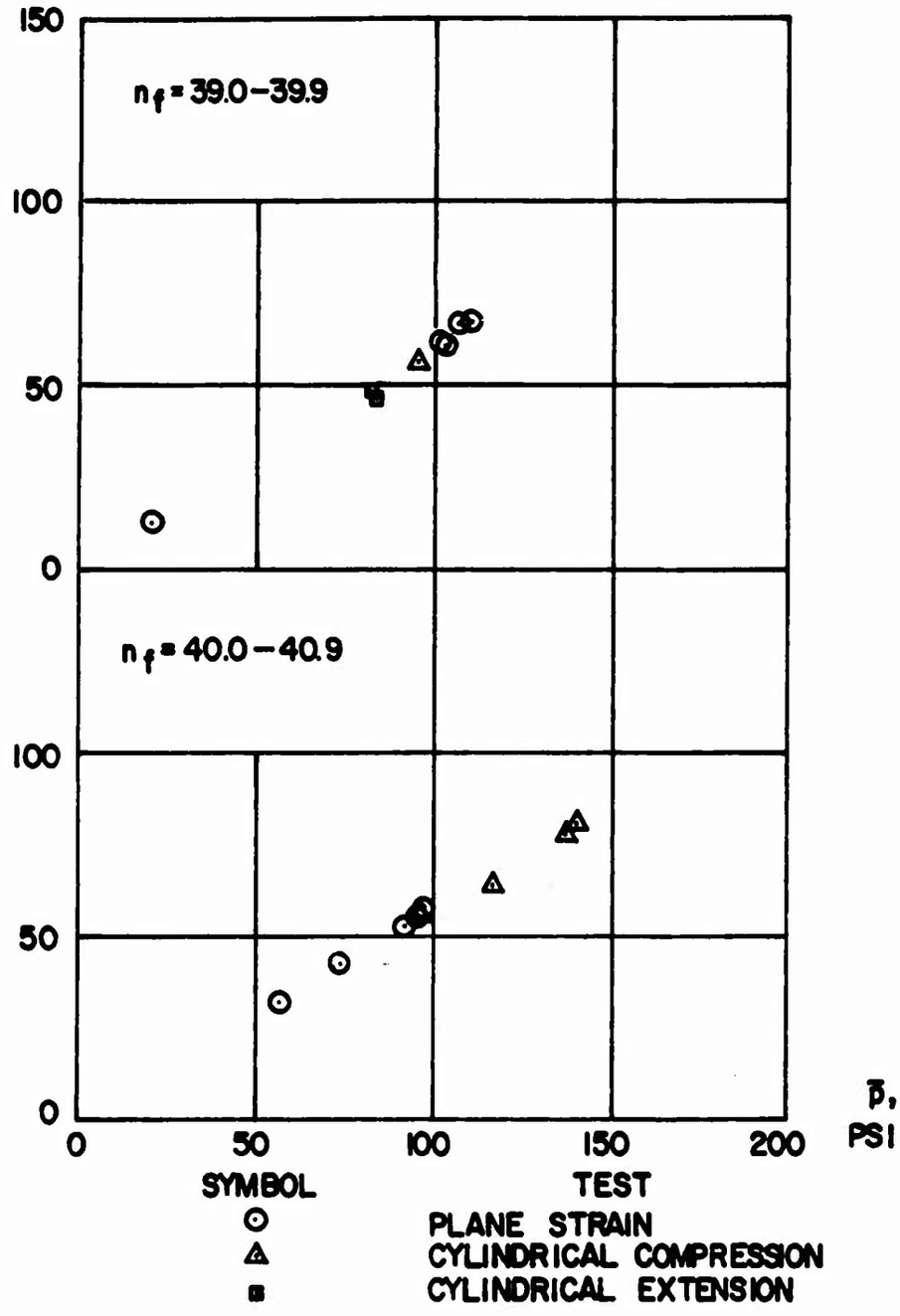

FIGURE 6.24 (c)

TRIAXIAL STRENGTH DATA FOR BRASTED SAND

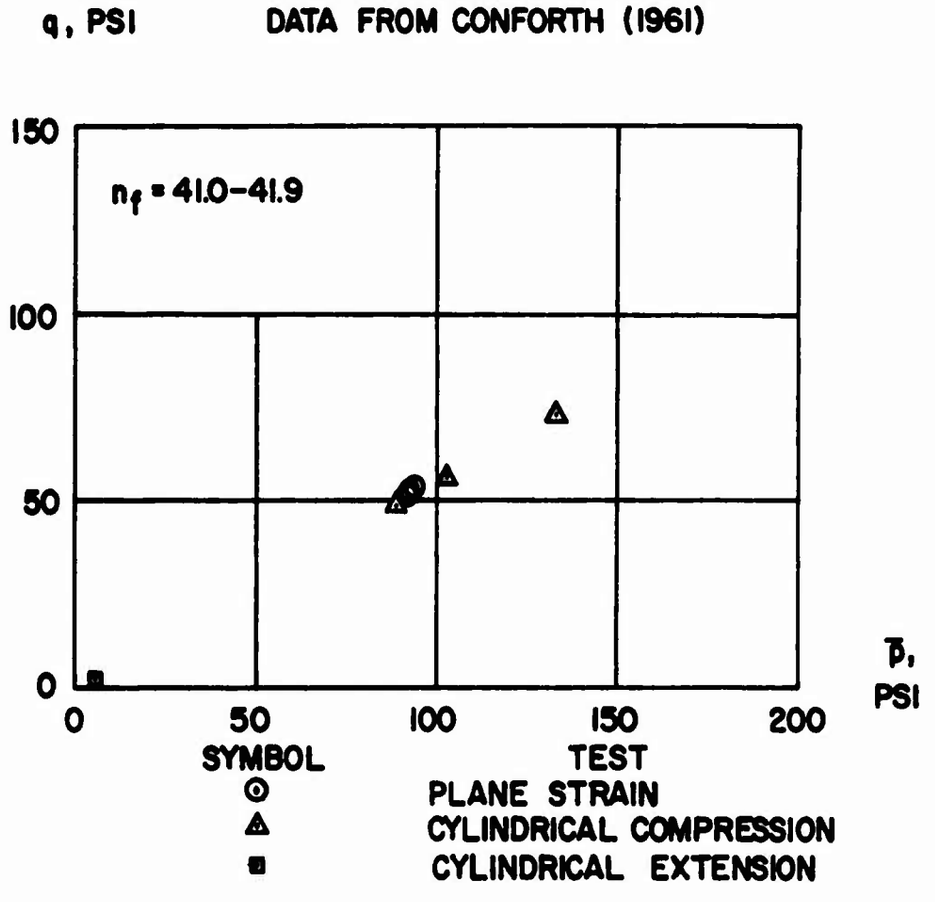

FIGURE 6.24(d)
TRIAXIAL STRENGTH DATA FOR
BRASTED SAND

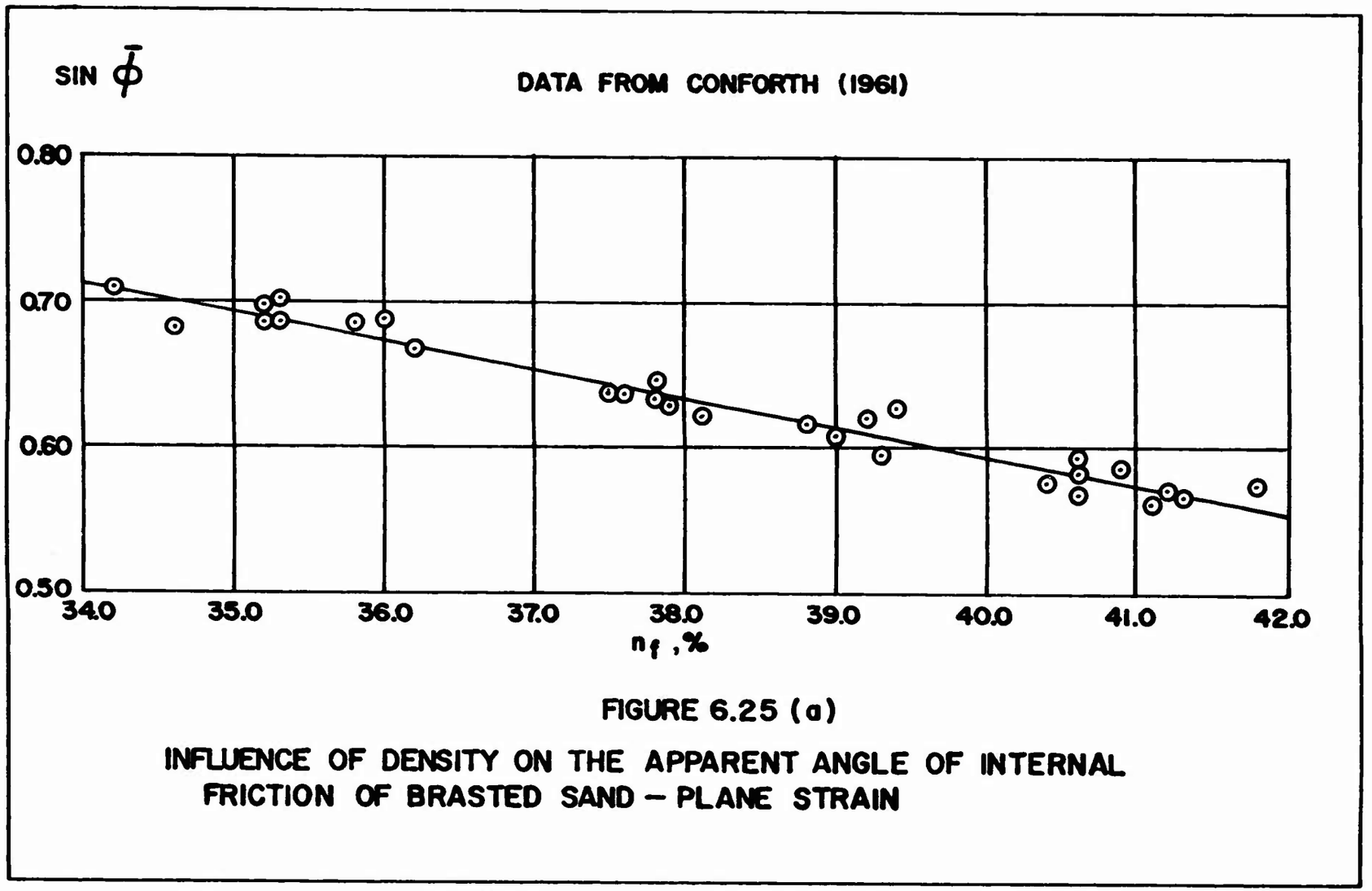

FIGURE 6.25 (a)

INFLUENCE OF DENSITY ON THE APPARENT ANGLE OF INTERNAL FRICTION OF BRASTED SAND – PLANE STRAIN

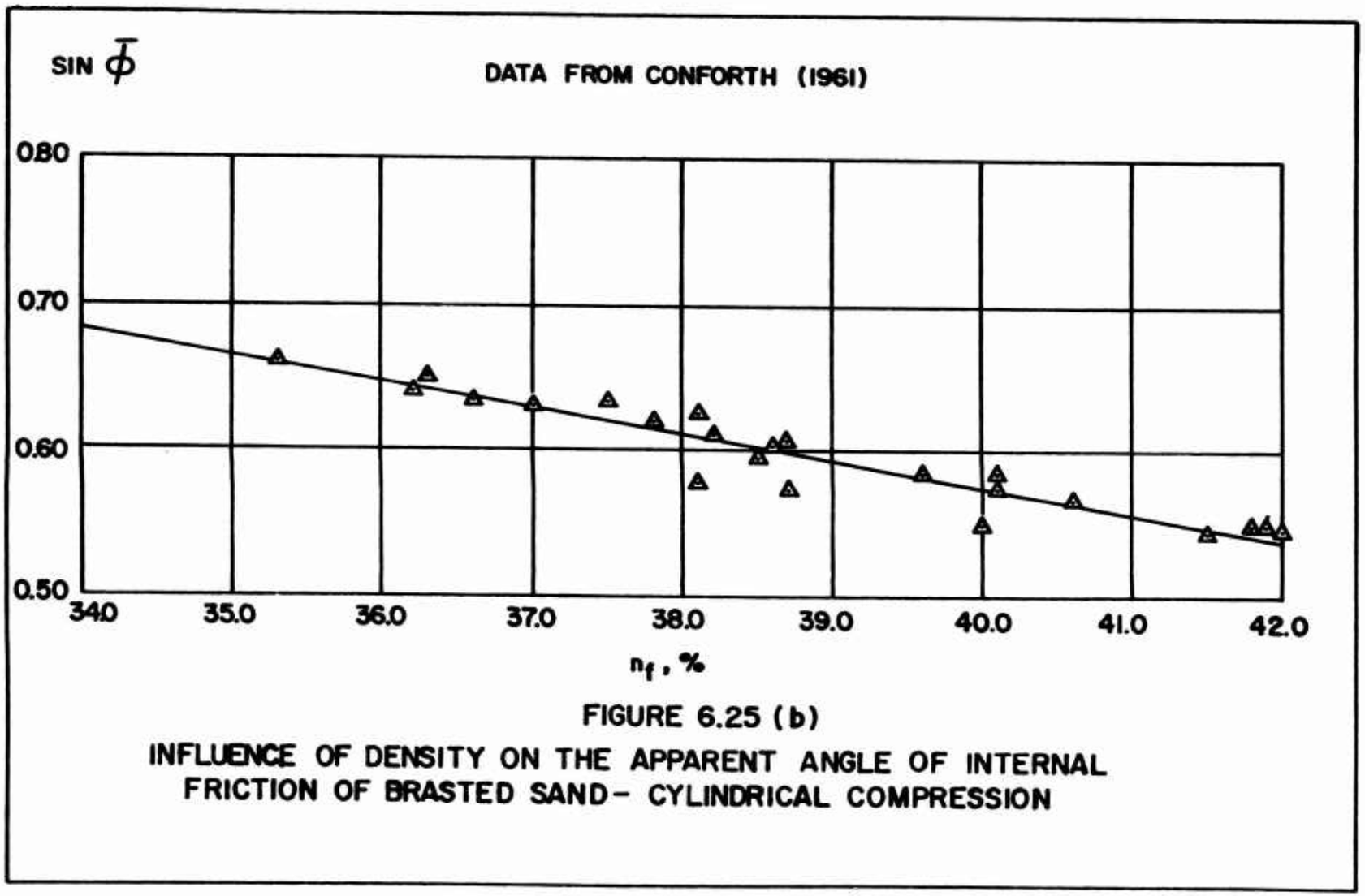

FIGURE 6.25 (b)

INFLUENCE OF DENSITY ON THE APPARENT ANGLE OF INTERNAL FRICTION OF BRASTED SAND- CYLINDRICAL COMPRESSION

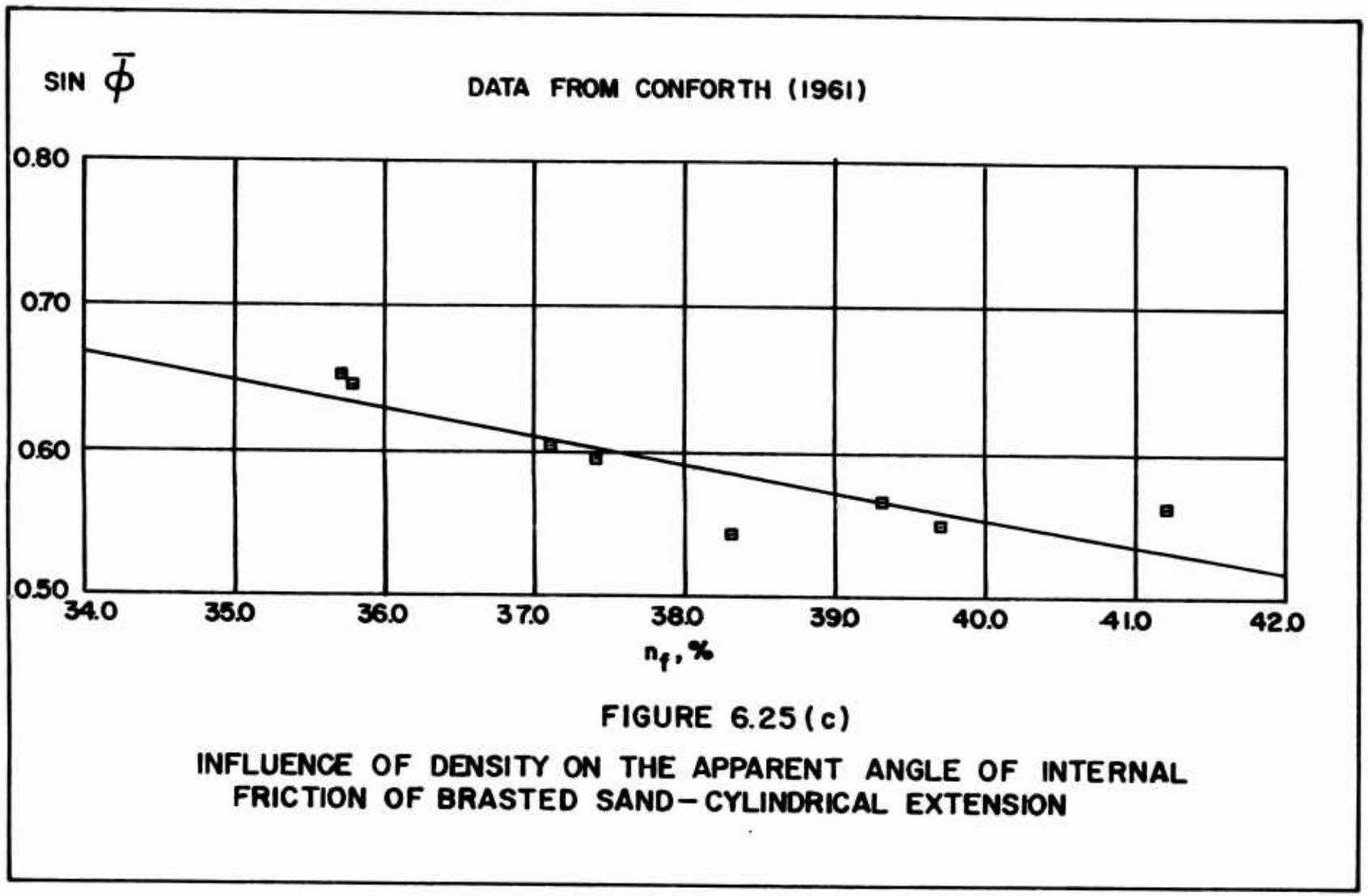

FIGURE 6.25 (c)

INFLUENCE OF DENSITY ON THE APPARENT ANGLE OF INTERNAL FRICTION OF BRASTED SAND – CYLINDRICAL EXTENSION

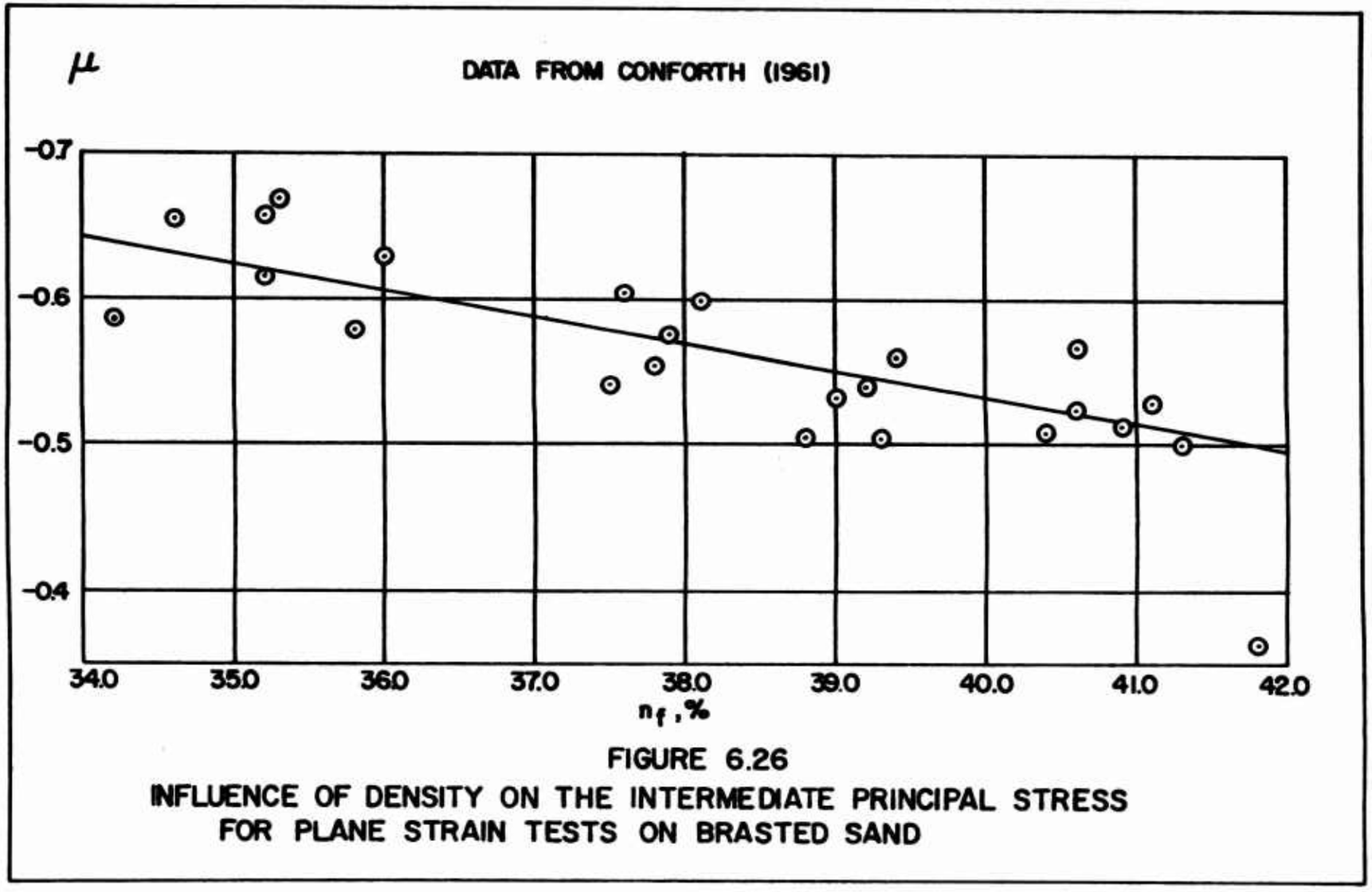

FIGURE 6.26
INFLUENCE OF DENSITY ON THE INTERMEDIATE PRINCIPAL STRESS FOR PLANE STRAIN TESTS ON BRASTED SAND

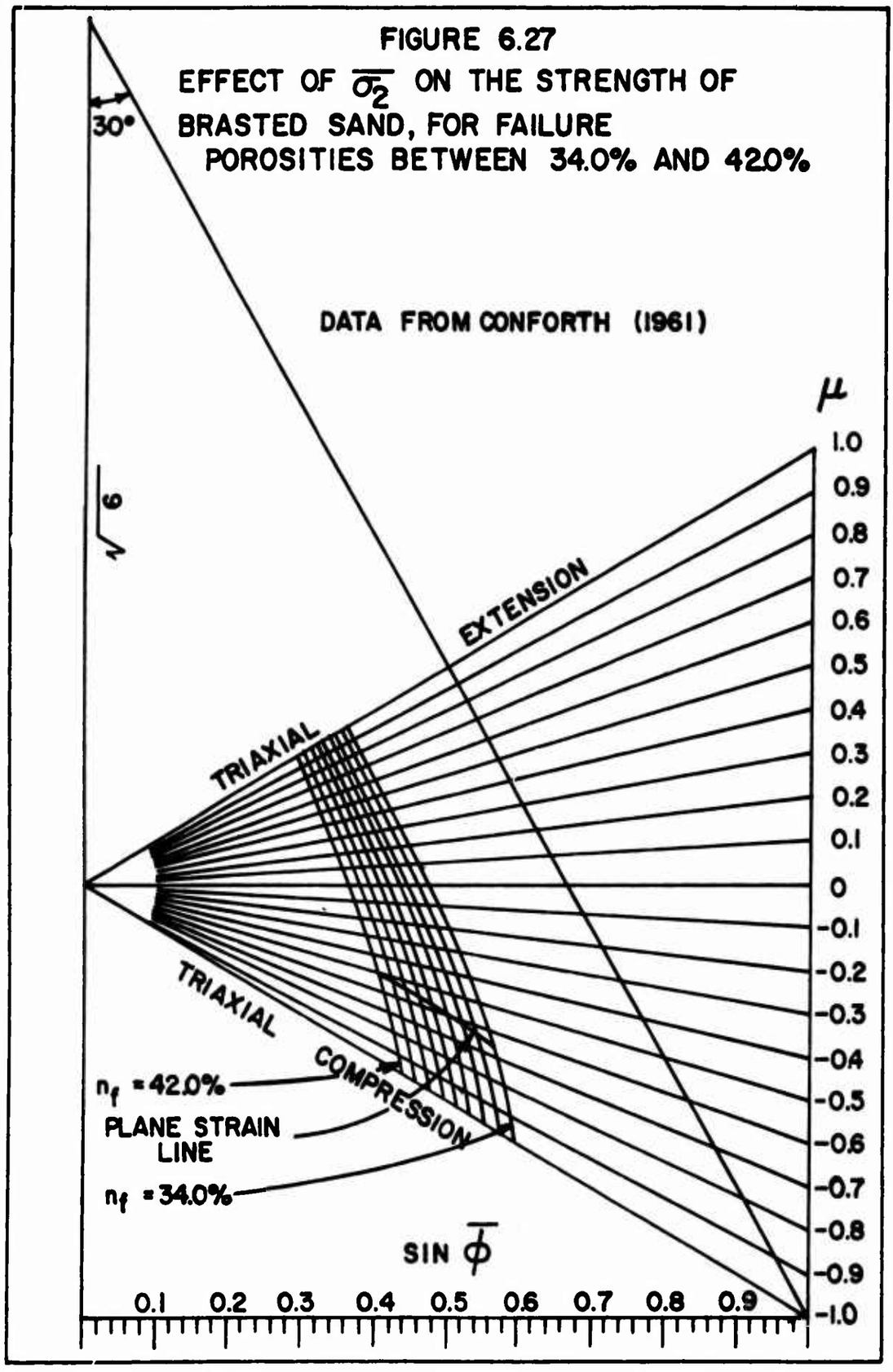

FIGURE 6.27
EFFECT OF $\overline{\sigma_2}$ ON THE STRENGTH OF BRASTED SAND, FOR FAILURE POROSITIES BETWEEN 34.0% AND 42.0%

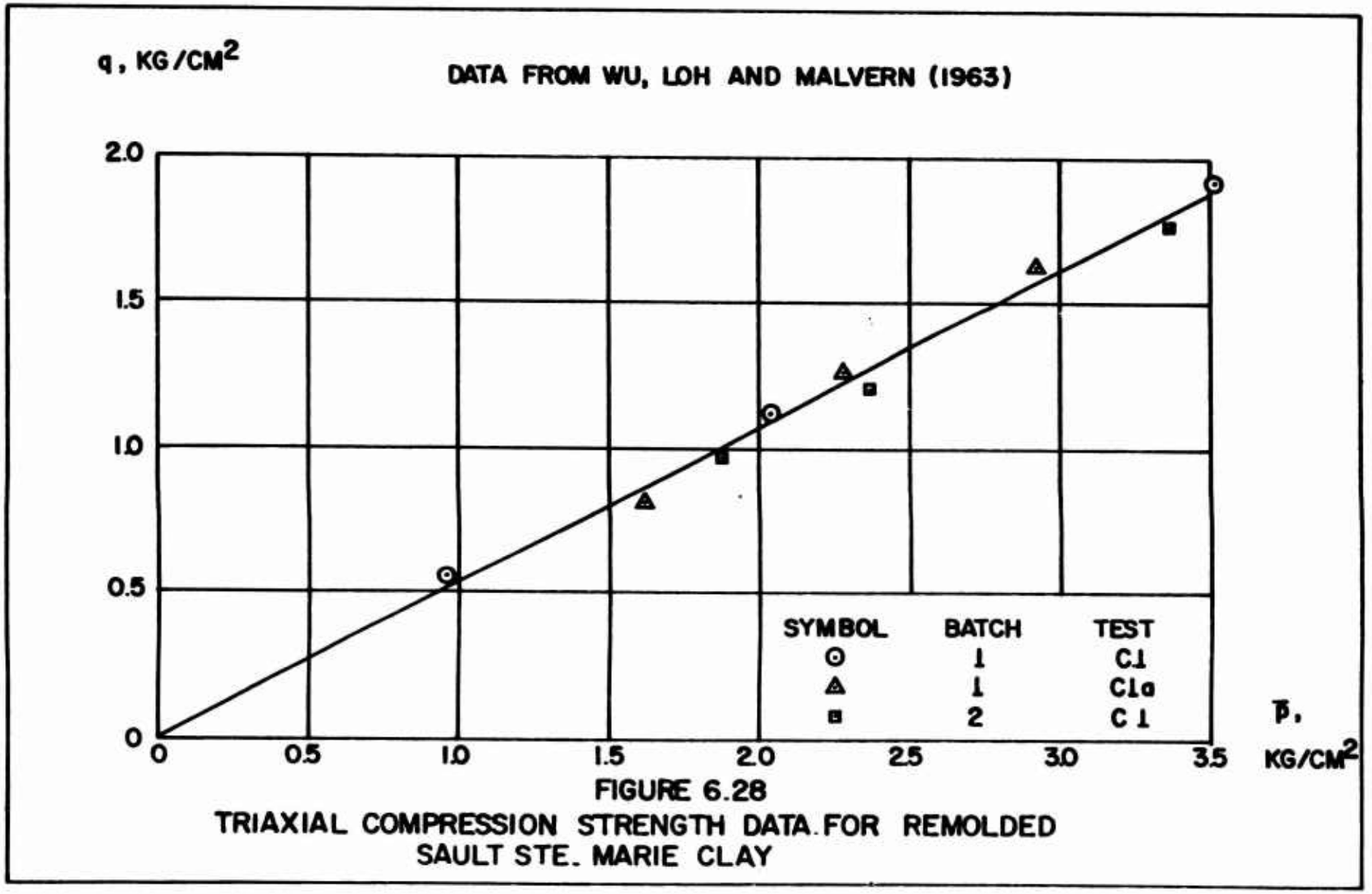

FIGURE 6.28
TRIAXIAL COMPRESSION STRENGTH DATA FOR REMOLDED SAULT STE. MARIE CLAY

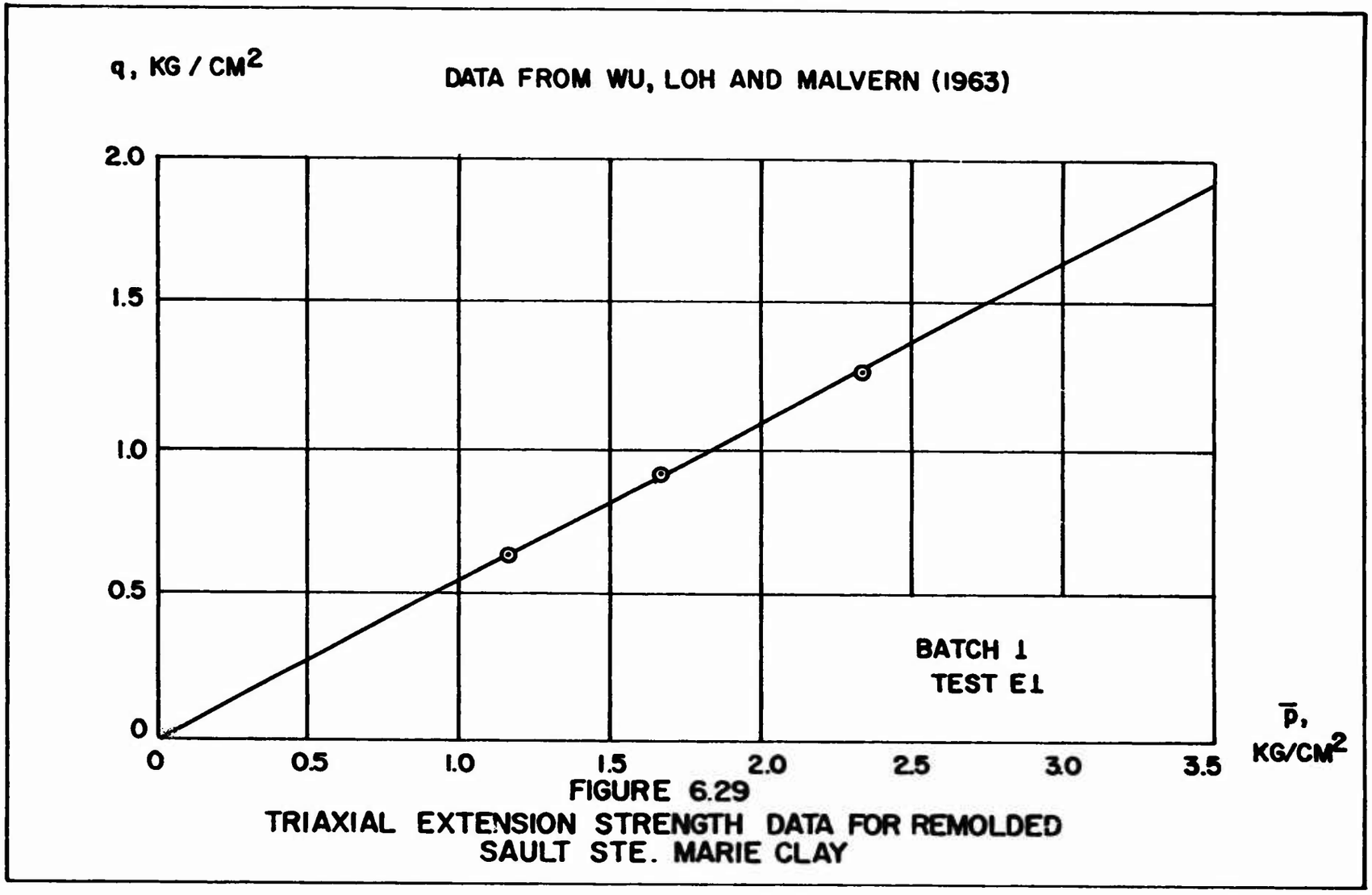

FIGURE 6.29

TRIAXIAL EXTENSION STRENGTH DATA FOR REMOLDED SAULT STE. MARIE CLAY

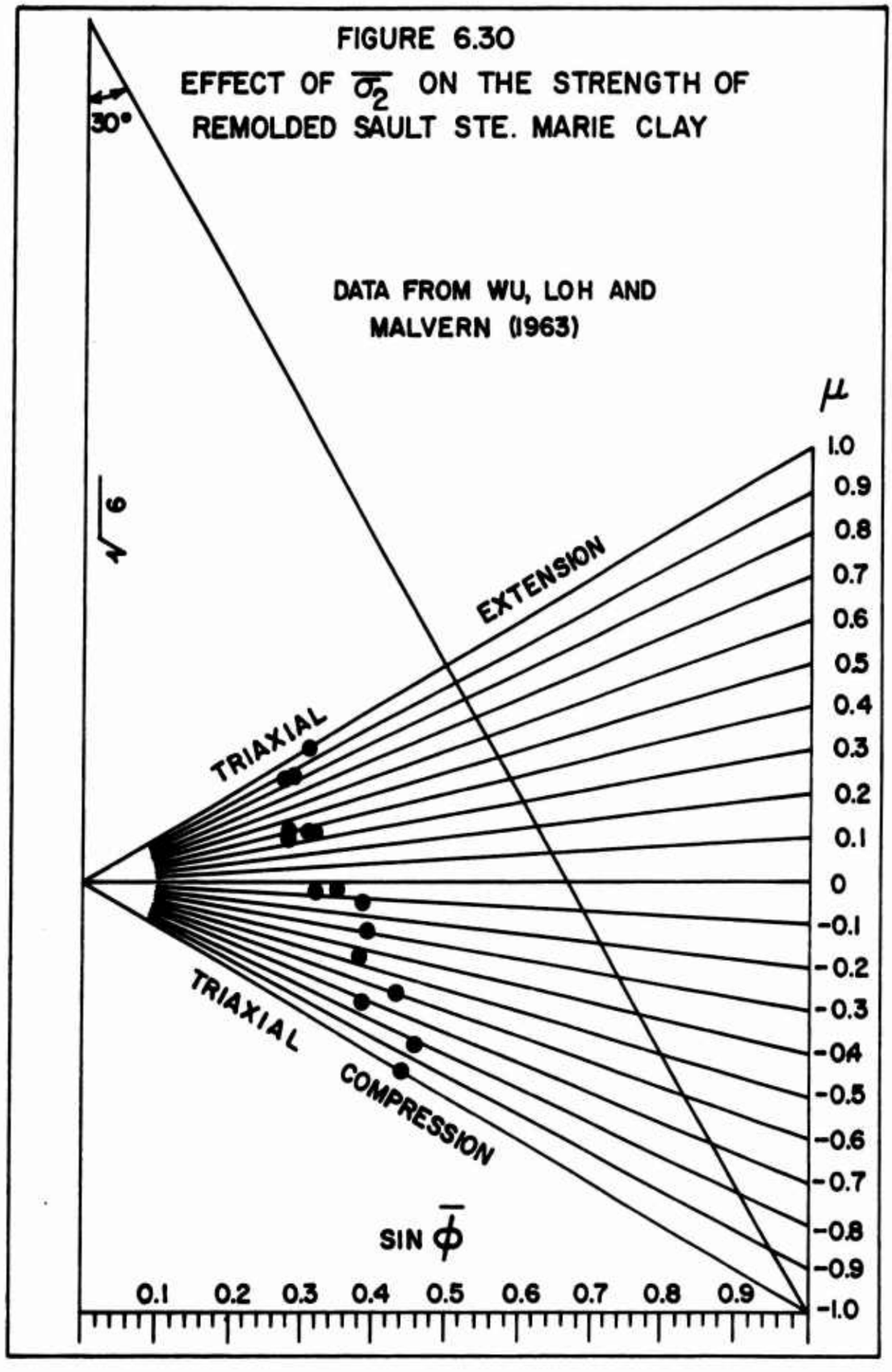
FIGURE 6.30
EFFECT OF $\overline{\sigma_2}$ ON THE STRENGTH OF
REMOLDED SAULT STE. MARIE CLAY
30°
DATA FROM WU, LOH AND
MALVERN (1963)
μ
1.0
0.9
0.8
0.7
0.6
0.5
0.4
0.3
0.2
0.1
0
-0.1
-0.2
-0.3
-04
-0.5
-0.6
-0.7
-0.8
-0.9
-1.0
$\sqrt{6}$
EXTENSION
TRIAXIAL
TRIAXIAL
COMPRESSION
SIN $\overline{\phi}$
0.1 0.2 0.3 0.4 0.5 0.6 0.7 0.8 0.9

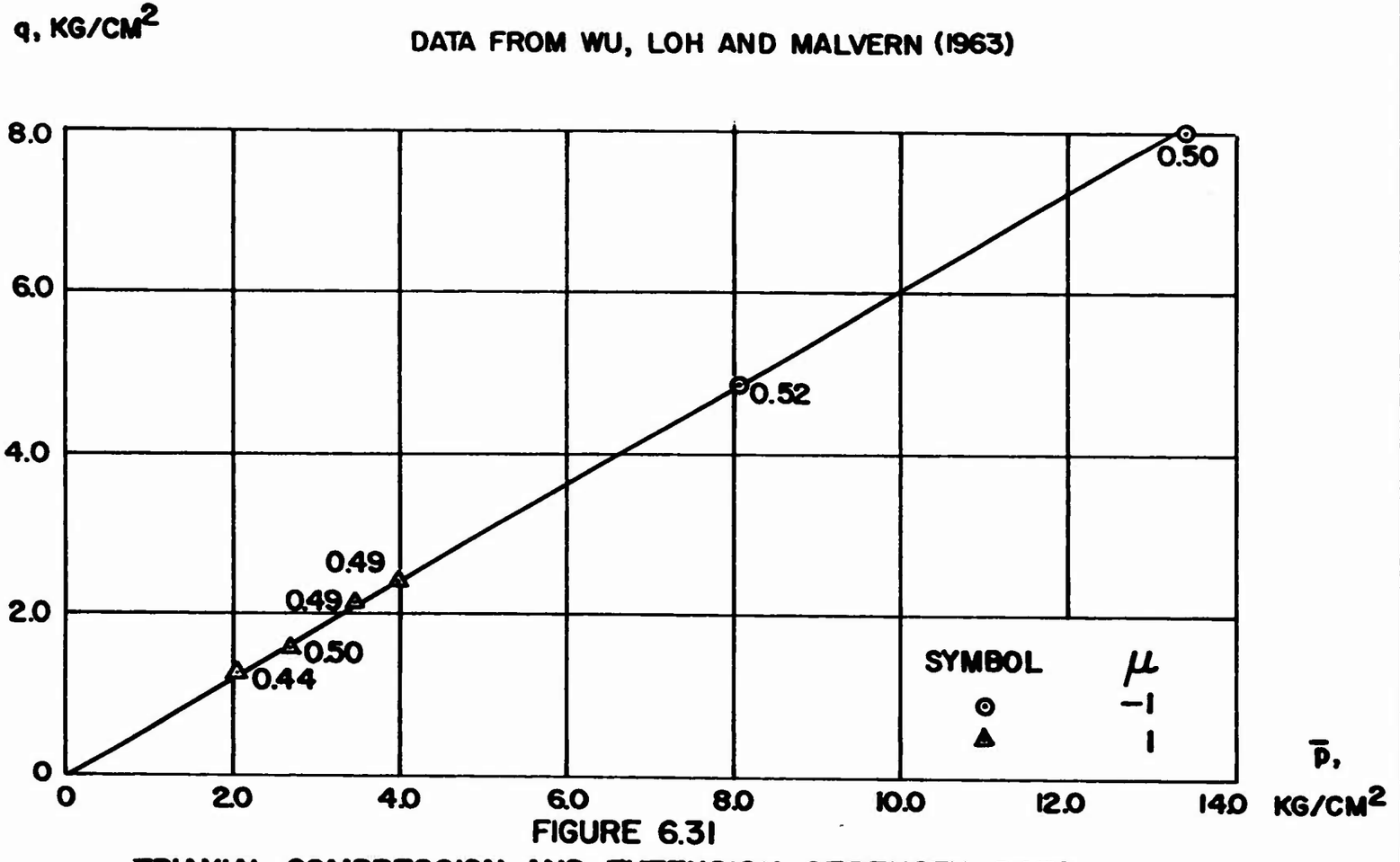

FIGURE 6.31

TRIAXIAL COMPRESSION AND EXTENSION STRENGTH DATA FOR THE 30-50 FRACTION OF STANDARD OTTAWA SAND

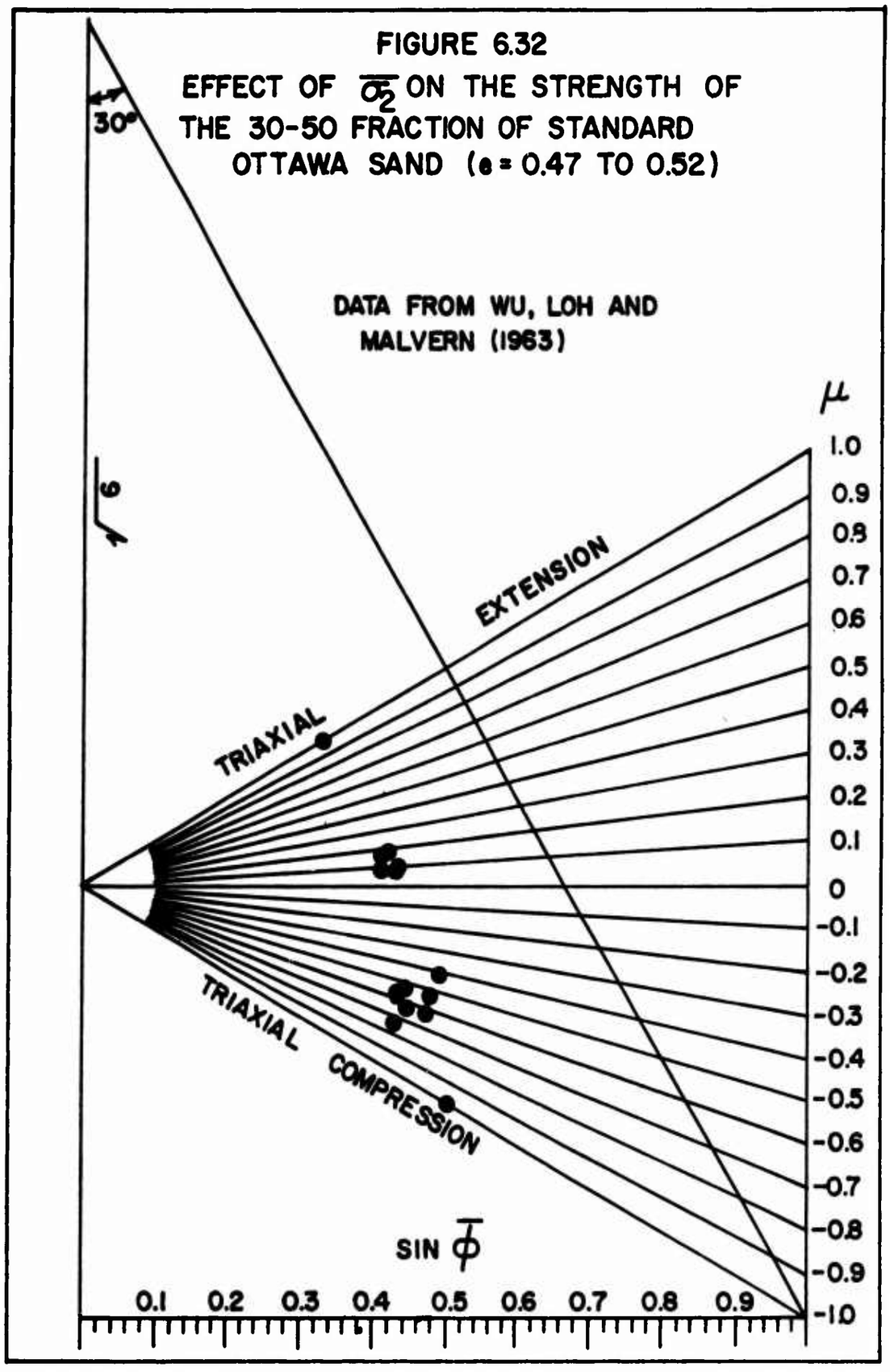

FIGURE 6.32
EFFECT OF $\overline{\sigma_2}$ ON THE STRENGTH OF THE 30-50 FRACTION OF STANDARD OTTAWA SAND (e = 0.47 TO 0.52)

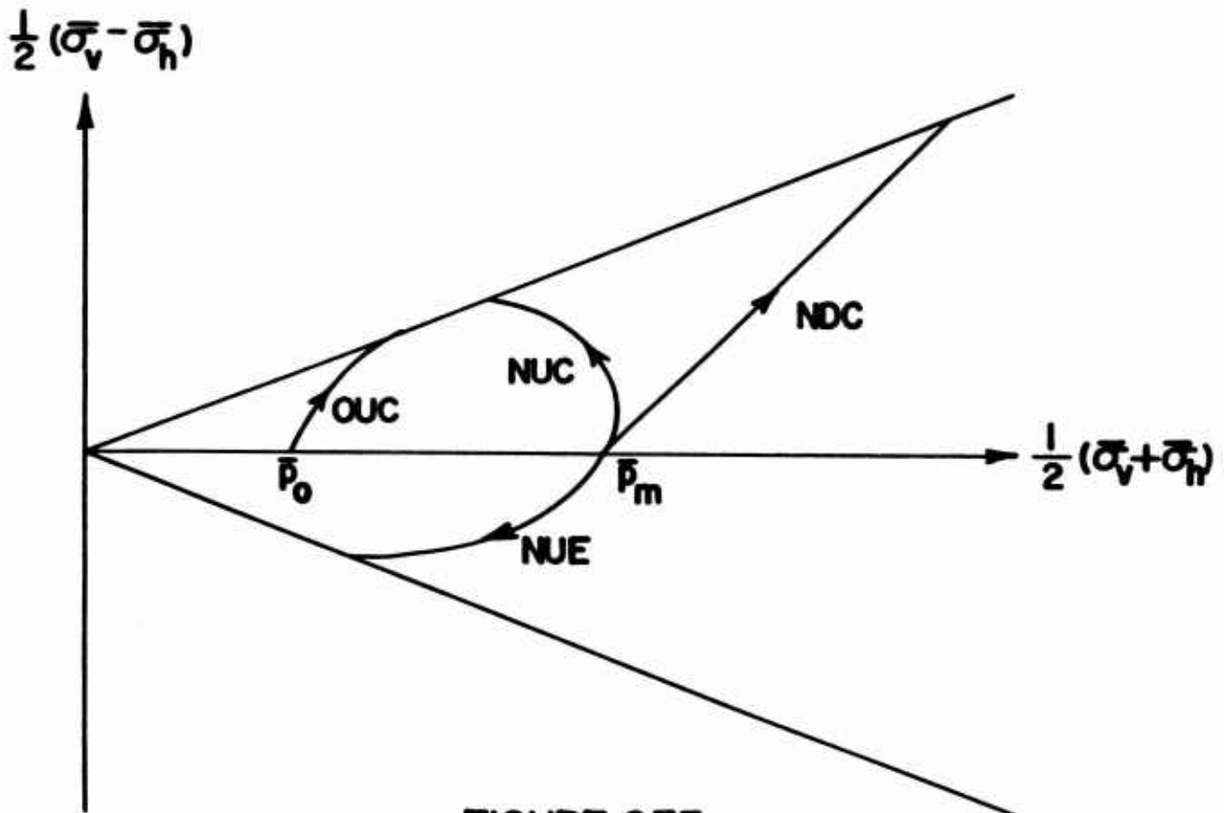

FIGURE 6.33

EFFECTIVE STRESS PATHS FOR ISOTROPICALLY CONSOLIDATED TRIAXIAL TESTS CONDUCTED BY SOWA (1963)

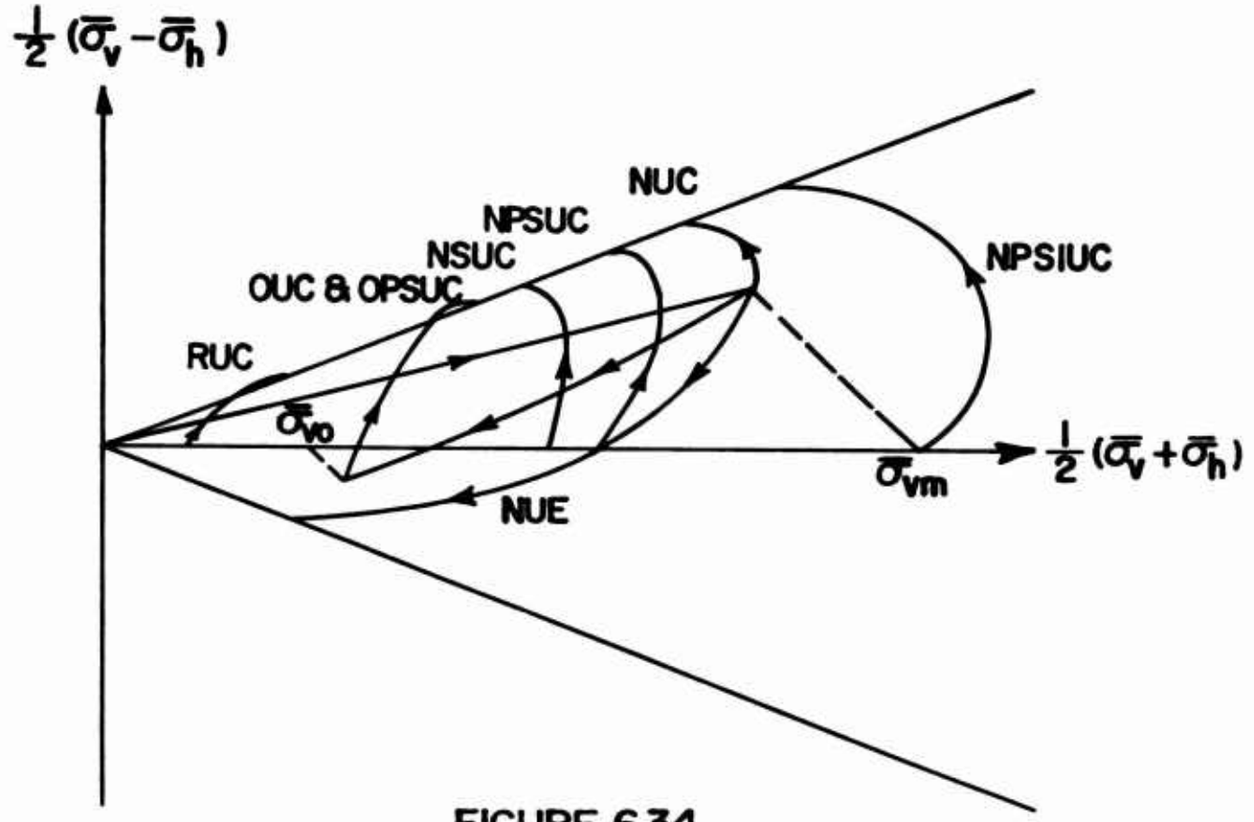

FIGURE 6.34

EFFECTIVE STRESS PATHS FOR K_o CONSOLIDATED TRIAXIAL TESTS CONDUCTED BY SOWA (1963)

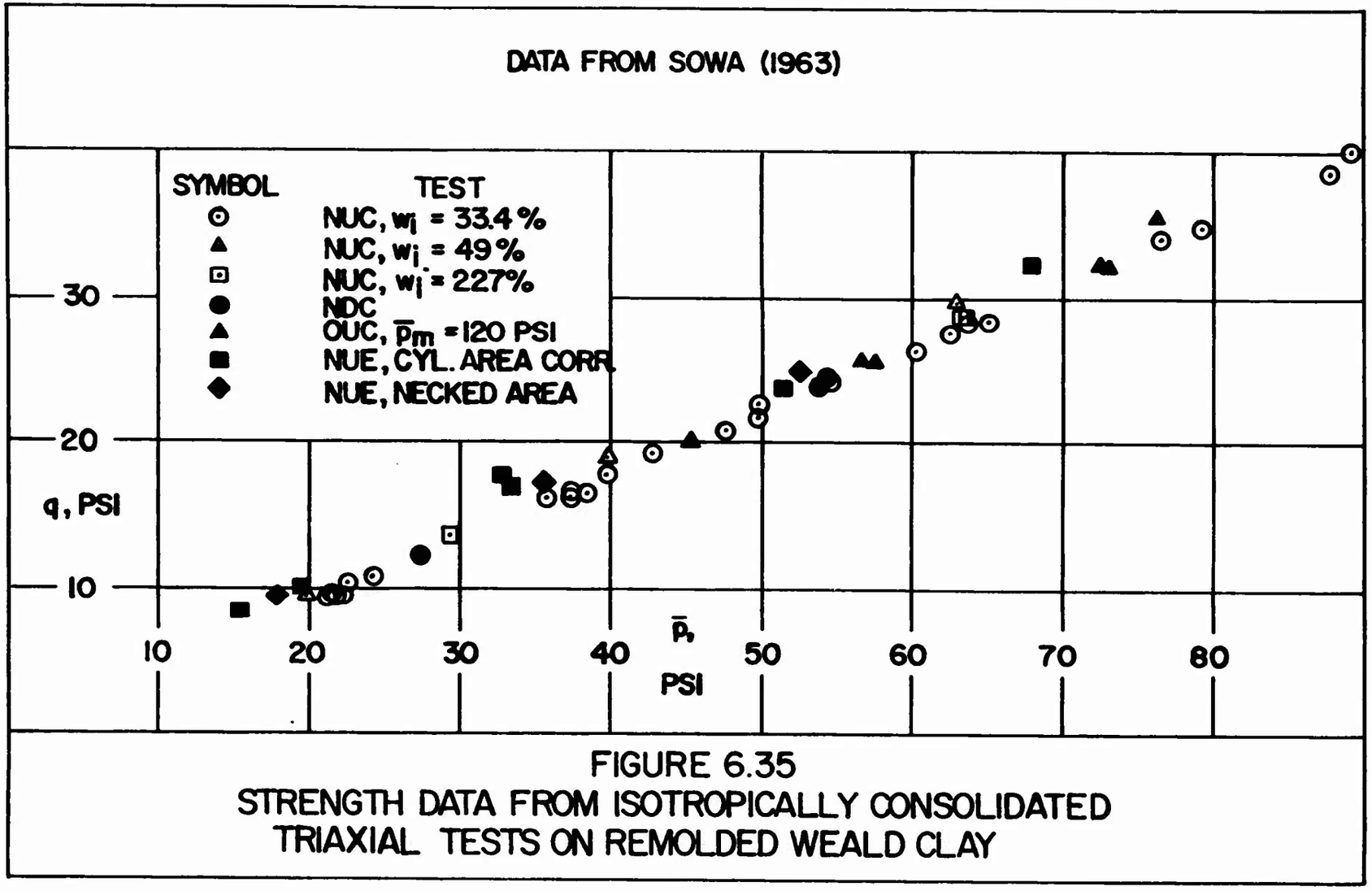

FIGURE 6.35
STRENGTH DATA FROM ISOTROPICALLY CONSOLIDATED
TRIAXIAL TESTS ON REMOLDED WEALD CLAY

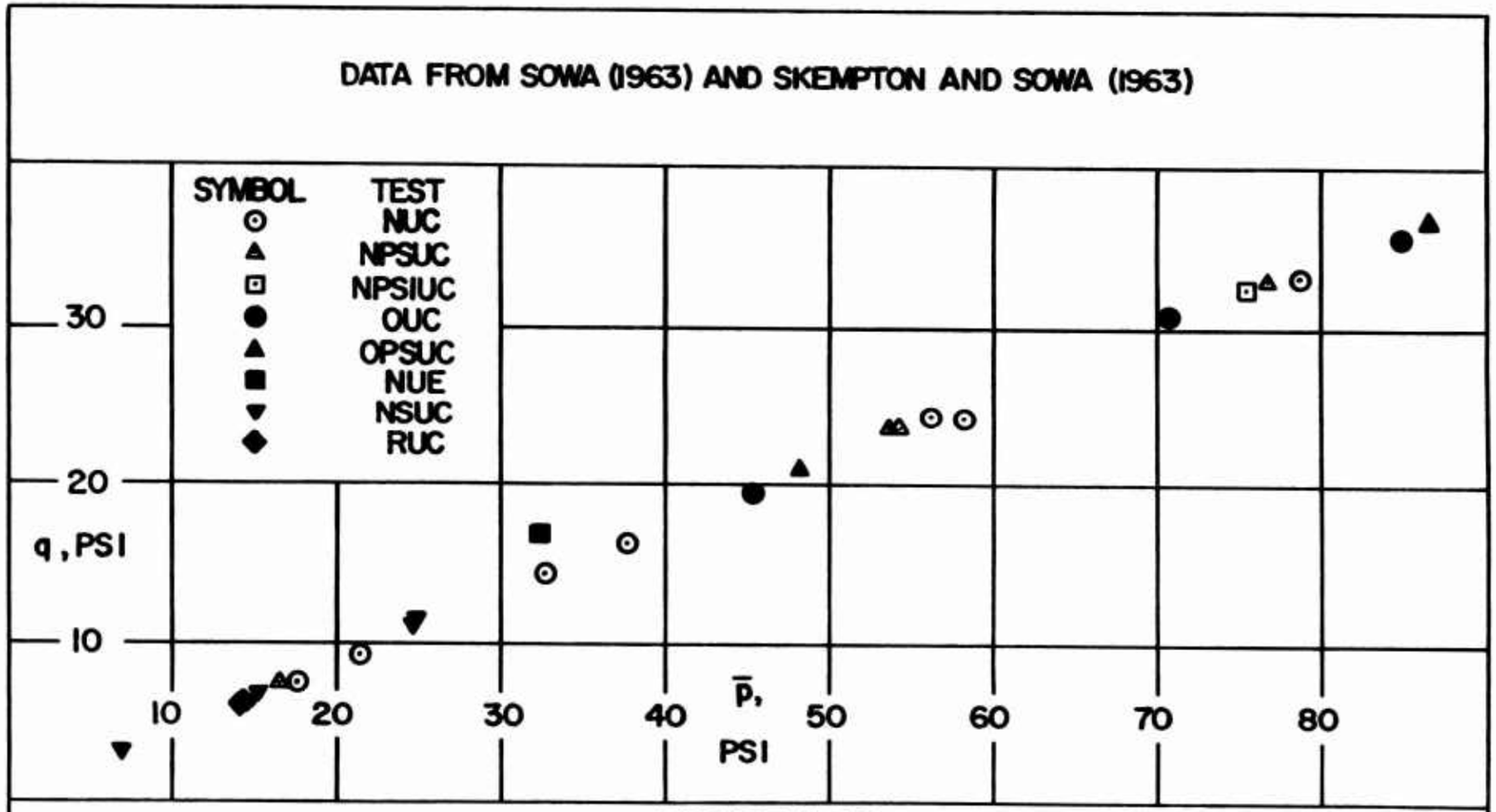

FIGURE 6.36
STRENGTH DATA FOR K_o CONSOLIDATED TRIAXIAL TESTS ON REMOLDED WEALD CLAY

DATA FROM WADE (1963)

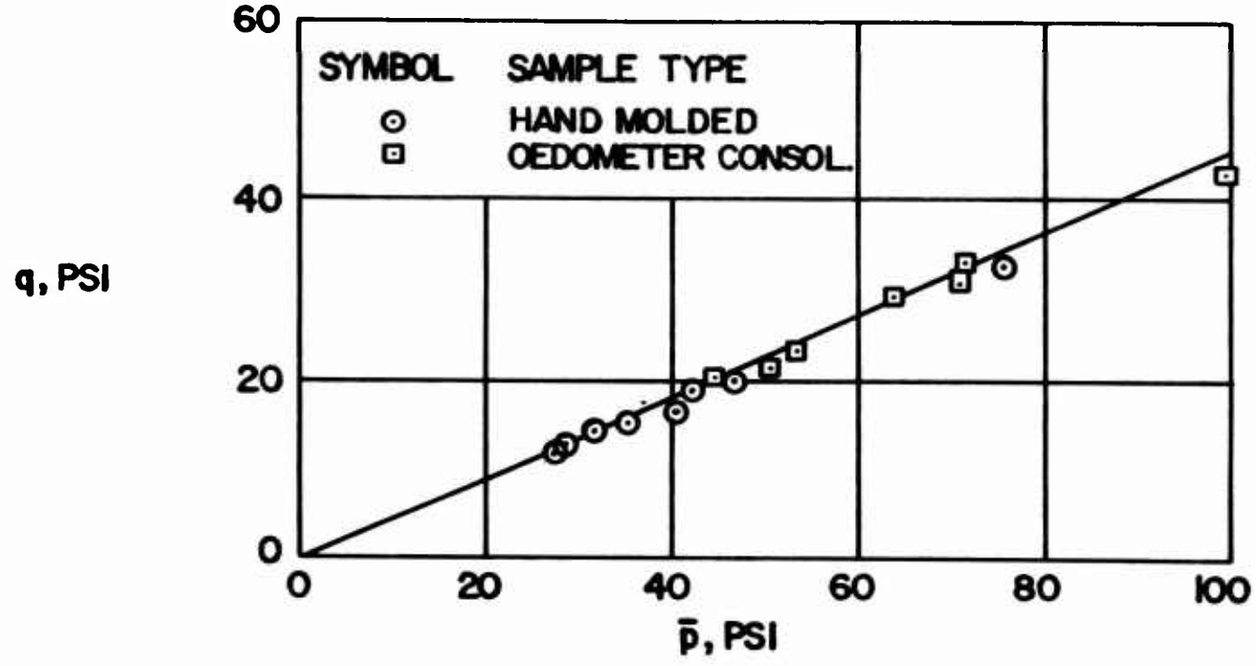

FIGURE 6.37

STRENGTH DATA FOR PLANE STRAIN TESTS ON REMOLDED WEALD CLAY

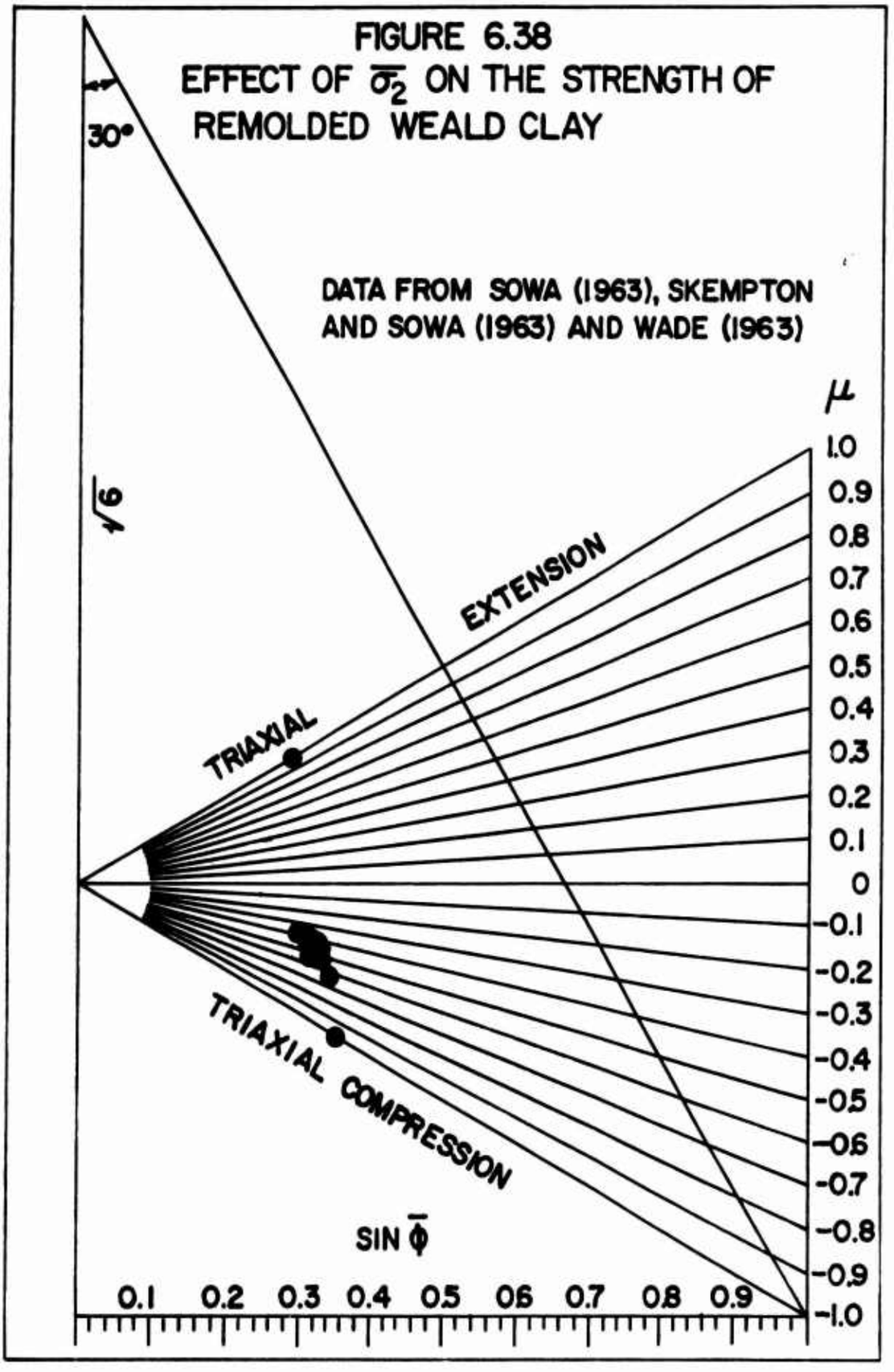

FIGURE 6.38
EFFECT OF $\bar{\sigma}_2$ ON THE STRENGTH OF REMOLDED WEALD CLAY

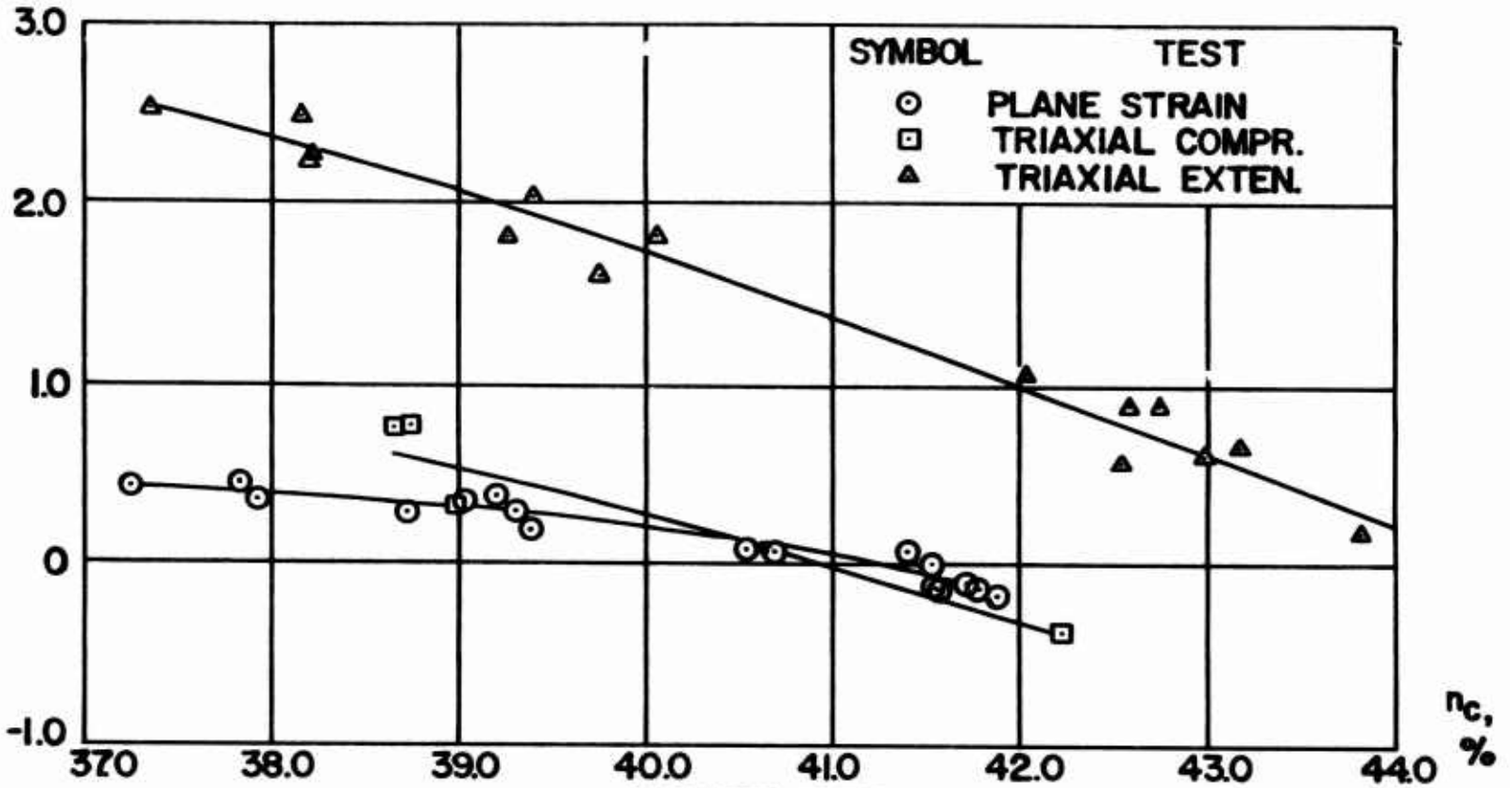

FIGURE 6.39
VOLUMETRIC STRAIN AT FAILURE IN PLANE STRAIN AND TRIAXIAL TESTS ON BELGIUM SAND

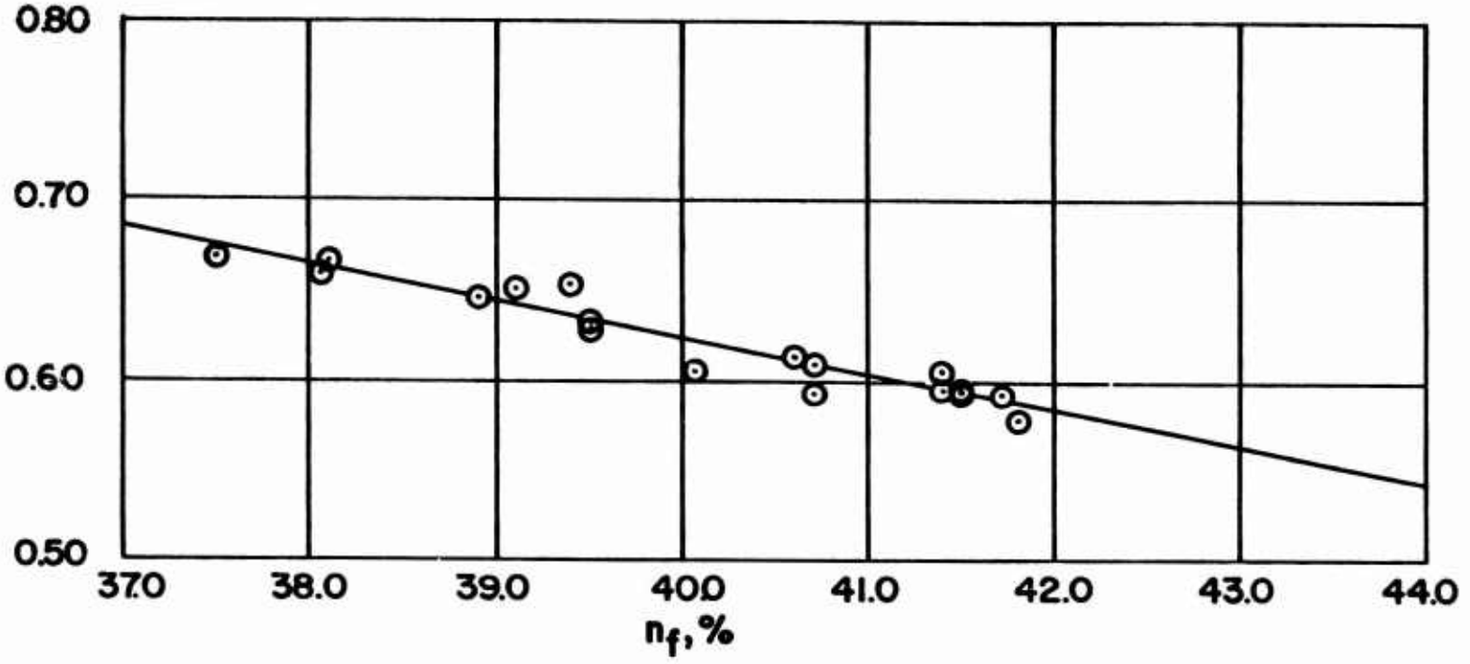

FIGURE 6.40 (a)

INFLUENCE OF DENSITY ON THE APPARENT ANGLE OF INTERNAL FRICTION OF BELGIUM SAND - PLAIN STRAIN

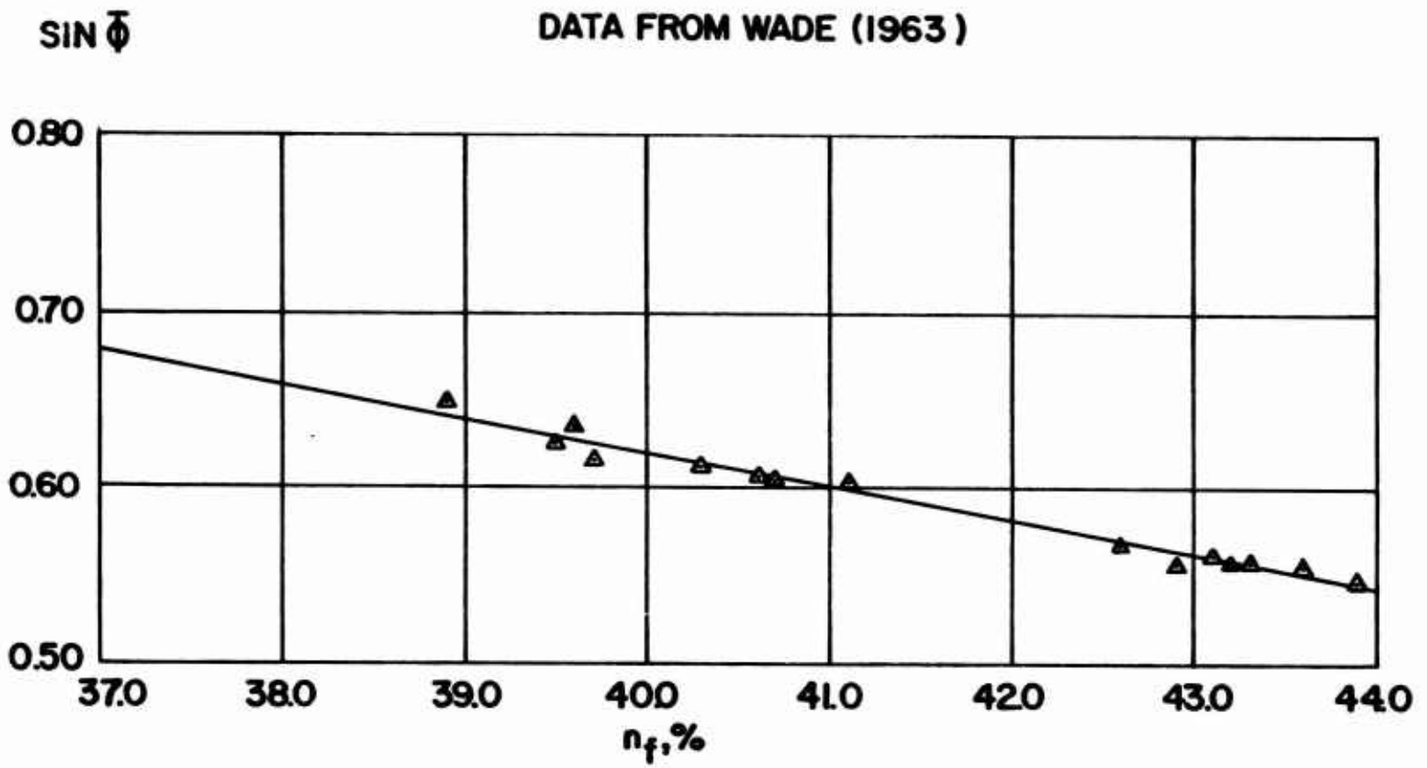

FIGURE 6.40(b)

INFLUENCE OF DENSITY ON THE APPARENT ANGLE OF INTERNAL FRICTION OF BELGIUM SAND – CYLINDRICAL COMPRESSION

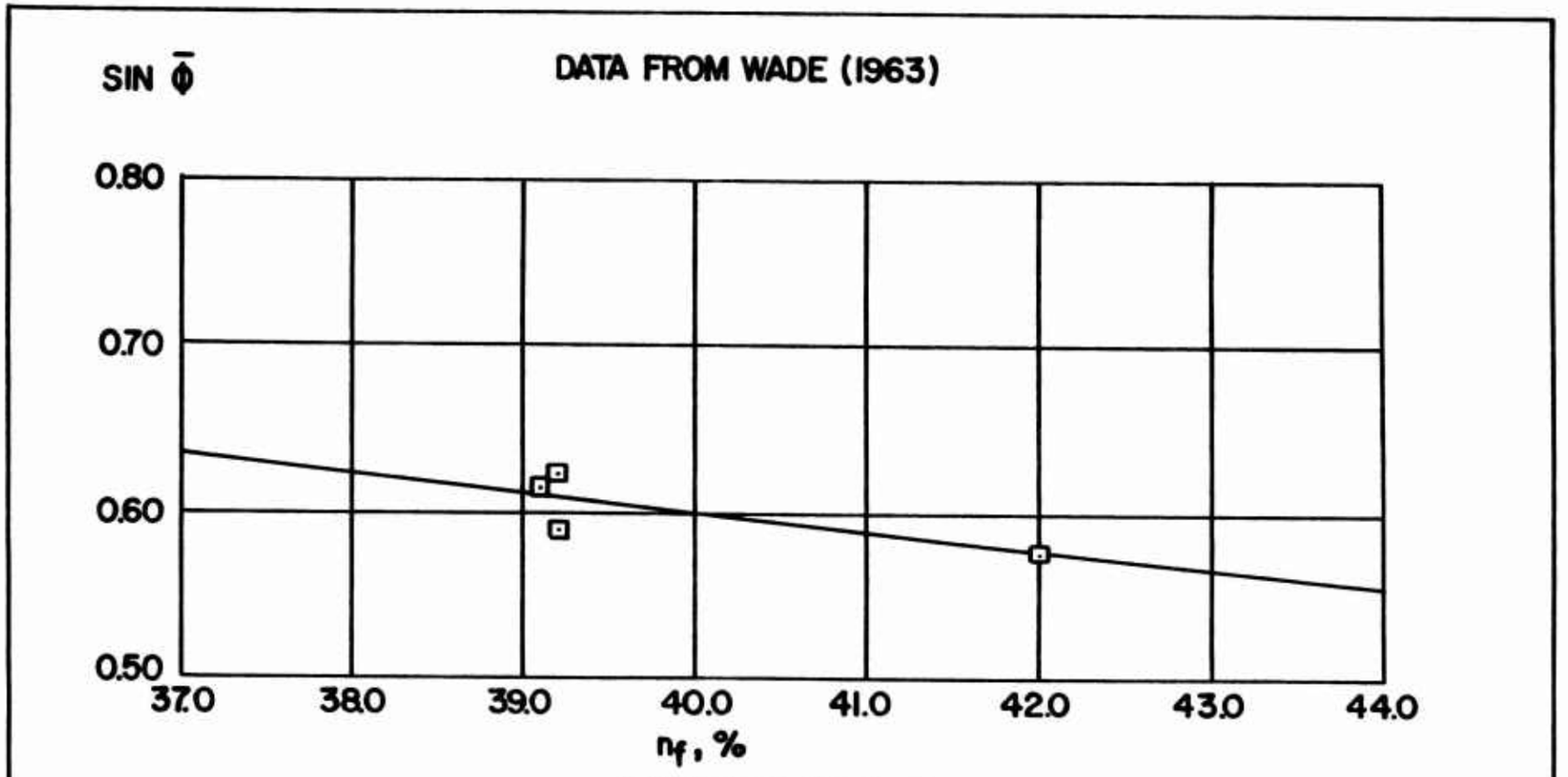

FIGURE 6.40 (c)

INFLUENCE OF DENSITY ON THE APPARENT ANGLE OF INTERNAL FRICTION OF BELGIUM SAND – CYLINDRICAL EXTENSION

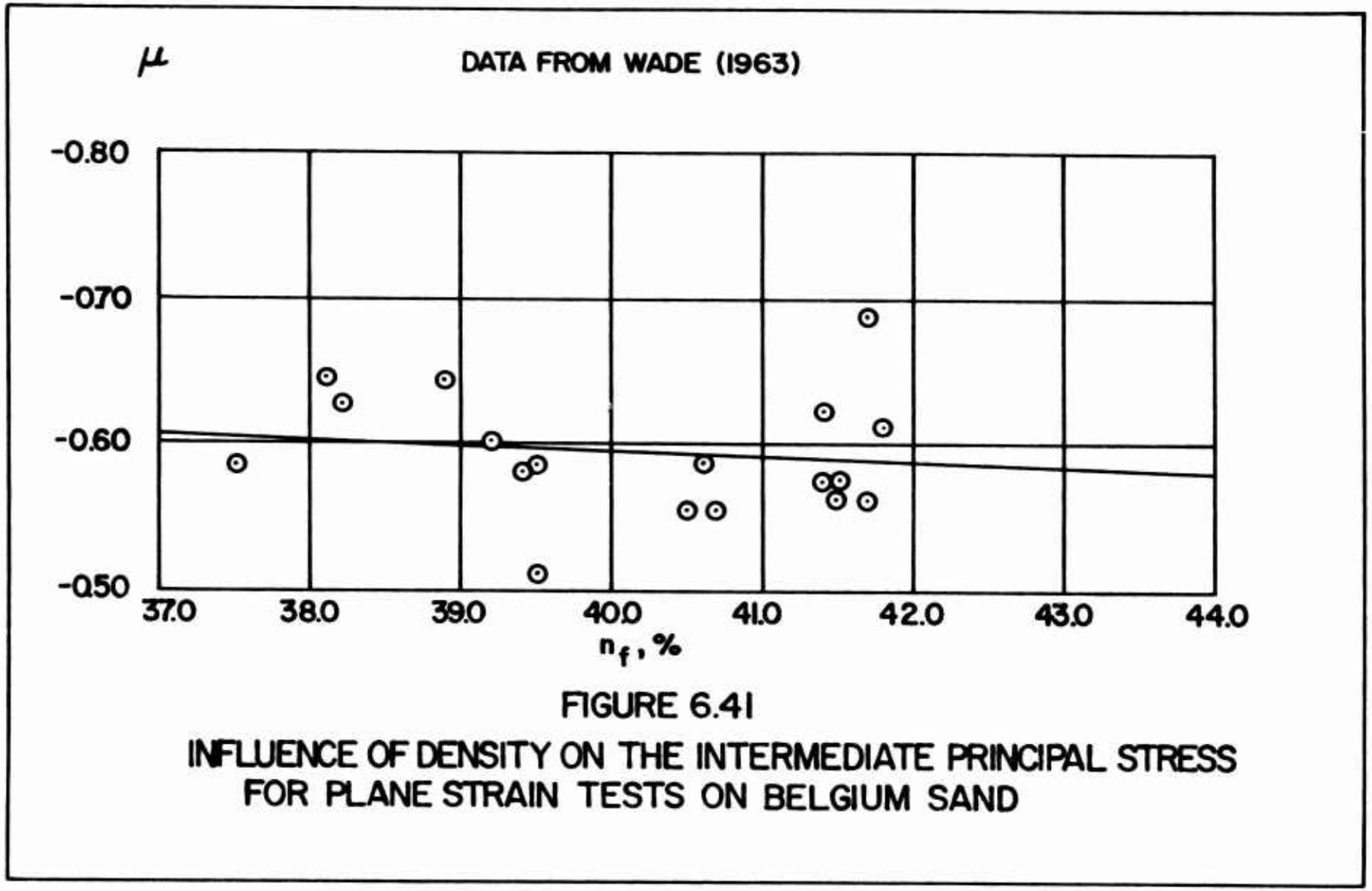

FIGURE 6.41

INFLUENCE OF DENSITY ON THE INTERMEDIATE PRINCIPAL STRESS FOR PLANE STRAIN TESTS ON BELGIUM SAND

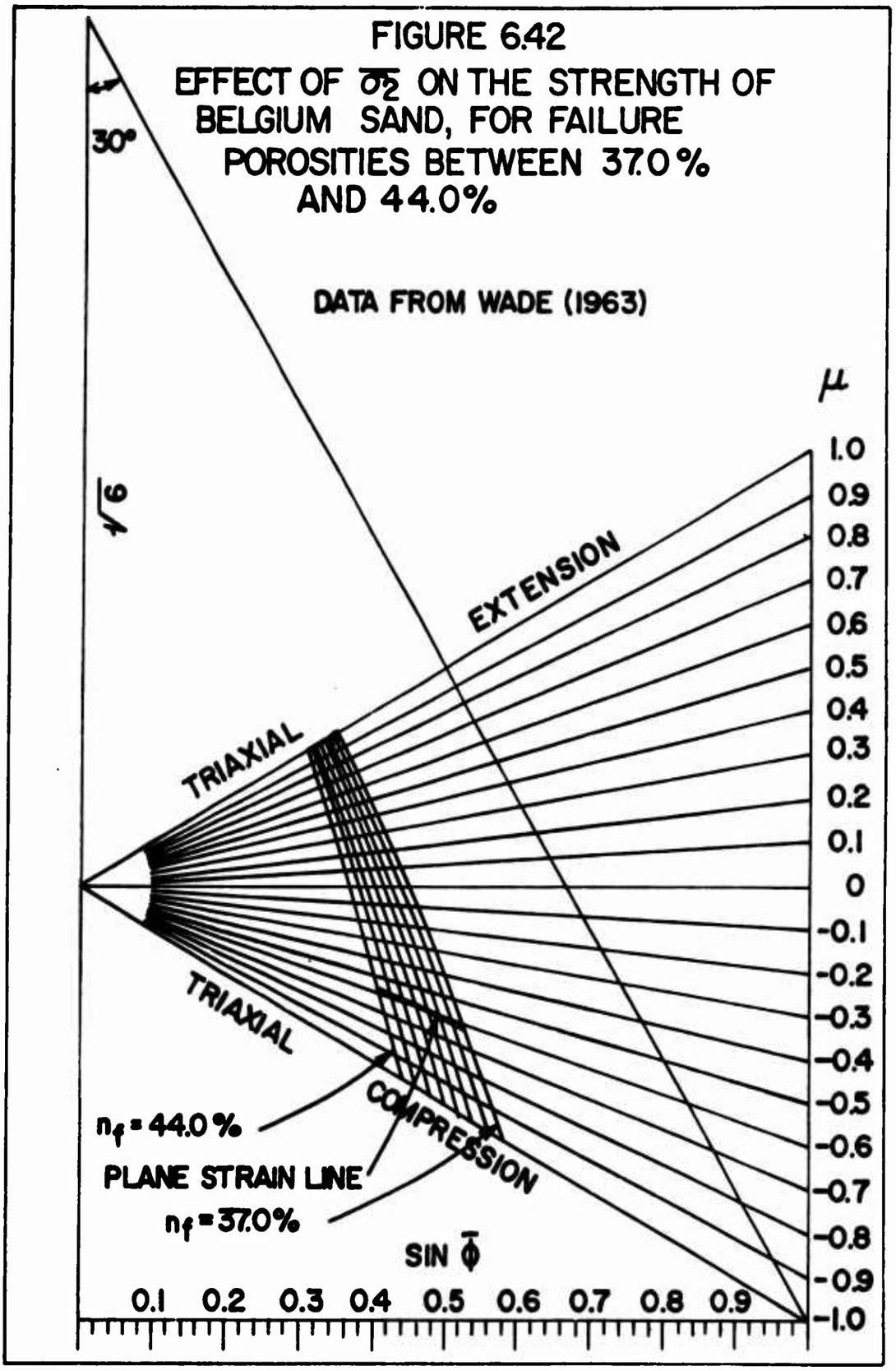

FIGURE 6.42
EFFECT OF $\bar{\sigma_2}$ ON THE STRENGTH OF BELGIUM SAND, FOR FAILURE POROSITIES BETWEEN 37.0 % AND 44.0%

DATA FROM WADE (1963)

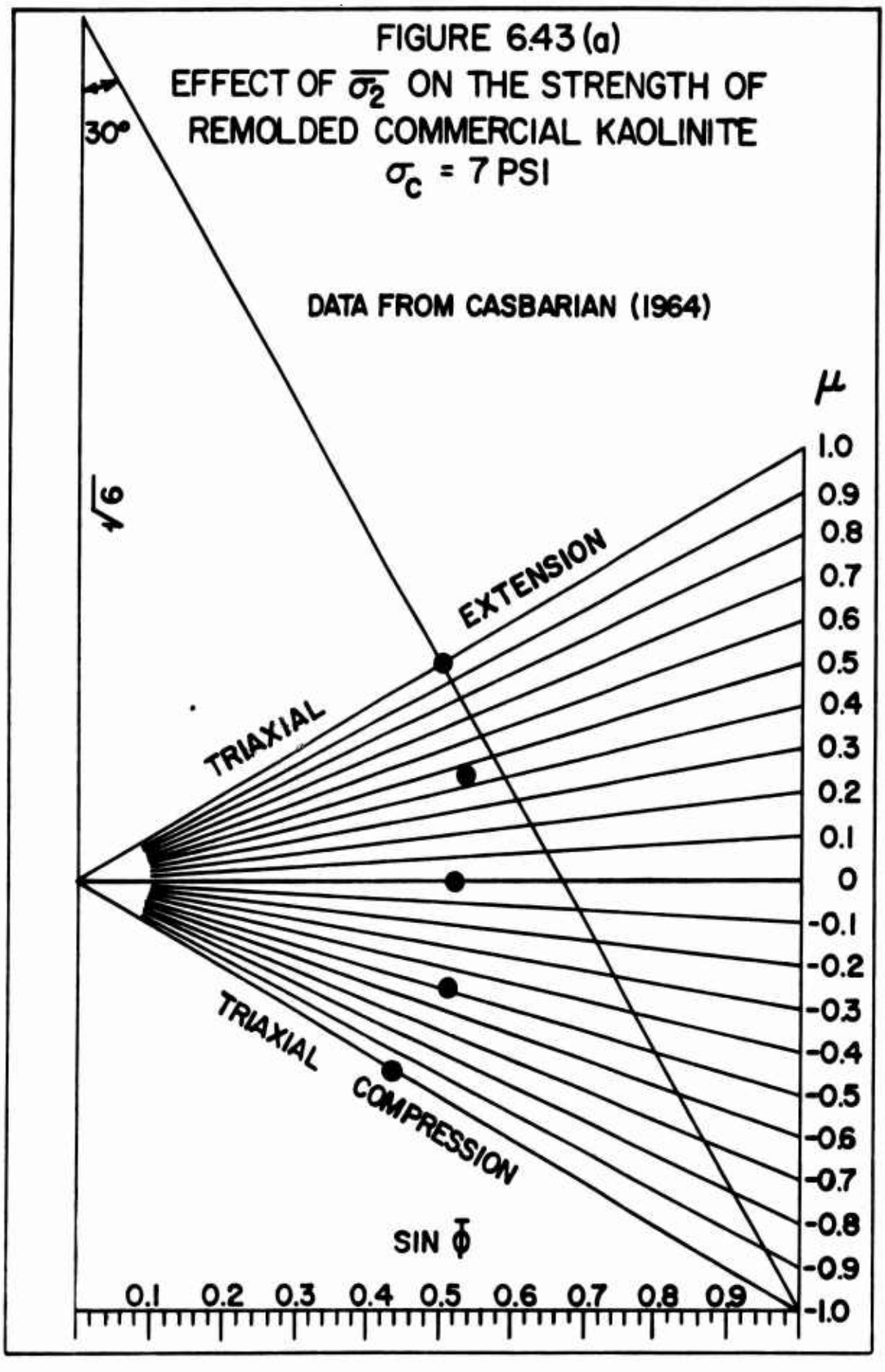
FIGURE 6.43 (a)
EFFECT OF $\overline{\sigma_2}$ ON THE STRENGTH OF
REMOLDED COMMERCIAL KAOLINITE
σ_c = 7 PSI
30°
DATA FROM CASBARIAN (1964)
$\sqrt{6}$
μ
1.0
0.9
0.8
0.7
0.6
0.5
0.4
0.3
0.2
0.1
0
-0.1
-0.2
-0.3
-0.4
-0.5
-0.6
-0.7
-0.8
-0.9
-1.0
EXTENSION
TRIAXIAL
TRIAXIAL
COMPRESSION
SIN $\bar{\phi}$
0.1 0.2 0.3 0.4 0.5 0.6 0.7 0.8 0.9

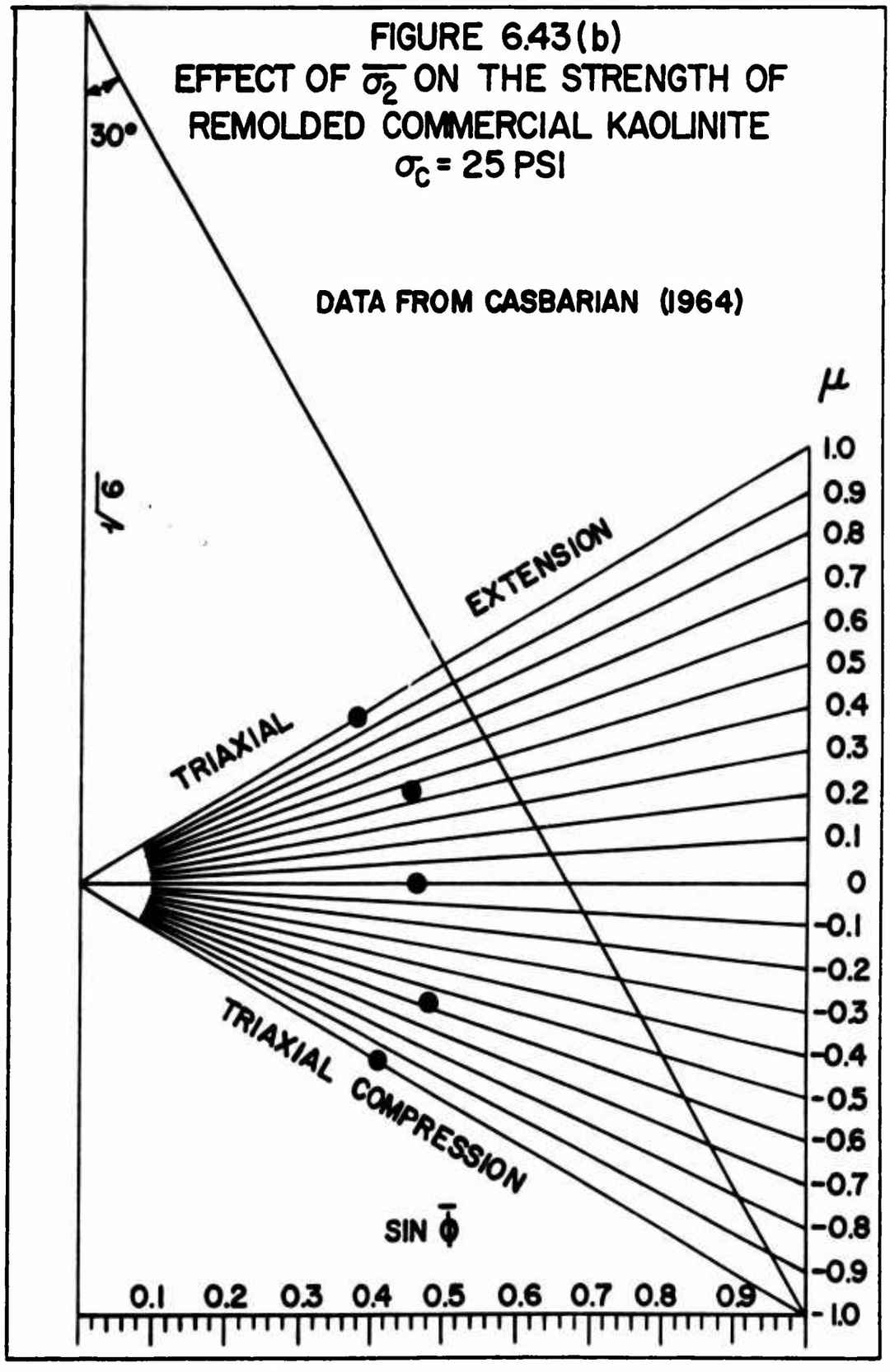

FIGURE 6.43(b)
EFFECT OF $\overline{\sigma_2}$ ON THE STRENGTH OF REMOLDED COMMERCIAL KAOLINITE
σ_c = 25 PSI

DATA FROM CASBARIAN (1964)

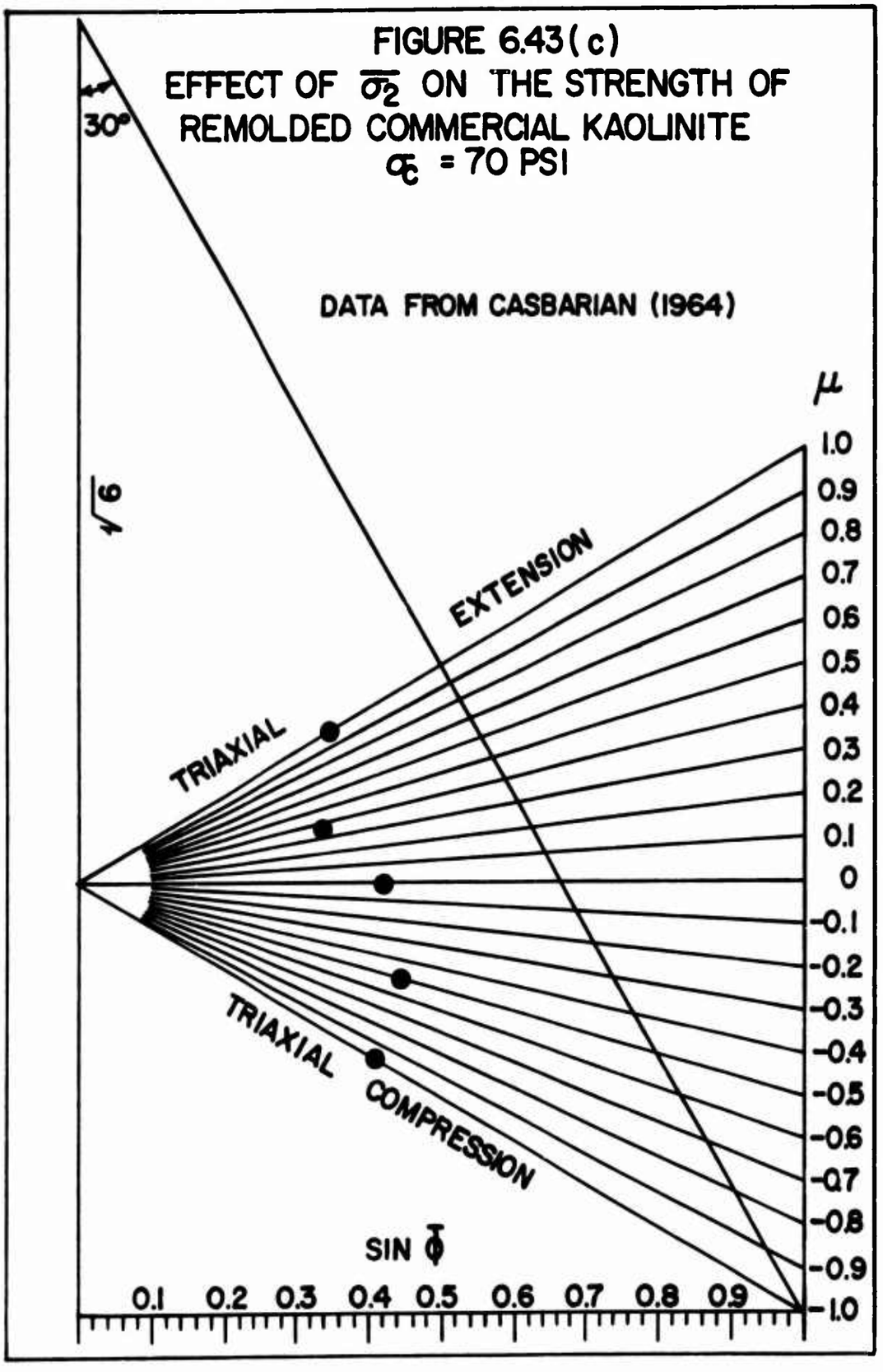

FIGURE 6.43(c)
EFFECT OF $\overline{\sigma_2}$ ON THE STRENGTH OF REMOLDED COMMERCIAL KAOLINITE
σ_c = 70 PSI

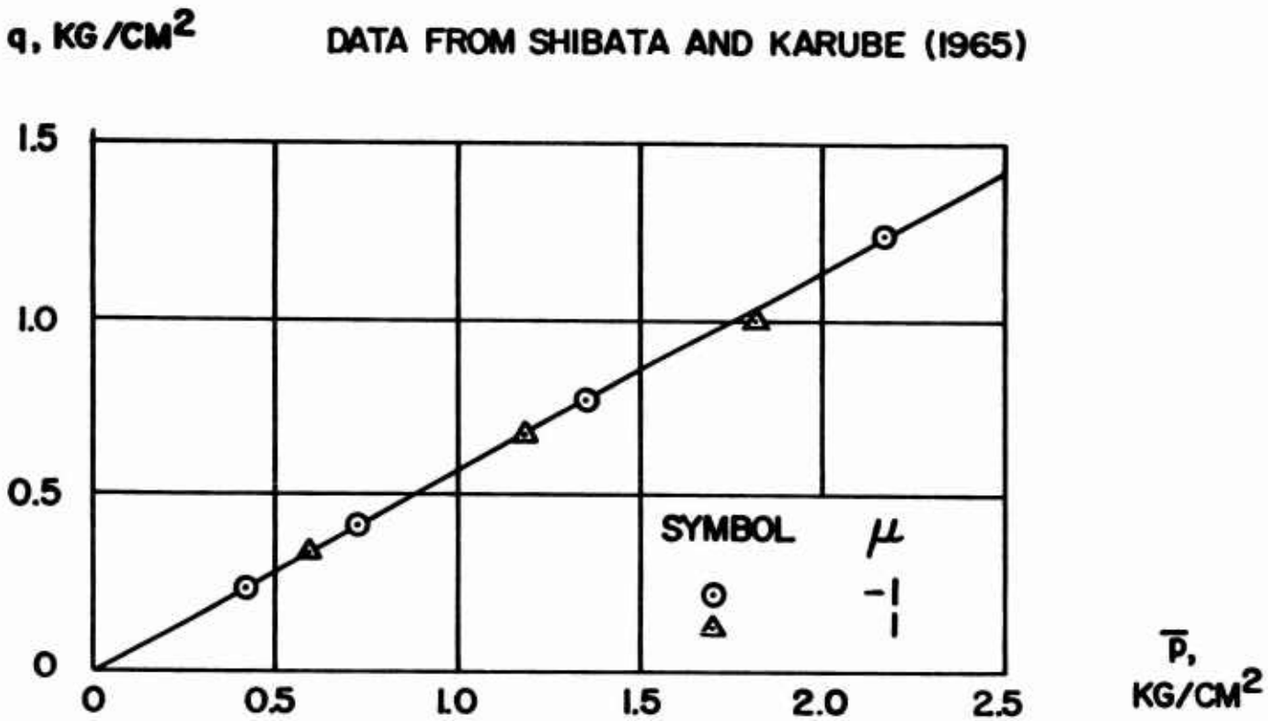

FIGURE 6.44

TRIAXIAL COMPRESSION AND EXTENSION STRENGTH DATA FOR REMOLDED OSAKA ALLUVIAL CLAY AT MAXIMUM PRINCIPAL EFFECTIVE STRESS RATIO

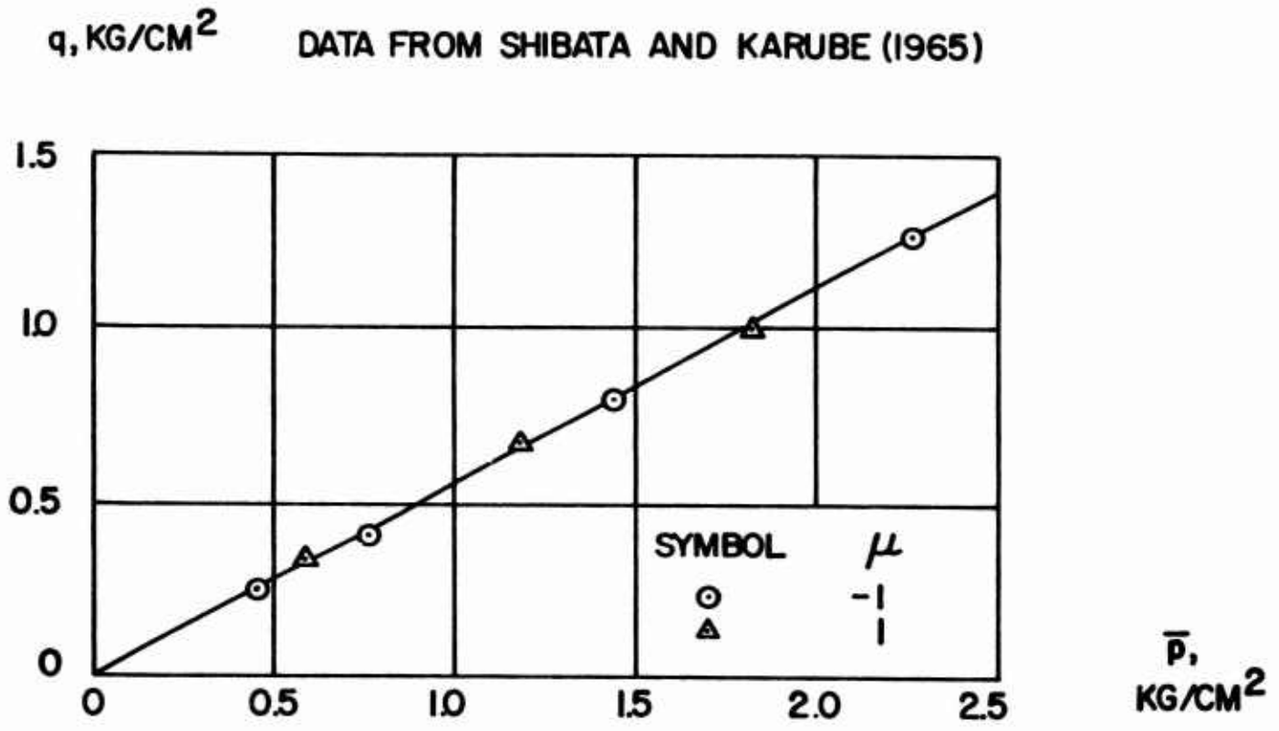

FIGURE 6.45
TRIAXIAL COMPRESSION AND EXTENSION STRENGTH DATA FOR REMOLDED OSAKA ALLUVIAL CLAY AT MAXIMUM PRINCIPAL STRESS DIFFERENCE

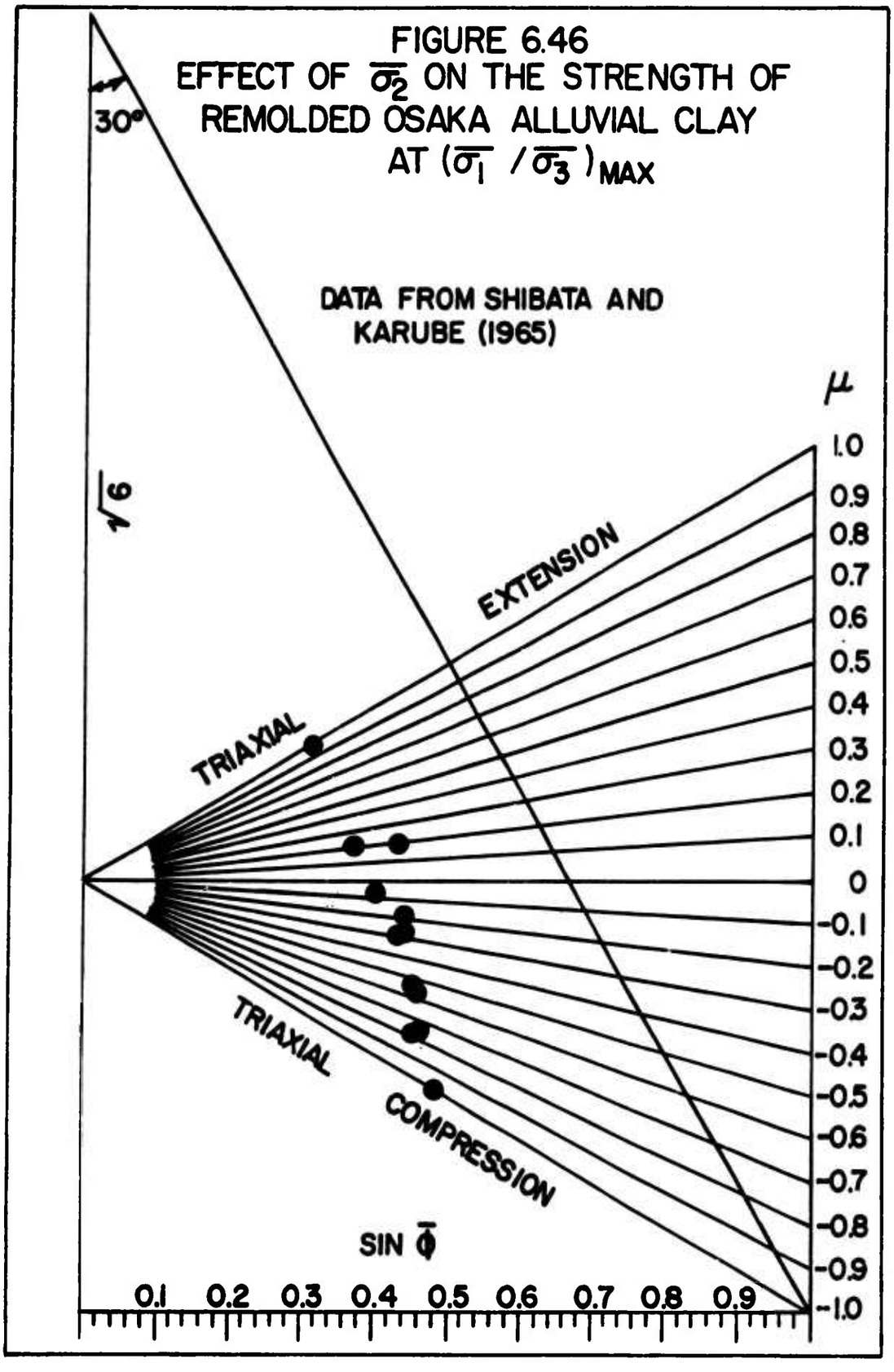

FIGURE 6.46
EFFECT OF $\overline{\sigma_2}$ ON THE STRENGTH OF REMOLDED OSAKA ALLUVIAL CLAY AT $(\overline{\sigma_1} / \overline{\sigma_3})_{MAX}$

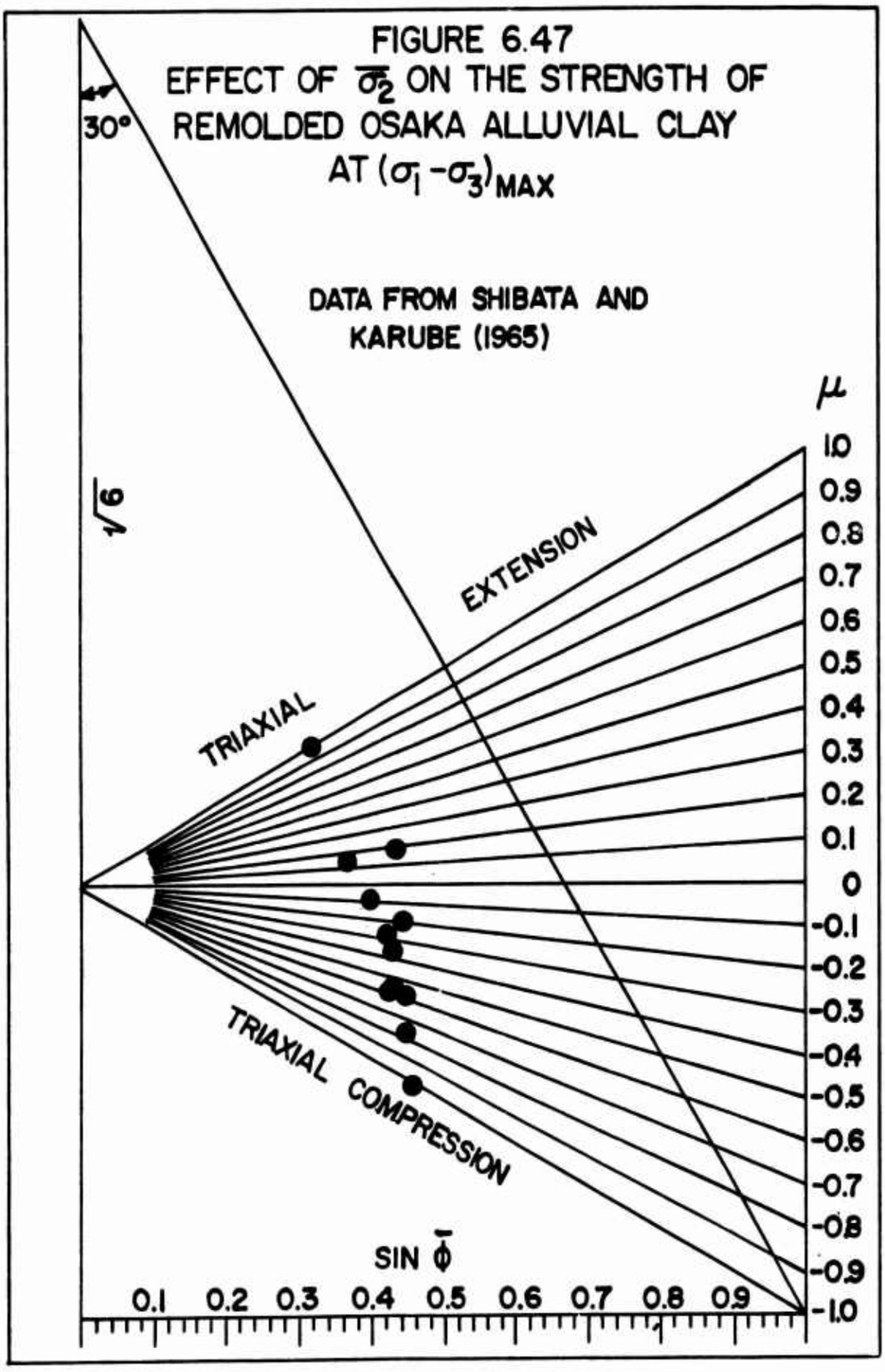

FIGURE 6.47
EFFECT OF $\bar{\sigma}_2$ ON THE STRENGTH OF REMOLDED OSAKA ALLUVIAL CLAY AT $(\sigma_1 - \sigma_3)_{MAX}$

DATA FROM SHIBATA AND KARUBE (1965)

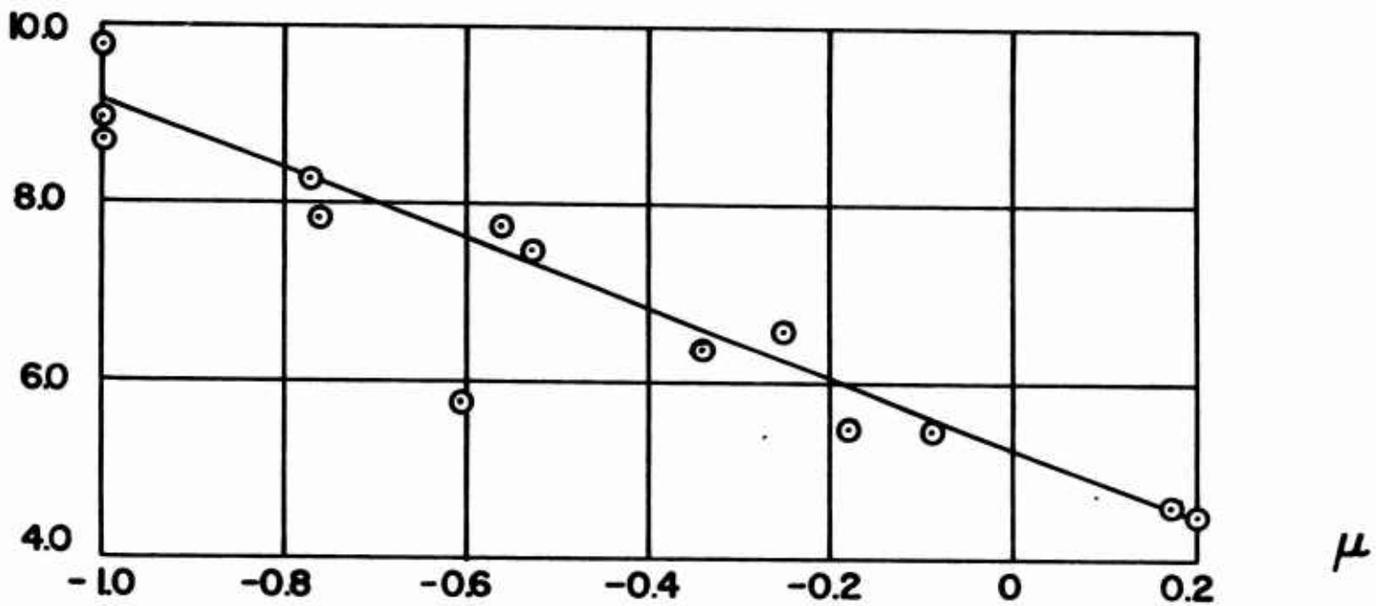

FIGURE 6.48

RELATION BETWEEN STRAIN AT MAXIMUM PRINCIPAL STRESS DIFFERENCE AND LODE'S PARAMETER FOR REMOLDED OSAKA ALLUVIAL CLAY

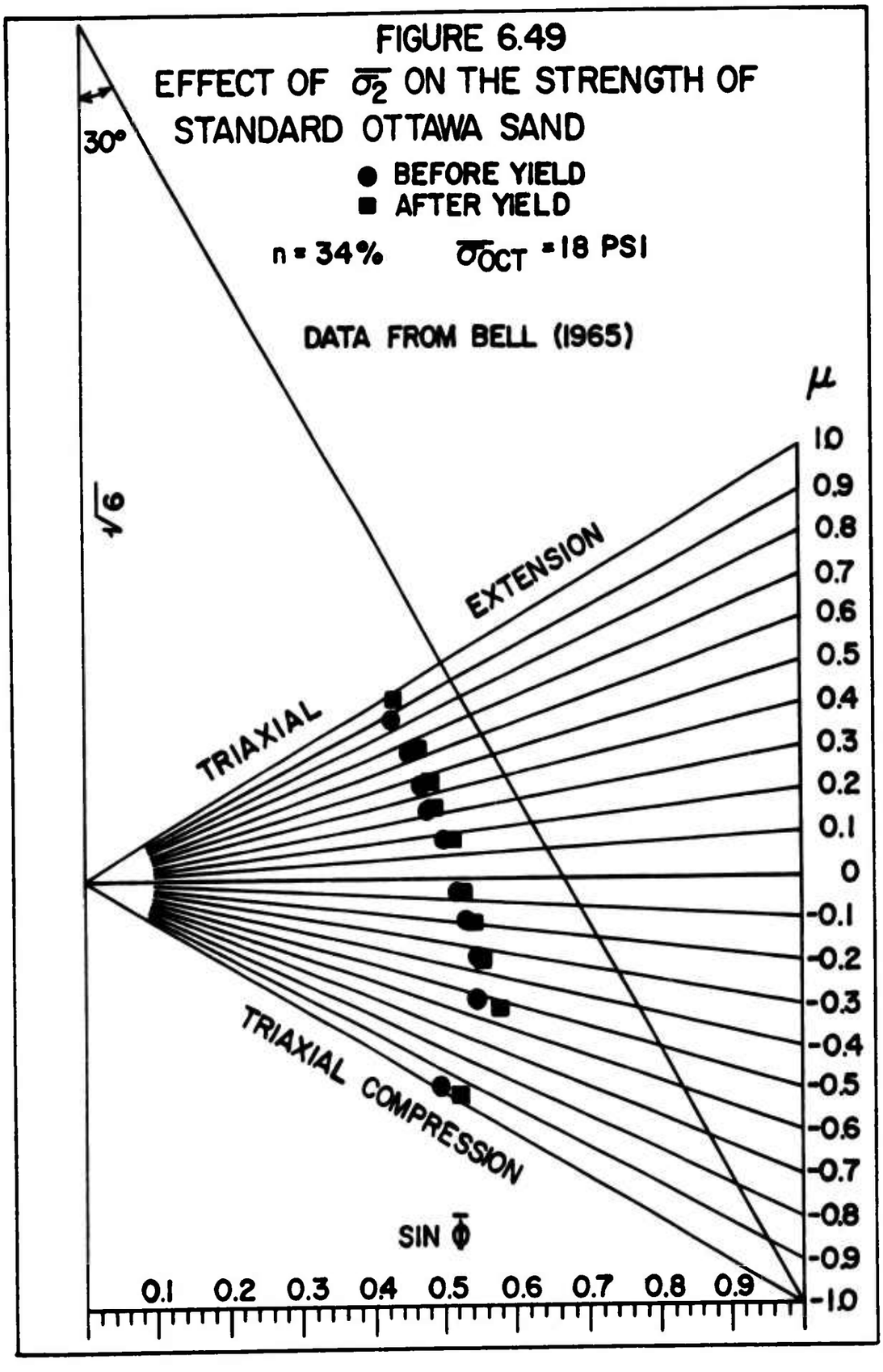

FIGURE 6.49
EFFECT OF $\overline{\sigma_2}$ ON THE STRENGTH OF STANDARD OTTAWA SAND

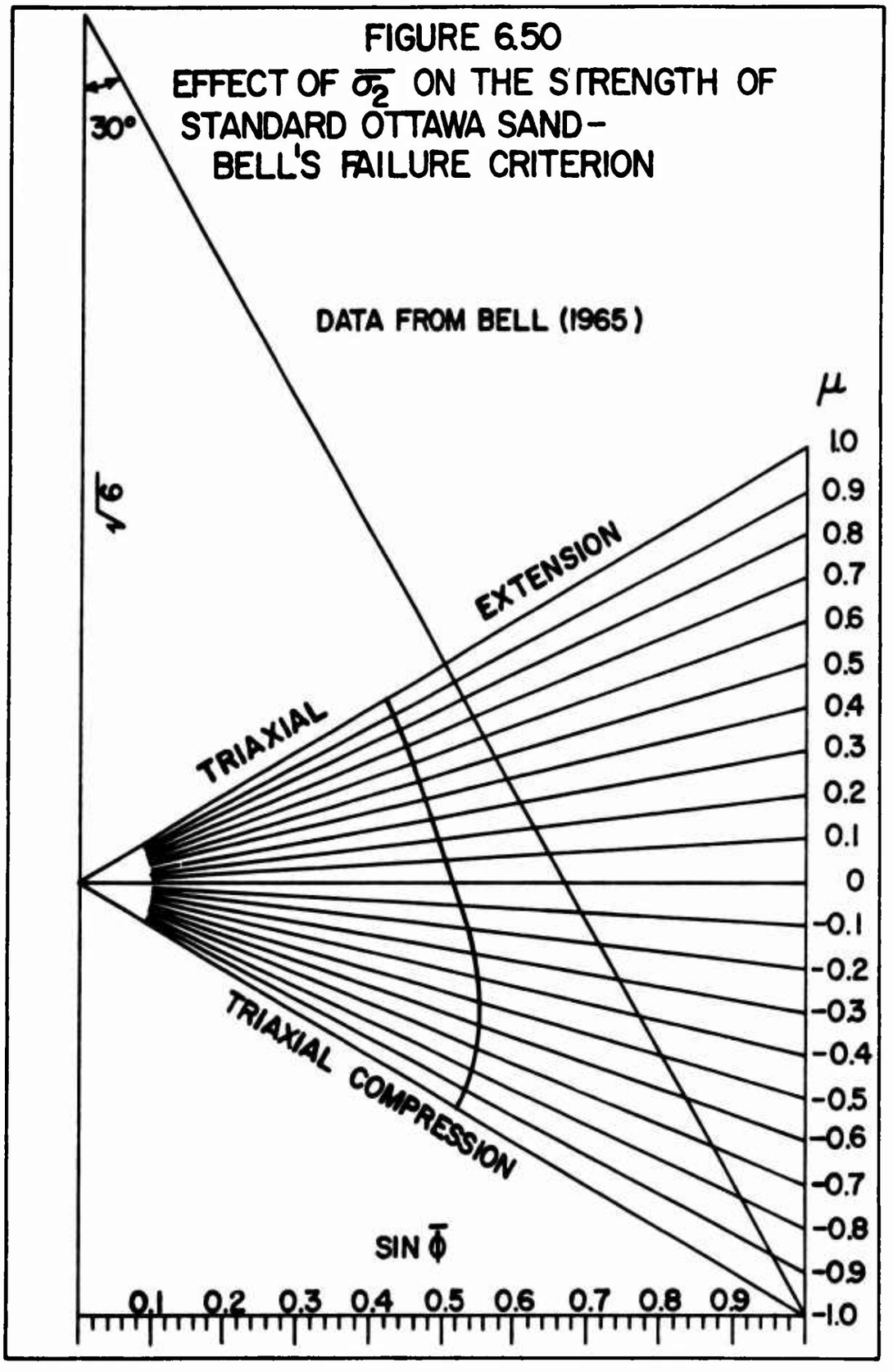

FIGURE 6.50
EFFECT OF $\bar{\sigma_2}$ ON THE STRENGTH OF STANDARD OTTAWA SAND - BELL'S FAILURE CRITERION

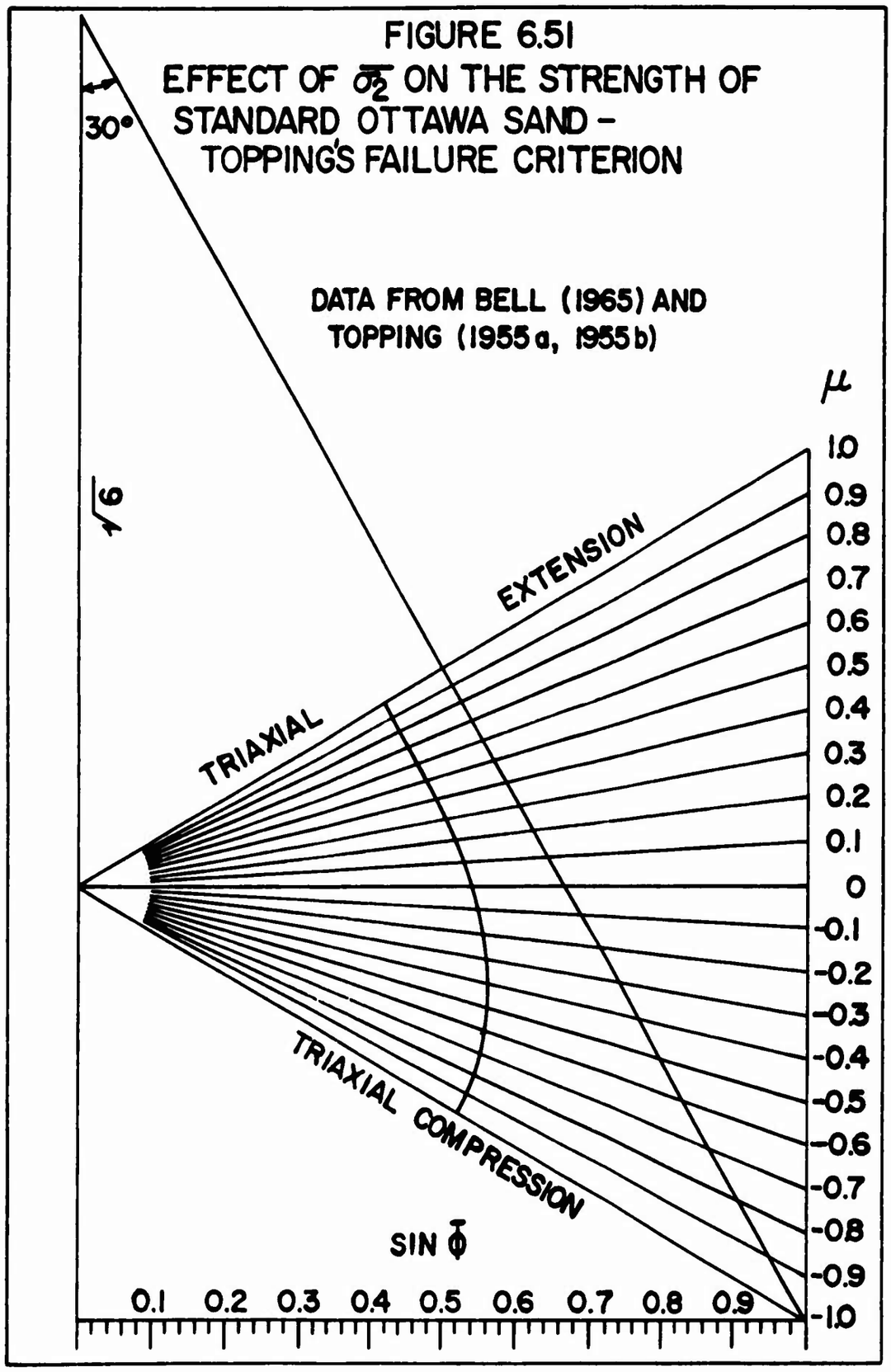
FIGURE 6.51
EFFECT OF $\bar{\sigma_2}$ ON THE STRENGTH OF STANDARD OTTAWA SAND - TOPPING'S FAILURE CRITERION
30°
DATA FROM BELL (1965) AND TOPPING (1955a, 1955b)
μ
1.0
0.9
0.8
0.7
0.6
0.5
0.4
0.3
0.2
0.1
0
-0.1
-0.2
-0.3
-0.4
-0.5
-0.6
-0.7
-0.8
-0.9
-1.0
$\sqrt{6}$
EXTENSION
TRIAXIAL
TRIAXIAL COMPRESSION
SIN $\bar{\phi}$
0.1 0.2 0.3 0.4 0.5 0.6 0.7 0.8 0.9

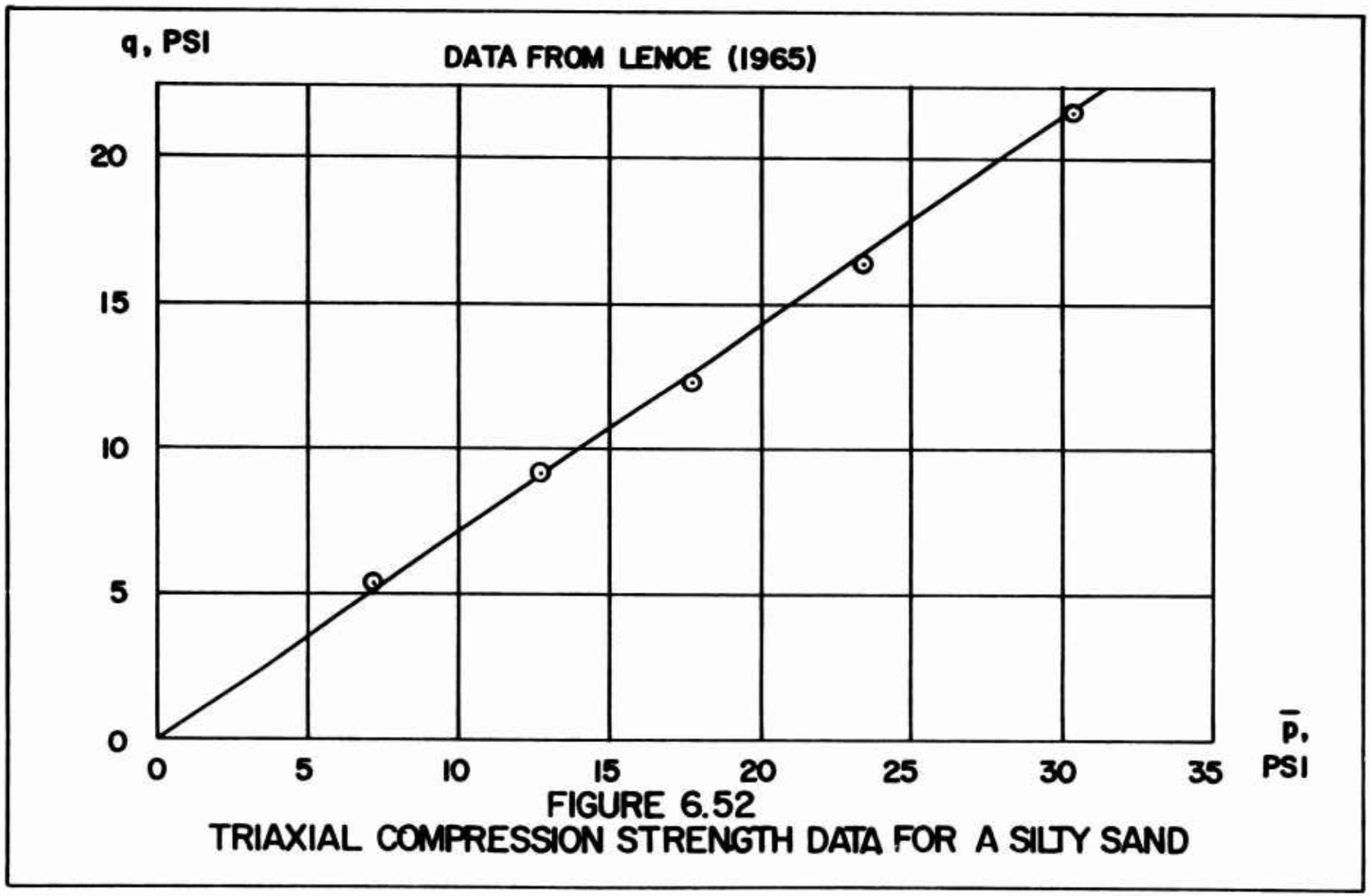

FIGURE 6.52
TRIAXIAL COMPRESSION STRENGTH DATA FOR A SILTY SAND

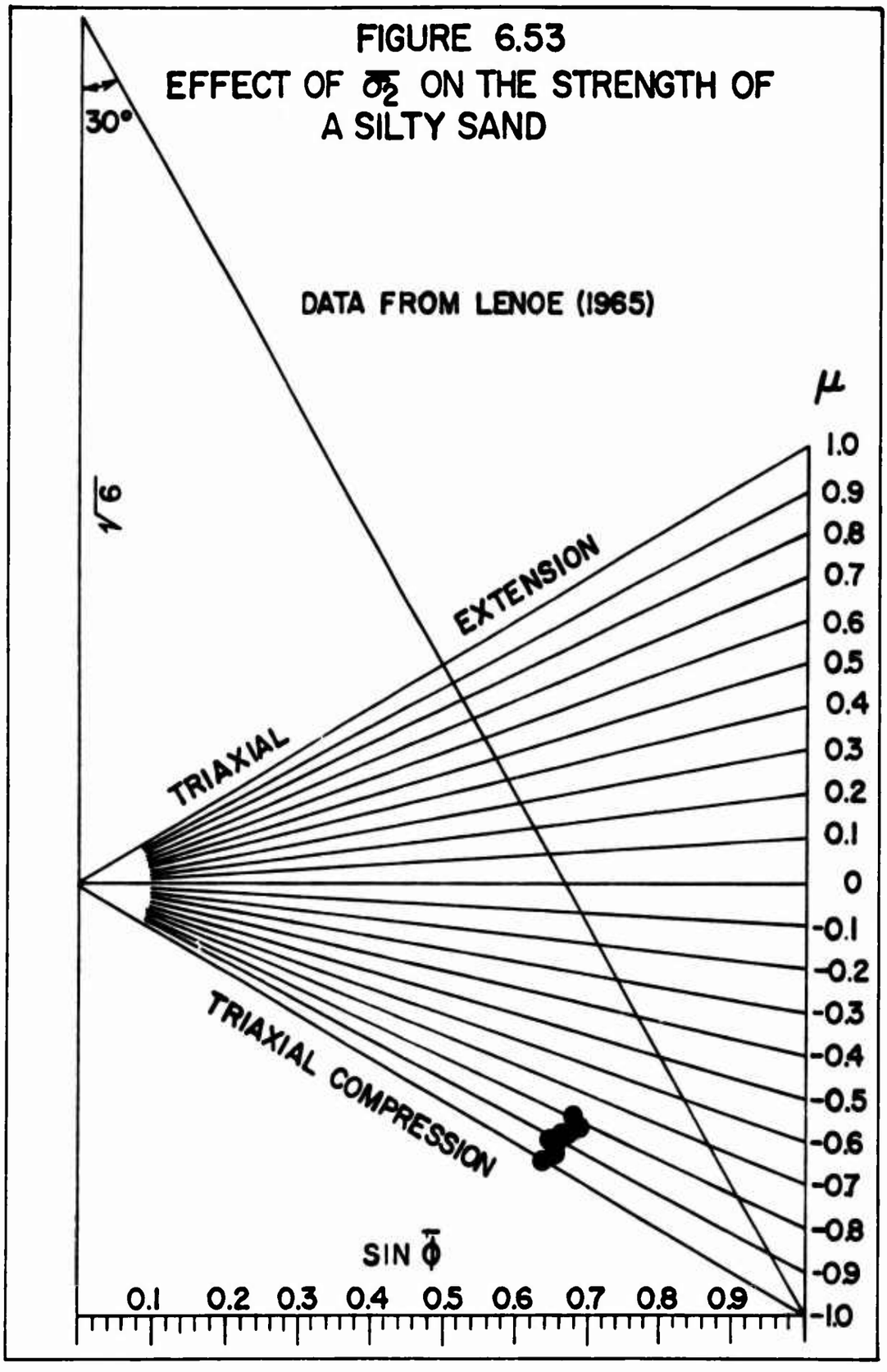
FIGURE 6.53
EFFECT OF $\bar{\sigma}_2$ ON THE STRENGTH OF A SILTY SAND
30°
DATA FROM LENOE (1965)
μ
1.0
0.9
0.8
0.7
0.6
0.5
0.4
0.3
0.2
0.1
0
-0.1
-0.2
-0.3
-0.4
-0.5
-0.6
-0.7
-0.8
-0.9
-1.0
$\sqrt{6}$
EXTENSION
TRIAXIAL
TRIAXIAL COMPRESSION
SIN $\bar{\phi}$
0.1 0.2 0.3 0.4 0.5 0.6 0.7 0.8 0.9

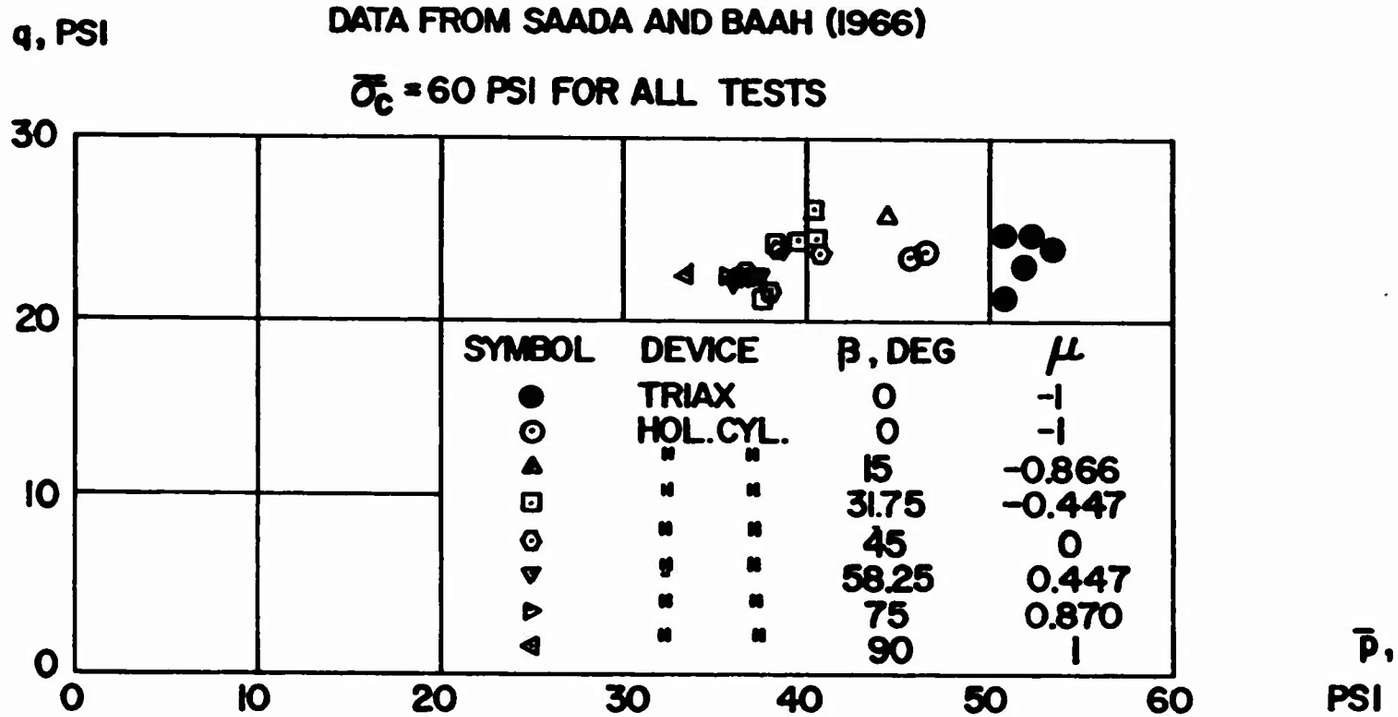

FIGURE 6.54

COMBINED INFLUENCE OF ANISOTROPY, THE INTERMEDIATE PRINCIPAL STRESS AND RATE OF APPLIED STRESS ON THE STRENGTH OF COMMERCIAL KAOLINITE

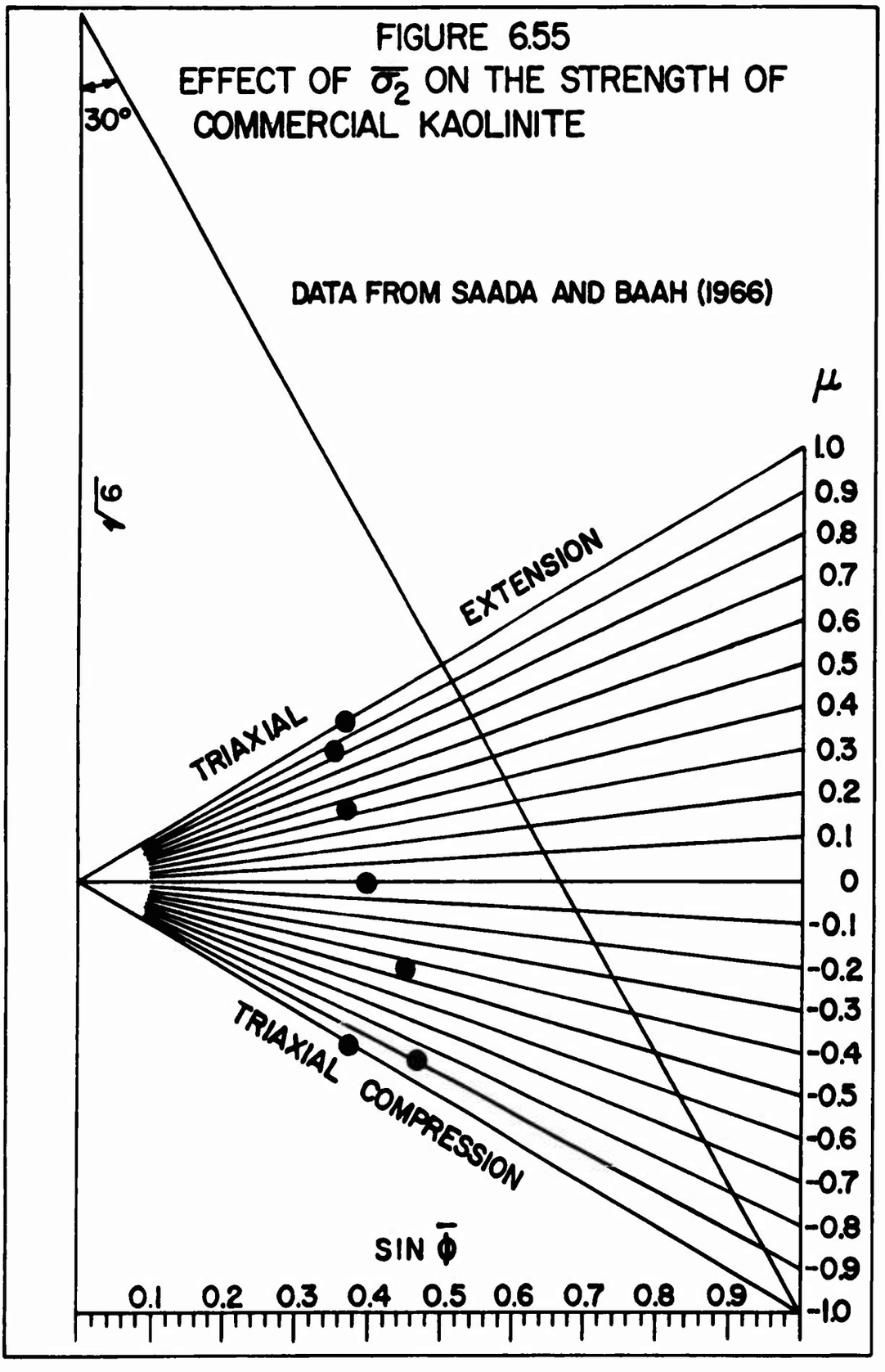

FIGURE 6.55
EFFECT OF $\overline{\sigma_2}$ ON THE STRENGTH OF COMMERCIAL KAOLINITE

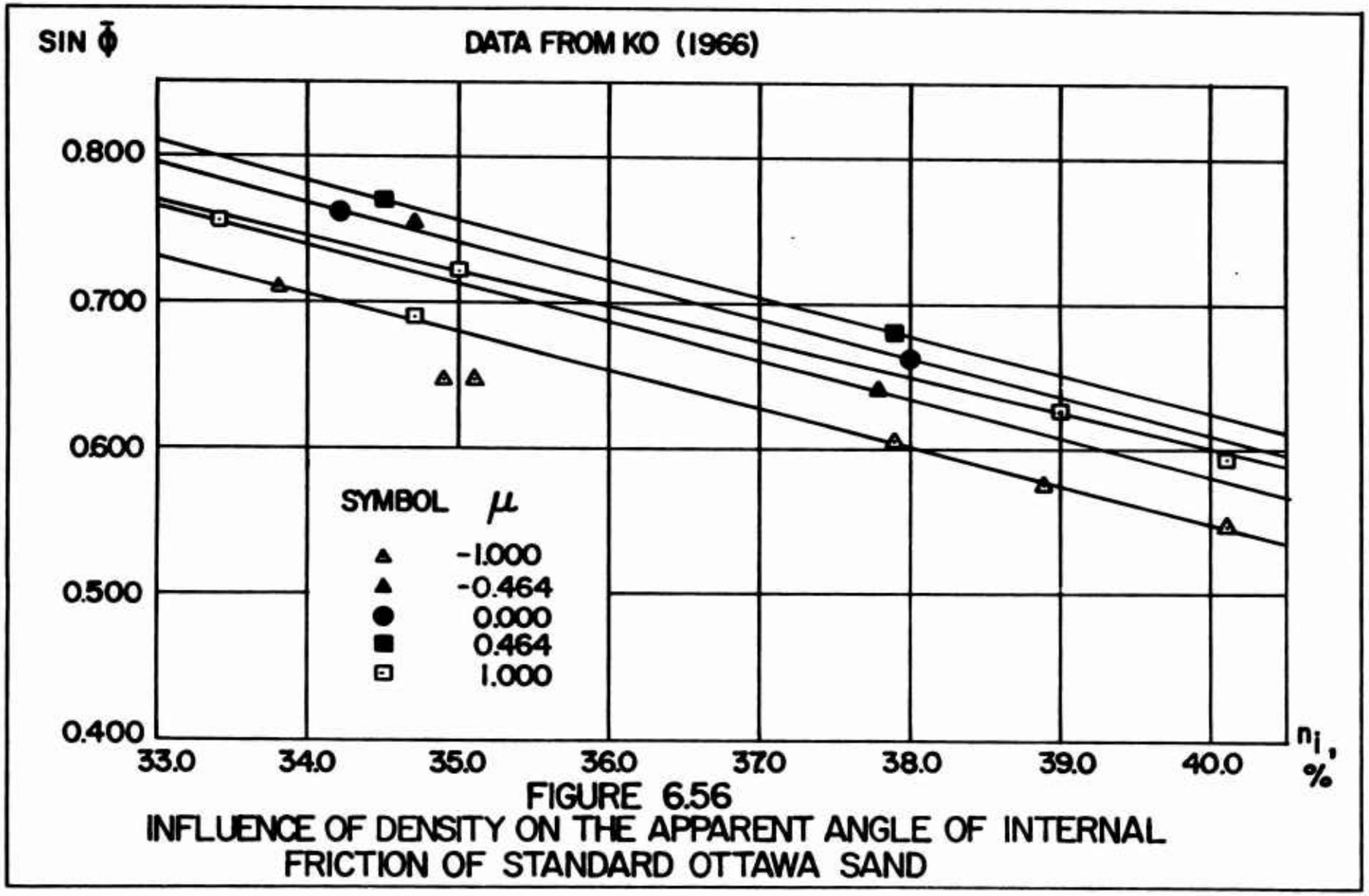

FIGURE 6.56
INFLUENCE OF DENSITY ON THE APPARENT ANGLE OF INTERNAL FRICTION OF STANDARD OTTAWA SAND

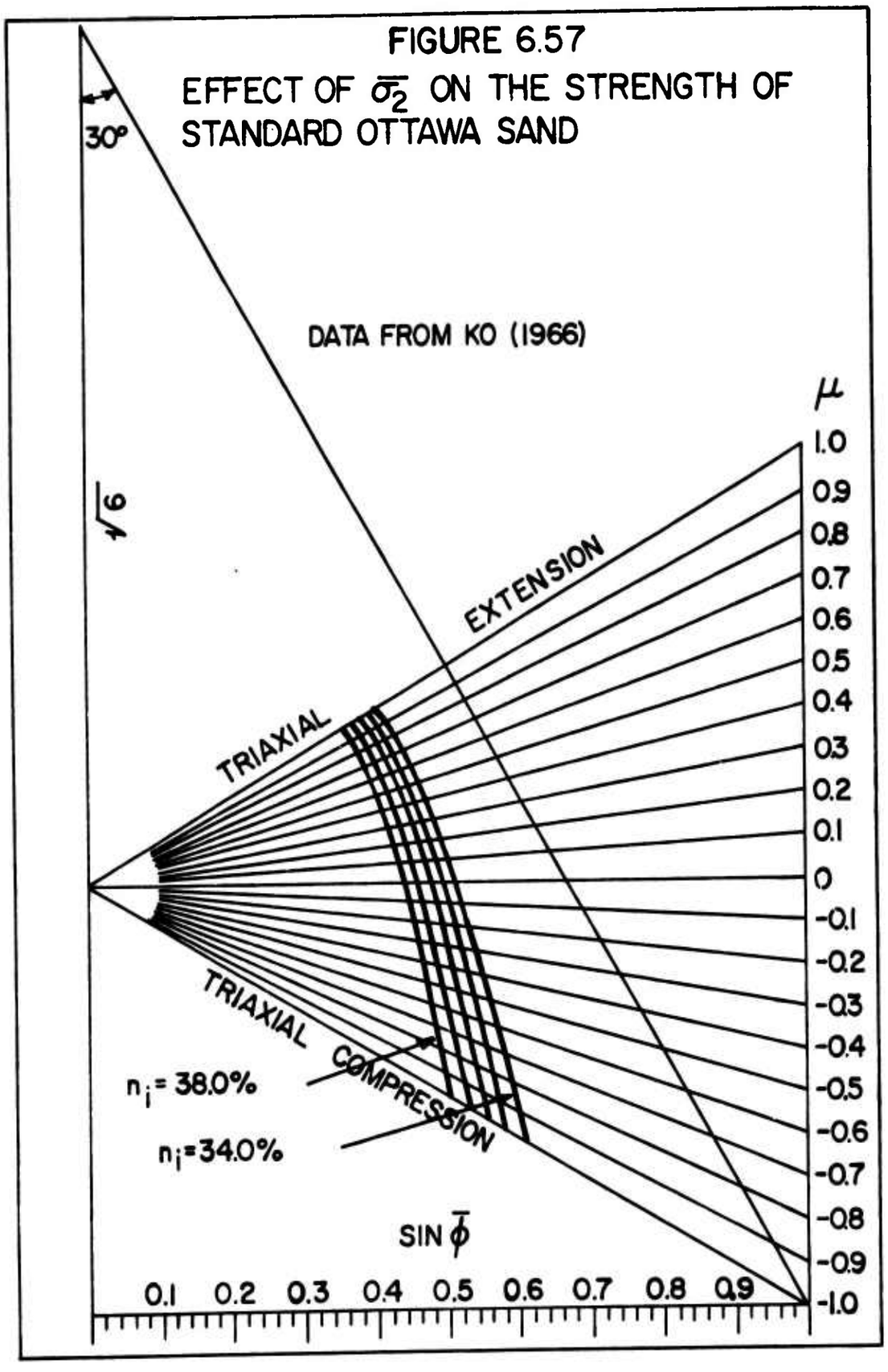

FIGURE 6.57
EFFECT OF $\bar{\sigma_2}$ ON THE STRENGTH OF STANDARD OTTAWA SAND

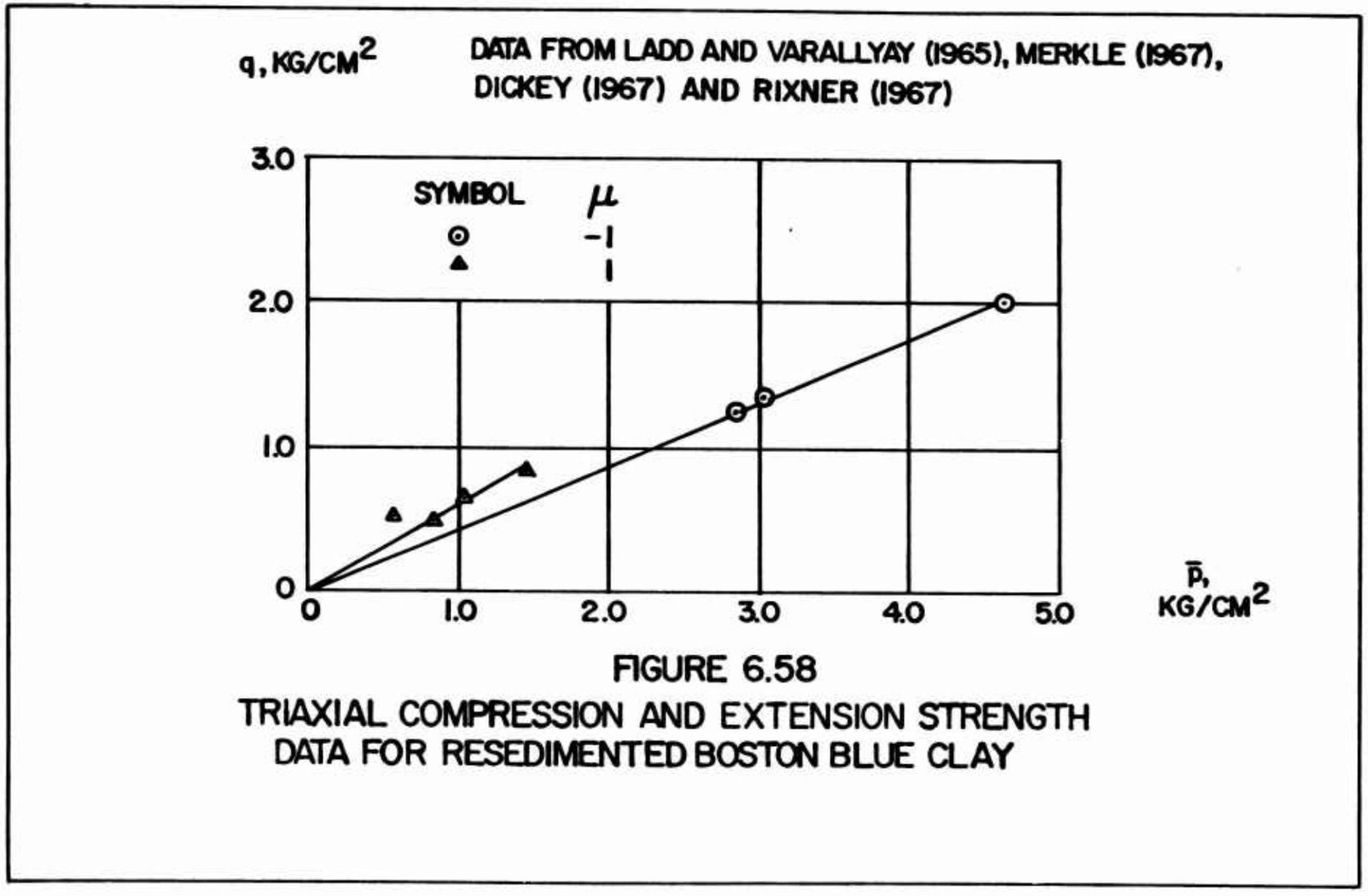

FIGURE 6.58

TRIAXIAL COMPRESSION AND EXTENSION STRENGTH DATA FOR RESEDIMENTED BOSTON BLUE CLAY

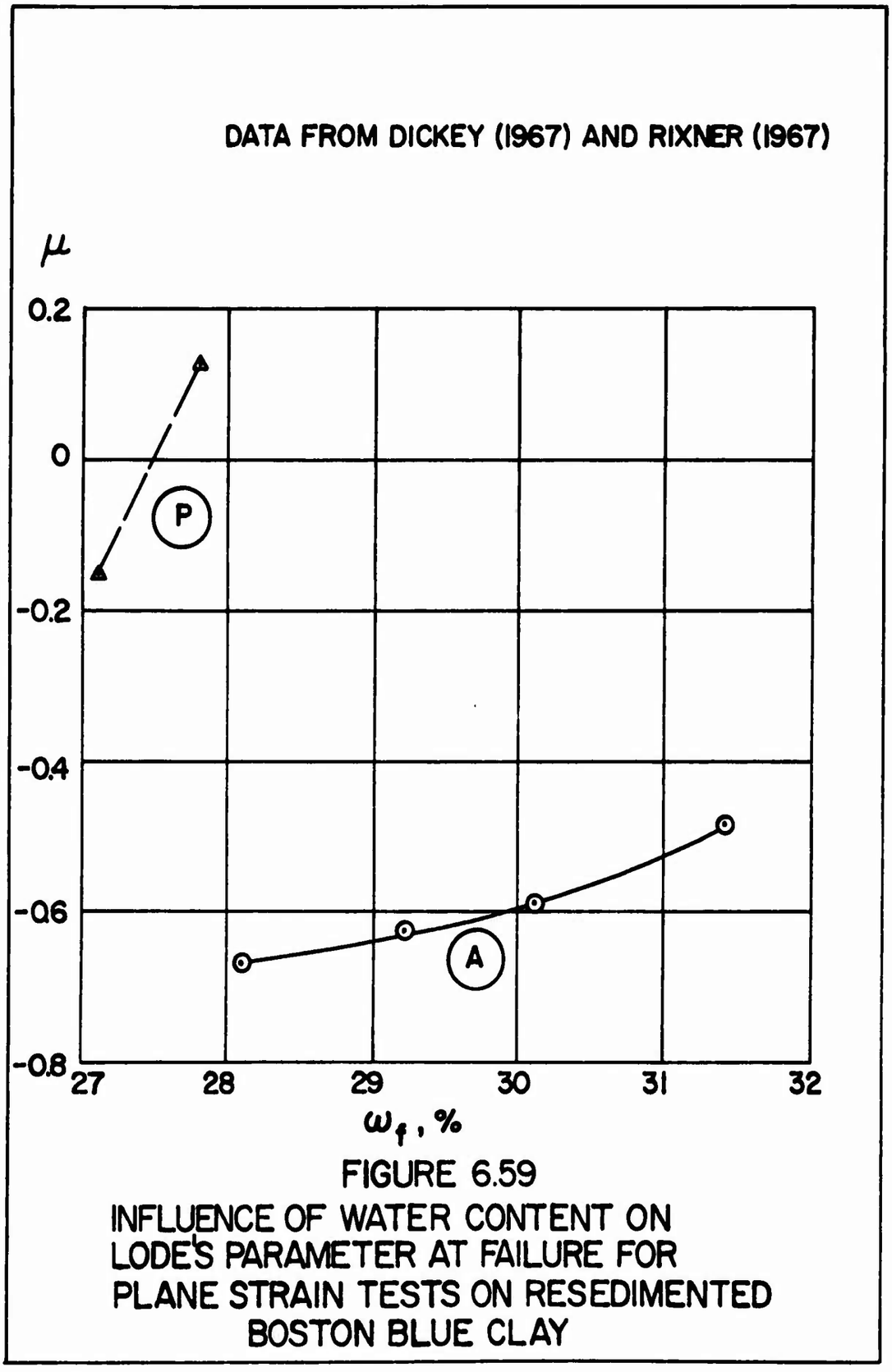

FIGURE 6.59

INFLUENCE OF WATER CONTENT ON LODE'S PARAMETER AT FAILURE FOR PLANE STRAIN TESTS ON RESEDIMENTED BOSTON BLUE CLAY

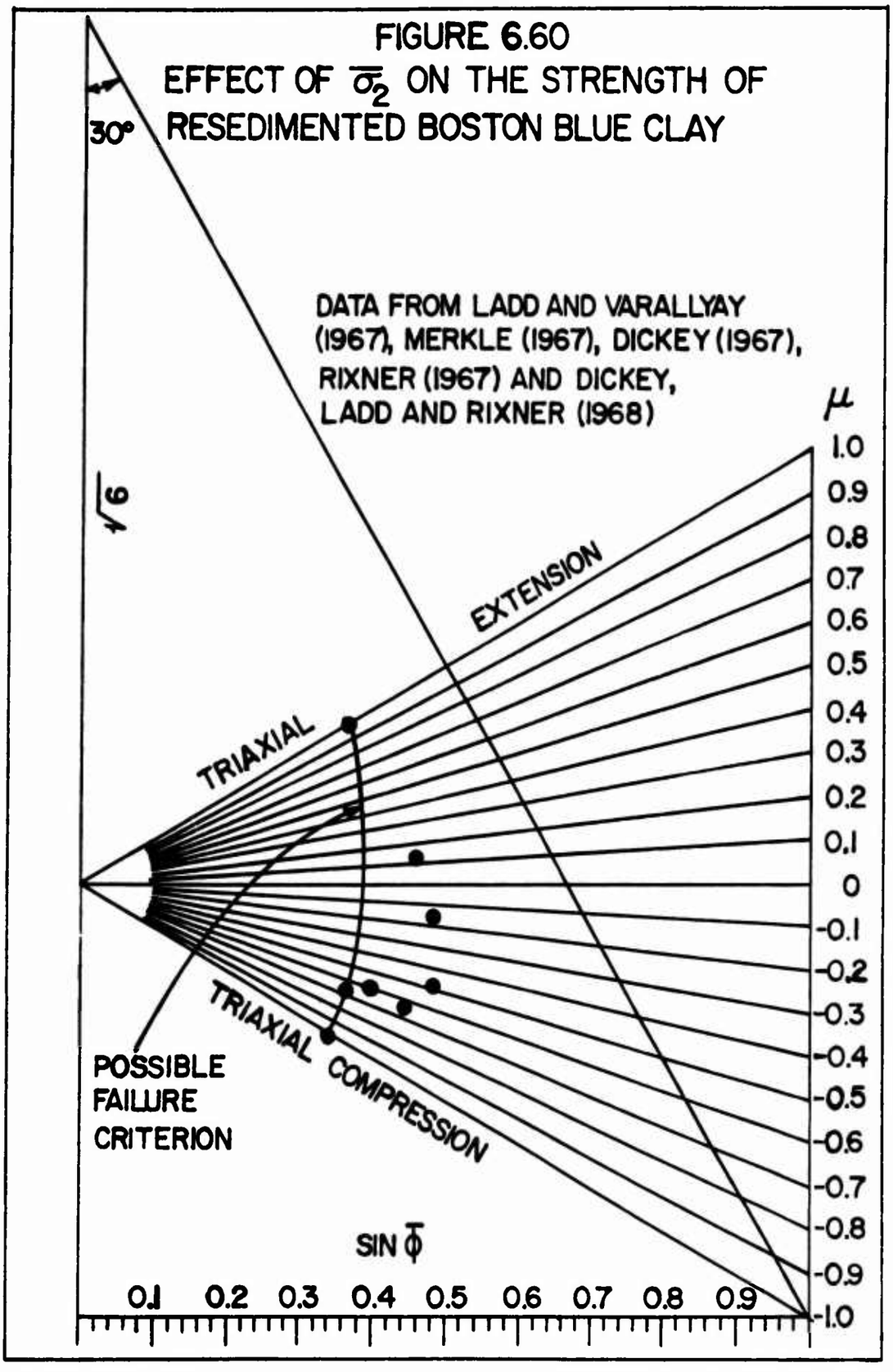

FIGURE 6.60
EFFECT OF $\overline{\sigma_2}$ ON THE STRENGTH OF RESEDIMENTED BOSTON BLUE CLAY

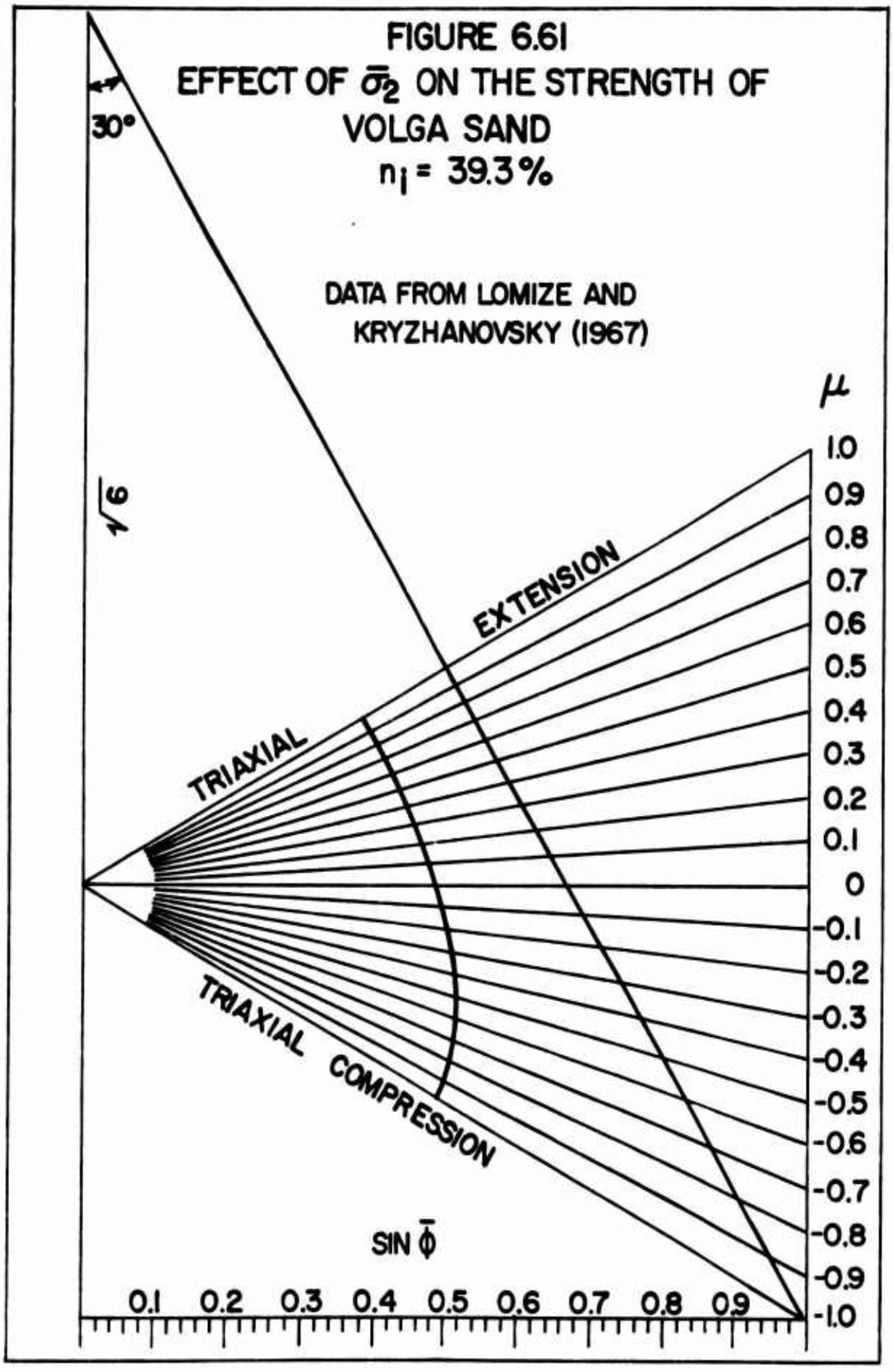
FIGURE 6.61
EFFECT OF $\bar{\sigma}_2$ ON THE STRENGTH OF VOLGA SAND
n_1 = 39.3%
DATA FROM LOMIZE AND KRYZHANOVSKY (1967)
30°
$\sqrt{6}$
μ
1.0
0.9
0.8
0.7
0.6
0.5
0.4
0.3
0.2
0.1
0
-0.1
-0.2
-0.3
-0.4
-0.5
-0.6
-0.7
-0.8
-0.9
-1.0
EXTENSION
TRIAXIAL
TRIAXIAL COMPRESSION
SIN $\bar{\phi}$
0.1 0.2 0.3 0.4 0.5 0.6 0.7 0.8 0.9

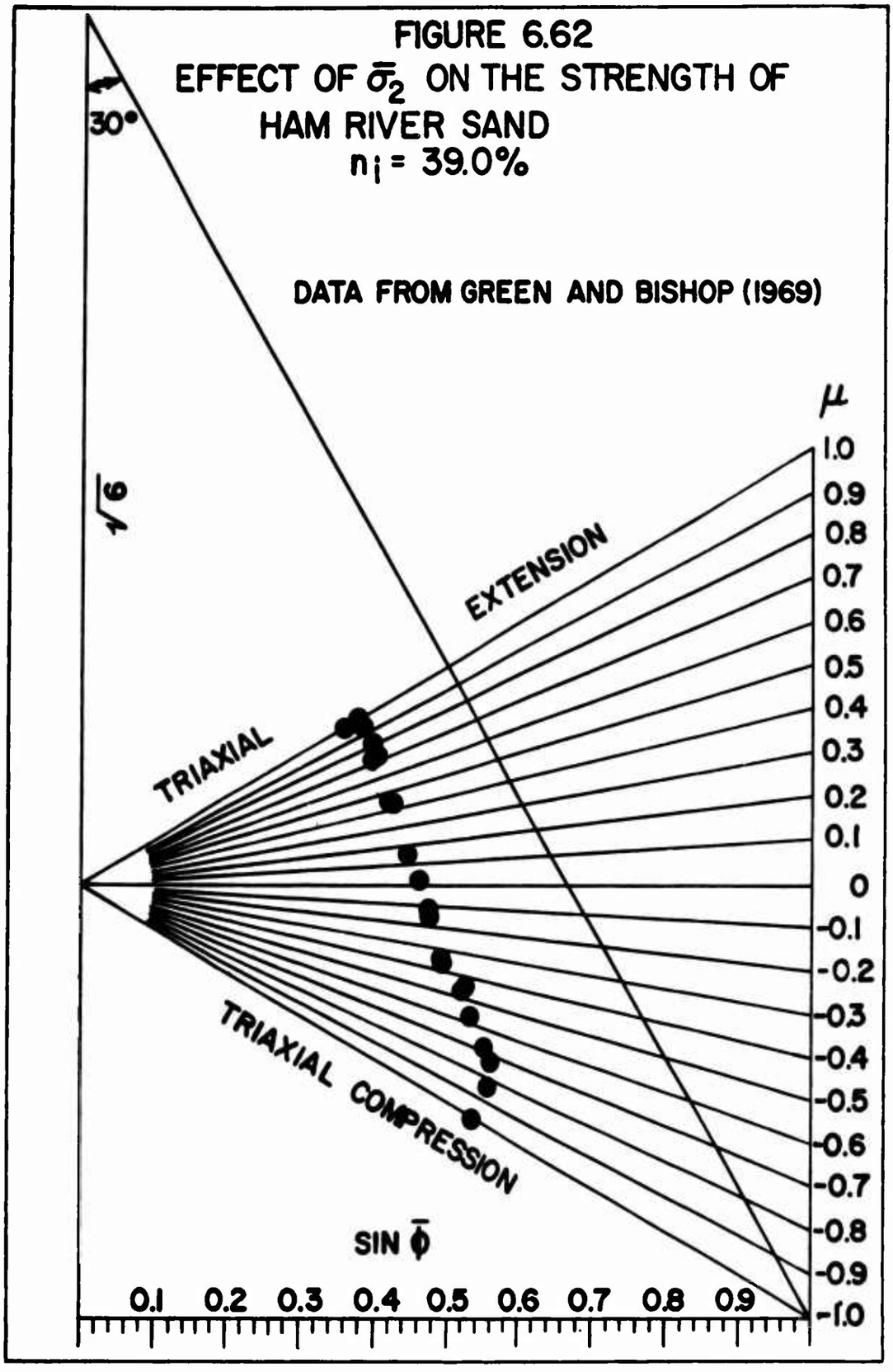

FIGURE 6.62
EFFECT OF $\bar{\sigma}_2$ ON THE STRENGTH OF HAM RIVER SAND
n_i = 39.0%

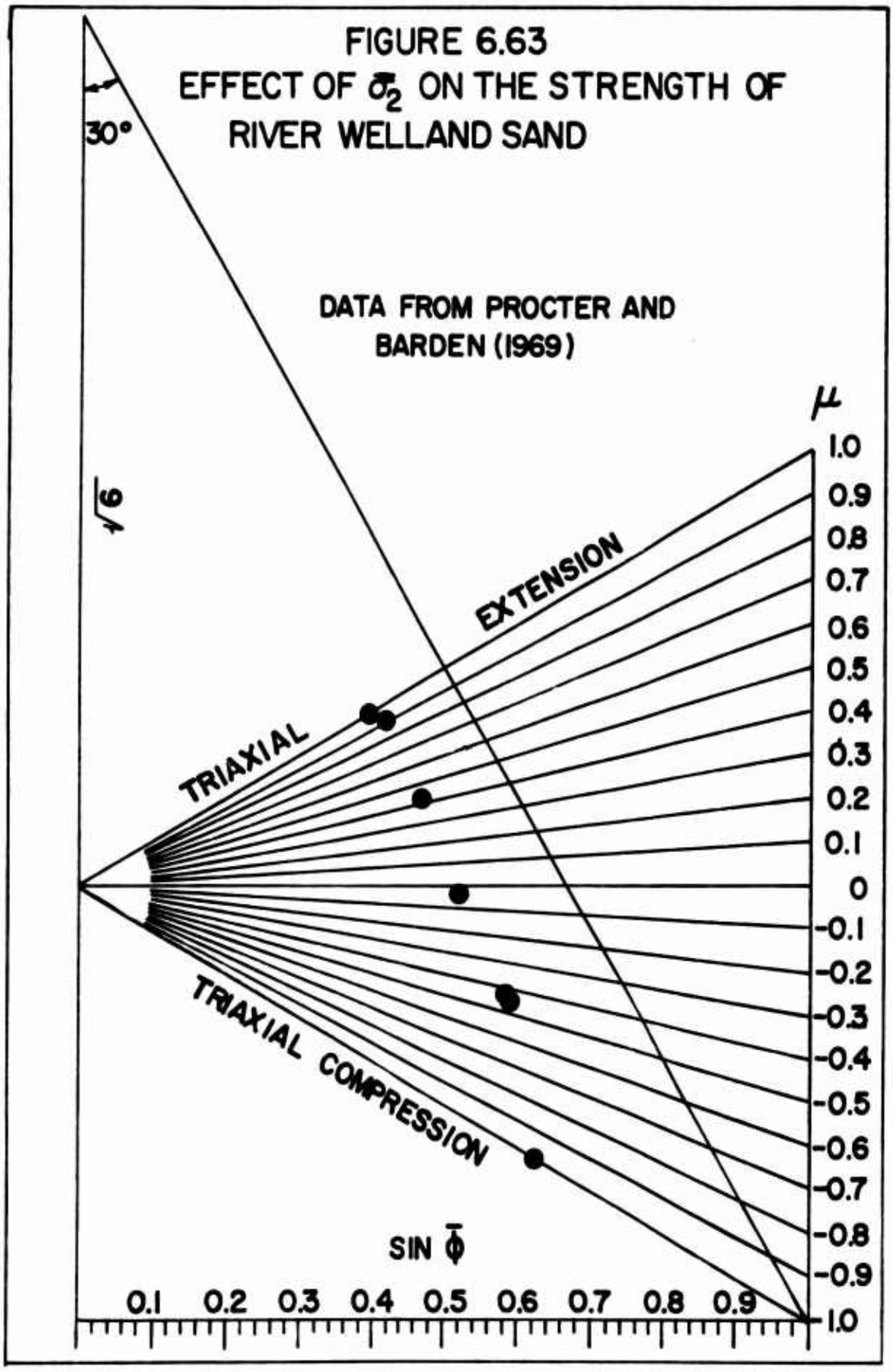
FIGURE 6.63
EFFECT OF $\bar{\sigma}_2$ ON THE STRENGTH OF
RIVER WELLAND SAND
30°
DATA FROM PROCTER AND
BARDEN (1969)
μ
1.0
0.9
0.8
0.7
0.6
0.5
0.4
0.3
0.2
0.1
0
-0.1
-0.2
-0.3
-0.4
-0.5
-0.6
-0.7
-0.8
-0.9
-1.0
$\sqrt{6}$
EXTENSION
TRIAXIAL
TRIAXIAL COMPRESSION
SIN $\bar{\phi}$
0.1 0.2 0.3 0.4 0.5 0.6 0.7 0.8 0.9

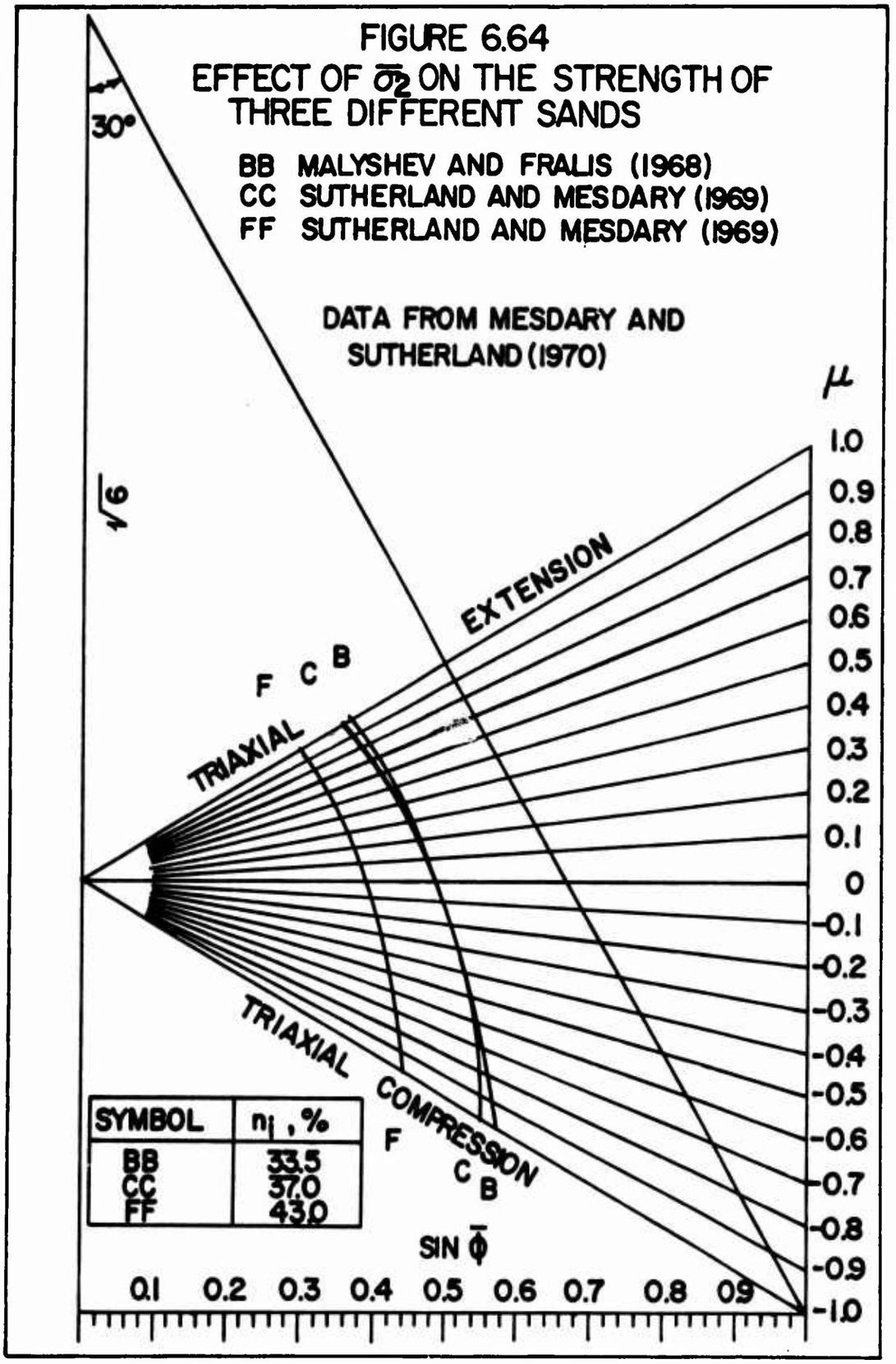

FIGURE 6.64
EFFECT OF $\bar{\sigma}_2$ ON THE STRENGTH OF THREE DIFFERENT SANDS

BB MALYSHEV AND FRALIS (1968)
CC SUTHERLAND AND MESDARY (1969)
FF SUTHERLAND AND MESDARY (1969)

DATA FROM MESDARY AND SUTHERLAND (1970)

CHAPTER 7

ANALYSIS OF MODIAP FOOTING TEST RESULTS

Purpose

This thesis was begun in the Fall of 1966 as a laboratory study of the load-settlement-time behavior of a rigid circular footing on the surface of resedimented Boston blue clay. At that time the Writer was in residence at the Massachusetts Institute of Technology on assignment by the Air Force Institute of Technology. Unfortunately, the Writer's reassignment by the Air Force prevented completion of all scheduled tests, thereby necessitating a reorientation of the thesis.

The footing tests were conducted under Project MODIAP (MODel Inter-American Program), sponsored jointly at M.I.T. by the U.S. Department of State, the Carnegie Corporation, the Creole Foundation, the Dow Chemical Company and the Shell Foundation. For a summary of work on the project up to 1966 see PEREZ-LA SALVIA, LUSCHER, ALVEREZ-STELLING AND GICOT (1966). Project MODIAP was initiated during the period February 1962 to August 1963 by Professor T.W. Lambe, with the assistance of Professor H.M. Horn. The two stated objectives of the project were: HORN (1963):

1) "to evaluate the ability of existing theories to predict total settlement, the time rate of settlement, and the pore pressures which build up in saturated deposits of soil which are subjected to surface loads, and

2) to attempt to formulate, if necessary, new theory which will make possible the prediction of load-settlement-pore pressure-time behavior of saturated soil."

Situations where settlement is not one-dimensional, and wherein the surface load is an appreciable portion of the bearing capacity of the loaded area were to receive particular attention. Large scale model tests were proposed in 1963, and it was the design, construction and proof testing of two identical three-foot diameter footing test bins which absorbed most of the Writer's time during the 1966-67 academic year. At the time the Writer left M.I.T. in May 1967, proof testing of the large bins was not quite complete and a structural modification was in progress. At this point the project had to be terminated due to lack of manpower. To the Writer's knowledge no further work has since been done with the large bins.

While fabrication of the large bins was in progress, the Writer ran a series of footing tests in a smaller device built and described by ALVEREZ-STELLING (1966). The original objectives of these tests were:

1) to provide information needed to design tests in the large bins, and
2) to provide information on possible scale effects.

The tests to be discussed in this chapter are seven bearing capacity tests, in which a two-inch diameter footing was loaded to failure in a short time (5.8 minutes average) in an attempt to minimize consolidation effects.

The purpose of this chapter is to propose a method for predicting initial settlement, based on an analysis of the MODIAP footing test results. The method is basically empirical, and is similar in principle to the current method of predicting undrained shear strength. Both methods hinge on the prediction of several parameters having physical significance, but both methods can also be viewed simply as curve-fitting.

Particular attention will be focused on the nonlinear or plastic component of initial settlement. The bearing capacity factor will be discussed, and the limit of usefulness

of elastic theory will be defined. Finally, the thesis will close with a discussion of how the results of Chapters 2 through 6 can be used in settlement predictions.

Empirical Settlement Curve

There are two important reasons for wanting to have a formula relating the load on a footing to the resulting settlement:

1) A formula facilitates settlement predictions.
2) The influence of soil and footing properties on settlement can be studied by studying their influence on the parameters in the settlement formula.

It was the latter reason that prompted the Writer to seek a general expression relating load and settlement in the MODIAP bearing capacity tests.

The general shape of a load-settlement curve is shown in Figure 7.1. The settlement δ corresponding to a given average contact pressure, q, is the sum of the elastic settlement, δ^E, which can be calculated by elastic theory, and the plastic settlement, δ^P, which is the nonlinear component of settlement.

$$\delta = \delta^E + \delta^P \tag{7.1}$$

The settlement magnification factor, ρ, is the ratio of plastic to elastic settlement at a given load.

$$\rho = \frac{\delta^P}{\delta^E} \tag{7.2}$$

The settlement magnification factor corresponding to an average contact pressure of 50 percent of the bearing capacity, q_{BC}, is denoted by the symbol ρ_{50} and is called the plastic settlement parameter. Using Equation (7.2), Equation (7.1) can be written in the form

$$\delta = \delta^E(1 + \rho) \tag{7.3}$$

Analyses of several sets of load-settlement and stress-strain curves, including those from MODIAP, show that a unique and simple relation exists between the load ratio, q/q_{BC}, and the settlement magnification factors ρ and ρ_{50}.

$$\frac{q}{q_{BC}} = \frac{1}{\frac{\rho_{50}}{\rho} + 1} \tag{7.4}$$

Notice that when $\rho = \rho_{50}$, $q/q_{BC} = 0.50$.

The elastic settlement, δ^E, can be calculated from the initial slope of the load-settlement curve, found by extrapolating a plot of $\log_{10}(q/\delta)$ VERSUS q back to zero load, as shown in Figure 7.3. Having the initial slope, the elastic settlement, the plastic settlement and the settlement magnification factor can be calculated. The parameters q_{BC} and ρ_{50} are then found by fitting a straight line to a plot of q VERSUS q/ρ, as shown in Figure 7.4, utilizing the fact that Equation (7.4) can be written in the form

$$q = q_{BC} - \rho_{50} \left(\frac{q}{\rho}\right) \tag{7.5}$$

The value of ρ_{50} is most conveniently calculated from the relationship shown in Figure 7.3,

$$\rho_{50} = \frac{q_{BC}}{\left(\frac{q}{\rho}\right)_o} \tag{7.6}$$

Equation (7.5) was suggested by J.G. MERKLE (1968) as an alternative to the Southwell plot described by TIMOSHIENKO AND GERE (1961, 191).

The previous analysis can be summarized by the following empirical settlement formula:

$$\frac{\delta}{B} = \frac{q}{M}\left(1 + \frac{\rho_{50}}{\frac{q_{BC}}{q} - 1}\right) \tag{7.7}$$

where B = a characteristic footing dimension

M = Terzaghi's coefficient of elastic subgrade reaction

The safety factor is then

$$\frac{q_{BC}}{q} = \left(\frac{1 + \theta}{2}\right) + \sqrt{\left(\frac{1 + \theta}{2}\right)^2 + (\rho_{50} - 1)\theta} \tag{7.8}$$

where

$$\theta = \frac{B\, q_{BC}}{\delta M} \tag{7.9}$$

Discussion of Test Data

Properties of the resedimented Boston blue clay used in the MODIAP footing tests are those obtained by MERKLE (1967) and tabulated in the discussion of Boston blue clay strength data in Chapter 6. The clay was consolidated in a 12 inch diameter oedometer, using a Karol-Warner Konbel loader, to obtain a cake about 4 1/2 inches in height. A 2 inch diameter brass footing, with its bottom surface roughened by concentric circular grooves, and which was rigid against both bending and tilting, was then placed on the surface of the cake. Then an air surcharge equal to the maximum average vertical consolidation stress (2.0 KG/CM^2) was applied to the surface of the clay and the footing by a flexible air bag. Finally, in the bearing capacity tests, the footing was loaded by dead weights until the time rate of settlement indicated that the test had progressed beyond failure into the penetration phase. Because the tests were load-controlled (as most field loading situations are), a maximum load was never reached. Instead, the test was

stopped when the rate of rotation of the pointer on the Ames dial which measured settlement indicated that penetration was occurring at a rapid and esentially constant rate. No external drainage was permitted during these tests, so the only drainage which could have led to consolidation or swelling in the neighborhood of the footing was internal pore water migration. However, the average test duration was only 5.8 minutes, which should have prevented most of the potential drainage without introducing appreciable viscous effects.

The footing test data, as recorded, are tabulated in Table 7.1 and plotted in Figure 7.2. The amount of scatter in Figure 7.2 is considered normal for load-controlled footing tests on soft clay.

The initial settlement under a given load is here defined as the maximum settlement which had occurred under that load at the time the next load increment was applied, that is the last settlement reading corresponding to a given load in Table 7.1. That value is the value called δ in the empirical settlement formula. The data used to determine the elastic subgrade modulus, M, are tabulated in Table 7.2. A typical semilogarithmic plot is shown in Figure 7.3. The resulting elastic subgrade moduli are shown below.

TEST	π MB KG/.001IN
102	14.9
103	11.4
104	8.4
105	15.7
107	4.6
108	1.7
109	11.4

The data used to determine the bearing capacity and plastic settlement parameter are tabulated in Table 7.3. A typical modified Southwell plot is shown in Figure 7.4. The resulting bearing capacities and plastic settlement parameters are shown below

TEST	P_{BC} KG	ρ_{50}
102	75.0	0.943
103	69.5	2.279
104	66.5	1.494
105	74.5	2.661
107	65.5	1.191
108	67.5	1.071
109	75.0	2.206

For the seven tests, the average values of the settlement parameters M, q_{BC} and ρ_{50} are:

$$\text{Elastic Subrade Modulus, } M = \frac{(10^3)(9.7285)}{20.2683} = 480 \text{ KG/CM}^2$$

$$\text{Bearing Capacity, } q_{BC} = \frac{70.5}{20.2683} = 3.478 \text{ KG/CM}^2$$

$$\text{Plastic Settlement Parameter, } \rho_{50} = 1.692$$

The unique relationship defined by Equation (7.4) is shown in nonlinear form in Figure 7.5 and in linear form in Figure 7.6. These two figures provide the experimental justification for Equation (7.4). Loads above the bearing capacity load are considered to be associated with the penetration phase and are omitted. Also omitted are data obtained at low loads, which show obvious seating effects. Data for these two figures are Tabulated in Table 7.4.

Figure 7.6 was constructed by using Equation (7.4). A more direct verification of the accuracy of the empirical settlement formula is obtained by using Equations (7.8) and (7.9) to compare measured and calculated loads. Data for this comparison are tabulated in Table 7.5 and plotted in Figure 7.7. Slight differences between Figures 7.6 and 7.7

are the result of truncation errors. Figure 7.7 clearly establishes the accuracy of the empirical settlement formula, for all safety factors greater than about 1.05. This includes all loads of practical interest.

Thus far the accuracy of the empirical settlement curve has been established, provided the elastic subgrade modulus, M, the bearing capacity, q_{BC}, and the plastic settlement parameter, ρ_{50}, are known. The practical usefulness of the curve depends on whether these three settlement parameters can be accurately predicted.

Predicting the Elastic Subgrade Modulus

Elastic theory gives the following formula for the elastic subgrade modulus for a rigid circular punch on the surface of an elastic halfspace, when B is the radius of the punch:

$$M = \frac{2E}{\pi(1 - \nu^2)} \qquad (7.10)$$

where

E = Young's modulus

ν = Poisson's ratio

When the material is incompressible, Poisson's ratio is 1/2, and Equation (7.10) reduces to

$$M = \frac{E}{1.179} \tag{7.11}$$

Elastic theory also gives the following expression for axial strain in a compressed cylinder:

$$\epsilon_1 = \frac{1}{E}\left[\sigma_1 - \nu(\sigma_2 + \sigma_3)\right] \tag{7.12}$$

When ν is 1/2 and σ_2 equals σ_3, which is the case in a cylindrical compression test on an incompressible material, Equation (7.12) reduces to

$$\epsilon_1 = \frac{1}{E}(\sigma_1 - \sigma_3) \tag{7.13}$$

or

$$E = \frac{\sigma_1 - \sigma_3}{\epsilon_1} \tag{7.14}$$

This is the definition of the modulus E for triaxial compression tests starting from zero shear given by LADD (1964). Data for determining the initial tangent modulus of remolded Boston

blue clay is tabulated in Table 7.6 and plotted in Figure 7.8, and the resulting expression relating elastic modulus to the major principal consolidation stress is

$$\frac{E_o}{\bar{\sigma}_{1C}} = 280 \qquad (7.15)$$

In the MODIAP footing tests the major principal consolidation stress was 2.0 KG/CM^2, so that the predicted value of the elastic subgrade modulus, M, for these tests is

$$M = \frac{280\ \bar{\sigma}_{1C}}{1.179} = \frac{560}{1.179} = 475\ KG/CM^2$$

The actual average value of M was 480 KG/CM^2. Thus, it appears that the elastic subgrade modulus can be accurately predicted by a combination of elastic theory and the results of isotropically consolidated undrained triaxial compression tests, for the case of initial settlement of a rigid circular footing on normally consolidated saturated Boston blue clay.

Predicting the Bearing Capacity

SKEMPTON (1951) recommended a bearing capacity factor of 6 for a shallow footing on clay, so that

$$q_{BC} = N_C s_U = 6\ s_U \tag{7.16}$$

where

s_U = undrained shear strength

The same three triaxial compression tests which were used to calculate the elastic subgrade modulus can also be used to determine the bearing capacity. They yielded the following values of $s_U/\bar{\sigma}_{1C}$:

TEST	$s_U/\bar{\sigma}_{1C}$
CIUC-1	0.263
CIUC-2	0.308
CIUC-3	0.287
Average	0.286

Therefore, the predicted value of bearing capacity for the MODIAP tests is

$$q_{BC} = (6)(0.286)\bar{\sigma}_{1C} = (6)(0.286)(2) = 3.43 \text{ KG/CM}^2$$

The actual average value of q_{BC} was 3.48 KG/CM^2. Thus, it appears that the bearing capacity of a rigid circular footing on normally consolidated saturated Boston blue clay can be accurately predicted by a combination of Skempton's bearing capacity factor and the results of isotropically consolidated undrained triaxial compression tests. As a matter of interest, the bearing capacities and bearing capacity factors for the seven individual tests are shown below.

TEST	q_{BC} KG/CM^2	N_C
102	3.70	6.47
103	3.43	6.00
104	3.28	5.73
105	3.68	6.43
107	3.23	5.65
108	3.33	5.82
109	3.70	6.47
Average	3.48	6.08

Predicting the Plastic Settlement Parameter

The plastic settlement parameter, ρ_{50}, is the parameter which distinguishes a local from a general bearing capacity failure; TERZAGHI and PECK (1967). It is the opinion of the Writer that the value of ρ_{50} is determined primarily by the overconsolidation ratio for saturated clays. Unfortunately, time did not permit an experimental investigation of the influence of overconsolidation ratio on the plastic settlement parameter, under Project MODIAP.

For the sake of comparison, values of the plastic settlement parameter for a few soils other than resedimented Boston blue clay are shown below.

SOIL	REFERENCE	ρ_{50}
Remolded London Clay	SKEMPTON (1951)	1.25
Yellow Clay, Wayne County, Michigan	HOUSEL (1928)	0.260
Expansive Clay, Lackland AFB	LACKLAND AFB (1968)	1.00
Wet Silty Clay	OSTERBERG (1948)	4.19

Information needed to accurately predict the plastic settlement parameter can be obtained in at least two ways:

1) by a series of model footing tests, in which over-consolidation ratio is the primary independent variable, and
2) by a parametric computer study using the finite element method.

The type of stress-strain relation to be used in a finite element parametric study will depend upon whether the soil is cross anisotropic or isotropic. When the soil is cross anisotropic, use should be made of the results of Chapter 5. When the soil is isotropic, a stress-strain relation can be formulated by extending the results of Chapter 6. Both cases will now be discussed in more detail.

Finite element computer programs are available which can accommodate a bilinear stress-strain relationship. When the soil is cross anisotropic, use can be made of a suggestion by D'APPOLONIA (1968) that the criterion for changing the slope of the stress-strain relationship at a point in the soil be the undrained shear strength at that point. The method for specifying the variation of undrained shear

strength with the angle β, between the major principal stress axis at failure and the material axis should be that introduced in Chapter 5, because the q_o effect will probably be the most important cause of variation in undrained shear strength with the angle β. The slopes of the bilinear stress-strain relationship can be determined as functions of the overconsolidation ratio by a series of conventional triaxial tests.

When the soil is isotropic, an empirical stress-strain relationship of deformation type can be formulated by extending the results of Chapter 6. The stress-strain equations for a homogeneous, isotropic, linearly elastic material are

$$\tau_{OCT} = K \epsilon_{VOL} \tag{7.17}$$

$$\tau_{OCT} = G \lambda_{OCT} \tag{7.18}$$

$$\mu = \eta \tag{7.19}$$

where

$$\tau_{OCT} = \frac{\sigma_1 + \sigma_2 + \sigma_3}{3} \tag{7.20}$$

$$\tau_{OCT} = \frac{1}{3}\sqrt{(\sigma_1 - \sigma_2)^2 + (\sigma_2 - \sigma_3)^2 + (\sigma_3 - \sigma_1)^2} \tag{7.21}$$

$$\mu = \frac{\sigma_2 - \left(\frac{\sigma_1 + \sigma_3}{2}\right)}{\left(\frac{\sigma_1 - \sigma_3}{2}\right)} \tag{7.22}$$

and

$$\epsilon_{VOL} = 3\epsilon_{OCT} = \epsilon_1 + \epsilon_2 + \epsilon_3 \tag{7.23}$$

$$\lambda_{OCT} = \frac{2}{3}\sqrt{(\epsilon_1 - \epsilon_2)^2 + (\epsilon_2 - \epsilon_3)^2 + (\epsilon_3 - \epsilon_1)^2} \tag{7.24}$$

$$\eta = \frac{\epsilon_2 - \left(\frac{\epsilon_1 + \epsilon_3}{2}\right)}{\left(\frac{\epsilon_1 - \epsilon_3}{2}\right)} \tag{7.25}$$

K is the bulk modulus and G is the shear modulus. It seems reasonable to formulate stress-strain relations for an isotropic soil in terms of the above octahedral stress and strain invariants, not only because they have fundamental physical significance, but also because the elastic stress-

strain relations then serve as a convenient reference point. Therefore, the following initial assumptions will be made:

1) The soil is isotropic.

2) The principal axes of stress and strain coincide.

3) The soil obeys a deformation-type stress-strain relationship, of the form

$$\epsilon_{VOL} = F_1 \ (\bar{\sigma}_{OCT}, \ \tau_{OCT}, \ \mu) \tag{7.26}$$

$$\lambda_{OCT} = F_2 \ (\bar{\sigma}_{OCT}, \ \tau_{OCT}, \ \mu) \tag{7.27}$$

$$\eta = F_3 \ (\bar{\sigma}_{OCT}, \ \tau_{OCT}, \ \mu) \tag{7.28}$$

The above stress-strain equations imply that contours of constant volumetric strain, octahedral shear strain or Lode's strain parameter are surfaces in principal stress space. Rendulic assumed that surfaces of constant volumetric strain (isochors) were surfaces of revolution, with the hydrostatic axis as the axis of revolution. Thus he was able to portray a volumetric stress-strain relationship by means of contours in a two-dimensional plot. However, he was not able to investigate the validity of his assumption.

Bell's discovery that contours of equal volumetric strain and equal octahedral shear strain, in an octahedral plane ($\bar{\sigma}_{OCT}$ = constant) stress plot, are approximately geometrically similar supplied a more realistic alternative to Rendulic's surface of revolution assumption. Bell's experimental data and the work of Lomize and Kryzhanovsky, and Topping suggest the following additional assumptions:

4) Contours of volumetric strain, ϵ_{VOL}, and octahedral shear strain, γ_{OCT}, in an octahedral plane are geometrically similar.

5) The shape of strain contours is the same for all octahedral planes, and the size of the contours is determined by the minimum void ratio ever attained and the present void ratio. In other words, the soil exhibits normalized behavior.

6) The shape of a strain contour in an octahedral plane is given by the expression

$$R = R_c \Gamma \tag{7.29}$$

where

$$\Gamma = \left(\frac{1 + R_E/R_C}{2}\right) + \left(\frac{1 - R_E/R_C}{2}\right) \cos 2\omega \qquad (7.30)$$

$$R = \sqrt{3}\ \tau_{OCT} \qquad (7.31)$$

$$\cos \omega = \mu/\sqrt{3} \qquad (7.32)$$

$$R_C = R(\mu = -1) \qquad (7.33)$$

$$R_E = R(\mu = 1) \qquad (7.34)$$

See Figures 6.5 and B.6.

7) Lode's stress and strain parameters are equal.

The resulting stress-strain equation, which can be represented by contours in a two-dimensional plot are

$$\epsilon_{VOL} = H_1\ (\bar{\sigma}_{OCT},\ \tau_{OCT}/\Gamma\ ) \qquad (7.35)$$

$$\lambda_{OCT} = H_2\ (\bar{\sigma}_{OCT},\ \tau_{OCT}/\Gamma\ ) \qquad (7.36)$$

$$\eta = \mu \qquad (7.37)$$

The contours represented by Equation (7.35) are undrained effective stress paths. Those represented by Equation (7.36) are strength mobilization contours. See Figure 7.9. Both sets of contours can be obtained from conventional triaxial compression and extension tests, and can be incorporated into a finite element computer program by means of fitted curves. Thus it should be possible to investigate the influence of any stress-strain parameter on any of the three settlement parameters.

The experimental data which suggested the above approach were for isotropically consolidated soils. The influence of anisotropic consolidation is not certain.

The above approach can perhaps be viewed as a generalization of the stress-strain theory developed by the Cambridge Group, with τ_{OCT} replaced by τ_{OCT}/Γ .

Useful Range of Elastic Theory in Predicting Initial Settlement

The useful range of elastic theory in predicting initial settlement depends on the value of the plastic settlement parameter. As the overconsolidation ratio increases the plastic settlement parameter decreases and the useful range of elastic theory increases. The useful range can be calculated by rewriting Equation (7.4). An elastic analysis will underestimate initial settlement by 50% ($\rho^E = 0.50\ \rho$) when the

settlement magnification factor is unity, and the safety factor is

$$(SF)_{EL} = \rho_{50} + 1 \qquad (7.38)$$

For the seven MODIAP tests, the limit of usefulness of elastic theory is shown below.

TEST	$(SF)_{EL}$
102	1.9
103	3.3
104	2.5
105	3.7
107	2.2
108	2.1
109	3.2

The average safety factor at which elastic theory is no longer useful for estimating initial settlement for these tests is 2.7. Since this is not a large safety factor, it appears that elastic theory is useful in many practical cases for predicting initial settlement. At this safety factor

the maximum shear stress along the footing axis, as predicted by elastic theory, is about 0.45 times the undrained shear strength for a rigid circular footing, and about 0.65 times the undrained shear strength for a uniform circular load, so there should be no difficulty in applying the stress path method proposed by LAMBE (1964).

Size Effects

If the settlement of a surface footing under a given pressure is not proportional to the size of the footing, it is due to variation of soil stress-strain characteristics with depth. The large MODIAP bins were not intended to investigate size effects, but rather to permit measurements of total stress, pore pressure and displacement at points within the clay, with devices which could be considered fairly small compared with the footing dimensions. It is doubtful if size effects would have been evident in the MODIAP tests, because the stress history of the clay was to have been essentially constant with depth.

Formulas based on simplified assumptions can be found in several textbooks, which attempt to reflect the influence of footing size on settlement. However, these formulas may not be applicable in many practical cases, because the assumed mode of variation of strength or compressibility with depth may be far from the truth. In practice, it is best to plot the undrained shear strength, the initial tangent modulus and the plastic strain parameter VERSUS depth, and then use average values of these parameters in predicting the values of the three settlement parameters.

Influence of Stress System

The model footing tests conducted by the Writer under project MODIAP and discussed in this chapter do not, by themselves, reveal the influence of stress system variables on load-settlement behavior, because they were all run on normally consolidated clay. Had their purpose been to investigate the influence of stress system variables, then in view of the information developed in Chapters 3-5, it is clear that they should have been run on clay at several stages of overconsolidation. The main reason for doing so is to observe the influence of anisotropic initial stresses,

i.e. the q_o effect. The end result would be a plot of the modulus of subgrade reaction, M, the ultimate bearing capacity, q_{BC}, and the plastic settlement parameter, ρ_{50}, as a function of the overconsolidation ratio, OCR = $\bar{\sigma}_{v,MAX}/\bar{\sigma}_{vo}$ for a given initial effective stress.

If all the footing tests are run on material at the same initial average effective stress,

$$\bar{p}_o \approx 1.5 \text{ KG/CM}^2$$

and if the modulus of subgrade reaction is proportional to the maximum past vertical effective stress,

$$M = 237.5\ \bar{\sigma}_{v,MAX}$$

$$= 237.5 \left(\frac{2OCR}{1+K_o}\right) \bar{p}_o$$

then the modulus of subgrade reaction can be calculated from the relationship between OCR and K_o. See D'APPOLONIA (1968, 73). These calculations are performed in Table 7.7.

The ultimate bearing capacity q_{BC} for anisotropic soils can be calculated from results presented by DAVIS AND CHRISTIAN (1971), provided the directional variation of

undrained shear strength is known, and that can be obtained by the method presented in Chapter 5. The results shown in Figure 7.10 were obtained by assuming that

$$\bar{\Phi} = 26^{o}$$

and that the pore pressure response is isotropic, with A_f varying with OCR in a manner similar to that for remolded Weald Clay; HENKEL (1958, Fig. 8). The assumption of isotropic strength parameters and pore pressure response was made here because of lack of conclusive test data to the contrary for resedimented Boston blue clay, but such an assumption is not essential to the method developed in Chapter 5. The calculations of ultimate bearing capacity are performed in Table 7.8.

An analysis of the results of a finite element computer study reported by D'APPOLONIA (1968) suggests a possible connection between the plastic settlement parameter ρ_{50} and the parameter

$$\mu_o = \frac{q_o - q_s}{p_s}$$

where

$$q_s = \frac{s_{uv} - s_{uh}}{2} = \frac{q_f(0) - q_f(90)}{2}$$

$$p_s = \frac{s_{uv} + s_{uh}}{2} = \frac{q_f(0) + q_f(90)}{2}$$

$$q_o = \left(\frac{\sigma_1 - \sigma_3}{2}\right)_o$$

The parameter μ_o is the ratio of the distance between the q_o point in Figure 7.10 and the midpoint of the horizontal axis of the polar strength plot, divided by one half the length of that axis. It appears that when the material is normally consolidated, and the parameter μ_o is near 1.0 (q_o point near the right hand portion of the polar strength plot), local yielding beneath the footing begins at fairly low contact stresses. But this zone of initial yielding directly beneath the footing is contained by the surrounding material which has not yet yielded and so ultimate failure is delayed. Because of the early initial yielding, the plastic settlement parameter ρ_{50} is relatively large. As the overconsolidation ratio increases, so does K_o; the q_o point moves in toward the origin of the polar strength plot, and the parameter μ_o decreases. Initiation of yielding is delayed, but yielding of the material which provides

lateral confinement for the material directly beneath the footing occurs sooner after the latter material begins to yield, and the transition to the penetration phase occurs more rapidly. A general bearing capacity failure results. Figure 7.11 is a plot of the plastic settlement parameter ρ_{50} VERSUS the parameter μ_o for seven cases investigated by D'APPOLONIA (1968). The values of ρ_{50} were measured graphically. There does appear to be a relationship between μ_o and ρ_{50}, and on this basis a relationship between μ_o and ρ_{50} for the Boston blue clay used in MODIAP has been estimated, using the one measured value obtained by the Writer and assuming a trend similar to that shown by D'Appolonia data. The resulting relationship between the overconsolidation ratio and the plastic settlement parameter is shown in Table 7.9.

The load-settlement curves in Figure 7.12 have been calculated using the values of M, q_{BC} and ρ_{50} from Tables 7.7, 7.8 and 7.9, which are also summarized below.

OCR	M	q_{BC}	ρ_{50}
	KG/CM^2	KG/CM^2	
1.0	475	3.24	1.69
1.5	677	4.38	1.05
2.0	843	5.37	0.63
3.0	1169	7.08	0.45
4.0	1477	8.58	0.36
5.0	1781	10.20	0.32

The difference between the ultimate bearing capacity for the normally consolidated case predicted here (3.24 KG/CM^2) and that predicted earlier (3.43 KG/CM^2) is due to a slight difference in the assumed pore pressure response, and to the use of the average of the vertical and horizontal strengths here, while the previous prediction used only the vertical strength. The difference in q_{BC} is small (6%). Plots of M, q_{BC} and ρ_{50} VERSUS OCR appear in Figure 7.13.

The above calculations illustrate how the information developed in Chapters 3, 4 and 5, dealing with anisotropy of the effective stress shear strength parameters, anisotropic pore pressure response and the q_o effect can be applied to the prediction of initial settlement. The information presented in Chapter 6 serves mainly to justify confidence in the reliability of the Revised Coulomb strength equation in the solution of practical problems.

Summary

A method for predicting initial settlement has been introduced, which depends on three empirical parameters: Terzaghi's elastic subgrade modulus, the bearing capacity

and the plastic settlement parameter. The plastic settlement parameter, which is introduced in this chapter, is the ratio of plastic to elastic settlement at a safety factor of two. The first two parameters can be accurately predicted by means of conventional triaxial compression tests. More information is needed to be able to accurately predict the plastic settlement parameter. Major steps toward obtaining this information are the method for determining undrained shear strength as a function of the orientation of the principal stresses at failure, introduced in Chapter 5, and general isotropic stress-strain equations introduced in this chapter by extending results presented in Chapter 6.

TABLE 7.1

MODIAP BEARING CAPACITY TEST DATA

t MIN	p KG	δ IN	t MIN	p KG	δ IN	t MIN	p KG	δ IN
	TEST NO. 101		1.75	44.6	.006	1.92	44.6	.019
0.00	0.0	.000	2.08	44.6	.007	2.12	44.6	.021
0.10	11.3	.003	2.25	55.5	.010	2.25	55.6	.027
0.35	11.3	.004	2.45	55.5	.013	2.50	55.6	.044
0.67	11.3	.005	2.72	66.7	.020	2.67	55.6	.051
0.83	22.4	.014	3.00	66.7	.034	2.75	61.9	.059
1.10	22.4	.018	3.25	66.7	.045	2.97	61.9	.079
1.37	22.4	.019	3.48	72.9	.066	3.25	61.9	.099
1.53	33.7	.035	4.17	72.9	.115	3.42	68.3	.119
1.75	33.7	.061	4.33	79.1	.150	3.58	68.3	.199
1.93	33.7	.068	5.75	79.1	.430	3.83	68.3	.264
2.05	45.0	.515	5.83	85.4	.480	3.92	74.6	.299
2.40	45.0	.525				4.18	74.6	.399
				TEST NO. 103		4.37	74.6	.424
	TEST NO. 102		0.00	11.1	.001	4.45	80.8	.449
0.00	11.1	.001	0.50	11.1	.001	4.62	80.8	.524
0.58	22.2	.001	0.58	22.2	.002	4.92	80.8	.584
0.90	22.2	.002	0.77	22.2	.003	5.00	86.9	.614
1.08	22.2	.002	1.08	22.2	.004			
1.25	33.5	.004	1.17	33.5	.009		TEST NO. 104	
1.55	33.5	.004	1.67	44.6	0.12	0.00	11.3	.001

(Continued)

TABLE 7.1

MODIAP BEARING CAPACITY TEST DATA

t MIN	P KG	δ IN	t MIN	P KG	δ IN	t MIN	P KG	δ IN
0.47	11.3	.002		TEST NO. 105		4.27	69.5	.102
0.62	22.4	.003	0.00	11.1	.001	4.57	69.5	.127
1.07	22.4	.004	0.37	11.1	.001	4.70	75.8	.137
1.20	33.5	.006	0.45	22.2	.002	4.92	75.8	.232
1.58	33.5	.010	0.93	22.2	.003	5.17	75.8	.322
1.75	44.6	.013	1.08	33.5	.004	5.27	82.2	.352
2.13	44.6	.021	1.48	33.5	.007	5.73	82.2	.502
2.25	50.8	.023	1.58	44.6	.008	5.92	82.2	.522
2.42	50.8	.030	1.77	44.6	.012	6.05	88.4	.552
2.67	50.8	.035	2.05	44.6	.014	6.47	88.4	.652
3.00	57.1	.040	2.18	50.7	.015	6.78	88.4	.692
3.42	57.1	.058	2.43	50.7	.020	6.92	94.6	.707
3.87	57.1	.068	2.73	50.7	.023			
4.00	63.4	.075	2.83	57.0	.025		TEST NO. 106	
4.22	63.4	.095	3.08	57.0	.032	0.00	11.1	.001
4.62	63.4	.125	3.28	57.0	.035	0.93	11.1	.001
4.83	69.7	.140	3.42	63.2	.038	1.07	22.2	.002
5.12	69.7	.225	3.60	63.2	.052	1.60	22.2	.003
5.38	69.7	.285	3.90	63.2	.062	1.78	33.5	.004
5.52	76.0	.325	4.00	69.5	.069	2.05	33.5	.006

(Continued)

TABLE 7.1

MODIAP BEARING CAPACITY TEST DATA

t MIN	P KG	δ IN	t MIN	P KG	δ IN	t MIN	P KG	δ IN
2.27	33.5	.007	7.45	82.2	.111	1.67	50.7	.041
2.43	44.6	.009	7.63	88.4	.119	1.83	50.7	.055
2.67	44.6	.012	7.90	88.4	.156	1.98	50.7	.062
3.10	44.6	.015	8.22	88.4	.181	2.13	57.0	.083
3.28	50.7	.016	8.37	94.6	.196	2.28	57.0	.098
3.72	50.7	.020		94.6	.386	2.40	57.0	.107
3.98	50.7	.022				2.50	63.2	.123
4.15	57.0	.023		TEST NO. 107		2.63	63.2	.155
4.33	57.0	.026	0.00	11.1	.002	2.80	63.2	.188
4.82	57.0	.032	0.18	11.1	.002	2.93	69.5	.218
4.95	63.2	.033	0.37	11.1	.003	3.10	69.5	.283
5.28	63.2	.039	0.48	22.4	.005	3.22	69.5	.308
5.47	63.2	.041	0.60	22.4	.007	3.32	75.8	.343
5.62	69.5	.044	0.77	22.4	.008	3.48	75.8	.433
6.00	69.5	.056	0.87	33.5	.011	3.77	75.8	.483
6.17	75.8	.061	1.03	33.5	.015	3.80	82.2	.513
6.42	75.8	.067	1.13	33.5	.016	3.97	82.2	.613
6.65	75.8	.083	1.27	44.6	.023	4.13	82.2	.658
6.80	82.2	.088	1.43	44.6	.033	4.22	88.4	.735
7.13	82.2	.101	1.55	44.6	.035			

(Continued)

TABLE 7.1

MODIAP BEARING CAPACITY TEST DATA

t MIN	P KG	δ IN	t MIN	P KG	δ IN	t MIN	P KG	δ IN
	TEST NO. 108		3.18	63.5	.331	3.33	33.2	.008
0.00	0.0	.000	3.40	63.5	.381	3.48	44.3	.010
0.15	11.1	.006	3.58	69.7	.431	3.62	44.3	.013
0.37	11.1	.007	3.70	69.7	.481	4.17	44.3	.017
0.67	11.1	.008	3.88	69.7	.531	4.32	55.4	.020
0.85	22.2	.014	4.02	75.9	.556	4.47	55.4	.029
1.07	22.2	.018	4.12	75.9	.631	4.90	55.4	.035
1.27	22.2	.019	4.38	75.9	.721	5.12	66.7	.043
1.43	33.3	.031	4.53	82.2	.821	5.28	66.7	.065
1.58	33.3	.037	4.62	82.2	.866	5.63	66.7	.087
1.78	33.3	.040	4.75	82.2	.921	5.82	73.1	.100
1.92	44.6	.051				5.98	73.1	.150
2.02	44.6	.069		TEST NO. 109		6.28	73.1	.200
2.23	44.6	.081	0.00	0.0	.000	6.45	79.4	.230
2.35	50.9	.096	0.22	11.1	.001	6.67	79.4	.315
2.47	50.9	.121	0.58	11.1	.001	6.95	79.4	.355
2.60	50.9	.136	0.97	22.2	.003	7.13	85.7	.380
2.70	57.2	.156	1.27	22.2	.003	7.27	85.7	.430
2.82	57.2	.206	1.60	22.2	.004	7.47	85.7	.465
2.92	57.2	.231	1.63	33.2	.005	7.60	91.9	.485
3.08	63.5	.281	2.98	33.2	.007	7.75	91.9	.535

(Continued)

TABLE 7.1

MODIAP BEARING CAPACITY TEST DATA

t MIN	P KG	δ IN	t MIN	P KG	δ IN	t MIN	P KG	δ IN
7.92	91.9	.570	8.35	98.0	.700	8.72	104.3	.825
8.03	98.0	.600	8.58	104.3	.750	8.88	104.3	.865
8.17	98.0	.650						

TABLE 7.2

DATA FOR DETERMINING THE ELASTIC SUBGRADE MODULUS, M

P KG	δ IN	P/δ KG/.001IN	P KG	δ IN	P/δ KG/.001IN	P KG	δ IN	P/δ KG/.001IN
	TEST NO. 102			TEST NO. 104				
11.1	.001	11.10	11.3	.002	5.65	82.2	.522	0.16
22.2	.002	11.10	22.4	.004	5.60	88.4	.692	0.13
33.5	.004	8.38	33.5	.010	3.35			
44.6	.007	6.37	44.6	.021	2.12		TEST NO. 107	
55.5	.013	4.27	50.8	.035	1.45	11.1	.003	3.70
66.7	.045	1.48	57.1	.068	0.84	22.4	.008	2.80
72.9	.115	0.63	63.4	.125	0.51	33.5	.016	2.09
79.1	.430	0.18	69.7	.285	0.24	44.6	.035	1.27
						50.7	.062	0.82
	TEST NO. 103			TEST NO. 105		57.0	.107	0.53
11.1	.001	11.10	11.1	.001	11.10	63.2	.188	0.34
22.2	.004	5.55	22.2	.003	7.40	69.5	.308	0.23
33.5	.009	3.72	33.5	.007	4.79	75.8	.483	0.16
44.6	.021	2.12	44.6	.014	3.19	82.2	.658	0.12
55.6	.051	1.09	50.7	.023	2.20			
61.9	.099	0.63	57.0	.035	1.63		TEST No. 108	
68.3	.264	0.26	63.2	.062	1.02	11.1	.008	1.39
74.6	.424	0.18	69.5	.127	0.55	22.2	.019	1.17
80.8	.584	0.14	75.8	.322	0.24	33.3	.040	0.83

(Continued)

TABLE 7.2

DATA FOR DETERMINING THE ELASTIC SUBGRADE MODULUS, M

P	δ	P/δ	P	δ	P/δ	P	δ	P/δ
KG	IN	KG/.001IN	KG	IN	KG/.001IN	KG	IN	KG/.001IN
				TEST NO. 109				
44.6	.081	0.55				73.1	.200	0.37
50.9	.136	0.37	11.1	.001	11.10	79.4	.355	0.22
57.2	.231	0.25	22.2	.004	5.55	85.7	.465	0.18
63.5	.381	0.17	33.2	.008	4.15	91.9	.570	0.16
69.9	.531	0.13	44.3	.017	2.61	90.0	.700	0.14
75.9	.721	0.11	55.4	.035	1.58	104.3	.865	0.12
82.2	.921	0.09	66.7	.087	0.77			

TABLE 7.3

DATA FOR DETERMINING THE BEARING CAPACITY, P_{BC}, AND THE PLASTIC SETTLEMENT PARAMETER, ρ_{50}

TEST	$\pi M \times 10^{-3}$ KG/IN	P KG	δ .001IN	δ^E .001IN	δ^P .001IN	ρ	P/ρ KG
102	14.9	11.1	1.000	0.745	0.255	0.342	32.46
		22.2	2.000	1.490	0.510	0.342	64.91
		33.5	4.000	2.248	1.752	0.779	43.00
		44.6	7.000	2.993	4.007	1.339	33.31
		55.5	13.000	3.724	9.276	2.491	22.28
		66.7	45.000	4.476	40.524	9.054	7.37
		72.9	115.000	4.893	110.107	22.503	3.24
		79.1	430.000	5.309	424.691	79.994	0.99
103	11.4	11.1	1.000	0.974	0.026	0.027	411.11
		22.2	4.000	1.947	2.053	1.054	21.06
		33.5	9.000	2.938	6.062	2.063	16.24
		44.6	21.000	3.912	17.088	4.368	10.21
		55.6	51.000	4.877	46.123	9.457	5.88
		61.9	99.000	5.430	93.570	17.232	3.59
		68.3	264.000	5.991	258.009	43.066	1.59
		74.6	424.000	6.544	417.456	63.792	1.17
		80.8	584.000	7.088	576.912	81.393	0.99

(Continued)

TABLE 7.3

DATA FOR DETERMINING THE BEARING CAPACITY, P_{BC}, AND THE PLASTIC SETTLEMENT PARAMETER, ρ_{50}

TEST	$\pi Mx10^{-3}$ KG/IN	P KG	δ .001IN	δ^E .001IN	δ^P .001IN	ρ	P/ρ KG
104	8.4	11.3	2.000	1.345	0.655	0.487	23.20
		22.4	4.000	2.667	1.333	0.500	44.80
		33.5	10.000	3.988	6.012	1.508	22.21
		44.6	21.000	5.310	15.690	2.955	15.09
		50.8	35.000	6.048	28.952	4.787	10.61
		57.1	68.000	6.798	61.202	9.003	6.34
		63.4	125.000	7.548	117.452	15.561	4.07
		69.7	285.000	8.298	276.702	33.346	2.09
105	15.7	11.1	1.000	0.707	0.293	0.414	26.81
		22.2	3.000	1.414	1.586	1.122	19.79
		33.5	7.000	2.134	4.866	2.280	14.69
		44.6	14.000	2.841	11.159	3.928	11.35
		50.7	23.000	3.229	19.771	6.123	8.28
		57.0	35.000	3.630	31.370	8.642	6.60
		63.2	62.000	4.025	57.975	14.404	4.39
		69.5	127.000	4.427	122.573	27.688	2.51
		75.8	322.000	4.828	317.172	65.694	1.15
		82.2	522.000	5.236	516.764	98.694	0.83
		88.4	692.000	5.630	686.370	121.913	0.73

(Continued)

TABLE 7.3

DATA FOR DETERMINING THE BEARING CAPACITY, P_{BC}, AND THE PLASTIC SETTLEMENT PARAMETER, ρ_{50}

TEST	$\pi M \times 10^{-3}$ KG/IN	P KG	δ .001IN	δ^E .001IN	δ^P .001IN	ρ	P/ρ KG
107	4.6	11.1	3.000	2.413	0.587	0.243	45.68
		22.4	8.000	4.870	3.130	0.643	34.84
		33.5	16.000	7.283	8.717	1.197	27.99
		44.6	35.000	9.696	25.304	2.610	17.09
		50.7	62.000	11.022	50.978	4.625	10.96
		57.0	107.000	12.391	94.609	7.635	7.47
		63.2	188.000	13.739	174.261	12.684	4.98
		69.5	308.000	15.109	292.891	19.385	3.59
		75.8	483.000	16.478	466.522	28.312	2.68
		82.2	658.000	17.870	640.130	35.821	2.29
108	1.7	11.1	8.000	6.529	1.471	0.225	49.33
		22.2	19.000	13.059	5.941	0.455	48.79
		33.3	40.000	19.588	20.412	1.042	31.96
		44.6	81.000	26.235	54.765	2.087	21.37
		50.9	136.000	29.941	106.059	3.542	14.37
		57.2	231.000	33.647	197.353	5.865	9.75
		63.5	381.000	37.353	343.647	9.200	6.90
		69.7	531.000	41.000	490.000	11.951	5.83
		75.9	721.000	44.647	676.353	15.149	5.01
		82.2	921.000	48.353	872.647	18.047	4.55

(Continued)

TABLE 7.3

DATA FOR DETERMINING THE BEARING CAPACITY, P_{BC}, AND THE PLASTIC SETTLEMENT PARAMETER, ρ_{50}

TEST	$\pi Mx10^{-3}$ KG/IN	P KG	δ .001IN	δ^E .001IN	δ^P .001IN	ρ	P/ρ KG
109	11.4	11.1	1.000	0.974	0.026	0.027	411.11
		22.2	4.000	1.947	2.053	1.054	21.06
		33.2	8.000	2.912	5.088	1.747	19.00
		44.3	17.000	3.886	13.114	3.375	13.13
		55.4	35.000	4.860	30.140	6.202	8.93
		66.7	87.000	5.851	81.149	13.869	4.81
		73.1	200.000	6.412	193.588	30.192	2.42
		79.4	355.000	6.965	348.035	49.969	1.59
		85.7	465.000	7.518	457.482	60.852	1.41
		91.9	570.000	8.061	561.939	69.711	1.32
		98.0	700.000	8.596	691.404	80.433	1.22
		104.3	865.000	9.149	855.851	93.546	1.11

TABLE 7.4

RELATION BETWEEN LOAD AND SETTLEMENT MAGNIFICATION

TEST	P KG	q/q_{BC}	$\rho/(\rho_{50}+\rho)$	ρ/ρ_{50}
102	22.2	0.296	0.266	0.363
	33.5	0.447	0.452	0.826
	44.6	0.595	0.587	1.420
	55.5	0.740	0.725	2.642
	66.7	0.889	0.906	9.601
	72.9	0.972	0.960	23.863
103	22.2	0.319	0.316	0.462
	33.5	0.482	0.475	0.905
	44.6	0.642	0.657	1.917
	55.6	0.800	0.806	4.150
	61.9	0.891	0.883	7.561
	68.3	0.983	0.950	18.897
104	33.5	0.504	0.502	1.009
	44.6	0.671	0.664	1.978
	50.8	0.764	0.762	3.204
	57.1	0.859	0.858	6.026
	63.4	0.953	0.912	10.416
105	11.1	0.149	0.135	0.156
	22.2	0.298	0.296	0.422
	33.5	0.450	0.461	0.857
	44.6	0.599	0.596	1.476
	50.7	0.680	0.697	2.301
	57.0	0.765	0.764	3.248
	63.2	0.848	0.844	5.413
	69.5	0.933	0.912	10.405

(Continued) TABLE 7.4

RELATION BETWEEN LOAD AND SETTLEMENT MAGNIFICATION

TEST	P KG	q/q_{BC}	$\rho/(\rho_{50}+\rho)$	ρ/ρ_{50}
107	11.1	0.169	0.169	0.204
	22.4	0.342	0.350	0.540
	33.5	0.511	0.501	1.005
	44.6	0.681	0.687	2.191
	50.7	0.774	0.795	3.883
	57.0	0.870	0.865	6.410
	63.2	0.965	0.914	10.650
108	11.1	0.164	0.174	0.210
	22.2	0.329	0.298	0.425
	33.3	0.493	0.493	0.973
	44.6	0.661	0.661	1.949
	50.9	0.754	0.768	3.307
	57.2	0.847	0.846	5.476
	63.5	0.941	0.896	8.590
109	22.2	0.296	0.323	0.478
	33.2	0.443	0.442	0.792
	44.3	0.591	0.605	1.530
	55.4	0.739	0.738	2.811
	66.7	0.889	0.863	6.287
	73.1	0.975	0.932	13.686

TABLE 7.5

COMPARISON OF MEASURED AND CALCULATED LOADS

TEST	P_{MEAS} KG	$(q/q_{BC})_{MEAS}$	δ_{MEAS} .001 IN	P_{CALC} KG	$(q/q_{BC})_{CALC}$
102	11.1	0.148	1	12.5	0.167
	22.2	0.296	2	21.6	0.288
	33.5	0.447	4	33.7	0.449
	44.6	0.595	7	44.3	0.590
	55.5	0.740	13	54.7	0.729
	66.7	0.889	45	67.8	0.904
	72.9	0.972	115	72.0	0.960
103	11.1	0.160	1	8.6	0.124
	22.2	0.319	4	22.1	0.318
	33.5	0.482	9	33.2	0.478
	44.6	0.642	21	45.3	0.652
	55.6	0.800	51	55.9	0.805
	61.9	0.891	99	61.4	0.884
	68.3	0.983	264	66.1	0.951
104	11.3	0.170	2	12.5	0.188
	22.4	0.337	4	20.3	0.305
	33.5	0.504	10	33.4	0.503
	44.6	0.671	21	44.3	0.666
	50.8	0.764	35	50.7	0.763
	57.1	0.859	68	57.0	0.858
	63.4	0.953	125	60.9	0.916

(Continued) TABLE 7.5

COMPARISON OF MEASURED AND CALCULATED LOADS

TEST	P_{MEAS} KG	$(q/q_{BC})_{MEAS}$	δ_{MEAS} .001 IN	P_{CALC} KG	$(q/q_{BC})_{CALC}$
105	11.1	0.149	1	10.8	0.145
	22.2	0.298	3	22.2	0.297
	33.5	0.450	7	34.0	0.456
	44.6	0.599	14	44.5	0.597
	50.7	0.680	23	51.6	0.693
	57.0	0.765	35	57.0	0.765
	63.2	0.848	62	62.9	0.845
	69.5	0.933	127	68.1	0.914
107	11.1	0.169	3	11.1	0.169
	22.4	0.342	8	22.6	0.345
	33.5	0.511	16	33.1	0.506
	44.6	0.681	35	44.9	0.685
	50.7	0.774	62	51.8	0.791
	57.0	0.870	107	56.7	0.866
	63.2	0.965	188	60.1	0.918
108	11.1	0.164	8	11.2	0.166
	22.2	0.329	19	21.5	0.319
	33.3	0.493	40	33.3	0.493
	44.6	0.661	81	44.6	0.661
	50.9	0.754	136	51.6	0.765
	57.2	0.847	231	57.1	0.846
	63.5	0.941	381	60.8	0.900

(Continued)

TABLE 7.5

COMPARISON OF MEASURED AND CALCULATED LOADS

TEST	P_{MEAS} KG	$(q/q_{BC})_{MEAS}$	δ_{MEAS} .001 IN	P_{CALC} KG	$(q/q_{BC})_{CALC}$
109	11.1	0.148	1	8.8	0.117
	22.2	0.296	4	23.0	0.307
	33.2	0.443	8	33.2	0.442
	44.3	0.591	17	45.0	0.600
	55.4	0.739	35	55.3	0.738
	66.7	0.889	87	65.0	0.866
	73.1	0.975	200	70.1	0.935

TABLE 7.6(a)

DATA FOR DETERMINING THE INITIAL TANGENT MODULUS, E_o, FOR REMOLDED BOSTON BLUE CLAY

REF	TEST	ϵ_1 %	$(\bar{\sigma}_1-\bar{\sigma}_3)/\bar{\sigma}_{1C}$	$(\bar{\sigma}_1-\bar{\sigma}_3)/\bar{\sigma}_{1C}\epsilon_1$
(1)	$\overline{\text{CIUC}}$-1	0.100	0.170	170
		0.135	0.228	169
		0.190	0.266	140
		0.230	0.328	143
		0.290	0.376	130
		0.460	0.444	96.5
		0.666	0.494	74.2
		0.945	0.505	53.4
		1.080	0.514	47.6
		1.270	0.522	41.1
		1.430	0.523	36.6
		3.440	0.525	15.3
(1)	$\overline{\text{CIUC}}$-2	0.020	0.072	360
		0.086	0.211	245
		0.216	0.426	197
		0.280	0.466	166
		0.430	0.533	124
		0.590	0.562	95.2
		0.800	0.587	73.4
		1.060	0.601	56.7
		1.390	0.607	43.7
		2.120	0.610	28.8
		2.340	0.615	26.3
		2.590	0.615	23.7
		2.777	0.615	22.1

(Continued)

TABLE 7.6(a)

DATA FOR DETERMINING THE INITIAL TANGENT MODULUS, E_o, FOR REMOLDED BOSTON BLUE CLAY

REF	TEST	ϵ_1 %	$(\bar{\sigma}_1-\bar{\sigma}_3)/\bar{\sigma}_{1C}$	$(\bar{\sigma}_1-\bar{\sigma}_3)/\bar{\sigma}_{1C}\epsilon_1$
(1)	$\overline{\text{CIUC}}$-3	0.040	0.097	242
		0.110	0.271	246
		0.210	0.353	168
		0.350	0.423	121
		0.520	0.465	89.4
		0.660	0.489	74.0
		0.820	0.513	62.6
		0.940	0.525	55.8
		1.110	0.534	48.1
		1.280	0.542	42.3
		1.710	0.553	32.3
		1.970	0.556	28.2
		2.490	0.562	22.6
		3.090	0.563	18.2
		3.690	0.574	15.6

TABLE 7.6(b)

DATA FOR DETERMINING THE INITIAL TANGENT MODULUS, E_o, FOR REMOLDED BOSTON BLUE CLAY

REF	S.F.	$(\sigma_1-\sigma_3)/(\sigma_1-\sigma_3)_f$	$E/\bar{\sigma}_{1C}$
(2)	5	0.200	242
	3	0.333	212
	2	0.500	174
	1.5	0.667	120
	1.2	0.833	72

REF	TEST	$E_o/\bar{\sigma}_{1C}$
(1)	$\overline{\text{CIUC}}$-1	170
(1)	$\overline{\text{CIUC}}$-2	345
(1)	$\overline{\text{CIUC}}$-3	325
(1)	Average	280
(2)		280

TABLE 7.7

PREDICTED INFLUENCE OF OVERCONSOLIDATION RATIO ON MODULUS OF SUBGRADE REACTION

OCR	K_o	$\bar{p}_o$ KG/CM^2	$\bar{\sigma}_{v,MAX}$ KG/CM^2	M KG/CM^2
1.0	0.50	1.50	2.00	475
1.5	0.58	1.50	2.85	677
2.0	0.69	1.50	3.55	843
3.0	0.83	1.50	4.92	1169
4.0	0.93	1.50	6.22	1477
5.0	1.00	1.50	7.50	1781

TABLE 7.8

PREDICTED INFLUENCE OF OVERCONSOLIDATION RATIO ON ULTIMATE BEARING CAPACITY

OCR	s_{uv} KG/CM^2	s_{uh} KG/CM^2	$\sqrt{s_{uv}\, s_{uh}}$ KG/CM^2	s_{u45} KG/CM^2	b/a	N_c'
1.0	0.63	0.45	0.53	0.50	0.94	5.08
1.5	0.69	0.77	0.73	0.74	1.01	5.14
2.0	0.80	0.99	0.89	0.91	1.02	5.14
3.0	1.07	1.29	1.17	1.16	0.99	5.14
4.0	1.37	1.49	1.43	1.43	1.00	5.14
5.0	1.70	1.70	1.70	1.70	1.00	5.14

The values of N_c' above are for a strip footing. The influence of anisotropy on N_c' is negligible, in this case.

OCR	$s_{uv}+s_{uh}$ KG/CM^2	N_c	q_{BC} KG/CM^2
1.0	1.08	6	3.24*
1.5	1.46	6	4.38
2.0	1.79	6	5.37
3.0	2.36	6	7.08
4.0	2.86	6	8.58
5.0	3.40	6	10.20

Values of N_c' from DAVIS AND CHRISTIAN (1971).

*This value agrees within 6% with the value 3.48 KG/CM^2 predicted previously, assuming isotropic behavior and a slightly different pore pressure response.

TABLE 7.9

PREDICTED INFLUENCE OF OVERCONSOLIDATION RATIO ON THE PLASTIC SETTLEMENT PARAMETER

OCR	s_{uv} KG/CM^2	q_o KG/CM^2	s_{uh} KG/CM^2	p_s KG/CM^2	q_s KG/CM^2	μ_o	ρ_{50}
1.0	0.63	0.50	0.45	0.540	0.090	0.759	1.69
1.5	0.69	0.40	0.77	0.730	-0.040	0.603	1.05
2.0	0.80	0.28	0.99	0.895	-0.095	0.419	0.63
3.0	1.07	0.14	1.29	1.180	-0.110	0.212	0.45
4.0	1.37	0.05	1.49	1.430	-0.060	0.077	0.36
5.0	1.70	0	1.70	1.700	0	0	0.32

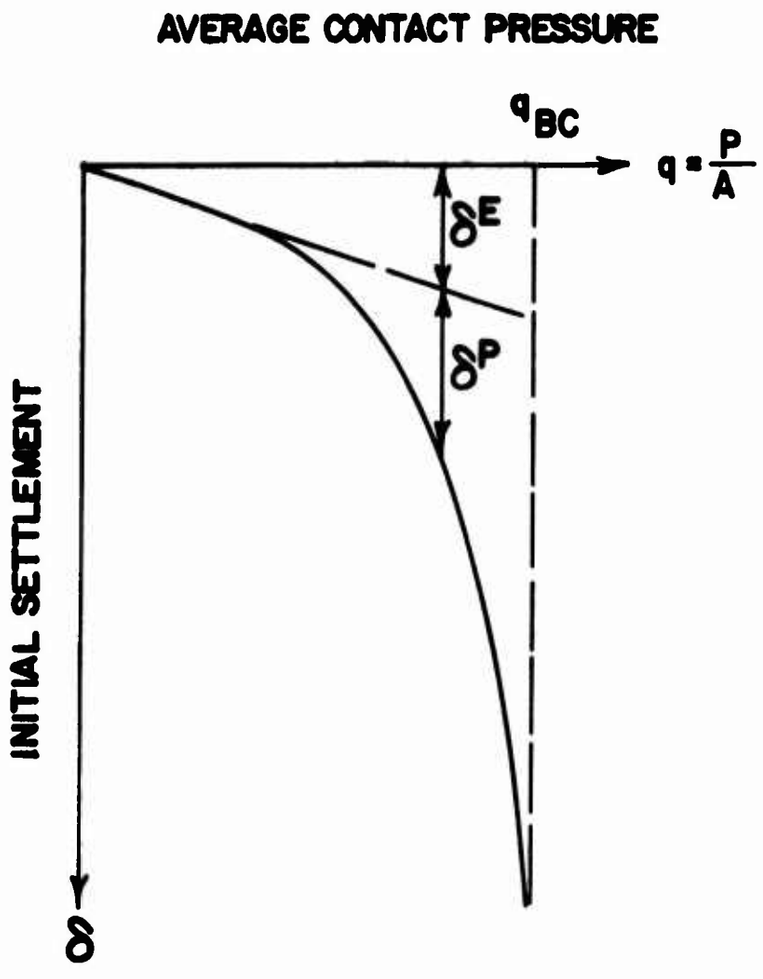

FIGURE 7.1

IDEALIZED INITIAL SETTLEMENT CURVE

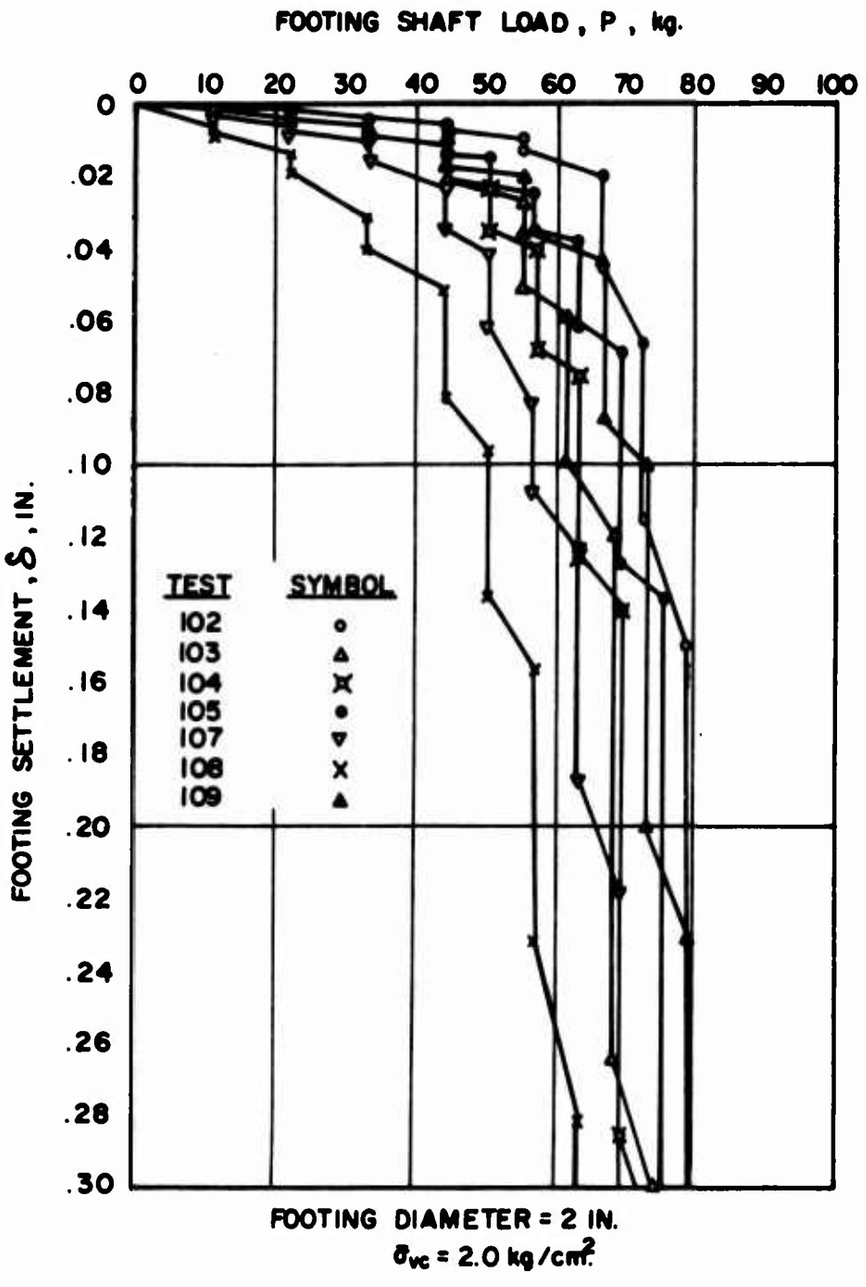

FIGURE 7.2

SETTLEMENT CURVES FOR MODIAP BEARING CAPACITY TESTS

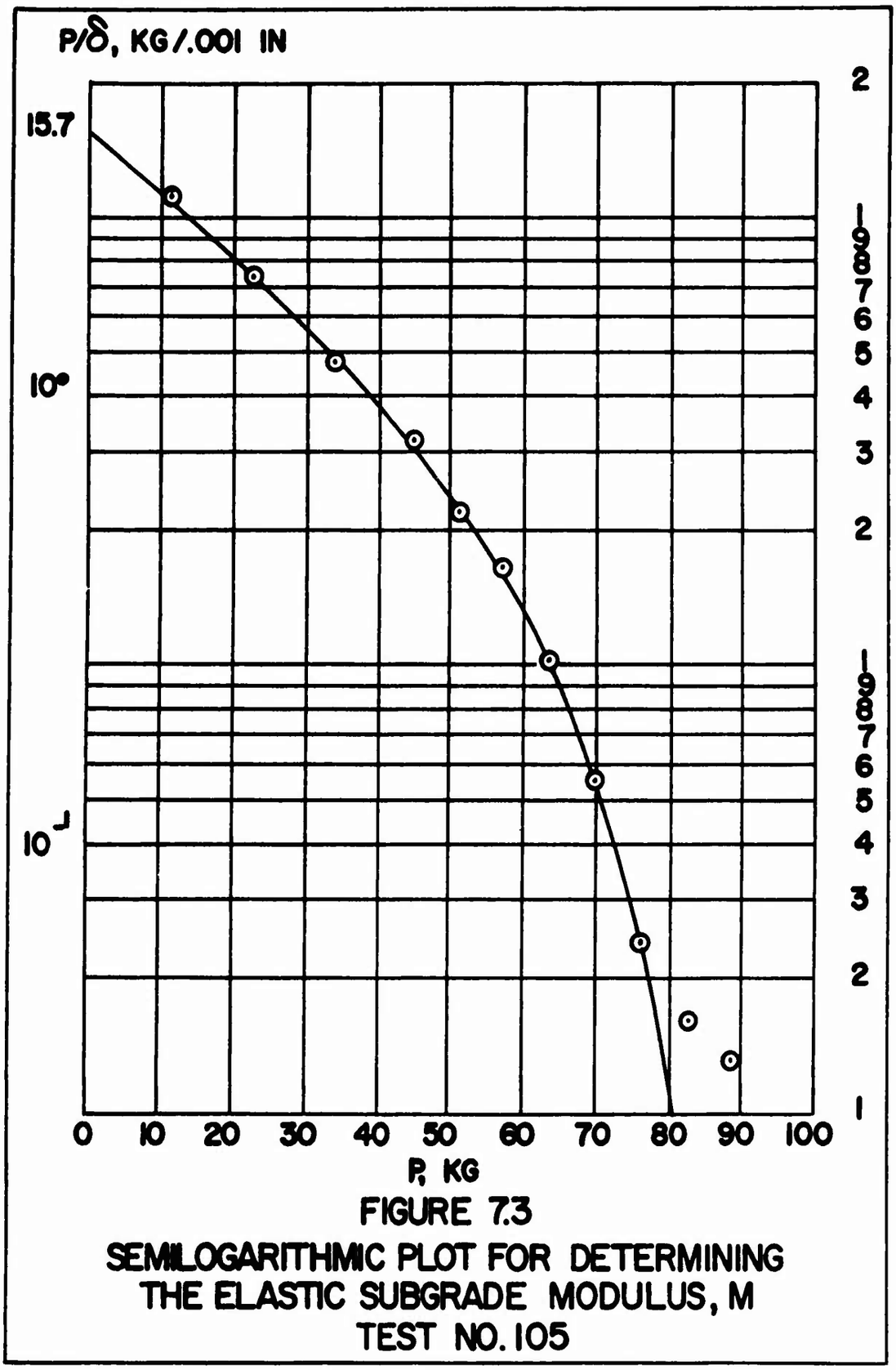

FIGURE 7.3

SEMILOGARITHMIC PLOT FOR DETERMINING THE ELASTIC SUBGRADE MODULUS, M TEST NO. 105

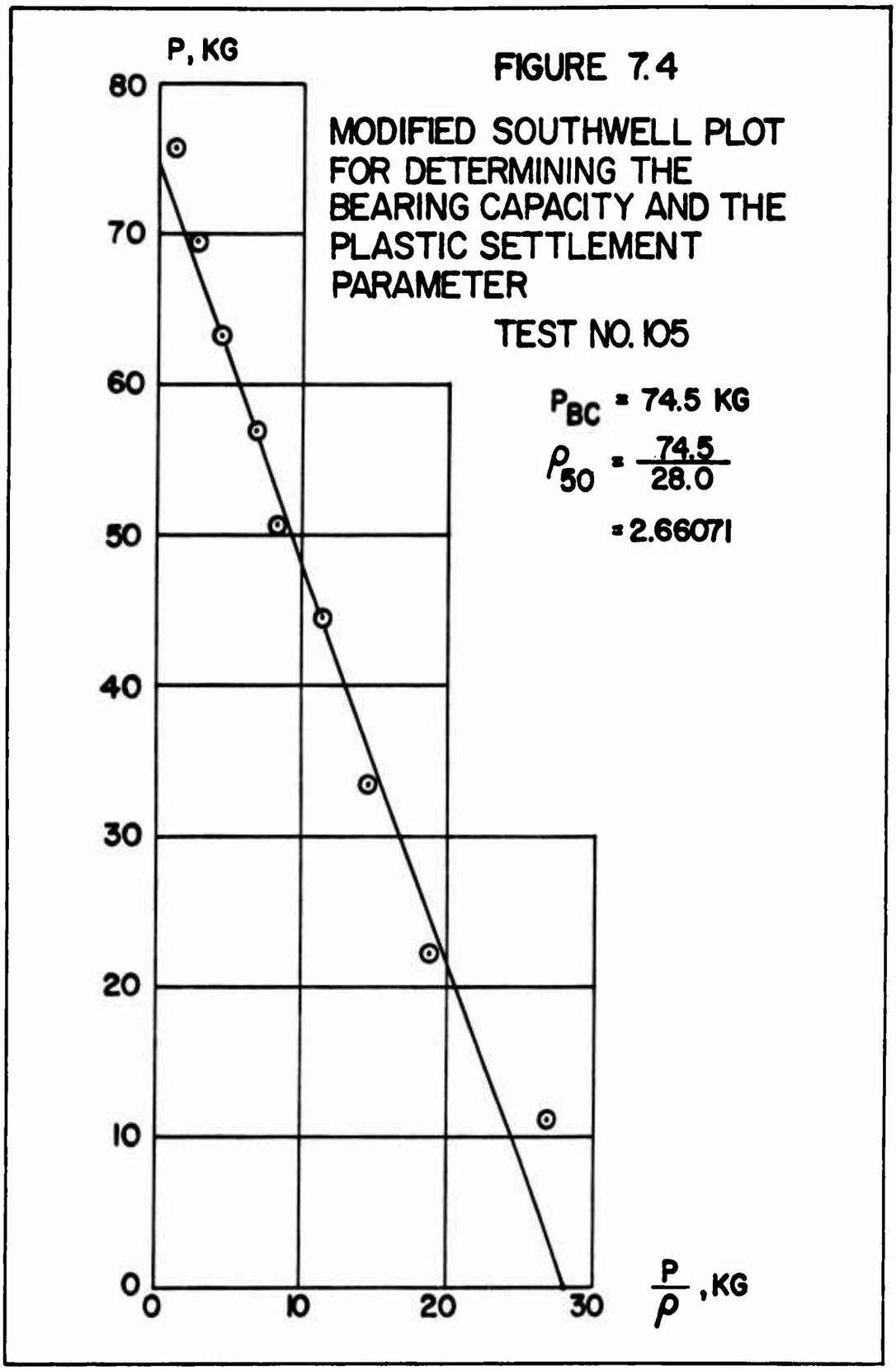

FIGURE 7.4

MODIFIED SOUTHWELL PLOT FOR DETERMINING THE BEARING CAPACITY AND THE PLASTIC SETTLEMENT PARAMETER

TEST NO. 105

$P_{BC} = 74.5$ KG

$\rho_{50} = \frac{74.5}{28.0}$

$= 2.66071$

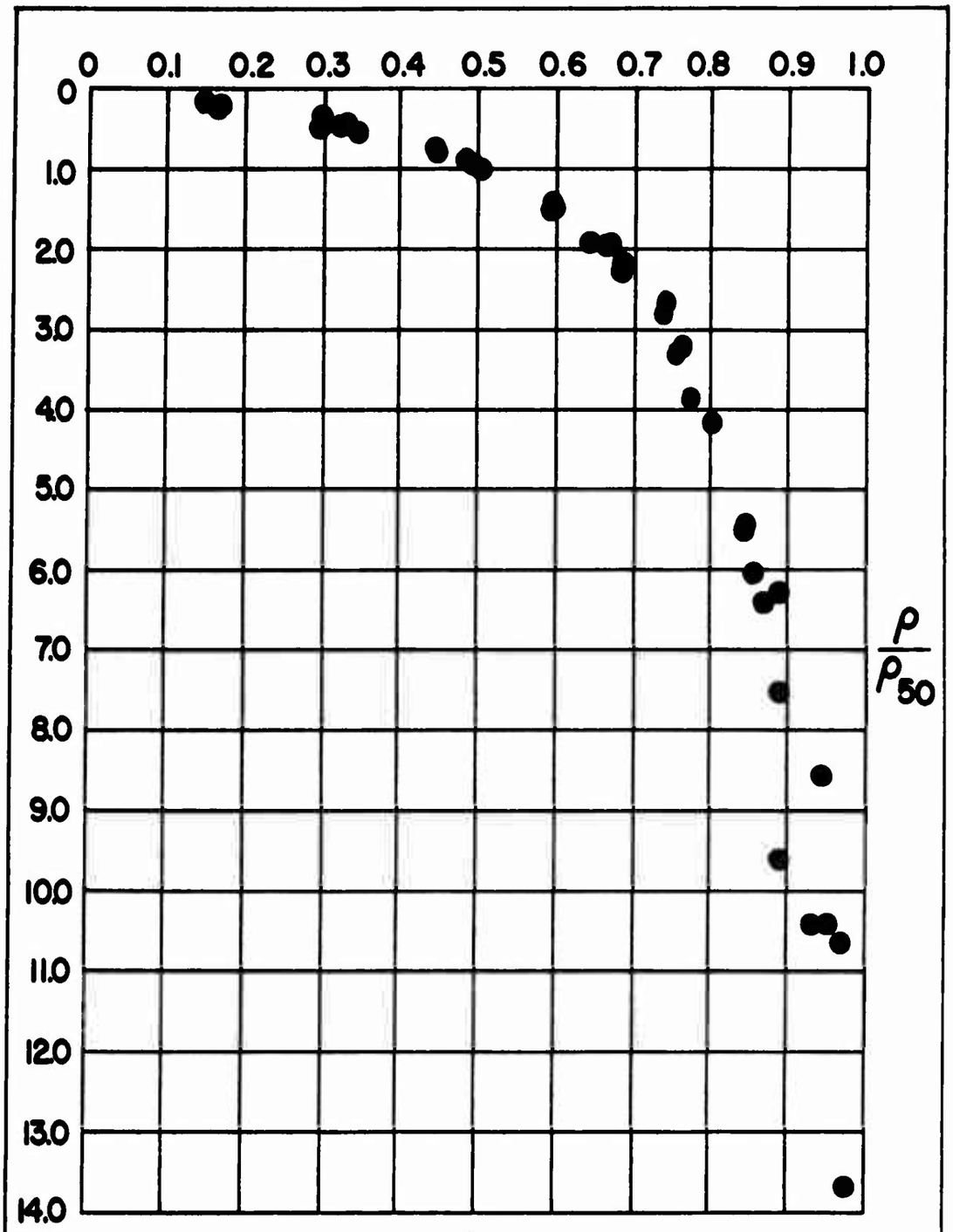

FIGURE 7.5
PLASTIC SETTLEMENT CURVE
FOR MODIAP FOOTING TESTS

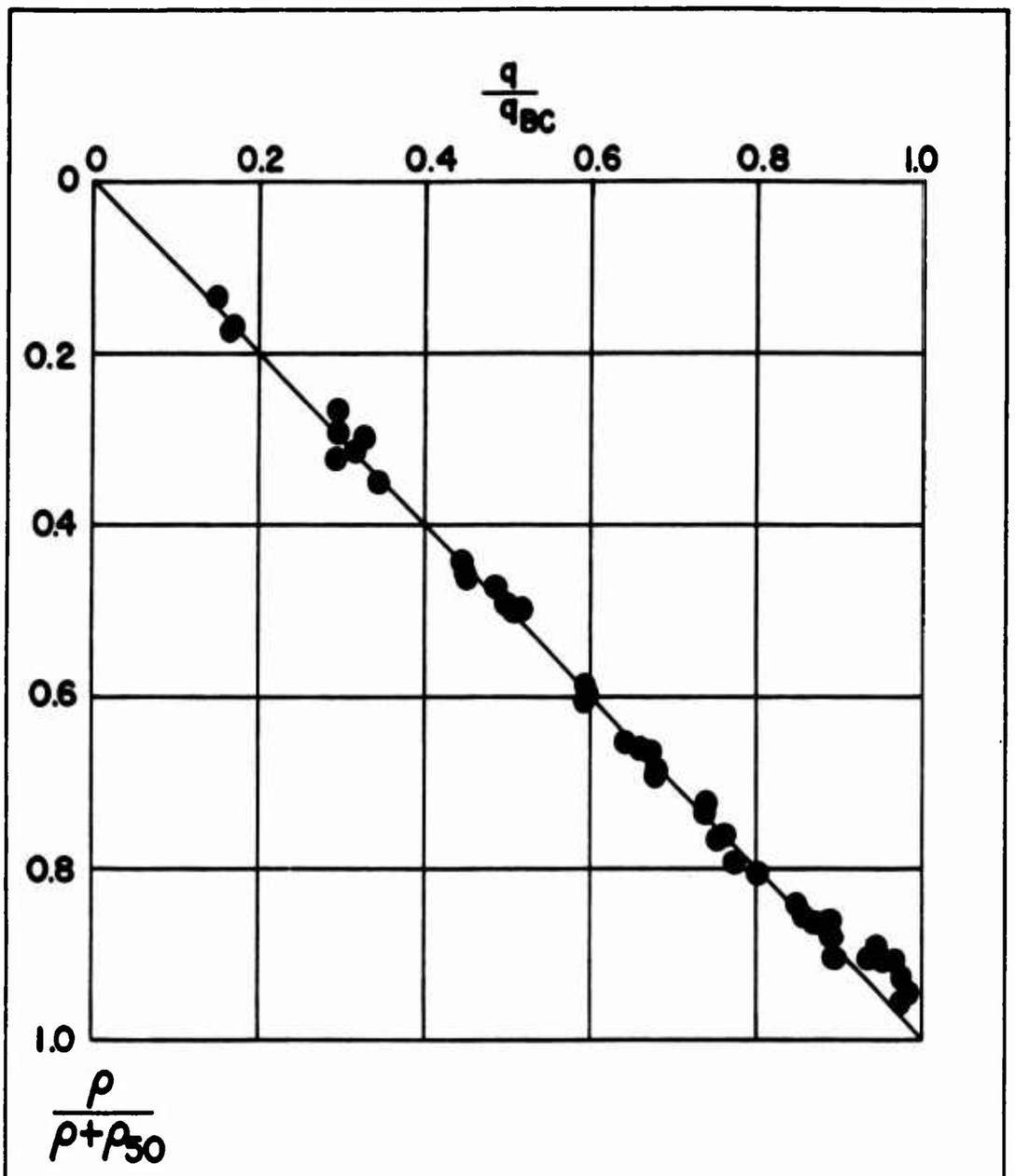

FIGURE 7.6

UNIFIED PLASTIC SETTLEMENT DIAGRAM FOR MODIAP FOOTING TESTS

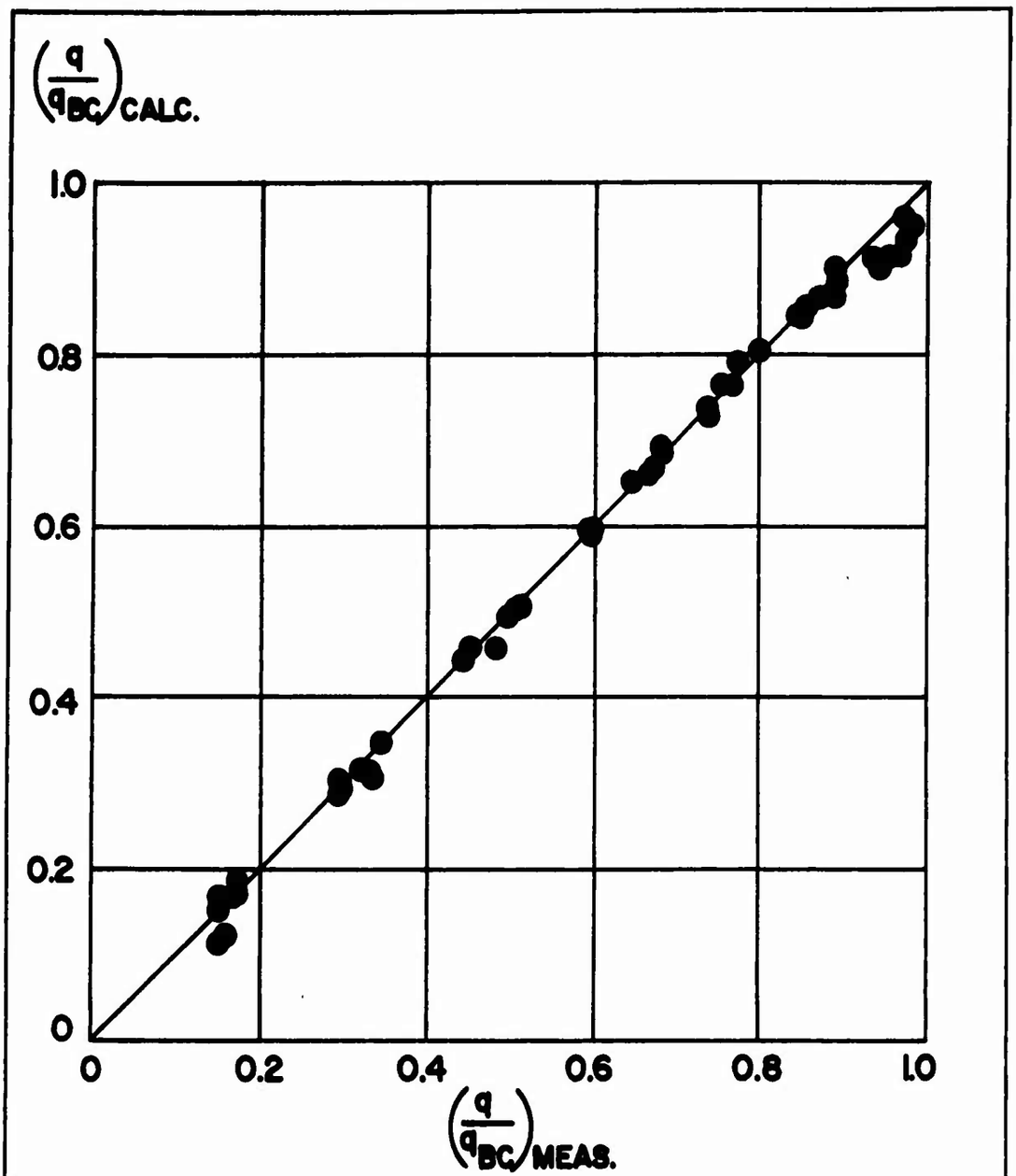

FIGURE 7.7

COMPARISON OF CALCULATED AND MEASURED LOADS FOR MODIAP FOOTING TESTS

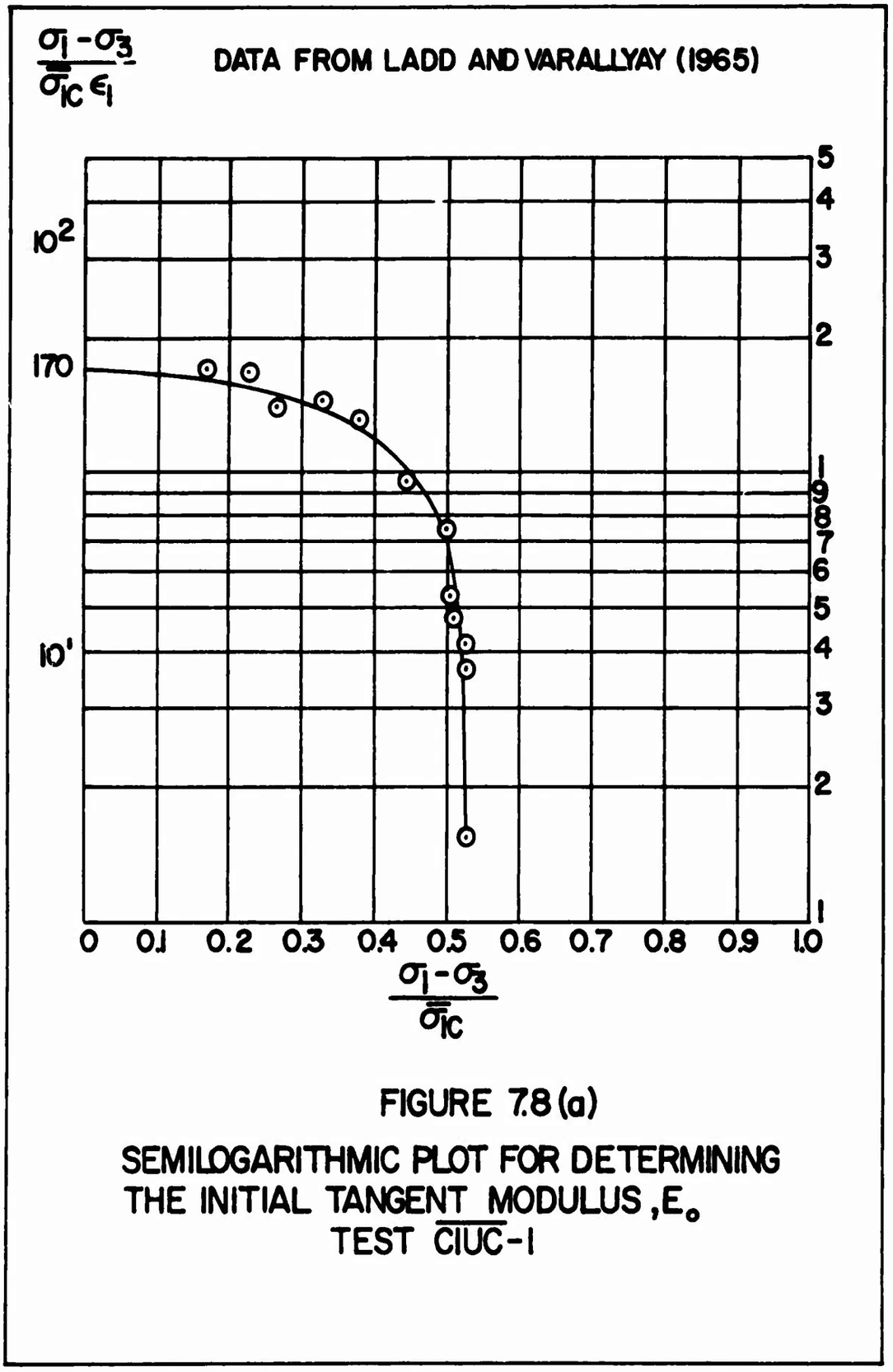

FIGURE 7.8 (a)

SEMILOGARITHMIC PLOT FOR DETERMINING THE INITIAL TANGENT MODULUS, E_o
TEST $\overline{CIUC}$-1

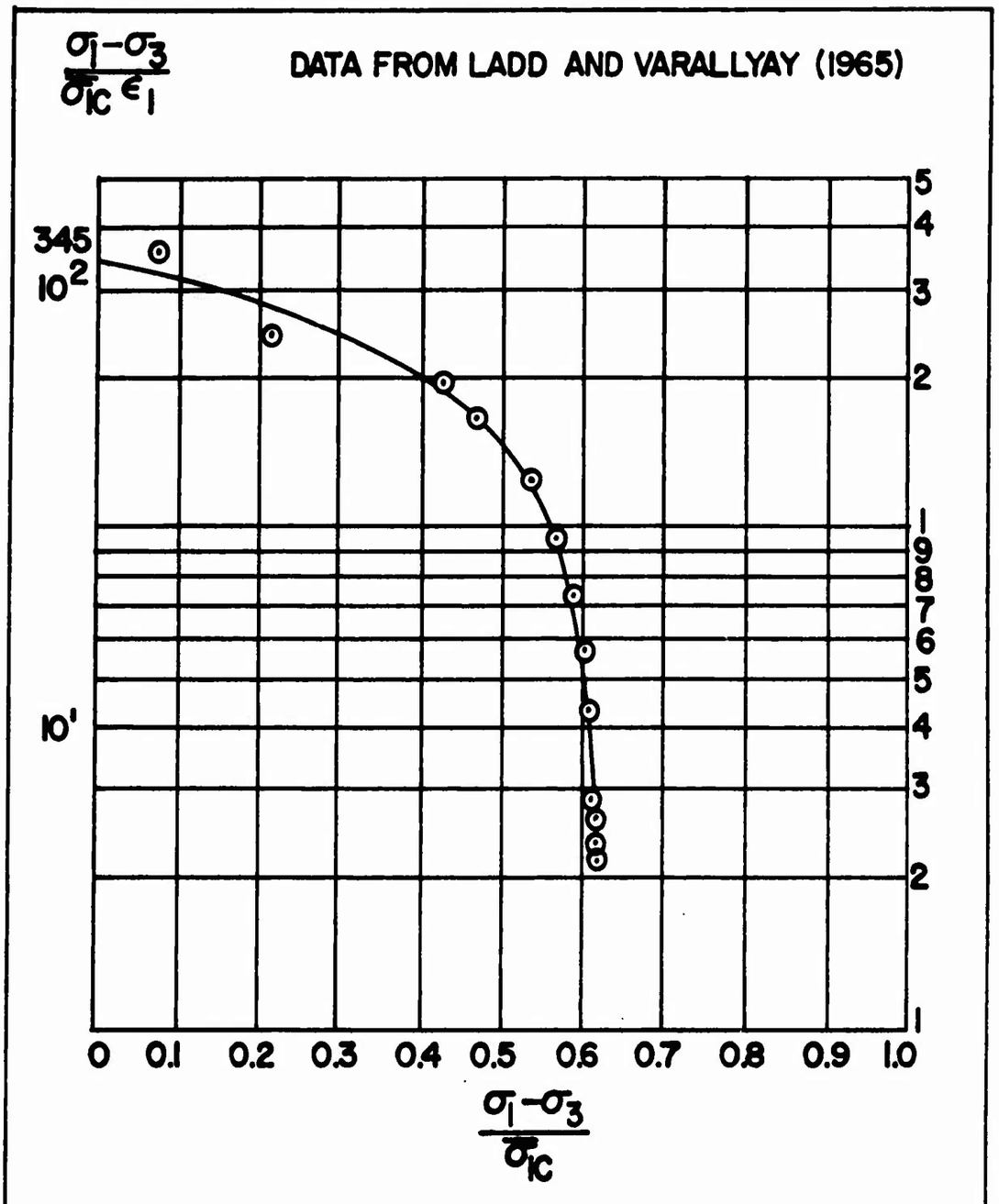

FIGURE 7.8(b)

SEMILOGARITHMIC PLOT FOR DETERMINING THE INITIAL TANGENT MODULUS, E_o
TEST $\overline{CIUC}$-2

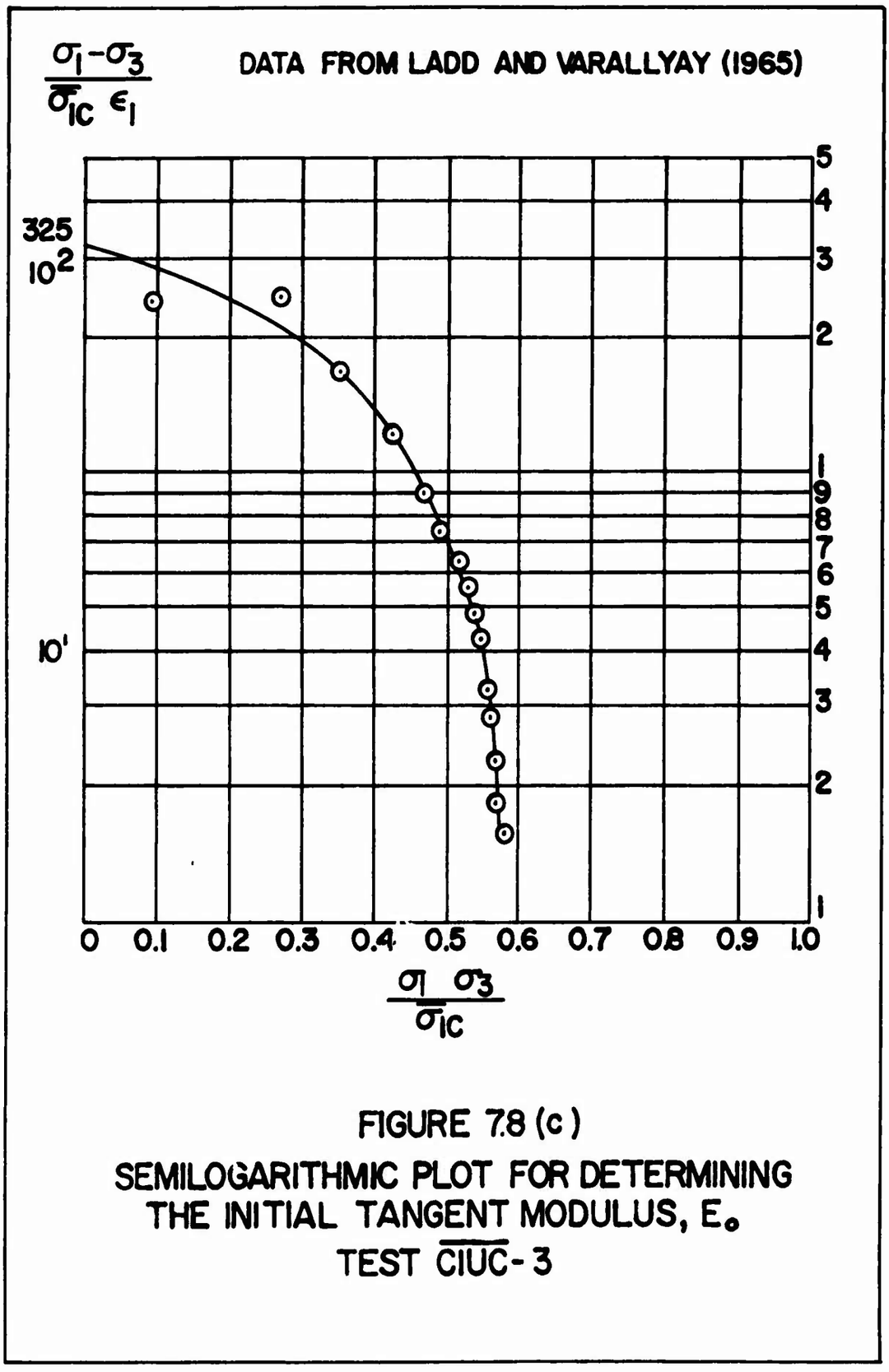

FIGURE 7.8 (c)

SEMILOGARITHMIC PLOT FOR DETERMINING THE INITIAL TANGENT MODULUS, E_o

TEST $\overline{CIUC}$-3

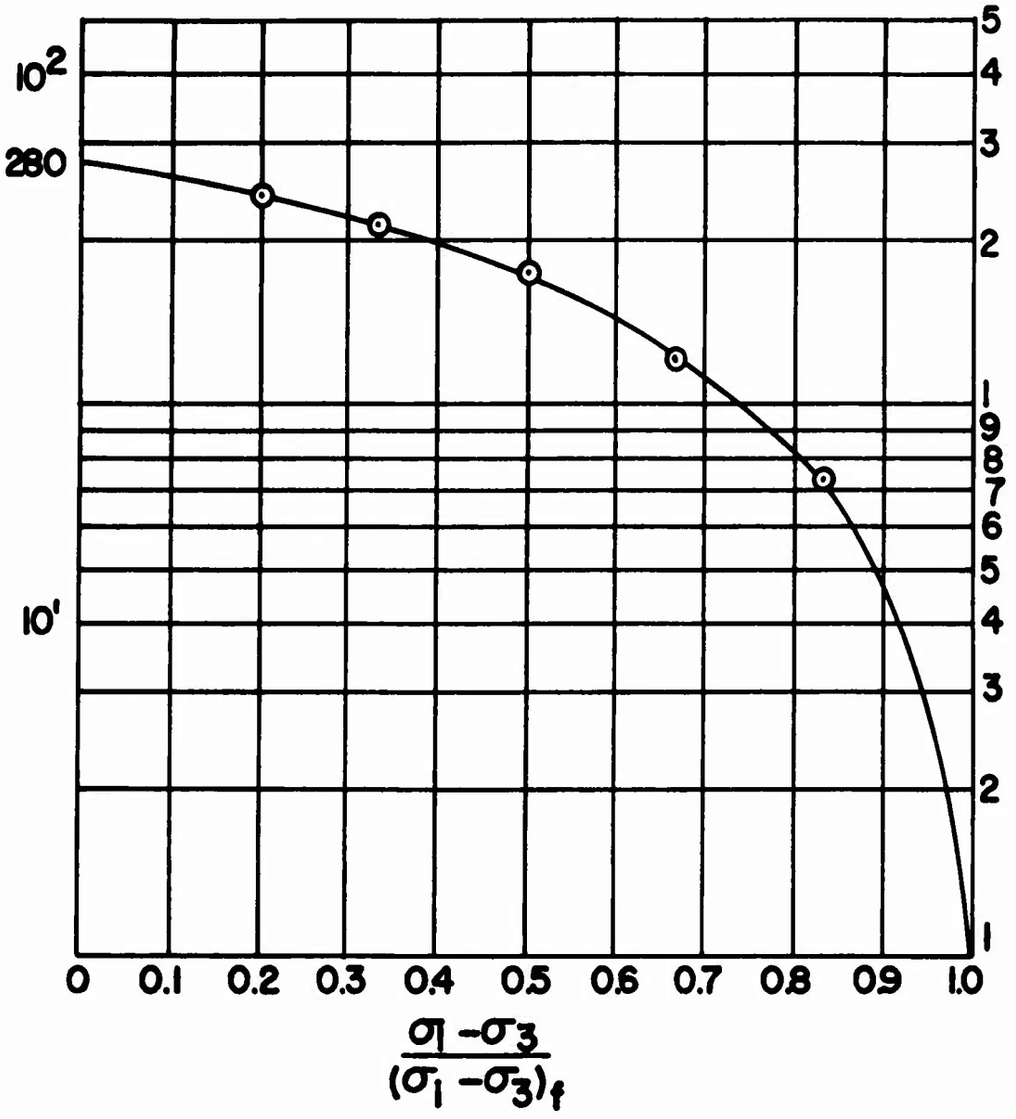

FIGURE 7.8(d)

SEMILOGARITHMIC PLOT FOR DETERMINING THE INITIAL TANGENT MODULUS, E_o REMOLDED BOSTON BLUE CLAY

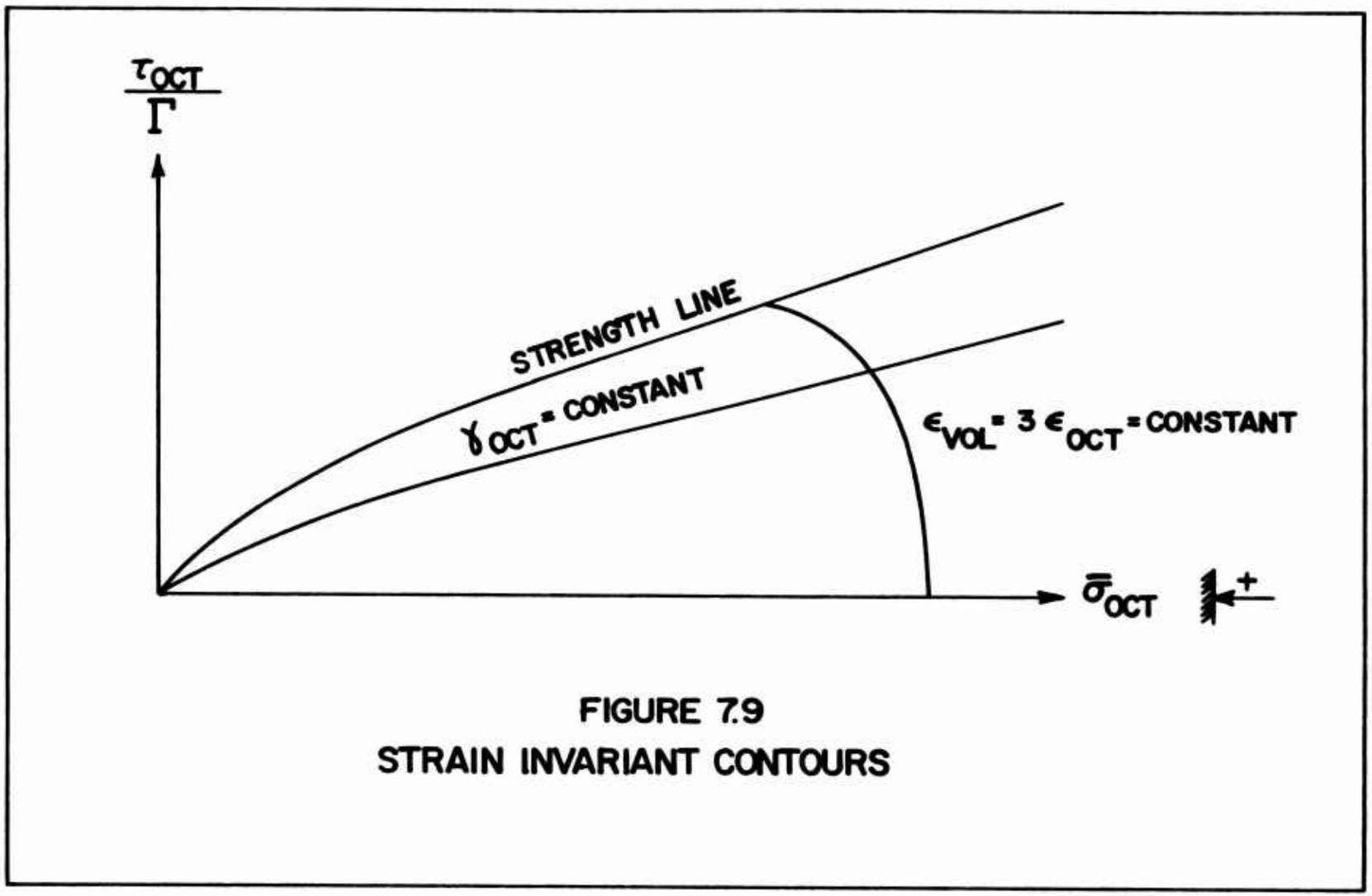

FIGURE 7.9
STRAIN INVARIANT CONTOURS

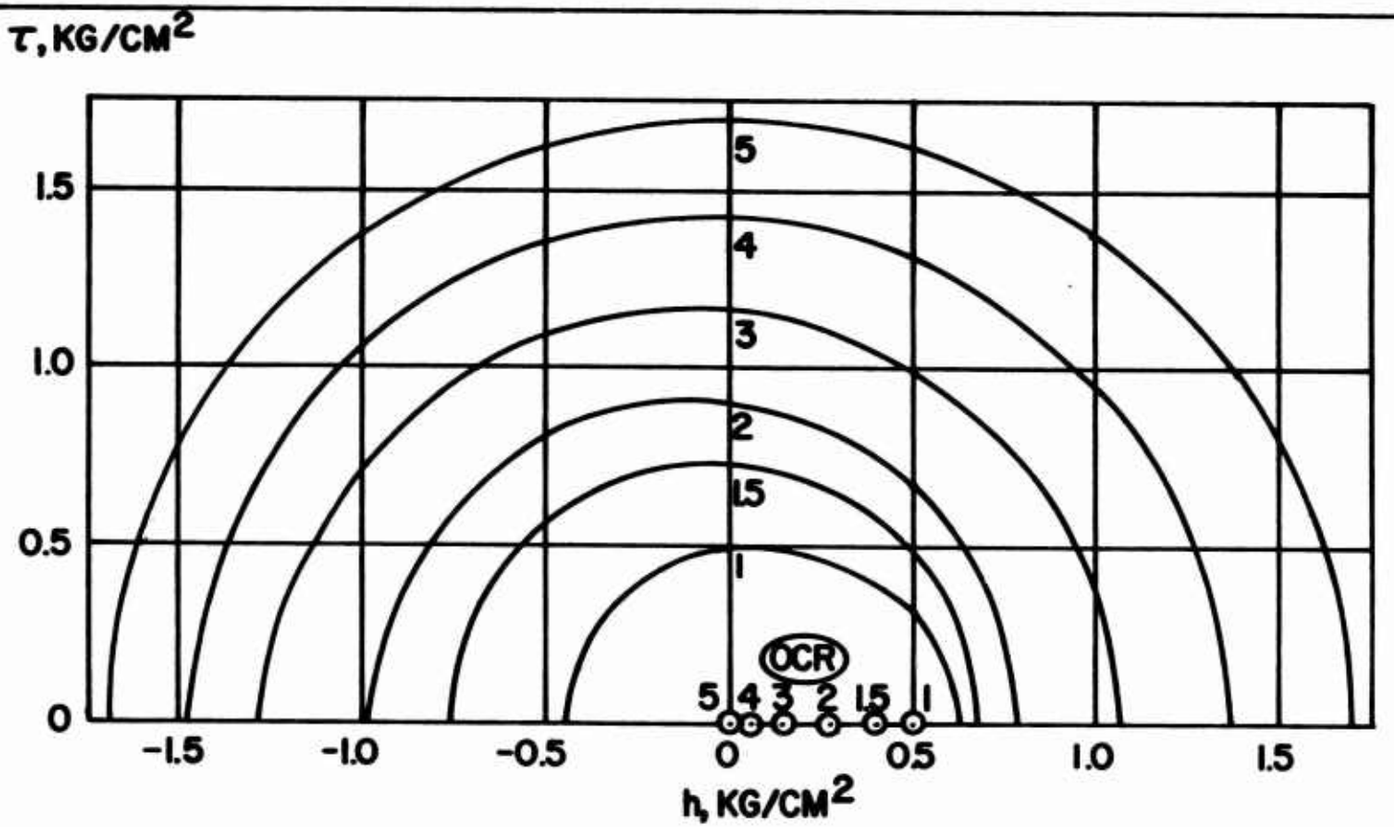

FIGURE 7.10
INFLUENCE OF OVERCONSOLIDATION ON THE DIRECTIONAL VARIATION OF UNDRAINED SHEAR STRENGTH

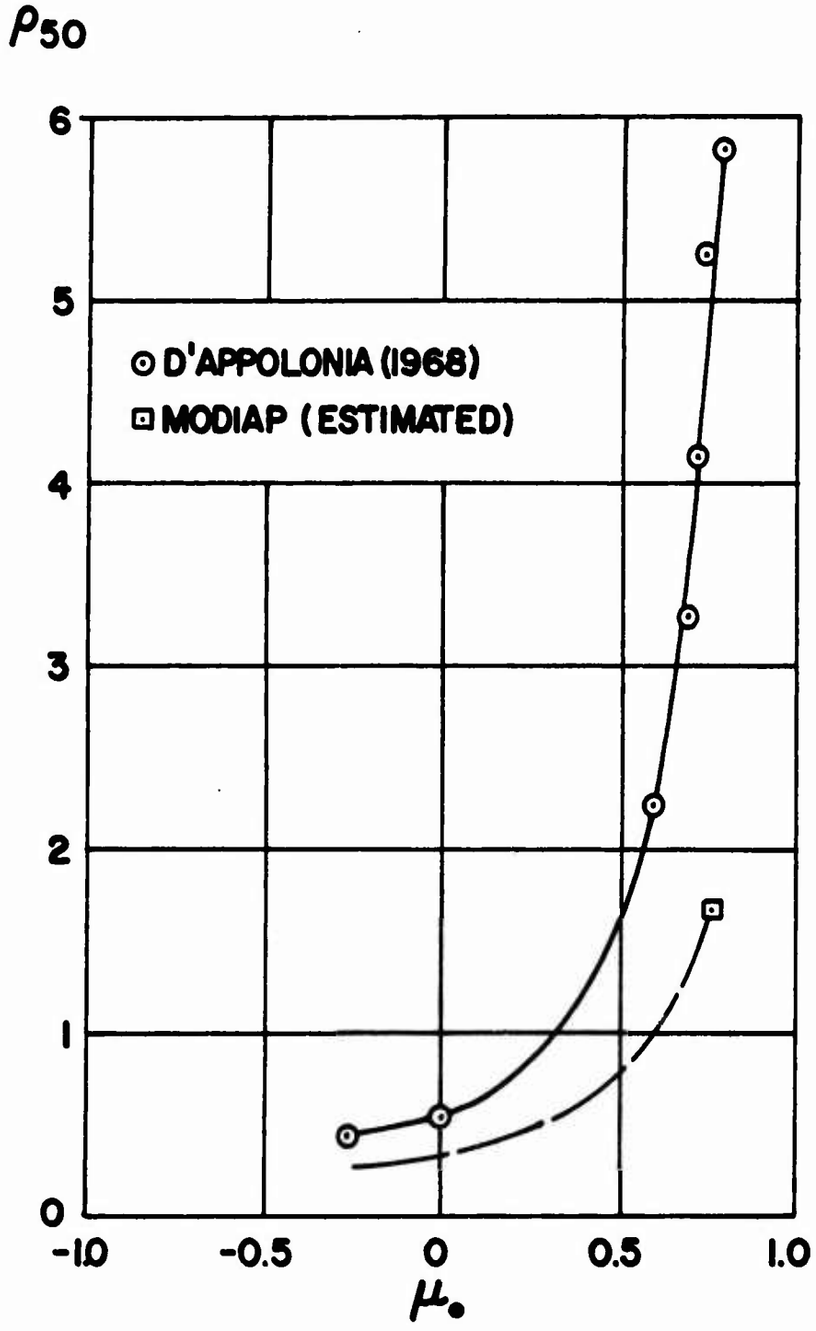

FIGURE 7.11
INFLUENCE OF INITIAL STRESS ON
THE PLASTIC SETTLEMENT PARAMETER

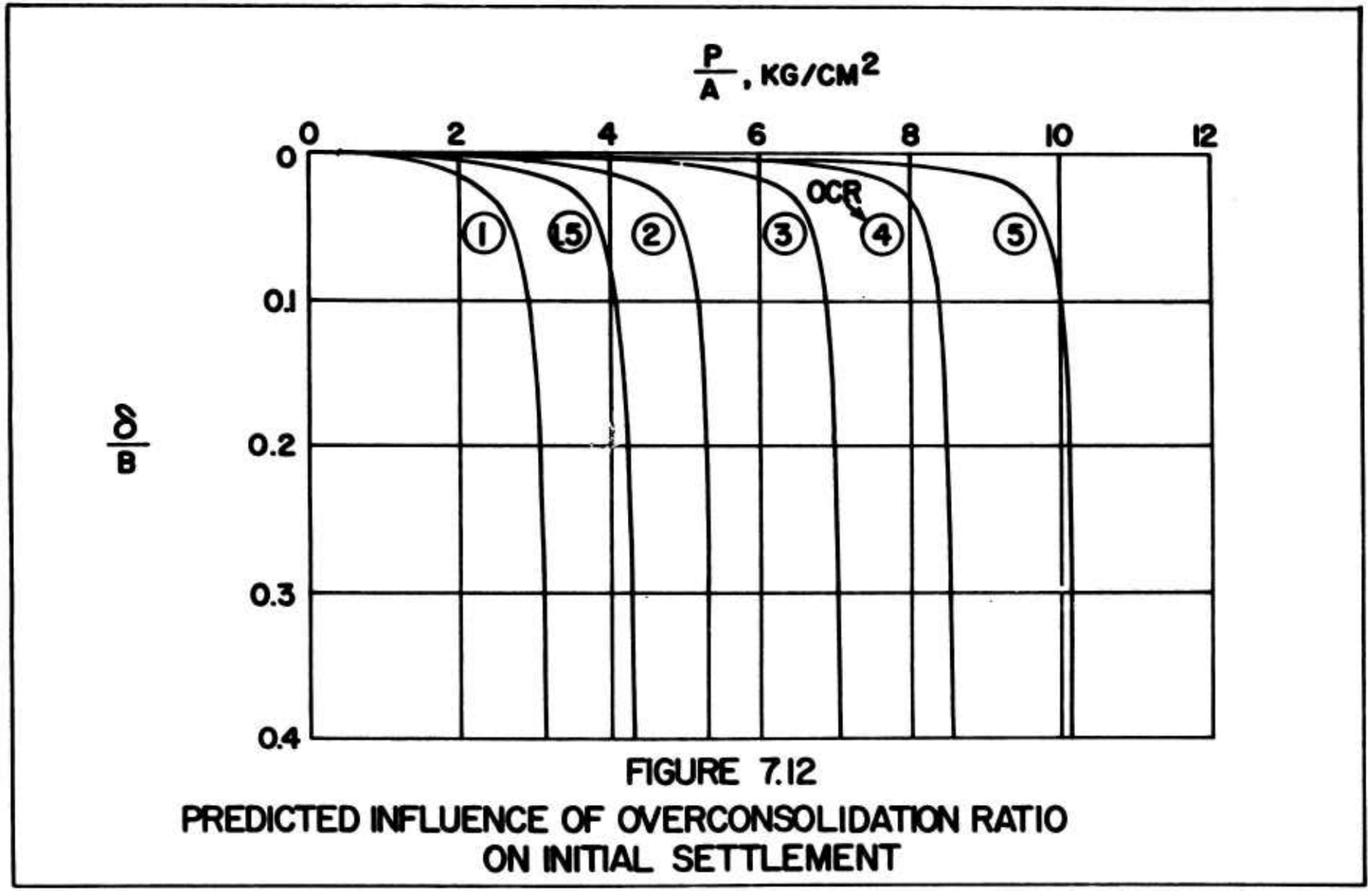

FIGURE 7.12

PREDICTED INFLUENCE OF OVERCONSOLIDATION RATIO ON INITIAL SETTLEMENT

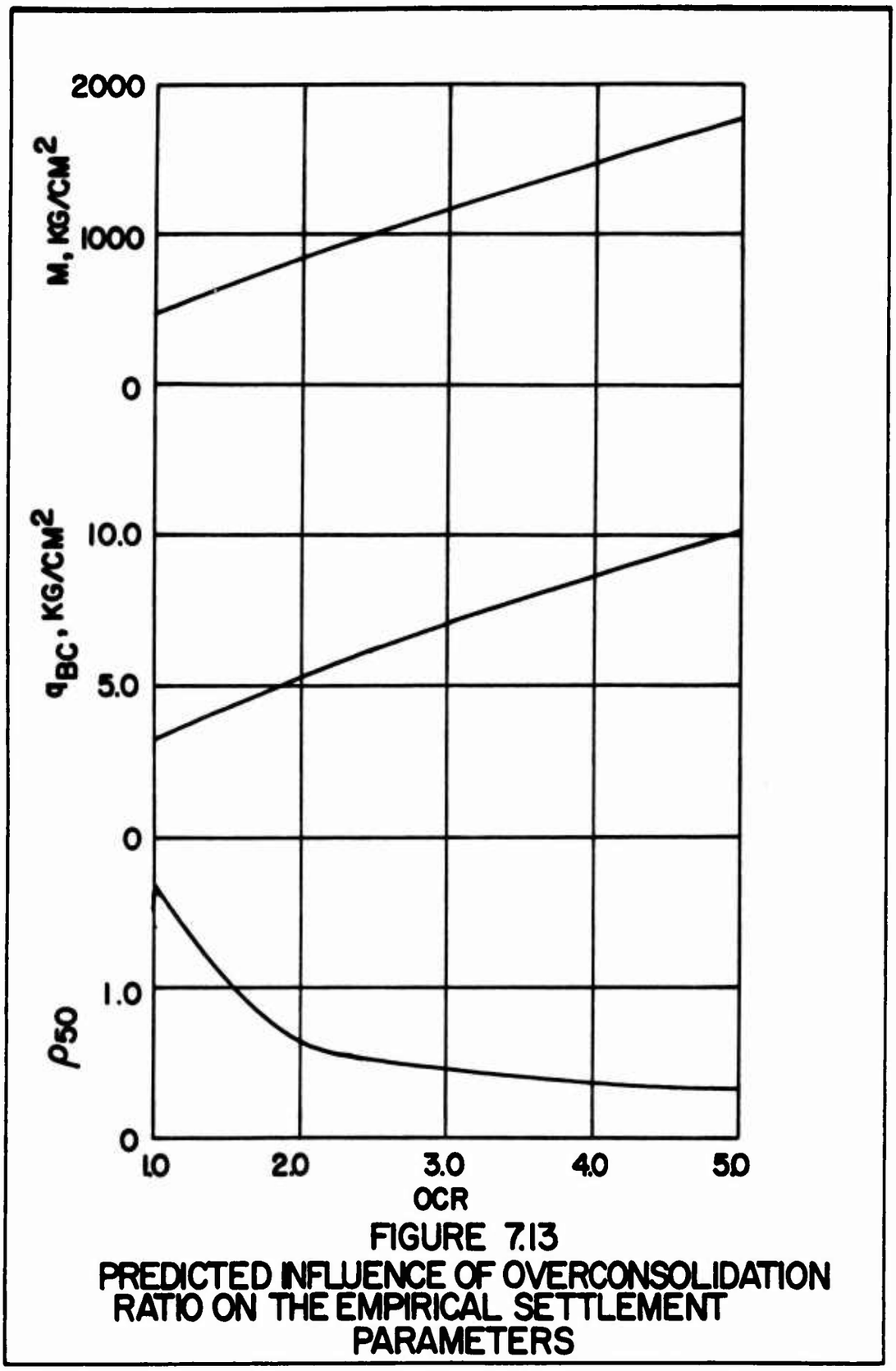

FIGURE 7.13
PREDICTED INFLUENCE OF OVERCONSOLIDATION RATIO ON THE EMPIRICAL SETTLEMENT PARAMETERS

CHAPTER 8

GENERAL SUMMARY

The objectives of this thesis are:

(a) On the basis of theory and available experimental data, explain the influence of stress system (i.e., anisotropy, pore pressure response, rotation of principal planes and the intermediate principal stress) on the undrained shear strength of saturated clay, in terms of effective stress.

(b) Use the developed theory to explain the influence of stress system on the results of model footing tests conducted under Project MODIAP at the Massachusetts Institute of Technology.

Detailed technical summaries appear at the ends of Chapters 3, 4, 5, 6 and 7. The purpose of this General Summary is to assess the relative importance of the four stress system variables considered:

1. anisotropy of the effective stress shear strength parameters,
2. anisotropic pore pressure response,
3. the q_o effect, and
4. influence of the intermediate principal stress.

The influence of the intermediate principal stress on the shear strength of both cohesive and granular soils can safely be neglected by the practicing engineer, provided his strength estimates are based on the results of triaxial compression tests. This is because the angle of shearing resistance is generally a minimum in triaxial compression, as compared with any other state of stress.

Most natural clays exhibit a directional variation of undrained shear strength, when tested in unconfined compression or consolidated undrained triaxial shear. Although relatively few investigators have obtained pore pressure measurements in the course of studying undrained shear strength anisotropy, they have all concluded that anisotropic pore pressure response was the main cause of anisotropic undrained shear strength, for the material which they tested.

Research on anisotropic pore pressure response should be given high priority among the research needs in soil mechanics and foundation engineering by ASCE.

To the Writer's knowledge, there never has been an investigation to determine the actual variation of cohesion and internal friction with failure plane orietation, so the relative importance of these two is unknown. Each is capable

of producing, by itself, a significant directional variation of the effective stress strength envelope.

The q_o effect is caused by the dependence of excess pore pressure on the applied principal total stress increments, rather than on the resulting changes in principal total stress. It leads to a directional variation of undrained shear strength even in soils which are isotropic with respect to both the effective stress shear strength parameters and pore pressure response. It must be considered in any investigation of undrained shear strength anisotropy. The q_o effect is probably the most important cause of undrained shear strength anisotropy in one-dimensionally normally consolidated and heavily overconsolidated clays, i.e. those for which K_o is either considerably less than or considerably greater than unity. Because of it, the IN-SITU directional variation of undrained shear strength may be far different from that exhibited by even the most carefully prepared isotropically consolidated laboratory test specimens. For this reason, whenever a series of triaxial tests is conducted to help predict the IN-SITU directional variation of undrained shear strength, the tests must include pore pressure measurements in order to be of any

substantial value, and the subsequent analysis must include consideration of the q_o effect in order to yield a reliable prediction of undrained shear strength. If an investigator is not willing to obtain pore pressure measurements, it is the Writer's opinion that he might just as well consider the undrained shear strength behavior of the material to be isotropic.

The analysis of model footing tests on clay in Chapter 7, together with theoretical considerations suggest that the influence of stress system on initial settlement is controlled primarily by the overconsolidation ratio, together with the maximum past vertical effective stress. This is because of the tendency of the soil skeleton to change volume when sheared, and thereby generate excess pore water pressure.

In the opinion of the Writer, the single most important fact brought out in this thesis is the strong influence of the q_o effect on undrained shear strength anisotropy. Because of it, no study of undrained shear strength anisotropy or its practical engineering consequences should ignore the importance of pore pressure response.

BIBILIOGRAPHY

Agarwal, K.B. (1967), "The Influence of Size and Orientation of Samples on the Strength of London Clay", Ph.D. Thesis, Univ. of London.

Alvarez - Stelling, J. (1966), "Settlement of Footings on Clay", M.S. Thesis, MIT.

Anderson, E.M. (1951), THE DYNAMICS OF FAULTING, Oliver and Boyd, Ltd.

Baker, W.H. and Krizek, R.J. (1970), "Mohr-Coulomb Strength Theory for Anisotropic Soils", ASCE PROC., Vol. 96, No. SM1, pp. 269-292.

Barber, E.S. (1948), discussion of "Shear Failure in Anisotropic Materials Possessing Any Values of Cohesion and Angle of Internal Friction", by R.J. Hank and L.E. McCarty, HRB PROC., Vol. 28, pp 455-456.

Bell, J.M. (1965), "Stress Strain Characteristics of Cohesionless Granular Materials Subjected to Statically Applied Homogeneous Loads in an Open Stress System", Ph.D. Thesis, Cal. Tech.

Bishop, A.W. (1948), "Some Factors Involved in the Design of a Large Earth Dam in the Thames Valley", PROC. 2nd ICSMFE, Vol. II, pp 13-18.

Bishop, A.W. (1954), "The Use of Pore-Pressure Coefficients in Practice", GEOTECHNIQUE, Vol. 4, No. 4, pp 148-152.

Bishop, A.W. (1957), discussion of Soil Properties and Their Measurement, PROC. 4th ICSMFE, Vol. III, p. 103-104.

Bishop, A.W. (1966), "The Strength of Soils as Engineering Materials", 6th Rankine Lecture, GEOTECHNIQUE, Vol. 16, No. 2, pp 91-128.

Bishop, A.W. (1967), discussion to Session 3, Shear Strength of Soils Other Than Clay, PROC. OSLO GEOT. CONF., Vol. 2, pp 201-204.

Bishop, A.W. and Eldin, A.K.G. (1953), "The Effect of Stress History on the Relation Between Φ and Porosity in Sand", PROC. 3rd ICSMFE, Vol. I, pp 100-105.

Bishop, A.W. and Little, A.L. (1967), "The Influence of the Size and Orientation of the Sample on the Apparent Strength of the London Clay at Maldon, Essex", PROC. OSLO GEOT. CONF., Vol. I, pp 89-96.

Bishop, A.W., Webb, D.L. and Lewin, P.I. (1965), "Undisturbed Samples of London Clay From the Ashford Common Shaft; Strength - Effective Stress Relationships", GEOTECHNIQUE, Vol. 15, No. 1, pp 1-31.

Bjerrum, L. and Flodin, N. (1960), "The Development of Soil Mechanics in Sweden", GEOTECHNIQUE, Vol. 10, pp 1-18.

Bjerrum, L. and Lo, K.Y. (1963), "Effect of Aging on the Shear Strength Properties of a Normally Consolidated Clay", GEOTECHNIQUE, Vol. 13, No. 2, pp 147-157.

Boker, R. (1915), "Die Mechanik der Bleibenden Formanderung in kristallinisch aufgebauten Korpern", MITTEILUNGEN UBER FORSCHUNGSARBEITEN AUF DEM GEBEITE DES INGENIEURWESSENS, Vol. 175/176, pp 1-51.

Bott, M.H.P. (1959), "The Mechanics of Oblique Slip Faulting", GEOL. MAG., Vol. 96, pp 109-117.

Brinch Hansen, J. and Gibson, R.E. (1949), "Undrained Shear Strengths of Anisotropically Consolidated Clays", GEOTECHNIQUE, Vol. 1, No. 3, pp 189-204.

Broms, B.B. and Ratnam, M.V. (1963), "Shear Strength of an Anisotropically Consolidated Clay", ASCE PROC., Vol 89, No. SM6, pp 1-26.

Casagrande, A. (1932), "The Structure of Clay and Its Importance in Foundation Engineering", J. BSCE; reprinted in CONTRIBUTIONS TO SOIL MECHANICS 1925-1940, pp 72-126.

Casagrande, A. (1934), discussion of "The Shearing Resistance of Soils", by L. Jurgenson, J. BSCE; reprinted in CONTRIBUTIONS TO SOIL MECHANICS 1925-1940, pp 218-225.

Casagrande, A. and Carrillo, N. (1944), "Shear Failure of Anisotropic Materials", J. BSCE; reprinted in CONTRIBUTIONS TO SOIL MECHANICS 1941-1953, pp 122-135.

Casbarian, A.O. (1964), "Effects of Rotation of the Principal Stress Axes and of the Intermediate Principal Stress on the Shear Strength of a Saturated Remolded Clay", Ph.D. Thesis, Cornell University.

Christian, J.T. (1966), "Plane Strain Deformation Analysis of Soil", Ph.D. Thesis, MIT.

Coleman, J.D. (1960), "Suction and the Yield and Failure Surface for Soil in the Principal Effective Stress Space", GEOTECHNIQUE, Vol. 10, No. 4, pp 181-183.

Conforth, D.H. (1961), "Plane Strain Failure Characteristics of a Saturated Sand", Ph.D. Thesis, Univ of London.

Conforth, D.H. (1964), "Some Experiments on the Influence of Strain Conditions on the Strength of Sand", GEOTECHNIQUE, Vol. 14, No. 2, pp 143-167.

Coulomb, C.A. (1776), "Essai sur une application des regles de maximis et minimis a quelques problemes de statique, relatifs a l'architecture", MEMOIRES DE MATHEMATIQUE ET DE PHYSIQUE, PRESENTES A L'ACADEMIE ROYALE DES SCIENCES PAR DIVERS SAVANTS, (Paris), Vol. 7, pp 343-382.

Courant, R. and Robbins, H. (1941), WHAT IS MATHEMATICS?, Oxford University Press.

D'Appolonia, D.J. (1968), "Prediction of Stress and Deformation for Undrained Loading Conditions", Ph.D. Thesis, MIT.

Davis, E.H. and Christian, J.T. (1971), "Bearing Capacity of Anisotropic Cohesive Soil", ASCE PROC., Vol. 97, No. SM5, pp 753-769.

Deresiewicz, H. (1958), "Mechanics of Granular Matter" in ADVANCES IN APPLIED MECHANICS, Vol, V, pp 233-306, Academic Press.

Dickey, J.W. (1967), "A Plane Strain Shear Device for Testing Clays", M.S. Thesis, MIT.

Dickey, J.W., Ladd, C.C. and Rixner, J.J. (1968), "A Plane Strain Shear Device for Testing Clays", MIT DEPT. OF CIV. ENG. RESEARCH REPORT R68-3, SOILS PUBLICATION NO. 237.

Dickson, L.E. (1922), FIRST COURSE IN THE THEORY OF EQUATIONS, Wiley.

Donath, F.A. (1961), "Experimental Study of Shear Failure in Anisotropic Rocks", BUL. GEOL. SOC. AM., Vol. 72, pp 985-990.

Donath, F.A. (1964), "Strength Variation and Deformation Behavior in Anisotropic Rock", in STATE OF STRESS IN THE EARTH'S CRUST, edited by W.R. Judd, American Elsevier, pp 281-298.

Donath F.A. and Cohen, C.I. (1960), "Anisotropy and Failure in Rocks" (Abstract), GEOL. SOC. AMER. BULL., Vol. 71, p 1851.

Drucker, D.C., Gibson, R.E., and Henkel, D.J. (1957), "Soil Mechanics and Work-Hardening Theories of Plasticity", ASCE TRANS., Vol. 122, p 338-346.

Duncan, J.M. and Seed, H.B. (1965), "The Effect of Anisotropy and Reorientation of Principal Stresses on the Shear Strength of Saturated Clay", U. of Cal. Dept. of C.E. Report No. TE-65-3, 177pp.

Duncan, J.M. and Seed, H.B. (1966a), "Anisotropy and Stress Reorientation in Clay", ASCE PROC., Vol. 92, No. SM5, pp 21-50.

Duncan, J.M. and Seed, H.B. (1966b), "Strength Variation Along Failure Surfaces in Clay", ASCE PROC., Vol. 92, No. SM6, pp 81-104.

Eden, W.J. (1955), "A Laboratory Study of Varved Clay From Steep Rock Lake, Ontario", AMERICAN JOURNAL OF SCIENCE, Vol. 253, No. 11, pp 659-674.

Eldin, A.K. (1951), "Fundamental Factors Controlling Shear Properties of Sands", Ph.D. Thesis, Univ of London.

Fisher, W.E. and Merkle, D.H. (1965), "The Great Alaska Earthquake", AFWL TR65-92, AD 627020 and 627096.

Fraser, A.M. (1957), "The Influence of Stress Ratio on Compressibility and Pore Pressure Coefficients in Compacted Soils", Ph.D. Thesis, Univ of London.

Fung, Y.C. (1965), FOUNDATIONS OF SOLID MECHANICS, Prentice-Hall.

Gibson, R.E. and Morgenstern, N. (1962), "A Note on the Stability of Cuttings in Normally - Consolidated Clays", GEOTECHNIQUE, Vol. 12, No. 3, pp 212-216.

Gilbert, G.D. (1954), "The Basic Shear Strength Properties of Weald Clay", Ph.D. Thesis, Univ of London.

Gilboy, G. (1928), "The Compressibility of Sand - Mica Mixtures", ASCE PROC., Vol. 54, pp 555-568.

Goldstein, H. (1950), CLASSICAL MECHANICS, Addison-Wesley.

Green, G.E. (1969), "Strength and Compressibility of Granular Materials Under Generalized Strain Conditions", Ph.D. Thesis, Univ of London.

Green, G.E. and Bishop, A.W. (1969), "A Note on the Strength of Sand Under Generalized Strain Conditions", GEOTECHNIQUE, Vol. 19, No. 1, pp 144-149.

Grim, R.E. (1953), CLAY MINERALOGY, McGraw Hill.

Habib, P. (1953), "Influence de la Variation de la Contrainte Principale Moyenne sur la Resistance au Cisaillement des Sols", (Influence of the Variation of the Intermediate Principal Stress on the Shearing Strength of Soils), PROC. 3rd ICSMFE, Vol. I, pp 131-136, translated by Cadet K.R. King at the USAF Academy.

Hafiz, M.A. (1950), "Strength Characteristics of Sands and Gravels in Direct Shear", Ph.D. Thesis, Univ. of London.

Hambly, E.C. (1969), "A New True Triaxial Apparatus", GEOTECHNIQUE, Vol. 19, No. 2, pp 307-309.

Handin, J. and Hager, R. (1957), "Experimental Deformation of Sedimentary Rocks", BULL. AMER. ASSOC. PETR. GEOL., Vol. 41, pp 1-50.

Hank, R.J. and McCarty, L.E. (1948), "Shear Failure in Anisotropic Materials Possessing Any Values of Cohesion and Angle of Internal Friction", HRB PROC., Vol. 28, pp 449-456.

Hanna, T.H. (1966), "Engineering Properties of Glacial - Lake Clays Near Sarnia, Ontario", ONTARIO HYDRO RESEARCH QUARTERLY, Vol. 18, No. 3, pp 1-12.

Hanna, T.H. (1967), discussion of "Shear Strength Properties of Two Stratified Clays", by K.Y. Lo and V. Milligan, ASCE PROC., Vol. 93, No. SM3, pp 183-188.

Harland, W.B. and Bayly, M.B. (1958), "Tectonic Regimes", GEOL. MAG., Vol. 95, pp 89-104.

Haythornthwaite, R.M. (1960a), "Stress and Strain in Soils", in PROC. 2nd SYMPOSIUM ON NAVAL STRUCTURAL MECHANICS: PLASTICITY, edited by E.H. Lee and P.S. Symonds, Pergamon, pp 185-192; see also report (same title) to U.S. Army Land Locomotion Research Laboratories, Warren, Michigan.

Haythornthwaite, R.M. (1960b), discussion of "Failure Hypotheses for Soils" by N.M. Newmark, ASCE RCSSCS, pp 989-992.

Haythornthwaite, R.M. (1960c), "Mechanics of Triaxial Test for Soils", ASCE PROC., Vol. 86, No. SM5, pp 35-62.

Haythornthwaite, R.M. (1963), discussion of "Study of Failure Envelope of Soils", by T.H. Wu, A.K. Loh and L.E. Malvern, ASCE PROC., Vol. 89, No. SM5, pp 119-120.

Henkel, D.J. (1956), "The Effect of Overconsolidation on the Behavior of Clays During Shear", GEOTECHNIQUE, Vol. 6, No. 4, pp 139-150.

Henkel, D.J. (1958), "The Correlation Between Deformation, Pore Water Pressure and Strength Characteristics of Saturated Clays", Ph.D. Thesis, Univ. of London.

Henkel, D.J. (1959), "The Relationships Between the Strength, Pore Water Pressure and Volume - Change Characteristics of Saturated Clays", GEOTECHNIQUE, Vol. 9, No. 3, pp 119-135.

Henkel, D.J. (1960a), "The Relationship Between the Effective Stresses and Water Content in Saturated Clays", GEOTECHNIQUE, Vol. 10, No. 2, pp 41-54.

Henkel, D.J. (1960b), "The Shear Strength of Saturated Remolded Clays", ASCE RCSSCS, pp 533-554.

Henkel, D.J. and Sowa, V.A. (1963), "The Influence of Stress History on the Stress Paths Followed in Undrained Triaxial Tests", ASTM STP 361, pp 280-292.

Henkel, D.J. and Wade, N.H. (1966), "Plane Strain Tests on a Saturated Remolded Clay", ASCE PROC., Vol. 92, No. SM6, pp 67-80.

Hildebrand, F.B. (1952), METHODS OF APPLIED MATHEMATICS, Prentice Hall.

Horn, H.M. (1963), "Investigation of the Load - Settlement Time Characteristics of Deposits of Saturated Soil (MODIAP)", a Proposal to the MIT Inter-American Program in Civil Engineering.

Horne, M.R. (1965), "The Behavior of an Assembly of Rotund, Rigid, Cohesionless Particles", Parts I and II, PROC. ROY. SOC. (London), Series A, Vol. 286, pp 62-97; Part III, Vol. 310 (1969), pp 21-34.

Housel, W.S. (1928), discussion of "The Science of Foundations", by K. Terzaghi, ASCE PROC., Vol. 54, No. 4, pp 1243-1251; see also TRANS., Vol. 93, (1929).

Hvorslev, M.J. (1936), "Conditions of Failure for Remolded Cohesive Soils", PROC. 1st ICSMFE, Vol. III, pp 51-53.

Hvorslev, M.J. (1937), "Uber die Festigkeitseigenschaften gestorter bindiger Boden" (On the strength properties of remolded cohesive soils), Thesis, 159 pp, published by Danmarks Naturvidenskabelige Samfund, Ingeniorvidenskabelige Skrifter, Series A, Nr. 45, Copenhagen.

Hvorslev, M.J. (1938), "The Shearing Resistance of Remolded Cohesive Soils", PROC. SOILS & FOUNDATIONS CONF., U.S. Engineer Dept., Boston, Section E, pp E1-E30.

Hvorslev, M.J. (1960), "Physical Components of the Shear Strength of Saturated Clays", ASCE RCSSCS, pp 169-273.

Jaeger, J.C. (1959), "The Frictional Properties of Joints in Rock", GEOFISICA PURA E APPLICATA, Vol. 43, pp 148-158.

Jaeger, J.C. (1960), "Shear Failure of Anisotropic Rocks", GEOLOGICAL MAGAZINE, Vol. XCVII, No. 1, pp 65-72.

Jaeger, J.C. and Cook, N.G.W. (1969), FUNDAMENTALS OF ROCK MECHANICS,Methuen.

Jakobson, B. (1952), "The Landslide at Surte on the Gota River", PROC. ROY. SWED. GEOT. INST., No. 5, 121 pp.

Jakobson, B. (1955), "Isotropy of Clays", GEOTECHNIQUE, Vol. 5, No. 1, pp 23-28.

Jakobson, B. (1957), "Some Fundamental Properties of Sand", PROC. 4th ICSMFE, Vol. 1, pp 167-171.

Johansen, K.W. (1958), "Brudbetingelser for sten og beton", (Failure Conditions for Rocks and Concrete), BYGNINGSSTATISKE MEDDELELSER, Vol. 19, Teknisk Forlag, Copenhagen, pp 25-44.

Johnson, W. and Mellor, P.B. (1962), PLASTICITY FOR MECHANICAL ENGINEERS, D. Van Nostrand.

Juarez - Badillo, E. (1963), "Pore Pressure Functions in Saturated Soils", ASTM STP 361, pp 226-249.

Kenney, T.C. (1963), "Stability of Cuts in Soft Soils", ASCE PROC., Vol. 89. No. SM5, pp 17-37.

Kirkpatrick, W.M. (1957), "The Condition of Failure For Sands", PROC. 4th ICSMFE, Vol. I, pp 172-178.

Kjellman, W. (1936), "Report on an Apparatus for Consumate Investigation of the Mechanical Properties of Soils", PROC. 1st ICSMFE, Vol. II, pp 16-20.

Klausner, Y. (1960), discussion of Shear Strength of Saturated, Remolded Clays, ASCE RCSSCS, pp 1056-1062.

Ko, H.Y. (1966), "Static Stress - Deformation Characteristics of Sand", Ph.D. Thesis, Cal. Tech.

Ko, H.Y. and Scott, R.F. (1967a), "A New Soil Testing Apparatus", GEOTECHNIQUE, Vol. 17, No. 1, pp 40-57.

Ko, H.Y. and Scott, R.F. (1967b), "Deformations of Sand in Hydrostatic Compressions", ASCE PROC., Vol. 93, No. SM3, pp 137-156.

Ko, H.Y. and Scott, R.F. (1967c), "Deformation of Sand in Shear", ASCE PROC., Vol. 93, No. SM5, pp 283-310.

Ko, H.Y. and Scott, R.F. (1968), "Deformation of Sand at Failure", ASCE PROC., Vol 94, No. SM4, pp 883-898.

Kolbuszewski, J.J. (1948), "An Experimental Study of the Maximum and Minimum Porosity of Sands", PROC. 2nd ICSMFE FE, Vol. I, pp 158-165.

Lackland AFB (1968), "Investigations for Building Foundations in Expansive Clays", Vol. I, conducted for Directorate of Civil Engineering, Hq. USAF by U.S. Army Engineer District, Fort Worth.

Ladanyi, B. (1960), "Etude des Relations entre les Contraines et les Deformations lors du Cisaillement des Sols Pulverulents", Extrait des ANNALES DES TRAVAUX PUBLICS DE BELGIQUE, No. 3.

Ladanyi, B. (1967), discussion of "Plane Strain Tests on a Saturated Remolded Clay", by D.J. Henkel and N.H. Wade, ASCE PROC., Vol. 93, No. SM5, pp 322-325.

Ladd, C.C. (1964), "Stress - Strain Modulus of Clay in Undrained Shear", ASCE PROC., Vol. 90, No. SM5, pp 103-132.

Ladd, C.C. and Lambe, T.W. (1963), "The Strength of Undisturbed Clay Determined From Undrained Tests", ASTM STP 361, pp 342-371.

Ladd, C.C. and Varallyay, J. (1965), "The Influence of Stress System on the Behavior of Saturated Clays During Undrained Shear", MIT DEPT. OF CIV. ENGR. RESEARCH REPORT R65-11, SOILS PUBLICATION NO. 177.

Lambe, T.W. (1951), SOIL TESTING FOR ENGINEERS, Wiley.

Lambe, T.W. (1953), "The Structure of Inorganic Soil", ASCE PROC., Vol. 79, Proc. Separate No. 315.

Lambe, T.W. (1963), "Pore Pressures in a Foundation Clay", ASCE TRANS., Vol. 128, Part I, pp 865-896.

Lambe, T.W. (1964), "Methods of Estimating Settlement", ASCE PROC., Vol. 90, No. SM5, pp 43-67.

Lambe, T.W. (1967), "Stress Path Method" ASCE PROC., Vol. 93, No. SM6, pp 309-331; closure Vol. 95, No. SM5, (1969), pp 1265-1266.

Lambe, T.W. and Whitman, R.V. (1969), SOIL MECHANICS, Wiley.

Lane, K.S. (1963), discussion of "Experience With Canadian Varved Clays", by V. Milligan, L.G. Soderman and A. Rutka, ASCE PROC., Vol. 89, No. SM3, pp 147-156.

Legget, R.F. (1958), "Soil Engineering at Steep Rock Iron Mines", PROC. INST. CIV. ENG., Vol. 11, pp 169-188.

Legget. R.F. and Bartley, M.W. (1953), "An Engineering Study of Glacial Deposits at Steep Rock Lake Ontario", ECONOMIC GEOLOGY, Vol. 48, pp 513-540.

Lenoe, E.M. (1966), "Deformation and Failure of Granular Media Under Three-Dimensional Stress", EXPERIMENTAL MECHANICS, Vol. 6, No. 2, pp 99-104.

Leussink, H. and Wittke, W. (1963), "Difference in Triaxial and Plain (sic) Strain Shear Strength", ASTM STP 361, pp 77-89.

Liam Finn, W.D. (1963), "The Effect of Lateral Restraint on the Stability of Cohesionless Material", PROC., ASSOC. OF ASPHALT PAVING TECHNOLOGISTS, Vol. 32, pp 475-490.

Liam Finn, W.D. and Mittal, H.K. (1963), "Shear Strength of a Soil in a General Stress Field", ASTM STP 361, pp 42-51.

Livneh, M. and Shklarsky, E. (1964), "Equations of Failure Stresses in Materials With Anisotropic Strength Parameters", HRB RECORD NO. 74, pp 44-54.

Lo, K.Y. (1965a), "Stability of Slopes in Anisotropic Soils", ASCE PROC., Vol. 92, No. SM4, pp 85-106; closure, Vol. 92, No. SM4, (1966), pp 77-82.

Lo, K.Y. (1965b), discussion of Effect of the Rotation of the Principal Stress Axes and of the Intermediate Principal Stress on the Shear Strength of a Remoulded Clay, PROC. 6th ICSMFE, Vol. III, pp 323-325.

Lo, K.Y. and Milligan, V. (1967), "Shear Strength Properties of Two Stratified Clays", ASCE PROC., Vol. 93, No. SM1, pp 1-15.

Lomize, G.M. and Kryzhanovsky, A.L. (1967), "On the Strength of Sand", PROC. OSLO GEOT. CONF., Vol. 1, pp 215-219.

Malyshev, M.V. (1967a), "A Generalization of the Mohr-Coulomb Strength Criterion for Soils", PROC. OSLO GEOT. CONF., Vol. 1, pp 221-224.

Malyshev, M.V. (1967b), written contribution to Session 3, Shear Strength of Soil Other Than Clay, PROC. OSLO GEOT. CONF., Vol. 2, pp 219-220.

Malyshev, M.V. and Fralis, A.D. (1968), "Conditions of Stability of Sand Soil", PROC. 3rd BUDAPEST CONF. ON SOIL MECH.

Marston, F.A. (1932), discussion of "The Structure of Clay and Its Importance in Foundation Engineering", by A. Casagrande, J. BSCE,; reprinted in CONTRIBUTIONS TO SOIL MECHANICS 1925-1940, pp 114-116.

Martin, R.T. (1962), "Research on the Physical Properties of Marine Soils", MIT DEPT. OF CIV. ENGR. RESEARCH REPORT R62-42, SOILS PUBLICATION NO. 127.

Mason, A.B. (1936), "Correlation of Surface Loading Tests With Unconfined Compression Tests for Cohesive Soils", PROC. 1st ICSMFE, Vol. II, pp 169-173.

Mason, A.B. (1939), "Influence of Anisotropic Properties of Clay Deposits on Settlements" D.Sc. Thesis, Harvard Univ.

Mason, A.B. (1940), "The Influence of Anisotropic Properties of Clay Sediments on Subsidence",PROC. CONF. ON SOIL MECH. AND ITS APPLICATION, Purdue Univ., pp 229-237.

Matthai, A.C. (1967), discussion of "Shear Strength Properties of Two Stratified Clays", by K.Y. Lo and V. Milligan, ASCE PROC., Vol. 93, No. SM6, pp 377-378.

Merkle, D.H. (1959), "The Safety of Civil Engineering Structures", M.S. Thesis, Cornell University.

Merkle, D.H. (1967), "The Load Settlement Time Behavior of a Rigid Circular Footing on Saturated Clay", unpublished report on project MODIAP at MIT.

Merkle, D.H. (1969), discussion of "Stress Path Method", by T.W. Lambe, ASCE PROC., Vol. 95, No. SM1, pp 383-385.

Merkle, J.G. (1966), "Studies of a Possible Yield Function for Graphite", pp 43-48 in the unclassified part of "Graphite Mechanics Program Progress Report No. 9", USAEC Report ORNL-CF-66-10-17.

Merkle, J.G. (1967), "An Engineering Approach to Multiaxial Plasticity", ORNL - 4138.

Merkle, J.G. (1968a), "Application of the Ellipsoidal Yield Function to Saturated Clay", unpublished notes at Oak Ridge National Laboratory.

Merkle, J.G. (1968b), "An Ellipsoidal Yield Function for Inelastic Nonmetallic Solids", unpublished notes at Oak Ridge National Laboratory.

Merkle, J.G. (1968c), private communication.

Merkle, J.G. (1970), "An Ellipsoidal Yield Function for Materials That Can Both Dilate and Compact Inelastically", NUCLEAR ENGINEERING AND DESIGN, Vol. 12, pp 425-451.

Mesdary, M.S. and Sutherland, H.B. (1970), Correspondence on "A Note on the Drained Strength of Sand Under Generalized Strain Conditions", by G.E. Green and A.W. Bishop, GEOTECHNIQUE, Vol. 20, No. 2, pp 210-212.

Meyerhof, G.C. (1965), discussion of "Stability of Slopes in Anisotropic Soils", by K.Y. Lo, ASCE PROC., Vol. 91, No. SM6, p 132.

Milligan, V., Soderman, L.Y. and Rutka, A. (1962), "Experience With Canadian Varved Clays", ASCE PROC., Vol. 88, No. SM4, pp 31-67.

Nadai, A. (1933), "Theories of Strength", ASME TRANS., JAM, Vol. 1, pp 111-129.

Nadai, A. (1950), THEORY OF FLOW AND FRACTURE OF SOLIDS, McGraw-Hill.

Newmark, N.M. (1960), "Failure Hypotheses for Soils", ASCE RCSSCS, pp 17-32.

Novozhilov, V.V. (1952), "O fixicheskom smisle invariantov napryazheniya, ispol' zuyemikh v teoriy plastichnosti" (On the Physical Significance of the Invariants of Stress Used in the Theory of Plasticity), JAMM, Vol. 16, pp 617-619; translated by C.A. Berg at MIT.

Obert, L. and Duvall, W.J (1967), ROCK MECHANICS AND THE DESIGN OF STRUCTURES IN ROCK, Wiley.

Osterberg, J.O. (1948), General Discussion, ASTM STP 79, pp 128-139.

Parkin, A.K. (1965), "On the Strength of Packed Spheres", JOURN. AUSTRALIAN MATH. SOC., Vol. 5, pp 443-452.

Parry, R.H.G. (1956), "Strength and Deformation of Clay", Ph.D. Thesis, Univ. of London.

Parry, R.H.G. (1960), "Triaxial Compression and Extension Tests on Remolded Saturated Clay", GEOTECHNIQUE, Vol. 10, No. 4, pp 166-180.

Peltier, M.R. (1957), "Recherches experimentale sur la courbe intrinseque de rupture des sols pulverulents", PROC. 4th ICSMFE, Vol. I, pp 179-182; translated by H.H. Einstein at MIT.

Perez-LaSalvia, H., Luscher, U., Alverez-Stelling, J. and Gicot, O. (1966), "Load-Settlement-Time Behavior of Footings on Clay-Final Report", MIT DEPT. OF CIVIL ENG. RESEARCH REPORT R66-27, SOILS PUBLICATION NO. 193.

Plant, J.R. (1955), "Shear Strength Properties of London Clay", MSc Thesis, Univ of London.

Procter, D.C. and Barden, L. (1969), Correspondence on "A Note on the Drained Strength of Sand Under Generalized Strain Conditions", by G.E. Green and A.W. Bishop, GEOTECHNIQUE, Vol. 19, No. 3, pp 424-426.

Ratnam, M.V. (1962), "A Study of the Effect of Anisotropic Consolidation on the Relationships Between Shear Strength, Water Content and Effective Stresses of a Kaolinite Clay", Ph.D. Thesis, Cornell Univ.

Rendulic, L. (1936a), "Relation Between Void Ratio and Effective Principal Stresses for a Remolded Silty Clay", PROC. 1st ICSMFE, Vol. 3, pp 48-51.

Rendulic, L. (1936b), "Porenziffer und Porenwasserdruck in Tonen", (Void Ratio and Pore Water Pressure in Clay), DER BAUINGENIEUR, Vol. 17, No. 51/52, pp 559-564; translated by D.H. Merkle and U. Luscher.

Rendulic, L. (1937), "Ein Grundgesetz der Tonmechanik und sein experimenteller Beweis", (A Fundamental Law of the Mechanics of Clay and its Experimental Proof), DER BAUINGERIEUR, Vol. 18, pp 459-467; translated by J. Varallyay at MIT.

Rennie, B.C. (1959), "On the Strength of Sand", JOURN. AUSTRALIAN MATH SOC., Vol. 1, pp 71-79.

Richart, F.E., Brandtzaeg, A. and Brown, R.L. (1928), "A Study of the Failure of Concrete Under Combined Compressive Stresses", BULL. NO. 185, Univ. of Ill. Eng. Exp. Sta.

Rixner, J.J. (1967), "The Influence of Plane Strain Conditions on the Strength Behavior of a Saturated Clay", M.S. Thesis, MIT.

Roscoe, K.H. (1969), "Some Soil Mechanics Concepts and the Possibility of Their Wider Application", Paper No. 81, INTL. CONF. ON STRUCTURE, SOLID MECHANICS AND ENGINEERING DESIGN, Southampton Univ., 27 pp.

Roscoe, K.H., Schofield, A.N. and Thurairajah, A. (1963), "An Evaluation of Test Data for Selecting a Yield Criterion for Soils", ASTM STP 361, pp 111-133.

Roscoe, K.H., Schofield, A.N. and Wroth, C.P. (1958), "On the Yielding of Soils", GEOTECHNIQUE, Vol. 8, No. 1, pp 22-53; correspondence Vol. 9, No. 2, (1959), pp 71-83.

Rowe, P.W. (1962), "The Stress-Dilatancy Relation for Static Equilibrium of an Assembly of Particles in Contact", PROC. ROY. SOC. (London), Series A, Vol. 269, pp 500-527.

Rutledge, P.C. (1939), "Theories of Failure of Materials Applied to the Shearing Resistance of Soils", presented at SPEE Civil Engineering Division Conference on Soil Mechanics at State College, Pennysylvania; published in PROC. CONF. ON SOIL MECH. AND ITS APPLICATION, Purdue Univ., (1940), pp 191-204.

Saada, A.S. (1962), "A Rheological Analysis of Shear and Consolidation of Saturated Clays", HRB BULL 342, pp 52-89.

Saada, A.S. (1967), "Stress-Controlled Apparatus for Tri-axial Testing", ASCE PROC., Vol. 93, No. SM6, pp 61-78.

Saada, A.S. and Baah, A.K. (1966), "Deformation and Failure of a Cross Anisotropic Clay Under Combined Stresses", Soil Mech. Lab., Case Inst. of Tech., Cleveland, Ohio.

Schmertmann, J.H. (1964), discussion of "Stability of Cuts in Soft Soils" by T.C. Kenny, ASCE PROC., Vol. 90, No. SM4, pp 183-189.

Schmertmann, J.H. (1966), discussion of "Stability of Slopes in Anisotropic Soils", by K.Y. Lo, ASCE PROC., Vol. 92, No. SM1, pp 203-207.

Schmid, W.E. (1960), discussion of "Failure Hypotheses for Soils" by N.M. Newmark, ASCE RCSSCS, pp 991-995.

Schmid, W.E., Klausner, Y. and Whitmore, C.F. (1960), "Reheological Shear and Consolidation Behavior of Clay Soils", Progress Report to the Office of Naval Research, Princeton University.

Scott, R.F. (1963), PRINCIPLES OF SOIL MECHANICS, Addison - Wesley.

Scott, R.F. and Ko, H.Y. (1969), "Stress-Deformation and Strength Characteristics", PROC. 7th ICSMFE, State of the Art Volume, pp 1-47.

Seed, H.B., Woodward, R.J. and Lundgren, R. (1964), "Clay Mineralogical Aspects of the Atterberg Limits", ASCE PROC., Vol. 90, No. SM4, pp 107-131.

Shibata, T. and Karube, D. (1965), "Influence of the Variation of the Intermediate Principal Stress on the Mechanical Properties of Normally Consolidated Clay", PROC. 6th ICSMFE, Vol. I, pp 359-363.

Shibata, T. and Karube, D. (1967), discussion of "Plane Strain Tests on a Saturated Remolded Clay", by D.J. Henkel and N.H. Wade, ASCE PROC., Vol. 93. No. SM5, pp 325-327.

Skempton, A.W. (1948), "The Effective Stresses in Saturated Clays Strained at Constant Volume", PROC. VII Int. Cong. of Applied Mechanics, Vol. 1, pp 378-392.

Skempton, A.W. (1951), "The Bearing Capacity of Clays", PROC. BRITISH BUILDING RESEARCH CONGRESS, Vol. I, pp 180-189.

Skempton, A.W. (1960a), "Terzaghi's Discovery of Effective Stress", in FROM THEORY TO PRACTICE IN SOIL MECHANICS, edited by L. Bjerrum, A. Casagrande, R.B. Peck and A.W. Skempton, Wiley, pp 42-53.

Skempton, A.W. (1960b), correspondence on "The Pore-Pressure Coefficients in Saturated Soils", GEOTECHNIQUE, Vol. 10, No. 4, pp 186-187.

Skempton, A.W. (1961), "Horizontal Stresses in an Over-consolidated Eocene Clay", PROC. 5th ICSMFE, Vol. I, pp 351-357.

Skempton, A.W. (1964), "Long - Term Stability of Clay Slopes", Fourth Rankine Lecture, GEOTECHNIQUE, Vol. 14, No. 2, pp 75-102.

Skempton, A.W. and Henkel, D.J. (1957), "Tests on London Clay From Deep Borings at Paddington, Victoria and the South Bank", PROC. 4th ICSMFE, Vol. I, pp 100-106.

Skempton, A.W. and Hutchinson, J. (1969), "Stability of Natural Slopes and Embankment Foundations", PROC. 7th ICSMFE, State of the Art Volume, pp 291-340.

Skempton, A.W. and Sowa, V.A. (1963), "The Behavior of Saturated Clays During Sampling and Testing", GEOTECHNIQUE, Vol. 13, No. 4, pp 269-290.

Soveri, U. and Hyyppa, J.M.I. (1959), RAKENNUSINSINOORI, (Helsinki, Finland).

Soveri, U. and Hyyppa, J.M.I. (1967), discussion of "Shear Strength Properties of Two Stratified Clays" by K.Y. Lo and V. Milligan, ASCE PROC., Vol. 93, No. SM5, pp 347-349.

Sowa, V.A. (1963), "A Comparison of the Effects of Isotropic and Anisotropic Consolidation on the Shear Behavior of a Clay", Ph.D. Thesis, Univ. of London.

Sowers, G.F. (1962), "Shallow Foundations", Chapter 6 in FOUNDATION ENGINEERING, edited by G.A. Leonards, McGraw-Hill.

Sowers, G.F. (1963), "Strength Testing of Soils", ASTM STP 361, pp 3-21.

Sutherland, H.B. and Mesdary, M.S. (1969), "The Influence of the Intermediate Principal Stress on the Strength of Sand", PROC. 7th ICSMFE, Vol. I, pp 391-399.

Taylor, D.W. (1948), FUNDAMENTALS OF SOIL MECHANICS, Wiley.

Teng, W.C. (1962), FOUNDATION DESIGN, Prentice-Hall.

Terzaghi, K. (1923), "Die Berechnung der Durchlassig - keitsziffer des Tones aus dem Verlauf der hydrodynamischen Spannungserscheinungen" (The Calculation of the Coefficient of Permeability of Clay From the Progress of Hydrodynamic Stress Phenomena); reprinted in FROM THEORY TO PRACTICE IN SOIL MECHANICS, edited by L. Bjerrum, A. Casagrande, R.B. Peck and A.W. Skempton, Wiley, (1960), pp 133-146.

Terzaghi, K. (1925), "Structure and Volume of Voids of Soils", pp 10-13 in ERDBAUMECHANIK AUF BODENPHYSIKALISHER GRUNDLAGE, translated by A. Casagrande in FROM THEORY TO PRACTICE IN SOIL MECHANICS, Wiley, (1960), pp 146-148.

Terzaghi, K. (1927), "Principles of Final Soil Classification", PUBLIC ROADS, Vol. 8, No. 3, pp 41-53.

Terzaghi, K. (1943), "Liner Plate Tunnels on the Chicago (Ill) Subway", ASCE TRANS., Vol. 108, pp 970-1097.

Terzaghi, K. (1944), "Ends and Means in Soil Mechanics", JOURNAL OF THE ENGINEERING INSTITUTE OF CANADA, Vol. 27, No. 12, pp 608-615.

Terzaghi, K. and Peck, P.B. (1967), SOIL MECHANICS IN ENGINEERING PRACTICE, 2nd edition, Wiley.

Thurston, C.W. and Deresiewicz, H. (1959), "Analysis of a Compression Test of a Model of a Granular Medium", ASME TRANS., JAM, Vol. 81, pp 251-258.

Timoshienko, S.P. and Gere, J.M. (1961), THEORY OF ELASTIC STABILITY, 2nd edition, Engineering Societies Monograph, McGraw-Hill.

Topping, A.D. (1955), "The Use of Experimental Constants in the Application of Theories of Strength to Rock", PROC. 2nd MIDWEST CONF. ON SOLID MECH., pp 178-192.

Trask, P.D. and Rolston, J.W. (1951), "Engineering Geology of the San Francisco Bay, California", GEOL. SOC. AM. BULLETIN, Vol. 62, pp 1078-1109.

Tschebotarioff, G.P. (1943), discussion of "Liner Plate Tunnels on the Chicago (Ill) Subway" by K. Terzaghi, ASCE TRANS., Vol. 108, pp 1075-1078.

Tschebotarioff, G.P. (1951), SOIL MECHANICS, FOUNDATIONS AND EARTH STRUCTURES, McGraw-Hill.

Tschebotarioff, G.P. and Bayliss, J.R. (1948), "The Determination of the Shearing Strength of Varved Clays and of Their Sensitivity to Remolding", PROC. 2nd ICSMFE, Vol. I, pp 203-207.

Uff, J.F. and Nash, J.K.T.L. (1967), "Anisotropy of Shale Due to Folding", PROC., OSLO GEOT. CONF., Vol. I, pp 301-303.

von Karman, T. (1911), "Festigkeitsversuche unter allseitigem Druck", ZEITSCRIFT DES VEREINS DEUTSCHER INGENIEURE, Vol. 55, pp 1749-1757.

Wade, N.H. (1963), "Plane Strain Failure Characteristics of a Saturated Clay", Ph.D. Thesis, Univ. of London.

Ward, W.H. (1957), discussion of Techniques of Field Measurement and Sampling, PROC., 4th ICSMFE, Vol. III, pp 123-124.

Ward, W.H., Marsland, A. and Samuels, S.G. (1965), "Properties of the London Clay at the Ashford Common Shaft; in-situ and Undrained Strength Tests", GEOTECHNIQUE, Vol. 15, No. 4, pp 321-344.

Ward, W.H., Samuels, S.G. and Butler, M.E. (1959), "Further Studies of the Properties of London Clay", GEOTECHNIQUE, Vol. 9, No. 2, pp 33-58.

Westerberg, N. (1921), "Jordtryck i Kohesionara jordarter", TEK. TIDSKR., Vol. 51, pp 25-29.

Westergaard, H.M. (1924), "Einfache Ableitung dar von Mohr gegebenen graphischen Darstellung des dreiachsigen Spannungszustandes", (A Simple Derivation of Mohr's Description of a Triaxial State of Stress), ZAMM, Vol. 4, pp 520-521; translated by D.H. Merkle.

Westergaard, H.M. (1952), THEORY OF ELASTICITY AND PLASTICITY, Harvard University Press (Dover reprint 1964).

Williams, A. (1958), "Oblique-slip Faults and Rotated Stress Systems", GEOL. MAG, Vol. 95, pp 207-218.

Williams, M.L. (1964), "Structural Analysis of Viscoelastic Materials", AIAA JOURN., Vol. 2, No. 5, pp 785-807.

Winter, G. (1961), "Properties of Steel and Concrete and the Behavior of Structures", ASCE TRANS., Vol. 126, Part II, pp 1054-1100.

Wood, C.C. (1958), "Shear Strength and Volume Change Characteristics of Compacted Soil Under Conditions of Plane Strain", Ph.D. Thesis, Univ. of London.

Wu, T.H. Loh, A.K. and Malvern, L.E. (1963), "Study of Failure Envelope of Soils", ASCE PROC., Vol. 89, No. SM1, pp 145-181.

Yong, R.N. and Warkentin, B.P. (1966), INTRODUCTION TO SOIL BEHAVIOR, Macmillan.

APPENDIX A

EXCESS PORE PRESSURE RESPONSE IN AN ISOTROPIC SOIL

If $\Delta\epsilon_1$, $\Delta\epsilon_2$ and $\Delta\epsilon_3$ are the principal strain increments at a point in an isotropic soil mass, caused by applied total stress increments $\Delta\sigma_1$, $\Delta\sigma_2$, $\Delta\sigma_3$, then the coefficients s_0, s_1, and s_2 in the equations

$$\begin{aligned}
\Delta\epsilon_1 &= s_0\,\Delta\bar{\sigma} + s_1\,\Delta\sigma_1' + s_2(\Delta\sigma_1')^2 \\
\Delta\epsilon_2 &= s_0\,\Delta\bar{\sigma} + s_1\,\Delta\sigma_2' + s_2(\Delta\sigma_2')^2 \\
\Delta\epsilon_3 &= s_0\,\Delta\bar{\sigma} + s_1\,\Delta\sigma_3' + s_2(\Delta\sigma_3')^2
\end{aligned} \qquad \text{(A.1)}$$

where

$$\begin{aligned}
\Delta\sigma_1' &= \Delta\sigma_1 - \Delta\sigma \\
\Delta\sigma_2' &= \Delta\sigma_2 - \Delta\sigma \\
\Delta\sigma_3' &= \Delta\sigma_3 - \Delta\sigma
\end{aligned} \qquad \text{(A.2)}$$

$$\Delta\sigma = \frac{\Delta\sigma_1 + \Delta\sigma_2 + \Delta\sigma_3}{3} \tag{A.3}$$

$$\Delta\bar{\sigma} = \Delta\sigma - \Delta u \tag{A.4}$$

can always be found, because the determinant

$$\begin{vmatrix} 1 & \Delta\sigma_1' & (\Delta\sigma_1')^2 \\ 1 & \Delta\sigma_2' & (\Delta\sigma_2')^2 \\ 1 & \Delta\sigma_3' & (\Delta\sigma_3')^2 \end{vmatrix}$$

is Vandermonde's determinant, which is zero if and only if the applied principal total stress increments are not all distinct.

When two of the applied total stress increments are equal, the corresponding principal strain increments in an isotropic soil will also be equal, and no inconsistency will arise in Equations (A.1). It will then be convenient to set the coefficient s_1 equal to zero, and obtain unique values for s_0 and s_2. Similarly, when all three applied total stress increments are equal, the three principal strain increments in an isotropic soil will also all be equal, and again no inconsistency will arise in Equations

(A.1). In this case, the deviator terms in Equation (A.1) will all be identically zero, so that a unique value of s_0 can be obtained.

When the soil is anisotropic, the same principal strain increments will not be equal under the above conditions, so that inconsistencies will arise in Equations (A.1) and no solutions will be possible. Hence, Equations (A.1) are appropriate only for an isotropic material. The coefficients s_0, s_1 and s_2 will therefore depend only on stress and strain invariants, and thus will be independent of the orientation of the applied principal total stress increments.

If Equations (A.1) are written for the case of undrained loading of a saturated isotropic clay, for which the volume change is zero, then summing the three equations yields

$$\Delta\epsilon_1 + \Delta\epsilon_2 + \Delta\epsilon_3 = 0 = 3\, s_0 (\Delta\sigma - \Delta u)$$

$$+ s_2 \left[(\Delta\sigma_1')^2 + (\Delta\sigma_2')^2 + (\Delta\sigma_3')^2 \right]$$

and therefore to the condition

$$\Delta u = \frac{\Delta\sigma_1 + \Delta\sigma_2 + \Delta\sigma_3}{3} + \frac{a}{9}\left[(\Delta\sigma_1 - \Delta\sigma_2)^2 + (\Delta\sigma_2 - \Delta\sigma_3)^2 + (\Delta\sigma_3 - \Delta\sigma_1)^2\right] \quad \text{(A.5)}$$

where

$$a = \frac{s_2}{s_0} \quad \text{(A.6)}$$

and because

$$(\Delta\sigma_1')^2 + (\Delta\sigma_2')^2 + (\Delta\sigma_3')^2 = \frac{1}{3}\left[(\Delta\sigma_1 - \Delta\sigma_2)^2 + (\Delta\sigma_2 - \Delta\sigma_3)^2 + (\Delta\sigma_3 - \Delta\sigma_1)^2\right] \quad \text{(A.7)}$$

Of course, the numerical values of the coefficients s_0, s_1 and s_2 are dependent upon the actual stress - strain relationship of the clay, the determination of which is beyond the scope of this thesis. It is the form of Equation (A.7) which is important here.

APPENDIX B

ANALYSIS OF STRESS IN SOIL

Purpose

In Chapter 1 it is predicted that there will be an increasing demand for the results of soil stress - strain tests to be cast in general form; in Chapter 3 the three-dimensional Mohr stress circle is used; and in Chapter 6 various soil failure criteria are examined, using devices such as two-dimensional plots in principal stress space. The purpose of this appendix is to present a thorough development of the concepts and equations employed in the analysis of stress, adapted for Soil Mechanics from Continuum Mechanics, Rheology and Plasticity, so that they may be conveniently referred to throughout the thesis.

Stress Transformation Equations

First, consider plane ABC of tetrahedron OABC in Figure B.1, having the outward unit normal vector

$$\bar{n} = \alpha_{n1}\bar{e}_1 + \alpha_{n2}\bar{e}_2 + \alpha_{n3}\bar{e}_3 \qquad (B.1)$$

Line OP is the shortest line from the coordinate origin to plane ABC, and is therefore normal to the plane, so that the normal unit vector $\bar{n}$ can be drawn along OP. Let the distance OP be h, and let the coordinates of any other point, R, which also lies in plane ABC be (x_1, x_2, x_3). Then since the line OP is normal to the plane, the projection of OR on $\bar{n}$ must be of magnitude h, i.e.

$$\bar{n} \cdot \overline{OR} = h \qquad (B.2)$$

or

$$\alpha_{n1}x_1 + \alpha_{n2}x_2 + \alpha_{n3}x_3 = \alpha_{ni}x_i = h \qquad (B.3)$$

Equation (B.3) is the equation of a plane in rectangular Cartesian coordinates, and it follows that

$$\begin{aligned} |\overline{OA}| &= A = \frac{h}{\alpha_{n1}} \\ |\overline{OB}| &= B = \frac{h}{\alpha_{n2}} \\ |\overline{OC}| &= C = \frac{h}{\alpha_{n3}} \end{aligned} \qquad (B.4)$$

Because the area of a cross section of a pyramid, taken parallel to the base, is proportional to the square of the perpendicular distance from the cross section to the appex, the volume of a pyramid is given by the well known formula

$$\text{volume} = \frac{\text{height}}{3} \times \text{base area}$$

Therefore, the volume of the tetrahedron OABC can be expressed in any of four ways:

$$V = \frac{h}{3} (\text{area ABC})$$

$$= \frac{A}{3} (\text{area BOC}) = \frac{B}{3} (\text{area AOC}) = \frac{C}{3} (\text{area AOB})$$

from which it follows that

$$\begin{aligned} \frac{\text{area BOC}}{\text{area ABC}} &= \frac{h}{A} = \alpha_{n1} \\ \frac{\text{area AOC}}{\text{area ABC}} &= \frac{h}{B} = \alpha_{n2} \\ \frac{\text{area AOB}}{\text{area ABC}} &= \frac{h}{C} = \alpha_{n3} \end{aligned} \qquad \text{(B.5)}$$

Consider now the stresses exerted BY the tetrahedron ON the surrounding material, shown in Figure B.2. The stress vectors $\bar{\sigma}_n$, $-\bar{\sigma}_1$, $-\bar{\sigma}_2$ and $-\bar{\sigma}_3$ are equal to the resultant forces exerted across faces ABC, BOC, AOC and AOB, respectively, divided by the area of the face on which they act. In the limit, as the dimensions of the tetrahedron approach zero, the stress vectors each represent a uniformly distributed force per unit area. Equilibrium considerations dictate that the vector sum of all forces acting on the tetrahedron be zero. Body forces, such as gravity and inertia, need not be included in the vector equilibrium equation for an infinitesimal tetrahedron, since their magnitudes are proportional to h^3, whereas the magnitudes of surface forces are proportional to h^2. The body forces therefore approach zero more rapidly than do the surface forces, as the tetrahedron dimensions approach zero. Therefore the following development is as applicable to problems of wave propagation as it is to the static problems considered in this thesis. The vector equilibrium equation for the infinitesimal tetrahedron is

$$-\bar{\sigma}_n(\text{area ABC}) + \bar{\sigma}_1(\text{area BOC}) + \bar{\sigma}_2(\text{area AOC})$$

$$+ \bar{\sigma}_3(\text{area AOB}) = 0$$

Dividing both sides of the above equation by (area ABC) yields

$$\bar{\sigma}_n = \alpha_{n1}\bar{\sigma}_1 + \alpha_{n2}\bar{\sigma}_2 + \alpha_{n3}\bar{\sigma}_3 = \alpha_{ni}\bar{\sigma}_i \tag{B.6}$$

Equation (B.6) is commonly referred to as Cauchy's equation.

Each of the stress vectors in Figure B.2 can be written in component form, and in particular,

$$\bar{\sigma}_1 = \sigma_{11}\bar{e}_1 + \sigma_{12}\bar{e}_2 + \sigma_{13}\bar{e}_3 = \sigma_{1j}\bar{e}_j$$

$$\bar{\sigma}_2 = \sigma_{21}\bar{e}_1 + \sigma_{22}\bar{e}_2 + \sigma_{23}\bar{e}_3 = \sigma_{2j}\bar{e}_j$$

$$\bar{\sigma}_3 = \sigma_{31}\bar{e}_1 + \sigma_{32}\bar{e}_2 + \sigma_{33}\bar{e}_3 = \sigma_{3j}\bar{e}_j$$

The above expressions can all be represented concisely by the single expression

$$\bar{\sigma}_i = \sigma_{ij}\bar{e}_j \tag{B.7}$$

which, when substituted into the concise form of Equation (B.6) yields

$$\bar{\sigma}_n = \alpha_{ni}\sigma_{ij}\bar{e}_j \tag{B.8}$$

or, in matrix form

$$\lfloor \sigma_n \rfloor = \{\alpha_n\}^T \underline{\sigma} \tag{B.9}$$

Since Equations (B.8) and (B.9) give the components of the stress row vector, $\bar{\sigma}_n$, the component of $\bar{\sigma}_n$ in the direction of the unit vector $\bar{m}$ in Figure B.2 must be

$$\sigma_{nm} = \bar{\sigma}_n \cdot \bar{m} = \{\alpha_n\}^T \underline{\sigma} \{\alpha_m\} \tag{B.10}$$

From Equation (B.10) it follows that the normal component of $\bar{\sigma}_n$, denoted σ_{nn}, is simply

$$\sigma_{nn} = \bar{\sigma}_n \cdot \bar{n} = \{\alpha_n\}^T \underline{\sigma} \{\alpha_n\} \tag{B.11}$$

Principal Stresses

It is of interest to investigate the change in σ_{nn} due to an infinitesimal change in $\bar{n}$. Figure B.3 shows

that, since $\bar{n}$ must remain a unit vector, it can only change direction, so that

$$d\bar{n} = d\lambda \bar{t} \tag{B.12}$$

where

$$\bar{t} \cdot \bar{n} = 0 \tag{B.13}$$

Equations (B.12) and (B.13) merely state that an infinitesimal change in the unit vector $\bar{n}$ must lie in a direction normal to $\bar{n}$. The increment in σ_{nn} due to $d\bar{n}$ can therefore be obtained from Equation (B.11) in the form

$$d\sigma_{nn} = \{d\alpha_n\}^T \underline{\sigma} \{\alpha_n\} + \{\alpha_n\}^T \underline{\sigma} \{d\alpha_n\}$$

$$= \{\alpha_n\}^T (\underline{\sigma} + \underline{\sigma}^T) \{d\alpha_n\} = d\lambda \{\alpha_n\}^T (\underline{\sigma} + \underline{\sigma}^T) \{\alpha_t\}$$

(B.14)

However, in view of the fact that there are assumed to be no distributed torques, the stress matrix is symmetric, so that

$$\underline{\sigma}^T = \underline{\sigma} \tag{B.15}$$

and therefore, by virtue of Equations (B.15) and (B.10), Equation (B.14) reduces to

$$d\sigma_{nn} = 2d\lambda \left\{\alpha_n\right\}^T \underline{\sigma} \left\{\alpha_t\right\} = 2d\lambda\sigma_{nt} \tag{B.16}$$

where σ_{nt} is the shearing component of $\bar{\sigma}_n$ in the direction of $\bar{t}$. From Equation (B.16) it can be immediately deduced that <u>stationary values of normal stress occur on planes of zero shear</u>. Therefore, to locate stationary values of normal stress, one seeks those directions for which the stress vector $\bar{\sigma}_n$ has no component normal to $\bar{n}$, and therefore for which

$$\bar{\sigma}_n = \sigma\, \bar{n} \tag{B.17}$$

Using Equation (B.9), Equation (B.17) can be written in matrix form as

$$\left\lfloor \sigma_n \right\rfloor = \left\{\alpha_n\right\}^T \underline{\sigma} = \sigma \left\{\alpha_n\right\}^T$$

or, transposing the above expression and using Equation (B.15),

$$\underline{\sigma}^T \left\{\alpha_n\right\} = \underline{\sigma} \left\{\alpha_n\right\} = \sigma \left\{\alpha_n\right\} \tag{B.18}$$

An even more convenient form is

$$(\underline{\sigma} - \sigma \underline{I}) \{\alpha_n\} = \{0\} \tag{B.19}$$

The expanded form of Equation (B.19) is

$$\begin{bmatrix} \sigma_{11} - \sigma & \sigma_{12} & \sigma_{13} \\ \sigma_{21} & \sigma_{22} - \sigma & \sigma_{23} \\ \sigma_{31} & \sigma_{32} & \sigma_{33} - \sigma \end{bmatrix} \begin{Bmatrix} \alpha_{n1} \\ \alpha_{n2} \\ \alpha_{n3} \end{Bmatrix} = \begin{Bmatrix} 0 \\ 0 \\ 0 \end{Bmatrix} \tag{B.20}$$

and since Equations (B.20) are a set of homogeneous linear equations, they possess a unique solution if and only if the determinant of the coefficient matrix, in this case referred to as the characteristic determinant, is zero. The equation expressing this condition is the characteristic equation

$$\begin{vmatrix} \sigma_{11} - \sigma & \sigma_{12} & \sigma_{13} \\ \sigma_{21} & \sigma_{22} - \sigma & \sigma_{23} \\ \sigma_{31} & \sigma_{32} & \sigma_{33} - \sigma \end{vmatrix} = 0 \tag{B.21}$$

Expansion of Equation (B.21) yields

$$(\sigma_{11} - \sigma)(\sigma_{22} - \sigma)(\sigma_{33} - \sigma) + \sigma_{12}\sigma_{23}\sigma_{31} + \sigma_{13}\sigma_{21}\sigma_{32}$$

$$- (\sigma_{11} - \sigma)\sigma_{23}\sigma_{32} - \sigma_{12}\sigma_{21}(\sigma_{33} - \sigma) - \sigma_{13}(\sigma_{22} - \sigma)\sigma_{31}$$

$$= -\sigma^3 + (\sigma_{11} + \sigma_{22} + \sigma_{33})\sigma^2 - \left(\begin{vmatrix} \sigma_{11} & \sigma_{12} \\ \sigma_{21} & \sigma_{22} \end{vmatrix} + \begin{vmatrix} \sigma_{22} & \sigma_{23} \\ \sigma_{32} & \sigma_{33} \end{vmatrix} \right.$$

$$\left. + \begin{vmatrix} \sigma_{33} & \sigma_{31} \\ \sigma_{13} & \sigma_{11} \end{vmatrix} \right) \sigma + \begin{vmatrix} \sigma_{11} & \sigma_{12} & \sigma_{13} \\ \sigma_{21} & \sigma_{22} & \sigma_{23} \\ \sigma_{31} & \sigma_{32} & \sigma_{33} \end{vmatrix} = 0$$

or

$$\sigma^3 - I_1\sigma^2 - I_2\sigma - I_3 = 0 \qquad \text{(B.22)}$$

where the stress invariants, I_1, I_2, I_3 are defined as follows:

$$I_1 = \sigma_{11} + \sigma_{22} + \sigma_{33} \qquad \text{(B.23)}$$

$$I_2 = -\left(\begin{vmatrix} \sigma_{11} & \sigma_{12} \\ \sigma_{21} & \sigma_{22} \end{vmatrix} + \begin{vmatrix} \sigma_{22} & \sigma_{23} \\ \sigma_{32} & \sigma_{33} \end{vmatrix} + \begin{vmatrix} \sigma_{33} & \sigma_{31} \\ \sigma_{13} & \sigma_{11} \end{vmatrix} \right) \tag{B.24}$$

$$I_3 = \begin{vmatrix} \sigma_{11} & \sigma_{12} & \sigma_{13} \\ \sigma_{21} & \sigma_{22} & \sigma_{23} \\ \sigma_{31} & \sigma_{32} & \sigma_{33} \end{vmatrix} \tag{B.25}$$

Equation (B.22) is a cubic equation, and therefore has three roots; COURANT AND ROBBINS (1941, 269). It can therefore be written

$$(\sigma - \sigma_1)(\sigma - \sigma_2)(\sigma - \sigma_3) = 0 \tag{B.26}$$

or

$$\sigma^3 - (\sigma_1 + \sigma_2 + \sigma_3)\sigma^2 + (\sigma_1\sigma_2 + \sigma_2\sigma_3 + \sigma_3\sigma_1)\sigma - \sigma_1\sigma_2\sigma_3 = 0 \tag{B.27}$$

and therefore

$$I_1 = \sigma_1 + \sigma_2 + \sigma_3 \tag{B.28}$$

$$I_2 = -(\sigma_1\sigma_2 + \sigma_2\sigma_3 + \sigma_3\sigma_1) \tag{B.29}$$

$$I_3 = \sigma_1\sigma_2\sigma_3 \tag{B.30}$$

Now

$$(\sigma_1 + \sigma_2 + \sigma_3)^2 = \sigma_1^2 + \sigma_2^2 + \sigma_3^2 + 2(\sigma_1\sigma_2 + \sigma_2\sigma_3 + \sigma_3\sigma_1)$$

and

$$(\sigma_1 - \sigma_2)^2 + (\sigma_2 - \sigma_3)^2 + (\sigma_3 - \sigma_1)^2 =$$

$$2(\sigma_1^2 + \sigma_2^2 + \sigma_3^2) - 2(\sigma_1\sigma_2 + \sigma_2\sigma_3 + \sigma_3\sigma_1)$$

and therefore

$$\begin{aligned} I_2 &= -(\sigma_1\sigma_2 + \sigma_2\sigma_3 + \sigma_3\sigma_1) \\ &= \frac{1}{2}\left[(\sigma_1^2 + \sigma_2^2 + \sigma_3^2) - (I_1)^2\right] \\ &= \frac{1}{6}\left\{\left[(\sigma_1 - \sigma_2)^2 + (\sigma_2 - \sigma_3)^2 + (\sigma_3 - \sigma_1)^2\right] - 2(I_1)^2\right\} \end{aligned} \tag{B.31}$$

Since $\underline{\sigma}$ is real and symmetric, the roots of Equation (B.22) are assured of being all real; HILDERBRAND (1952, 31). It is therefore convenient to define the deviatoric stress matrix, $\underline{s}$ by the expressions

$$\underline{\sigma} = \underline{s} + \frac{I_1}{3}\underline{I} \tag{B.32}$$

$$\sigma = s + \frac{I_1}{3} \tag{B.33}$$

Equation (B.19) then becomes

$$\left[\left(\underline{s} + \frac{I_1}{3}\underline{I}\right) - \left(s + \frac{I_1}{3}\right)\underline{I}\right]\{\alpha_n\} = \{0\}$$

or simply

$$(\underline{s} - s\,\underline{I})\,\{\alpha_n\} = \{0\} \tag{B.34}$$

The invariants of the deviatoric stress tensor are

$$J_1 = s_{11} + s_{22} + s_{33} = s_1 + s_2 + s_3 = 0 \tag{B.35}$$

$$J_2 = -\left(\begin{vmatrix} s_{11} & s_{12} \\ s_{21} & s_{22} \end{vmatrix} + \begin{vmatrix} s_{22} & s_{23} \\ s_{32} & s_{33} \end{vmatrix} + \begin{vmatrix} s_{33} & s_{31} \\ s_{13} & s_{11} \end{vmatrix}\right)$$

$$= -(s_1 s_2 + s_2 s_3 + s_3 s_1)$$

$$= \frac{s_1^2 + s_2^2 + s_3^2}{2}$$

$$= \frac{1}{6}\left[(s_1 - s_2)^2 + (s_2 - s_3)^2 + (s_3 - s_1)^2\right]$$

$$= \frac{1}{6}\left[(\sigma_1 - \sigma_2)^2 + (\sigma_2 - \sigma_3)^2 + (\sigma_3 - \sigma_1)^2\right] \qquad \text{(B.36)}$$

$$J_3 = \begin{vmatrix} s_{11} & s_{12} & s_{13} \\ s_{21} & s_{22} & s_{23} \\ s_{31} & s_{32} & s_{33} \end{vmatrix} = s_1 s_2 s_3 \qquad \text{(B.37)}$$

and therefore Equation (B.22) reduces to

$$s^3 - J_2 s - J_3 = 0 \qquad \text{(B.38)}$$

The s^2 term is absent from Equation (B.38) because J_1 is zero, and Equation (B.38) is therefore referred to as the reduced characteristic or reduced cubic equation; DICKSON (1922, 45).

The solution to Equation (B.38) begins by assuming that

$$s = z + \frac{J_2}{3z} \qquad \text{(B.39)}$$

which means that

$$z^2 - sz + \frac{J_2}{3} = 0 \qquad \text{(B.40)}$$

Equation (B.40) implies that s is the sum of two values of z, the product of which is $\frac{J_2}{3}$. Substitution of Equation (B.39) into Equation (B.38) yields a quadratic equation for z^3:

$$s^3 - J_2 s - J_3$$

$$= \left(z^3 + J_2 z + \frac{J_2^2}{3z} + \frac{J_2^3}{27z^3}\right) - J_2 \left(z + \frac{J_2}{3z}\right) - J_3$$

$$= z^3 + \left(\frac{J_2}{3}\right)^3 \frac{1}{z^3} - J_3 = 0$$

or

$$(z^3)^2 - J_3 z^3 + \left(\frac{J_2}{3}\right)^3 = 0 \qquad \text{(B.41)}$$

The solution to Equation (B.41) is

$$z^3 = \frac{J_3}{2} \pm \sqrt{\left(\frac{J_3}{2}\right)^2 - \left(\frac{J_2}{3}\right)^3} \qquad \text{(B.42)}$$

The question immediately arises whether the quantity under the radical is positive or negative, which can be answered by evaluating the ratio

$$\frac{\frac{J_3}{2}}{\left(\frac{J_2}{3}\right)^{3/2}}$$

Since the roots of Equation (B.22), and therefore of Equation (B.38) are known to be real, it can be assumed that

$$s_1 \geq s_2 \geq s_3$$

so that if

$$\frac{s_1 + s_3}{2} = r \tag{B.43a}$$

$$\frac{s_1 - s_3}{2} = q \tag{B.43b}$$

and

$$\mu = \frac{s_2 - r}{q} = \frac{s_2 - \frac{s_1 + s_3}{2}}{\frac{s_1 - s_3}{2}} \tag{B.44}$$

then $s_1 = r + q$

$s_2 = r + \mu q$

$s_3 = r - q$

In addition, Equation (B.35) requires that

$$s_1 + s_2 + s_3 = 3r + \mu q = 0$$

so that the deviator stress parameters r and q are related by the expression

$$r = -\frac{\mu}{3} q$$

and therefore the principal deviator stresses can all be expressed in terms of the parameters μ and q as follows:

$$s_1 = (1 - \frac{\mu}{3}) q$$

$$s_2 = \frac{2\mu}{3} q \qquad \text{(B.45)}$$

$$s_3 = -(1 + \frac{\mu}{3}) q$$

Substitution of Equations (B.45) into the ratio in question reduces it it a function of μ only, as follows.

$$\frac{J_3}{2} = -\frac{\mu}{3}\left(1 - \frac{\mu^2}{9}\right)q^3 = -\frac{\mu(9 - \mu^2)}{27}\, q^3$$

$$\frac{J_2}{3} = \frac{q^2}{18}\left[(1 - \mu)^2 + (1 + \mu)^2 + 4\right] = \frac{3 + \mu^2}{9}\, q^2$$

$$\frac{\frac{J_3}{2}}{\left(\frac{J_2}{3}\right)^{3/2}} = -\frac{\mu(3 + \mu)(3 - \mu)}{(3 + \mu^2)^{3/2}} \qquad \text{(B.46)}$$

According to Equation (B.44) the parameter μ varies between -1 (when $s_2 = s_3$) and +1 (when $s_2 = s_1$). The ratio in Equation (B.46) therefore also varies between +1 and -1, as can be verified by direct calculation, and therefore the radicand in Equation (B.42) is nonpositive. This being the case, the roots of Equation (B.41) are complex, and can therefore be represented by an Argand diagram as shown in Figure B.4(a).

The two complex roots of Equation (B.41) shown in Figure (B.4a) are

$$z^3 = \frac{J_3}{2} \pm i \sqrt{\left(\frac{J_2}{3}\right)^3 - \left(\frac{J_3}{2}\right)^2}$$

$$= \left(\frac{J_2}{3}\right)^{3/2} e^{\pm i3\omega}$$

where

$$\cos 3\omega = \frac{\frac{J_3}{2}}{\left(\frac{J_2}{3}\right)^{3/2}} = -\frac{\mu(3+\mu)(3-\mu)}{(3+\mu^2)^{3/2}} \qquad \text{(B.48)}$$

Equation (B.48) is plotted in Figure (B.4b)

The desired values of z are therefore

$$z = \sqrt{\frac{J_2}{3}}\, e^{\pm i\omega_j} \quad (j = 1,2,3)$$

where

$$\omega_1 = \omega - \frac{2\pi}{3}$$

$$\omega_2 = \omega \qquad \text{(B.49)}$$

$$\omega_3 = \omega + \frac{2\pi}{3}$$

$$\omega = \frac{1}{3} \cos^{-1} \frac{\frac{J_3}{2}}{\left(\frac{J_2}{3}\right)^{3/2}} \qquad \text{(B.50)}$$

and the three roots of s are the sums of complex conjugate pairs of z values.

$$s_j = \sqrt{\frac{J_2}{3}} \left(e^{i\omega_j} + e^{-i\omega_j}\right) = 2\sqrt{\frac{J_2}{3}} \cos \omega_j \quad (j = 1,2,3)$$

Therefore, if we let

$$\tau_{OCT}^2 = \frac{2J_2}{3} = \frac{1}{9} \left[(s_1 - s_2)^2 + (s_2 - s_3)^2 + (s_3 - s_1)^2\right] \qquad \text{(B.51)}$$

then the roots of Equation (B.38) are

$$s_j = \sqrt{2}\, \tau_{OCT} \cos \omega_j \quad (j = 1,2,3) \qquad \text{(B.52)}$$

The geometrical and physical significance of τ_{OCT} will be explored later.

In order to calculate the principal stresses, σ_1, σ_2 and σ_3 when the stresses

$$\underline{\sigma} = \begin{bmatrix} \sigma_{11} & \sigma_{12} & \sigma_{13} \\ \sigma_{21} & \sigma_{22} & \sigma_{23} \\ \sigma_{31} & \sigma_{32} & \sigma_{33} \end{bmatrix}$$

are given one does the following:

1. Calculate I_1 from Equation (B.23).
2. Calculate the deviatoric stresses from Equation (B.32).
3. Calculate J_2 from Equation (B.36).
4. Calculate τ_{OCT} from Equation (B.51).
5. Calculate J_3 from Equation (B.37).
6. Calculate ω_2 from Equation (B.50).
7. Calculate ω_1 and $_3$ from Equations (B.49).
8. Calculate s_1, s_2, and s_3 from Equations (B.52).
9. Calculate σ_1, σ_2 and σ_3 from Equation (B.32).

Principal Stress Directions

Once the principal stresses have been calculated, the direction cosines associated with each can be obtained from three separate solutions of Equation (B.20), in which σ is successively set equal to σ_1, σ_2 and σ_3. In each

solution, at least one of the equations will be redundant, so that a corresponding number of the direction cosines will be arbitrary. The directions thus obtained are those of the principal stress axes. They are mutually orthogonal, because the matrix $\underline{\sigma}$ is symmetric, which means that planes of zero shear stress must occur at right angles to one another.* Thus, if

$$\underline{\alpha} = \left[\{\alpha_1\} \,\vdots\, \{\alpha_2\} \,\vdots\, \{\alpha_3\} \right] \tag{B.53}$$

where $\{\alpha_1\}$, $\{\alpha_2\}$ and $\{\alpha_3\}$ are the three principal directions, then

$$\underline{\alpha}^T \underline{\alpha} = \underline{I} \tag{B.54}$$

Cayley - Hamilton Theorem

Using Equation (B.53), Equation (B.18) can now be written

$$\underline{\sigma}\ \underline{\alpha} = \underline{\alpha}\ \underline{\Sigma} \tag{B.55}$$

---

*A mathematical proof is also easily performed; HILDERBRAND (1952; 31).

where

$$\underline{\Sigma} = \begin{bmatrix} \sigma_1 & 0 & 0 \\ 0 & \sigma_2 & 0 \\ 0 & 0 & \sigma_3 \end{bmatrix} \tag{B.56}$$

and therefore, by virtue of Equation (B.54)

$$\underline{\alpha}^T \, \underline{\sigma} \, \underline{\alpha} = \underline{\Sigma} \tag{B.57}$$

$$\underline{\alpha} \, \underline{\Sigma} \, \underline{\alpha}^T = \underline{\sigma} \tag{B.58}$$

It is a simple matter to generalize Equations (B.57) and (B.58) for higher powers of $\underline{\sigma}$ and $\underline{\Sigma}$. For example,

$$\underline{\alpha} \, \underline{\Sigma}^2 \, \underline{\alpha}^T = (\underline{\alpha} \, \underline{\Sigma} \, \underline{\alpha}^T)(\underline{\alpha} \, \underline{\Sigma} \, \underline{\alpha}^T) = \underline{\sigma}^2$$

and so forth.

If Equation (B.22) is written for each of the principal stresses, σ_1, σ_2 and σ_3 and the result put in matrix form, the result is

$$\underline{\Sigma}^3 - I_1 \, \underline{\Sigma}^2 - I_2 \, \underline{\Sigma} - I_3 \, \underline{I} = \underline{0} \tag{B.59}$$

Premultiplication by $\underline{\alpha}$ and postmultiplication by $\underline{\alpha}^T$ then yields

$$\underline{\sigma}^3 - I_1 \underline{\sigma}^2 - I_2 \underline{\sigma} - I_3 \underline{I} = 0 \qquad \text{(B.60)}$$

Equation (B.60) states that the stress matrix satisfies its own characteristic equation, and is a particular form of the Cayley - Hamilton theorem. A similar equation holds for the deviatoric stress matrix, $\underline{s}$.

$$\underline{s}^3 - J_2 \underline{s} - J_3 \underline{I} = 0 \qquad \text{(B.61)}$$

and since

$$\mathrm{Tr}(\underline{s}) = s_1 + s_2 + s_3 = 0$$

it follows that

$$J_3 = \frac{1}{3} \mathrm{Tr}(\underline{s}^3) = \frac{s_1^3 + s_2^3 + s_3^3}{3} \qquad \text{(B.62)}$$

The following expressions for the stress invariants are of interest.

$$\frac{I_1}{3} = \frac{\sigma_1 + \sigma_2 + \sigma_3}{3}$$

$$\tau_{OCT}^2 = \frac{s_1^2 + s_2^2 + s_3^2}{3} \qquad \text{(B.63)}$$

$$J_3 = \frac{s_1^3 + s_2^3 + s_3^3}{3}$$

Simplification of Stress Analysis by Using Principal Stress Axes as Coordinate Axes

One of the many reasons for investigating the directions of the principal stress axes is that many of the previous expressions, as well as further analyses, are considerably simplified if the coordinate axes at a point coincide in direction with the principal stress axes. For example, when this is the case,

$$\underline{\sigma} = \underline{\Sigma} = \begin{bmatrix} \sigma_1 & 0 & 0 \\ 0 & \sigma_2 & 0 \\ 0 & 0 & \sigma_3 \end{bmatrix} \qquad \text{(B.64)}$$

It is particularly convenient to work only with the principal stresses when a material has isotropic stress - strain

properties, because then the directions of the principal axes have no influence on stress - strain behavior.

Stress Dyadic

Cauchy's equation (B.6) originally suggested the treatment of stress as a dyadic; WESTERGAARD (1952, 56).

$$\bar{\bar{\sigma}} = \sigma_{ij}\, \bar{e}_i\, \bar{e}_j \qquad \text{(B.65)}$$

The dyadic $\bar{\bar{\sigma}}$ is an entity, the component of which in any direction is a vector, in the same way that a vector is an entity, the component of which in any direction is a scalar. A dyadic is, of course, a tensor of order 2, since a tensor of order n is an entity, the component of which in any direction is a tensor of order n - 1.

Equation (B.6) can thus be written

$$\bar{\sigma}_n = \bar{n} \cdot \bar{\bar{\sigma}} \qquad \text{(B.66)}$$

and Equation (B.10) as

$$\sigma_{mn} = \bar{m} \cdot \bar{n} \cdot \bar{\bar{\sigma}} \qquad \text{(B.67)}$$

When the coordinate axes coincide with the principal stress axes, Equation (B.65) reduces to

$$\bar{\bar{\sigma}} = \sigma_1 \bar{e}_1 \bar{e}_1 + \sigma_2 \bar{e}_2 \bar{e}_2 + \sigma_3 \bar{e}_3 \bar{e}_3 \qquad \text{(B.68)}$$

so that

$$\bar{\sigma}_n = \bar{n} \cdot \bar{\bar{\sigma}}$$

$$= \sigma_1 \alpha_{n1} \bar{e}_1 + \sigma_2 \alpha_{n2} \bar{e}_2 + \sigma_3 \alpha_{n3} \bar{e}_3$$

(B.69)

and

$$\sigma_{nm} = \bar{m} \cdot \bar{\sigma}_n$$

$$= \sigma_1 \alpha_{n1} \alpha_{m1} + \sigma_2 \alpha_{n2} \alpha_{m2} + \sigma_3 \alpha_{n3} \alpha_{m3}$$

(B.70)

Stresses on an Octahedral Plane

In particular, when

$$\bar{m} = \bar{n} = \bar{n}_{OCT} = \frac{1}{\sqrt{3}} (\bar{e}_1 + \bar{e}_2 + \bar{e}_3) \qquad \text{(B.71)}$$

so that the plane under consideration is an octahedral plane, making equal angles with each of the principal stress axes, then Equation (B.70) yields

$$\sigma_{nn} = \sigma_{OCT} = \frac{\sigma_1 + \sigma_2 + \sigma_3}{3} = \frac{I_1}{3} \tag{B.72}$$

whereas Equation (B.69) yields

$$\bar{\sigma}_{OCT} = \frac{1}{\sqrt{3}} \left(\sigma_1 \bar{e}_1 + \sigma_2 \bar{e}_2 + \sigma_3 \bar{e}_3\right) \tag{B.73}$$

The stress vector $\bar{\sigma}_{OCT}$ can be resolved into components normal and parallel to the octahedral plane, by writing

$$\bar{\sigma}_{OCT} = \sigma_{OCT} \bar{n}_{OCT} + \bar{\tau}_{OCT} \tag{B.74}$$

so that the octahedral shear stress is

$$\bar{\tau}_{OCT} = \bar{\sigma}_{OCT} - \sigma_{OCT} \bar{n}_{OCT}$$

$$= \frac{1}{\sqrt{3}} \left[\left(\sigma_1 - \frac{I_1}{3}\right) \bar{e}_1 + \left(\sigma_2 - \frac{I_1}{3}\right) \bar{e}_2 + \left(\sigma_3 - \frac{I_1}{3}\right) \bar{e}_3\right]$$

$$= \frac{1}{\sqrt{3}} \left(s_1 \bar{e}_1 + s_2 \bar{e}_2 + s_3 \bar{e}_3\right) \tag{B.75}$$

and therefore the magnitude of the octahedral shear stress is given by

$$\tau_{OCT}^2 = \bar{\tau}_{OCT} \cdot \bar{\tau}_{OCT} = \frac{s_1^2 + s_2^2 + s_3^2}{3} \qquad (B.76)$$

which is identical to the second of Equations (B.63)

The stress vector acting on the octahedral plane whose normal unit vector is given by Equation (B.71) thus has projections $\left(\frac{\sigma_1}{\sqrt{3}}, \frac{\sigma_2}{\sqrt{3}}, \frac{\sigma_3}{\sqrt{3}}\right)$ along the principal stress axes, and can be resolved into components normal and parallel to the octahedral plane, of magnitude σ_{OCT} and τ_{OCT} respectively. The shear component, $\bar{\tau}_{OCT}$, has projections $\left(\frac{s_1}{\sqrt{3}} \quad \frac{s_2}{\sqrt{3}} \quad \frac{s_3}{\sqrt{3}}\right)$ along the principal stress axes.

Octahedral Plane Stress Plot

The form of Equation (B.73) suggests that the vector

$$\bar{\sigma} = \sqrt{3}\, \bar{\sigma}_{OCT} = \sigma_1 \bar{e}_1 + \sigma_2 \bar{e}_2 + \sigma_3 \bar{e}_3 \qquad (B.77)$$

be plotted in principal stress space, as shown in Figure (B.5). The vector $\bar{\sigma}$ can be expressed as

$$\bar{\sigma} = \frac{I_1}{\sqrt{3}} \bar{n}_{OCT} + \bar{\tau} \tag{B.78}$$

where

$$\frac{I_1}{\sqrt{3}} \bar{n}_{OCT} = \frac{I_1}{3} (\bar{e}_1 + \bar{e}_2 + \bar{e}_3) \tag{B.79}$$

$$\bar{\tau} = \sqrt{3}\, \bar{\tau}_{OCT} = s_1 \bar{e}_1 + s_2 \bar{e}_2 + s_3 \bar{e}_3 \tag{B.80}$$

The deviator stress vector, $\bar{\tau}$, lies in a plane normal to $\bar{n}_{OCT}$, i.e. in an octahedral plane, and when viewed by looking in along the $-\bar{n}_{OCT}$ direction, appears as shown in Figure B.6. It is convenient to establish rectangular Cartesian coordinates XYZ, with the origin 0' at the tail of the $\bar{\tau}$ vector, the Z axis pointing in the $\bar{n}_{OCT}$ direction, and the X and Y axes lying in the octahedral plane containing $\bar{\tau}$. The unit vector $\bar{e}_z$ is obviously equal to $\bar{n}_{OCT}$.

$$\bar{e}_z = \frac{1}{\sqrt{3}} \bar{e}_1 + \frac{1}{\sqrt{3}} \bar{e}_2 + \frac{1}{\sqrt{3}} \bar{e}_3 \tag{B.81}$$

The direction cosines of $\bar{e}_x$ are determined from the conditions

$$
\begin{aligned}
\bar{e}_x \cdot \bar{n}_{OCT} &= 0 \\
\bar{e}_x \cdot \bar{e}_2 &= 0 \\
\bar{e}_x \cdot \bar{e}_1 &> 0 \\
\bar{e}_x \cdot \bar{e}_x &= 1
\end{aligned}
\tag{B.82}
$$

which, by inspection, indicates that

$$
\bar{e}_x = \frac{1}{\sqrt{2}}\,\bar{e}_1 - \frac{1}{\sqrt{2}}\,\bar{e}_3 \tag{B.83}
$$

The direction cosines of $\bar{e}_y$ are easily determined by the condition that the XYZ system be right handed, so that

$$
\bar{e}_y = \bar{e}_z \times \bar{e}_x = \frac{1}{\sqrt{6}} \begin{vmatrix} \bar{e}_1 & \bar{e}_2 & \bar{e}_3 \\ 1 & 1 & 1 \\ 1 & 0 & -1 \end{vmatrix}
$$

$$
-\frac{1}{\sqrt{6}}\,\bar{e}_1 + \frac{2}{\sqrt{6}}\,\bar{e}_2 - \frac{1}{\sqrt{6}}\,\bar{e}_3 \tag{B.84}
$$

The coordinates (X,Y) are therefore

$$x = \bar{\tau} \cdot \bar{e}_x = \frac{s_1 - s_3}{\sqrt{2}}$$

$$y = \bar{\tau} \cdot \bar{e}_y = \frac{2s_2 - s_1 - s_3}{\sqrt{6}} \qquad \text{(B.85)}$$

In view of Equation (B.35), Equation (B.85) can be written

$$y = \sqrt{3}\, \tau_{OCT} \cos \omega_2 = \frac{3}{\sqrt{6}}\, s_2 = \sqrt{\frac{3}{2}}\, s_2$$

which yields again the second of Equations (B.52),

$$s_2 = \sqrt{2}\, \tau_{OCT} \cos \omega_2$$

The angle ω_2, in Figure B.7 is therefore the same angle used to solve the reduced characteristic equation; c.f. Equation (B.41). In addition,

$$\cot \omega_2 = \frac{2s_2 - s_1 - s_3}{\sqrt{3}\,(s_1 - s_3)} = \frac{s_2 - \left(\frac{s_1 + s_3}{2}\right)}{\sqrt{3}\left(\frac{s_1 - s_3}{2}\right)} = \frac{\mu}{\sqrt{3}} \qquad \text{(B.86)}$$

The octahedral shear stress, τ_{OCT}, controls the length of the vector $\bar{\tau}$ in an octhahedral plane stress plot, and the ratio μ controls its orientation. Thus the relationship between the angle ω_2, Lode's parameter μ, and the invariants τ_{OCT} and J_3 is made clear.

As a consequence of the above results, the projections of $\bar{\tau}$ along the projected axes 1 and 3 in Figure B.6 are seen to be $\sqrt{\frac{3}{2}}\, s_1$ and $\sqrt{\frac{3}{2}}\, s_3$, respectively, so that Figure B.6 is a graphical representation of Equations B.52. The interior of the triangle ABC represents that portion of the octahedral plane for which all three principal stresses are positive (compressive). Reference to Figure B.1 shows that point B represents the point $(0, \sigma_2, 0)$, so that at B

$$\sigma_2 = 3\sigma_{OCT}$$
$$s_2 = 2\sigma_{OCT}$$

and therefore in Figure B.6,

$$0'B = \sqrt{\frac{3}{2}}\ (2\sigma_{OCT}) = \sqrt{6}\ \sigma_{OCT}$$

$$= 0'A = 0'C$$

Figure B.6 is the basis for the construction of octahedral plane stress plots in Chapter 6.

Physical Interpretation of the Octahedral Invariants τ_{OCT} and ψ_2

Before concluding this appendix with a discussion of Mohr's representation of a traixial state of stress, a physical interpretation will be given to the parameters τ_{OCT} and ω_2, similar to a suggestion made by NOVOZHILOV (1952).

Although it is not necessary to have the condition

$$s_1 \geq s_2 \geq s_3$$

be satisfied in plotting the stress point in Figure B.6, if it is satisfied, the projection of $\bar{\tau}$ on the X axis will be $\frac{s_1 - s_3}{\sqrt{2}} = \sqrt{2}\,\tau_{MAX}$. Lode's parameter μ thus controls the ratio τ_{MAX}/τ_{OCT}, or vice versa, through the relation

$$\frac{\tau_{MAX}}{\tau_{OCT}} = \sqrt{\frac{3}{2}}\,\sin\omega_2 = \frac{3}{\sqrt{2(3+\mu^2)}}$$

which has already been used in Equation (B.48).

Equation (B.69) gives an expression for the stress vector, $\bar{\sigma}_n$, acting on a plane with unit normal $\bar{n}$.

$$\bar{\sigma}_n = \alpha_{n1}\,\sigma_1\,\bar{e}_1 + \alpha_{n2}\,\sigma_2\,\bar{e}_2 + \alpha_{n3}\,\sigma_3\,\bar{e}_3 \qquad \text{(B.69)}$$

The tangential component of $\bar{\sigma}_n$ has the same magnitude as the vector

$$\bar{\sigma}_n \times \bar{n} = \begin{vmatrix} \bar{e}_1 & \bar{e}_2 & \bar{e}_3 \\ \alpha_{n1}\,\sigma_1 & \alpha_{n2}\,\sigma_2 & \alpha_{n3}\,\sigma_3 \\ \alpha_{n1} & \alpha_{n2} & \alpha_{n3} \end{vmatrix}$$

$$= \alpha_{n2}\,\alpha_{n3}(\sigma_2 - \sigma_3)\bar{e}_1 + \alpha_{n3}\,\alpha_{n1}(\sigma_3 - \sigma_1)\bar{e}_2$$

$$+ \alpha_{n1}\,\alpha_{n2}(\sigma_1 - \sigma_2)\bar{e}_3$$

so that the square of the magnitude of the resultant shear stress is

$$\tau_n^2 = \alpha_{n1}^2\,\alpha_{n2}^2(\sigma_1 - \sigma_2)^2 + \alpha_{n2}^2\,\alpha_{n3}^2(\sigma_2 - \sigma_3)^2$$

$$+ \alpha_{n3}^2\,\alpha_{n1}^2(\sigma_3 - \sigma_1)^2 \qquad \text{(B.87)}$$

The above derivation of Equation (B.87) is considerably shorter than that resulting from a straightforward application of the Pythagorean theorem.

It can easily be demonstrated that

$$\int_S \alpha_{ni}^2 \, \alpha_{nj}^2 \, ds = \frac{1}{15} \quad (i \neq j)$$

where S is the surface of a unit sphere, so that the root mean square shear stress at a point, τ_{RMS}, is found from the equation

$$\tau_{RMS}^2 = \int_S \tau_n^2 \, ds$$

$$= \frac{1}{15} \left[(\sigma_1 - \sigma_2)^2 + (\sigma_2 - \sigma_3)^2 + (\sigma_3 - \sigma_1)^2 \right]$$

$$= \frac{3}{5} \tau_{OCT}^2 = \frac{1}{5} R^2 \qquad \text{(B.88)}$$

where R is the radius of the octahedral stress point in Figure B.6. The above result was obtained by NOVOZHILOV (1952) by another method.

As a matter of interest, if an attempt is made to calculate the components of the vector $\bar{\tau}_n$ from the formula

$$\bar{\tau}_n = \bar{n} \times \bar{\sigma}_n \times \bar{n}$$

one obtains the well known result

$$\bar{\tau}_n = (\bar{n} \cdot \bar{n})\bar{\sigma}_n - (\bar{\sigma}_n \cdot \bar{n})\bar{n}$$

$$= \bar{\sigma}_n - (\bar{\sigma}_n \cdot \bar{n})\bar{n}$$

by virtue of a mathematical identify. Thus, while the expression $\bar{\sigma}_n \times \bar{n}$ provides a quick means of evaluating the magnitude of the vector $\bar{\tau}_n$, it offers no real help in calculating the components of the shear stress vector itself.

Mohr's Representation of a Triaxial State of Stress

The most useful two-dimensional representation of a triaxial state of stress is that due to Mohr; WESTERGAARD (1924). The mathematical justification of the Mohr circle construction is based on interpreting the equations

$$\left.\begin{aligned} \alpha_{n1}^2 + \alpha_{n2}^2 + \alpha_{n3}^2 &= 1 \\ \sigma_1 \alpha_{n1}^2 + \sigma_2 \alpha_{n2}^2 + \sigma_3 \alpha_{n3}^2 &= \bar{\sigma}_n \cdot \bar{n} = \sigma_{nn} \\ \sigma_1^2 \alpha_{n1}^2 + \sigma_2^2 \alpha_{n2}^2 + \sigma_3^2 \alpha_{n3}^2 &= \bar{\sigma}_n \cdot \bar{\sigma}_n = \sigma_{nn}^2 + \tau_n^2 \end{aligned}\right\} \qquad (B.89)$$

as a set of simultaneous linear equations in the variables α_{n1}^2, α_{n2}^2, α_{n3}^2. The determinant of the matrix of coefficients is, again, Vandermonds's determinant, which appeared in Appendix A. Application of Cramer's rule to Equations (B.89) thus yields the following solutions:

$$\tau_n^2 + (\sigma_{nn} - \sigma_2)(\sigma_{nn} - \sigma_3) = \alpha_{n1}^2(\sigma_1 - \sigma_2)(\sigma_1 - \sigma_3) \quad \text{(B.90a)}$$

$$\tau_n^2 + (\sigma_{nn} - \sigma_1)(\sigma_{nn} - \sigma_3) = \alpha_{n2}^2(\sigma_2 - \sigma_1)(\sigma_2 - \sigma_3) \quad \text{(B.90b)}$$

$$\tau_n^2 + (\sigma_{nn} - \sigma_1)(\sigma_{nn} - \sigma_2) = \alpha_{n3}^2(\sigma_3 - \sigma_1)(\sigma_3 - \sigma_2) \quad \text{(B.90c)}$$

When one of the direction cosines is zero, the corresponding equation in (B.90) reduces to a particularly simple form:

$$\alpha_{n1} = 0 : \text{(B.90a)} \rightarrow \tau_n^2 + (\sigma_{nn} - \sigma_2)(\sigma_{nn} - \sigma_3) = 0 \quad \text{(B.91a)}$$

$$\alpha_{n2} = 0 : \text{(B.90b)} \rightarrow \tau_n^2 + (\sigma_{nn} - \sigma_1)(\sigma_{nn} - \sigma_3) = 0 \quad \text{(B.91b)}$$

$$\alpha_{n3} = 0 : \text{(B.90c)} \rightarrow \tau_n^2 + (\sigma_{nn} - \sigma_1)(\sigma_{nn} - \sigma_2) = 0 \quad \text{(B.91c)}$$

Each of Equations (B.91) describes a circle in Figure B.8b, with its center on the normal stress axis, as shown below:

Equation	Center	Radius*	Curve +
B.91a	$\frac{\sigma_2 + \sigma_3}{2}$	$\frac{\sigma_2 - \sigma_3}{2}$	B'C'
B.91b	$\frac{\sigma_1 + \sigma_3}{2}$	$\frac{\sigma_1 - \sigma_3}{2}$	C'A'
B.91c	$\frac{\sigma_1 + \sigma_2}{2}$	$\frac{\sigma_1 - \sigma_2}{2}$	A'B'

* Assuming that $\sigma_1 \geq \sigma_2 \geq \sigma_3$

\+ See Figure B.7

Referring to Figure B.8, the following mappings are thus effected, from the unit sphere to a two-dimensional plot:

Curve on Unit Sphere	Mohr Mapping
AB	A'B'
BC	B'C
CA	C'A

Point D' in Figure B.8b, which corresponds to Point D in Figure B.8a, is located from the conditions

$$\alpha_{n1} = 0$$
$$\alpha_{n2} = \cos \Phi$$
$$\alpha_{n3} = \sin \Phi$$

Under these conditions, the second of Equations (B.89) reduces to the familiar form

$$\sigma_{nn} = \sigma_2 \cos^2 \Phi + \sigma_3 \sin^2 \Phi$$

$$= \left(\frac{\sigma_2 + \sigma_3}{2}\right) + \left(\frac{\sigma_2 - \sigma_3}{2}\right) \cos 2\Phi$$

which justifies locating Point D' as shown. Points E', F' and G' are located in a similar fashion.

Point P' in Figure B.8b, which corresponds to Point P in Figure B.8a, can be located by noticing that Point P lies at the intersection of arc DE, for which $\alpha_{n3} = \sin \Phi =$ constant, and arc FG, for which $\alpha_{n1} = \cos \theta =$ constant. Points D', E', F' and G' are assumed to have already been located, as described above. When $\alpha_{n3} = \sin \Phi =$ constant, Equation (B.90c) remains the equation of a circle, with center at $\frac{\sigma_1 + \sigma_2}{2}$ and radius such that the circle connects Point D' and E', as it must. Thus is arc D'E' located,

and similarly arc F'G' with its center at $\frac{\sigma_2 + \sigma_3}{2}$. Point P' is located at the intersection of arcs D'E' and F'G', and has coordinates (σ_{nn}, τ_n).

Since σ_{OCT} and τ_{OCT} are the normal and shear stresses acting on a plane whose normal makes equal angles with each of the principal axes, σ_{OCT} and τ_{OCT} can be found graphically by setting

$$\theta_{OCT} = \cos^{-1}\left(\frac{1}{\sqrt{3}}\right) = \cos^{-1}(0.5773503) = 54^{\circ}44'52''$$

$$\Phi_{OCT} = 35^{\circ}15'53''$$

Note that

$$\cos\theta_{OCT} = \sqrt{\frac{1}{3}}$$

$$\sin\theta_{OCT} = \sqrt{\frac{2}{3}}$$

so that

$$\sin 2\theta_{OCT} = 2\sin\theta_{OCT}\cos\theta_{OCT} = \frac{2\sqrt{2}}{3}$$

$$\cos 2\theta_{OCT} = 2\cos^2\theta_{OCT} - 1 = -\frac{1}{3}$$

Thus, when

$$\sigma_2 = \sigma_3$$

$$\left.\begin{aligned} \sigma_{OCT} &= p - \frac{1}{3} q \\ \tau_{OCT} &= \frac{2\sqrt{2}}{3} q \end{aligned}\right\} \qquad \text{(B.92)}$$

and when $\sigma_2 = \sigma_1$,

$$\left.\begin{aligned} \sigma_{OCT} &= p + \frac{1}{3} q \\ \tau_{OCT} &= \frac{2\sqrt{2}}{3} q \end{aligned}\right\} \qquad \text{(B.93)}$$

A typical construction for determining σ_{OCT} and τ_{OCT} graphically is shown in Figure B.9.

In applications dealing with cross anistropy, such as those considered in Chapter 3, it is more convenient to employ the spherical coordinates δ and ψ, shown in Figure B.10, than to use the coordinates δ and Φ shown in Figure B.8a. In this case, the three direction cosines are

$$\left.\begin{aligned} \alpha_{n1} &= \cos\delta \\ \alpha_{n2} &= \sin\delta \sin\psi \\ \alpha_{n3} &= \sin\delta \cos\psi \end{aligned}\right\} \qquad (B.94)$$

and therefore, the last two of Equations (B.89) assume the form

$$\sigma_{nn}^2 + \tau_n^2 = \sigma_1^2 \cos^2\delta + \sigma_2^2 \sin^2\delta \sin^2\psi + \sigma_3^2 \sin^2\delta \cos^2\psi$$

$$\sigma_{nn} = \sigma_1 \cos^2\delta + \sigma_2 \sin^2\delta \sin^2\psi + \sigma_3 \sin^2\delta \cos^2\psi$$

In view of the fact that the equation of a circle in (σ, τ) space, with its center on the σ axis, has the form

$$(\sigma^2 + \tau^2) - a\,\sigma = b$$

where $\frac{a}{2}$ is the location of the center of the circle (see Figure B.7), one is led to form the expression

$$(\sigma_{nn}^2 + \tau_n^2) - a\,\sigma_{nn} = \sigma_1(\sigma_1 - a)\cos^2\delta$$

$$+ \sigma_2(\sigma_2 - a)\sin^2 \delta \sin^2 \psi + \sigma_3(\sigma_3 - a)\sin^2 \delta \cos^2 \psi$$

$$= \cos^2 \delta \left[\sigma_1(\sigma_1 - a)\right] + \sin^2 \delta \left[\sigma_2(\sigma_2 - a) \sin^2 \psi\right.$$

$$\left. + \sigma_3(\sigma_3 - a)\cos^2 \psi\right] \qquad \text{(B.95)}$$

When the angle ψ is constant, the angle δ can be eliminated from Equation (B.95) by setting

$$\sigma_1(\sigma_1 - a) = \sigma_2(\sigma_2 - a)\sin^2 \psi + \sigma_3(\sigma_3 - a)\cos^2 \psi = b \qquad \text{(B.96)}$$

which will be satisfied, provided

$$a = \frac{\left(\frac{\sigma_2^2 + \sigma_3^2}{2}\right) - \left(\frac{\sigma_2^2 - \sigma_3^2}{2}\right) \cos 2\psi - \sigma_1^2}{\left(\frac{\sigma_2 + \sigma_3}{2}\right) - \left(\frac{\sigma_2 - \sigma_3}{2}\right) \cos 2\psi - \sigma_1} \qquad \text{(B.97)}$$

Thus, the relation between σ_{nn} and τ_n along a meridian of longitude in Figure B.10 is also circular, in the Mohr circle mapping.

When $\tau_n = 0$, $\delta = 0$, and Equation (B.95) reduces to

$$\sigma_{nn}(\sigma_{nn} - a) = \sigma_1(\sigma_1 - a)$$

so that

$$\sigma_{nn} = \sigma_1$$

When $\psi = 0^\circ$, Equation (B.97) reduces to

$$a = \frac{\sigma_3^2 - \sigma_1^2}{\sigma_3 - \sigma_1} = \sigma_1 + \sigma_3$$

and when $\psi = 90^\circ$, Equation (B.97) reduces to

$$a = \frac{\sigma_2^2 - \sigma_1^2}{\sigma_2 - \sigma_1} = \sigma_1 + \sigma_2$$

The center of the circular arc A'H' in Figure B.10b is at J', and is located as follows:

1. S_{12} and S_{13} are the centers of circles A'B' and A'C' respectively.
2. Draw a circle through S_{12} and S_{13}, with center on the normal stress axis.
3. With H' determined by ψ, draw line H'A', intersecting the circle S_{12} S_{13} at I'. The angle I'S_{12} S_{13} should be ψ.
4. Draw I'J' perpendicular to line H'A'. The center of the circular arc H'A' is at J'.

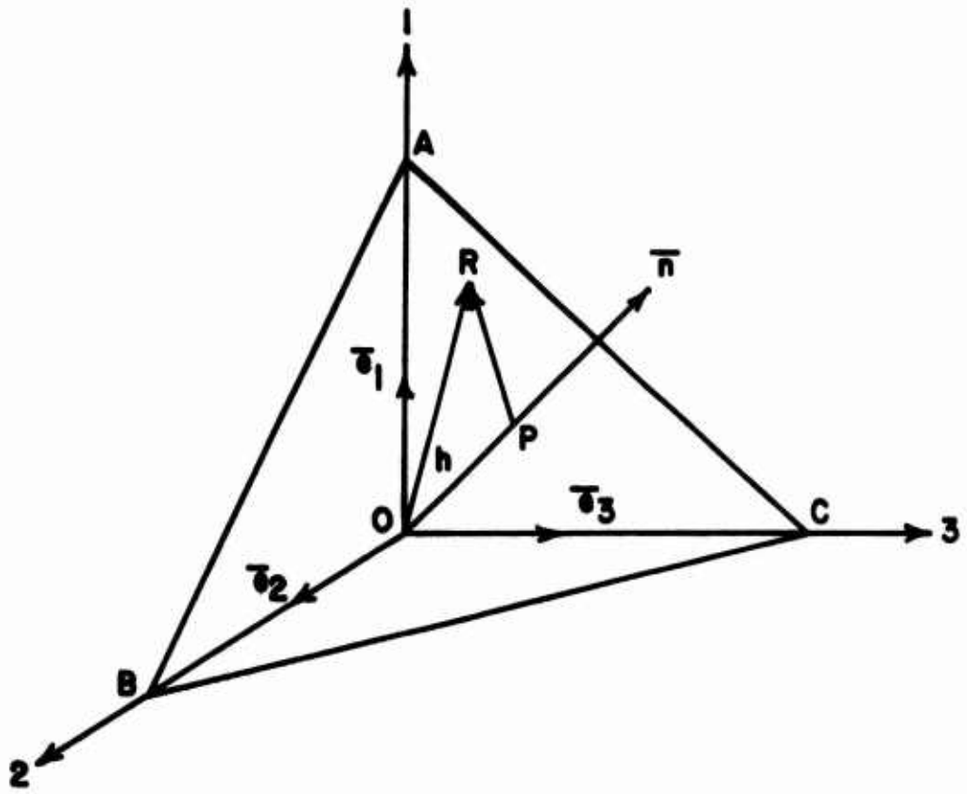

FIGURE B.1
TETRAHEDRON OABC

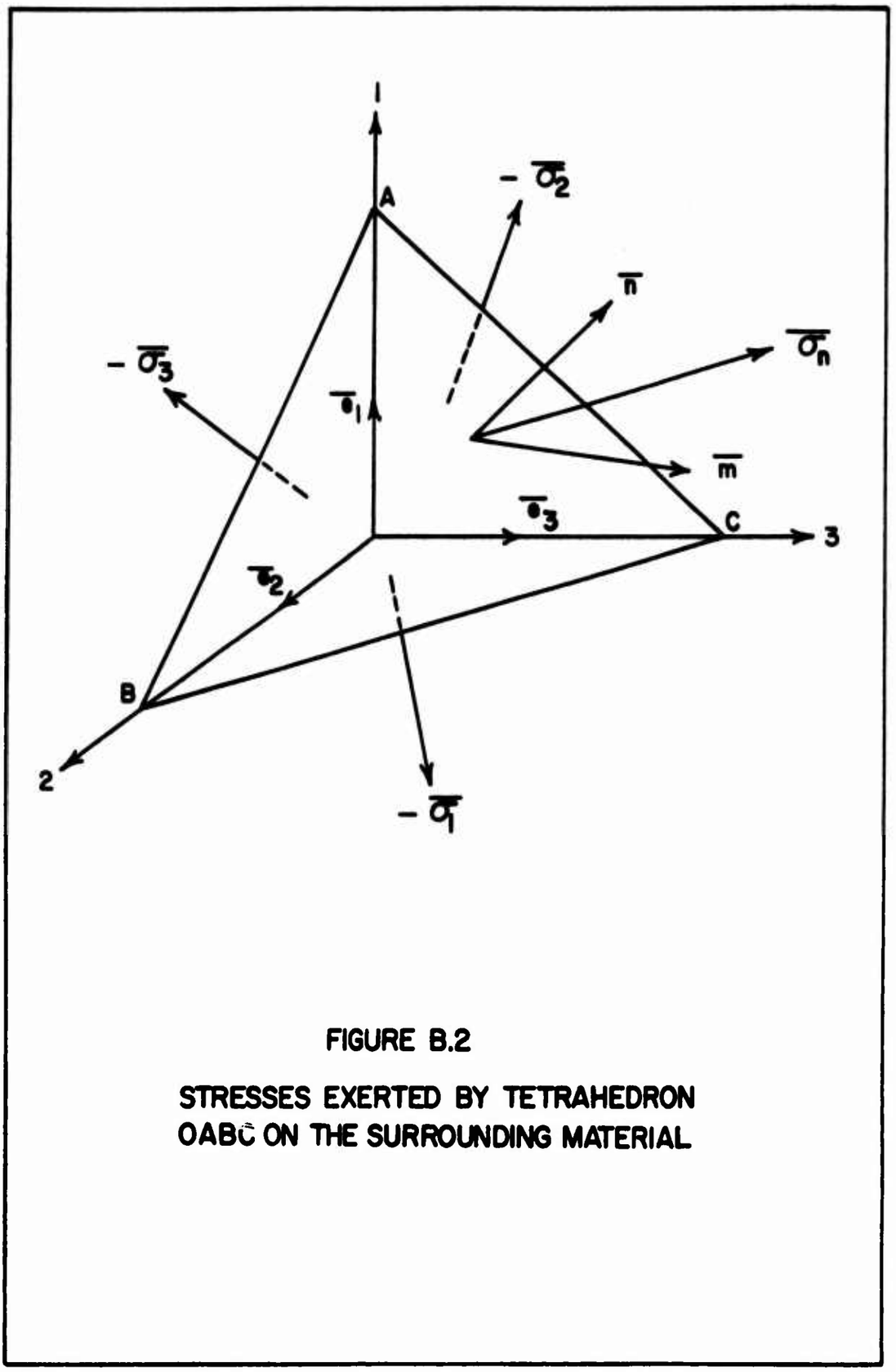

FIGURE B.2

STRESSES EXERTED BY TETRAHEDRON OABC ON THE SURROUNDING MATERIAL

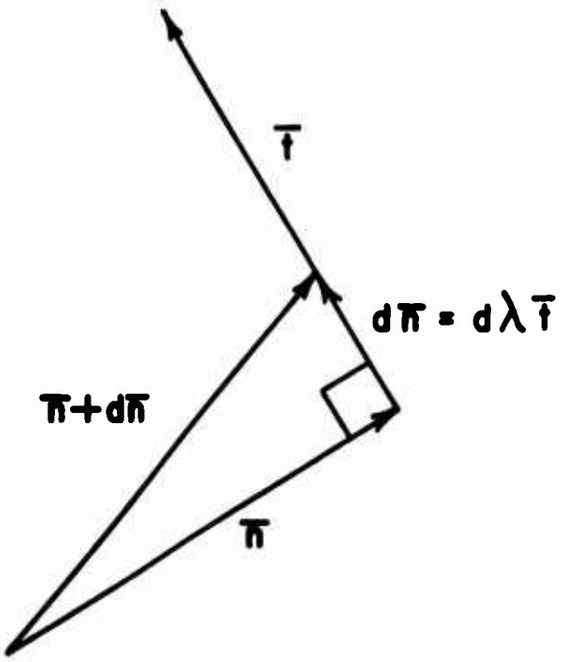

FIGURE B. 3

INFINITESIMAL CHANGE IN A UNIT VECTOR

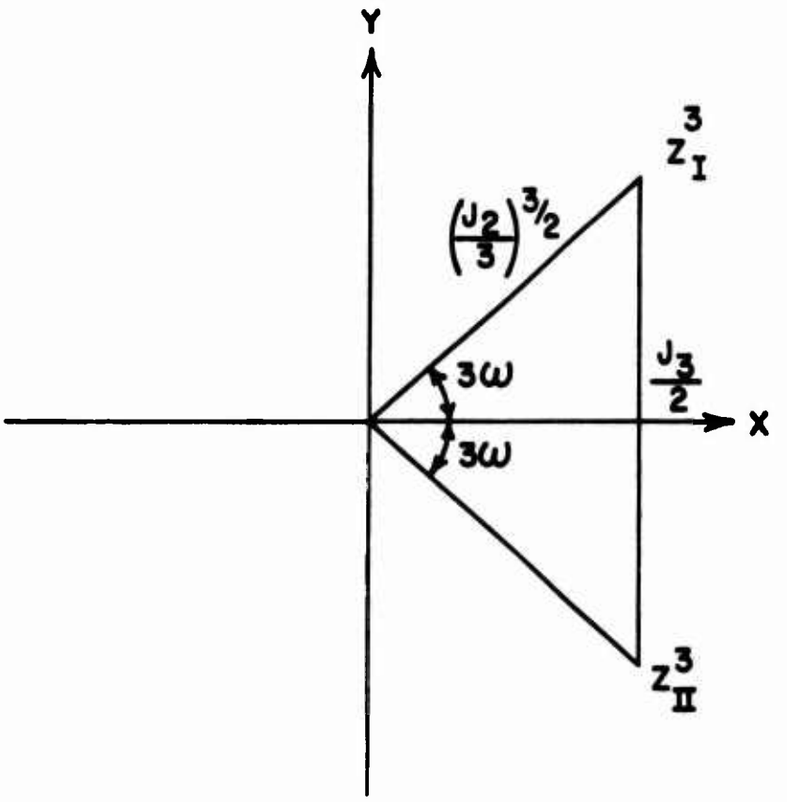

FIGURE B.4 (a)

REPRESENTATION OF THE ROOTS OF EQUATION (B.41) IN AN ARGAND DIAGRAM

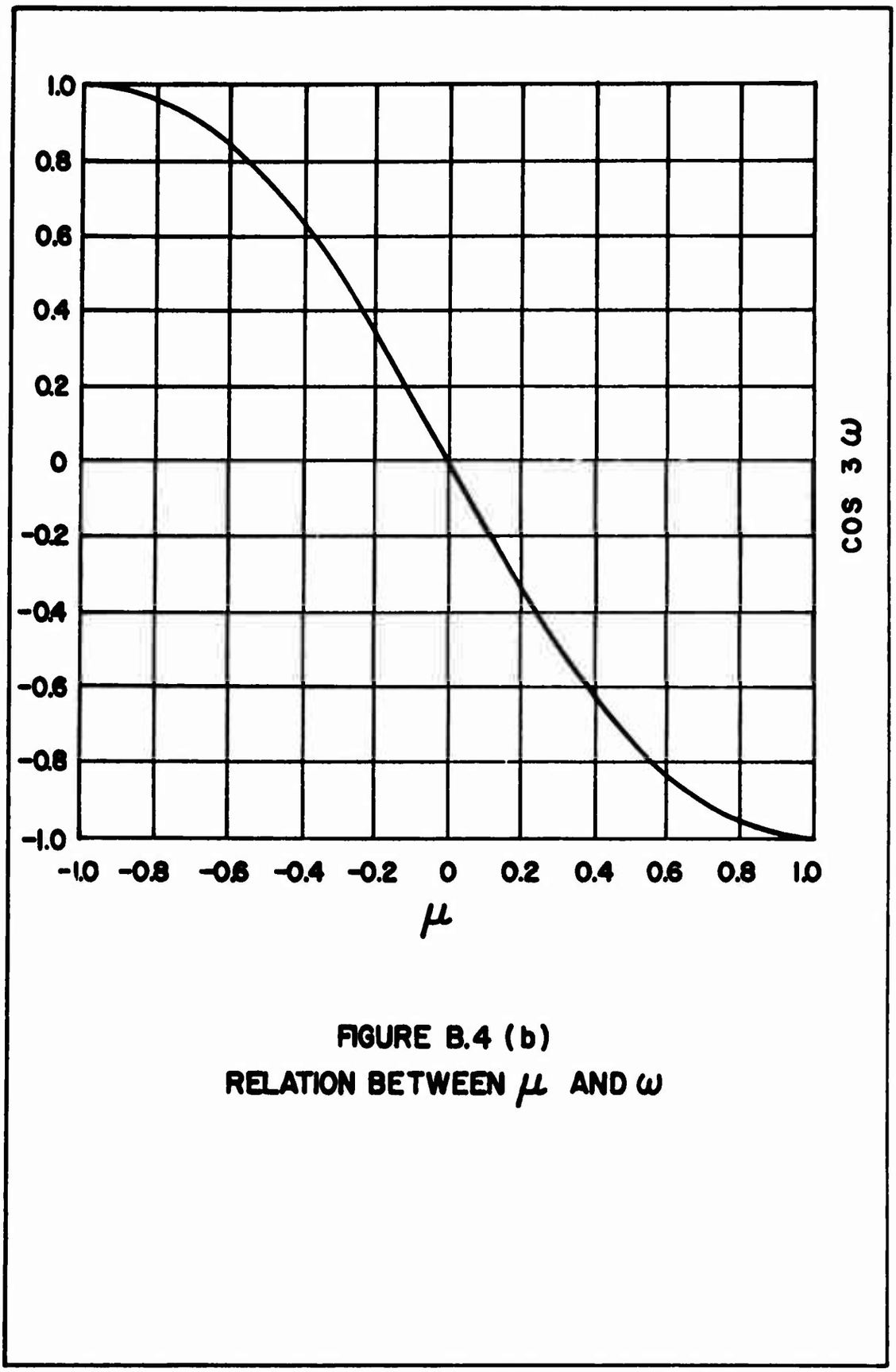

FIGURE B.4 (b)
RELATION BETWEEN μ AND ω

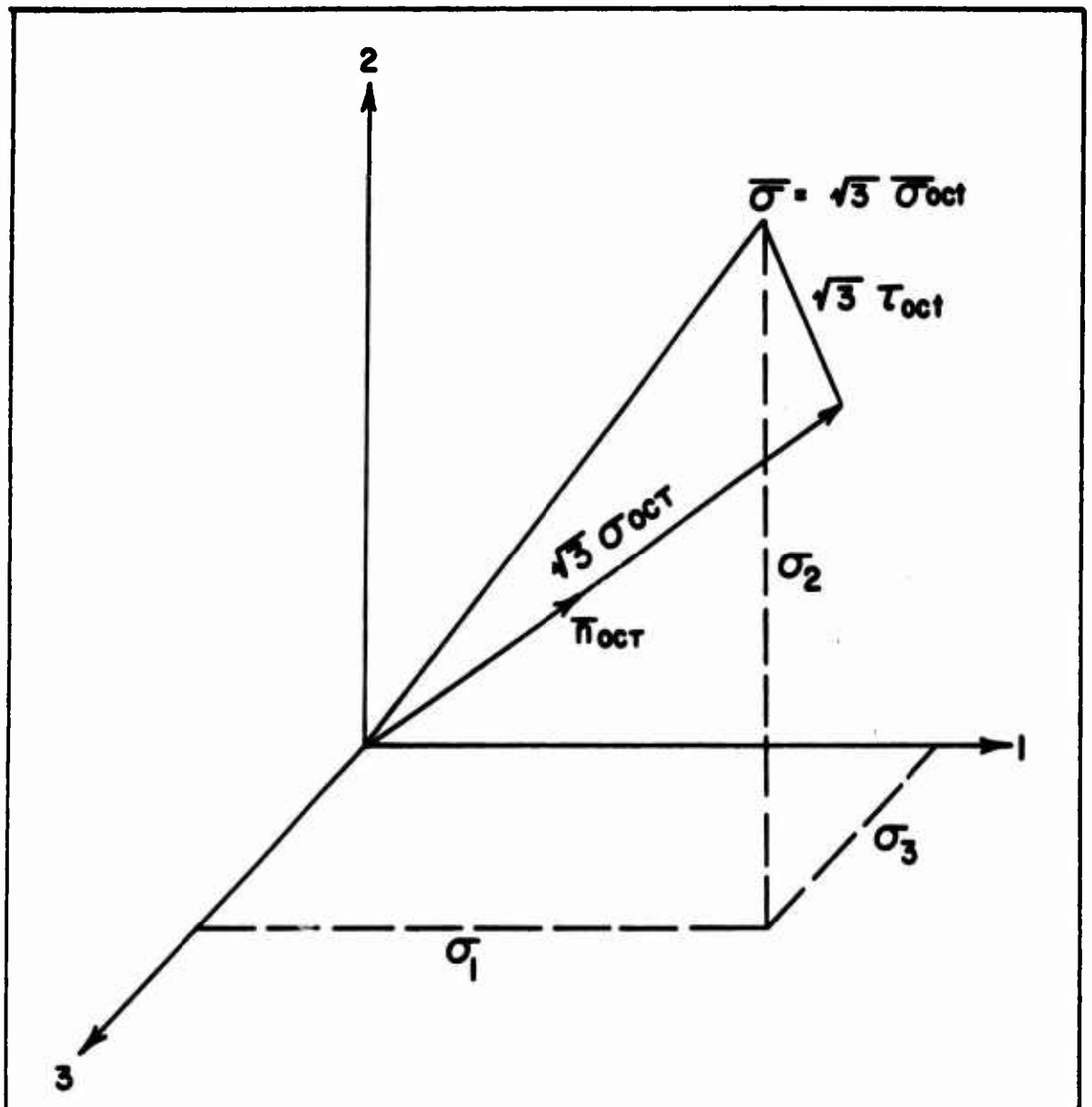

FIGURE B.5

SCALED OCTAHEDRAL STRESS VECTOR
IN PRINCIPAL STRESS SPACE

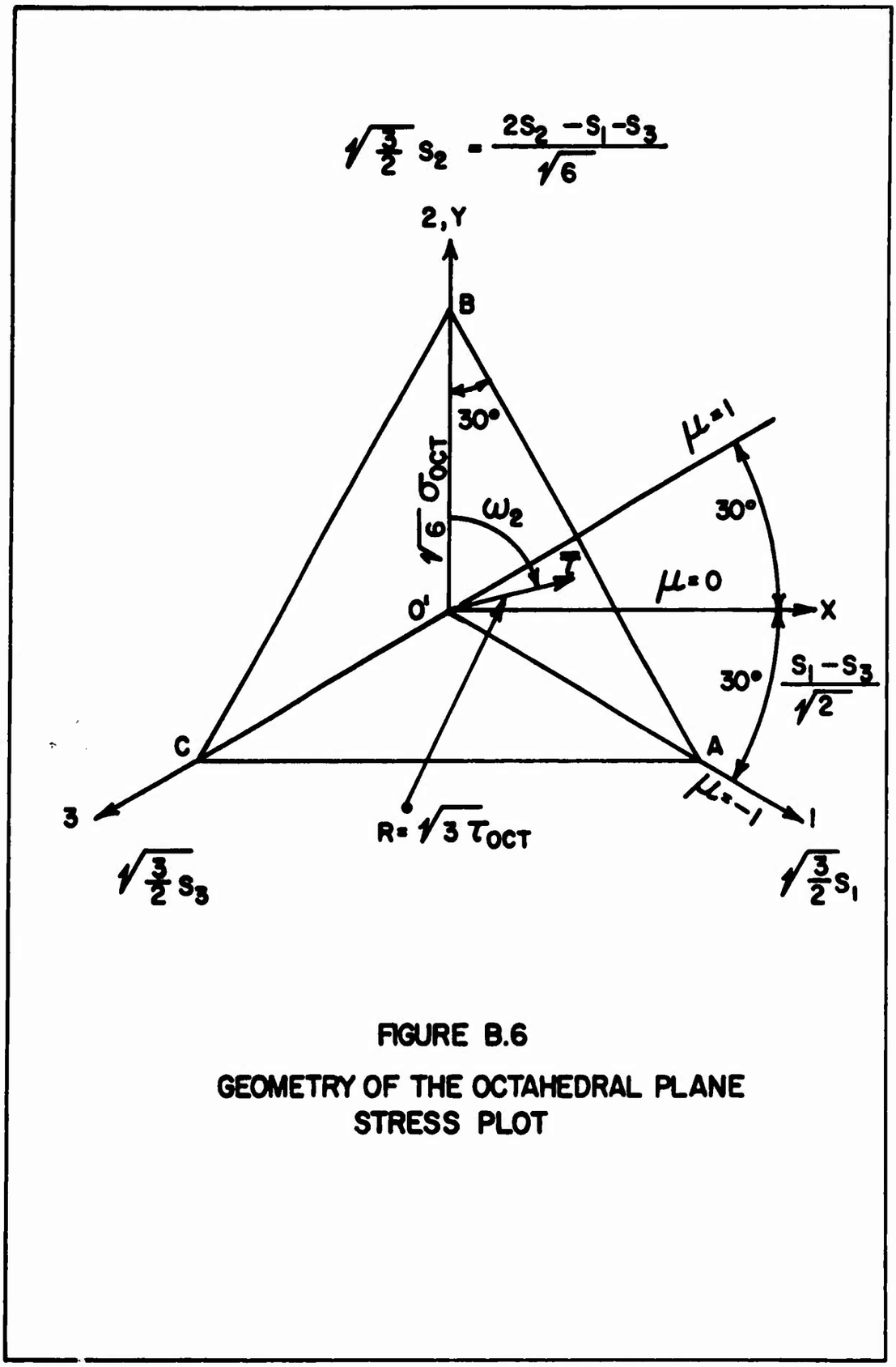

FIGURE B.6

GEOMETRY OF THE OCTAHEDRAL PLANE
STRESS PLOT

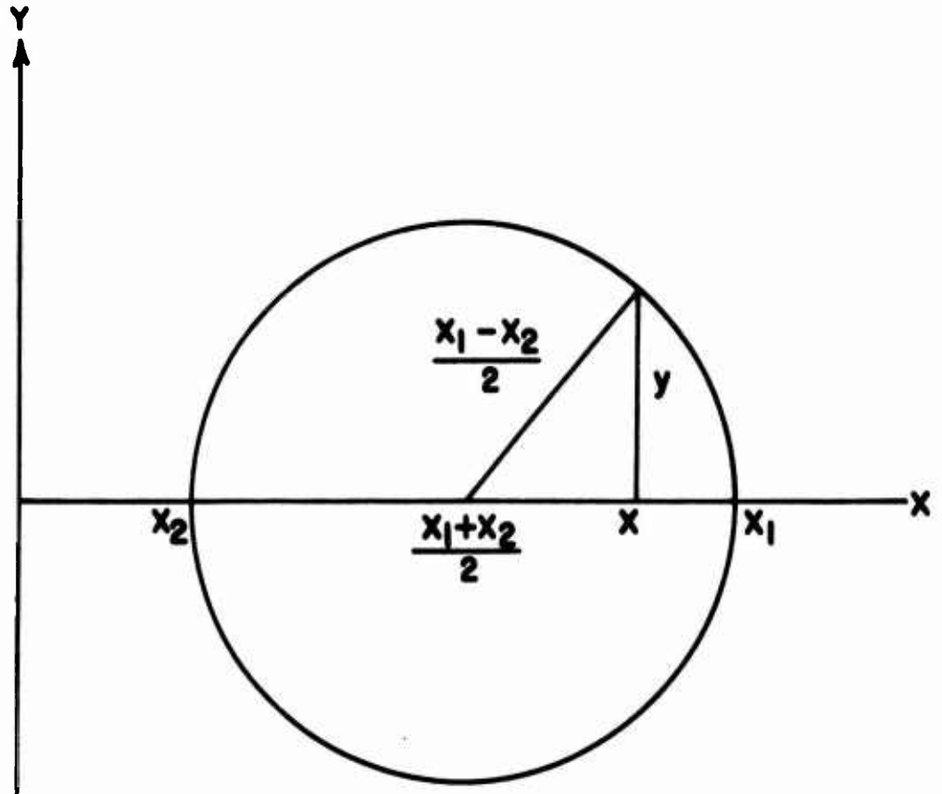

$$y^2 + \left[x - \left(\frac{x_1+x_2}{2}\right)\right]^2 = \left(\frac{x_1-x_2}{2}\right)^2$$

$$\left(y^2+x^2\right) - \left(x_1+x_2\right)x + x_1x_2 = 0$$

$$y^2 + \left(x - x_1\right)\left(x-x_2\right) = 0$$

CHARACTERISTICS

1. COEFFICIENT OF BOTH y^2 AND x^2 IS UNITY.
2. NO LINEAR TERM IN y.
3. CENTER AT $\frac{1}{2}(x_1+x_2)$
4. RADIUS $\frac{1}{2}(x_1-x_2)$

FIGURE B.7

EQUATION OF A CIRCLE WITH CENTER ON THE X AXIS

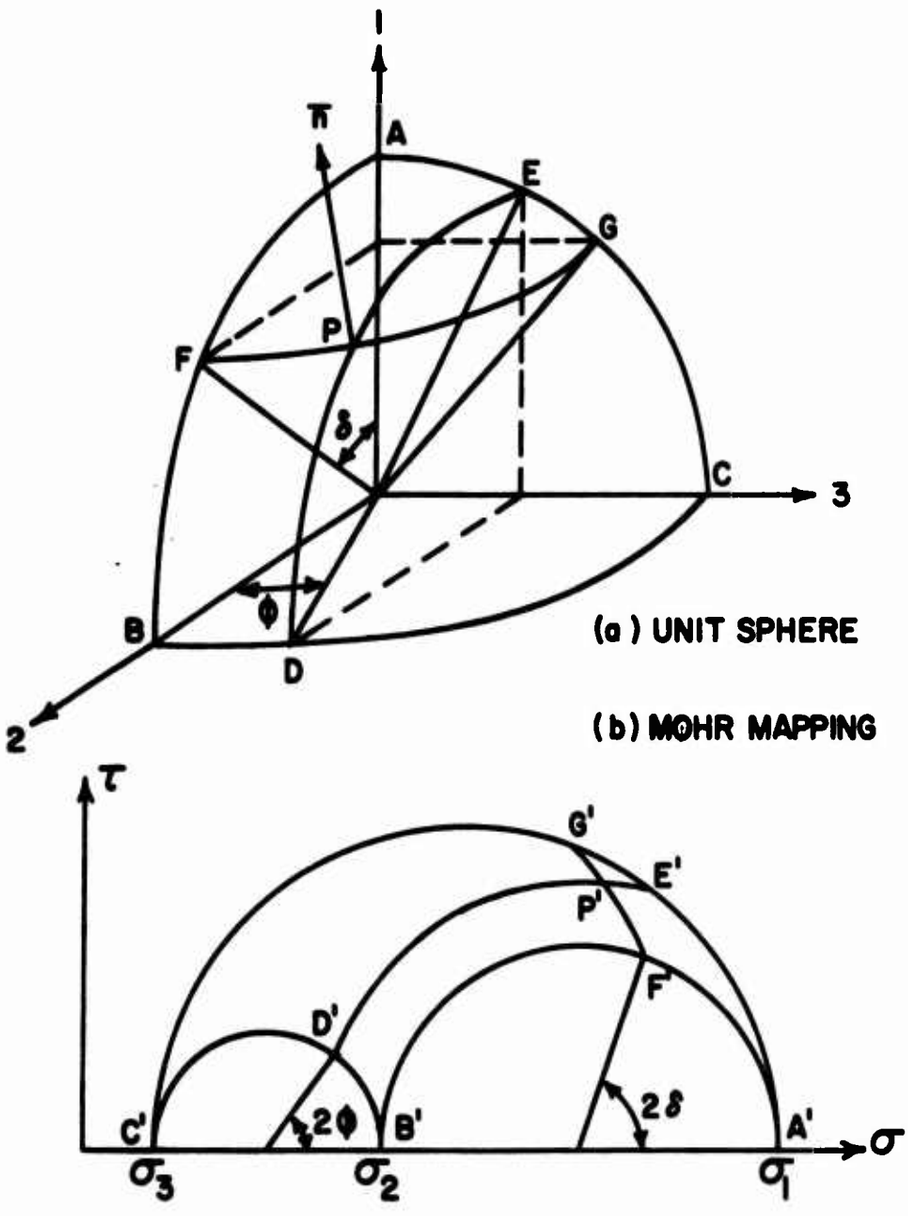

FIGURE B.8

MOHR CIRCLE CONSTRUCTION FOR TRIAXIAL STRESS

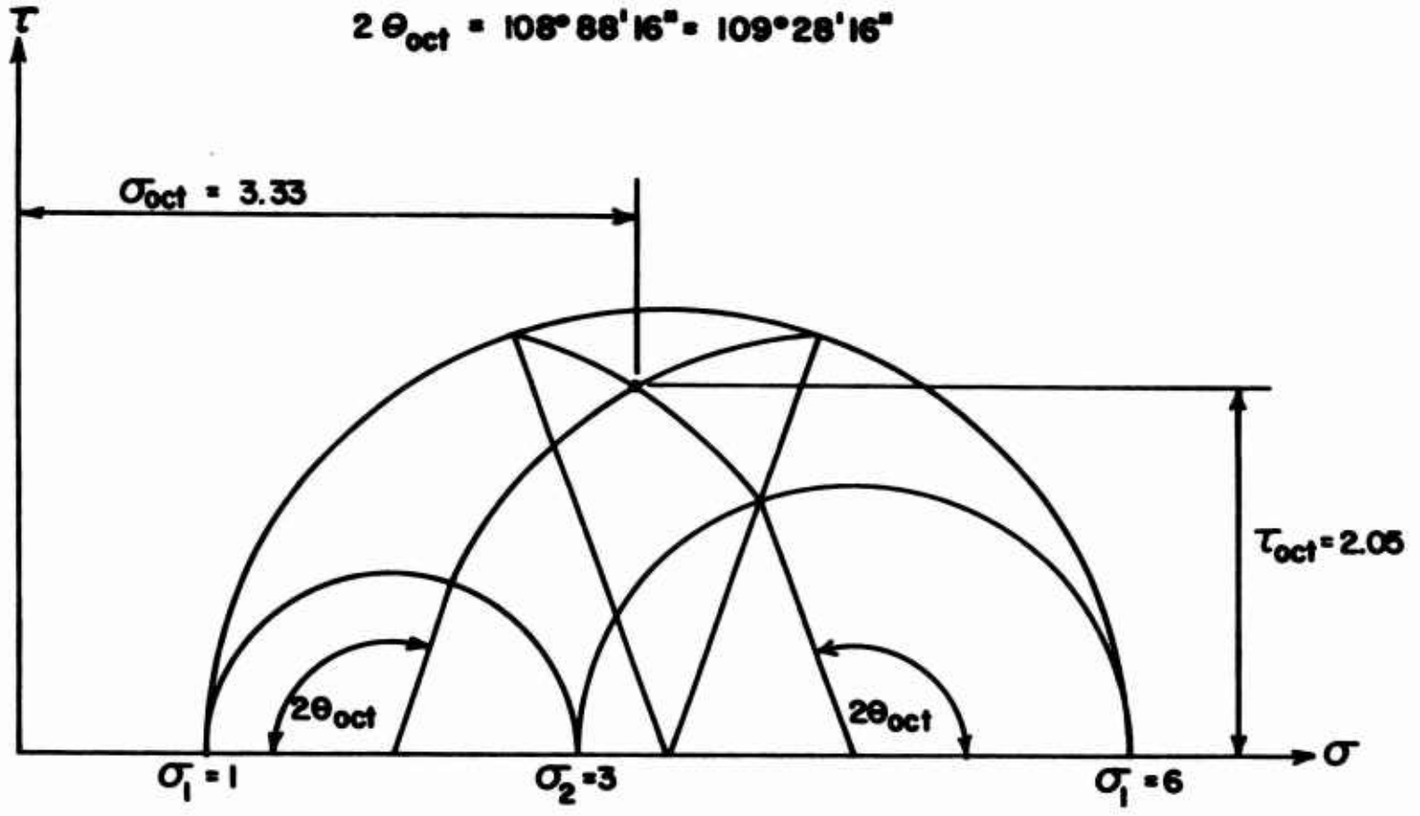

FIGURE B.9

GRAPHICAL DETERMINATION OF OCTAHEDRAL STRESSES

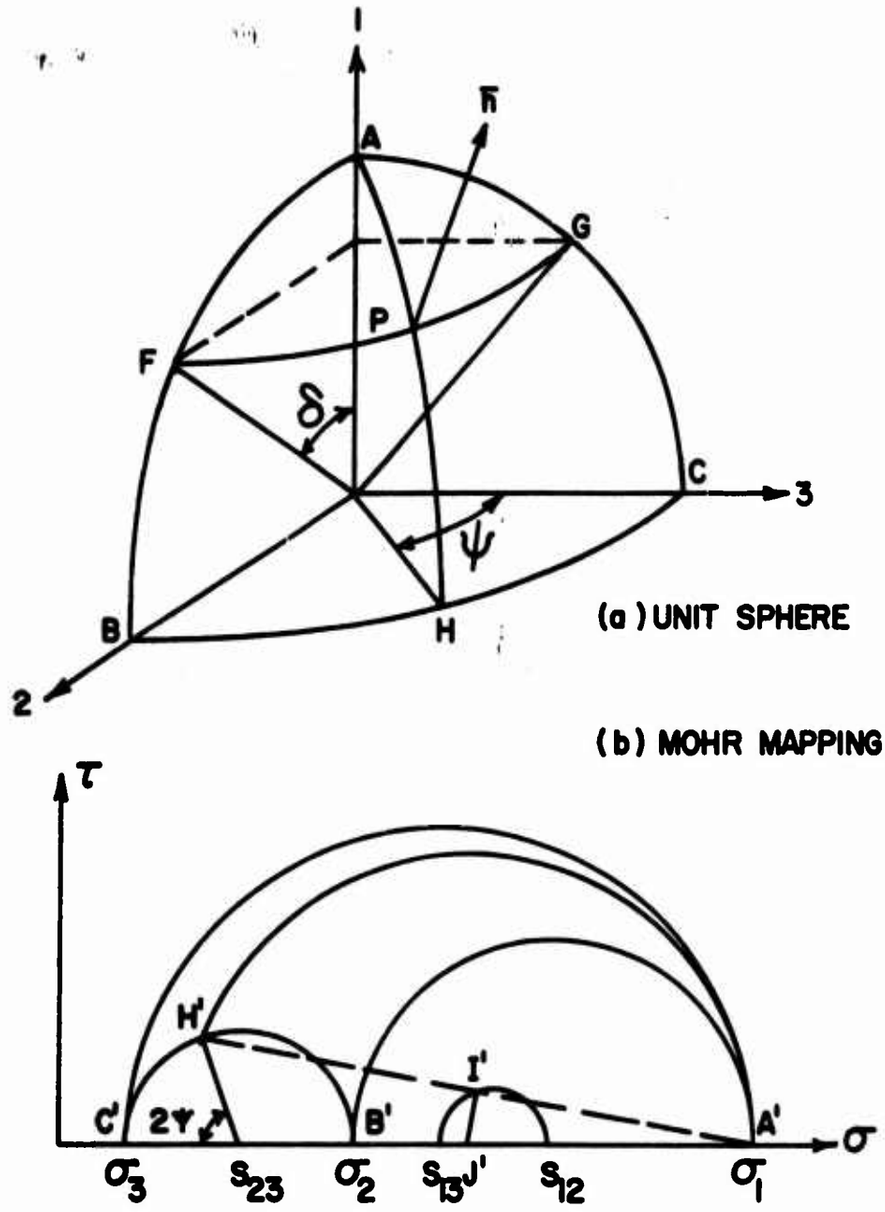

FIGURE B.10

MOHR MAPPING OF A MERIDIAN OF LONGITUDE ON A UNIT SPHERE

APPENDIX C

STRENGTH OF A FACE-CENTERED CUBIC PACKING OF EQUAL ROUGH RIGID SPHERES

Data presented in Chapter 6, dealing with the influence of the intermediate principal stress on shear strength, show that many soils exhibit a significant increase in the effective angle of shearing resistance as Lode's parameter begins to exceed -1. Such results are so common that they probably do reflect true soil behavior, rather than imperfect test technique. If so, a physical explanation is of interest, which is the object of this appendix.

This has been achieved by analyzing the strength of a face-centered cubic packing of equal, rough, rigid spheres. The same packing has been analyzed by several other investigators, including RENNIE (1959), THURSTON AND DERESIEWICZ (1959) and PARKIN (1965). The results obtained here differ in detail from those of Parkin, due to a different assumption concerning the magnitude of contact friction forces at the instant of slipping. Parkin assumed all contact friction forces to be equal in magnitude, whereas here it will only be assumed that each contact friction force is equal to f

times the corresponding contact normal force, at the instant of slipping. The results obtained here are algebraically simpler than those of Parkin, and therefore permit a more direct physical interpretation. In particular, it will be possible to offer a simple physical explanation for variation of the effective angle of shearing resistance with the relative value of the intermediate principal stress.

Consider a face-centered cubic array of equal spheres, in which the centers of non-contacting spheres of diameter d are located a distance $\sqrt{2}d$ apart in each of three mutually perpendicular directions, starting from the center of any sphere in the array. In addition, consider the cube formed by the centeres of eight non-contacting spheres, of side length $\sqrt{2}d$. There is, in addition, a sphere with its center at the center of each of the six faces of the cube. (See Figure C.1)

A second way of viewing a face-centered cubic array is in a direction normal to one of the cube axes and making 45° angles with each of the other two axes. Viewed from this angle, the face-centered cubic array appears as a series of layers, each of which is a square array with the centers of contacting spheres located a distance d apart in each of

two perpendicular directions, starting from the center of any sphere in the layer. Each sphere in one layer rests in the depression between four contacting spheres in the layer beneath, hence the term "pyramidal". (See Figure C.2)

Still a third way of viewing a face-centered cubic array is in a direction making equal angles with each of the three cube axes. Viewed from this angle, the face-centered cubic array appears again as a series of layers, each of which is now a hexagonal array with the centers of contacting spheres located a distance d apart in each of three directions parallel to the sides of an equilateral triangle, starting from the center of any sphere in the layer. Each sphere in one layer rests in the depression between three contacting spheres in the layer beneath, which depression is in turn located above a similar but unfilled depression in the layer beneath it. The same translation brings any hexagonal layer into the position of the contacting layer immediately above it. (See Figure C.3) This is one of two possible close-packed arrays composed of hexagonal layers. The other, called hexagonal close packed, is the same as described above, except that each sphere in one layer is located directly over a sphere

in the second layer beneath it; DERESIEWICZ (1958). The hexagonal or tetrahedral viewpoint is common in studies of the molecular structure of clay minerals.

Perhaps the easiest way of illustrating the unity of the above three views of the face-centered cubic array is by means of Figure C.4. From it one can see that the characteristic 3x3 matrices, used to obtain the coordinates of any sphere center, starting from any other sphere center, and commonly associated with the face-centered cubic, pyramidal and tetrahedral - hexagonal unit elements, can be obtained from each other by simple rotational coordinate transformations, or even by simple vector addition.

In the strength analysis to follow it will be convenient to consider the pyramidal unit element shown in Figure C.5. In the center of the element is a sphere (the center sphere), which has its center at the coordinate origin. It contacts each of the eight corner spheres, and is also tangent to the element sides at the four points where the 2 and 3 axes enter and leave the element.

Since the pyramidal element diagonal is 2d, and the length and width are both d, the height must be $\sqrt{2}d$, so that the total volume is

$$V = \sqrt{2}\, d^3 \qquad (C.1)$$

The volume of solids equals the volume of two spheres of diameter d.

$$V_s = \frac{\pi d^3}{3} \qquad (C.2)$$

The solid density, i.e. the volume of solids per unit of total volume is

$$D = \frac{V_s}{V} = \frac{\pi}{3\sqrt{2}} = 0.74 \qquad (C.3)$$

The porosity, i.e. the volume of voids per unit of total volume is

$$n = (1 - D) \times 100\% = 26\% \qquad (C.4)$$

and the void ratio, i.e. the volume of voids per unit volume of solids is

$$e = \frac{1}{D} - 1 = \frac{3\sqrt{2}}{\pi} - 1 = 0.35 \qquad (C.5)$$

As with any other finite element analysis, (the spheres being the finite elements in this case) three basic sets of equations describe the mechanical response of the pyramidal array:

1. equilibrium equations, which relate contact forces to boundary stresses,

2. force-deformation equations, which state that a contact friction force equals f times the corresponding contact normal force, and acts in the direction of slip, and

3. continuity equations, which state that each corner sphere remains in contact with the center sphere during slip.

It is convenient to perform the deformation analysis first, in which it is assumed that the element in Figure C.5 is part of a continuum, composed of identical but randomly oriented elements, and that this particular element is one for which the 1, 2 and 3 axes coincide with the principal strain axes. It will aid the reader to keep in mind that this is what one might call a strain-controlled analysis, because we shall specify the principal strains and then calculated the associated boundary stresses. Referring to Figure C.6, and treating compressive normal strains as positive, the displacement of point S can be written

$$\bar{u}_s = -\frac{\epsilon_1 d}{\sqrt{2}}\bar{e}_1 - \frac{\epsilon_2 d}{2}\bar{e}_2 - \frac{\epsilon_3 d}{2}\bar{e}_3 \tag{C.6}$$

It is convenient to let

$$\begin{aligned} \epsilon_2 &= -2\Delta \sin\theta \\ \epsilon_3 &= -2\Delta \cos\theta \end{aligned} \tag{C.7}$$

so that the displacement of point S becomes

$$\bar{u}_s = -\frac{\epsilon_1 d}{\sqrt{2}}\bar{e}_1 + \Delta d(\sin\theta\,\bar{e}_2 + \cos\theta\,\bar{e}_3) \tag{C.8}$$

The requirement that sphere S remain in contact with the center sphere during slip leads to the requirement (for infinitesimal strains) that the displacement of point S occur in a plane normal to line OS, hence normal to the direction

$$\bar{n}_s = \frac{\bar{e}_1}{\sqrt{2}} + \frac{\bar{e}_2}{2} + \frac{\bar{e}_3}{2} \tag{C.9}$$

Thus, setting $-\bar{u}_s \cdot \bar{n}_s = 0$ yields

$$\epsilon_1 = \Delta(\sin\theta + \cos\theta) \tag{C.10}$$

so that the strain tensor becomes

$$\epsilon_{ij} = \begin{bmatrix} \epsilon_1 & 0 & 0 \\ 0 & \epsilon_2 & 0 \\ 0 & 0 & \epsilon_3 \end{bmatrix} = \Delta \begin{bmatrix} \sin\theta + \cos\theta & 0 & 0 \\ 0 & -2\sin\theta & 0 \\ 0 & 0 & -2\cos\theta \end{bmatrix} \tag{C.11}$$

where, because the corner spheres are assumed to be initially in contact, and therefore cannot move toward each other*:

$$0 \leq \theta \leq \frac{\pi}{4} \tag{C.12}$$

Under this restriction,

$$\epsilon_1 > \epsilon_2 \geq \epsilon_3 \tag{C.13}$$

The displacement of point S will therefore be in the direction

---

*This assumption was made by Parkin, It will be relaxed here later.

$$\bar{t}_s = \frac{-(\sin\theta + \cos\theta)\bar{e}_1 + \sqrt{2}\sin\theta\,\bar{e}_2 + \sqrt{2}\cos\theta\,\bar{e}_3}{F} \qquad (C.14)$$

where

$$F = \sqrt{3 + \sin 2\theta} \qquad (C.15)$$

Proceeding next to the force-deformation analysis, we see that the contact friction force exerted on the center sphere by S must act in the direction given by Equation (C.14). The directions of the other contact friction forces are given by expressions identical in form, except for changes in sign of components.

Finally the equilibrium analysis, which Rennie performed by an elegant application of the Divergence Theorem, will be accomplished here in a more conventional manner. The self-equilibrating contact normal forces p, q, r and s, corresponding to the corner sphere pairs P - P', Q - Q', R - R' and S - S' in Figure C.5, and the contact normal force t (which is zero if $\theta > 0$) must each act along a line from the origin to the center of the corresponding contacting sphere. Consequently the contribution to the boundary stresses from the contact normal forces will be

$$\sigma_{ij}^{n} = \begin{bmatrix} \sigma_{11}^{n} & \sigma_{12}^{n} & \sigma_{13}^{n} \\ \sigma_{21}^{n} & \sigma_{22}^{n} & \sigma_{23}^{n} \\ \sigma_{31}^{n} & \sigma_{32}^{n} & \sigma_{33}^{n} \end{bmatrix}$$

where, referring to Figure C.5, σ_{ij} is the stress component acting in the (-)j direction on a rectangular cross section of the entire pyramidal element containing the origin and with its outward normal pointing in the (+)i direction, Thus,

$$\sigma_{11}^{n} = \frac{\frac{1}{\sqrt{2}}(p + q + r + s)}{d^2} \qquad \sigma_{12}^{n} = \frac{\frac{1}{2}(-p + q - r + s)}{d^2} = \sigma_{21}^{n}$$

$$\sigma_{22}^{n} = \frac{\frac{1}{2}(p + q + r + s)}{\sqrt{2}\, d^2} \qquad \sigma_{23}^{n} = \frac{\frac{1}{2}(-p - q + r + s)}{\sqrt{2}\, d^2} = \sigma_{32}^{n}$$

$$\sigma_{33}^{n} = \frac{\frac{1}{2}(p + q + r + s)}{\sqrt{2}\, d^2} \qquad \sigma_{31}^{n} = \frac{\frac{1}{\sqrt{2}}(p - q - r + s)}{\sqrt{2}\, d^2} = \sigma_{13}^{n}$$

so that

$$\sigma_{ij}^{n} = \frac{1}{d^2}\begin{bmatrix} \frac{p+q+r+s}{\sqrt{2}} & \frac{-p+q-r+s}{2} & \frac{p-q-r+s}{2} \\ \frac{-p+q-r+s}{2} & \frac{p+q+r+s}{2\sqrt{2}} & \frac{-p-q+r+s}{2\sqrt{2}} \\ \frac{p-q-r+s}{2} & \frac{-p-q+r+s}{2\sqrt{2}} & \frac{p+q+r+s}{2\sqrt{2}} \end{bmatrix}$$

When $\theta = 0$, σ_{22}^{n} is increased by an amount $t/\sqrt{2}d^2$, where t is arbitrary but has no influence on the deformation. If we assume that the intermediate principal axes of stress and strain coincide, then

$$\sigma_{21} = \sigma_{23} = 0$$

so that

$$-p+q-r+s = 0$$

$$-p-q+r+s = 0$$

Adding and subtracting the above equations yields

$$p = s$$

$$q = r$$

so that the contribution to the stress tensor due to the contact normal forces reduces to

$$\sigma_{ij}^{n} = \frac{1}{d^2} \begin{bmatrix} \sqrt{2}(p+q) & 0 & p-q \\ 0 & \frac{p+q}{\sqrt{2}} & 0 \\ p-q & 0 & \frac{p+q}{\sqrt{2}} \end{bmatrix} \qquad \text{(C.16)}$$

Note that $\sigma_{ij}^{n} \epsilon_{ij} = 0$, since the contact normal forces do no work during slipping.

Next, we assume that at the instant of slipping each contact friction force equals the coefficient of friction f, times the corresponding contact normal force*. Therefore, the contribution tc the boundary stresses from the contact friction forces will be

---

*Parkin assumed each contact friction force to be equal to f times the smaller of p or q, which results in an expression for strain energy density which depends on p - q.

$$\sigma_{ij}^{f} = \begin{bmatrix} \sigma_{11}^{f} & \sigma_{12}^{f} & \sigma_{13}^{f} \\ \sigma_{21}^{f} & \sigma_{22}^{f} & \sigma_{23}^{f} \\ \sigma_{31}^{f} & \sigma_{32}^{f} & \sigma_{33}^{f} \end{bmatrix}$$

where, again referring to Figure C.5:

$$\sigma_{11}^{f} = \frac{2f(\sin\theta + \cos\theta)(p+q)}{Fd^2} \qquad \sigma_{12}^{f} = 0 = \sigma_{21}^{f}$$

$$\sigma_{22}^{f} = \frac{-2\sqrt{2}\, f \sin\theta\, (p+q)}{\sqrt{2}\, Fd^2} \qquad \sigma_{23}^{f} = 0 = \sigma_{32}^{f}$$

$$\sigma_{33}^{f} = \frac{-2\sqrt{2}\, f \cos\theta\, (p+q)}{\sqrt{2}\, Fd^2} \qquad \sigma_{31}^{f} = \frac{2f\,(\sin\theta + \cos\theta)(p-q)}{\sqrt{2}\, Fd^2}$$

$$= \sigma_{13}^{f}$$

so that

$$\sigma_{ij}^{f} = \frac{2f}{Fd^2}\begin{bmatrix} (\sin\theta + \cos\theta)(p+q) & 0 & \frac{(\sin\theta + \cos\theta)(p-q)}{\sqrt{2}} \\ 0 & -\sin\theta(p+q) & 0 \\ (\sin\theta + \cos\theta)(p-q) & 0 & -\cos\theta(p+q) \end{bmatrix}$$

The work per unit volume done during slip is therefore

$$W_f = \sigma_{ij}^{f} \epsilon_{ij} = \frac{2fF\Delta(p+q)}{d^2} \qquad (C.18)$$

Since the energy dissipated by friction during slip is independent of $(p - q)$, the major and minor principal stress axes will not need to rotate during slip to achieve a minimum energy condition. At the instant of slip, the total boundary stresses will be

$$\sigma_{ij} = \frac{\sqrt{2}}{d^2} \begin{bmatrix} (p+q)\left[1 + \frac{2f}{F}(\sin\theta + \cos\theta)\right] & 0 & \left(\frac{p-q}{\sqrt{2}}\right)\left[1 + \frac{\sqrt{2}f}{F}(\sin\theta + \cos\theta)\right] \\ 0 & (p+q)\left[\frac{1}{2} - \frac{\sqrt{2}f}{F}\sin\theta\right] & 0 \\ \left(\frac{p-q}{\sqrt{2}}\right)\left[1 + \frac{\sqrt{2}f}{F}(\sin\theta + \cos\theta)\right] & 0 & (p+q)\left[\frac{1}{2} - \frac{\sqrt{2}f}{F}\cos\theta\right] \end{bmatrix}$$

(C.19)

Equation (C.19) indicates that the value of $(\sigma_1 + \sigma_3)$ at the instant of slip is independent of (p-q), and therefore of the orientation of the major and minor principal stress axes, but the same is not true of $(\sigma_1 - \sigma_3)$, which increases as $|p - q|$ increases. Therefore, the smallest value of $(\sigma_1 - \sigma_3)$ which will induce slip, for a given value of $(\sigma_1 + \sigma_3)$, corresponds to the condition

$$p - q = 0 \tag{C.20}$$

in which case the principal axes of stress and strain all coincide, and the total stress tensor reduces to

$$\sigma_{ij} = \frac{2\sqrt{2}p}{d^2} \begin{bmatrix} 1 + \frac{\sqrt{2}f}{F}(\sin\theta + \cos\theta) & 0 & 0 \\ 0 & \frac{1}{2} - \frac{\sqrt{2}f}{F}\sin\theta & 0 \\ 0 & 0 & \frac{1}{2} - \frac{\sqrt{2}f}{F}\cos\theta \end{bmatrix} \tag{C.21}$$

The angle of shearing resistance can now be calculated from the expression

$$\sin \Phi = \frac{\sigma_1 - \sigma_3}{\sigma_1 + \sigma_3} = \frac{F + 2\sqrt{2}\, f(\sin \theta + 2 \cos \theta)}{3F + 2\sqrt{2}\, f \sin \theta} \qquad (C.22)$$

and Lode's parameter at the instant of slip is

$$\mu = \frac{2\sigma_2 - (\sigma_1 + \sigma_3)}{\sigma_1 - \sigma_3} = - \frac{F + 6\sqrt{2} f \sin \theta}{F + 2\sqrt{2}\, f(\sin \theta + 2 \cos \theta)} \qquad (C.23)$$

When the spheres are frictionless, $f = 0$ and Equation (C.22) yield's Rennie's result

$$\sin \Phi = \frac{1}{3} \quad (f = 0) \qquad (C.24)$$

When $\theta = \frac{\pi}{4}$, Equation (C.23) yields $\mu = -1$ (triaxial compression) and Equation (C.22) yields*

$$\sin \Phi = \frac{1 + 3f}{3 + f} \qquad (C.25)$$

---

*This expression agrees with that of ROWE (1962, 508); see also HORNE (1965, 63).

When $\theta = 0$ (plane strain) Equation (C.22) yields

$$\sin \Phi = \frac{\sqrt{3} + 4\sqrt{2}f}{3\sqrt{3}} \qquad (C.26)$$

and Equation (C.23) yields

$$\mu = -\frac{\sqrt{3}}{\sqrt{3} + 4\sqrt{2}} \qquad (C.27)$$

When $\theta = 0$ the intermediate principal stress becomes arbitrary, because of the arbitrary contact force t which has no influence on slip, and therefore Φ remains constant at the value given by Equation (C.26) and μ exceeds the value given by Equation (C.27).

It is interesting, and in fact extremely revealing to inquire what would happen to the boundary stresses if the corner spheres were initially separated by an infinitesimal amount, so that small compressive strains would be possible in the 2 and 3 directions, thus permitting negative values of θ in Figure (C.6). Having removed the previous strain restriction, we next observe that the slip strains are related to the relative values of the principal stresses. It is therefore convenient to normalize the principal stresses with respect to the average principal stress, which is

$$\sigma_{OCT} = \frac{\sigma_1 + \sigma_2 + \sigma_3}{3} = \frac{2\sqrt{2}p}{d^2}\left[\frac{2}{3}\right] \qquad (C.28)$$

The ratios of the principal stresses at failure to the average principal stress at failure are

$$\left.\begin{aligned} \rho_1 &= \frac{\sigma_1}{\sigma_{OCT}} = \frac{3}{2} + \frac{3f}{\sqrt{2}}\left(\frac{\sin\theta + \cos\theta}{\sqrt{3 + \sin 2\theta}}\right) \\ \rho_2 &= \frac{\sigma_2}{\sigma_{OCT}} = \frac{3}{4} - \frac{3f}{\sqrt{2}}\left(\frac{\sin\theta}{\sqrt{3 + \sin 2\theta}}\right) \\ \rho_3 &= \frac{\sigma_3}{\sigma_{OCT}} = \frac{3}{4} - \frac{3f}{\sqrt{2}}\left(\frac{\cos\theta}{\sqrt{3 + \sin 2\theta}}\right) \end{aligned}\right\} \qquad (C.29)$$

and the ratios of the principal deviator stresses at failure to the average principal stress at failure are

$$\left.\begin{aligned} \Psi_1 &= \frac{\sigma_1 - \sigma_{OCT}}{\sigma_{OCT}} = \rho_1 - 1 \\ \Psi_2 &= \frac{\sigma_2 - \sigma_{OCT}}{\sigma_{OCT}} = \rho_2 - 1 \\ \Psi_3 &= \frac{\sigma_3 - \sigma_{OCT}}{\sigma_{OCT}} = \rho_3 - 1 \end{aligned}\right\} \qquad (C.30)$$

By direct expansion it can be demonstrated that the failure (slip) criterion obeyed by the face-centered cubic packing is

$$2\left(\Psi_1 - \frac{1}{2}\right)^2 + \left(\Psi_2 - \Psi_3\right)^2 = \frac{9f^2}{2} \qquad (C.31)$$

Figure B.6 then shows that one can select the following dimensionless coordinates in a normalized octahedral plane stress plot:

$$\left.\begin{aligned} y &= \frac{\Psi_2 - \Psi_3}{\sqrt{2}} \\ x &= \sqrt{\frac{3}{2}}\,\Psi_1 \end{aligned}\right\} \qquad (C.32)$$

The failure criterion, expressed in terms of dimensionless rectangular Carterian coordinates in the octahedral plane, therefore takes the form

$$\left(\sqrt{\frac{2}{3}}\,x - \frac{1}{2}\right)^2 + \frac{1}{2}\left(\sqrt{2}\,y\right)^2 = \frac{9f^2}{4}$$

or

$$\left(\frac{x - \frac{1}{2}\sqrt{\frac{3}{2}}}{\frac{3f}{2}\sqrt{\frac{3}{2}}} \right)^2 + \left(\frac{y}{\frac{3f}{2}} \right)^2 = 1 \qquad \text{(C.33)}$$

Equation (C.33) is the equation of an ellipse in the octahedral plane, with its center at the point ($x = \frac{1}{2}\sqrt{\frac{3}{2}}$, $y = 0$), its major axis coinciding with the X axis, and major and minor semiaxes of length $\frac{3f}{2}\sqrt{\frac{3}{2}}$ and $\frac{3f}{2}$.

When f is less than one third, the ellipse will cross the +X axis twice, indicating two possible modes of failure in triaxial compression ($\mu = -1$) and none in triaxial extension ($\mu = 1$). In fact, however, the axial <u>strain</u> in one case is compression ($\theta = \frac{\pi}{4}$) and in the other case extension ($\theta = -\frac{3\pi}{4}$). When $f = 1/3$, failure occurs under pure hydrostatic stress when $\theta = -\frac{3\pi}{4}$. This is because the stress tensor σ_{ij}^{n} is not hydrostatic.

The failure surface in stress space described by Equation (C.33) is a cone, with its apex at the origin and having an elliptical octahedral cross-section. It is because the octahedral cross-section is an ellipse that the angle of shearing resistance varies with the relative value of the

intermediate principal stress. This particular sphere packing simply does not obey the Mohr - Coulomb failure criterion.

Having defined a failure or yield criterion for a face-centered cubic packing of equal, rough rigid spheres, we shall now see if the associated slip strains obey the normality condition of classical plasticity theory. We therefore write the failure criterion in the form

$$\frac{1}{2}(2\Psi_1 - 1)^2 + (\Psi_2 - \Psi_1)^2 - \frac{9f^2}{2} = 0$$

and then, since

$$2\Psi_1 - 1 = 2\rho_1 - 3 = \rho_1 - \rho_2 - \rho_3$$

$$\Psi_2 - \Psi_3 = \rho_2 - \rho_3$$

the failure criterion can be written in the form

$$H(\rho_{ij}) = \frac{1}{2}(\rho_1 - \rho_2 - \rho_3)^2 + (\rho_2 - \rho_3)^2 - \frac{9f^2}{2} = 0 \qquad (C.34)$$

The scalar components of the gradient of H are

$$\left.\begin{aligned}
\frac{\partial H}{\partial \rho_1} &= (\rho_1 - \rho_2 - \rho_3) = \frac{3\sqrt{2}f}{F}(\sin\theta + \cos\theta) \\
\frac{\partial H}{\partial \rho_2} &= -(\rho_1 - \rho_2 - \rho_3 + 2(\rho_2 - \rho_3) = -\frac{6\sqrt{2}\,f}{F}\sin\theta \\
\frac{\partial H}{\partial \rho_3} &= -(\rho_1 - \rho_2 - \rho_3) - 2(\rho_2 - \rho_3) = -\frac{6\sqrt{2}\,f}{F}\cos\theta
\end{aligned}\right\} \quad (C.35)$$

Comparison of Equation (C.35) with Equation (C.11) shows that the normality condition is satisfied, provided the yield criterion is written in terms of <u>normalized</u> stress components. This fact establishes a connection between the mechanics of particulate and continuous media.

There appears to be no reason why other packings of discrete frictional elements should not behave in a similar manner. The basic reason for satisfaction of the normality condition in terms of normalized stresses is that each contact friction force (a) acts along the direction of slip, and (b) equals f times the corresponding contact normal force, which acts normal to the direction of slip.

In particular, it can be shown that the failure criterion for a general quadratic packing, where α is the contact angle, is

$$\left[\frac{x - \sqrt{\frac{3}{2}}\,(3\cos^2\alpha - 1)}{(\sqrt{3}\cos\alpha)\left(\frac{3f}{\sqrt{2}}\sin\alpha\right)}\right]^2 + \left[\frac{y}{\frac{3f}{\sqrt{2}}\sin\alpha}\right]^2 = 1$$

and that the normality condition is satisfied in terms of normalized stresses. The body-centered cubic array obeys the extended von Mises failure criterion.

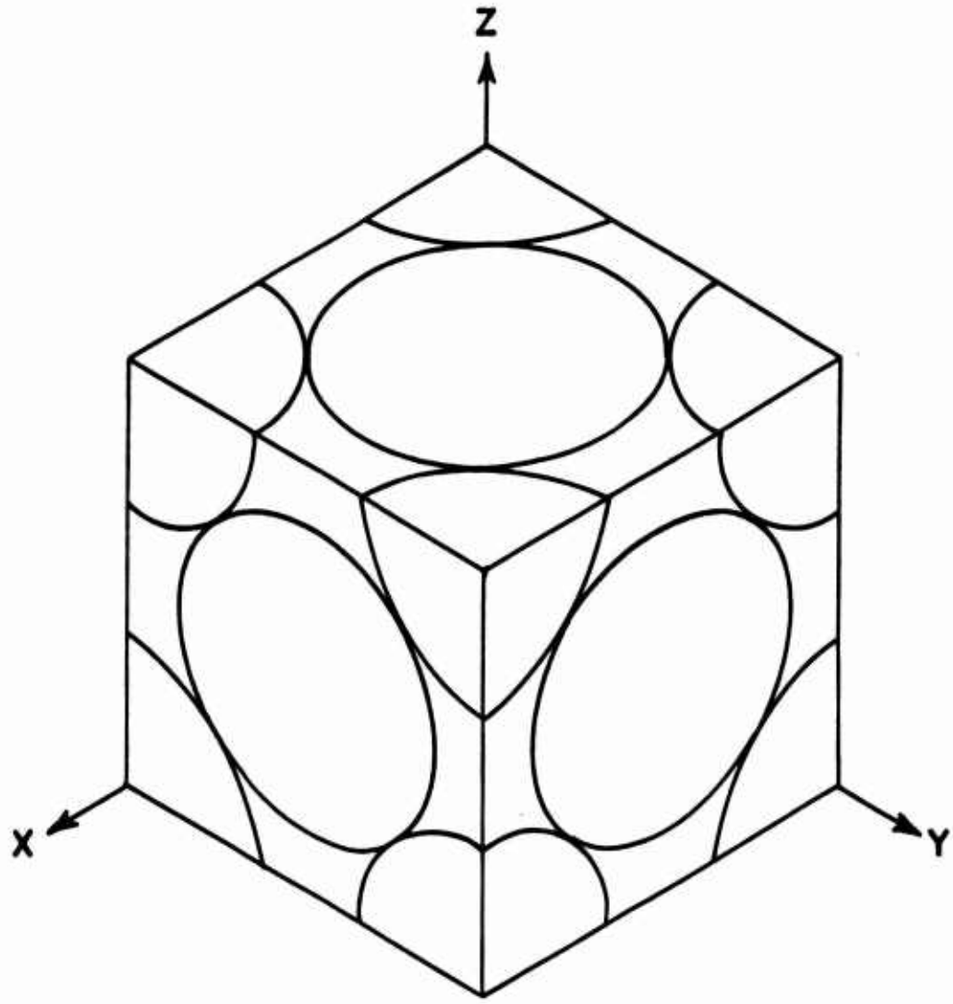

FIGURE C.1

FACE-CENTERED CUBIC ARRAY
OF EQUAL SPHERES

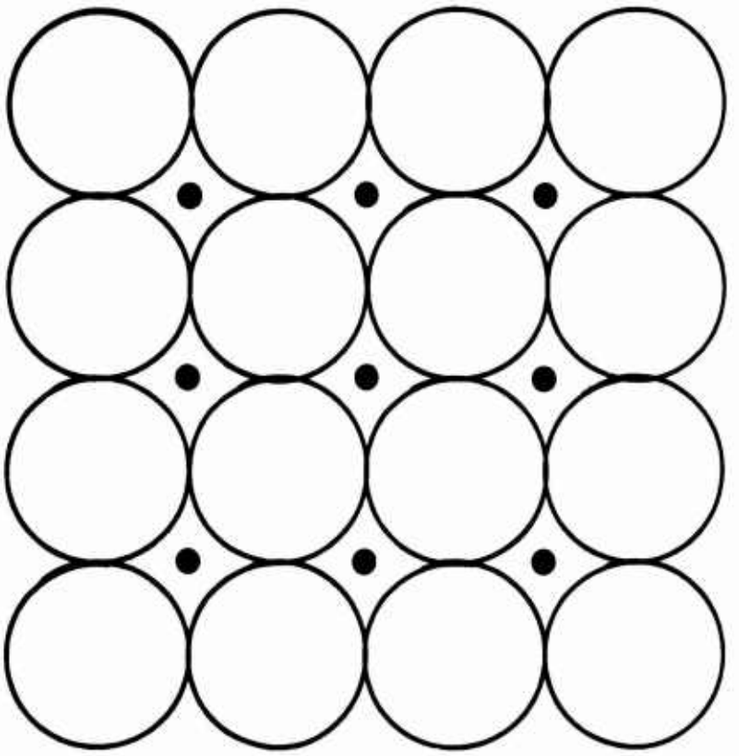

● DENOTES A DEPRESSION FILLED BY A SPHERE IN THE LAYER ABOVE

FIGURE C.2

PYRAMIDAL VIEW OF THE FACE-CENTERED CUBIC ARRAY OF EQUAL SPHERES

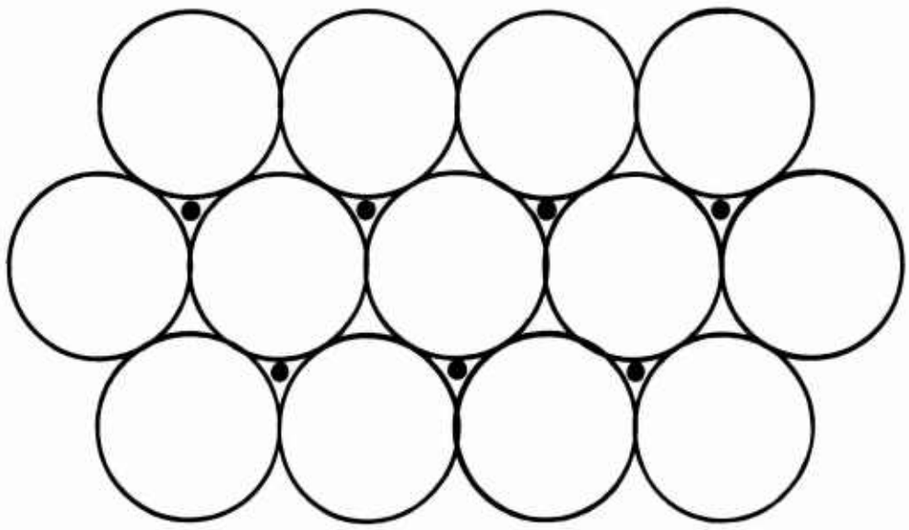

● DENOTES A DEPRESSION FILLED BY A SPHERE IN THE LAYER ABOVE

FIGURE C.3

HEXAGONAL OR TETRAHEDRAL VIEW OF THE FACE-CENTERED CUBIC ARRAY OF EQUAL SPHERES

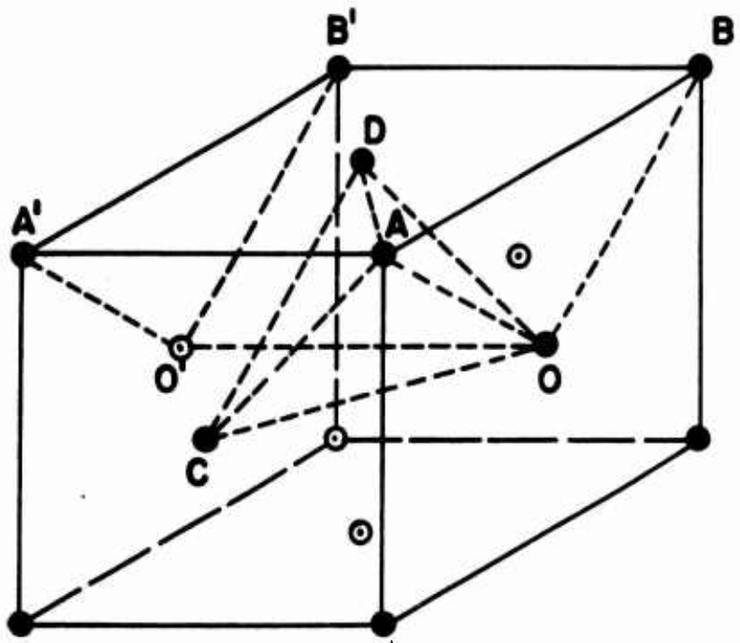

FIGURE C.4

THREE VIEWS OF THESAME DENSE PACKING OF EQUAL SPHERES: FACE-CENTERED CUBIC, PYRAMIDAL AND TETRAHEDRAL

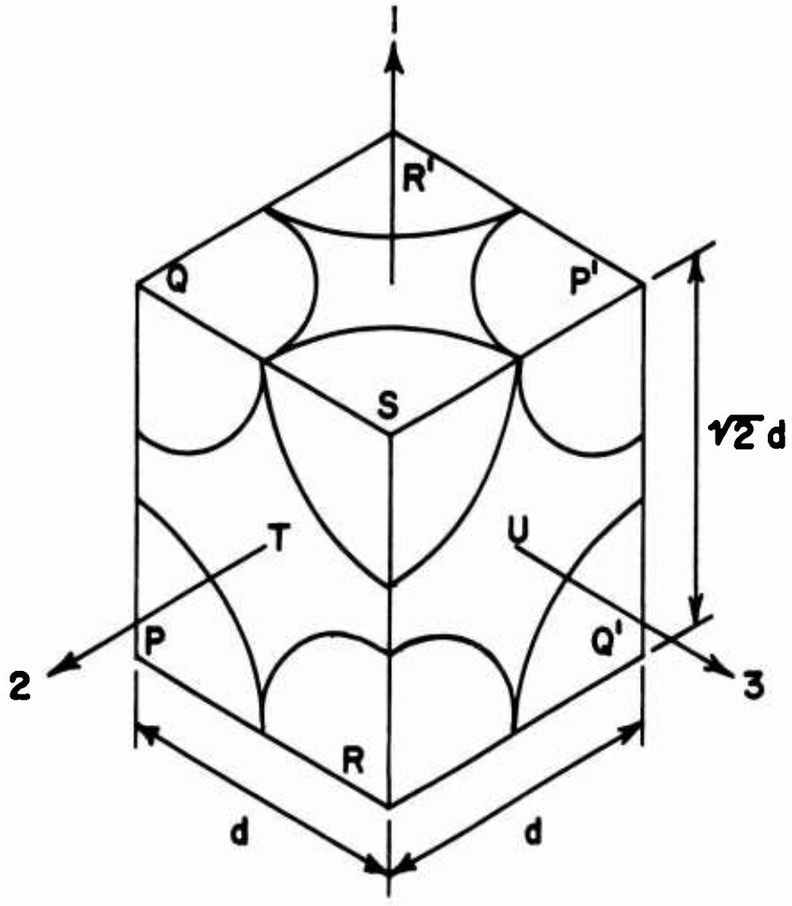

FIGURE C.5

UNIT ELEMENT CONSIDERED IN THE STRENGTH ANALYSIS OF A FACE-CENTERED CUBIC (PYRAMIDAL) PACKING OF EQUAL ROUGH RIGID SPHERES

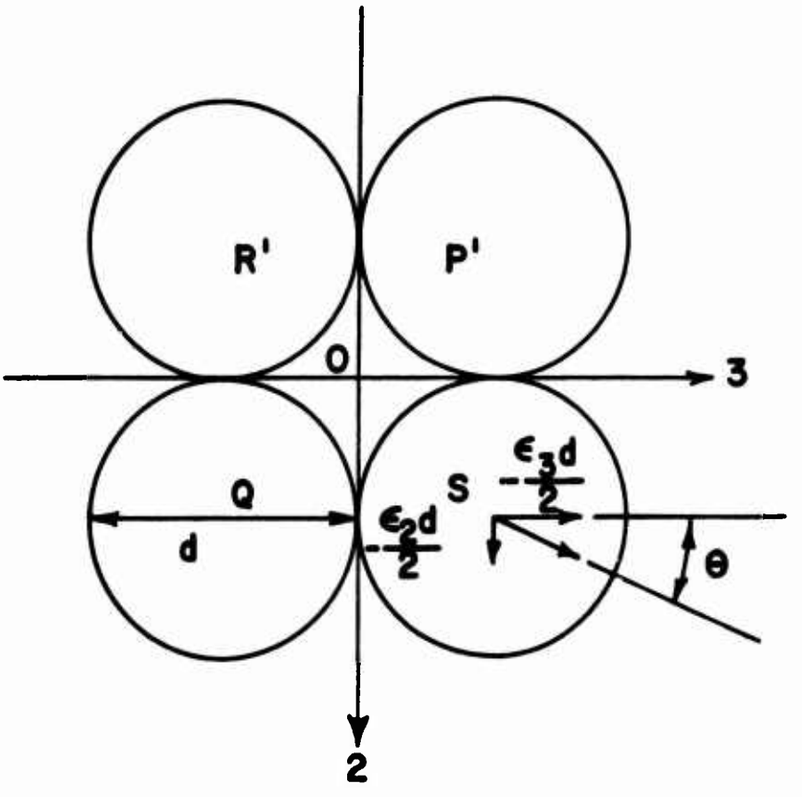

$\epsilon_2 = -2\Delta \sin\theta$

$\epsilon_3 = -2\Delta \cos\theta$

FIGURE C.6

ASSUMED DEFORMATION PATTERN